Spatial organisation of the immunoglobulin heavy chain locus and inter-chromosomal gene networks driving B cell development

Olga Mielczarek

University of Cambridge
Murray Edwards College
Babraham Institute

September 2017

This dissertation is submitted for the degree of Doctor of Philosophy

Declaration

This dissertation is the result of my own work and includes nothing which is the outcome of work done in collaboration except as declared in the Preface and specified in the text. It is not substantially the same as any that I have submitted, or, is being concurrently submitted for a degree or diploma or other qualification at the University of Cambridge or any other University or similar institution except as declared in the Preface and specified in the text. I further state that no substantial part of my dissertation has already been submitted, or, is being concurrently submitted for any such degree, diploma or other qualification at the University of Cambridge or any other University of similar institution except as declared in the Preface and specified in the text. It does not exceed the prescribed word limit (60,000 words) for the Degree Committee of Biology.

Olga Mielczarek

September 2017

Dla Babci i Dziadka

Acknowledgements

I would like to thank everyone who played a significant role in helping me complete my PhD:

Most of all, my supervisor Anne for enabling me to carry out a PhD in her lab, for guidance, support and availability to discuss science at any time. Peter R-G for being my assessor and his insightful advice.

Mike from whom I inherited a promising project and who was always helpful and willing to dig out information from the back of his head. Luca and Zhan for a great collaboration that elevated my work to new heights. Louise, Dan, Biola and Stefan for initial training in lab techniques and invaluable scientific help.

Steven, Csilla, Simon A, Felix and Hashem for massive help with bioinformatics. Especially Steven and Csilla from whom I learned a great deal and thanks to whom I befriended the command line. Also thanks to Peter and Louise for help with R.

Anne S-P for chats and laughs and occasional help with statistics, without which in fact I would be doomed. Also, for R and Graphpad magic. And not the least for being the best cake eater a baker could wish for.

Simon W for guidance on microscopy, Arthur for assistance with cell sorting, Kristina for sequencing, animal technicians at the BSU and technical services and support, without whom this work would not have been possible. Thanks to Matt for printing this very thesis, for admin support and general helpfulness.

The PE stars Tacita and Mike who initiated me in the joys of public engagement. Not everyone gets to design their own DNA puzzle!

Fellow students Bryony, Amanda and Jayeta for morning bus chats, lifts home, many cups of tea and a healthy dose of moral support. Also Alice, Izi, Louise, Jo, Peter and Sam for being fantastic colleagues and for becoming my friends. Boo for always being hyper and never failing to make me laugh.

My best friends Ola, Dorass, Lu, Irma, Misiek and Ola B for being the greatest forever. Nathan for making excellent shepherd's pie, being the most patient person I know and always being my beacon. My mum and sis for visiting me in Cambridge frequently, being fun and super supportive all the time.

By far the biggest thanks goes to my grandparents who were my most ardent cheerleaders and always asked about my progress. Najbardziej dziękuję Babci i Dziadkowi za bycie moimi największymi fanami. Żadna rozmowa nie obyła się bez zapytania o moja prace.

Summary

B lymphocytes produce a wide array of antibodies to recognize a countless number of antigens. This highly diverse repertoire is produced during B cell development in the bone marrow from the immunoglobulin heavy chain (Igh) and light chain (Igk and Igl) loci. The mouse Igh is a large (~3Mb) multigene locus that contains 195 variable (V), 10 diversity (D) and 4 joining (J) genes that undergo developmentally regulated V(D)J recombination to produce the variable region of the antibody.

Gene expression depends on spatial organisation of chromatin. To ensure that all V genes have a chance to recombine, they are brought into physical proximity to the D-J region by locus contraction and DNA looping. Not all V genes recombine with equal frequencies and we aim to investigate how dynamic changes in 3D structure of the Igh locus facilitate V(D)J recombination.

Chromosome conformation capture techniques have revolutionised studies of genome conformation. I have applied a novel form of enriched Hi-C to study both intra-locus (cis) and genome-wide (trans) interactions of the immunoglobulin loci in pro-B and pre-B cells. This method provides a higher resolution than Hi-C and is less biased than 4C and 5C.

I have mapped all cis interactions within the Igh locus to produce a comprehensive view of the structure of the locus prior to recombination. This approach has shown that the 3' superanchor (3'CBEs) and the Intergenic Control Region 1 (IGCR1) containing CTCF sites are the two most interacting regions in the locus making long-range contacts with all V genes. A second major conformational feature is that the distal V genes form a large tightly looped domain forming the centre of mass of the locus to which the 3'CBEs and IGCR1 loop. Thanks to a collaboration on polymer modelling, 5000 single conformations were simulated based on the ensemble Hi-C data. This showed that every structure is different, supporting a model of dynamic and flexible organisation of the locus rather than hierarchical subdomains therein. Moreover, there is only a slight trend for V genes interacting more often with the D-J region to have higher recombination scores, supporting an 'equal opportunity for all' model in which participation of V genes in V(D)J recombination is not constrained by linear genomic distance from the DJ region. Nevertheless, CTCF binding level does contribute to V gene recombination frequency.

I have also discovered that Igh and Igk loci participate in a highly specialised network of genome-wide (trans) interactions involving genes encoding B cell-specific factors essential for activation and maintenance of B cell identity, including Pax5, Foxo1, Ebf1, and Runx1. I have validated these by 3D DNA FISH and found that at the pro-B cell stage the Igh is involved in many trans interactions, whereas Igk does not make any contacts. In contrast, Igk gains numerous trans interactions at the pre-B cell stage, many of which overlap with the interactions Igh participates in at both developmental stages. Together, these findings reveal a complex developmentally regulated orchestration of genome conformation changes that underpins B cell development.

Table of Acknowledgement of Assistance

1) Initial training in techniques and laboratory practice and subsequent mentoring:
   - Anne Corcoran – supervisor
   - Dan Bolland – mentor
   - Peter Rugg-Gunn – assessor
   - General training in techniques – Dan Bolland, Biola Javierre, Louise Matheson, Amanda Baizan-Edge, Peter Chovanec

2) Data obtained from a technical service provider (e.g. DNA sequencing, illustrations, simple bioinformatics information etc)
   - Bioanalyzer assay for DNA library QC – Kristina Tabbada
   - Illumina sequencing – Kristina Tabbada
   - FACS sorting – Arthur Davis
   - DNA sequencing: Beckman Coulter
   - Oligonucleotide synthesis: Sigma-Aldrich

3) Data produced jointly (e.g. where it was necessary or desirable to have two pairs of hands)
   - Capture Hi-C libraries were made jointly with Louise Matheson

4) Data/materials provided by someone else (e.g. one-off analysis, bioinformatics analysis, where parallel data or technical provision in a very different area is needed to provide a connected account in the thesis)
   - BSU staff looked after mice
   - Capture baits were made with Mike Stubbington, Dan Bolland and Louise Matheson
   - $Rag^{-/-Bal}$ pro-B cells were harvested by Mike Stubbington and Dan Bolland, $Rag^{-/-Mom}$ pro-B cells, Rag/81X pre-B cells and thymocytes were harvested jointly with Louise Matheson
   - Mapping and filtering of Hi-C and Capture Hi-C data from the first sequencing run was done by Steve Wingett
   - Custom scripts for custom genome generation, merging of bam files and averaging of the interaction matrices were written by Steven Wingett
   - Guidance on Homer was given by Steven Wingett and Csilla Varnai
   - Guidance on Seqmonk was given by Simon Andrews
   - Guidance on Cytoscape was given by Boo Virk
   - Statistics to identify significant trans interactions was done by Anne Segonds-Pichon
   - Polymer modelling was done by Luca Giorgetti and Yinxiu Zhan

129Sv	129Sv mouse strain
3'RR	3' regulatory region
3C	Chromosome conformation capture
4C	Chromosome conformation capture on chip
5C	3C carbon copy
Ac	Acetylation
AID	Activation-induced deaminase
APC	Antigen presenting cell
BAC	Bacterial artificial chromosome
BCR	B-cell receptor
C	Constant gene
C57BL/6	C57 black 6 mouse strain
CBE	CTCF-binding element
CDR	Complementarity determining region
CHi-C	Capture Hi-C
ChIP-seq	Chromatin immunoprecipitation followed by high throughput sequencing
CLP	Common lymphoid progenitor
CSR	Class switch recombination
Ct	Cycle threshold
D	Diversity gene
DHS	DNase I hypersensitive site
DMEM	Dulbecco's modified Eagle medium
DNase	Deoxyribonuclease
dNTP	Deoxynucleotide triphosphate
DP	CD4 CD8 double positive
DSB	Double-stranded break
DTT	Dithiothreitol
EDTA	Ethylenediaminetetraacetic acid
ELP	Early lymphoid progenitor
ESC	Embryonic stem cell
Eμ	Immunoglobulin heavy-chain intronic enhancer
F1	First generation
FACS	Fluorescence-activated cell sorting
FCS	Foetal calf serum
FISH	Fluorescence in situ hybridisation
FITC	Fluorescein isothiocyanate
FrOSt1a	Friend of site 1 a
FrOSt1b	Friend of site 1 b
H3K27me3	Histone 3 lysine 27 tri-methylation
H3K4Ac	Histone 3 lysine 4 acetylation
H3K4me2/3	Histone 3 lysine 4 di/tri-methylation
H3K9ac	Histone 3 lysine 9 acetylation
H3K9me2	Histone 3 lysine 9 di/tri-methylation
HMM	Hidden Markov Model
HS	(DnaseI) Hypersensitive site
HSC	Haematopoietic stem cell
ICE	Iterative correction of eigenvector decomposition
IFN-y	Interferon gamma
Ig	Immunoglobulin
IGCR1	Intergenic control region 1
Igh	Immunoglobulin heavy-chain

Igκ	Immunoglobulin kappa light-chain
Igλ	Immunoglobulin lambda light-chain
J	Joining gene
LAD	Lamina-associated domain
LB	Luria-Bertani media
LMPP	Lymphoid-primed multipotent progenitor
MACS (bioinformatics)	Model-based Analysis for ChIP-Seq
MACS (cell preparation)	Magnetic cell sorting
MAR	Matrix attachment region
MHC	Major histocompatibility complex
MLP	Multilineage progenitor
MPP	Multipotent progenitor
N-nucleotides	Non-templated nucleotides
NGS	Next-generation sequencing
NHEJ	Non-homologous end-joining
P-nucleotides	Palindromic nucleotides
PAIR	PAX5-activated intergenic repeat
PBS	Phosphate-buffered saline
PCA	Principal component analysis
PCI	Phenol:chloroform:isoamyl alcohol
PCR	Polymerase chain reaction
PE	Phycoerythrin
PerCP-Cy5.5	Peridinin chlorophyll A protein-cyanine 5.5
Pre-BCR	Pre-B-cell receptor
qPCR	Quantitative polymerase chain reaction
RAG	Recombination activating gene
RNA Pol II	RNA polymerase II
RNA-seq	High throughput sequencing of RNA
RSS	Recombination signal sequence
SDS	Sodium dodecyl sulfate
SHM	Somatic hypermutation
shRNA	Short hairpin RNA
SPRI	Solid phase reversible immobilisation
SSC	Saline sodium citrate
T2C	Targeted chromatin capture
TAD	Topologically-associated domain
TCR	T cell receptor
TdT	Terminal deoxynucleotidyl transferase
TF	Transcription factor
V	Variable gene

Contents

List of figures

List of tables

1

1. Introduction

The work presented in this thesis explores the nuclear dynamics of V(D)J recombination and early B cell development. I focused on the spatial organisation of the Igh locus, determining the DNA interactions that underline the generation of a diverse immunoglobulin repertoire. I have also examined a network of interactions between the Igh locus and other genes. Here, I first introduce early B cell development and the process of V(D)J recombination. Subsequently I provide an overview of genome organisation in 3D and the methods used to investigate chromatin conformation. Finally, I present the current models of the spatial arrangement of the Igh locus and the interactions of its elements.

1.1. Adaptive immunity

The adaptive immune system comprises humoral immunity mediated by B lymphocytes and cellular immunity mediated by T lymphocytes. A shared key property of these cells is the ability to generate a wide array of highly antigen-specific receptors and to retain a memory of encountered pathogens. These are the T cell receptors (TCR) produced by T cells and the Immunoglobulins (Ig) produced by B cells. TCRs are exclusively transmembrane proteins, whereas immunoglobulins can be alternatively spliced and expressed either on the cell surface as the B cell receptor (BCR) or as secreted antibodies. The TCRs on the surface of T cells bind epitopes processed by the antigen presenting cells (APCs) and displayed via the major histocompatibility complex II (MHC II) proteins. Helper T (Th) cells ($CD4^+$) start producing TCRs specific to the presented antigen and cytotoxic T cells ($CD8^+$) induce apoptosis of infected cells. The Th cells activate B cells expressing a receptor specific to the antigen that activated the Th cells. The TCR recognizes the antigen molecules bound to the MHC II on the B cell, which stimulates clonal expansion of B cells through the interaction of the CD40 ligand (CD40L) on the Th cell surface and the CD40 molecule on the B cell surface. This ensures proliferation of B cells producing highly antigen-specific BCRs. Secreted antibodies bind to antigens without the need of presentation. They bind to antigens on the surface of pathogens interfering with their function, stimulate phagocytosis and activate the complement system promoting inflammation. The antibody-mediated response against new pathogens

might be weak and slow, however, specialized long-lived memory B cells are able to retain the information about previously encountered antigens and mount a stronger and faster secondary response upon subsequent infection with the same or a similar pathogen (reviewed in Flajnik and Kasahara 2010; Boehm 2011).

In order to target a large variety of pathogens, the immunoglobulins must be able to recognize a vast number of antigens. The human antibody repertoire is estimated to be ~10^{11} unique BCRs and immunoglobulins with high binding specificities (Georgiou et al. 2014). If each were encoded by a separate gene it would exceed the capacity of the genome. Instead, to provide the antibody receptor diversity, combinatorial rearrangements of DNA segments from the immunoglobulin heavy chain (Igh) and light chain (Igk and Igl) loci are generated during V(D)J recombination, followed by editing and selection of the the primary antibody repertoire for high specificity and against auto-reactivity.

1.2. Early B cell development

In order to become highly specialized mature cells that produce one type of antibody and have immunological memory, B cells first undergo a strictly regulated multistep developmental process characterized by two stages: specification (induction of B lineage-specific gene expression) and commitment (repression of alternative lineage gene expression).

B lymphocytes arise from self-renewing hematopoietic stem cells (HSCs) in the bone marrow (**Figure 1**). HSCs are precursors for lymphoid, erythroid and myeloid lineages and are characterized by high expression of the receptor for stem cell factor c-kit while lacking the expression of cell surface markers specific to any of the three lineages (Kim et al. 1998). PU.1 transcription factor is essential for cell maintenance of HSCs as well as for differentiation, where low levels of PU.1 promote B cell lineage while high levels of PU.1 promote myeloid lineage (Iwasaki et al. 2005; DeKoter and Singh 2000). Similarly, E2A is involved both in HSC maintenance and in the activation of lymphoid genes (Dias et al. 2008a), but also later for surrogate light chain and activation-induced cytidine deaminase (AID) expression (Sayegh et al. 2003; Greenbaum et al. 2004). Other transcription factors such as Ikaros, BCL11A and MYB have a strictly lymphoid-priming role (Ng et al. 2009; Yu et al. 2012; Greig et al. 2010) and activate Runx1 and Foxo1 expression (Huang et al. 2008; Yu et al. 2012). The earliest differentiated progeny of HSCs are multipotent progenitors (MPPs; also termed multilineage progenitors (MLPs)), which have multilineage differentiation potential but have lost the capacity for extensive self-renewal (Adolfsson et al. 2001). A subset of MPPs expressing high levels of tyrosine kinase receptor FLT3 are defined as lymphoid-primed MPPs (LMPPs), which are no longer able to differentiate into erythroid cells (Adolfsson et al. 2005). FLT3 signalling is required for the upregulation of lymphoid genes, including Il7r, Rag1 and Ebf1 (Dolence et al. 2014), which are directly activated by E2A, PU.1 and Ikaros (Lin et al. 2010; Reynaud et al. 2008). LMPPs expressing Rag1 and TdT, but not Il7r are defined as early

lymphoid progenitors (ELPs), which are restricted to the lymphoid lineage (Igarashi et al. 2002) and their survival requires BCL11A (Yu et al. 2012). ELPs give rise to the common lymphoid progenitors (CLPs) able to differentiate into B lymphocytes, T lymphocytes and natural killer cells (Kondo et al. 1997). The Ly6d marker identifies B cell-biased lymphoid progenitors (Ly6d+) within the CLPs (Inlay et al. 2009). The recombination of immunoglobulin loci has been reported to start in CLPs that have exited the cell cycle (Rumfelt et al. 2006).

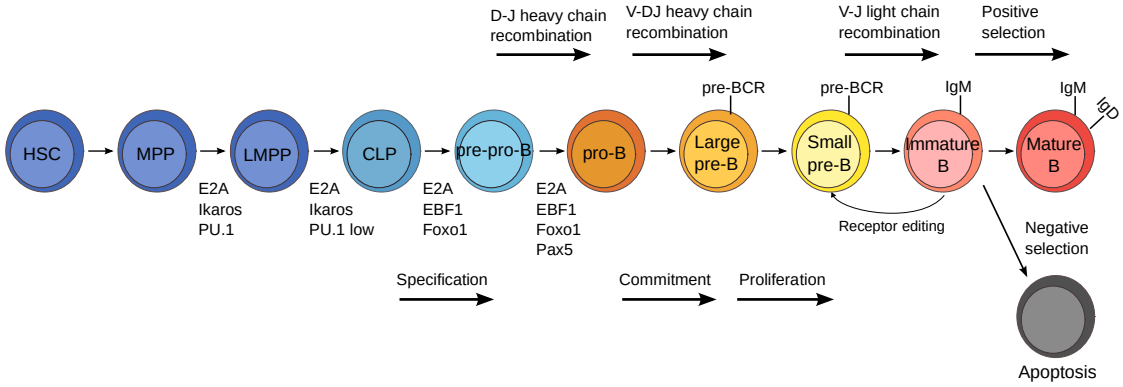

Figure 1. B cell development in the bone marrow. The timing of lymphocyte commitment to the B lineage, proliferation and immunoglobulin genes rearrangement is indicated by the arrows below and above the diagram. Crucial transcription factors promoting progression through early developmental stages are indicated between cells.

CLPs give rise to the first clearly distinguishable B cell population termed pre-pro-B cells, which are characterized by the expression of a B cell-associated cell surface marker B220 (Li et al. 1996) and E2A-mediated expression of Ebf1 and Foxo1 which are involved in a positive feedback loop (Mansson et al. 2012). Low expression of Il7r allows for high level of Rag1 and Rag2 expression activated by Foxo1, Ikaros, and E2A (Amin and Schlissel 2008; Johnson et al. 2008). Ebf1 is a B lineage-specifying factor repressing the T lineage-specifying factor Notch1 (Nechanitzky et al. 2013). D-J recombination of the immunoglobulin heavy chain locus (Igh) takes place in CLPs and pre-pro-B cells (Rumfelt et al. 2006), followed by V-DJ recombination in committed pro-B cells (progenitor B cells) (Alt and Baltimore 1982). Pro-B cell commitment is marked by the expression of the lineage commitment factor Pax5, and its target CD19 (Fuxa and Busslinger 2007), which initiates a new feedback loop between Pax5, Ebf1, Irf4 and Irf8 (Decker et al. 2009; Schebesta et al. 2007; Lin et al. 2010). In early pre-B cells, the recombination of the heavy chain is completed successfully when its polypeptide is expressed on the cell surface in association with a surrogate light chain (SLC), comprising the pre-BCR (Mårtensson and Ceredig 2000). Signalling through the pre-BCR prompts B cells to re-enter the cell cycle and proliferate, which coincides with downregulation and degradation of Rag1 and Rag2, upregulation of IL7R signalling (Zhang et al. 2006b) and downregulation of Foxo1 by very high levels of EBF1 (Amin and Schlissel 2008; Timblin and Schlissel 2013). As B cells exit the cell cycle again, re-activation of Rag1 and Rag enables recombination of the immunoglobulin light chain locus (Igk or Igl) in late

pre-B cells (Hardy et al. 2007). If the light chain polypeptide is functional and dimerises with the heavy chain, a new BCR is expressed on the cell surface. These newly formed immature B cells enter an important checkpoint: selection against auto reactivity (Hardy and Hayakawa 2001). Autoreactive B cells undergo receptor editing by further light chain recombination to produce a non-autoreactive receptor (Nemazee 2006). The light chain recombination is first attempted on both Igk loci, then on both Igl loci. If unsuccessful, cells undergo apoptosis. The immature B cells express IgM and leave the bone marrow to mature in peripheral lymphoid organs, where thanks to alternative splicing they express IgM and IgD as mature recirculating follicular B cells (Allman et al. 2001; Rolink et al. 2004). Upon activation by antigen and T cell-secreted cytokines, the antibody sequence undergoes affinity maturation. B cells can change the class of the immunoglobulin they express in the process of class switch recombination (CSR) catalysed by a B cell-specific enzyme activation-induced cytidine deaminase (AID). CSR leads to a switch to another constant gene, and efficient CSR is dependent on both the Igh intronic enhancer (Eμ) (Sakai et al. 1999) and the 3' regulatory region (3'RR) (Pinaud et al. 2001). AID also catalyses somatic hypermutation (SHM) of the VDJ sequence by introducing C to T mutations (Maul and Gearhart 2010).

1.3. Immunoglobulin loci and V(D)J recombination

The antibody molecule consists of four polypeptides: two identical heavy chains and two identical light chains, where the light chain can consist of either a kappa or a lambda chain (**Figure 2**) (Schroeder and Cavacini 2010). Each antibody chain contains an antigen-binding variable domain on its N-terminus and a constant domain on its C-terminus. The adjacent variable domains of the heavy and light chains are collectively termed complementarity-determining region (CDR) (Wu and Kabat 1970; Capra and Kehoe 1975) and are the products of V(D)J recombination. The constant domain anchors the BCR to the B cell surface or allows secreted antibodies to interact with other cells. Constant regions of the heavy chain determine the antibody isotype (class) (M, D, G, A or E).

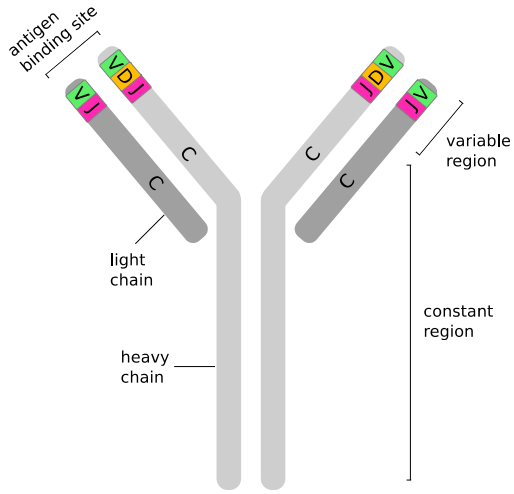

Figure 2. Structure of an antibody. An antibody consists of two identical heavy chains and two identical light chains, which are joined by disulphide bonds and non-covalent interactions. The heavy chain variable region is encoded by the recombined VDJ sequence, whereas the light chain variable region is encoded by the recombined VJ sequence. The two variable regions contain complementary determining regions (CDRs), which together form an antigen-binding site characterised by unique antigen-binding specificity. The constant region enables dimerization of the two heavy and two light chains, anchors the antibody on the cell surface and transmits signals to the immune system.

1.3.1. Coding and regulatory elements of the Igh locus

The murine Igh locus is a large (~3Mb) complex genomic region close to the telomere of the long arm of chromosome 12. The full sequence of the C57BL/6 mouse strain Igh locus has been assembled and characterized by our lab (Johnston et al. 2006) revealing its repetitive nature, especially in the V region. There are 195 variable (V) genes (spanning 2.5Mb), 12 diversity (D) genes (60kb), 4 joining (J) genes (1.5kb) and 8 constant (C) genes (180kb) (**Figure 3**). The V genes belong to 16 families based on sequence homology and are grouped into proximal V genes (nearer the 3' end; for example V7183 and VQ52 families), middle V genes (for example VS107, VSM7, VGAM and J606 families) and distal V genes (nearer the 5' end of the locus; for example VJ558 and V3609 families) (Brodeur and Riblet 1984; Johnston et al. 2006). 128 out of 195 V genes recombine with significant frequency above the detection threshold and are considered active (Bolland et al. 2016). D genes are classified into four families: DFL16.1, DSP, DST4 and DQ52. 10 out of 12 D genes recombine productively (Bolland et al. 2016). 9 D genes are clustered together, 85kb downstream of the V genes, while the DQ52 gene is 18kb further away, less than 1kb upstream of the four J genes (Ye 2004). 8 C genes are spread over 180kb downstream of J genes. Each V, D and J gene is flanked by a recombination signal sequence (RSS), which determines their recombination capacity depending on its similarity to a consensus sequence (Cowell et al. 2002). To ensure unidirectional recombination, the J and the V genes are flanked by a 23RSS and the D genes by 12RSSs. Transcriptional promoters are present upstream of every V, D and C gene. All

elements are in the same orientation on the same DNA strand. The locus contains several cis-regulatory elements including enhancers and insulators.

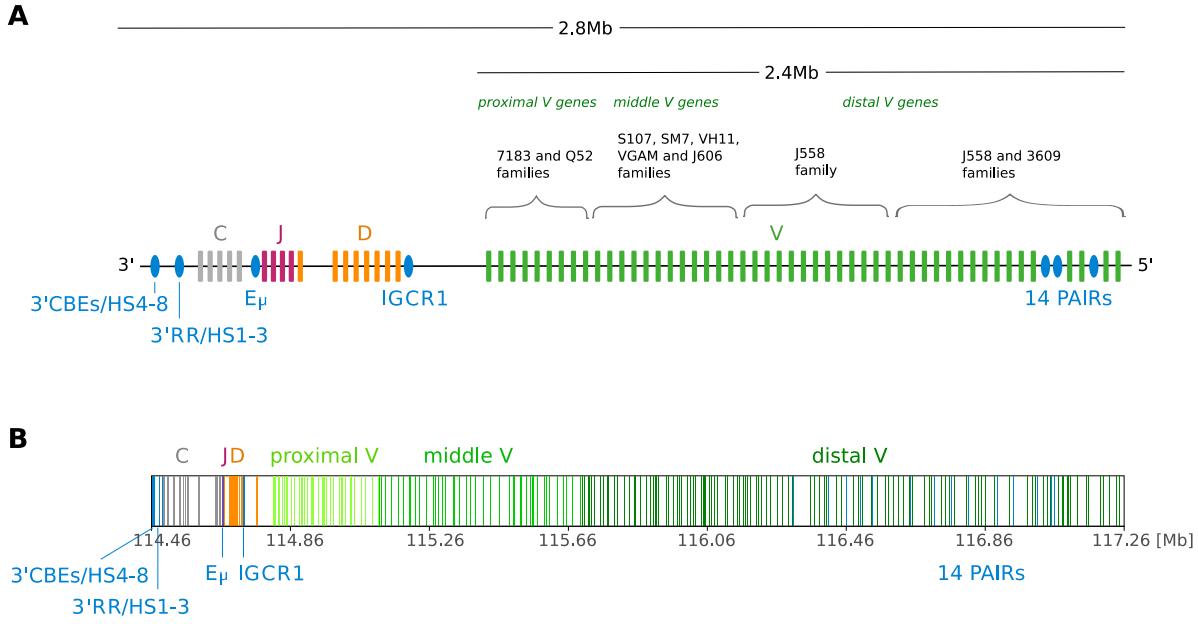

Figure 3. Linear arrangement of the Igh locus. A. The mouse Igh locus is 2.8Mb long and harbours 8 Constant (C) genes, 4 Joining (J) genes, 12 Diversity (D) genes and 195 Variable (V) genes. The V genes belong to 16 families based on sequence homology and are broadly divided into 3'-proximal, middle and 3'-distal genes. At the 3' end of the locus there are 8 DHS sites with enhancer properties, 4 of which comprise the 3' Regulatory Region (3'RR), and 7-10 CTCF-binding sites forming the 3' superanchor (3'CBEs). The intronic enhancer Eμ is located between the C and J genes. The Intergenic Control Region 1 (IGCR1) at the end of D gene cluster contains 2 CTCF-binding sites that act as an insulator. There are ~110 CTCF-binding sites in the V gene region, and towards the 5' end of the locus are 14 Pax5-Activated Intergenic Repeat (PAIR) elements characterized by high levels of non-coding transcription and active chromatin marks. This figure in not to scale. **B.** Igh locus annotation to scale. Every vertical line represents a gene or a regulatory element. The two D genes between the IGCR1 and the proximal V genes are inactive D genes DST4.2 and DFL16.2 (not depicted in A). Genomic coordinates are mouse chr12 mm9 genome assembly.

3' superanchor (3'CBEs/HS4-8)

A recently identified superanchor at the 3' end of the Igh locus is a structural and functional feature characterized by the presence of multiple densely clustered CTCF binding elements (CBEs), DNA hypomethylation and a strategic position at a domain boundary (Benner et al. 2015). The 3' end of the Igh locus contains 8 DNase hypersensitive sites (HS1-8) (Dariavach et al. 1991; Zhou et al. 2002; Garrett et al. 2005). HS5-8 overlap with 7 CBEs and there are a further 9 CBEs within 120kb of HS8, while the 3' superanchor has been proposed to be composed of 10 CBEs (Benner et al. 2015). The exact number of CTCF sites in this region differs slightly between published CTCF ChIP-seq datasets (Lin et al. 2012; Ebert et al. 2011; Degner et al. 2011; Benner et al. 2015; Bolland et al. 2016). The 3' superanchor, referred to here as 3'CBEs/HS4-8, denotes the 3' boundary of the Igh locus domain and is involved in DNA interactions with the V genes, most probably via the numerous CTCF sites present in that region (Benner et al. 2015; Zhang et al. 2012). This dual role reflects the ability of CTCF to act as both an insulator and a contact mediator (reviewed in Ong and Corces 2014). All

CTCF sites in the 3'CBEs/HS4-8 are in convergent orientation to the CTCF sites in the V region, which is a favoured configuration among genomic contacts (Rao et al. 2014a; Sanborn et al. 2015; Fudenberg et al. 2016). It has been proposed that the interactions between the 3' superanchor and the V genes give an equal opportunity to all Vs to be used in V(D)J rearrangement (Medvedovic et al. 2013, Benner et al. 2015). CTCF binding to the Igh is lymphocyte-specific but invariant during early stages of B cell development (Lin et al. 2012; Ebert et al. 2011; Degner et al. 2011) and the chromatin at the 3'CBEs bears active marks and is demethylated prior to pro-B cell stage, which suggests other epigenetic mechanisms allowing 3'CBEs interactions with V genes (Benner et al. 2015; Giambra et al. 2008).

3' Regulatory Region (3'RR/HS1-3)

HS1-3 at the 3' end of the Igh locus, between the 3' superanchor and the constant genes, make up the 3' Regulatory Region (3'RR/HS1-3). Often HS4-7 from the 3' superanchor are also attributed to the 3'RR. Deletion of HS1-4 results in a lack of CSR, reduced SHM and aberrant mono-allelic transcription after rearrangement (Pinaud et al. 2001; Shi and Eckhardt 2001; Dunnick et al. 2009; Vincent-Fabert et al. 2010), whereas deletion of HS5-7 results in increased proximal V gene usage and reduced overall Igh locus compaction (Volpi et al. 2012). In this thesis, the designation 3'CBEs/HS4-8 and 3'RR/HS1-3 is geographical as well as based on the step-wise activation of this region. The HS4 and sequences downstream gain open chromatin marks in pro-B cells whereas the HS1-3 enhancer is activated after pre-B cell stage and it persists in mature splenic B cells (Garrett et al. 2005; Giambra et al. 2008).

hRE1 and hRE2 elements between the constant genes Cy1 and Cy2b are new putative regulatory elements with PAX5-binding sites and HS properties. hRE1, which also binds YY1, has been shown to enhance transcription in vitro and in a pro-B cell specific manner (Predeus et al. 2014).

Intronic enhancer Eμ

The intronic enhancer Eμ, which is located between the J and C genes, was the first eukaryotic enhancer element described (Banerji et al. 1983; Alt and Baltimore 1982). It comprises a 220bp enhancer core and two flanking matrix attachment regions (MARs) (Cockerill et al. 1987). The core sequence contains binding sites for multiple transcription factors including YY1, E2A and PU.1, but not CTCF (Greenbaum et al. 2004; Ebert et al. 2011; Degner et al. 2011; Nikolajczyk et al. 1999; Mullen et al. 2011; Medvedovic et al. 2013). Eμ promotes the expression of a rearranged VDJ product (Gillies et al. 1983; Sakai et al. 1999) and plays a role in allelic exclusion (Li and Eckhardt 2009), but has no effect on SHM (Perlot et al. 2005). It promotes deposition of the active chromatin mark H3K4Ac, but not H3K9me2 and H3K4me2 (Chakraborty et al. 2009b). The Eμ is required for effective D-J recombination and for V-DJ recombination of distal V genes, but V(D)J recombination is not completely abolished in its absence (Perlot et al. 2005; Afshar et al. 2006; Bolland et al. 2007; Chakraborty et al. 2009b). It remains unclear whether the defect in V-DJ recombination in the

absence of Eμ is a secondary effect of reduced D-J recombination. Reduced overall compaction of the Igh locus has been reported in the absence of Eμ (Chakraborty et al. 2009b; Guo et al. 2011a; Gerasimova et al. 2015).

Intergenic control region 1 (IGCR1)

The intergenic control region 1 (IGCR1) is strategically positioned just upstream of the D genes and contains two CTCF-binding sites (Degner et al. 2009; Featherstone et al. 2010; Guo et al. 2011b). The two CBEs are oppositely oriented and mediate interactions with the downstream 3' superanchor as well as with upstream CTCF sites in the V region (Guo et al. 2011b; Zhang et al. 2012; Medvedovic et al. 2013). The IGCR1 acts as an insulator to prevent premature V-DJ recombination (Featherstone et al. 2010) and in pro-B cells it insulates proximal V genes to promote distal V gene usage and equalize recombination opportunity for all Vs (Guo et al. 2011b). The two CBEs in the IGCR1 act in a cooperative fashion (Lin et al. 2015).

PAX5-activated intergenic repeats (PAIRs)

14 Pax5-activated intergenic repeat (PAIR) elements lie in the distal V3609 gene cluster and are the only regulatory elements in the V region described to date (Ebert et al. 2011). PAIRs are ~450kb long, are bound by Pax5, CTCF, cohesin, YY1 and E2A, are characterized by PAX5-dependent active chromatin marks (H3K9ac, H3K4me2 and H3K4me3) and give rise to Pax5-regulated non-coding antisense transcription only at the pro-B cell stage.

1.3.2. Mechanism of V(D)J recombination

V(D)J recombination is catalyzed by the endonuclease complex RAG encoded by the recombination activation genes Rag1 and Rag2. The RAG complex is sufficient *in vitro* (McBlane et al. 1995) and essential *in vivo* (Mombaerts et al. 1992; Shinkai et al. 1992) to initiate V(D)J recombination. RAG expression is restricted to developing lymphocytes and it becomes expressed in CLPs. Ikaros and E2A activate the Rag1 gene promoter, whereas PAX5, MYB, LEF1 and GATA-3 activate the Rag2 promoter (Chen et al. 2011). The RAG complex binds to the RSS of the J gene via RAG1 in a sequence-specific manner enhanced by RAG2 (Ciubotaru et al. 2003; Shimazaki et al. 2012), and recruits a D gene and its RSS. The high-mobility group-box protein 1 (HMGB1) acts as a cofactor and increases RAG affinity for the RSSs (van Gent et al. 1997). RAG cleaves the DNA precisely between the RSSs and the coding sequence by hydrolysis of the top strand to introduce a nick with a free 3'-hydroxyl group, which performs a nucleophilic attack on the bottom strand to produce a double strand break (DSB) (reviewed in Schatz and Swanson 2011) (**Figure 4**). A hairpin loop is formed between the two DNA strands at the gene end, which is facilitated by HMGB1 (Swanson 2002; Bergeron et al. 2005). The coding sequences are joined together by the non-homologous end joining (NHEJ) machinery and the intervening region is excised (Rooney et al. 2004). Asymmetric nicking during hairpin repair can introduce the addition of germline-

encoded palindromic (P-) nucleotides (Meier and Lewis 1993). Repertoire diversity is further increased by terminal deoxynucleotidyl transferase (TdT) that inserts non-template (N-) nucleotides in recombination junctions as well as by variable cutting back of the coding ends (Benedict et al. 2000).

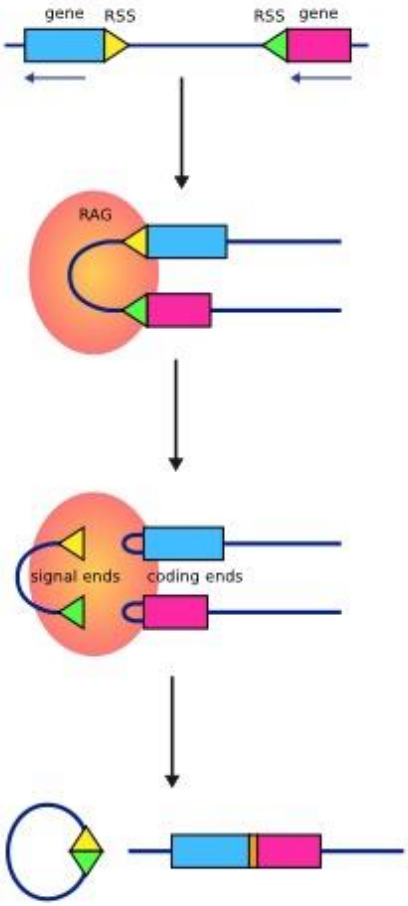

Figure 4. The mechanism of RAG cleavage in V(D)J recombination. The RAG complex (orange ellipse) composed of RAG1 and RAG2 binds to one RSS and creates a nick. The second RSS is then recruited and nicked and both RSSs (yellow and green triangles) are cleaved to create double strand breaks (DSB) between the genes and the RSSs. The coding (gene) ends (blue and pink rectangles) form hairpins, which are processed by the non-homologous end joining NHEJ machinery into a coding joint. During this process additional N- and P-nucleotides are incorporated by TdT (orange rectangle between blue and pink rectangles). The signal ends are blunt and form a signal joint in a form of an excision circle. Figure adapted from Fugmann *et al*. 2000.

1.3.3. Immunoglobulin heavy chain recombination

The D-J recombination commences in CLPs and early pre-pro-B lymphoid progenitors and is completed by the early pro-B cell stage on both Igh alleles (Rumfelt et al. 2006) (**Figure 5**). Next, only one Igh allele undergoes V-DJ recombination in committed pro-B cells. A successful recombination event is achieved when the newly produced heavy chain polypeptide pairs with a surrogate light chain and is expressed as a pre-B cell receptor (pre-BCR) on the cell surface (Mårtensson and Ceredig 2000). The second allele undergoes allelic

exclusion (Corcoran 2005). If this first V-DJ recombination event is unsuccessful, then recombination is attempted on the remaining allele. Signaling by the pre-BCR leads to a proliferative burst (Rolink et al. 2000) and temporary suppression of RAG, after which cells exit the cell cycle again (Bassing et al. 2002) and the Igk locus undergoes a single recombination event (V-J) in pre-B cells to generate the immunoglobulin light chain. Pairing of heavy and light chains generates the BCR.

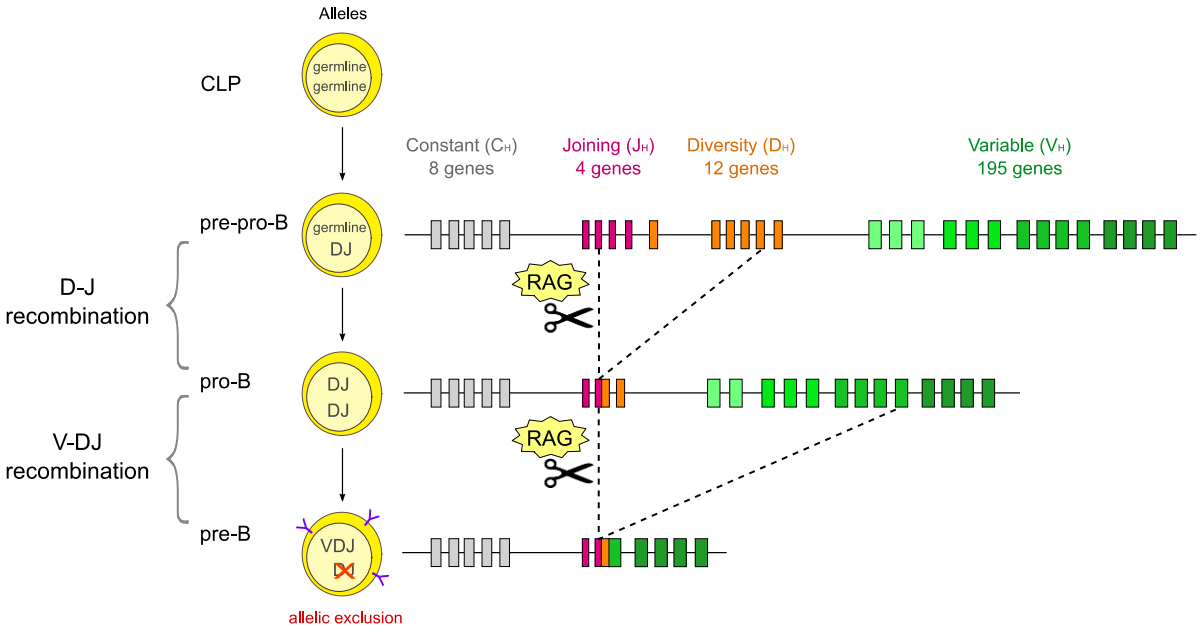

Figure 5. V(D)J recombination of the immunoglobulin heavy chain locus. D-J recombination begins at the pre-pro-B cell stage (Ly6d^{+} B-biased CLPs) and completes by the pro-B cell stage on both Igh alleles. In pro-B cells, V-DJ recombination initiates on only one of the alleles, and if successful, the second DJ-recombined allele undergoes allelic exclusion. If the first V-DJ recombination is unsuccessful, then the second allele recombines. V(D)J recombination is catalysed by the RAG recombinase complex.

1.4. Nuclear dynamics

1.4.1. Chromatin organisation

Chromatin is non-randomly organized in the nucleus as indicated by the earliest studies of organization of chromosomes in eukaryotes by light microscopy (reviewed in Cremer and Cremer 2010). The initial discovery of a rosette-like structure of chromatin (Paulson and Laemmli 1977) was confirmed by early FISH studies proposing chromatin to behave in a random walk fashion with 0.5-5Mb loops attached to a fixed backbone (Trask 1991). Almost two decades of research into chromatin organisation has revealed complex structural and functional compartmentalisation of the genome (reviewed in Bickmore and van Steensel 2013).

1.4.1.1. Chromosome territories

Chromosomes occupy individual discrete territories in the nucleus (Koss 1998; Nagele et al. 1999; Bolzer et al. 2005; Roix et al. 2003; Parada et al. 2002; Meaburn and Misteli 2007; Cremer and Cremer 2010). The majority of gene interactions are therefore intra-chromosomal (Lieberman-Aiden et al. 2009), however, genes can loop out of their chromosome territories to interact in trans with other genomic regions. Examples include the Igh locus and myc genes in activated B cells (Osborne et al. 2007), multiple co-regulated erythroid genes (Schoenfelder et al. 2010), HoxB genes upon activation (Chambeyron and Bickmore 2004), Shh gene when expressed in the limb bud (Amano et al. 2009) and IFN-gamma-upregulated MHC genes (Volpi et al. 2000).

1.4.1.2. A and B compartments

Genome-wide DNA interaction profiling revealed that the chromatin spatially separates into an alternating pattern of large domains termed A and B compartments. Gene-rich euchromatic A compartments tend to reside towards the periphery on the chromosome territory, whereas gene-poor heterochromatic B compartments tend to reside near the centre of the chromosome territory (Lieberman-Aiden et al. 2009; Yaffe and Tanay 2011; Nagano et al. 2017; Belaghzal et al. 2017). As structural entities, the size of compartments remains largely invariant during development and between cell types, however over 30% of compartments change between active (A compartment) and inactive (B compartment) status (Nagano et al. 2015; Dixon et al. 2015). A/B compartments are also the most prominent feature of chromatin organisation in plants and yeast, which lack topologically-associated domains described below (Feng et al. 2014; Wang et al. 2015; Liu et al. 2017; Hsieh et al. 2015).

1.4.1.3. Topologically-associated domains (TADs)

The mammalian genome is compartmentalised into topologically associated domains (TADs) of several megabases in size (Lieberman-Aiden et al. 2009; Dixon et al. 2012; Nora et al. 2012; Sexton et al. 2012). These spatially constrained functional units tend to interact internally more than externally. TADs have defined domain boundaries often occupied by CTCF and cohesin insulating two adjacent functional genomic regions (Dixon et al. 2012; Symmons et al. 2014; Rao et al. 2014d). TADs have been shown to be largely invariant between different cell types, although their insulation can vary depending on the transcriptional activity of genes and intra-domain DNA interactions can change considerably in a tissue- and developmental stage-specific manner (Dixon et al. 2012; Nora et al. 2012; Phillips-Cremins et al. 2013; Le Dily et al. 2014; Dixon et al. 2015). However, ‘facultative’ TADs have also been identified and characterise Hox gene activation (Noordermeer et al. 2011). TADs have been recently shown to be functionally but not structurally privileged (Zhan et al. 2017b) and their size can change with the introduction of new functionally-relevant elements (Franke et al. 2016). The size of TADs and sub-TADs is driven by the functional properties of the regulatory microenvironments they insulate and there does not

seem to be a universally privileged TAD scale. TADs also correspond to genomic units of replication timing (Pope et al. 2014).

The Igh locus forms its own ~2.8Mb TAD (Lin et al. 2012; Zhang et al. 2012; Benner et al. 2015; Montefiori et al. 2016) (**Figure 6**). At the 3' end its boundary is demarcated by the 3' superanchor (3'CBEs/HS4-8) (Medvedovic et al. 2013; Benner et al. 2015; Montefiori et al. 2016), whereas at the 5' end, although a massive drop in DNA interactions has been observed after the last V gene (Medvedovic et al. 2013), no regulatory elements have been identified there (Perlot et al. 2010). The Zfp386 gene, which is just outside the 5' boundary of the Igh TAD, has been shown to interact largely with downstream sequences (Medvedovic et al. 2013).

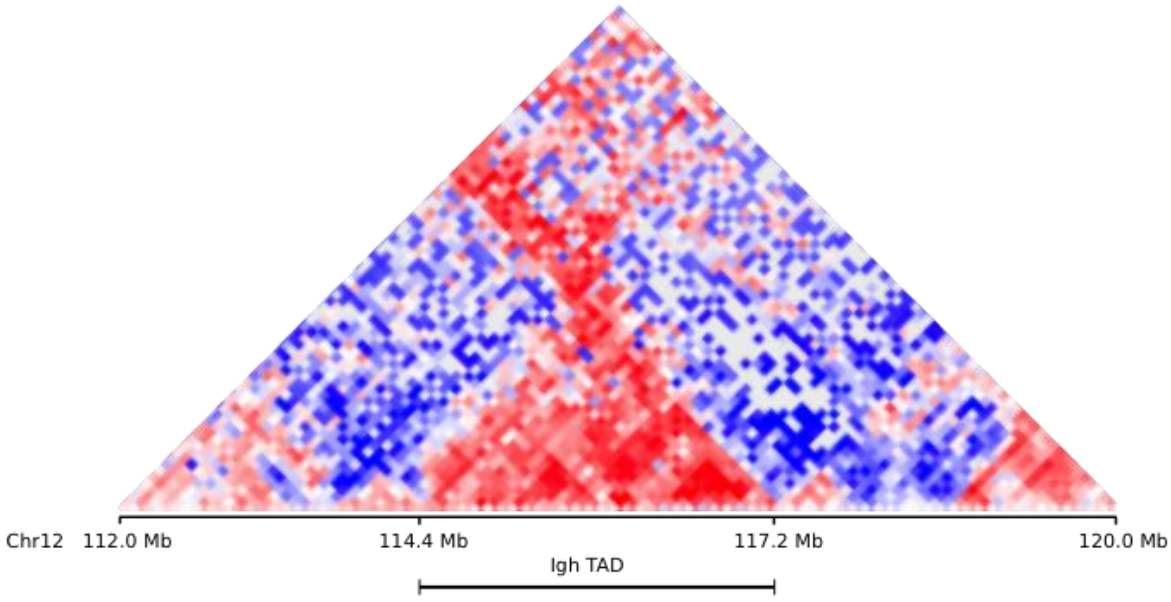

Figure 6. The Igh TAD. Hi-C interactions of the genomic region containing the Igh locus, illustrating the well-defined Igh TAD. Hi-C data is from an AMuLV pro-B cell line D345 from Zhang *et al*. 2012. Normalised observed/expected interaction frequencies were plotted in Juicebox software in 100kb bins with 10kb step.

1.4.1.4. Architectural proteins - the role of CTCF

CTCF (CCCTC-binding factor) is a highly conserved zinc finger protein, which interacts with other CTCF-bound sites and is the only known insulator protein in vertebrates (Bell et al. 1999; Wallace and Felsenfeld 2007; Phillips and Corces 2009). CTCF has been implicated in determining TAD boundaries and localising at the bases of DNA loops (Dixon et al. 2012; Sanyal et al. 2012; Tang et al. 2015a; Rudan et al. 2015; Sanborn et al. 2015; Fudenberg et al. 2016; Zhan et al. 2017b). CTCF-CTCF interactions create domains that insulate gene activities from neighbouring regions and also mediate DNA loop formation facilitating interactions between genes and regulatory elements. Examples of CTCF-mediated interactions controlling gene expression include beta-globin, MHC class II and Kcnq5 loci (Palstra et al. 2003; Majumder et al. 2008; Ren et al. 2012). The directionality of CTCF-binding elements (CBEs) is important and they preferentially interact when positioned in

convergent orientation (oppositely directed and facing each other) (Rao et al. 2014d; Sanborn et al. 2015; Gómez-Marín et al. 2015; Fudenberg et al. 2016). Notably, this convergent orientation favours RAG recombinase activity in off-target sites (Hu et al. 2015). CTCF binding to the genome has been shown to be mostly invariant during development. Multiple sites genome-wide are bound in embryonic stem cells and only a proportion of these lose CTCF binding with developmental progression, albeit retaining it at lineage-specific sites (Beagan et al. 2017).

It is challenging to study the genome architecture upon global loss of CTCF and out of two recent reports, which used the auxin-inducible degron system for acute CTCF depletion in mouse embryonic stem cells, one has shown the genome conformation to be largely preserved (Kubo et al. 2017), whereas another observed a loss in TAD border insulation (Nora et al. 2017). Both studies found that A and B compartments remain invariant in the absence of CTCF.

CTCF sites flanking the Igh TAD are also bound by CTCF in non-lymphocytes, but CTCF binding within the Igh locus is lymphocyte-specific, although enriched throughout B cell development (Degner et al. 2009). There are ~120 CBEs dispersed throughout the Igh locus (Degner et al. 2011; Ebert et al. 2011; Bolland et al. 2016). Surprisingly, a pro-B cell-specific conditional knockout of CTCF under the mb1-cre promoter control showed no effect on the Igh locus (Ribeiro de Almeida et al. 2011), although recombination and contraction of the Igk locus were reduced at the subsequent developmental stage (pre-B cells), suggesting that CTCF deposited at the pre-pro-B cell stage maintained its role in pro-B cells. A conditional CTCF knockout under an earlier RAG promoter control resulted in a complete absence of pro-B cells, supporting this model (Heath et al. 2008). As described above, CTCF sites in the Igh show both insulation and interaction-mediating properties (Featherstone et al. 2010; Guo et al. 2011b; Benner et al. 2015).

Most CTCF-bound sites are also bound by cohesin (Parelho et al. 2008; Rubio et al. 2008; Wendt et al. 2008). This four-protein complex forms a ring around the DNA sequence it associates with (reviewed in Nasmyth and Haering 2009; Rankin and Dawson 2016) and facilitates the interactions between two convergent CTCF elements (Hnisz et al. 2016). Cohesin itself is loaded onto the chromatin by Nipbl (Tonkin et al. 2004; Krantz et al. 2004) but its binding to DNA is stabilised by CTCF (Wendt et al. 2008; Parelho et al. 2008). Like CTCF, cohesin has been shown to be enriched at TAD boundaries (Dixon et al. 2012; Van Bortle et al. 2014) and at bases of DNA loops. CTCF and cohesin often together mediate genomic interactions, such as for example in the beta-globin and IFN-gamma loci (Chien et al. 2011; Hadjur et al. 2009). This, however, is not a rule, as shown for the Oct4 locus where the binding of cohesin coincided with the binding of a transcription activator Mediator (Kagey et al. 2010), as well as for oestrogen-regulated genes that bound cohesin and oestrogen receptor alpha (Schmidt et al. 2010). Cohesin plays a role in the architecture of antigen receptor loci as exemplified by mediating long-range interactions in the Tcra locus (Seitan et al. 2011) (reviewed in Seitan et al. 2012). In the Igh locus, cohesin binding seems to

be more dynamic than that of CTCF, being most enriched at the pro-B stage (Degner et al. 2009). A model has emerged that CTCF-binding denotes potential sites of interactions, but contacts are determined by cohesin binding (Holwerda and de Laat 2013). Genome-wide loss of cohesin binding does not affect genome compartentalisation (Seitan et al. 2013; Rao et al. 2017), however it has been recently reported that deletion of cohesin loading factor Nipbl1 results in widespread disruption of loop domains (Rao et al. 2017). This was not observed by previous studies ablating one of cohesin subunits (Seitan et al. 2013; Sofueva et al. 2013; Zuin et al. 2014).

YY1, first discovered as a transcriptional repressor binding to the Eμ (Ephrussi et al. 1985; Church et al. 1985; Shi et al. 1991), is another ubiquitously expressed zinc finger protein participating in mediating DNA looping and it is able to associate with CTCF at the protein level i*n vitro* (Donohoe et al. 2007). Particularly, YY1 binding has been shown to co-localise with CTCF binding at highly conserved sites of increased transcriptional activation (Schwalie et al. 2013). YY1 binding to DNA loop anchors is much more dynamic and cell type-specific than that of CTCF (Beagan et al. 2017). In contrast to CTCF, a pro-B cell-specific conditional knockout of YY1 under the mb1-cre promoter control resulted in reduced Igh locus contraction, reduced V-DJ recombination and an arrest at pro-B to pre-B transition, which could not be rescued by the introduction of a rearranged Igh (Liu et al. 2007). YY1-binding sites in the Igh locus tend to co-localize with PAX5-, but not CTCF-binding sites (Ebert et al. 2011; Revilla-i-Domingo et al. 2012; Medvedovic et al. 2013). YY1 has been shown to play a broad regulatory role at multiple stages of B cell development (Kleiman et al. 2016). In the Igk locus, YY1 is involved in the recruitment of EZH2 and ensuring a diverse V-J_k repertoire (Pan et al. 2013).

1.4.2. Epigenetic factors that regulate immunoglobulin loci rearrangement

1.4.2.1. Accessibility hypothesis

Cleavage of different antigen receptor loci genes in different lymphocytes and in a developmental stage-specific mono-allelic manner must be strictly regulated to confine the generation of double-stranded breaks in space and time. The accessibility hypothesis proposed that this specificity is achieved by altering the access of each immunoglobulin locus to the RAG recombinase complex through remodelling of the chromatin structure (Yancopoulos and Alt 1985). Indeed, whilst the TCR loci remain inactive in B lymphocytes, the Igh and Igk/Igl loci are activated at consecutive stages of B cell development (reviewed in Outters et al. 2015; Cobb et al. 2006). The activation of the Igh locus is characterised by extensive sense and antisense non-coding germline transcription from the Eμ, J and D genes in pre-pro-B cells, followed by transcription over the V genes in pro-B cells, consistent with the timings of D-J and V-DJ recombination (Lennon and Perry 1985; Kim 1990; Thompson 1995; Bolland et al. 2004; 2007). Step-wise histone acetylation (Chowdhury and Sen 2001; Johnson et al. 2003),

deposition of H3K4me3 marks (Chakraborty et al. 2007; Morshead et al. 2003), removal of repressive mark H3K9me2 (Johnson et al. 2003), gain of DNase hypersensitivity (Maes et al. 2001) and DNA demethylation (Storb and Arp 1983) of the locus all coincide with V(D)J recombination (**Figure 7**).

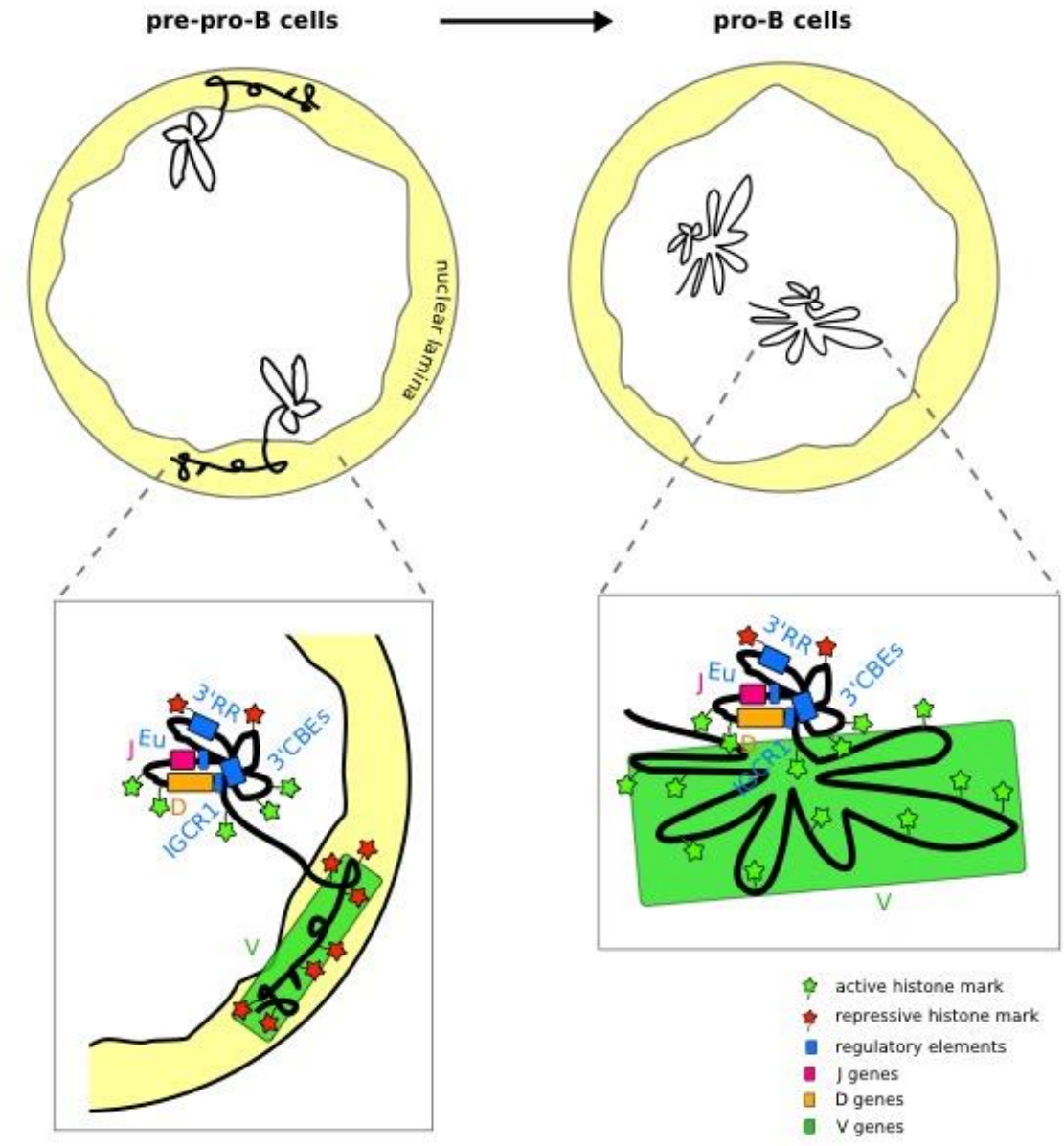

Figure 7. Contraction and relocation of the Igh locus. In pre-pro-B cells the Igh locus (black ribbon) in tethered to the nuclear lamina via the V gene region, which carries repressive chromatin marks, whereas the 3' end is facing the inside of the nucleus and carries active chromatin marks over the J and D genes (insert). The 3' end is looped and the IGCR1 insulates the J and D genes from pre-mature V-DJ recombination. In pro-B cells, the Igh locus relocates to the centre of the nucleus and undergoes overall compaction. The V region becomes highly looped, gains active chromatin marks and interacts with the D-J region and the 3'CBEs superanchor (insert). The 3'RR is inactive until the next developmental stage.

Prior to D-J recombination, the Iμ transcript from the intronic enhancer Eμ (Lennon and Perry 1985; Kim 1990) and the μ_0 transcript from the PDQ52 promoter extend across the J,

Eμ and C regions (Thompson 1995). D antisense transcription begins from the Eμ enhancer and elongates through J and D genes in the opposite direction (Bolland et al. 2007). This non-coding transcription moves nucleosomes to create a highly accessible environment over the J and D genes. Sense non-coding transcription from the V gene promoters precedes V-DJ recombination (Yancopoulos and Alt 1985; Corcoran et al. 1998). The antisense transcription starts from the VJ606 and VJ558 family regions, as well as from the PAIR elements and is pro-B cell specific (Ebert et al. 2011). PAIR4, PAIR6 and PAIR11 transcripts are the most highly expressed (Verma-Gaur et al. 2012). It has been proposed that the chromatin opening capacity of non-coding transcription makes relevant parts of the Igh locus accessible at appropriate stages of the recombination process (Featherstone et al. 2010).

The Igh locus is largely DNA methylated in pro-B cells, with only Eμ and the last D gene (DQ52) showing tissue-specific demethylation. Highly localised Eμ-dependent demethylation at newly formed DJ junctions may distinguish these sites for V-DJ recombination (Selimyan et al. 2013). Substantial demethylation also occurs at the 3' superanchor at the locus boundary (Benner et al. 2015).

In non-B cells the Igh locus carries the repressive marks H3K9me2 and H3K27me3 (Morshead et al. 2003; Chakraborty et al. 2009b). In B cells, these repressive marks are sequentially substituted by H3K9 acetylation of the J, D and V regions coinciding with their ordered recombination (Chowdhury and Sen 2001; Espinoza and Feeney 2005; Maes et al. 2006). Activating H3K4me3 marks are gained at newly recombined DJ segments (Subrahmanyam et al. 2012), while repressive H3K9me2 marks in the V region are removed in a PAX5-dependent manner to facilitate V-DJ recombination (Johnson et al. 2004). IL7R signalling mediates the promotion of sense non-coding transcription (Corcoran et al. 1998) and distal V gene acetylation (Bertolino et al. 2005).

The expression of RAG recombinase strictly precedes the recombination events and is tightly controlled during the cell cycle, with high levels in G1 and low levels in G0 (Li et al. 1996; Jiang et al. 2005). RAG expression begins in CLPs and is attenuated during pro-B to pre-B transition to allow for a proliferative burst. It is resumed in pre-B cells to catalyse the recombination of light chain loci (Bassing et al. 2002). RAG expression is initiated by E2A and Ikaros (Hsu et al. 2003; Wei et al. 2005) and is later enhanced by PAX5 (Lauring and Schlissel 1999).

1.4.2.2. Subnuclear localisation - locus relocation

Prior to the pro-B stage the Igh locus is situated in a repressive chromatin environment and is anchored to the lamina via its 5' end (V genes), but the the 3' end (D and J genes) is oriented towards the centre of the nucleus. This may explain some level of D-J recombination prior to pro-B stage (Fuxa et al. 2004). FISH studies haves shown that prior to V-DJ recombination the Igh locus relocates from repressive heterochromatin at the periphery of the nucleus to euchromatin in the centre (Kosak et al. 2002; Rother et al. 2016) (**Figure 7**). The ability to recombine is not a prerequisite for relocation, as the Igh relocates in $Rag^{-/-}$ B cells (Kosak et al. 2002; Rother et al. 2016). However, relocation is absent or reduced in several knockout

mouse models of key B cell lineage transcription factors, such as Ebf1$^{-/-}$, E2A$^{-/-}$ and Il7r$^{-/-}$, but not in Pax5$^{-/-}$ and Yy1$^{-/-}$ (Kosak et al. 2002; Hewitt et al. 2010; Lin et al. 2012; Sayegh 2005; Guo et al. 2011a). After V(D)J recombination, the non-functional Igh locus has been shown to be recruited to pericentromeric heterochromatin and decontracted (Hewitt et al. 2008). However, a recent study has reported that the Igh returns to contacting the lamina in pre-B cells, albeit in a contracted state, thus relocation might be specifically linked with the developmental regulation of V-DJ recombination (Rother et al. 2016).

It was originally reported that the Igk locus also relocates in pro-B cells, suggesting additional mechanisms preventing Igk recombination before the pre-B cell stage (Kosak et al. 2002; Fitzsimmons et al. 2007). However, a recent study has shown that the Igk locus does not relocate from the periphery until the pre-B cell stage, when V-J$_k$ recombination takes place, prompting the authors to propose that relocation has a previously unsuspected role in ordered recombination (Rother et al. 2016).

1.4.2.3. Locus contraction

Simultaneously with relocation, the Igh locus undergoes large-scale contraction in pro-B cells to bring all V genes into close spatial proximity with D and J genes (Fuxa et al. 2004; Sayegh 2005; Liu et al. 2007; Reynaud et al. 2008; Rother et al. 2016) (**Figure 7**). This was determined by measuring the reduction in the distance between FISH probes positioned at the opposite ends of the locus (Fuxa et al. 2004). Upon locus contraction, the Igh elements become juxtaposed and confined to a much smaller space than might be expected from their genomic distance. Detection of DNA looping in Igh elements showed that distal V genes frequently loop closer to the C region than proximal V genes, which are closer in linear sequence (Sayegh 2005). These changes in the spatial organisation of the locus are accompanied by the deposition of active chromatin marks (Johnson et al. 2003). Locus contraction has been shown to be impaired in the absence of key transcription factors such as PAX5, YY1, E2A and Ikaros (Fuxa et al. 2004; Reynaud et al. 2008; Medvedovic et al. 2013).

PAX5 has binding sites at the HS4, at both hRE elements, at the Eμ, at the 3' end of D genes as well as multiple binding sites in the distal V region, particularly at the PAIRs and at approximately 20 V gene RSSs (Ebert et al. 2011; Bolland et al. 2016). Most PAX5 sites in the 3' part of the locus overlap with YY1-binding sites (Medvedovic et al. 2013; Bolland et al. 2016). Pax5 expression is necessary but not sufficient for locus contraction as ectopic Pax5 expression in T cells showed increased chromatin accessibility over distal Vs, Igh relocation and proximal V-DJ recombination, but not locus contraction. On the other hand, reconstitution of Pax5 expression in Pax5$^{-/-}$ pro-B cells induced locus contraction, which suggests an additional unknown factor expressed only in pro-B cells and not in T cells (Fuxa et al. 2004). PAX5 has been proposed to mediate subdomain formation via very long-range DNA looping in the Igh locus (Montefiori et al. 2016; Gerasimova et al. 2015), whereas YY1 is thought to facilitate the overall locus contraction (Gerasimova et al. 2015; Medvedovic et al. 2013).

The role of E2A and Ikaros in Igh locus contraction may be indirect as these factors act early in development. A lack of E2A causes a developmental arrest at pre-pro-B cell stage (Bain 1994; Zhuang 1994; Dias et al. 2008b) and a lack of Ikaros leads to ablation of all lymphocyte formation (Georgopoulos et al. 1994; Wang et al. 1996). E2A and Ikaros have very few binding sites in the Igh locus, although E2A binds to the PAIR elements (Ebert et al. 2011).

1.4.2.4. Recombination factories

The J genes and the Eμ show high enrichment for active histone mark H3K4me3 and DNase hypersensitivity. The PHD domain of RAG2 specifically binds H4K4me3 and this depends on the amount of H3K4me3 deposited over the Eμ and Js (Liu et al. 2007; Matthews et al. 2007). This interaction in turn is thought to increase the cleavage capacity of RAG1 (Deng et al. 2015). It has been suggested that this open active chromatin environment creates a RAG-rich subnuclear hub termed 'recombination centre', which provides a focal point for D-J recombination, followed by the looping of V genes to the DJ segment for V-DJ recombination (Subrahmanyam and Sen 2010; Ji et al. 2010; Schatz and Ji 2011). Therefore, the recombination centre is a region on the Igh locus sequence where RAG catalyses the recombination reaction.

On the other hand, subnuclear foci enriched for transcriptionally active RNA polymerase II, that exist even in absence of transcription, have been termed 'transcription factories' (Jackson et al. 1993; Iborra et al. 1996; Mitchell and Fraser 2008). Upon activation of transcription, genes move to associate with pre-assembled transcription factories (**Figure 8**A). Co-regulated genes have been shown to physically associate in shared transcription factories (Schoenfelder et al. 2010; Park et al. 2014). RAG and RNA PolII are thought to bind in the V region but it has been challenging to measure their enrichment levels by ChIP-seq (Ji et al. 2010; Choi et al. 2013; Teng et al. 2015).

Recent work from our lab has shown that the RAG complex colocalizes with RNA Pol II in subnuclear compartments and that the Igh is anchored in a transcription factory (Jo Martins, unpublished data). It has been suggested that the non-coding transcript originating from the Eμ, which is transcribed continuously in pro-B cells (Bolland et al. 2007), supports recombination by recruiting the recombination centre into a transcription factory (reviewed in Stubbington and Corcoran 2013), creating a 'recombination factory'. A recombination factory comprises a transcription factory defined as a nuclear focus rich in RNA Pol II and a recombination centre defined as a RAG-binding region over the J genes (**Figure 8**B). Together, they provide the open chromatin state and the catalytic enzymes required for recombination.

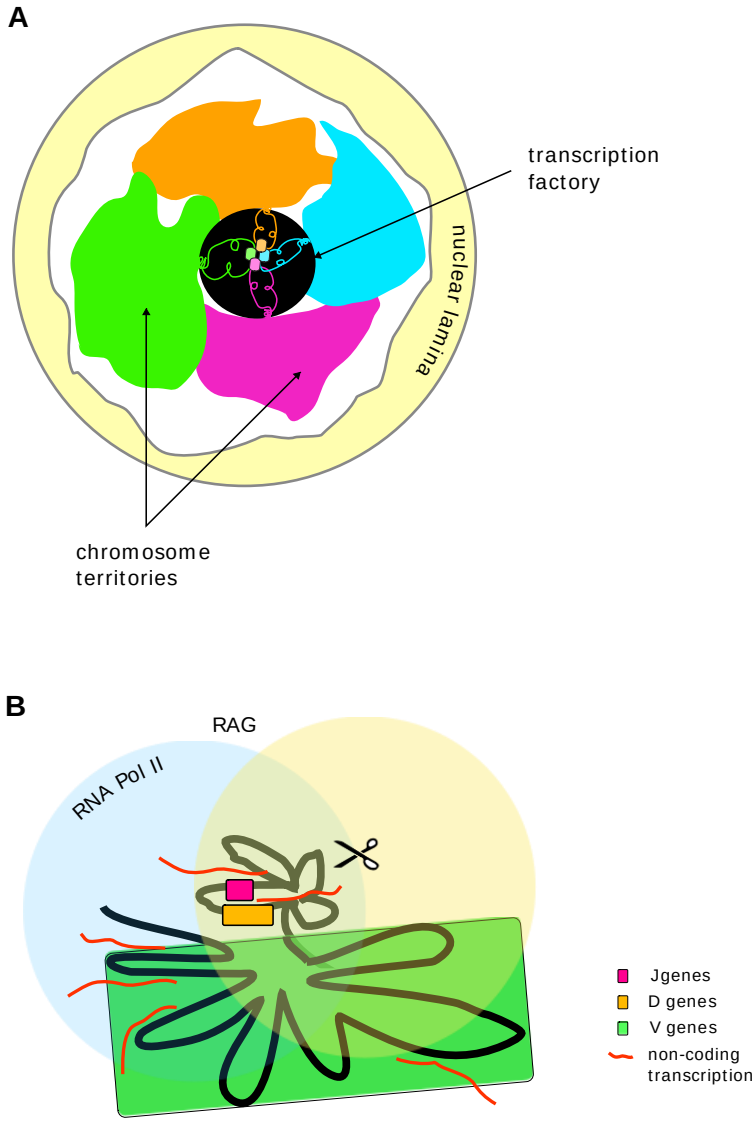

Figure 8. Transcription and recombination factories. **A.** A transcription factory containing transcribing genes looped out of their chromosome territories. **B.** A recombination factory around the recombining Igh locus is enriched for Pol II and the RAG complex.

1.4.2.5. Local determinants of V gene usage

While locus contraction and DNA looping enable all V genes to contact the DJ region, the ultimate usage of all active V genes in V(D)J rearrangements depends on the local chromatin context at the V genes and their RSSs. Recent assays developed to quantify the primary antibody repertoire have shown that V genes recombine with dramatically varied frequencies (Arnaout et al. 2011; Choi et al. 2013; Bolland et al. 2016; Lin et al. 2016). Work in our lab demonstrated that active V gene recombination is governed by two distinct local chromatin states at the RSSs defined by specific genetic and epigenetic factors. Binding of either PAX5 and IRF4 or CTCF and RAD21 to the V genes' RSSs characterises chromatin states of actively recombining V genes (Bolland et al. 2016). Whereas lack of binding of either of those two groups of factors characterises an inactive chromatin state of V genes that

do not recombine. Analysis of interspersed V gene families and their active recombination led to the discovery that these chromatin states are based on she evolution of V genes and not on geographical location along the Igh locus."

1.4.3. Probing the 3D conformation of the genome

Fluorescence in-situ hybridisation (FISH) has been used extensively to interrogate the spatial organisation of the genome. It has allowed for visualisation of chromosome territories (Bolzer et al. 2005) and their intermingling (Branco and Pombo 2006), as well as observations that certain genes loop out of their chromosome territories upon activation (Volpi et al. 2000; Chambeyron and Bickmore 2004; Osborne et al. 2007; Amano et al. 2009; Schoenfelder et al. 2010). FISH was also used to demonstrate the re-location from the nuclear periphery of the immunoglobulin and β-globin loci upon activation (Kosak et al. 2002; Rother et al. 2016; Ragoczy et al. 2006). This method detected the recruitment of erythroid genes located on the opposite ends on the chromosome into a shared transcription factory (Osborne et al. 2004) as well as co-localisation of the three immunoglobulin loci in plasma cells during highest rates of antibody transcript production (Park et al. 2014).

Chromosome Conformation Capture methods

The chromosome conformation capture (3C) technique has been developed to alleviate some limitations of the FISH method, such as low resolution and a low number of loci that can be assayed in one experiment. 3C relies on cross-linking of chromatin in a population of cell nuclei, subsequent digestion with a restriction enzyme and ligation of paired DNA molecules, followed by cross-link reversal and analysis of ligation products, which comprise sequences that were in physical proximity in the nucleus at the time of cross-linking (**Figure 9**) (Dekker 2002; Splinter et al. 2004; Miele et al. 2006). The frequency with which a given interaction between two loci occurs in a population of cells is measured by the relative amount of a particular ligation product. This is detected by qPCR using gene specific primers (Hagege et al. 2007). It is therefore a 'one-to-one' method as it only allows the investigation of ligation events between two particular restriction fragments of interest. Originally, the 3C method was employed to study the conformation of an entire yeast chromosome III showing that it forms a contorted ring (Dekker 2002). The technique was adapted for the mammalian system and used to study interactions of various loci including the alpha-globin and beta-globin (Vernimmen et al. 2009; Tolhuis et al. 2002; Splinter et al. 2006). Quantitative 3C requires rigorous controls to account for PCR bias (Palstra et al. 2003; Hagege et al. 2007). In practice, multiple primer pairs are designed to probe for genes of interest and also for intervening sequences to demonstrate a specific interaction. To overcome the low throughput restrictions, a multiplexed 3C-seq method was developed (Soler et al. 2010; Stadhouders et al. 2012; 2013), which utilises next-generation sequencing (NGS) to detect multiple 3C interactions in one experiment.

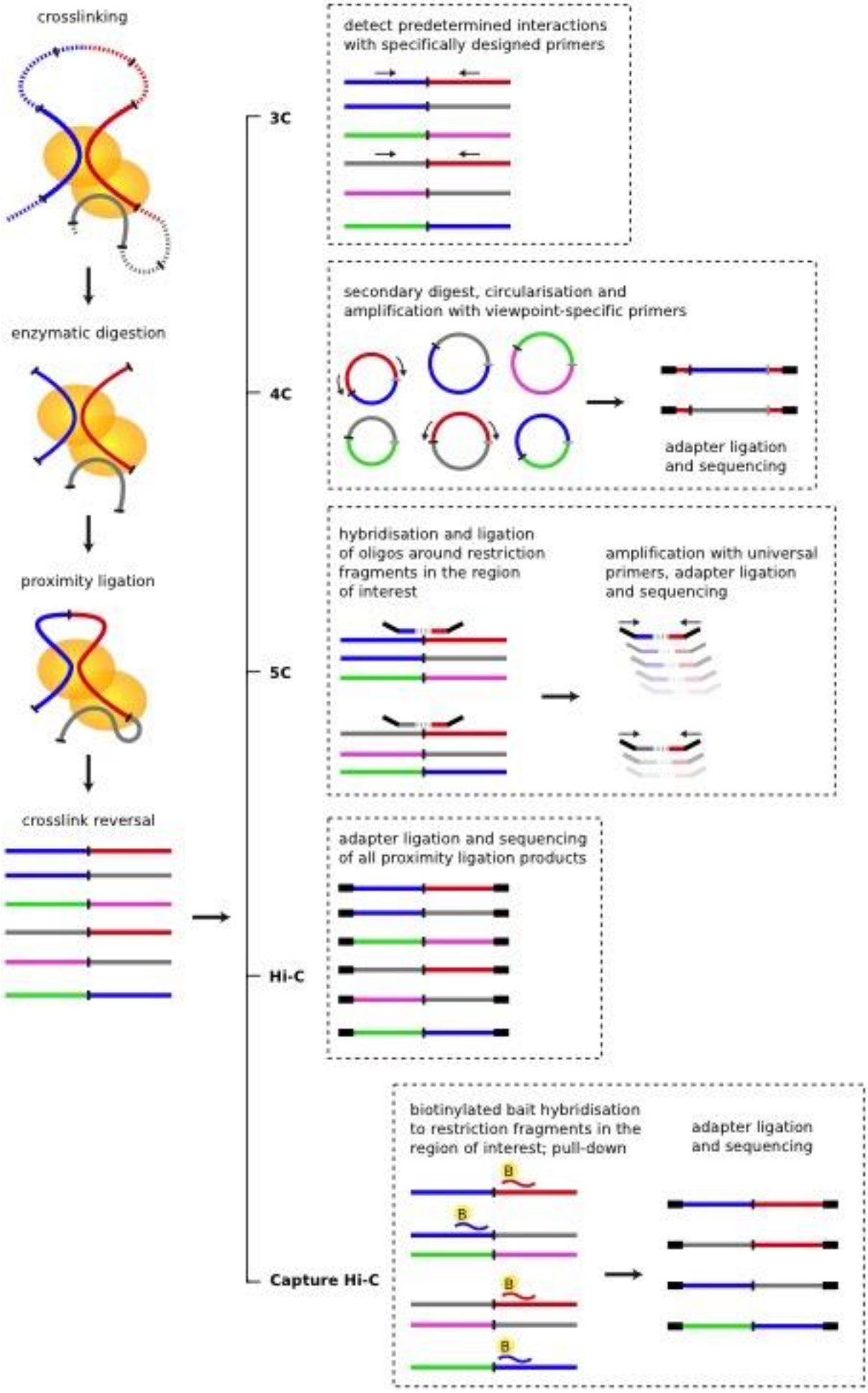
crosslinking
enzymatic digestion
proximity ligation
crosslink reversal
3C
4C
5C
Hi-C
Capture Hi-C
detect predetermined interactions with specifically designed primers
secondary digest, circularisation and amplification with viewpoint-specific primers
adapter ligation and sequencing
hybridisation and ligation of oligos around restriction fragments in the region of interest
amplification with universal primers, adapter ligation and sequencing
adapter ligation and sequencing of all proximity ligation products
biotinylated bait hybridisation to restriction fragments in the region of interest; pull-down
adapter ligation and sequencing
B

Figure 9. Chromosome conformation capture methods. 3C-based methods start with chemical crosslinking (orange ovals) of chromatin and fragmentation with a restriction enzyme, followed by proximity-based ligation of DNA ends and crosslink reversal. This creates a pool of paired sequences that represent regions that were in close spatial proximity in the nucleus at the time of crosslinking. Religated molecules are then processed according to each 3C-derivative. For 3C, predetermined interactions are detected by PCR amplification of both interaction ends. For 4C, the religated DNA molecules are circularised and amplified with primers specific for a viewpoint of interest, capturing all other ends ligated to the viewpoint. For 5C, an array of nucleotides designed to cover all restriction fragment in a region of interest is hybridised to the interaction junctions, ligated together and PCR amplified. PCR amplification is directly proportional to interaction frequency. For Hi-C, all molecules with religated junctions are sequenced. For capture Hi-C (enriched Hi-C), interactions from a region of interest are extracted from the Hi-C ensemble by hybridisation to RNA baits, DNA baits, bait-coated beads or a microarray.

The 3C protocol has rapidly evolved into higher throughput approaches. 4C (chromosome conformation capture on chip) allows for probing of all interactions involving a viewpoint of interest ('one-to-all'). It involves trimming of the ligated restriction junctions obtained from a 3C assay using a secondary restriction enzyme. Trimmed fragments are circularised and inverse-amplified using primers for the region of interest (viewpoint) and analysed on a microarray (Zhao et al. 2006; Simonis et al. 2006). This method was used to establish the existence of active and inactive chromatin domains (Simonis et al. 2006), characterise epigenetic regulation of imprinted loci (Zhao et al. 2006) and demonstrate co-localisation of co-regulated genes (Schoenfelder et al. 2010). A 4C-seq approach uses the same library preparation but it is analysed by NGS, providing higher resolution and more accurate quantification (van de Werken et al. 2012; Splinter et al. 2012; de Wit and de Laat 2012; Medvedovic et al. 2013). Capture-C, a multiplex 4C-seq, achieves the highest possible resolution of single restriction fragment and mitigates the use of viewpoint primers by capturing viewpoint sequences using short DNA bait hybridisation and pull-down (Hughes et al. 2014; Davies et al. 2016). ChIP-loop-4C is a method that includes a chromatin immunoprecipitation step to enrich for a subset of interactions between loci that were bound to specific proteins of interest. Cross-linked chromatin is incubated with antibody complexes bound to magnetic beads, pulled down and processed like 4C material (Horike et al. 2005; Guo et al. 2011a).

5C (chromosome conformation capture carbon copy) is a ‘many-to-many' method that gives a map of all interactions within a chosen genomic region (usually 500kb-5Mb) by using multiple primers specific for the majority of restrictions sites in the sequence of interest (Dostie et al. 2006; Dostie and Dekker 2007; Nora et al. 2012). Primers complementary to the sequence immediately adjacent to each restriction junction are hybridised to a 3C library. Two primers that anneal facing each other across a ligation junction are ligated, amplified using the universal T7 promoters attached to the 5C primers in a multiplex PCR reaction and analysed by NGS. In principal, the amount of a particular 5C product is directly proportional to the frequency of interactions involving two given restriction fragments (‘carbon copy’). However, it is not possible to identify any PCR duplicates resulting from over-amplification that might have occurred. 5C is much higher throughput than 3C, but relies on multiple primers and doesn't reach the resolution of 4C.

Hi-C is an 'all-to-all' primer-free approach that captures all chromatin interactions genome-wide (Lieberman-Aiden et al. 2009). Essentially, this method enables investigation of all interactions captured by a 3C protocol in a high throughput, highly quantitative manner. After chromatin fixation and digestion, the DNA ends are filled in with biotin-conjugated nucleotides, which can be pulled down after ligation and cross-link reversal to select only for interaction junctions and avoid analysis of undigested fragments. The library is then sonicated, size selected for ~400bp fragments and adapters are ligated for subsequent NGS analysis of all ligation junctions. This method is a significant improvement of 3C enabling instant genome-wide analysis. Interactions are usually analysed in fixed-width bins of 10-100kb. Hi-C does not suffer from primer bias and thanks to sonication each interaction sequence is unique and exact duplicates can be excluded as PCR artefacts. However, these highly complex libraries pose significant sequencing and computational challenges in analysis of interaction frequencies at high resolution. An average Hi-C experiment uses ~30-50 million cells and obtains ~50-100 million sequencing reads, which represents less than 1% of all possible interactions genome-wide. The highest resolution Hi-C maps to date analysed interactions in 1kb bins using ~2 billion sequences (Rao et al. 2014d).

The 3D organisation of the genome revealed by Hi-C has been validated by Genome Architecture Mapping (GAM) (Beagrie et al. 2017). This independent, proximity ligation-free assay relies on DNA sequencing from thin nuclear cryosections. Sequences that often co-reside in the same cryosection correspond to frequently detected Hi-C contacts. GAM provided a much needed verification of Hi-C findings and has given informative interaction data at 30kb resolution using as few as 400 cells.

Chromosome conformation capture studies are performed on material from a population of cells, which produces data that represents average interaction frequencies, but does not provide information on mutually exclusive interactions or contacts involving more than two loci simultaneously. The advantage of FISH imaging of single nuclei has been exploited to validate a subset of interactions observed with 3C-based methods. Computational modelling approaches based on polymer physics have proven valuable in translating the chromosome conformation capture data from an ensemble of cells into multiple possible single structures (Giorgetti et al. 2014; Brackley et al. 2016; Naumova et al. 2013; Barbieri et al. 2012; Rosa and Everaers 2008). This gives a set of all potential single conformations that might have constituted the experimental pool.

The ultimate goal of being able to study interactions at high resolution in single cells has been pioneered by single cell Hi-C (Nagano et al. 2013) and subsequent studies using F1 hybrid nuclei to reconstruct the 3D structures of all chromosomes (Nagano et al. 2017; Stevens et al. 2017). Thus far, single cell Hi-C can probe interactions at domain resolution (100kb-1Mb).

The demand to interrogate chromatin interactions of particular loci of interest in detail at high resolution prompted the development of enriched Hi-C methods, where a subset of interactions involving the region of interest is baited for in the Hi-C pool. This substantially

reduces the sequencing burden needed to achieve high read coverage on the region of interest. Promoter Capture Hi-C enriched for interactions involving most promoters in the genome using the Agilent SureSelect bead capture system (Dryden et al. 2014; Schoenfelder et al. 2015a; Mifsud et al. 2015; Jäger et al. 2015; Martin et al. 2015; Wilson et al. 2016; Javierre et al. 2016). Similarly, HiCap baited for promoters with the Roche NibleGen capture probes (Sahlén et al. 2015). These experiments enriched for thousands of restriction fragments genome-wide and obtained 4C-like profiles for each bait (viewpoint). On the other hand, multi-megabase loci have been enriched for using tiled, lawn-like bait systems to be able to interrogate all-to-all interactions in a region of interest. This includes the T2C method enriching for the SAMD4A locus with the NibleGen Capture array (Kolovos et al. 2014; 2016) and the Capture Hi-C method baiting for a large region around the Sox9 locus (Franke et al. 2016) and for 14 colorectal cancer risk loci (Jäger et al. 2015) using the Agilent SureSelect beads.

1.4.4. Chromatin interactions in the Igh locus

Translating individual observations of Igh locus contraction (Fuxa et al. 2004) and DNA looping (Sayegh 2005) into a comprehensive model of the 3D structure of this enormous locus has been a major challenge. The first study to assess the overall 3D structure of the Igh used 11 small (10kb) FISH probes distributed evenly along the locus, combined with mathematical modelling (Jhunjhunwala et al. 2008). They showed that the distal V region was positioned close to the Eμ-J region more frequently in $Rag^{-/-}$ pro-B cells than in earlier $E2A^{-/-}$ pre-pro-B cells. In contrast, the proximal V region was the same distance from the Eμ-J in pro-B and pre-pro-B cells. This revealed a major conformational change in the Igh locus when it is poised for recombination, suggesting that the distal V genes are brought close to the Eμ-J region to have the same opportunity to recombine as the proximal Vs. Also, the distal and the proximal V regions interacted with the 3' end of the locus with similar frequency. Furthermore, they observed that the FISH probe located in the IGCR1 was buried within the C region in pre-pro-B cells, keeping the D and J genes away from the Vs, but in pro-B cells it interacted with the V region, suggesting IGCR1's insulator function and a role in step-wise recombination, which was later confirmed by 3C (Degner et al. 2009; Featherstone et al. 2010; Guo et al. 2011b). This early study also reported a larger variability of distance measurements in pro-B cells than in pre-pro-B cells suggesting more variety in the interaction landscape at this stage. This supports the model that in order to produce a wide repertoire of antibodies, every Igh allele in every B cell has a different conformation to recombine different V genes, called an ‘equal opportunity for all’ model.

1.4.4.1. The role of CTCF

As mentioned previously, chromatin interactions preferentially involve CTCF motifs that are positioned in convergent orientation (Rao et al. 2014; Gómez-Marín et al. 2015). Indeed, the ~10 3'CBEs around HS4-8 at the 3’ end of the Igh locus are in convergent orientation to the

>100 CTCF-binding sites in the V region and have been proposed to act as a superanchor recruiting V genes to the 3' end of the Igh locus (Benner et al. 2015). Additionally, the two CBEs in the IGCR1 are in divergent orientation: CBE2 is in convergent orientation to the 3' superanchor whereas CBE1 is in convergent orientation to the CBEs in the V region. Thus, CBE1-to-V, CBE2-to-3'CBEs and 3'CBEs-to-V are likely to be the major interaction points in the locus.

1.4.4.2. The 3' domain

Studies by Guo *et al*. 2011a and Degner *et al.* 2011 investigating chromatin interactions in the Igh locus by 3C, 4C+microarray and ChIP-loop 4C, found that the IGCR1, 3'RR/HS1-3 and 3'CBEs/HS4-8 all interact with the Eμ (**Figure 10** light blue arches) and the 3'CBEs/HS4-8 interact very strongly with the IGCR1 (Guo et al. 2011a; Degner et al. 2011) (**Figure 10** dark grey arch), but no interaction was detected between the IGCR1 and the 3'RR/HS1-3 (Degner et al. 2011). Together with D and J genes these interactions form a highly structured 3' domain bordered by CTCF-bound sites at the 3'CBEs and the IGCR1. These loops likely shape the 3' end of the Igh locus with little variability between single B cells. These interactions were shown to be CTCF-dependent by deleting the IGCR1 (Guo et al. 2011b), as the interactions between 3'CBEs/HS4-8 and IGCR1, Eμ and IGCR1, and between Eμ and 3'CBEs/HS4-8 were lost, but the interaction between the Eμ and the 3'RR/HS1-3 remained as these two sites do not bind CTCF. A previous shRNA CTCF knockdown study did not detect a reduction in IGCR1-Eμ interaction (Degner et al. 2011). These two studies proposed that the V genes reside in a separate domain, preventing premature V-DJ recombination.

To generate a comprehensive high-resolution interaction profile of the Igh locus Medvedovic *et al.* 2013 performed numerous 4C-seq experiments using 16 different viewpoints, focussing on the regulatory elements located at the 3' end and the PAIR elements in the distal V region. They suggested that the 3' domain is more extended, encompassing elements from the 3'CBEs to 3' of middle V genes (Medvedovic et al. 2013). This model is consistent with previous findings that proximal V genes recombine normally in the absence of locus contraction (Fuxa et al. 2004). They also confirmed that the Igh forms a TAD in pro-B cells as more reads overall mapped within the Igh in pro-B cells than in $Pax5^{-/-}$ pro-B cells. They found that interactions between the 3'RR/CBEs, Eμ and IGCR1 still formed in the absence of locus contraction and were also present in thymocytes, which supports previous claims.

1.4.4.3. The role of Eμ

Additionally to Eμ interactions within the 3' end of the locus, Guo et al. 2011a also identified interactions between the Eμ and Q52 (the first V genes) (**Figure 10** green arch), 5'V7183 (a region at the 5' end of the proximal V genes) (**Figure 10** light blue arch) and 3'VJ558 (at the beginning of the J558 region) (**Figure 10** thick red arch). This confirmed that the proximal and middle V genes re-position close to the J-Eμ region prior to recombination.

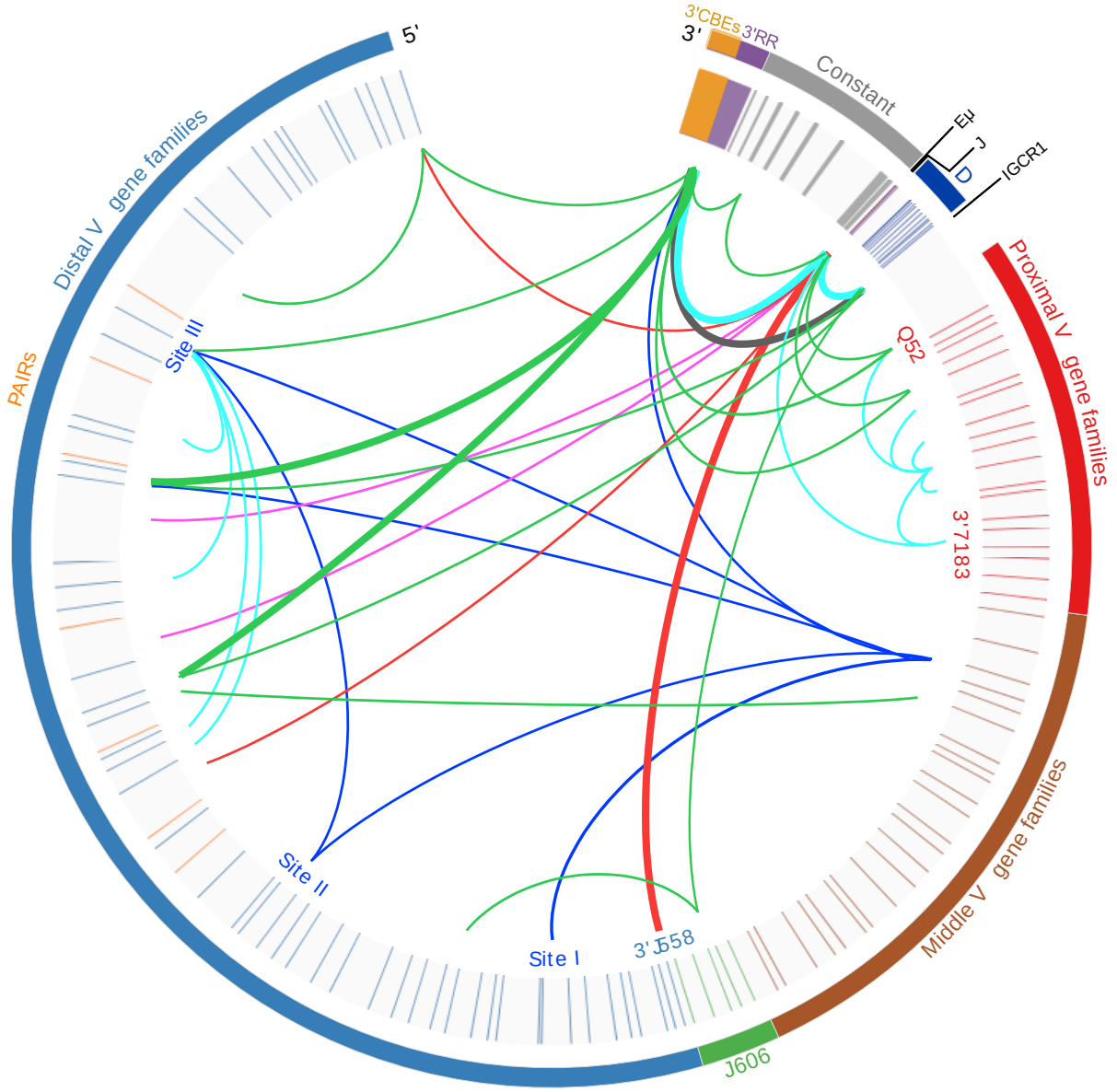

Figure 10. Interactions in the Igh reported to date. The outer circle shows regulatory elements and groups of genes in the Igh locus. The vertical lines in the inner circle show positions of C, J, D and V genes. The 3'RR and 3'CBEs are depicted as regions. The orange lines in the distal V gene families denote PAIR elements. The arches inside the circles depict genomic interactions by connecting regions involved in direct physical contacts. Interactions reported by more than one study are shown as thick arches. The interactions between the 3'CBEs superanchor and all V genes are not depicted. Red – Jhunjhunwala *et al.* 2008, light blue – Guo *et al.* 2011a, dark grey – Guo *et al.* 2011b, purple – Verma-Gaur *et al.* 2012, green– Medvedovic *et al.* 2013, dark blue – Montefiori *et al.* 2016. Figure adapted and updated from Stubbintgon and Corcoran 2013.

Importantly, deletion of Eμ caused a loss of locus relocation and contraction (Guo et al. 2011a; Chakraborty et al. 2009b; Gerasimova et al. 2015). However, Medvedovic *et al.* 2013 did not observe changes in interactions between the 3'CBEs/HS4-8 and the V region in models lacking either Eμ, 3'RR/HS1-3 or IGCR1 (Medvedovic et al. 2013). It is not clear why these results differ since both groups used 4C techniques and more experiments are needed to clarify the involvement of the Eμ in long-range interactions. Guo *et al*. 2011a reported that all

Eμ-interacting sequences bind YY1 and Eμ deletion does not impair YY1 binding to these sites. They also reported that all YY1 binding colocalised with CTCF binding, however analysis by our lab of publicly available ChIP-seq datasets did not find an overlap (Bolland et al. 2016).

1.4.4.4. Local interactions in the V region

Experiment from a seciprocal viewpoint at the 5'V7183 and an additional one at V10 (near J558.72.173) identified local medium-range interactions in the V region, which were also present in Eμ-deficient pro-B cells that have diminished locus contraction (Guo et al. 2011a) (**Figure 10** light blue arches). The authors proposed that these local V loops form before locus contraction and are CTCF-mediated. A subsequent CTCF knockdown study reported disruption of these local V interactions, but preservation of the Eμ-5'7138 interaction (Gerasimova et al. 2015). In the absence of locus contraction in $Pax5^{-/-}$ pro-B cells the interaction between the IGCR1 and proximal Vs was maintained, but a long-range interaction between 5'V7183 and 3'VJ558 was lost. Eμ-dependent interactions Eμ-5'7183, Eμ-3'J558 and 5'7183-3'J558 were reduced in a YY1 knockdown experiment, whereas local contacts in distal Vs were not disturbed (Gerasimova et al. 2015). Similarly, Medvedovic *et al*. 2013 reported that PAIR elements in the distal V region were involved in specific local interactions in pro-B cells and these loops were maintained in the absence of locus contraction in $Pax5^{-/-}$ pro-B cells. Specifically, PAIR4, 5 and 8 were interacting with the whole J558 cluster and their interaction patterns were very similar to each other. On the contrary, the J606 viewpoint had a very different pattern of interactions and these were diminished in the absence of locus contraction, suggesting it is outside the putative PAIRs domain. They did not confirm the previously identified Eμ-PAIRs interactions (Verma-Gaur et al. 2012) (**Figure 10** red arch), however they found interactions, albeit not of high frequency, between PAIR4, 5 and 8 and the IGCR1 and 3'CBEs/HS4-8 in pro-B cells, but not in $Pax5^{-/-}$ pro-B cells (Medvedovic et al. 2013) (**Figure 10** green and thick green arches). This suggests that indeed CTCF might mediate long-range interactions comprising locus contraction.

1.4.4.5. Flexible looping of V genes

The high-resolution 4C-seq by Medvedovic *et al.* 2013 observed that the distal Vs interact with 3' elements at relatively low frequencies and with very similar patterns (Medvedovic et al. 2013). They concluded that the 3' domain of the locus encompassing the 3'CBEs-D genes as well as most of the proximal V genes forms a more rigid structure, whereas the middle and distal V genes flexibly loop into the proximity of the 3' end to enable all V genes to recombine. However, the observed low frequency of distal V interactions might be due to a lack of correction for overall read coverage and genomic distance in 4C-seq experiments. Benner *et al.* 2015 proposed a model where the 3'CBEs/HS4-8 superanchor contacts all V genes, but did not incorporate the contacts of the IGCR1 in their model. 3'CBEs-V interactions were clearly identifiable thanks to corrections applied to Hi-C analysis (Benner et al. 2015).

1.4.4.6. PAX5-mediated subdomains

The most recent study by Montefiori *et al*. 2016 carried out a first all-to-all interaction assay on the Igh locus using 5C (Montefiori et al. 2016), followed by validation by FISH. They report seven main interaction sites in the Igh locus that define three topological subdomains linked by long-range loops (**Figure 10** dark blue arches). Subdomain A (0.6Mb) contains all 3' elements, J, D and most of proximal V genes as well as an interaction anchor Site I at the end of proximal Vs. Subdomain B (0.7Mb) contains middle V genes and interaction anchor sites FrOSt1a at the end of middle Vs, FrOSt1b around the J558.9.99 and Site II around the J558.19.109. Subdomain C (0.8Mb) contains distal V genes and interaction anchors Site II.5 around PAIR6-8 and Site III around PAIR10-11. Sites I, II and III frequently interacted with each other simultaneously, and sites I, II, III and FrOSt1a bind CTCF. They focused on characterising the interactions within the V region between the three subdomains and showed that even long-range (over 1Mb) interactions involving Sites I, II and III are Eμ-independent. Additionally, Sites II.5 and III overlap with PAIR elements and therefore bind PAX5, and accordingly, their interactions were diminished in $Pax5^{-/-}$ pro-B cells, whereas interaction between Site I in the middle Vs and Site II downstream of PAIRs was not. This suggests that there are fairly long-range 'local' locus contraction-independent V interactions. They infer that since some looping between sites I, II and III is present in non-B cells they reflect constitutive conserved interactions always present in the Igh to a certain extent and propose that pro-B cells could utilize those constitutive interactions and just increase their frequency with the 3' domain in pro-B cells to maximise locus contraction. Evidently, a separate 'switch' is needed to dissolve the IGCR1's insulating activity and initiate V-DJ recombination. Overall, they postulate that Igh locus contraction is mediated by Site I interactions with five other sites in the V region and that these interactions are mediated by PAX5, and are not in the form of stochastic flexible looping of all V genes onto the D-J region as proposed by Medvedovic *et al*. 2013 and Benner *et al*. 2015 (Medvedovic et al. 2013; Benner et al. 2015)

1.4.4.7. Timing and environment of V(D)J recombination

Using live imaging of fluorescently labelled Igh loci and computer modelling, a major advance beyond FISH techniques on fixed cells, Lucas *et al.* 2014 determined first passage times of interactions between V and D genes. This study revealed that a V gene interacts with the DJ region within minutes of D-J recombination, much faster than expected (Lucas et al. 2014). Importantly, space was an influential factor in V genes localising to the DJ region and, within the same space, DJ and V regions come together much faster if there are 100 V genes compared with one V gene. As the DJ region pairs most rapidly with the closest V gene, and the nuclear environment can be described as viscoelastic, they proposed that the DJ region resides in a cavity surrounded by equally distant V genes and that the viscous nuclear environment causes V genes to bounce back and forth rapidly until a specific synapsis is established by the RAG machinery. This ties well with the 'equal opportunity for all' model (Jhunjhunwala et al. 2008).

1.4.4.8. Models proposed to date

Before it was even possible to interrogate the spatial conformation of DNA it was clear that V genes reside in a different chromatin environment than the D and J genes to prevent premature V-DJ recombination (Storb and Arp 1983; Lennon and Perry 1985; Maes et al. 2001; Johnson et al. 2003; Morshead et al. 2003; Bolland et al. 2004). Early FISH studies showed that the distal V genes come into close proximity with the DJ region upon locus contraction in pro-B cells to have the same chance to recombine as the proximal V genes (Sayegh 2005; Jhunjhunwala et al. 2008). Subsequently, several studies proposed a hierarchical organisation of the Igh locus folding. There is an overall consensus that the 3' domain is defined by the interactions between the 3'CBEs superanchor and the IGCR1, which involve CTCF, as well as between these elements and the 3'RR and Eμ potentially involving YY1 and PAX5 (Guo et al. 2011a; Degner et al. 2011; Guo et al. 2011b; Medvedovic et al. 2013; Kumar et al. 2013; Gerasimova et al. 2015; Montefiori et al. 2016). These interactions are also present to a large extent in pre-pro-B cells and other lymphocytes. This 3' domain also encompasses the proximal V gene family V7183, which is able to participate in V(D)J recombination even in the absence of locus contraction in cells lacking PAX5, YY1 or Eμ.

The V region is characterised by local shorter-range loops as well as very long-range loops that bring the V genes closer to the DJ region. The local intra-V interactions have been observed within the proximal Vs around the last V7183 genes (Guo et al. 2011a) and in the distal Vs around the PAIR elements (Guo et al. 2011a; Medvedovic et al. 2013; Gerasimova et al. 2015; Montefiori et al. 2016), and these loops are independent of locus contraction. In contrast, local interactions detected around the VJ606 genes in the middle Vs were absent in uncontracted $Pax5^{-/-}$ pro-B cells (Medvedovic et al. 2013). A large-scale contraction of the Igh locus is necessary for optimal V-DJ recombination and involves physical juxtaposition of distal V genes closer to the D and J genes. Medvedovic *et.al*. 2013 proposed that flexible dynamic long-range looping of V genes to the 3' end is responsible for the highly diverse Igh repertoire, supports the 'equal opportunity for all' model where V genes bounce back and forth to the DJ (Lucas et al. 2014) and reflects the heterogeneity of pro-B cells ensemble. Benner *et al.* 2015 suggests that all long-range V gene interactions are via the 3' superanchor and are mediated by CTCF (Benner et al. 2015). On the other hand, Gerasimova *et al.* 2015 and Montefiori *et al*. 2016 favour three V gene subdomains juxtaposed onto each other by PAX5 and YY1 (Gerasimova et al. 2015; Montefiori et al. 2016). In particular, they propose that CTCF mediates local V interactions, PAX5 anchors several long-range loops in distal Vs and YY1 further compacts these domains.

There remains scope for further investigation of looping between the Igh elements, particularly to elucidate all-to-all interactions at higher resolution using the best possible current method of enriched Hi-C. It remains to be determined whether the IGCR1 also acts as a superanchor and what is the organisation of the V genes in pro-B cells compared to an uncontracted locus.

1.5. Hypothesis

The work described in this thesis addresses a hypothesis in three parts. Firstly, that the 3D conformation of the immunoglobulin heavy chain locus is key for efficient V(D)J recombination and is therefore governed by non-random spatial relationships between the J, D and V genes and key regulatory elements of the Igh locus - the 3' superanchor (3'CBEs), the 3' Regulatory Region (3'RR), the Intronic Enhancer (Eμ) and the Intergenic Control Region 1 (IGCR1). Since all V genes have one goal: to rearrange with a DJ segment, I hypothesised that an average interaction frequency map will reveal the overarching structural patterns facilitating recombination.

Secondly, I hypothesised that there are multiple correct conformations of the Igh locus and that precisely this heterogeneous ensemble of individual conformations contribute the variety of V(D)J recombination events to generate a diverse antibody repertoire.

Thirdly, that Ig loci and/or genes driving B cell development might participate in a genome-wide network of physical interactions because they bind the same transcription factors and co-regulate each other on a transcriptional level. Therefore, they might frequently reside in close proximity that would manifest itself as inter-chromosomal interactions.

1.6. Aims

During my PhD I set out to test the presented hypotheses by completing five aims:

1. To apply Capture Hi-C - a new multi-bait system, to enrich Hi-C material for interactions involving the 2.8Mb Igh locus as well as other Ig loci and selected genes driving B cell development.
2. To resolve the spatial conformation of the immunoglobulin heavy chain locus by producing a high resolution unbiased map of all-to-all chromatin contact frequencies.
3. To use polymer modelling to obtain all possible single Igh 3D structures from ensemble data and to correlate V gene position in single structures with their recombination frequency to identify the spatial determinants driving V gene choice.
4. To obtain a sufficiently high depth of Capture Hi-C to be able to investigate inter-chromosomal contacts of immunoglobulin loci and other selected genes.
5. To validate any newly discovered genome-wide interactions using an independent imaging method.

2

2. Materials and methods

2.1. Animals

All mice were bred by Biological Services Unit staff at the Babraham Institute under project license PPL80/2529 approved by the UK Home Office. This includes strains: wild type C57BL/6 mice, $Rag1^{tmBal}$ mice (Matthias and Baltimore 1993) and $Rag1^{tmMom}$ mice (Mombaerts et al. 1992) both in C57BL/6, collectively referred to as $Rag^{-/-}$ throughout this thesis, Vh81X mice (Martin et al. 1997) in BALB/c on $Rag1^{-/-}$ background referred to as Rag/81X, and $cE\mu^{-/-}Rag2^{-/-}$ mice in 129Sv (Perlot et al. 2005) referred to as $E\mu^{-/-}$. Mice were taken at 6-12 weeks old and killed according to Schedule 1 of the Animals (Scientific Procedures) Act 1986.

2.2. Cell collection

2.2.1. B cells harvesting from the bone marrow

Femurs and tibias were dissected from mice and kept on ice at all times. Bones were cleaned and the ends and caps were cut off. A 25-gauge syringe and a 2.5ml needle were used to flush the bone marrow with ice-cold RPMI-1640 medium (Invitrogen) supplemented with 5% FCS and 24mM HEPES into a Falcon tube. Cell aggregates were separated by repeated pipetting using a 10ml pipette. Cell suspension was decanted to separate from debris. Cells were collected by centrifugation at 1300rpm at 4°C for 5min and resuspended in ice-cold PBS.

2.2.2. Thymocyte harvesting

Thymi were dissected from wild type mice and kept in ice-cold RPMI-1640 medium (Invitrogen) supplemented with 5% FCS and 24mM HEPES. Thymi were disrupted with forceps and flushed with ice-cold PBS through a 70μm cell strainer (Becton Dickinson) into a Falcon tube to obtain a single cell suspension. Cells were collected by centrifugation at 1300rpm at 4°C for 5min, resuspended in ice-cold PBS and strained again. For Hi-C library

preparation cells from 4 thymi were pooled to form one biological replicate. For 3D DNA FISH cells from one thymus were FACS sorted for double-positive ($CD4^+$, $CD8^+$) T cells and then used to prepare microscope slides.

2.3. Magnetic-activated cell sorting (MACS)

2.3.1. MACS enrichment

To enrich for $CD19^+$ cells from bone marrow suspension, after collection, bone marrow cells were washed in PBS, filtered through a 70µm cell strainer and centrifuged at 1300rpm at 4°C for 5min. This wash was then repeated twice using a 40mm cell strainer. Cells were resuspended in MACS buffer (0.5% v/v FCS, 2mM EDTA in PBS) at $100x10^6$ cells/ml. Magnetic microbeads conjugated to anti-CD19 antibodies (Miltenyi Biotec) were added to the cell suspension at 50µl of beads per $100x10^6$ cells and incubated at 4°C for 15min with mixing every 5min. Cells were centrifuged at 1300rpm at 4°C for 5min and resuspended in MACS buffer at $100x10^6$ cells/ml. Up to 2ml of sample was then placed on a large selection (LS) MACS column (Miltenyi Biotec) that was previously placed on a magnet and calibrated with 5ml of MACS buffer. The flow-through containing unlabelled cells was discarded and columns were washed three times with 3ml of MACS buffer. The column-bound fraction contained the $CD19^+$ B lymphocyte population, which was eluted by removing the column from the magnet and flushing with 5ml of MACS buffer.

2.3.2. MACS depletion

To efficiently sort pure cell populations by FACS, bone marrow suspension was first depleted of non-B cells. Bone marrow cells were washed in PBS, filtered through a 70µm cell strainer and centrifuged at 1300rpm at 4°C for 5min. This wash was then repeated twice using a 40µm cell strainer. Cells were resuspended in PBS at $25x10^6$ cells/ml and stained with the following biotinylated antibodies (at dilutions indicated in brackets): TER119 (1:400, eBioscience, to remove erythrocytes); CD11b (1:1600, eBioscience, myeloid cells); GR1 (1:1600, eBioscience, myeloid cells); LY6c (1:400, AbD Serotec, T cells and myeloid cells); CD3e (1:800, eBioscience, T cells). Cells were incubated on ice for 20min, washed in PBS to remove unbound antibodies, then resuspended in PBS at $100x10^6$ cells/ml. 50µl of streptavidin magnetic beads (Miltenyi Biotec) were added per every $100x10^6$ cells. Samples were incubated at 4°C for 15min, shaking every 5min to prevent beads from settling. Samples were then washed with PBS, filtered through a 40µm cell strainer and resuspended in MACS buffer (0.5% v/v FCS, 2mM EDTA in PBS) at $100x10^6$ cells/ml. Up to 2ml of sample was placed on a large selection (LS) MACS column (Miltenyi Biotec) that was previously placed on a magnet and calibrated with 5ml of MACS buffer. The flow-through containing unlabelled B cells was collected in a Falcon tube.

2.4. Fluorescence-activated cell sorting (FACS)

For B cells, MACS depleted cells were resuspended at $20x10^6$ cells/ml and stained for FACS to sort a desired cell population using the following fluorochrome-conjugated antibodies: B220-BV421 (1:200, Biolegend), CD19-PercpCy5.5 (1:400, BD Pharmingen), CD43-FITC (1:200, BD Pharmingen) and CD25-PE (1:800, BD Pharmingen). Cells were stained on ice for 45min, washed and sorted on a FACSAria machine (Becton Dickinson) as follows:

$Rag^{-/-}$ pro-B cells and $E\mu^{-/-}$ pro-B cells: $B220^+$, $CD19^+$, $CD43^+$
Rag/81X pre-B cells: $B220^+$, $CD19^+$, $CD43^-$, $CD25^+$

For DP T cells, thymocytes prepared as in 2.2.2 were washed in PBS, resuspended at $20x10^6$ cells/ml and stained with CD8-FITC (1:400, eBioscience) and CD4-PercpCy5.5 (1:800, eBioscience) on ice for 45 min. Cells were then washed and sorted on a FACSAria machine for $CD4^+$, $CD8^+$ cells.

2.5. General molecular biology techniques

2.5.1. Isolation of genomic DNA

Genomic DNA (gDNA) was isolated using the DNeasy kit (Qiagen) according to the manufacturer's instructions. gDNA quantification and quality was measured using a NanoDrop spectrophotometer (Thermo Scientific).

2.5.2. Bacterial artificial chromosomes for Capture Hi-C baits and DNA FISH probes

BACs for Capture Hi-C baits

BACs (bacterial artificial chromosomes) were purchased from BACPAC Resources Centre (https://bacpacresources.org/) and covered the following regions of interest: **Igh locus** (RP23-149L24, RP23-109B20, RP24-251F12, RP23-404D8, RP23-145K3, RP23-373N4, RP23-24I12, RP23-147E23, RP23-206K17, RP23-18L19, RP24-282L18, RP23-70F21, RP23-197F8, RP23-257D2, RP23-354D10, RP23-101G12, RP23-230L2, RP23-123N21, RP23-172K2, RP24-386J17), **Igk locus** (RP23-34P19, RP24-322E13, RP23-255N3, RP23-234A12, RP23-173G20, RP23-185M15, RP24-76K4, RP23-321G20, RP23-29F15, RP24-405O23, RP23-211L5, RP23-344N8, RP23-279O6, RP24-179E20, RP24-568F14, RP23-124O23, RP24-144F12, RP24-475M8, RP24-314D, RP23-367A13, RP23-64J23, RP23-175B24, RP23-66O20, RP23-435I4), **Igl locus** (RP23-247I1 and RP23-272P19), **Pax5** (RP23-397E2), **Foxo1** (RP24-212F1), **Il7r** (RP24-282H6), **Rag1&Rag2** (RP23-325I3), **Hist1** (RP23-

141E23), **Vmrn** (RP24-66A14), **Hbb** (RP24-344M21), **Yy1** (RP23-351K4), **Tcf3** (RP23-126H18), **Ikzf1** (RP23-373H2) **Nanog** (RP24-464B14), **p27kip** (RP23-45G16).

BACs for DNA FISH probes

Igh(DJ) (RP23-109B20), **Igh(V)** (RP23-70F21), **Igk** (RP24-179E20 and RP23-124O23), **Pax**5 (RP23-397E2), **Foxo**1 (RP24-212F17), **Ebf**1 (RP23-298N21), **Runx**1 (RP23-465H23), **Bach**2 (RP23-67O11), **Myc** (RP23-98D8).

2.5.3. Growth of bacterial cultures

Bacterial cultures were streaked out on Luria-Bertani (LB) agar plates supplemented with 25mg/L chloramphenicol as per BACPAC instructions and grown overnight at 37^{o}C. A single bacterial colony was transferred into 5ml of LB with 25mg/L chloramphenicol and grown at 37^{o}C for 8h while shaking at 200rpm. The 5ml culture was transferred into a 1L flask containing 200ml of LB with 25mg/L chloramphenicol and grown at 37^{o}C overnight while shaking at 200rpm. To make glycerol stocks, 500µl of bacterial culture was added to 500µl of 60% glycerol and stored at -80^{o}C.

2.5.4. BAC DNA purification

BAC DNA was extracted from bacterial culture using a Macherey-Nagel NucleoBond BAC 100 kit according to manufacturer's instructions for low-copy plasmid purification (Maxi/BAC). Purified BAC DNA was resuspended in 300µl of H_2O, warmed up to 37^{o}C to facilitate solubility of large DNA molecules and concentration was determined using a NanoDrop spectrophotometer.

2.5.5. Polymerase chain reaction

PCR amplification reactions were set up in a final volume of 25µl and typically contained 100-500ng of DNA, 0.5µl of Hot Start Taq DNA polymerase (Qiagen), 2.5µl of 10x reaction buffer, 0.2µM primers and 0.2mM each dATP, dTTP, dCTP and dGTP. The template was amplified with a hot start enzyme activation and initial denaturation at 95°C for 15min, followed by 35 cycles of denaturation at 94°C for 30s, annealing at appropriate temperature for 1min and extension at 72°C for 30s per 1kb of expected product, followed by final extension at 72°C for 10min.

Table 1. Primers used for genotyping of Rag1^{tmMom}, Rag1^{tmBal} and Rag/81X mice.

Primer	Sequence (5' → 3')
Rag1^{tmMom} F WT	GAGGTTCCGCTACGACTCTG
Rag1^{tmMom} R Common	CCGGACAAGTTTTTCATCGT
Rag1^{tmMom} R mutant	TGGATGTGGAATGTGTGCGAG
Rag1^{tmBal} F Common	GAAATCCATCTCCTGCCAGA
Rag1^{tmBal} R WT	GGCTTGACACATGGTGGTTA
Rag1^{tmBal} R NeoR	CCGCTTCCATTGCTCAGCGG
VH81X F	CGCGCGGCCGCGTGGAGTCTGGGGGAGGCT
VH81X R	CCCAGACATCGAAGTACCAGCTACTACCATG

Reactions for final PCR amplification of Hi-C libraries were performed in a final volume of 50µl and contained 2.5µl of streptavidin bead-bound Hi-C library, 0.3µl of Phusion high fidelity DNA polymerase (Thermo Scientific) to minimize amplification errors, 5µl of 5x Phusion HF Buffer, 0.25µM primers and 0.25mM each dATP, dTTP, dCTP and dGTP. The template was amplified with a hot start enzyme activation and initial denaturation at 98°C for 30s, followed by an appropriate number of cycles (see results section) of denaturation at 98°C for 10s, annealing at 65°C for 30s and extension 72°C for 30s, followed by final extension at 72°C for 7min.

2.5.6. Real-time qPCR

DNA was amplified using Applied Biosystems SYBR Green PCR Master Mix (Life Technologies) in a Bio-Rad C1000^{TM} Thermal cycler. Reactions were set up in 25µl and contained 12.5µl of SYBR Green PCR Master Mix (Life Technologies), 0.4µM primers and 10-20ng of template DNA. Standard curves were created using serial dilutions of kidney genomic DNA obtained from Bryony Stubbs. Each sample was run in triplicate. PCR reactions were subjected to a hot start enzyme activation at 95°C for 10min and 40 cycles of denaturation at 95°C for 15s and annealing/extension at 60°C for 1min.

Data was analyzed according to the comparative threshold cycle (Ct) method, where the amount of target, normalized to an experimental control, is given by $2^{\Delta Ct}$. Ct indicates the PCR cycle number at which the amount of amplified target reaches a fixed threshold and 2 refers to assumed primer efficiency. The ΔCt value is determined by subtracting the average control Ct value from the average target Ct value.

2.5.7. Agarose gel electrophoresis

Constant-field electrophoresis was carried out in a horizontal submerged agarose gel tank as described by Sambrook and Russell (2001). 0.8-2% w/v agarose gels containing 40mg/L ethidium bromide were prepared in TBE. DNA was visualized with UV light (300nm) and imaged using a Gel Doc system (Bio-Rad).

2.6. Chromosome conformation capture: Hi-C and Capture Hi-C

Chromosome conformation capture experiments were based on to the protocol by Stefan Schoenfelder and Mayra Furlan-Magaril (Schoenfelder et al. 2015a).

2.6.1. Hi-C libraries preparation

Chromatin fixation, cells lysis and restriction enzyme digestion

20-50x10^6 cells (CD19 MACS enriched $Rag^{-/-}$ pro-B cells, CD19 MACS enriched Rag/81X pre-B cells or thymocytes from whole thymus) were fixed for exactly 10 minutes at room temperature (RT) in 37ml of DMEM supplemented with 10% FBS (Invitrogen) and containing a final concentration of 2% formaldehyde (Agar Scientific). The reaction was quenched with 1M glycine added to a final concentration of 0.125M and incubation for 5min at RT followed by 15min incubation on ice. Cells were centrifuged at 1500rpm at 4°C for 10min, washed in ice cold 1x PBS and snap frozen in liquid nitrogen then stored at -80ºC.

Fixed cell pellet was resuspended in lysis buffer (10mM Tris-HCl pH=8, 0.2% NP-40, 10mM NaCl, 1 protease inhibitor cocktail tablet (Roche complete, EDTA free), H2O) and incubated on ice for 30min with occasional mixing. Cells were centrifuged at 1800rpm at 4°C for 5min and the cell pellet was resuspended in ice-cold 1.25X NEB2 buffer (1ml buffer/30x10^6 cells). Samples were split into four 250µl aliquots and a further 108µl of ice-cold 1.25x NEB2 buffer was added to each aliquot. To remove proteins not directly cross-linked to DNA, 11µl of 10% SDS was added to each aliquot and they were incubated at 37ºC for 1h with shaking at 950rpm. To quench the SDS, 75µl of 10% Triton X-100 was added and incubated for a further 1h at 37°C.

To digest the cross-linked chromatin, 1500U of HindIII (New England Biolabs) were added to each aliquot and incubated overnight at 37ºC with shaking at 950rpm. Digestion efficiency was assessed using primers spanning HindIII sites. If the digestion is complete or near-complete, products generated by primers spanning a HindIII site should be detectable at a much lower level than products generated by primers not spanning HindIII sites.

Biotin incorporation

Restriction fragment ends in cross-linked digested chromatin were filled-in and biotinylated by the addition of 6µl 10x NEB Buffer 2, 2µl nuclease-free water, 37.5µl of 0.4mM biotin-14-dATP (Life Technologies), 1.5µl each of 10mM dCTP, dGTP, dTTP and 50U of Klenow DNA polymerase I large fragment (New England Biolabs). Reactions were incubated at 37ºC for 75min. Samples were mixed by shaking at 700rpm for 5s every 30s.

Ligation and cross-link reversal

541µl of ligation reaction mix (100µl of 10x NEB ligation buffer, 10µl of 100x BSA, 250U of T4 DNA ligase (Invitrogen) and 429µl of H_2O) was added to biotinylated samples and incubated at 16ºC for 4h, then at RT for 30min.

Cross-links were reversed by adding 600µg of Proteinase K (Qiagen) to each sample and incubated overnight at 65ºC. 100µg of RNaseA (Qiagen) was added to each sample and incubated at 37C for 1h.

All steps up to this point were carried out in undisrupted nuclei.

DNA purification

DNA was purified by a phenol (Sigma-Aldrich) extraction followed by two phenol-chloroform (Sigma-Aldrich) extractions and precipitated with 0.1 volume of 3M NaOAc and 2.5 volume of 100% ethanol at -20°C overnight. DNA was centrifuged at 35000rpm at 4°C for 30min and washed three times with 70% ethanol then resuspended in buffer TLE. DNA concentration was measured using Quant-iT™ PicoGreen® dsDNA Assay Kit according to manufacturer's instruction.

Quality control

Previously reported interactions have been detected by PCR to confirm the accuracy of previous steps. Histone 1 cluster (Hist1) interaction was used as a short-range control interaction and interaction between Hox genes served as a long-range control interaction.

Fill-in of restriction ends during biotinylation replaces the HindIII restriction site (AAGCTT) with an NheI restriction site (GCTAGC). This can be used to assess the proportion of ligation junctions that were successfully biotinylated. PCR products of control interactions described above were digested with both enzymes individually and in combination. An expected result is full digestion with NheI and no digestion with HindIII (double digestion test). Digestion reactions contained PCR amplicon of a known control interaction and 50U of enzyme, 1.5µl of appropriate buffer and 1.5µl of BSA if required and were incubated at 37°C for 1h.

Shearing of library and end repair

To avoid pulling down unligated biotinylated fragments, biotin-14-dATP from those DNA ends was removed using the exonuclease activity of T4 DNA polymerase. Hi-C material was divided into 5µg aliquots and mixed with 10µg of BSA, 1x NEB Buffer 2, 0.1mM dATP and 15U of T4 DNA polymerase (New England Biolabs) in a total reaction volume of 100µl and incubated at 20ºC for 4h. The enzymatic reaction was stopped by addition of 2µl of 0.5M EDTA pH 8.0 and DNA purified by phenol-chloroform extraction followed by ethanol precipitation.

Pellets were resuspended in 130µl of nuclease-free water per 10µg of material and sheared by sonication using an E220 ultrasonicator (Covaris) according to manufacturer's instructions using the following settings: 10% duty factor, 140W peak incident power, 200 cycles per burst, 55s treatment time.

Sheared ends were repaired by adding 6.5U of Klenow (New England Biolabs), 65U of T4 DNA polynucleotide kinase (New England Biolabs), 19.5U of T4 DNA polymerase (New England Biolabs), 1x T4 ligase buffer (Invitrogen) and 0.25mM each of dATP, dCTP, dGTP and dTTP in 170µl reactions and incubated at RT for 30min. The DNA was purified using a PCR Purification Kit (Qiagen) according to the manufacturer's instructions and eluted from the columns with 30µl of TLE (Tris Low EDTA: 10mM Tris-HCl pH 8.0, 0.1mM EDTA) twice to give final volume of 60µl per every 10µg of material.

dATP-tailing and size selection

3' A overhangs were added to the repaired ends of DNA fragments in 50µl reactions containing 10µg of Hi-C material, 1x NEB Buffer 2, 0.25mM dATP and 17.5U of Klenow fragment 3′→5′ exo- (New England Biolabs) and incubated at 37ºC for 30min, followed by inactivation at 65ºC for 20min.

Fragments of the desired length (200bp-600bp) were selected by double-sided SPRI bead selection using Ampure XP beads (Beckman Coulter) according to the manufacturer's instructions. First selection was performed with 0.6 volumes (60µl) of beads to remove high molecular-weight DNA fragments. The unbound fraction was used to perform the second selection with 0.9 volumes of beads (additional 30µl of beads). Bound DNA of desired sizes was eluted from the beads with 50µl of TLE. All DNA from one biological replicate was pooled at this stage and DNA concentration was measured using Quant-iT™ PicoGreen® dsDNA Assay Kit according to manufacturer's instructions. The yield was between 10-30µg per library.

Pull-down of biotinylated fragments

Fragments containing biotinylated ligation junctions were pulled-down using streptavidin-coated beads. The libraries were divided between multiple tubes of 5µg of DNA each and mixed with 150µl of Dynabeads MyOne Streptavidin C1 beads (Life Technologies) and processed according to the manufacturer's instructions. The binding step was performed with beads suspended in 300µl of 2x binding and wash buffer (5mM Tris-HCl pH=8, 0.5mM EDTA, 1M NaCl) and 300µl of Hi-C material in TLE. Beads were finally washed with 200µl of 2x T4 ligase buffer and then resuspended in 50µl 1x T4 ligase buffer.

Adapter ligation

Paired-end sequencing TruPE adapters (Table 2) were annealed together to produce double-stranded adapters by mixing 15µl of both adapters (each at 100µM) with 70µl of nuclease-free water and heated to 90ºC for 5 minutes followed by 15min at 70ºC and then cooled to RT on

the bench. These are non-standard short adapters and don't contain barcodes allowing for multiplexing the libraries during sequencing. The barcodes were added later, during the Capture Hi-C baits hybridisation step.

4µl of annealed adapters and 1400U of T4 DNA ligase (New England Biolabs) were added to the streptavidin bead suspension containing biotinylated Hi-C material and reactions were incubated at RT for 2h. Beads with Hi-C material were recovered using a magnetic separator, washed twice with 400µl of wash buffer (5mM Tris-HCl pH=8, 0.5mM EDTA, 1M NaCl, 0.05% Tween), once with 200µl of wash buffer without Tween, once with 200µl of 1x NEB Buffer 2, once with 60µl of 1x NEB Buffer 2 and resuspended in 40µl of 1x NEB Buffer 2. Aliquots from the same biological replicate were pooled.

Table 2. Short 33bp adapter sequences ligated to Hi-C library fragments before final library amplification.

Adapter	Sequence (5' → 3')
Capture Hi-C TruPE adapter 1	[Phos]GATCGGAAGAGCACACGTCTGAACTCCAGTCAC
Capture Hi-C TruPE adapter 2	ACACTCTTTCCCTACACGACGCTCTTCCGATCT

Amplification of Hi-C library

Test PCR reactions were set up to determine the optimal number of cycles to amplify the Hi-C libraries. 2.5µl of bead suspension were used as template with 0.3µM each TruPE PCR primer 1.0.33 and TruPE PCR primer 2.0.33 (Table 3), 1x Phusion Buffer and 0.25mM each of dATP, dCTP, dGTP and dTTP in 25µl reactions. An initial denaturation step of 98ºC for 30s was followed by a varying number of cycles (typically 7, 9 and 12) of 98ºC for 10s, 65ºC for 30s and 72ºC for 30s, followed by final extension for 7min at 72ºC. A number of cycles for final library amplification was chosen according to where the band of the amplified library was barely visible on a gel or one cycle less, in order to not over-amplify the material.

The remaining bead-bound Hi-C material was split into 2.5µl aliquots for use as template in PCR reactions as described above with the determined number of cycles. After library amplification, beads were immobilized using a magnetic separator and the supernatant containing the amplified library was pooled with all other supernatants from the same Hi-C library (biological replicate). DNA was purified and PCR primers removed using 0.9 volumes of Ampure XP beads (Beckman Coulter) following manufacturer's instructions and eluted in 100µl of TLE.

Hi-C libraries were analysed using Bioanalyzer High-Sensitivity DNA Assay (Agilent) by the Next Generation Sequencing Facility at the Babraham Institute to check for product size and library concentration.

Table 3. Primer sequences for final Hi-C library amplification

Primer	Sequence (5' → 3')
Capture Hi-C Tru-PE PCR primer 1.0.33	ACACTCTTTCCCTACACGACGCTCTTCCGATCT
Capture Hi-C Tru-PE PCR primer 1.0.33	GTGACTGGAGTTCAGACGTGTGCTCTTCCGATC

2.6.2. Generation of short biotinylated RNA baits for target capture

Digestion with HindIII

BAC DNA was digested with 40U of HindIII per 5µg of BAC DNA. DNA was purified by phenol-chloroform extraction, ethanol precipitated at -20ºC overnight, centrifuged at 14000rpm form 20min at 4C. The pellet was washed with 70% ethanol, air dried and resuspended in 6µl of 10mM Tris pH 7.5. DNA concentration was determined by NanoDrop spectrophotometer.

T7 promoter adapters annealing and bait DNA shearing

Adapters containing T7 promoter sequence were produced by annealing two oligonucleotides (**Table 4**) as described above for Capture Hi-C TruPE adapters. Adapters were then ligated to digested BAC DNA in 130µl reactions pooling up to 6 BACs together by adding 150ng of each BAC DNA, 0.8µM annealed adapters and 400U of T4 DNA ligase (New England Biolabs) and incubated at 16ºC overnight. The reaction was inactivated at 65°C for 10min.

Table 4. T7 DNA polymerase promoter oligonucleotides.

Adapter	Sequence (5' → 3')
T7-1	TCTAGTCGACGGCCAGTGAATTGTAATACGACTCACTATAGGGCGA
T7-2	[Phos]AGCTTCGCCCTATAGTGAGTCGTATTACAATTCACTGGCCGTCGACTAGA[SpcC3][a]

a [SpcC3] indicated a C3 spacer, underline indicates overhanging HindIII complementary end

To generate 200bp bait fragments, BAC DNA was sheared by sonication using an E220 ultrasonicator (Covaris) with the following parameters: 10% duty factor, 175 W peak incident power, 200 cycles per burst, 180s treatment time. Sheared ends were repaired and DNA purified and size-selected for 180bp-300bp fragments using 0.7 and 1.0 volumes of SPRI beads.

Bait transcription and biotinylation

Biotinylated RNA baits were generated by using size-selected BAC DNA fragments as a template in 20µl *in vitro* transcription reactions using T7 MegaScript kit (Life Technologies). Each reaction contained 1x reaction buffer, 5.5µl of template DNA (typically between 100ng-500ng), 2.5mM biotin-UTP (Roche), 5mM rUTP, 7.5mM each rATP, rCTP, rGTP and 2µl of T7 enzyme mix. Reactions were incubated at 37ºC overnight. Template DNA was removed by incubation with 2U of TURBO DNase (Life Technologies) at 37ºC for 15min. Biotinylated RNA baits were purified using Ambion MEGAclear kit (Life Technologies) according to the manufacturer's instructions. RNA yield was determined using NanoDrop spectrophotometer.

2.6.3. Capture Hi-C libraries generation - baits hybridisation

500ng of Hi-C material was used for hybridisation with biotinylated RNA baits. The Hi-C libraries were dried using a SpeedVac vacuum concentrator (Thermo Scientific) at 45ºC for 15-20min and resuspended in 3.5µl of H_2O. Hi-C material was mixed with 2.5µg of mouse Cot-1 DNA (Life Technologies), 2.5µg of sheared salmon sperm DNA (Life Technologies) and 30µM of each blocking oligo (**Table 5**) in a 10µl reaction and incubated at 95ºC for 5min followed by 5min at 65ºC. 13µl of 2x hybridisation buffer (10x SSPE, 10x Denhardt's solution, 10mM EDTA, 0.2% SDS) were pre-warmed to 65ºC. 500ng of RNA baits in 5.5µl volume was mixed with 20U of SUPERase-In (Life Technologies) and pre-warmed to 65°C. Hi-C material was mixed with hybridisation buffer and baits and incubated at 65ºC for 24h in a thermocycler with a heated lid.

60µl of Dynabeads MyOne Streptavidin T1 beads (Life Technologies) were washed 3 times and resuspended in 200µl of 1M NaCl, 10mM Tris-HCl pH 7.5 and 1mM EDTA. Beads were combined with the hybridisation reaction and incubated at RT for 30min to capture only fragments from the Hi-C that hybridised to the biotinylated baits. Beads were recovered using a magnetic separator and washed once with 500µl of 1x SSC/0.1% SDS for 15min at RT, followed by three washes of 10min each at 65ºC with 500µl of pre-warmed 1x SSC/0.1% SDS. Finally beads were quickly washed with 200µl of 1x NEB Buffer 2 at RT and resuspended in 30µl of NEB Buffer2.

Test PCRs were performed to determine the optimal number of cycles as described above and the final PCR was performed to amplify the Capture Hi-C libraries. In this step, the PCR primers used added barcoded adapters to each library so that samples could be multiplexed on a single flow-cell lane for sequencing (Table 6). Barcoded adapters were also added to pre-capture Hi-C libraries.

Fragments of desired length (200bp-600bp) were selected by double-sided size selection using Ampure XP beads (Beckman Coulter) according to the manufacturer's instructions. First selection was performed with 0.5 volumes of beads to remove high molecular-weight DNA fragments. The unbound fraction was used to perform the second selection with 1 volume of beads to remove low molecular-weight DNA fragments. Bound DNA of desired

sizes was eluted from the beads with 20µl of TLE. All DNA from each biological replicate was pooled.

Capture Hi-C libraries were also analysed using Bioanalyzer High-Sensitivity DNA Assay (Agilent) by the Next Generation Sequencing Facility at the Babraham Institute to check for product size and library concentration. KAPA Library Quantification Kit (KAPA Biosystems) was also used to independently assess the library concentration in a 10µl reaction containing 6µl of KAPA qPCR master mix containing primers and 1µl of library diluted 1:1000 or 1µl of KAPA standard.

Table 5. Blocking oligos used in Capture Hi-C bait hybridisation step.

Blocking oligo	Sequence (5' → 3')
P7_b2_f_IBR_Schellenberg	GTGACTGGAGTTCAGACGTGTGCTCTTCCGATCdd
P7_b2_r_IBR_Schellenberg	AGATCGGAAGAGCACACGTCTGAACTCCAGTCAC
P5_b1_f_IBR_Schellenberg_33	ACACTCTTTCCCTACACGACGCTCTTCCGATCTdd
P5_b1_r_IBR_Schellenberg_33	AGATCGGAAGAGCGTCGTGTAGGGAAAGAGTGT

Table 6. TruSeq adapter sequences used as primers in the final amplification of Capture Hi-C libraries.

Primer	Sequence (5' - 3')
TruSeq universal adapter	AATGATACGGCGACCACCGAGATCTACACTCTTTCCCTACACGACGCTCTTCCGATCT
TruSeq universal adapter with index (reverse complement)	CAAGCAGAAGACGGCATACGAGATXXXXXXGTGACTGGAGTTCAGACGTGTGCTCTTCCGATC

Underline indicates the position of a unique 6bp index

2.7. Hi-C and Capture Hi-C sequencing and reads processing

Hi-C and Capture Hi-C libraries we sequenced as 100bp paired-end reads on Illumina HiSeq by the Next Generation Sequencing Facility at the Babraham Institute. Hi-C libraries were sequenced once, multiplexing 5 libraries on one lane. Each Capture Hi-C library was sequenced three times, multiplexing 4 libraries on one lane. Capture Hi-C data from each sequencing run was processed separately and data belonging to the same biological replicate was combined after custom genome generation (section 2.8.1).

Reads processing by HiCUP

Sequenced reads were mapped, filtered and quality assessed using the Hi-C User Pipeline (HiCUP) software developed by Steven Wingett at the Babraham Institute (Wingett et al.

2015). Hi-C experiments produce molecules reflecting genomic interactions and so are composed on two ligated together DNA fragments that are not adjacent in linear sequence and harbour a digested and subsequently filled-in restriction site between them. These dual reads are referred to as di-tags that have two 'ends'. They demand to be mapped unconventionally compared to most paired-end reads. Forward and reverse reads are processed separately. First, sequences were de-multiplexed based on unique indices in the sequencing adapters used for each library. Second, if reads extended beyond the restriction junction, they were truncated at the restriction site to eliminate the part of the read that comes from a different location in the genome. Third, these trimmed reads were mapped uniquely using Bowtie2 (MAPQ>30) or, in the presence of a possible secondary alignment, if the difference in alignment scores between the primary alignment and the next best alignment was greater than 10 and the probability of misalignment reported by Samtools was less than 1:1000, then these reads were also included. Reads were mapped to the mm9 (NCBI37) mouse reference genome assembly. Forward and reverse reads were mapped independently and then re-paired to form di-tags. Fourth, sequences representing experimental artefacts and uninformative di-tags were removed: di-tags that are products of re-ligation of adjacent fragments, contiguous sequences encompassing more than one restriction junction coming from incomplete digestion, self-ligated (circularised) fragments, internal fragments without restriction junction and dangling ends without a ligation partner were filtered out and remaining di-tag were considered valid read pairs. Fifth, di-tags were removed when the mapped reads were positioned further away from the putative restriction site than allowed by the experimental size-selection step. Sixth, reads with identical starts and ends were removed, retaining one copy, because as the library has been sonicated, identical reads represent PCR duplicates. Mapped and filtered valid read pairs from each library were stored in a BAM format.

2.8. Bioinformatic analysis of Capture Hi-C datasets

2.8.1. Normalisation of Capture Hi-C datasets using HOMER

Generation of custom genome files

Capture Hi-C datasets were filtered to retain only read pairs with at least one end mapping to the baited regions. Custom genome chr_i.dat files were created to generate mini chromosomes with starts and ends matching the start and end of BACs used for generating the baits. This was done using a custom script written by Steven Wingett and was necessary for subsequent data analysis in HOMER. Capture Hi-C datasets from three separate sequencing runs belonging to the same biological replicate were merged and de-duplicated again (**Table 7**). Using the *hicup2homer* conversion script in HiCUP the Capture Hi-C BAM files were converted to 'HiC summary' file format accepted by the Hi-C analysis tool HOMER (Heinz et al. 2010).

Creating interaction frequency matrices using HOMER

Capture Hi-C datasets, in the form of custom genome, were analysed using the Hi-C analysis tool HOMER (Heinz et al. 2010) to produce normalised interaction frequency matrices at 20kb resolution for the Igh locus in $Rag^{-/-}$ pro-B cells, Rag/81X pre-B cells and Thymus. HOMER employs an iterative correction method for matrix balancing, which corrects for multiple biases inherent to Hi-C experiments collectively referred to as observability of the analysed restriction fragments or genomic bins, or as sequencing coverage biases. A background model at 20kb resolution was generated and the *analyzeHiC* function was used to produce interaction frequency matrices in 20kb bins with or without distance correction (the *-simpleNorm* option was used to omit distance correction, default settings were used otherwise). Output matrices were visualised in Java TreeView (Saldanha 2004).

2.8.2. Identification of significant inter-chromosomal interactions

To find statistically significant inter-chromosomal interactions from viewpoints of interest, a set of 7 virtual 4C experiments has been performed. For the Ig loci, all HindIII fragments in each baited region were taken as a viewpoint (Igh - 3.1Mb, Igk - 3.5Mb, Igl - 410Mb), whereas for other baited regions of interest (Pax5 - 207kb, Foxo1 - 150kb, Il7r - 170kb and Rag1Rag2 - 215kb) a 500kb genomic bin was taken as a viewpoint (chr4:44500001-45000000 for Pax5, chr3:52000001-52500000 for Foxo1, chr15:9000001-9500000 for Il7r and chr2:101000001-101500000 for Rag1Rag2). The virtual 4Cs were carried out in Seqmonk software using raw Capture Hi-C data processed by HiCUP as described in section 2.7. The genome was binned into 500kb bins and 'other ends' of all read pairs mapping to each viewpoint were extracted and quantified in 500kb bins, creating seven 4C-like datasets. Trans interactions yield far fewer reads than cis interactions, hence a lower resolution was required. The first 3Mb of every chromosome's centromeric end were omitted, which is a standard approach when mapping NGS data to avoid these repetitive regions. Other ends from the same chromosome as the viewpoint were eliminated. Modified z-score analysis using the median was performed to identify the highest outlier bins with z-score > 3.5, representing the most frequent interactions with the viewpoint. An interaction between the viewpoint and a 500kb bin was considered significant if its z-score was greater than 3.5 in all biological replicates. For 500kb bins that satisfied this condition an average z-score was calculated.

A/B compartment analysis

A/B compartments were identified in non-enriched Hi-C datasets with help from Csilla Varnai. The genome was binned into 500kb bins and the *runHiCpca.pl* function in HOMER was used to identify the first and second principal component in Hi-C datasets. H3K4me3 ChIP-seq dataset (GSE80155) was used to determine the sign on the PCA eigenvectors. Default parameters were used except *-pc 2 -active H3K4me3*.

Hierarchical clustering

Hierarchical clustering of trans interactions was performed using heatmap.2 function in R using the default distance function ('Euclidean'), the default clustering function ('complete') and dendrogram clustering was applied to both columns and rows.

2.9. Polymer modelling of the Igh locus

A polymer modelling method described previously by Giorgetti *et al*. (Giorgetti et al. 2014) was used to model all possible single conformation of the Igh locus based on the interaction frequency matrices outputted from HOMER. This was done by Yinxiu Zhan and Luca Giorgetti at the Friedrich Miescher Institute for Biomedical Research in Basel, Switzerland. Briefly, the model describes the DNA fibre as self-avoiding polymer chain of beads and the Igh locus was divided into beads of diameter *a=20kb* corresponding to 20kb bins in the interaction maps. The Monte Carlo model turns the interactions frequencies from ensemble data into interaction potentials (energies) restricted by hard-core repulsion of *0.6a*. The interaction is considered specific when the distance between beads does not exceed *1.5a*. The interaction potentials are iteratively optimised by Monte Carlo sampling, starting with values *p=1* for adjacent beads and random values for other bead pairs. The sampling modifies the interactions potential values until the simulated potentials converge with the experimental interaction frequencies. A full set of possible single conformation is found when all interaction potentials pooled together reflect the experimental interaction frequencies.

2.10. 3D DNA fluorescent *in situ* hybridisation (FISH)

FISH experiments were based on to the 3D DNA FISH protocol developed and optimized for B cells by Dan Bolland (Bolland et al. 2013).

2.10.1. Direct labelling of fluorescent probes

BAC DNA was nick-translated and incorporated with aminoallyl-dUTP (Ambion) in a 100µl reaction containing 2µg of BAC DNA, 10µl of 10x NTB buffer (0.5 M Tris-HCl, pH=7.5), 10µl of 0.1M DTT (Invitrogen), 8µl of d(GAC)TP mix 0.5mM each, 2µl of 0.5mM dTTP, 12µl of 0.5mM aminoallyl-dUTP, 20U of DNA polymerase I (New England Biolabs) and 2µl of 10U/µl DNase I (Roche) at appropriate dilution (1:30 here) to obtain nick-translated products of length 150bp-1000bp. The reaction was incubated at 16ºC for 2h. The efficiency of nick-translation was checked by running 1µl of sample on 2% w/v agarose gel while keeping the rest of the reaction on ice. Nick-translation reaction was terminated by heating to 75ºC for 5 min. Nick-translated DNA was then purified using a PCR purification kit (Qiagen)

and ethanol precipitated at -20ºC overnight. Precipitated DNA was centrifuged at 14,000 rpm at 4ºC for 30min. The pellet was washed with ethanol and air dried. Nick-translated DNA pellet was resuspended in 6µl of H_2O and concentration was measured by NanoDrop prectrophotometer. To couple the DNA with a fluorescent dye, DNA was heated to 95C for 5min, then mixed with 2µl of AlexaFluor dye dissolved in DMSO (Sigma Aldrich) and 3µl of 0.2M $NaHCO_3$ and incubated in the dark for 1h at RT. 40µl of H_2O was added to the sample and fluorescent-labelled DNA was purified using a PCR purification kit (Qiagen) with an extra PE wash. DNA was eluted in 50µl of H_2O and fluorescent dye incorporation was measured using the 'proteins and labels' option of the NanoDrop prectrophotometer. Expected incorporation was 5-10 dyes per 100bp.

2.10.2. Microscope slides preparation

FACS sorted cells were washed with PBS and placed on Poly-L-lysine coated slides (Sigma Aldrich) by dropping a droplet containing 200,000 cells in the middle of the slide. Cells were left for 3min at RT to settle. Slides were fixed by submerging the slide in 4% paraformaldehyde (Sigma Aldrich) for 10min at RT. All reactions were carried out in 100ml coplin jars by transferring slides between jars. The fixation reaction was quenched in 155mM glycine for 10min at RT. Cells were permeabilised for 10min at RT in 0.1% saponin/0.1% Triton in 1x PBS. Cells were washed in PBS for 5min at RT and stored in 50% glycerol at -20ºC for 7 days.

2.10.3. DNA FISH probes hybridisation

Probe precipitation

20ng of each (two or three) fluorescent dye-labelled DNA FISH probe was mixed with 2µg of Cot-1 mouse DNA (Invitrogen) and 9.7µg of salmon sperm DNA (Sigma) in 100µl H_2O and ethanol precipitated for 1h at -20ºC. The probe was centrifuged at 14,000 rpm for 30min at 4ºC, then washed with ethanol and air dried. The pellet was resuspended in 5µl of formamide (Sigma Aldrich) and incubated in the dark at 37ºC for 30min with shaking at 1000 rpm. Resuspended probe was mixed with 5µl of 20% dextran sulphate in 2x SSC and incubated in the dark at 37ºC for 10min.

Probe hybridisation

The slides were taken out of 50% glycerol, washed in PBS for 5min in RT and calibrated in 20% glycerol/1x PBS at RT for 10min. Slides were washed twice in 1x PBS at RT for 5min. Slides were incubated in 0.1M HCl at RT for 30min and washed in 1x PBS at RT for 5min. Cells were permeabilised by incubating the slide in 0.5% saponin/0.5% Triton/1x PBS at RT for 30min and then washed twice in PBS for 5min at RT. Slides were equilibrated in 50% formamide/2x SSC for at least 10min at RT. Before placing fluorescent-labelled probes onto the cells, the slide was briefly washed in PBS to wash off excess formamide and pat dried.

10µl of probe was pipetted onto a coverslip, which was then inverted and placed onto the cells on the slide and sealed around with Fixogum rubber cement (Marabu). To hybridise the probe, the slide was heated on a hot plate at 78°C for exactly 2min and incubated in a humid box in the dark at 37°C for at least 16h. From this point all incubations were done in the dark. The rubber cement was peeled off and slides placed in 2x SSC for 10min until the coverslip slid off. To remove unspecifically bound probe the slide was incubated in 50% formamide/2x SSC at 45°C for 15min, then in 0.2x SSC at 63°C for 15min, followed by 5min in 2xSSC at 45°C, 5min in 2x SSC at RT and 5min in PBS at RT. Cell nuclei were stained with DAPI (5µg/ml in 2x SSC) (Invitrogen) for exactly 2min at RT and washed in PBS for 5min at RT. For final fixation slides were incubated in 3.7% formaldehyde/1x PBS for exactly 5min at RT, then the quenched in 155mM glycine for at least 30min at RT and washed in PBS for 5 min at RT. A 22x50mm coverslip with a drop of Vectashield Antifade (Vector Labs) or ProLong Diamond (Thermo Fisher) mounting medium was mounted onto the slide, sealed with nail varnish and kept in the dark for 20min. Slides were kept at 4°C overnight or imaged immediately.

2.10.4. Fluorescent signal acquisition using Metacyte

Fluorescent signals were acquired by MetaSytems Metacyte imaging system using a Zeiss Axio Imager Z2 microscope. Metacyte automatically imaged fields of view with multiple cells, capturing the fluorescent signals across 15 focal planes every 0.5µm in all nuclei in view, averaging 5 nuclei per field and capturing a total of 300-800 fields. Fluorescent signals were acquired using wavelengths of 488nm (green), 555nm (red), 647nm (far red) and 358nm (DAPI) (acquisition parameters: max integration time 0.24s for DAPI, 0.76s for Alexa Fluor 488 and 555, 1.76s for Alexa Fluor 647. Acquisition time is automatically adjusted by Metacyte according to signal brightness. Signal saturation area 4µm^2 for DAPI and 1µm for Alexa Fluor 488, 555 and 647).

2.10.5. Fluorescent signal analysis using Metafer

Metafer software analysed every captured nucleus by identifying the number of fluorescent signals and recording their position coordinates in relation to nuclear volume (analysis parameters: min cell area 20µm^2, max cell area 100µm. Spot selection: absolute spot area 0.25µm^2, max spot area 0.1µm, min spot distance 0.1µm, min spot intensity 30%. Signals recorded on 3 axis for each spot. Cells with zero spots rejected). DAPI fluorescence was measured to determine nuclear volume. Only cells harbouring two fluorescent signals of each wavelength were selected. Cartesian coordinates of each signal in 3D were exported from Metafer and distances between all signal pairs (red1-green1, red1-green2, red2-green1, red2-green2) were calculated using a custom script written by Felix Krueger. The shortest distance in each cell was taken for further analysis. For tripartite interactions, the distances between a

red and a green signal below 1μm were identified and the presence of a far red signal within 1μm of either red or green signal was assessed.

2.10.6. Statistical analysis of FISH distances

The differences between $Rag^{-/-}$ pro-B cells, $E\mu^{-/-}$ pro-B cells, Rag/81X pre-B cells and Thymus in the number of cells with two or three closest fluorescent signals closer than 1μm were analysed using Fisher's exact test with Bonferroni correction for multiple testing. To analyse the differences between all distances separating two closest fluorescent signals in these three genotypes, Kruskal-Wallis test with Dunn's correction for multiple testing was used. To analyse the differences between all distances separating two closest fluorescent signals in $Rag^{-/-}$ pro-B cell and $E\mu^{-/-}$ pro-B cells, Mann-Whitney test was used.

2.11. Other datasets used in the analysis

Nuclear RNA-seq datasets in $Rag^{-/-}$ pro-B cells and Rag/81X pre-B cells were generated by Louise Matheson in our lab and mapped with Bowtie2 by Felix Krueger. Reads were quantified in 500kb bins as well as over genes adjusted for gene length as log2 and normalised between datasets. Bins that had 0 or 1 read were removed from analysis. The difference in read counts between paired datasets was analysed using a paired t-test with Bonferroni correction for multiple comparisons. The difference in read counts between non-paired datasets was analysed using one-way ANOVA with Sidak's multiple comparisons test.

ChIP-seq datasets for CTCF in $Rag^{-/-}$ pro-B cells (GSE27214) (Ebert et al. 2011) and H3K4me3 (GSE80155) (Bolland et al. 2016) were mapped with Bowtie and peaks were called using MACS2 in the narrow peak mode (Zhang et al. 2008) by Hashem Koohy. Correlation between ChIP signal levels and the V beads interaction frequency with D beads was performed by Yinxiu Zhan. An average of all ChIP-seq peak summits in 20kb beads was calculated and correlated with V beads interaction frequencies with D beads using Pearson's correlation.

3

3. The first high-resolution unbiased spatial conformation model of the immunoglobulin heavy chain locus

3.1. Introduction

A highly diverse repertoire of immunoglobulin heavy chains is produced by somatic recombination of one V, one D and one J gene out of an array of over 200 genes in the large 2.8Mb mouse Igh locus. It has become apparent that chromatin is organised in a non-random fashion inside the nucleus and that genomic regions make functionally relevant contacts even if separated by large linear distances or on different chromosomes (Lettice et al. 2002; Tolhuis et al. 2002; Schoenfelder et al. 2009). The Igh locus was therefore a key representative paradigm to investigate how the 3D structure of genomic loci relates to their function. Initially, imaging methods such as fluorescence in-situ hybridisation (FISH) were utilised to study gene positions in relation to each other and the nuclear membrane. The first detected structural feature suggesting that V(D)J recombination requires major reshaping of chromatin was a massive locus contraction, i.e. a change from an extended to a globular form, during transition from pre-pro-B cell to pro-B cell stage (Fuxa et al. 2004; Rother et al. 2016). The advent of the chromosome conformation capture (3C) method and its derivatives (4C, 5C and HiC) alleviated the low resolution of FISH and enabled the identification of a multitude of functional contacts genome-wide. These assays allow for investigation of the spatial conformation of genomic loci by cross-linking and digestion of chromatin, followed by re-ligation of DNA fragments that were in close physical proximity prior to fixation (reviewed in Schmitt et al. 2016; Davies et al. 2017).

The interactions of the Igh genes and regulatory elements have been extensively studied using 3C and 4C (Guo et al. 2011a; 2011b; Kumar et al. 2013; Medvedovic et al. 2013; Rother et al. 2016; Degner et al. 2011; Verma-Gaur et al. 2012) and recently by 5C (Montefiori et al. 2016). Early studies have focused on probing for interactions from the intronic enhancer Eμ as a viewpoint and have shown that it interacts extensively with other elements in the 3' half of the Igh locus, but is also capable of long-range looping to the V

region. Other viewpoints analysed included the 3' regulatory region (3'RR/HS1-3), the 3' HS4-8 sites and the IGCR1, which have been shown to interact with each other in pro-B cells, but also in earlier stages of B cell development as well as in other lymphocytes, suggesting a generally highly organised structure of the 3' end of the Igh locus. Notably, the 3' HS4-8 and the IGCR1 often exhibited more frequent interactions than the intervening Eμ (Guo et al. 2011b; Medvedovic et al. 2013). Various viewpoints in the V region have also been probed, but the distal Vs were extremely difficult to investigate due to their repetitiveness and therefore low mappability in NGS studies. These 3C-based investigations produced two somewhat divergent views of the spatial organisation of the Igh locus. On one hand, all studies agree on a high level of looping in the locus at the pro-B cell stage, on long-range interactions bringing the 3' and the 5' ends closer together, on the presence of very frequent interactions between the 3' regulatory elements and on the existence of loops in the distal V region that are independent of locus contraction. On the other hand, some studies favour a highly defined overarching 3-loop structure: a 3' domain, a proximal V domain and a distal V domain (Guo et al. 2011a; Gerasimova et al. 2015; Montefiori et al. 2016), whereas others take a less rigid view and propose that the V genes loop to the 3' end in a flexible fashion with interactions varying greatly from cell to cell (Medvedovic et al. 2013). Reports also disagree on the level of contribution of the various regulatory elements to locus contraction, with some reporting that the loss of Eμ and the loss of the IGCR1 reduce locus contraction (Guo et al. 2011a; 2011b; Gerasimova et al. 2015), whereas others did not see any effect (Medvedovic et al. 2013).

Thanks to Hi-C the Igh locus has been visualised as one topologically-associating domain (TAD), but the resolution of Hi-C experiments was not high enough to interrogate the interactions of particular elements of the locus (Lin et al. 2012; Benner et al. 2015). A recent 5C study was the first to focus on visualising all interactions throughout the Igh. 5C relies on a large number of primers to probe for every restriction fragment in the interrogated region, but the Igh locus, particularly the V gene region, is quite repetitive, which makes it one of the most poorly mappable regions in the genome. Therefore, designing unique good quality 20bp primers for all 887 HindIII fragments in the Igh locus is currently impossible. The 5C study was able to design 225 primers along the Igh and build an interaction map at 150kb resolution plotted using a sliding window of 15kb steps. Subsequent FISH analysis led them to identify PAX5-dependent and PAX5-independent interactions. This prompted them to propose a proximal V domain, an unstructured middle V domain and a distal V domain, whose folding is PAX5-dependent (Montefiori et al. 2016). A 4C study, on the other hand, achieved 20kb resolution with 5kb step, albeit only from several hand-picked viewpoints (Medvedovic et al. 2013).

Although much effort has been expended on elucidating the spatial organisation of the Igh locus, a comprehensive, unbiased, high resolution and all-to-all structure is still lacking. Hi-C material requires immense sequencing depth to be able to sample interactions in large loci at high resolution (Rao et al. 2014d). To alleviate the need for sequencing the whole

genome, multiple studies devised methods to extract ligation products from Hi-C material that only contained interactions involving a region of interest. These include Capture-C (Hughes et al. 2014; Davies et al. 2016), T2C (Kolovos et al. 2014; 2016) and Promoter Capture Hi-C (Mifsud et al. 2015; Schoenfelder et al. 2015a). The Capture Hi-C assay used in this thesis is based on the Promoter Capture Hi-C protocol and was devised by Stefan Schoenfelder and Mike Stubbintgon, who designed a set of baits to enrich the Hi-C material for interactions involving the Igh locus. I carried out these experiments incorporating the in-nucleus ligation strategy and blocking oligos improving bait pull-down. This method provided read coverage of every single HindIII fragment in the Igh and gave 45-fold enrichment over Hi-C.

Previous 4C-based studies have not used any coverage or distance correction to normalise the detected ligation product counts. However, normalisation has been shown to be an essential step in Hi-C-derived experiments (reviewed in Ay and Noble 2015; Schmitt et al. 2016). Enriching for a genomic region several megabases in size using a lawn-like bait system was a very novel approach at the start of my experiments and no accepted analysis methods existed in the field. I have used the Hi-C analysis tool HOMER to perform coverage correction to account for biases in Hi-C datasets and obtain normalised interaction frequencies between all elements of the Igh locus at 20kb resolution. This is the first study that provides a comprehensive all-to-all interaction landscape of the Igh locus just prior to recombination. Furthermore, the interaction frequencies obtained from this ensemble Capture Hi-C analysis have been modelled using polymer modelling by my collaborators Luca Giorgetti and Yinxiu Zhan at the Friedrich Miescher Institute for Biomedical Research in Basel, Switzerland. Their polymer model (Giorgetti et al. 2014) allowed us to elucidate all possible single conformations from the ensemble data. This revealed that there is no one dominant structure that can describe the organisation of the Igh locus, but rather an ensemble of many structures. Pro-B cells are a heterogeneous population in which different cells are recombining different V genes with different D-J segments to generate a diverse antibody repertoire, and this is the first analysis ever attempted to obtain a glimpse of what the Igh locus might fold like in single cells prior to recombination.

This chapter outlines my efforts to elucidate the architecture of the Igh locus, identify hallmarks of its organisation and shed light on the link between chromatin interactions and V gene usage in V(D)J recombination.

3.2. Generation of Capture Hi-C libraries in pro-B cells, pre-B cells and thymocytes

$Rag^{-/-}$ models facilitate study of Ig loci prior to recombination

I was interested in resolving the spatial conformation of the poised Igh just prior to V(D)J recombination in order to elucidate the DNA contacts that likely govern the frequency of V gene rearrangement. This cannot be achieved by investigating wild type pro-B cells, because V(D)J recombination is initiated in CLPs and at the pro-B cell stage most cells have already undergone D-J recombination on both alleles and are undergoing V-DJ recombination on the first or second allele. Individual pro-B lymphocytes are therefore at different stages of V(D)J rearrangement and most cells have parts of the Igh locus sequence missing due to excision of intervening regions after D-J and V-D joining. To investigate the Igh locus at the pro-B cell stage, whilst preserving its germline sequence, cells from $Rag^{-/-}$ mice were used to generate Capture Hi-C libraries. Both strains of Rag mice used lack a functional recombination activation gene 1 (Rag1) endonuclease and therefore lack the RAG enzyme complex (Mombaerts et al. 1992; Matthias and Baltimore 1993). This results in B cell arrest at the pro-B stage and an inability to undergo V(D)J recombination. However, the Igh locus in these cells is activated and poised for recombination. It is contracted (Kosak et al. 2002; Fuxa et al. 2004; Guo et al. 2011a), is bearing active histone marks (Chowdhury and Sen 2001; Maes et al. 2006) and exhibits non-coding transcription across the locus (Bolland et al. 2004; Verma-Gaur et al. 2012). $Rag^{-/-}$ mice are therefore a widely accepted model for studying the spatial organisation of the Igh locus in pro-B cells. The $Rag^{-/-\ Bal}$ strain carries a single nucleotide mutation in the RSS-recognition sequence (a missense Hist-609 to Leu substitution) (Matthias and Baltimore 1993) and the $Rag^{-/-\ Mom}$ strain carries a 1.4kb deletion encompassing both the nuclear localisation signal and the zinc-finger-like motif of the Rag1 gene (Mombaerts et al. 1992). Samples generated from these two strains are collectively referred to as $Rag^{-/-}$ pro-B cells in this thesis.

To study the Ig loci at the next developmental stage in the context of genome-wide inter-chromosomal interactions (discussed in chapter 4), I used Rag/81X mice (Martin et al. 1997) whose B lymphocytes are arrested at the pre-B cell stage. These mice have the $Rag^{-/-\ Mom}$ mutation, but they also carry an 81X transgene, which is a functionally rearranged Igμ chain with the 81X V gene (V 7183.2.3) and also contains the Eμ enhancer. Progression to the pre-B cell stage is conferred by the expression of the transgene, which ensures pre-BCR expression and cell proliferation, thus circumventing the need for V(D)J recombination of the Igh locus. Consequently, these B lymphocytes become arrested at the pre-B cell stage and are unable to undergo V_k-J_k light chain recombination.

As a negative control, I used thymocytes from wild type mice. A proportion of T lymphocytes may undergo D-J recombination (Born et al. 1988), but the Igh locus V region is decontracted and V-DJ recombination does not occur. T lymphocytes have the advantage of originating from the same progenitors as B lymphocytes and have proven an excellent

comparison when investigating genome-wide contacts of Ig loci (discussed in chapter 4) allowing the dissection of B cell-specific observations and more widely applicable characteristics of lymphocyte development.

Capture Hi-C libraries processing and quality control

Experimental procedures for generating Hi-C and Capture Hi-C libraries are described in section 2.6 and shown in **Figure 11**. Each Hi-C library was prepared using 20-50x10^6 ex-vivo cells pooled from multiple mice. Libraries from $Rag^{-/-}$ pro-B cells and Rag/81X pre-B cells were generated using bone marrow enriched for $CD19^+$ cells. B lymphocytes in these mouse strains are arrested at pro-B and pre-B cell stage, respectively, and contain no mature B cells, therefore all $CD19^+$ cells are the cells of interest. T lymphocyte libraries were made from whole thymus. In collaboration with Louise Matheson, I prepared three Capture Hi-C libraries from $Rag^{-/-}$ pro-B cells (one replicate from $Rag^{-/-\ Bal}$ and two replicates from $Rag^{-/-\ Mom}$), two libraries from Rag/81X pre-B cells and two T lymphocyte libraries.

The quality of the libraries was confirmed at several stages during library preparation. First, the efficiency of chromatin digestion by HindIII was determined to be ~80% by amplifying the digested material and an undigested control using primers spanning HindIII restriction sites (**Table 7**). Second, after biotin incorporation, end ligation and cross-link reversal, the Hi-C material was confirmed to contain two known interactions, one between Hox genes and one between Hist1 genes (**Figure 12**A). Third, biotin incorporation into the ligation junctions was confirmed by a double digestion test using Hox and Hist1 PCR products (**Figure 12**B), which were successfully digested by NheI after relegation (filled-in HindIII ends produce an NheI site). Fourth, an aliquot of the Hi-C material was used to determine the optimal number of PCR cycles for the final library amplification, to produce a sufficient amount of material for sequencing while minimising duplicate products (**Figure 12**C). Finally, the Capture Hi-C and Hi-C libraries were analysed using Bioanalyzer High-Sensitivity DNA Assay, both before and after bait capture and final amplification to add full-length sequencing adapters, to confirm the correct size of the sequences (average insert size ~420bp) (**Figure 12**D,E).

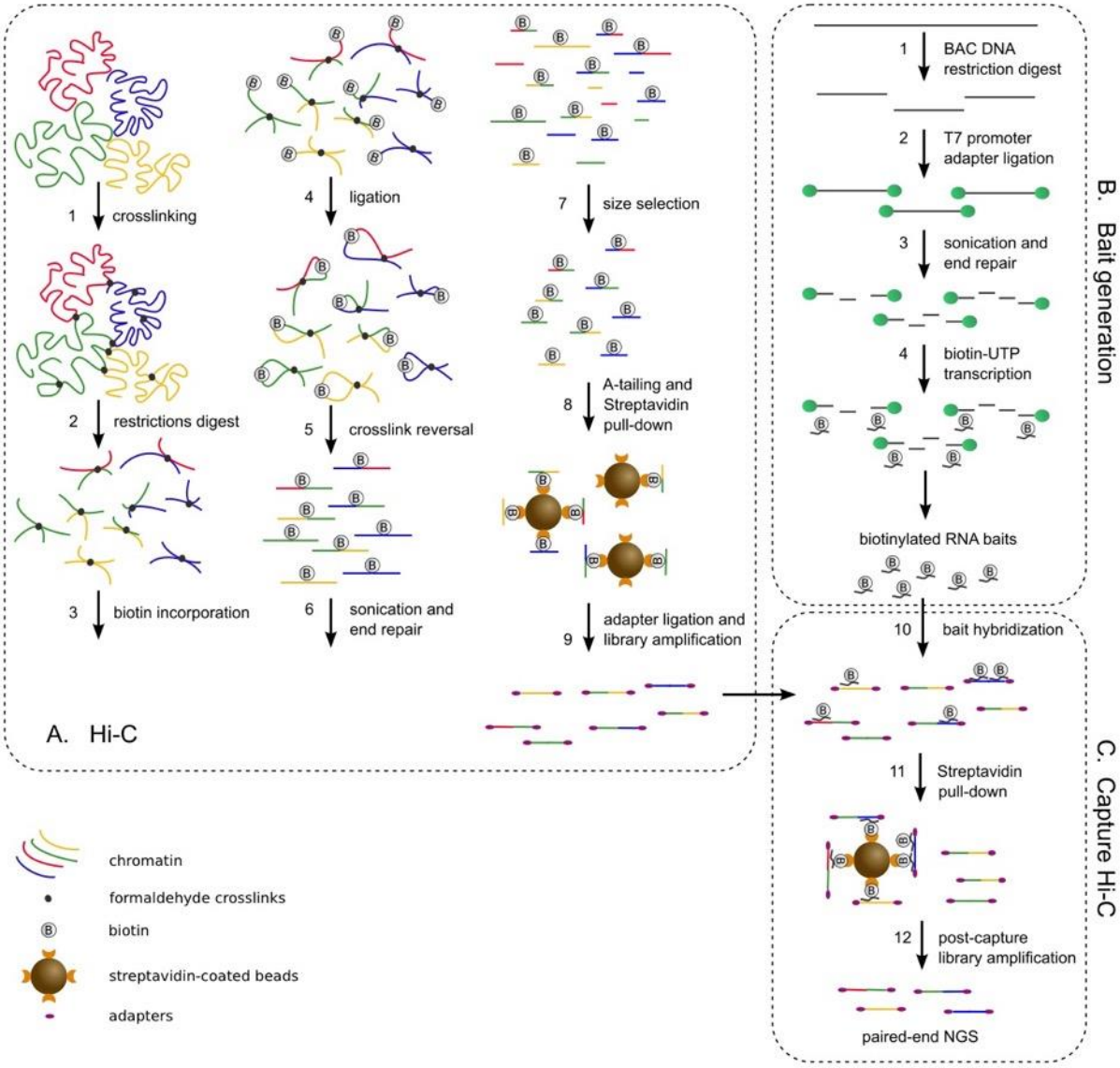

Figure 11. Capture Hi-C workflow. See methods section 2.6 for detailed protocol description. **A.** Hi-C library preparation steps (1-9). **B.** Small biotinylated RNA baits preparation steps (1-4). Green ovals represent T7 adapters. Short wavy lines represent RNA. Small grey circles represent biotin molecules. **C.** Capture step: Hi-C library enrichment by bait hybridization and pull-down.

Table 7. Chromatin digestion efficiency. RT-qPCR results to test the efficiency of chromatin digestion by the HindIII enzyme. Cross-linked digested chromatin was amplified using HindIII site-spanning primer pairs (J606, J558, 3609 and ERCC) and a control primer pair DQ52 that did not span a HindIII restriction site. The amplification levels for HindIII-spanning primers decreased in the digested chromatin samples whereas there was no difference in amplification levels for DQ25 primer pair. The percentage of digestion was calculated according to the formula: $100\text{-}100/2^{(CTs\text{-}CTc)D\text{-}(CTs\text{-}CTc)UD}$. CTs - primers spanning HindIII sites, CTc - control. Tested for $Rag1^{-/-Bal}$ pro-B replicate 3 only as the digestion protocol is well established in the lab.

primer pair	sample	avg CT	% of digestion
DQ52	undigested (UD)	24.47	n/a
	digested (D)	24.26	
J606	undigested (UD)	24.58	
	digested (D)	26.43	77.69
J558	undigested (UD)	24.22	
	digested (D)	25.92	68.60
3609	undigested (UD)	25.59	
	digested (D)	28.20	92.33
ERCC	undigested (UD)	25.69	
	digested (D)	28.10	91.80

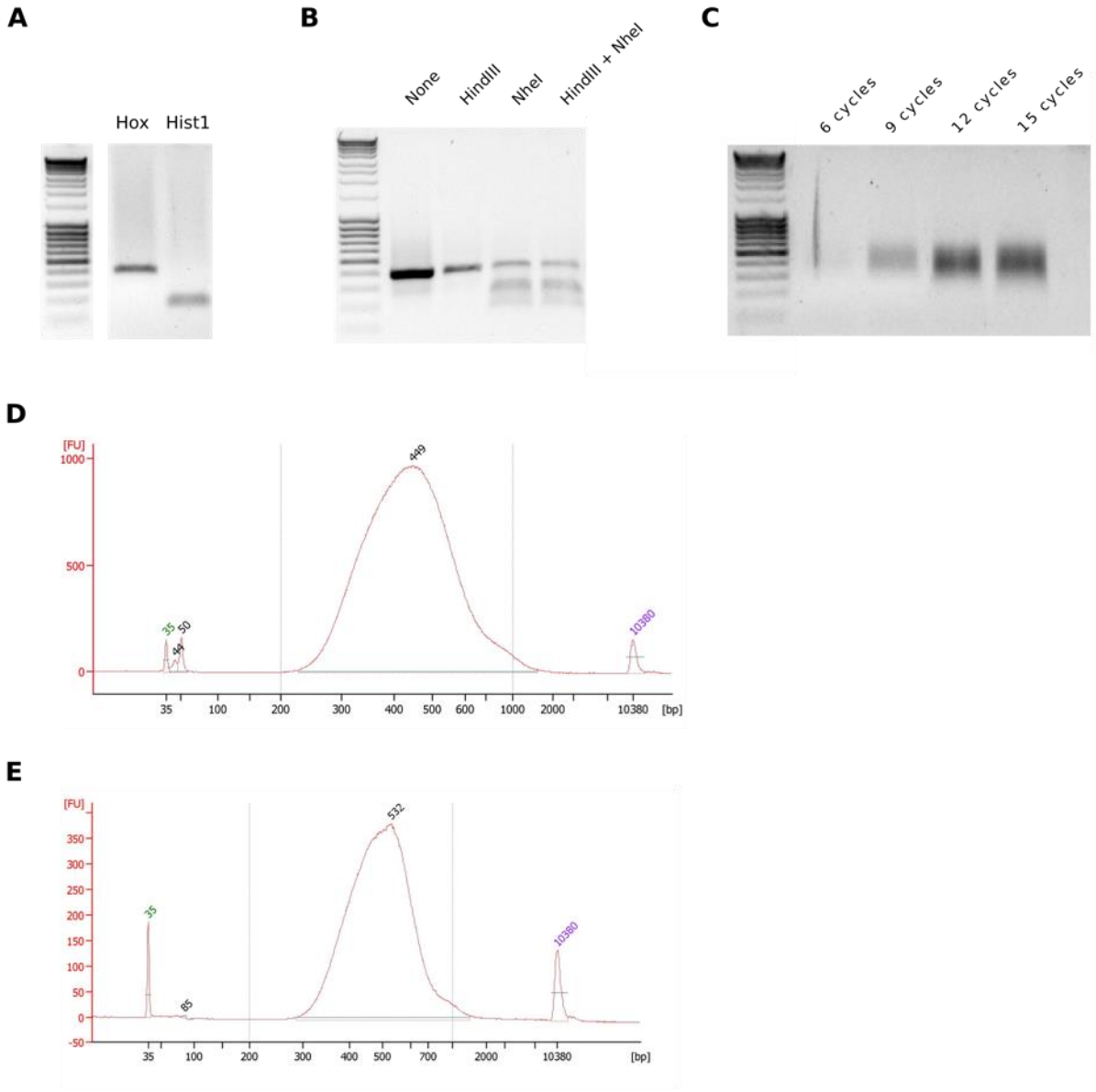

Figure 12. Quality control for Hi-C library preparation and final quantification of Hi-C and Capture Hi-C library. Data shown is for Rag1$^{-/-Bal}$ pro-B replicate 3 library as a representative of all samples. **A.** Detection of known short-range (Hist1) and long-range (Hox) interactions by PCR in the Hi-C material after the cross-link reversal step. **B.** Double digestion test using the Hox interaction PCR product from (A) to confirm proper ends fill-in during biotin incorporation step. The result was analysed by gel electrophoresis. Enzymes used in each reaction are indicated above the lanes. One band indicates undigested DNA whereas two bands indicate digested chromatin by the above enzyme. Only NheI should be able to digest properly filled-in fragments. **C.** PCR amplifications to determine the number of final post-hybridisation PCR cycles for Capture Hi-C library amplification. Reaction products were analysed by gel electrophoresis. The number of cycles used for each reaction in indicated above the lanes. **D and E.** Agilent 2100 Bioanalyzer High Sensitivity DNA Assay output for Hi-C (D) and Capture Hi-C (E) library quantification. The x axis shows fragment lengths and the y axis shows the fluorescent signal intensity as a measure of the concentration of fragments at each length. Peaks at 35bp and 10.38kb correspond to standards used to calibrate the assay. Approximately 100bp of each fragment is taken up by the adapter. True fragment lengths are between 200bp and 1000bp.

3.2.1. Regions enriched in Capture Hi-C experiments

Baits were designed to cover all three immunoglobulin loci as well as several selected genes important in B cell development and control regions (**Figure 13**) (short biotinylated baits generation is described in section 2.6.2 and **Figure 11**B). The analysis in this chapter focuses on the baited Igh locus and chapter 4 extends the analysis to include the Igk, Igl, Foxo1, Pax5, Il7r and Rag1Rag2 baited regions. Regions baited for Nanog, Hbb, Yy1, p27kip, Ikzf1 and Tcf3 were not investigated further during my PhD as they were either alternative negative controls or their pull-down level was not satisfactory. The Igh locus baits were made using 20 overlapping BACs and covered all HindIII fragment ends in the 3.1Mb genomic region chr12:114312294-117466000, which encompasses the 2.8Mb Igh locus (chr12:114461473-117247870) and an additional 130kb downstream and 200kb upstream of the locus (**Figure 14**).

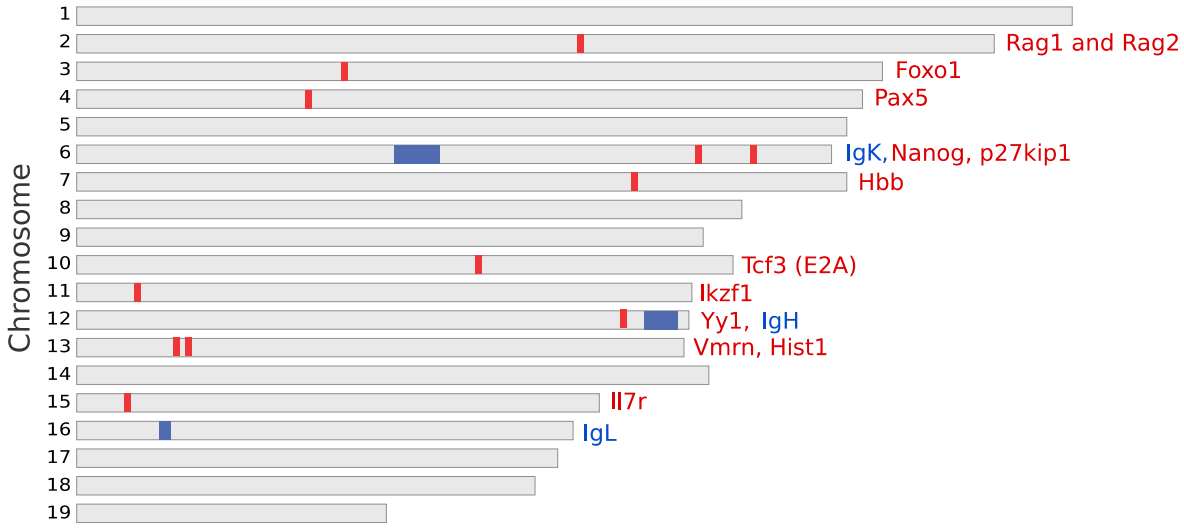

Figure 13. Regions enriched in Capture Hi-C. Shown are approximate positions of regions used to produce baits and loci of interest within them. Red rectangles show baits generated using one BAC; Blue rectangles show baits generated using multiple BACs. Drawing not to scale.

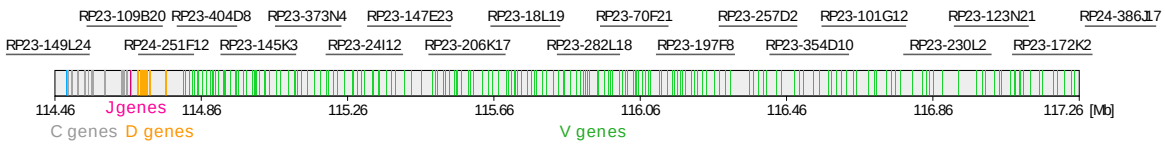

Figure 14. Positions of BACs covering the Igh locus. Baits for the Igh were generated using 20 overlapping BACs depicted above the locus schematic. The Igh locus schematic shows coloured vertical lines corresponding to C, J, D and V genes and coordinates along chr12.

3.2.2. Sequencing, mapping and quality control of Capture Hi-C libraries

Hi-C and Capture Hi-C libraries were sequenced on a Hiseq Illumina platform as 100bp paired-end reads and processed using HiCUP software (Wingett et al. 2015) as described in section 2.7 and outlined in **Figure 15**. Each Capture Hi-C library has been sequenced three times, multiplexing 4 libraries on a lane and processed independently by HiCUP. Hi-C libraries have been sequenced once, multiplexing 5 libraries on a lane, because they only served as a control to calculate fold enrichment over baited regions in Capture Hi-C and to compare read coverage distribution pre- and post-capture.

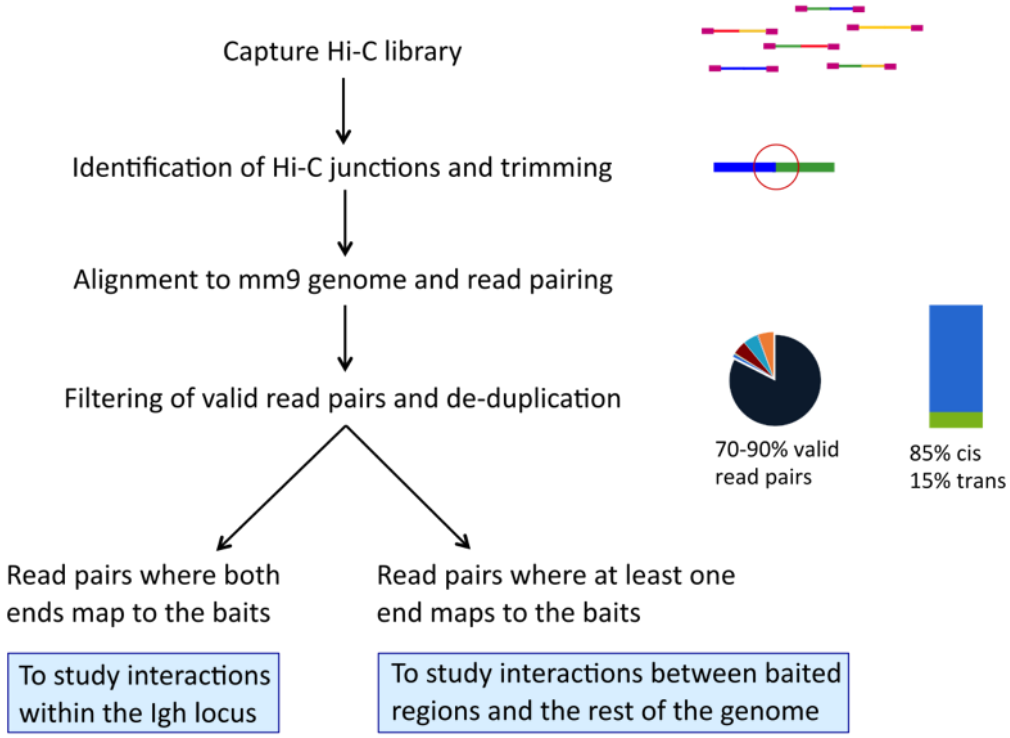

Figure 15. HiCUP workflow. See methods section 2.7 and chapter 3 section 3.2.2 for detailed description of HiCUP processing. Mock example HiCUP statistics are shown as a pie chart and a bar plot on the right. They represent good quality library statistics with 70-90% valid pairs and *cis:trans* ratio of 85:15%. The bifurcation of the workflow shows different outputs that can be obtained from HiCUP and used for analysis of *cis* or *trans* interactions.

Hi-C and Capture Hi-C paired-end reads are in the form of 'di-tags', which are characterised by a filled-in HindIII restriction junction in the middle and two reads on either side that come from regions that are not immediately adjacent in the linear genomic sequence. One end of every di-tag of interest maps to the baited region and the 'other end' might map either to a baited or a non-baited sequence. The forward and reverse reads were mapped separately and then re-paired. **Table 8** provides a summary of all sequencing runs and a breakdown of read pair numbers in each step of processing by HiCUP. First, for each read in *Total read pairs*, a HindIII restriction junction was identified and the read was trimmed if the

sequence extended beyond a second junction. Next, the forward and reverse reads were mapped uniquely to the mouse genome and re-paired, giving *Uniquely mapped pairs*. The percentage of *Uniquely mapped pairs* is higher in Hi-C datasets than in Capture Hi-C datasets, most likely because the Ig loci sequences are ones of the most poorly mappable regions of the genome due to their repetitive nature. To identify *Valid pairs* (*bona fide* genomic interaction products), di-tags were filtered to remove spurious read pairs representing experimental artefacts (re-ligation, incomplete digestion, multiple restriction fragments, single restriction fragments) (Belton et al. 2012). A high proportion of valid pairs indicates a good quality library. Valid pairs were de-duplicated to remove identical di-tags, which, in a sonicated library, are products of PCR over-amplification. A very high percentage of *De-duplicated pairs* shows that the libraries consisted predominantly of unique ligation events. Even after merging all 3 technical replicates (sequencing runs) the duplication level was extremely low (a very high *% unique reads after merging*) suggesting that the datasets were of high complexity and could potentially be sequenced to an even greater depth to obtain new unique read pairs.

HiCUP also reports the proportion of *cis* and *trans* di-tags (read pairs representing intra-chromosomal interactions - *cis*, and inter-chromosomal interactions - *trans*) as one of the quality measures (**Table 8** and **Figure 16**). My library generation protocol used an in-nucleus ligation strategy and so the cis:trans ratio was expected to be 85%:15% (Nagano et al. 2015), compared to 45%:55% for an in-solution ligation protocol (Lieberman-Aiden et al. 2009; van Berkum et al. 2010). Another existing enriched Hi-C protocol observed 20%-30% of trans interactions (Kolovos et al. 2016), whereas a single cell Hi-C protocol observed only 6.5% of trans contacts (Nagano et al. 2017).

Overall, the Capture Hi-C libraries generated here are of very good quality, achieving a high proportion of unique alignments, a high proportion of valid read pairs and high cis:trans ratios. To assess the biological replicates for each cell type, a principal component analysis (PCA) based on Hi-C read coverage was performed and showed that biological replicates are very similar (**Figure 17**), although a slight batch effect was observed for $Rag^{-/-}$ pro-B samples. To address this, all subsequent analyses have been performed separately on each biological replicate and an average per cell type was reported. The analysis of cis interactions showed all three biological replicates to be similar, whereas for trans interactions, only contacts significant in each of the three replicates were taken for further analysis.

Capture Hi-C has been extensively tested to demonstrate that it captures true meaningful genomic interactions (Schoenfelder et al. 2015a). Here, histone 1 cluster (Hist1) and vomeronasal cluster (Vmrn) baits served as controls (**Figure 18**). Other ends of all reads in the baited Hist1 viewpoint at chr13:23527157-23754469 were quantified in 20kb bins and an interaction enrichment can be observed over 1Mb upstream, around another Hist1 cluster that was not baited. This interaction skips over an additional bait for the vomeronasal gene cluster in the intervening region. This shows that a previously reported interaction between the Hist1 cluster on chromosome 13 and another Hist1 cluster upstream is readily detected in

my Capture Hi-C data (Schoenfelder et al. 2015a). Notably, this also shows that interactions between baited regions are not preferentially detected and Capture Hi-C picks up true biologically relevant genomic contacts.

Table 8. HiCUP read processing summary. See chapter 3 section 3.2.2 for detailed description of read processing by HiCUP. Capture Hi-C libraries have been sequenced three times and each sequencing run is indicated by a grey box on the left. Hi-C libraries have been sequenced once. *Total read pairs* show the total number of sequences obtained in a sequencing run per library. *Uniquely mapped pairs* show read pairs that passed unique mapping criteria and are also expressed as a percentage of *Total read pairs*. *Valid pairs* show bona fide read pairs after filtering out of experimental artefacts, and are also expressed as a percentage of *Uniquely mapped reads*. *De-duplicated pairs* show read pairs after removal of PCR duplicates, and are also expressed as a percentage of *Valid pairs*. *% cis* shows the proportion of read pairs with both ends mapping to the same chromosome. *% trans* shows the proportion of read pairs with ends mapping to locations on different chromosomes. The grey rectangle on the right (*Merged Capture Hi-C sequencing runs 1-3*) indicates a point where reads for each biological replicate from the three sequencing runs were merged. *% unique reads after merging* shows that there was very little duplication between the sequencing runs.

		Library	Total read pairs	Uniquely mapped pairs	% Uniquely mapped pairs	Valid pairs	% Valid pairs	De-duplicated pairs	% De-duplicated pairs	% cis	% trans		% unique reads after merging	Total valid pairs per biol rep
Capture Hi-C libraries	sequencing run 1	$Rag^{-/-Mom}$ pro-B biol rep 1	23,384,191	6,932,499	29.65%	5,787,496	83.48%	5,748,333	99.32%	87.3%	12.70%	Merged Capture Hi-C sequencing runs 1-3	99.39%	20,326,427
		Rag/81X pre-B biol rep 1	30,318,935	9,229,123	30.44%	8,492,299	92.02%	8,418,766	99.13%	84.1%	15.88%		98.95%	30,700,186
		Thymus biol rep 1	26,931,579	9,464,463	35.14%	8,312,233	87.83%	8,272,307	99.52%	83.4%	16.58%		99.79%	29,467,898
		$Rag^{-/-Bal}$ pro-B biol rep 3	35,434,809	12,097,626	34.14%	10,474,130	86.58%	10,375,135	99.05%	88.7%	11.30%		99.46%	39,562,609
		$Rag^{-/-Mom}$ pro-B biol rep 2	46,706,466	15,907,915	34.06%	13,232,089	83.18%	13,065,987	98.74%	86.2%	13.77%		99.04%	43,244,062
		Rag/81X pre-B biol rep 2	34,336,545	10,330,830	30.09%	9,456,266	91.53%	9,336,425	98.73%	80.4%	19.64%		98.75%	33,648,952
		Thymus biol rep 2	27,860,318	9,052,281	32.49%	7,973,540	88.08%	7,899,257	99.07%	82.9%	17.08%		99.52%	30,398,961
	sequencing run 2	$Rag^{-/-Mom}$ pro-B biol rep 1	32,322,617	9,779,220	30.26%	8,165,396	83.50%	8,056,535	98.67%	87.3%	12.72%			
		Rag/81X pre-B biol rep 1	43,945,460	13,651,842	31.07%	12,569,912	92.07%	12,366,068	98.38%	84.2%	15.82%			
		Thymus biol rep 1	37,653,545	13,477,035	35.79%	11,840,222	87.85%	11,718,688	98.97%	83.4%	16.56%			
		$Rag^{-/-Bal}$ pro-B biol rep 3	49,862,398	16,633,585	33.36%	14,414,224	86.66%	14,220,806	98.66%	88.7%	11.30%			
		$Rag^{-/-Mom}$ pro-B biol rep 2	53,893,089	17,966,784	33.34%	14,960,856	83.27%	14,728,421	98.45%	86.2%	13.76%			
		Rag/81X pre-B biol rep 2	45,343,441	13,323,734	29.38%	12,203,398	91.59%	11,999,258	98.33%	80.4%	19.63%			
		Thymus biol rep 2	40,388,315	12,848,704	31.81%	11,325,103	88.14%	11,179,412	98.71%	83.0%	17.05%			
	sequencing run 3	$Rag^{-/-Mom}$ pro-B biol rep 1	25,635,537	7,928,908	30.93%	6,607,646	83.34%	6,521,559	98.70%	87.3%	12.72%			
		Rag/81X pre-B biol rep 1	34,506,111	10,940,551	31.71%	10,068,924	92.03%	9,915,352	98.47%	84.2%	15.82%			
		Thymus biol rep 1	29,891,118	10,910,167	36.50%	9,577,421	87.78%	9,476,903	98.95%	84.2%	15.82%			
		$Rag^{-/-Bal}$ pro-B biol rep 3	51,717,151	17,527,977	33.89%	15,180,729	86.61%	14,966,668	98.59%	84.2%	15.82%			
		$Rag^{-/-Mom}$ pro-B biol rep 2	55,815,651	18,877,127	33.82%	15,708,227	83.21%	15,449,654	98.35%	84.2%	15.82%			
		Rag/81X pre-B biol rep 2	45,843,293	13,677,607	29.84%	12,529,601	91.61%	12,313,269	98.27%	84.2%	15.82%			
		Thymus biol rep 2	40,339,393	13,021,951	32.28%	11,470,555	88.09%	11,320,292	98.69%	84.2%	15.82%			
Hi-C libraries	sequencing run 1	$Rag^{-/-Mom}$ pro-B biol rep 1	25,673,508	15,291,166	59.56%	10,647,110	69.63%	10,587,165	99.44%	87.7%	12.26%			
		Rag/81X pre-B biol rep 1	22,097,881	13,007,892	58.86%	11,422,741	87.81%	11,361,486	99.46%	84.7%	15.28%			
		Thymus biol rep 1	25,073,034	15,244,010	60.80%	12,092,872	79.33%	12,031,870	99.50%	83.5%	16.54%			
		$Rag^{-/-Bal}$ pro-B biol rep 3	33,883,698	20,549,191	60.65%	15,794,844	76.86%	15,700,339	99.40%	88.7%	11.35%			
		$Rag^{-/-Mom}$ pro-B biol rep 2	32,640,130	19,668,705	60.26%	13,708,894	69.70%	13,617,672	99.33%	86.6%	13.43%			
		Rag/81X pre-B biol rep 2	23,966,161	14,200,583	59.25%	12,336,595	86.87%	12,259,413	99.37%	81.0%	19.01%			
		Thymus biol rep 2	33,984,315	19,887,551	58.52%	15,859,336	79.75%	15,761,235	99.38%	83.1%	16.95%			

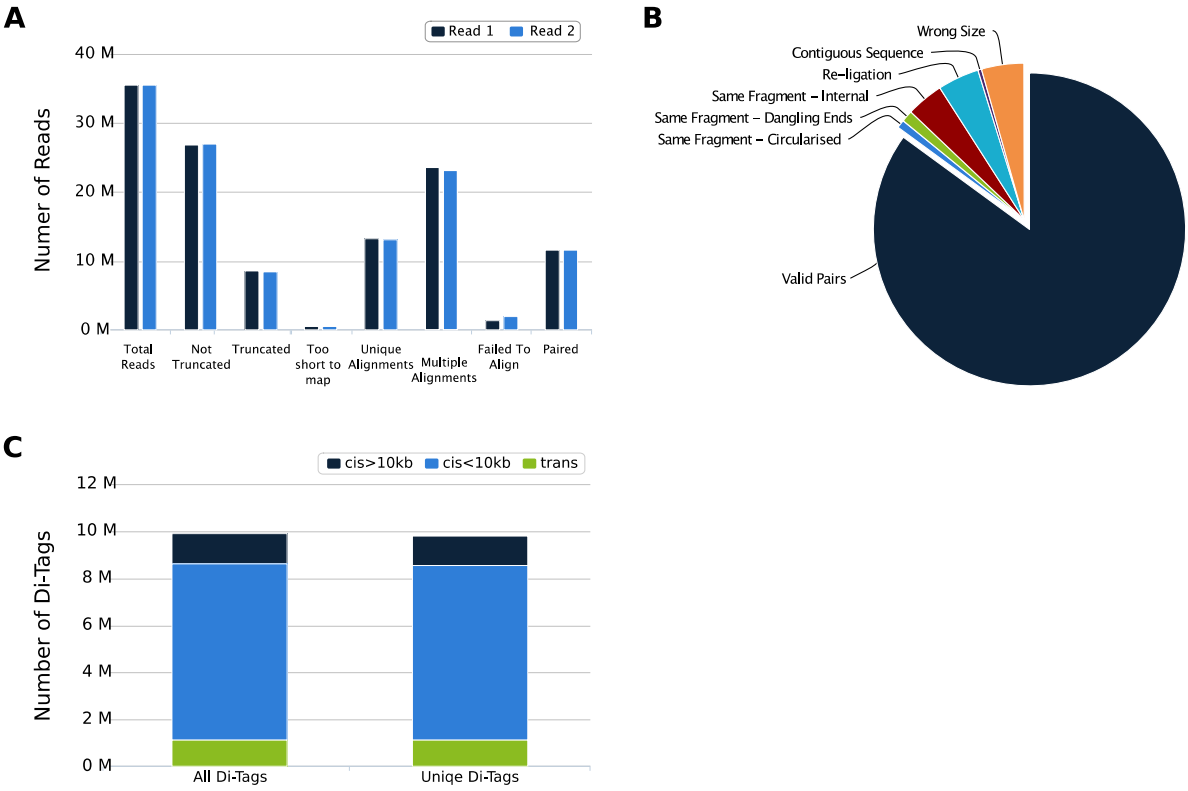

Figure 16. HiCUP metrics. Metrics for Rag1$^{-/-Bal}$ pro-B replicate 3 library from sequencing run 1 are shown. See chapter 3 section 3.2.2 for detailed description of read processing by HiCUP. **A.** Step by step representation of reads passing every stage of analysis. **B.** Break-down of types of invalid read pairs. **C.** *Cis:trans* ratio.

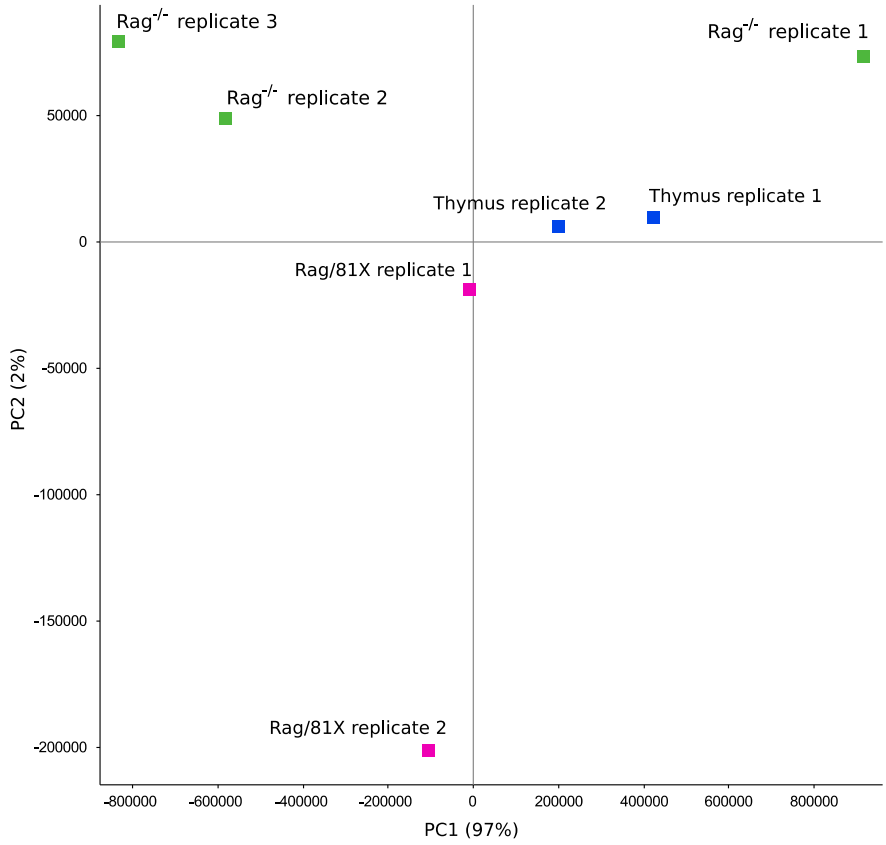

Figure 17. Principal component analysis (PCA) shows clustering of Capture Hi-C biological replicates. PCA analysis was performed in Seqmonk based of Hi-C read coverage. Rag$^{-/-}$ replicates cluster well by PC2, Rag/81X replicates cluster well by PC1 and Thymus replicates cluster well by PC1 and PC2. Any deviation might be caused by cell collection by different people and library preparation on different days.

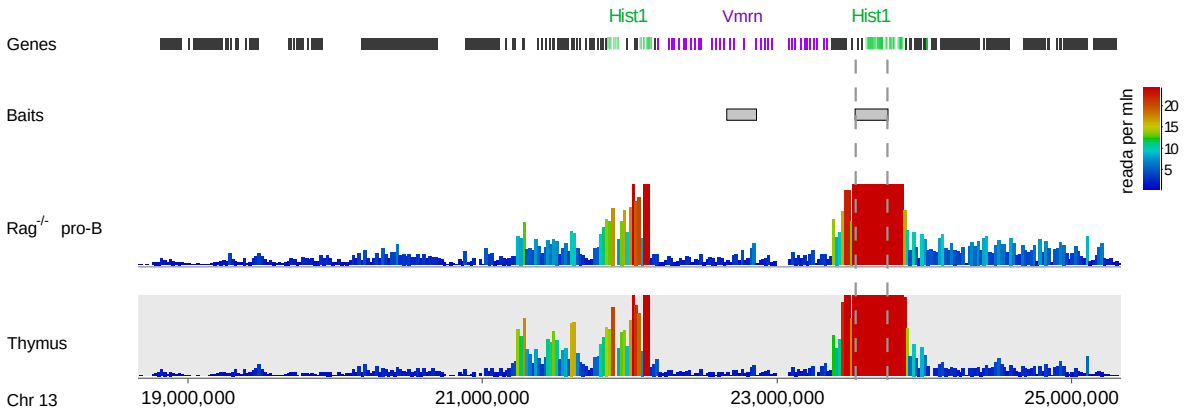

Figure 18. Control interaction between Hist1 clusters on chromosome 13 was readily detected by Capture Hi-C. The histone 1 genes (Hist1) and the vomeronasal genes (Vmrn) are marked in green and purple, respectively. The regions enriched in Capture Hi-C are indicated by grey horizontal rectangles corresponding to the BACs used for bait generation. A virtual 4C from the Hist1 baited region (viewpoint indicated by vertical dashed lines) was performed in Seqmonk. All other ends of reads mapping to the viewpoint were quantified in 20kb bins genome-wide for Rag$^{-/-}$ pro-B and thymus libraries. Reads were quantified as an average of biological replicates and adjusted per million reads. The number of reads in 20kb bins is represented by the height and the colour of the bars along chr13. There is a peak over the left Hist1 cluster indicating that this region interacts with the viewpoint. There is no peak over the vomeronasal cluster.

3.2.3. Capture Hi-C gives 45-fold enrichment over Hi-C

The purpose of enrichment of a Hi-C library is to achieve greater sequencing depth within a region of interest and to circumvent the burden of sequencing the extremely complex Hi-C library, as well as reduce the computational power required for analysis. I confirmed that the baited regions have been successfully and uniformly enriched, with the exception of Ikzf1 bait which failed (**Figure 19**). Capture efficiency was on average 12.5% (**Table 9**) as determined by the proportion of di-tags in the final Capture Hi-C library with at least one end mapping to the baited regions. This largely depends on the fraction of HindIII fragments being baited as well as on the efficiency of bait hybridisation, blocking oligos, streptavidin pull-down and purification steps. There are 844,500 HindIII fragments in the mouse genome and my baits cover 2868 HindIII fragments, which means that 0.34% of HindIII fragments in the genome was covered by 12.5% of the di-tags in the dataset. Hi-C libraries are by nature extremely complex and for the mouse genome the possible number of Hi-C ligation events between HindIII fragments is over 300 billion in each cell, whereas average Hi-C datasets have 100-200 million di-tags. Capture Hi-C libraries capture a much higher percentage of possible ligation events, as they had 4 million di-tags covering the 2868 baited HindIII fragments, which could make 4 million ligation events.

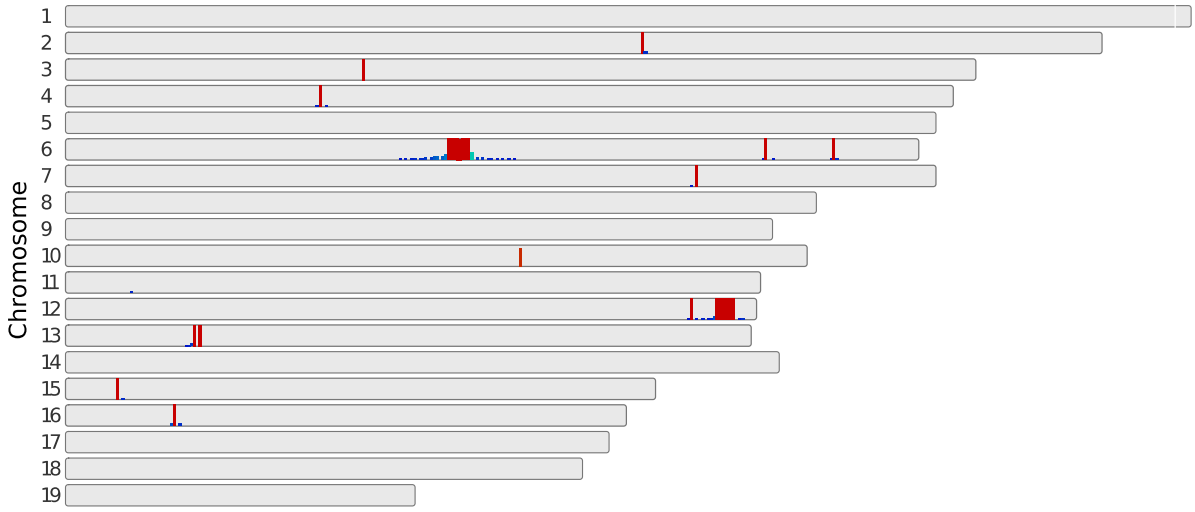

Figure 19. Baited regions showed high read enrichment. Data for $Rag^{-/-Mom}$ pro-B replicate 1 is shown. All reads in the post-HiCUP Capture Hi-C library were quantified in 500kb bins across the genome. Red bars indicate massive read enrichment over the baited regions compared to the rest of the genome. All baits were highly enriched apart from the Ikaros bait (Ikzf1) on chr11, which did not give any enrichment.

Table 9. Table 9. Bait capture efficiency in Capture Hi-C libraries.

Capture Hi-C library	Total valid pairs	Total valid pairs over baited regions	Capture efficiency
Rag$^{-/-Mom}$ pro-B biol rep 1	20,326,427	2,500,125	12.3%
Rag/81X pre-B biol rep 1	30,700,186	3,908,430	12.7%
Thymus biol rep 1	29,467,898	3,503,939	11.9%
Rag$^{-/-Bal}$ pro-B biol rep 3	39,562,609	4,436,374	11.2%
Rag$^{-/-Mom}$ pro-B biol rep 2	43,244,062	5,040,101	11.7%
Rag/81X pre-B biol rep 2	33,648,952	4,655,520	13.8%
Thymus biol rep 2	30,398,961	3,920,256	12.9%

Here, Capture Hi-C has achieved 45-fold enrichment of read coverage over Hi-C (**Table 10** and **Figure 20**). The enrichment level was calculated by dividing the number of reads per million covering baited regions in Capture Hi-C by the number of reads per million covering baited regions in Hi-C before capture. I anticipated that enriching for the Igh locus would be particularly useful, because it is one of the most lowly mappable regions in the genome. Also, on average there are 320 HindIII fragments per 1Mb in the mouse genome, whereas in the Igh baited region there are 286 HindIII fragments per 1Mb, making it slightly disadvantaged in terms of visibility when probing for interactions. Indeed, **Figure 21** illustrates that the Igh locus has lower overall read coverage than the neighbouring regions. The mappability track shows that in the distal parts of the Igh locus there are regions with significant dips in mappability of 100bp reads. An enrichment of 45-fold makes it the highest covered Hi-C dataset over the whole of the Igh locus in pro-B lymphocytes ever generated.

Table 10. Capture Hi-C fold enrichment over Hi-C.

Capture Hi-C library	Reads pairs per milion over baited regions in Hi-C	Reads pairs per milion over baited regions in Capture Hi-C	Fold enrichment
Rag$^{-/-Mom}$ pro-B biol rep 1	3,373	170,854	51x
Rag/81X pre-B biol rep 1	3,653	177,423	49x
Thymus biol rep 1	3,894	154,841	40x
Rag$^{-/-Bal}$ pro-B biol rep 3	3,598	160,577	45x
Rag$^{-/-Mom}$ pro-B biol rep 2	3,588	159,074	44x
Rag/81X pre-B biol rep 2	3,748	177,808	47x
Thymus biol rep 2	3,872	164,823	43x

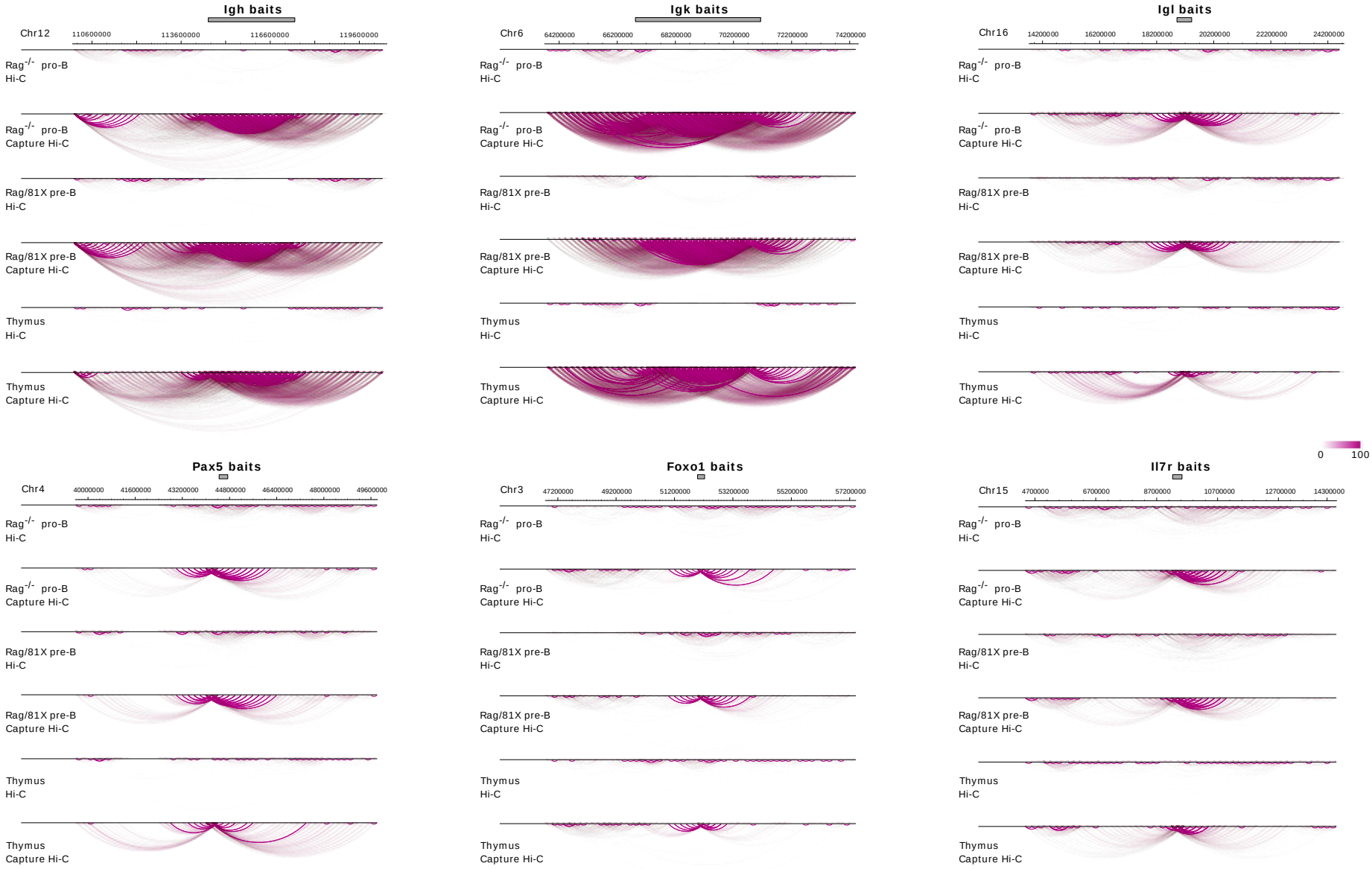
Igh baits
Chr12
110600000
113600000
116600000
119600000
Rag-/- pro-B Hi-C
Rag-/- pro-B Capture Hi-C
Rag/81X pre-B Hi-C
Rag/81X pre-B Capture Hi-C
Thymus Hi-C
Thymus Capture Hi-C
Igk baits
Chr6
64200000
66200000
68200000
70200000
72200000
74200000
Rag-/- pro-B Hi-C
Rag-/- pro-B Capture Hi-C
Rag/81X pre-B Hi-C
Rag/81X pre-B Capture Hi-C
Thymus Hi-C
Thymus Capture Hi-C
Igl baits
Chr16
14200000
16200000
18200000
20200000
22200000
24200000
Rag-/- pro-B Hi-C
Rag-/- pro-B Capture Hi-C
Rag/81X pre-B Hi-C
Rag/81X pre-B Capture Hi-C
Thymus Hi-C
Thymus Capture Hi-C
0
100
Pax5 baits
Chr4
40000000
41600000
43200000
44800000
46400000
48000000
49600000
Rag-/- pro-B Hi-C
Rag-/- pro-B Capture Hi-C
Rag/81X pre-B Hi-C
Rag/81X pre-B Capture Hi-C
Thymus Hi-C
Thymus Capture Hi-C
Foxo1 baits
Chr3
47200000
49200000
51200000
53200000
55200000
57200000
Rag-/- pro-B Hi-C
Rag-/- pro-B Capture Hi-C
Rag/81X pre-B Hi-C
Rag/81X pre-B Capture Hi-C
Thymus Hi-C
Thymus Capture Hi-C
Il7r baits
Chr15
4700000
6700000
8700000
10700000
12700000
14300000
Rag-/- pro-B Hi-C
Rag-/- pro-B Capture Hi-C
Rag/81X pre-B Hi-C
Rag/81X pre-B Capture Hi-C
Thymus Hi-C
Thymus Capture Hi-C

Figure 20. Capture Hi-C gives 45-fold enrichment over Hi-C. Interactions were quantified between 200kb bins genome-wide, using randomly selected 5 million read pairs from each dataset to adjust to the same number of overall read counts. All interactions in 10Mb regions around the baited sequences are plotted. Horizontal grey rectangles above the genomic positions indicate the baited regions. Data shown is from $Rag^{-/-Mom}$ pro-B replicate 2, Rag/81X pre-B replicate 2 and Thymus replicate 2. The colour scale from 0 to 100 indicates that all interaction counts between two given bins higher than 100 are depicted in the darkest purple. The arc plots were visualised using the WashU EpiGenome Browser (Zhou 2013).

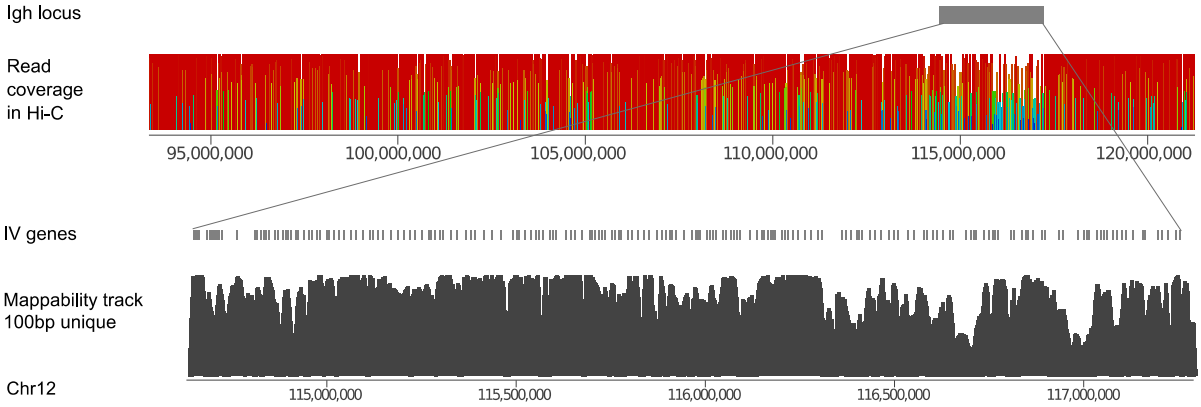

Figure 21. The Igh locus has lower read coverage in Hi-C than the rest of the genome. The top panel shows read coverage in Hi-C library for $Rag^{-/-Mom}$ pro-B replicate 1 over the telomeric 25Mb of chromosome 12. Reads were quantified in 100kb bins. The colour and height of the bars indicates read count magnitude (red-high, blue-low). Igh has lower read coverage than the surrounding sequences on chr12. The bottom panel zooms in on the Igh locus and shows an *in silico* mappability track of 100bp fragments generated every 1bp along the V region and mapped uniquely to mm9. The fragments were quantified in 100kb bins with 10kb step. The height of the bars indicates the magnitude of fragment count. Grey vertical lines above the mappability track indicate positions of the V genes.

3.2.4. Capture Hi-C bait pull-down preserves the Hi-C read coverage pattern over Igh

I confirmed that the bait pull down step did not introduce any biases and that the baits generated from 20 different BACs covering the Igh locus have enriched the Hi-C material with equal efficiency (**Figure 22**). I compared the read coverage patterns along the Igh locus between the Hi-C and Capture Hi-C libraries in all three cell types and they showed a very similar pattern. This demonstrates that there was little spurious cross-hybridisation or inefficient baits. To further investigate this in a quantitative manner, the read coverage over the Igh locus in Hi-C was compared to the read coverage in Capture Hi-C and it showed that they were highly positively correlated (**Figure 23**).

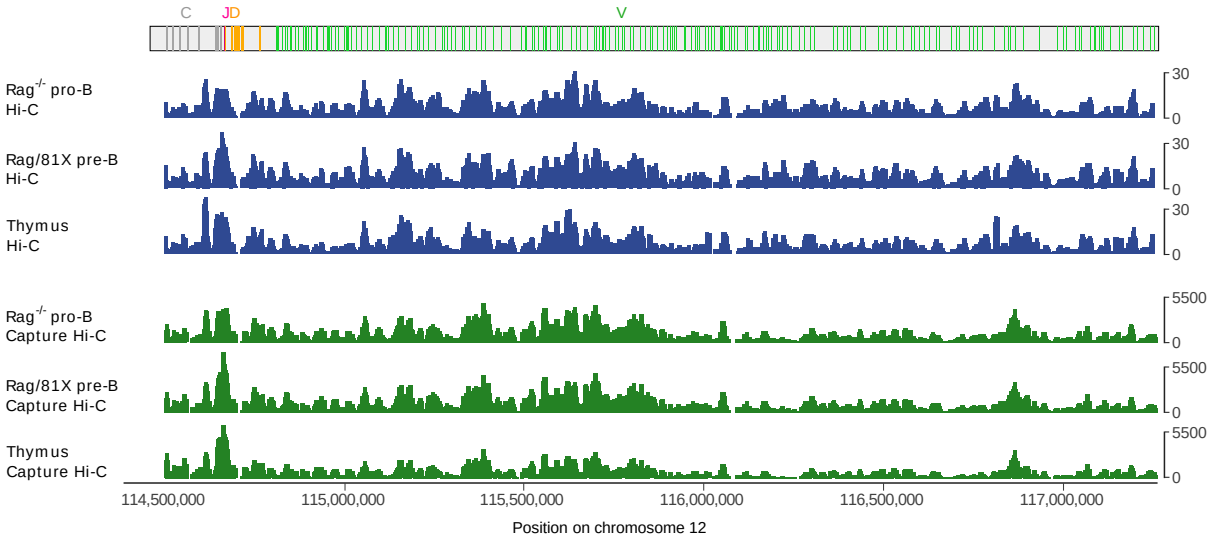

Figure 22. Read coverage pattern in Hi-C is preserved in Capture Hi-C libraries. Reads from biological replicates were averaged, quantified in 10kb sliding windows with 1kb step and adjusted per million reads in the library. The top panel shows the read coverage of the Igh locus in Hi-C libraries and the bottom panel in Capture Hi-C libraries. Grey vertical lines above the data tracks indicate positions of C, J, D, V genes and regulatory elements

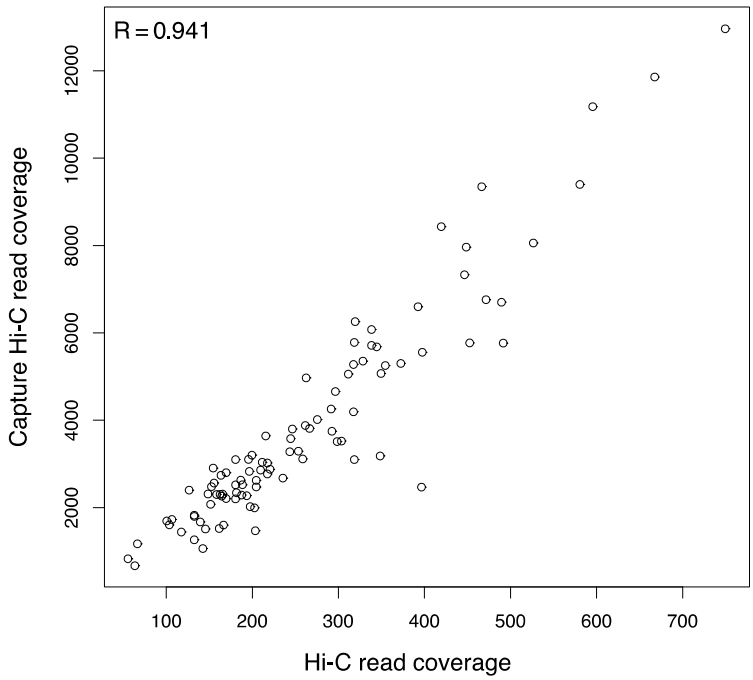

Figure 23. Read coverage patterns in Hi-C and Capture Hi-C are highly correlated. Reads were quantified in 30kb bins over the Igh locus (chr12:114,330,000-117,450,000). For Capture Hi-C, a custom genome dataset was used. Representative data is shown for Rag1-/-Bal pro-B replicate 3 from sequencing run 1. R - Pearson's correlation coefficient.

3.3. A normalised contact frequency map of the Igh locus

3.3.1. Igh locus has more intra-locus interactions when poised for recombination

The 2.8Mb long Igh locus resides in its own TAD of around 3Mb (Benner et al. 2015; Medvedovic et al. 2013; Lin et al. 2012; Zhang et al. 2012). At the pro-B cell stage, when V-DJ recombination is occurring, the locus undergoes a large-scale spatial contraction resulting in the 5' end becoming positioned much closer to the 3' end than in earlier developmental stages or in non-B cells (Fuxa et al. 2004; Rother et al. 2016). I observed that the Igh interacts much more internally than with its neighbouring sequence on chromosome 12 in $Rag^{-/-}$ pro-B cells compared to thymocytes (**Figure 24**). This analysis takes advantage of Capture Hi-C picking up interactions not only within the baited regions but also between the baited regions and the rest of the genome. The Igh makes more contacts with the surrounding sequence in the thymus than in pro-B cells. In pro-B cells, the Igh has more intra-locus interactions and the 3' and 5' boundaries of the Igh TAD are sharper. The regions immediately adjacent to the Igh have higher interaction counts than in the thymus, which is consistent with 4C-like profiles of interactions from a particular viewpoint. Also, these interactions drop more dramatically with distance in pro-B cells compared to thymus, suggesting fewer outside-locus interactions.

To investigate the interactions within the Igh locus in detail and at higher resolution, read count normalisation is required to account for read coverage biases.

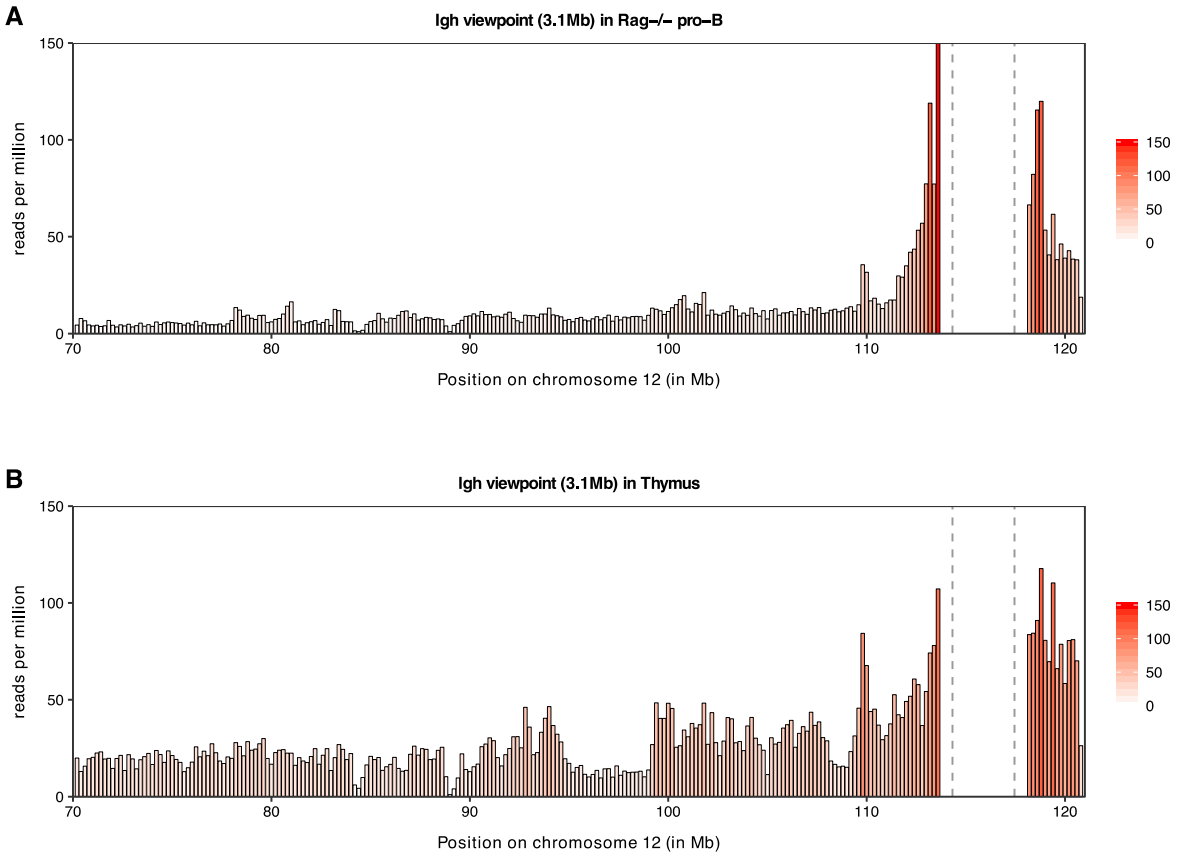

Figure 24. Igh locus makes more intra-locus contacts and interacts less with its surrounding sequences on chr12 in pro-B cells compared to the thymus. Interactions from the Igh viewpoint to its neighbouring sequences at the telomeric end of chr12 in Rag$^{-/-}$ pro-B cells (A) and in the thymus (B). Virtual 4C was performed in Seqmonk. Reads with at least one end mapping to the 3.1Mb Igh viewpoint were extracted, quantified in 200kb bins as an average of biological replicates and adjusted per million reads in the library. The colour and the height of the bars indicate the magnitude of read counts. The Igh viewpoint is indicated by grey dashed lines. 3 bins on each side of the viewpoint were omitted for clarity. The peak at 110Mb is the Yy1 baited region.

3.3.2. Correcting for biases

Hi-C experiments, like most next-generation sequencing methods, are subject to systematic biases that may influence the detection of true interaction frequencies between two restriction fragments (Lieberman-Aiden et al. 2009; Yaffe and Tanay 2011; Imakaev et al. 2012). These biases include chromatin accessibility, mappability/sequencing coverage, restriction fragment length and density and GC content, and are collectively referred to as visibility biases. Many approaches have been developed to alleviate the problem of uneven overall read coverage in Hi-C datasets (reviewed in Schmitt et al. 2016).

Capture Hi-C is a novel method and analysis pipelines only now start to account for enriched Hi-C data types. There are analysis algorithms specific for Promoter Capture Hi-C data such as CHiCAGO (Cairns et al. 2016) and GOTHiC (Mifsud et al. 2017), but they have been developed to analyse 4C-like interaction profiles from a single baited viewpoint/restriction fragment. These programs are able to analyse thousands of baits in one experiment (Schoenfelder et al. 2015a; Dryden et al. 2014), provided that the baits are

designed to cover single small viewpoints as the programs create an interaction profile over adjacent non-baited other ends. They therefore do not support the analysis of large regions baited in a lawn-like fashion where every restriction fragment has been baited and serves as a viewpoint. There are very few studies that have enriched the Hi-C material for large multi-megabase regions using consecutive baits (Jager et al. 2015; Franke et al. 2016; Kolovos et al. 2016) and at the time of my experiments none were published. This type of experimental design creates a 'mini Hi-C' for the region of interest and should in theory be analysed like a Hi-C dataset, applying bias normalisation. The results are presented in a form of a symmetric interaction frequency matrix (all-vs-all) with the region of interest on the diagonal and interaction frequencies between them off the diagonal. The first enriched Hi-C study for a large region (Franke et al. 2016) applied a matrix balancing method based on the Sinkhorn and Knopp algorithm optimised for large datasets at very high resolution, implemented in the recent Juicer software (Rao et al. 2014b). The second study (Kolovos et al. 2016) and the original Hi-C study (Lieberman-Aiden et al. 2009) applied a very simple coverage normalisation by dividing the number of reads for each interaction by the sum of total reads mapped to both ends involved in the interaction, which is a single step of the Sinkhorn and Knopp matrix balancing. A multi-step, iterative Sinkhorn and Knopp matrix balancing method known as ICE (Imakaev et al. 2012) has become the most widely used approach for Hi-C data analysis (Schmitt et al. 2016) and I decided to use the HOMER package (Heinz et al. 2010), which utilises this strategy and is an extensively used multifunctional software for Hi-C analysis (Lin et al. 2010; 2012; Qian et al. 2014; Kaikkonen et al. 2014; Benner et al. 2015; Nagano et al. 2015; Robin et al. 2015; Cairns et al. 2016; Karathia et al. 2016; Orlanski et al. 2016; Freire-Pritchett et al. 2017).

Assuming that the entire interaction space is probed in an unbiased manner, each restriction fragment (or bin) should be observed the same number of times in the experiment. This means that the total number of reads covering each fragment (or bin), i.e. the sum of reads in each row and column in a symmetric matrix, should be equal. The probability of detecting an interaction between bins A and B in a given raw Hi-C dataset (observed) is:

$$p(observed) = \frac{Reads\ between\ A\ and\ B}{Total\ reads\ in\ dataset}$$

whereas the probability of detecting an interaction between bins A and B in an ideal unbiased Hi-C dataset (expected), where all bins have equal visibility, is the product of visibilities of A and B:

$$p(expected) = \frac{Total\ reads\ in\ A}{Total\ reads\ in\ dataset} \times \frac{Total\ reads\ in\ B}{Total\ reads\ in\ dataset}$$

therefore, we are looking for:

$$\frac{observed}{expected} = \frac{Reads\ between\ A\ and\ B}{(\frac{Total\ reads\ in\ A}{Total\ reads\ in\ dataset}) \times (\frac{Total\ reads\ in\ B}{Total\ reads\ in\ dataset}) \times Total\ reads\ in\ dataset}$$

HOMER software creates a background model in which it produces expected interaction frequencies between genomic bins of chosen length based on the assumption that all bins

should have equal visibility. This model produces a set of correction factors for each matrix that allows for subsequent plotting of a normalised interaction frequency matrix with elements displayed as observed/expected interaction frequencies. To this end, HOMER employs the ICE iterative correction of matrix balancing method (Imakaev et al. 2012). In an ideal scenario there would be no visibility biases and so the observed raw contact counts captured by Hi-C would be the true contact counts. However, due to the aforementioned biases in reality: $(\text{observed contact})_{AB} = (\text{true contact})_{AB} \times \text{bias}_A \times \text{bias}_B$. The iterative matrix balancing method calculates the biases until they become equal to 1, which means the sum of reads in each row and column of the interaction matrix will be equal (a doubly stochastic matrix). To achieve this, it identifies the first bias by dividing the sum of all reads in each row and column by the average of all reads in each row and column (coverage/avg) and then multiplies each value in the observed interaction matrix by the two respective biases (one for row and one for column). The correction carries on iteratively until convergence is achieved.

BACs used to generate the baits covering the Igh locus start at genomic location 114,312,294Mb on chromosome 12. For the purpose of Capture Hi-C bins being comparable to Hi-C bins, all analysis was done starting from position 114,330,000Mb. The region chr12:114,330,000-117,450,000 was binned into 20kb non-overlapping bins and used to generate HOMER matrices. The J, D and V genes as well as the regulatory elements in the Igh locus falling into each 20kb bin are listed in **Table 11**.

Table 11. Igh genes and regulatory elements in 20kb bins. Beads 0-139 used in polymer modelling (section 3.4) are in column one. The start and end of the 20kb bins in the entire baited region used for the generation of interaction frequency matrices are in columns two and three as positions on chromosome 12 in bp. The Igh elements present within the coordinates of each 20kb bin are listed in column four.

bead number	bin start	bin end	Igh elements
	114330000	114349999	
	114350000	114369999	
	114370000	114389999	
	114390000	114409999	
	114410000	114429999	
	114430000	114449999	
0	114450000	114469999	HS8, HS7 HS6 HS5 HS4 HS3b
1	114470000	114489999	HS3b HS1,2
2	114490000	114509999	HS3a Ca Ce
3	114510000	114529999	Ce Cg2a
4	114530000	114549999	Cg2b
5	114550000	114569999	hRE2 hRE1 Cg1
6	114570000	114589999	
7	114590000	114609999	Cg3
8	114610000	114629999	
9	114630000	114649999	Cd
10	114650000	114669999	Cd Cm Emu_core J4 J3 J2 J1 DQ52
11	114670000	114689999	cRSS_1 3'_DST4 DST4 P6_D DSP2.5
12	114690000	114709999	DSP2.5 P5_D DSP2.3_inv DSP2.3 cRSS_2 D1ps3'/P4_D DSP2.x_3'_inv DSP2.x_3' cRSS_3 P3_D DSP2.x_5'_inv DSP2.x_5' cRSS_4 cRSS_5/P2_D DSP2.2_inv DSP2.2
13	114710000	114729999	DSP2.2 cRSS_6 Dpsi2 D1ps5' DSP2.9 cRSS_7 Dpsi1 D6.1 cRSS_8 DFL16.1 cRSS_9 cRSS_10 IGCR_CBE2 cRSS_11 IGCR_CBE1
14	114730000	114749999	
15	114750000	114769999	DST4.2 cRSS_12 P1_D DFL16.2
16	114770000	114789999	
17	114790000	114809999	
18	114810000	114829999	7183.1pg.1 Q52.1pg.2 7183.2.3_(81X) Q52.2.4 7183.3pg.5
19	114830000	114849999	7183.4.6 7183.5pg.7 Q52.3.8
20	114850000	114869999	Q52.3.8 7183.6pg.9 7183.7.10
21	114870000	114889999	PG.1.11 Q52.4pg.12
22	114890000	114909999	Q52.5.13 7183.8pg.14 7183.9.15 7183.10pg.16
23	114910000	114929999	Q52.6pg.17 Q52.7.18 7183.11pg.19
24	114930000	114949999	7183.12.20
25	114950000	114969999	PG.2.21 Q52.8.22 PG.3.23 7183.13pg.24
26	114970000	114989999	7183.14.25 7183.15pg.26
27	114990000	115009999	7183.16.27 PG.4.28 Q52.9.29
28	115010000	115029999	PG.5.30 7183.17pg.31
29	115030000	115049999	PG.6.32 Q52.10.33 Q52.11.34
30	115050000	115069999	7183.18.35
31	115070000	115089999	7183.19.36
32	115090000	115109999	7183.20.37
33	115110000	115129999	7183.21pg.38 Q52.12pg.39 Q52.13.40 PG.7.41
34	115130000	115149999	S107.1.42
35	115150000	115169999	S107.2pg.43
36	115170000	115189999	SM7.1.44 X24.1.45
37	115190000	115209999	36-60.1.46 PG.8.47
38	115210000	115229999	VH11.1.48
39	115230000	115249999	SM7.2.49
40	115250000	115269999	X24.2pg.50
41	115270000	115289999	36-60.2pg.51 PG.9.52 VH11.2.53
42	115290000	115309999	SM7.3.54 VH16.1.55
43	115310000	115329999	PG.10.56
44	115330000	115349999	VGAM3.8-1-57 PG.11.58 VGAM3.8-2-59
45	115350000	115369999	PG.12.60
46	115370000	115389999	VGAM3.8-3-61
47	115390000	115409999	S107.3.62
48	115410000	115429999	SM7.4.63
49	115430000	115449999	36-60.3.64
50	115450000	115469999	S107.4.65
51	115470000	115489999	
52	115490000	115509999	36-60.4.66 36-60.5.67 3609N.1pg.68
53	115510000	115529999	PG.13.69 36-60.6.70
54	115530000	115549999	VGAM3.8-4-71
55	115550000	115569999	36-60.7pg.72 PG.14.73 36-60.8.74
56	115570000	115589999	PG.15.75 PG.16.76
57	115590000	115609999	PG.16.76 3609N.2.77 VH12.1.78
58	115610000	115629999	J606.1.79
59	115630000	115649999	J606.1.79 J606.2.80
60	115650000	115669999	J606.3.81
61	115670000	115689999	J606.4.82
62	115690000	115709999	J606.5.83 3609.1.84 J558.1.85
63	115710000	115729999	VH10.1.86 PG.17.87 J558.2.88
64	115730000	115749999	VH10.2pg.89
65	115750000	115769999	J558.3.90 VH10.3.91
66	115770000	115789999	PG.18.92 J558.4.93
67	115790000	115809999	J558.5pg.94 VH15.1.95
68	115810000	115829999	J558.6.96
69	115830000	115849999	J558.7pg.97
70	115850000	115869999	J558.8.98 J558.9.99 J558.10pg.100
71	115870000	115889999	J558.11pg.101
72	115890000	115909999	J558.12.102 J558.13.103
73	115910000	115929999	J558.14pg.104 J558.15pg.105 J558.16.106
74	115930000	115949999	J558.17pg.107 J558.18.108
75	115950000	115969999	J558.19.109
76	115970000	115989999	J558.20pg.110 J558.21pg.111 J558.22.112
77	115990000	116009999	J558.23.113
78	116010000	116029999	J558.24pg.114 J558.25pg.115 J558.26.116
79	116030000	116049999	J558.27pg.117 J558.28pg.118
80	116050000	116069999	J558.29pg.119 J558.30pg.120 J558.31.121
81	116070000	116089999	J558.32pg.122 J558.33pg.123 J558.34.124
82	116090000	116109999	J558.34.124
83	116110000	116129999	J558.35pg.125 J558.36.126
84	116130000	116149999	J558.37.127 J558.38pg.128
85	116150000	116169999	J558.39.129 J558.40pg.130
86	116170000	116189999	J558.41pg.131 J558.42.132 J558.43.133
87	116190000	116209999	J558.44pg.134 J558.45pg.135
88	116210000	116229999	J558.46pg.136 J558.47.137
89	116230000	116249999	J558.47.137 3609.2pg.138
90	116250000	116269999	3609.3.139
91	116270000	116289999	J558.48pg.140
92	116290000	116309999	J558.49.141 3609.4.142 PAIR1
93	116310000	116329999	PAIR1
94	116330000	116349999	
95	116350000	116369999	J558.50.143 J558.51pg.144
96	116370000	116389999	J558.51pg.144 J558.52.145
97	116390000	116409999	J558.53.146 3609.5.147 PAIR2
98	116410000	116429999	PAIR2
99	116430000	116449999	J558.54.148 J558.55.149
100	116450000	116469999	PAIR3
101	116470000	116489999	J558.56.150
102	116490000	116509999	3609.6pg.151 PAIR4 J558.57pg.152
103	116510000	116529999	
104	116530000	116549999	3609.7.153 PAIR5
105	116550000	116569999	J558.58.154
106	116570000	116589999	J558.59.155 J558.60pg.156
107	116590000	116609999	J558.61.157
108	116610000	116629999	J558.62pg.158 J558.63pg.159
109	116630000	116649999	3609.8pg.160 PAIR6
110	116650000	116669999	PG.19.161
111	116670000	116689999	J558.64.162
112	116690000	116709999	J558.65.163 3609.9.164
113	116710000	116729999	PAIR7
114	116730000	116749999	J558.66.165 J558.67.166
115	116750000	116769999	3609.10pg.167 PAIR8
116	116770000	116789999	J558.68pg.168
117	116790000	116809999	3609.11.169
118	116810000	116829999	PAIR9
119	116830000	116849999	J558.69.170 J558.70pg.171 J558.71pg.172
120	116850000	116869999	J558.71pg.172 J558.72.173
121	116870000	116889999	3609.12.174
122	116890000	116909999	PAIR10
123	116910000	116929999	
124	116930000	116949999	J558.73pg.175 PAIR11
125	116950000	116969999	
126	116970000	116989999	J558.74.176
127	116990000	117009999	J558.75.177 3609.13pg.178 PAIR12
128	117010000	117029999	J558.76pg.179
129	117030000	117049999	J558.77.180 3609.14pg.181
130	117050000	117069999	PAIR13 PAIR14
131	117070000	117089999	J558.78.182 3609.15pg.183 J558.79.184
132	117090000	117109999	3609.16pg.185 J558.80.186 J558.81.187
133	117110000	117129999	J558.82pg.188
134	117130000	117149999	
135	117150000	117169999	J558.83.189 J558.84.190
136	117170000	117189999	
137	117190000	117209999	J558.85.191 J558.86pg.192
138	117210000	117229999	J558.87.193
139	117230000	117249999	J558.88.194 J558.89pg.195
	117250000	117269999	
	117270000	117289999	
	117290000	117309999	
	117310000	117329999	
	117330000	117349999	
	117350000	117369999	
	117370000	117389999	
	117390000	117409999	
	117410000	117429999	
	117430000	117449999	

3.3.3. Igh locus spatial organisation - normalising Capture Hi-C matrices

HOMER was designed to take genome-wide datasets as input and so Capture Hi-C data had to be presented in the form of mini chromosomes which correspond to the baited regions. The $Rag^{-/-}$ pro-B cell and thymus Capture Hi-C datasets were filtered to retain only di-tags with both ends mapping to the baited regions, and a custom genome was created comprising mini chromosomes with starts and ends matching the starts and ends of BACs used for bait generation (described in section 2.8.1 and shown in **Figure 15**). These custom genome datasets were analysed in HOMER to produce normalised contact maps at 20kb resolution over the Igh locus. I generated a background model at 20kb resolution and used the *analyzeHiC* function to produce normalised interaction frequency matrices (**Figure 25** and **Figure 30**). Two forms of matrices were constructed, with and without correcting for genomic distance.

First, the *-simpleNorm* option in the *analyzeHiC* function gave observed/expected matrices corrected for coverage biases described above without taking the distance between the bins into consideration (**Figure 25**). This type of matrix is a 'natural' representation of chromatin contacts, because genomic distance is a big determinant of contact frequencies. Interaction frequency between regions in cis decreases, on average, as their genomic distance increases. Close cis interactions around the matrix diagonal are the most frequent and moving further away from the diagonal the interaction frequency gradually decreases. However, if regions that are far apart in genomic sequence interact very frequently, then an enrichment can be observed far from the diagonal. In $Rag^{-/-}$ pro-B cells there is a much higher enrichment of interactions far from the diagonal (**Figure 25**A) than in the thymus (**Figure 25**B). This is a reflection of locus contraction and means that V, D, and J genes as well as regulatory elements such as 3'RR, Eμ and IGCR1 interact frequently with each other over long distances.

Second, the *-norm* option in the *analyzeHiC* function was used to apply distance correction (**Figure 30**). This created observed/expected matrices where the expected contact frequencies were a function of distance between the interacting bins. Contacts along the diagonal are not enriched here, because bins in close proximity are expected to interact very frequently. The overall pattern of enrichment of interactions between the Igh elements in $Rag^{-/-}$ pro-B cells was clearly higher than expected from linear distance (**Figure 30**A). This shows that despite the large distances between the elements in the Igh locus they are contacting each other more frequently than expected and overall make more contacts in pro-B cells than in the thymus (**Figure 30**B).

A

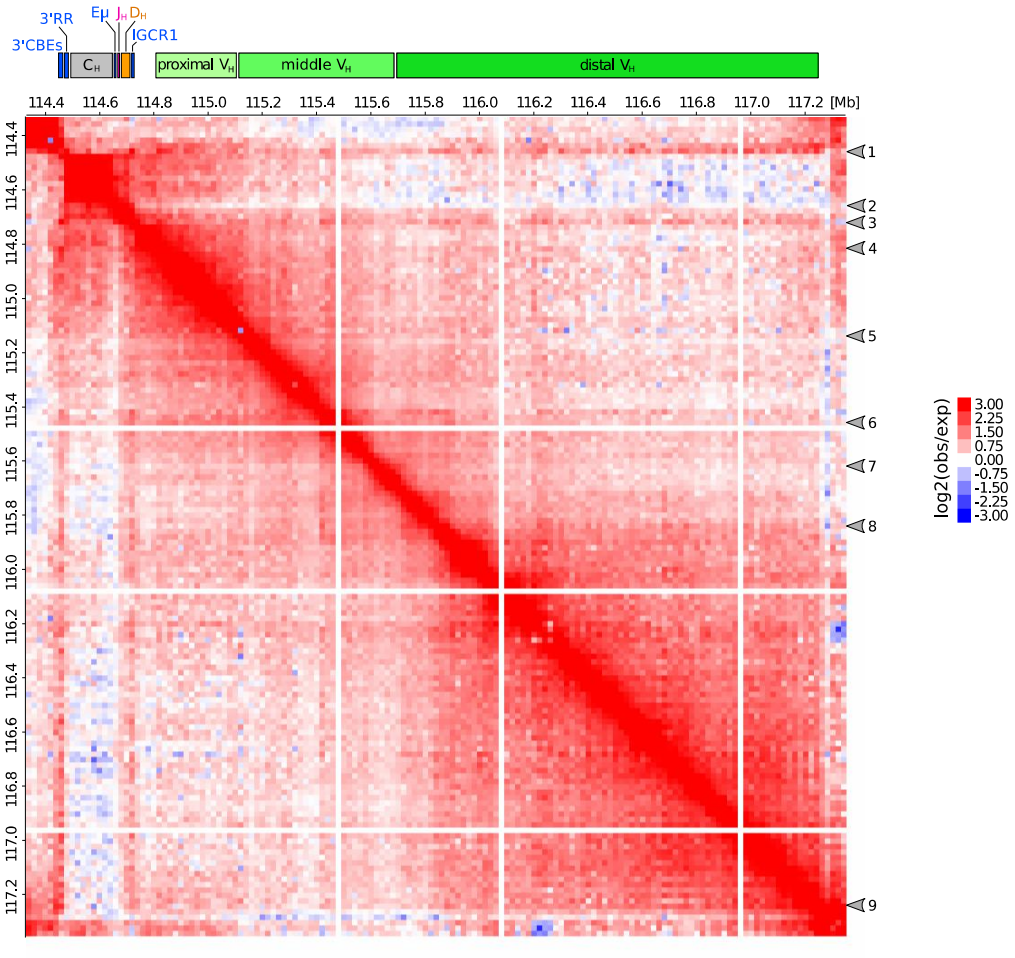
3'RR
Eμ
JH
DH
3'CBEs
IGCR1
CH
proximal VH
middle VH
distal VH
114.4 114.6 114.8 115.0 115.2 115.4 115.6 115.8 116.0 116.2 116.4 116.6 116.8 117.0 117.2 [Mb]
1
2
3
4
5
6
7
8
9
log2(obs/exp)
3.00
2.25
1.50
0.75
0.00
-0.75
-1.50
-2.25
-3.00

B

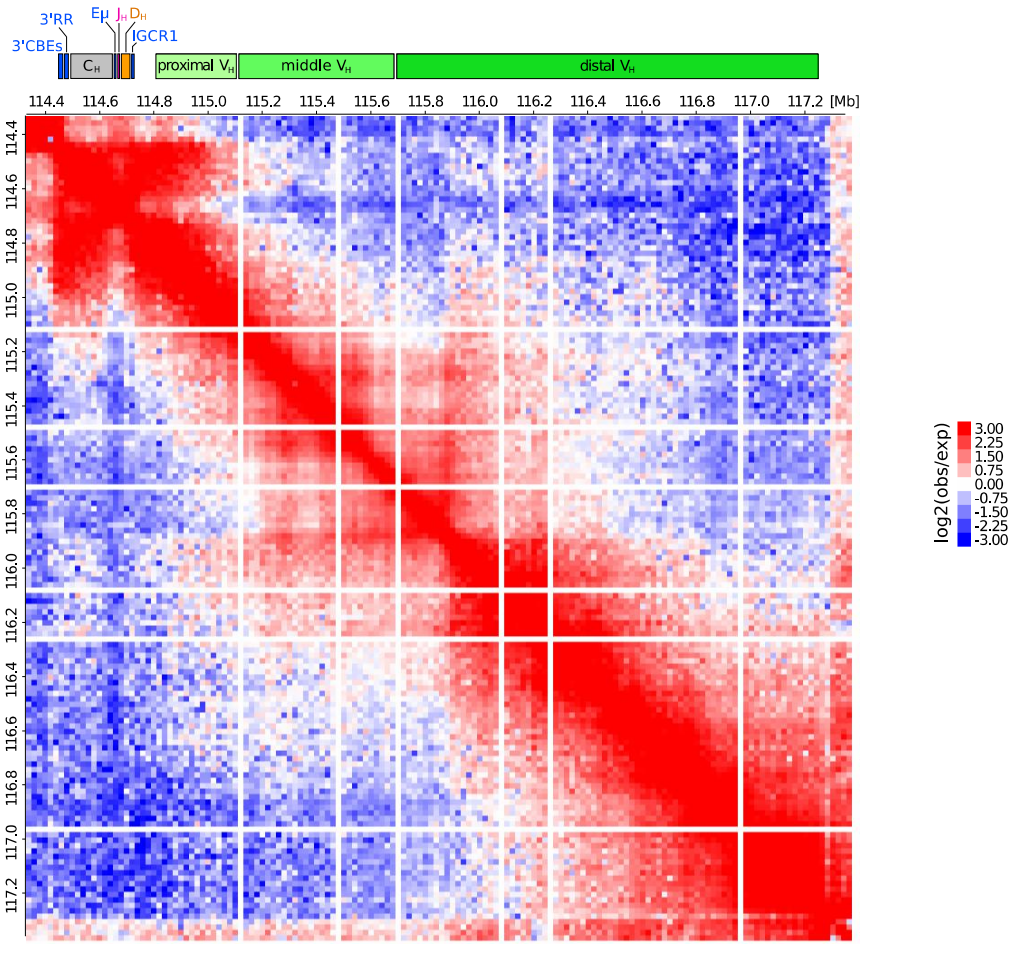
3'RR
Eμ
JH
DH
3'CBEs
IGCR1
CH
proximal VH
middle VH
distal VH
114.4 114.6 114.8 115.0 115.2 115.4 115.6 115.8 116.0 116.2 116.4 116.6 116.8 117.0 117.2 [Mb]
log2(obs/exp)
3.00
2.25
1.50
0.75
0.00
-0.75
-1.50
-2.25
-3.00

Figure 25. Interaction frequency matrices of the Igh locus corrected for read coverage. Matrices generated in HOMER and visualized in Java TreeView. The Igh locus baited region (chr12:114,330,000-117,450,000) was divided into 20kb bins and pairwise interactions are plotted for $Rag^{-/-}$ pro-B cells (A) and thymus (B). An average of biological replicates was taken. The Igh locus elements are annotated above the heatmaps. Genomic coordinates are given above and on the left of each matrix. Each matrix entry (square) represents a normalized interaction frequency between a pair of bins. Log2(obs/exp) values indicate fold enrichment or depletion. Pairwise interactions observed at frequency higher than expected (enriched) are depicted in red, whereas interactions observed at frequency lower than expected (depleted) are depicted in blue. Matrix entries near the diagonal represent pairwise interactions between bins that are proximal in linear genomic distance, whereas entries far off the diagonal represent pairwise interactions between bins that are distal in linear genomic distance. White lines are unusually lowly covered bins excluded by HOMER, and so were last 5 bins (117,350,000-117,450,000). Grey arrows indicate regions discussed in the text (arrow 1 – 3'CBEs/HS4-8, arrow 2 – Eμ, arrow 3 – IGCR1, arrow 4 – start of V genes, arrow 5 – end of proximal V genes, arrow 6 – last S107 gene S107.4.65, arrow 7 – first J606 gene J606.1.89, arrow 8 – start of distal V domain at J558.7pg.97, arrow 9 – end of Igh TAD at 117.27Mb).

I will be mostly discussing the coverage corrected and not distance corrected interaction matrices. The distance corrected matrices only report interactions that have higher contact frequency than what is expected given their distance, whereas I am interested in the absolute interaction frequency profile of the Igh elements as this is the true representation of the Igh locus spatial conformation.

HindIII is a '6-cutter' as it recognises a 6bp sequence A|AGCT|T. The 887 HindIII fragments over the Igh locus were covered on average by 1,471,530 reads in $Rag^{-/-}$ pro-B cells and 1,252,721 reads in the thymus, which gives approximately 1500 reads per single HindIII fragment. HindIII fragments vary hugely in size from as small as 100bp to as large as 33kb within the Igh locus alone. I analysed the data in 20kb bins as this was optimal for achieving high resolution and a desire to keep the bins a fixed width for the purpose of polymer modelling (section 3.4). High resolution data is characterised by high sparsity and HOMER excludes bins that are not sufficiently covered (at least 1/5 of the mean). Here, the white lines in the interaction matrices are bins with unusually low coverage that have been excluded by HOMER as they contain very few, very large or no HindIII fragments. In the $Rag^{-/-}$ pro-B matrix (**Figure 25**A) the non-informative bins are: 115.47-115.49Mb, which contains a large 15kb HindIII fragment; 116.07-116.09Mb, which has no HindIII fragment ends as a very large 33kb HindIII fragment spans it; 116.95-116.97Mb, which contains a large 10kb HindIII fragment; and the last five bins in the matrix 117.35-117.45Mb.

The custom genome approach that only retains intra-locus di-tags deprives the bins near the ends of the baited regions of a substantial number of reads (outward interactions). Indeed, the last 10 bins in the matrix upstream of 117.25Mb, falling outside on the Igh TAD, had a very low read coverage. Five of them were excluded from the analysis by HOMER and the remaining five most probably had their interaction frequencies somewhat overcorrected as they show highly enriched interactions with bins downstream of the 3' end of the locus. This is most likely due to asymmetry of contact possibilities in the baited region, as the middle bins have more contact options upstream and downstream than the edge bins, whose outward contacts were artificially eliminated. On the other hand, precisely because these bins fall

outside the Igh locus, which is contracted in pro-B cells and the 3' and 5’ ends are relatively close to each other, the regions immediately adjacent to the Igh TAD boundaries might inevitably be in close spatial proximity. It is therefore difficult to assess whether this phenomenon is an experimental artefact or a true reflection of locus contraction.

To quantify the differences in read coverage between Capture Hi-C and Hi-C, I examined the correlations between read coverage values and between HOMER correction factors (**Figure 35**). This was performed on the Igh baited region divided into 104 30kb bins. The last 6 bins (99-104), corresponding to the last 10 bins in the 20kb matrix, were identified as outliers (**Figure 35**A and B left). Bin 98 was also a slight outlier but it is within the Igh locus and contains the last V gene (J558.89pg.195) so it was retained. After removal of the 6 outlier bins the read coverage and the correction factors in Capture Hi-C were highly positively correlated with Hi-C data (**Figure 35** A and B right).

3.3.4. CTCF-binding elements might mediate Igh looping

The CCCTC-binding factor (CTCF) has been implicated as a major factor in determining TAD boundaries and anchoring the bases of DNA loops (Sanyal et al. 2012; Tang et al. 2015b; Rudan et al. 2015; Sanborn et al. 2015; Fudenberg et al. 2016; Zhan et al. 2017a). The directionality of CTCF-binding elements (CBEs) is important because they preferentially interact when in convergent orientation (oppositely directed and facing each other) (Rao et al. 2014c; de Wit et al. 2015a; Sanborn et al. 2015; Fudenberg et al. 2016). Out of the ~120 CTCF-binding elements in the Igh locus (Degner et al. 2011; Ebert et al. 2011; Bolland et al. 2016) (**Figure 36**) there are ~110 CBEs dispersed in the V region and are either positioned at the promoters of proximal and middle V genes or are intergenic in the distal V region. There are 7 CBEs located just downstream of the 3’RR/HS1-3 (around HS4-8 and downstream, referred to as 3'CBEs/HS4-8) that are in convergent orientation with the CBEs in the V region. The IGCR1 harbours 2 divergent CBEs, one in convergent orientation with the CTCF sites in the V region and a second one convergent with the CTCF sites in the 3'CBEs/HS4-8.

Three major features of the Igh locus spatial conformation in pro-B cells emerged from the Capture Hi-C experiments. First, the 3'CBEs/HS4-8 bin (114.45-114.47Mb) interacts with all V genes. Second, the IGCR1 bin (114.71-114.73Mb) also interacts with all V genes. Third, there is a highly looped distal V domain (**Figure 25**A arrows 1, 3, 8 and 9).

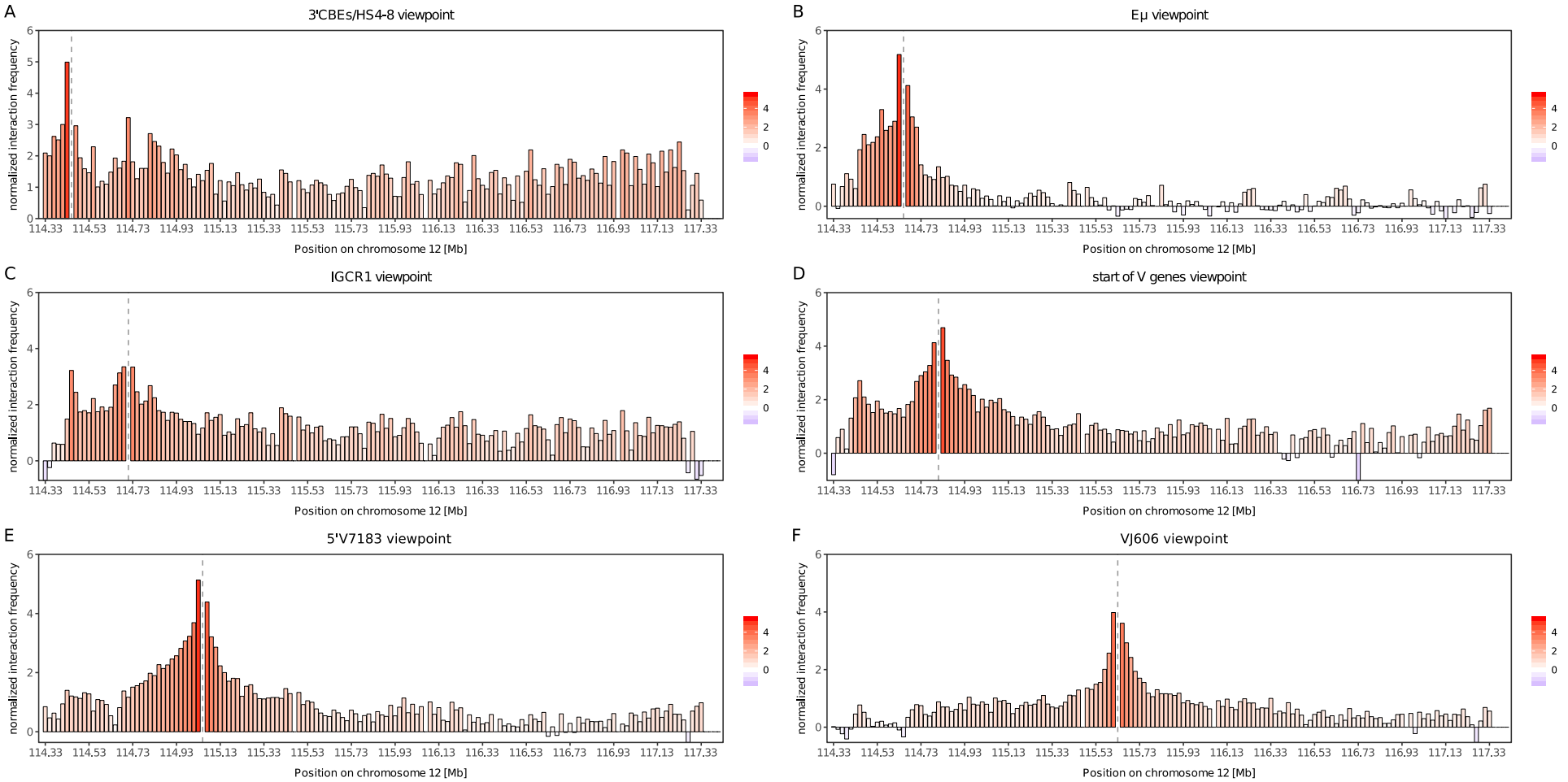

Figure 26. Virtual 4C interaction tracks for selected viewpoints extracted from the Rag$^{-/-}$ pro-B coverage corrected interaction matrix in Figure 25A. Reads quantified as described in figure 25. Normalised interaction frequency corresponds to the log2(obs/exp) values and is depicted using the same colour scheme. The 20kb bin containing the viewpoint has been omitted for clarity. **A**. Interaction profile from the 3'CBE/HS4-8 viewpoint (114.45-114.47Mb). **B.** Interaction profile from the Eμ viewpoint (114.65-114.67Mb). **C.** Interaction profile from the IGCR1 viewpoint (114.71-114.73Mb). **D**. Interaction profile from the Start of V genes viewpoint (114.81-114-83Mb). **E.** Interaction profile from the 5'V7183 viewpoint (115.05-115.07Mb). **F.** Interaction profile from the VJ606 viewpoint (115.63-115.65Mb). Continued in Figure 27.

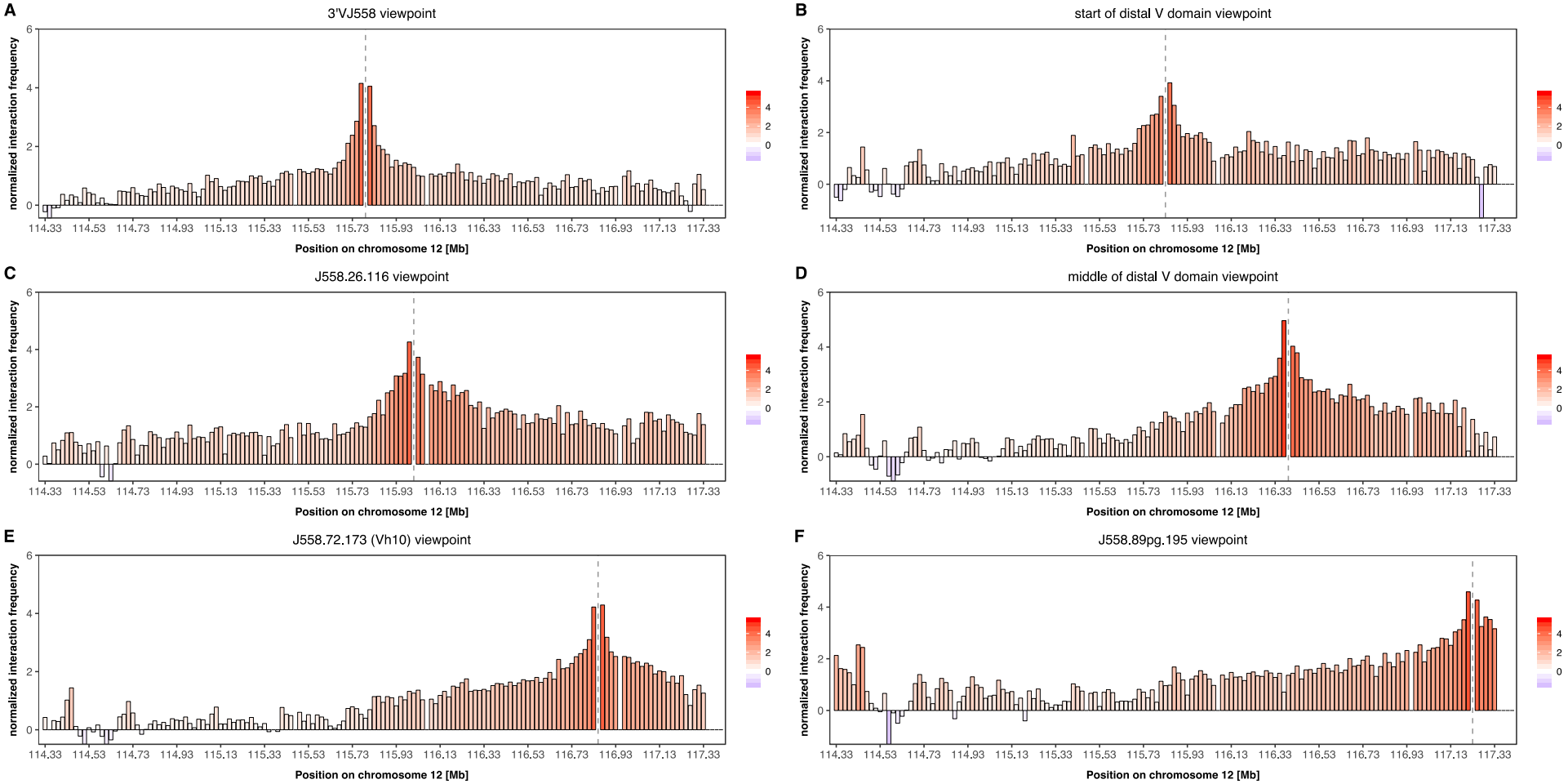

Figure 27. Virtual 4C interaction tracks for selected viewpoints extracted from the Rag$^{-/-}$ pro-B coverage corrected interaction matrix in Figure 25A. Continued from Figure 26. Reads quantified as described in figure 15. Normalised interaction frequency corresponds to the log2(obs/exp) values and is depicted using the same colour scheme. The 20kb bin containing the viewpoint has been omitted for clarity. **A.** Interaction profile from the 3'VJ558 viewpoint (115.79-115.81Mb). **B**. Interaction profile from the Start of distal V domain viewpoint (115.83-115.85Mb). **C.** Interaction profile from the J558.26.116 viewpoint (116.01-116.03Mb). **D**. Interaction profile from the Middle of distal V domain viewpoint (116.39-116.41Mb). **E.** Interaction profile from the J558.72.173 (Vh10) viewpoint (116.85-116.87Mb). **F**. Interaction profile from the J558.89pg.195 viewoint (117.23-117.25Mb).

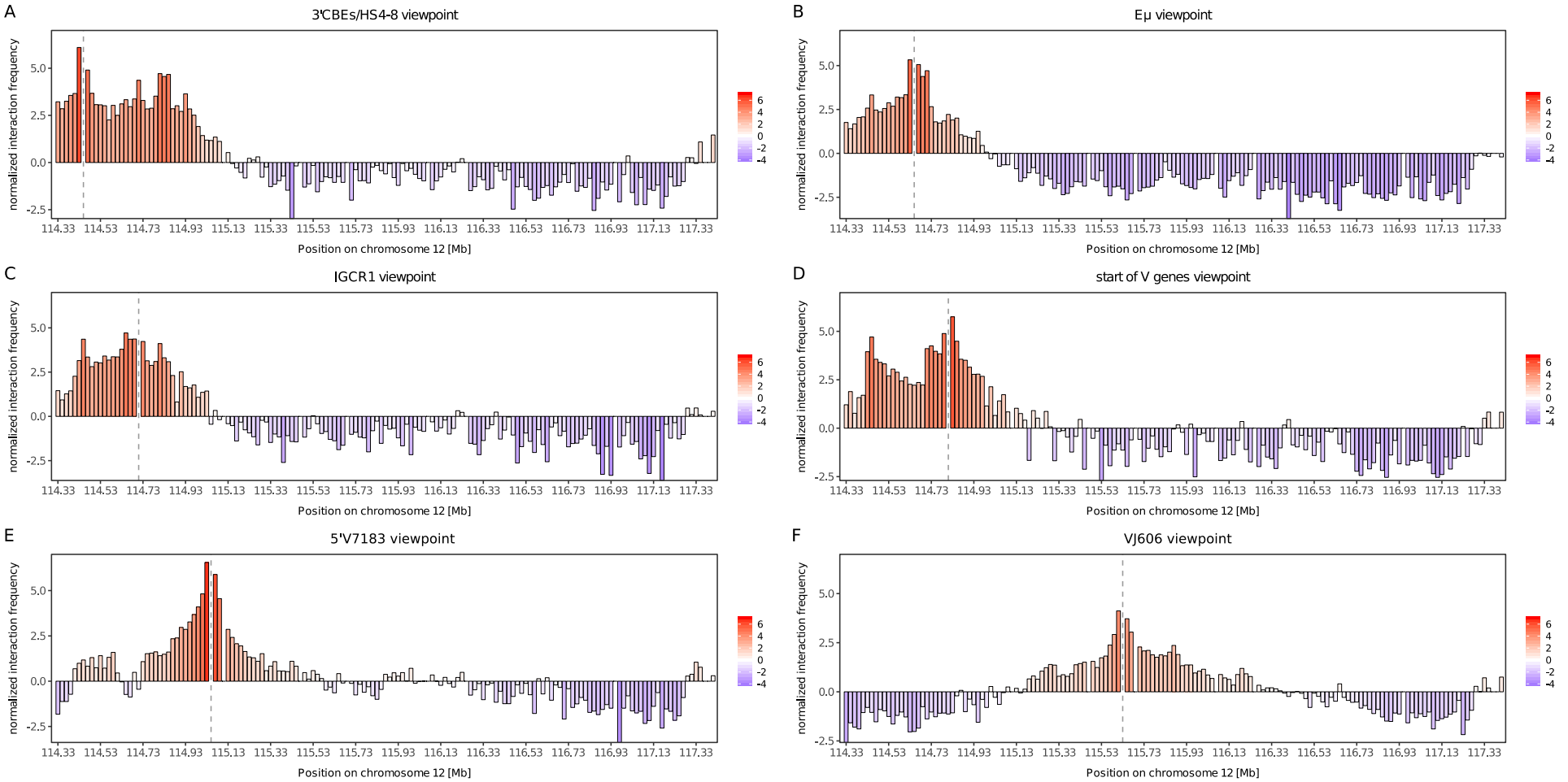

Figure 28. Virtual 4C interaction tracks for selected viewpoints extracted from the thymus coverage corrected interaction matrix in Figure 25B. Reads quantified as described in figure 25. Normalised interaction frequency corresponds to the log2(obs/exp) values and is depicted using the same colour scheme. The 20kb bin containing the viewpoint has been omitted for clarity. **A.** Interaction profile from the 3'CBE/HS4-8 viewpoint (114.45-114.47Mb). **B**. Interaction profile from the Eμ viewpoint (114.65-114.67Mb). **C**. Interaction profile from the IGCR1 viewpoint (114.71-114.73Mb). **D**. Interaction profile from the Start of V genes viewpoint (114.81-114-83Mb). **E**. Interaction profile from the 5'V7183 viewpoint (115.05-115.07Mb). **F**. Interaction profile from the VJ606 viewpoint (115.63-115.65Mb). Continued in Figure 29.

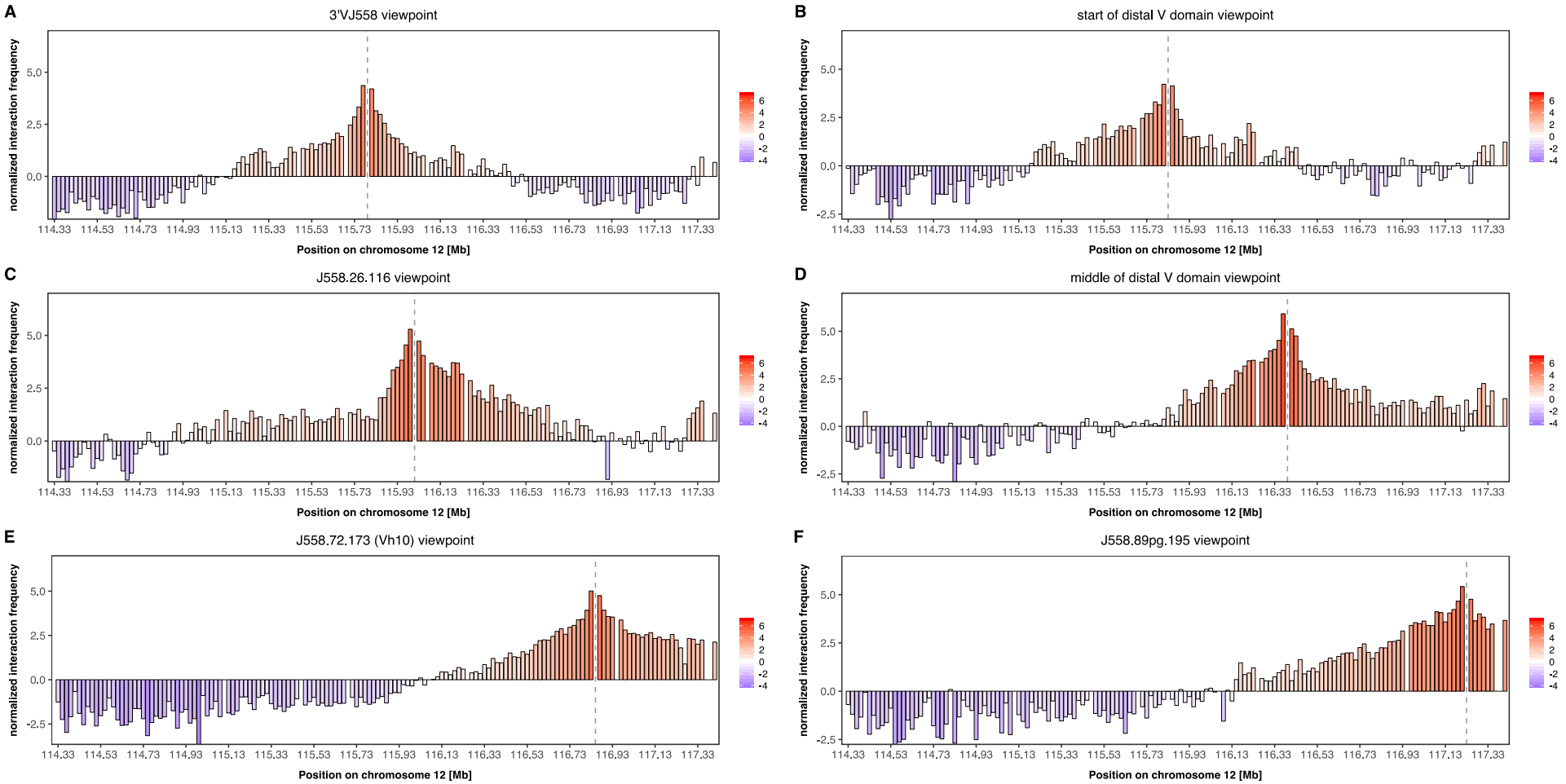

Figure 29. Virtual 4C interaction tracks for selected viewpoints extracted from the thymus coverage corrected interaction matrix in Figure 25B. Continued from Figure 28. Reads quantified as described in figure 25. Normalised interaction frequency corresponds to the log2(obs/exp) values and is depicted using the same colour scheme. The 20kb bin containing the viewpoint has been omitted for clarity. **A**. Interaction profile from the 3'VJ558 viewpoint (115.79-115.81Mb). **B**. Interaction profile from the Start of distal V domain viewpoint (115.83-115.85Mb). **C**. Interaction profile from the J558.26.116 viewpoint (116.01-116.03Mb). **D**. Interaction profile from the Middle of distal V domain viewpoint (116.39-116.41Mb). **E**. Interaction profile from the J558.72.173 (Vh10) viewpoint (116.85-116.87Mb). **F**. Interaction profile from the J558.89pg.195 viewpoint (117.23-117.25Mb).

3’CBEs interactions

In pro-B cells, the 3'CBEs/HS4-8 bin contacts all V genes with similar frequencies (**Figure 25**A arrow 1 and **Figure 26**A) and its 7 CTCF motifs that are convergent with the CTCF motifs in the V region make it a conspicuous focal point for contacts. The most frequent interaction of the 3'CBEs/HS4-8 was with the IGCR1 (arrow 3) and the second most frequent interaction upstream was with the bin at 144.81Mb containing the first five V genes (arrow 4), including the most highly recombining V genes 7183.2.3 (V81X) and Q52.2.4 (Bolland et al. 2016). It also interacts frequently with immediately adjacent bins: the upstream 3'RR/HS1-3 bin and the downstream bins containing a further 11 CTCF-binding sites (based on ChIP-seq from Ebert et al. 2011).

In the distal V region, the 3'CBEs/HS4-8 interacts most frequently with the last V bin at 117.23Mb marking the end of the Igh locus (arrow 9), after which interactions drop considerably (**Figure 26**A). These 7 CBEs at HS4-8 plus another 3 CBEs further downstream have been identified by Benner *et al.* as a superanchor using non-enriched Hi-C (Benner et al. 2015). Moreover, the bin 3' of the 3'CBEs/HS4-8 (114.43-114.45Mb, containing 1 CTCF site) interacted with V genes more frequently than the bin 5' of the 3'CBEs/HS4-8 (containing the 3’RR/HS1-3) (**Figure 25**A above and below arrow 1). Together with the convergent orientation of these CTCF elements, my data strongly support the dependency of long-range interactions on CTCF-binding sites.

The 3'RR/HS1-3, which is an enhancer important for class switch recombination in later B cells, interacts very frequently with the 3’CBEs/HS4-8 bin as mentioned above, but it does not contain CTCF sites and does not interact frequently with the V region. The 3'RR/HS1-3 interacts more frequently than the 3'CBEs/HS4-8 with the bins between itself and the IGCR1, which can be observed in the previous 4C-seq experiment from these two viewpoints (Medvedovic et al. 2013). This forms a tight, highly looped 3' end domain (**Figure 25**A between arrows 1 and 3).

The study that proposed the 3' superanchor (Benner et al. 2015) observed a sharp end of the Igh TAD after the last V gene, which might involve the CTCF-binding sites near the last V genes and possibly a single CTCF site 18kb after the last V (J558.89pg.195). My data also shows a clear Igh TAD boundary at 117.25Mb (arrow 9). As shown earlier, the bins upstream of the last V gene had unusually low read coverage, which indicates that they belong to the next TAD and interact mostly outwards, away from the Igh.

Collectively, this data supports the conclusion that 7 CTCF-binding elements downstream of the 3'RR interact with high frequency with the IGCR1 and with all V genes. The 3’CBEs-IGCR1 interaction creates a tightly looped 3' domain containing the 3'RR and the Eμ. The 3’CBEs-IGCR1-V interactions might facilitate bringing V genes into close proximity with D genes for recombination.

IGCR1 interactions

The IGCR1, whose role is to insulate the V genes from the D-J region prior to D-J recombination (Guo et al. 2011b), harbours 2 divergent CBEs and contacts all V genes with very similar frequencies (**Figure 25**A arrow 3 and **Figure 26**C). Two bins downstream of the IGCR1 contain most D genes (114.67-114.71Mb) and also interact frequently with all V genes (**Figure 25**A two bins above arrow 3). The bin 114.67-14.69Mb, rather than the IGCR1 itself, seems to be the general boundary of V-D looping. The interaction frequency of the IGCR1 along the V genes was more uniform than that of the 3'CBEs/HS4-8, without a marked increase at the first and last V gene (**Figure 26**A and C).

The IGCR1 interacts frequently with three bins downstream of itself (containing the D and J genes) and with the 3'CBEs/HS4-8 (**Figure 26**C). Between these two regions, there is only a slight increase in IGCR1's interactions with the bin containing putative enhancers hRE1 and hRE2 (114.55-11457Mb) (Predeus et al. 2014). Notably, the IGCR1 does not interact very frequently with the 11 CTCF sites downstream of the 3'CBEs/HS4-8. Markedly, both the 3'CBEs/HS4-8 and the IGCR1 were enriched for interactions with every bin along the Igh locus as demonstrated by the lack of negative values in the virtual 4C diagrams (**Figure 26**A and C). The 20kb resolution achieved here shows clearly that the 3'CBEs/HS4-8 and the IGCR1 are indeed the interactive focal points in the Igh locus. One bin downstream of the 3'CBEs/HS4-8 and two bins downstream of the IGCR1 seem to form local interaction boundaries. I was not able to determine whether the IGCR1's 3' CBE2 interacts only downstream and the 5' CBE1 interacts only upstream, as they are both in the same HindIII fragment.

The IGCR1 seems to also be the start of a small proximal V subdomain encompassing all proximal V genes up to the end of the 7183 gene family (7183.21g.38) at 115.13Mb (arrow 5). This domain could in fact start as far as at the 3'CBEs/HS4-8 bin, but the Eμ is evidently poorly enriched for interactions with all features upstream of the IGCR1 (**Figure 25**A arrow 2 and **Figure 26**B). The Eμ is a part of the tight 3' end domain between the IGCR1 and the 3'CBEs/HS4-8, but it seems distinctly sequestered from contacting the V genes, whereas the D genes just 5' of the Eμ readily contact all V genes. Work from our lab identified putative CTCF-binding sites around DST4 and DSP2.5 genes, which might further explain the interactivity of the D region compared to the Eμ (Bryony Stubbs, PhD thesis, unpublished). The 20kb bin containing the Eμ also contains two constant genes, but does not show the interaction pattern of the downstream constant genes, which are enriched for interactions with proximal Vs and depleted for interactions with middle and distal Vs.

Eμ interactions

To further investigate the behaviour of the Eμ, I re-analysed the Capture Hi-C data in HOMER using shifted bin coordinates, so that the three HindIII fragments over the J genes and the Eμ belonged to either a bin containing only D genes or a bin containing only constant genes (**Figure 37**A). When the original Eμ bin coordinates (114.65-114.67Mb) were shifted

downstream further over the C genes (114.648100-114.668100Mb) and did not contain the DQ52 gene, the interaction profile of the Eμ-containing bin remained similar to the original coordinates (**Figure 37**B). It was still not enriched for interactions with proximal V genes. However, I noted an increased depletion for interactions with the distal V genes in accordance with the behaviour of other C gene bins. Intriguingly, when the original Eμ bin coordinates were shifted upstream further over D genes, the Eμ-containing bin became slightly enriched for interactions along the locus (**Figure 37**C). This enrichment however was not as high as that of the upstream D bins. In this binning, the Eμ bin and the first C gene bin were both the least enriched bins for interactions with the proximal Vs. This analysis shows that the bin containing the Eμ has the tendency to loop out of the 3' domain regardless of it being in a bin with D genes or constant genes. Eμ might reside in very accessible chromatin to be able to bind the large RNA Pol II complex, as well as for the nearby J genes to bind the large RAG1/2 complex. Indeed, it has been shown that Eμ-J is by far the most enriched region for the active chromatin marks H3K4me3, H3K4me2 and H3K9Ac in pro-B cells (Chakraborty et al. 2009a; Malin et al. 2010; Ebert et al. 2013).

Distance correction confirms enrichment for long-range interactions

The matrix corrected for distance still shows enrichment for interactions throughout the Igh locus, confirming that these contacts are non-random and are more frequent than expected from genomic proximity (**Figure 30**A). The interactions between the 3'CBEs/HS4-8 and the V region as well as between the IGCR1 and the V region are still the most enriched interactions in the locus (**Figure 30**A, **Figure 31**A and C). The immediate area around the IGCR1 bin is not enriched for contacts in distance corrected heatmaps, suggesting that the IGCR1 does not interact with the proximal Vs and the D-J region more than expected from genomic proximity (**Figure 31**C). The interaction of the IGCR1 with the 3'CBEs/HS4-8 is very highly enriched, as is the interaction between the 3'CBEs/HS4-8 and the first V gene at 114.81Mb. The subdomain between the IGCR1 and the 3'CBEs/HS4-8 remains enriched in the distance corrected map despite its small size, especially the region encompassing the Eμ, hRE1 hRE2, and HS1-3. This suggests that the Eμ might preferentially reside close to the 3'RR.

A

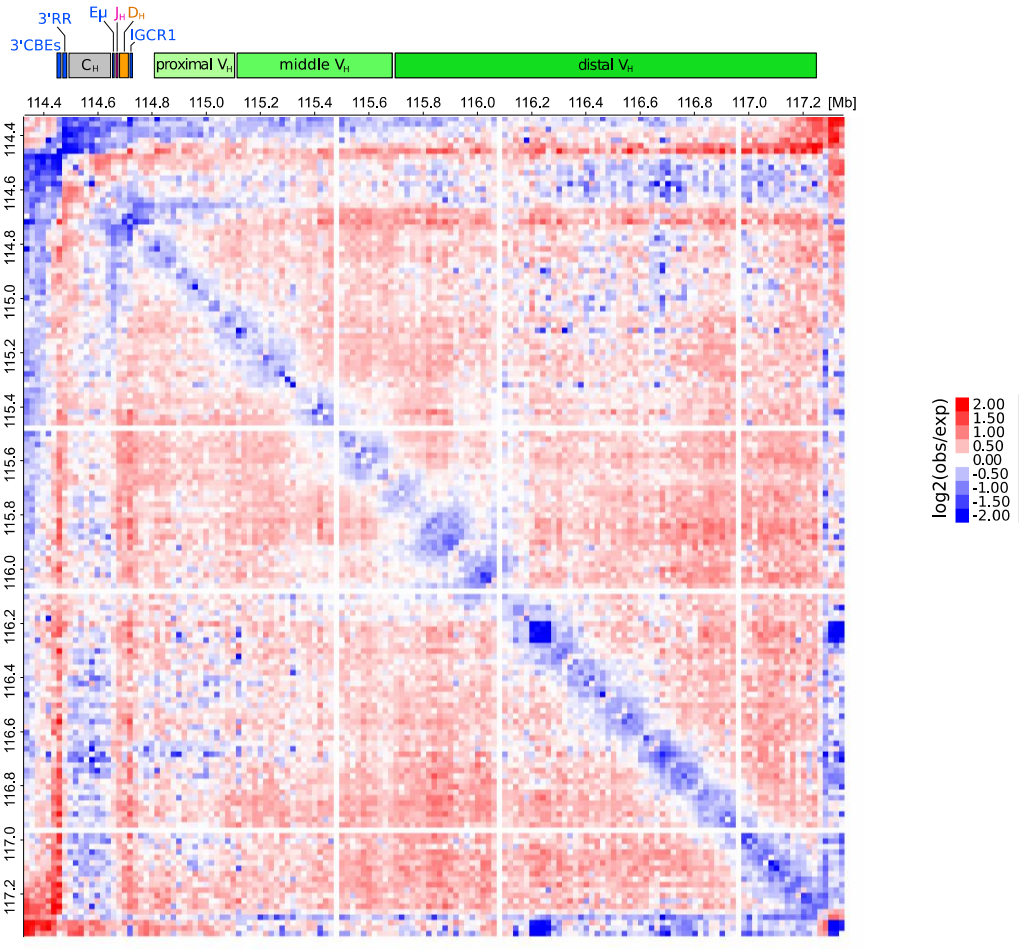
3'RR
Eμ
JH DH
3'CBEs
IGCR1
CH
proximal VH
middle VH
distal VH
114.4 114.6 114.8 115.0 115.2 115.4 115.6 115.8 116.0 116.2 116.4 116.6 116.8 117.0 117.2 [Mb]
log2(obs/exp)
2.00
1.50
1.00
0.50
0.00
-0.50
-1.00
-1.50
-2.00

B

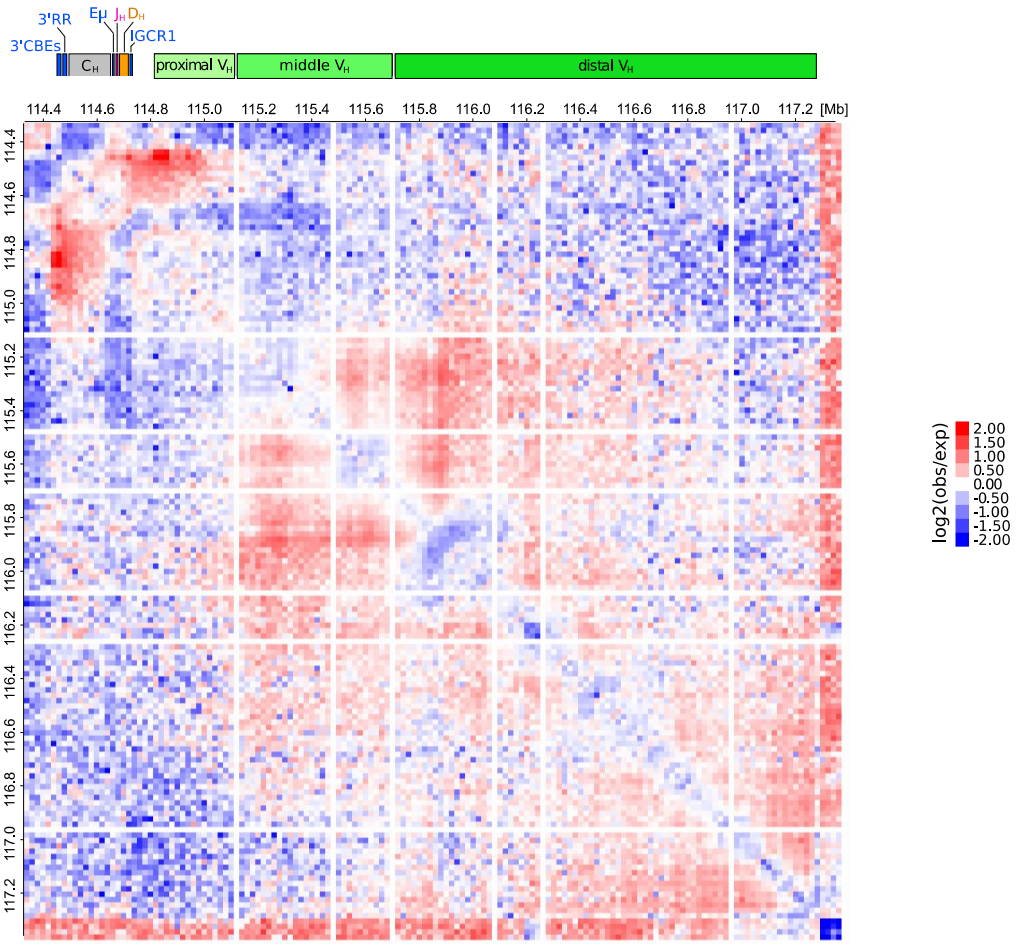
3'RR
Eμ
JH DH
3'CBEs
IGCR1
CH
proximal VH
middle VH
distal VH
114.4 114.6 114.8 115.0 115.2 115.4 115.6 115.8 116.0 116.2 116.4 116.6 116.8 117.0 117.2 [Mb]
log2(obs/exp)
2.00
1.50
1.00
0.50
0.00
-0.50
-1.00
-1.50
-2.00

Figure 30. Interaction frequency matrices of the Igh locus corrected for read coverage and distance. Matrices generated in HOMER and visualized in Java TreeView. The Igh locus baited region (chr12:114,330,000-117,450,000) was divided into 20kb bins and pairwise interactions are plotted for $Rag^{-/-}$ pro-B cells (A) and thymus (B). An average of biological replicates was taken. The Igh locus elements are annotated above the heatmaps. Genomic coordinates are given above and on the left of each matrix. Each matrix entry (square) represents a normalized interaction frequency between a pair of bins. Log2(obs/exp) values indicate fold enrichment or depletion. Pairwise interactions observed at frequency higher than expected accounting for genomic distance separating the bins (enriched) are depicted in red, whereas interactions observed at frequency lower than expected accounting for genomic distance separating the bins (depleted) are depicted in blue. Matrix entries near the diagonal represent pairwise interactions between bins that are proximal in linear genomic distance, whereas entries far off the diagonal represent pairwise interactions between bins that are distal in linear genomic distance. White lines are unusually lowly covered bins excluded by HOMER, and so were last 5 bins (117,350,000-117,450,000).

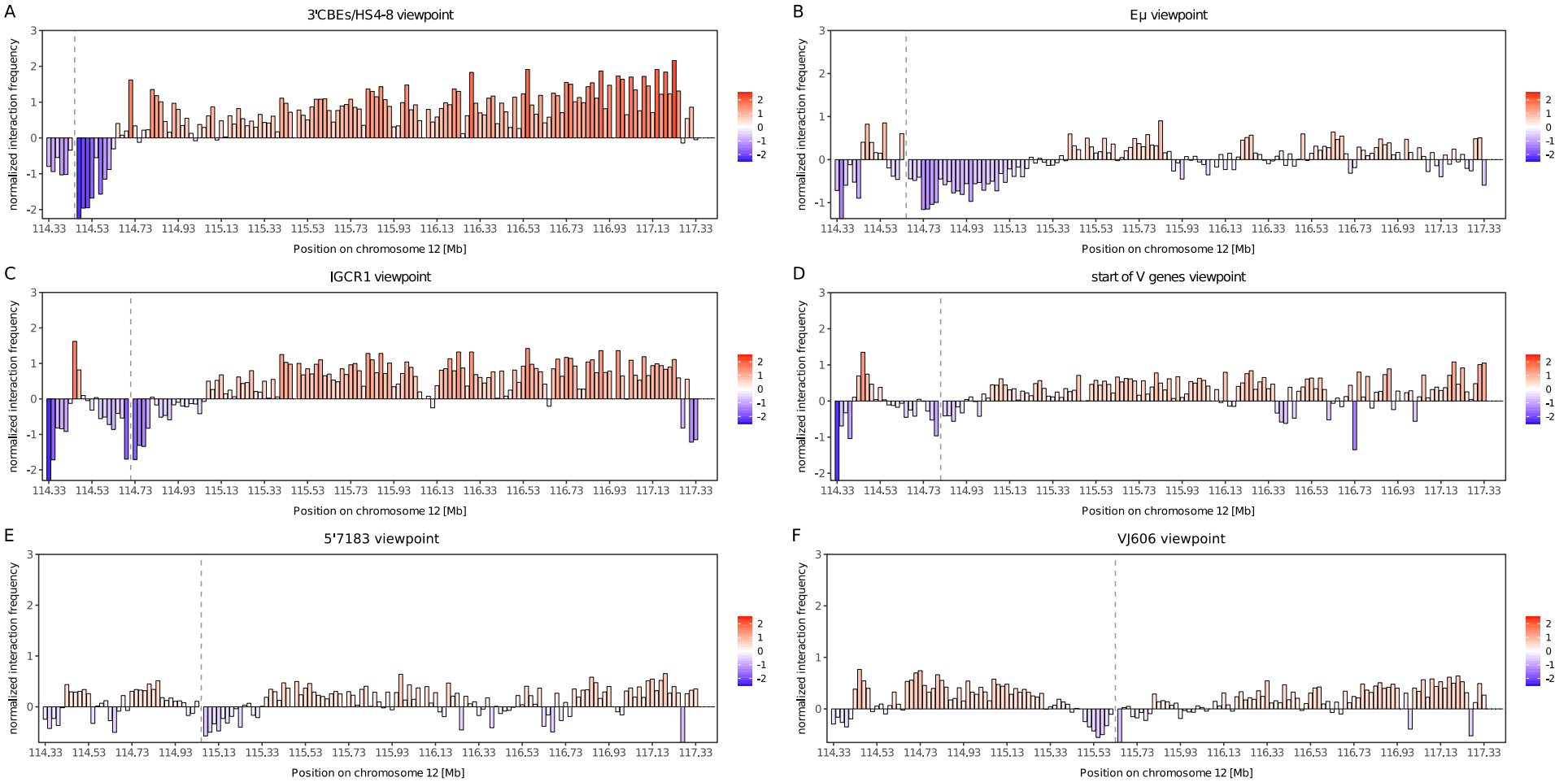

Figure 31. Virtual 4C interaction tracks for selected viewpoints extracted from the Rag$^{-/-}$ pro-B coverage corrected and distance corrected interaction matrix in Figure 30A. Reads quantified as described in figure 30. Normalised interaction frequency corresponds to the log2(obs/exp) values and is depicted using the same colour scheme. The 20kb bin containing the viewpoint has been omitted for clarity. **A**. Interaction profile from the 3'CBE/HS4-8 viewpoint (114.45-114.47Mb). **B**. Interaction profile from the Eμ viewpoint (114.65-114.67Mb). **C**. Interaction profile from the IGCR1 viewpoint (114.71-114.73Mb). **D.** Interaction profile from the Start of V genes viewpoint (114.81-114-83Mb). **E.** Interaction profile from the 5'V7183 viewpoint (115.05-115.07Mb). **F.** Interaction profile from the VJ606 viewpoint (115.63-115.65Mb). Continued in Figure 32.

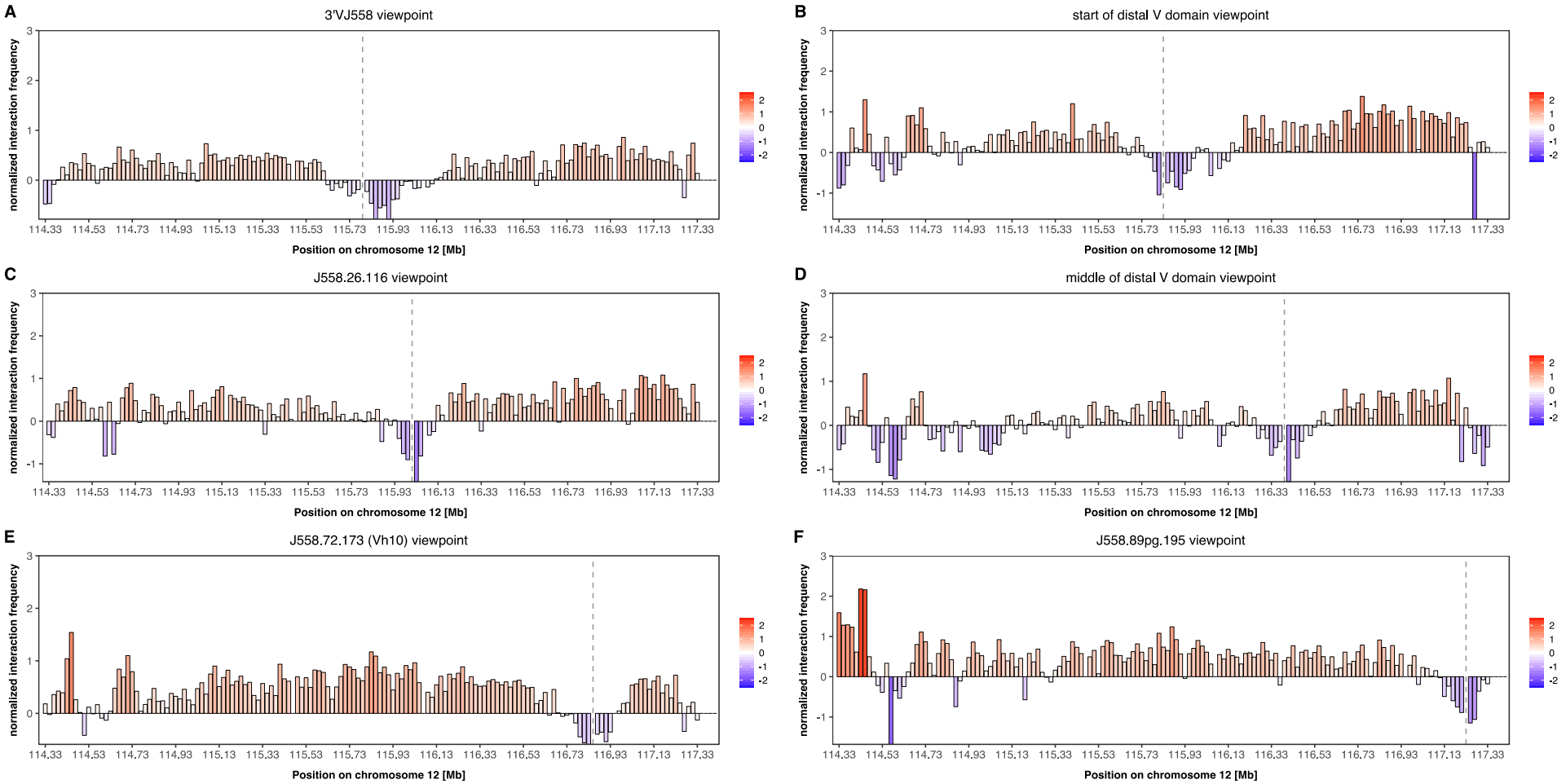

Figure 32. Virtual 4C interaction tracks for selected viewpoints extracted from the Rag$^{-/-}$ pro-B coverage corrected and distance corrected interaction matrix in Figure 30A. Continued from Figure 31. Reads quantified as described in figure 30. Normalised interaction frequency corresponds to the log2(obs/exp) values and is depicted using the same colour scheme. The 20kb bin containing the viewpoint has been omitted for clarity. **A**. Interaction profile from the 3'VJ558 viewpoint (115.79-115.81Mb). **B**. Interaction profile from the Start of distal V domain viewpoint (115.83-115.85Mb). **C**. Interaction profile from the J558.26.116 viewpoint (116.01-116.03Mb). **D**. Interaction profile from the Middle of distal V domain viewpoint (116.39-116.41Mb). **E**. Interaction profile from the J558.72.173 (Vh10) viewpoint (116.85-116.87Mb). **F**. Interaction profile from the J558.89pg.195 viewpoint (117.23-117.25Mb).

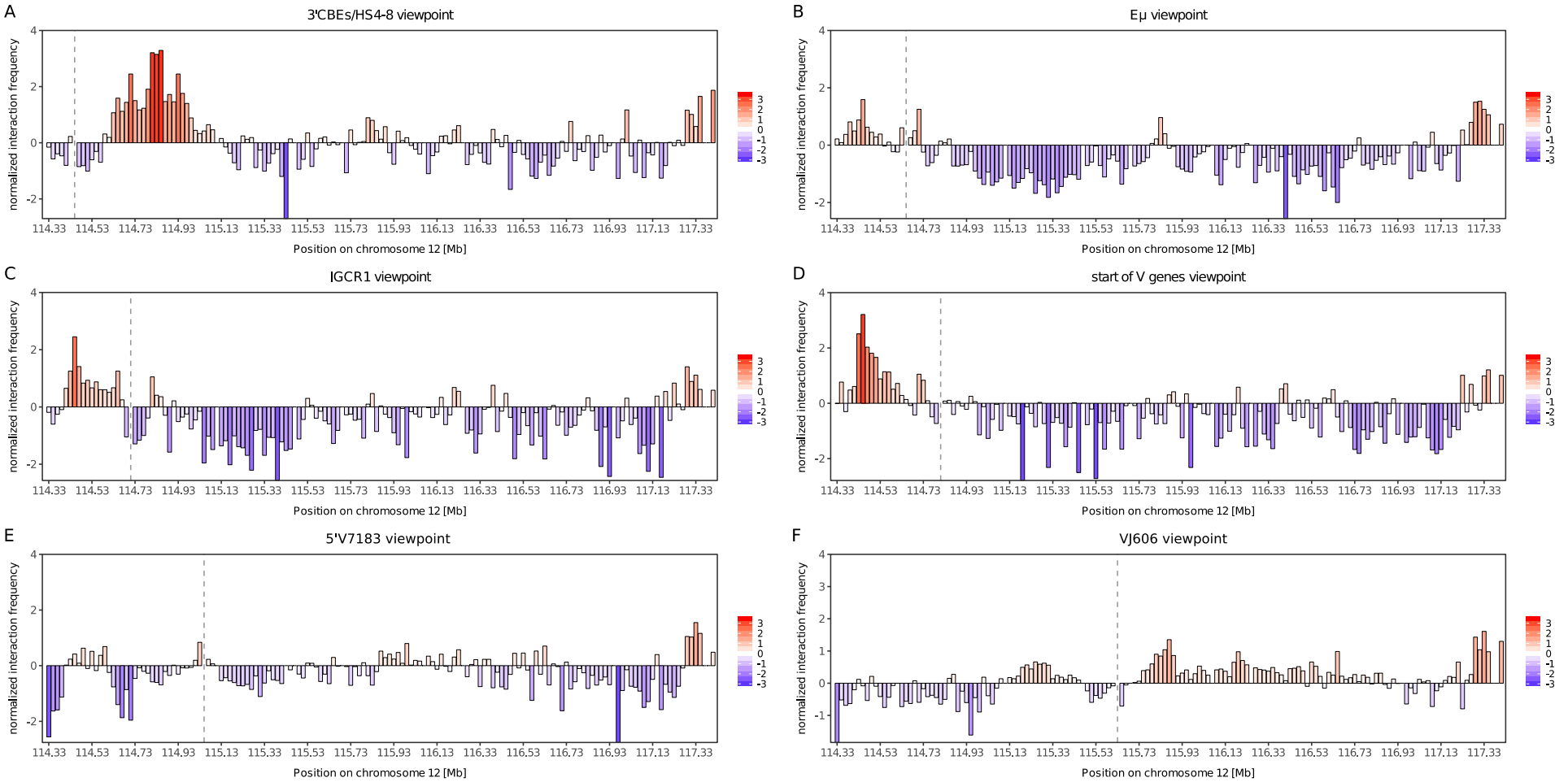

Figure 33. Virtual 4C interaction tracks for selected viewpoints extracted from the thymus coverage corrected and distance corrected interaction matrix in Figure 30B. Reads quantified as described in figure 30. Normalised interaction frequency corresponds to the log2(obs/exp) values and is depicted using the same colour scheme. The 20kb bin containing the viewpoint has been omitted for clarity. **A**. Interaction profile from the 3'CBE/HS4-8 viewpoint (114.45-114.47Mb). **B**. Interaction profile from the Eμ viewpoint (114.65-114.67Mb). **C.** Interaction profile from the IGCR1 viewpoint (114.71-114.73Mb). **D.** Interaction profile from the Start of V genes viewpoint (114.81-114-83Mb). **E**. Interaction profile from the 5'V7183 viewpoint (115.05-115.07Mb). **F**. Interaction profile from the VJ606 viewpoint (115.63-115.65Mb). Continued in Figure 34.

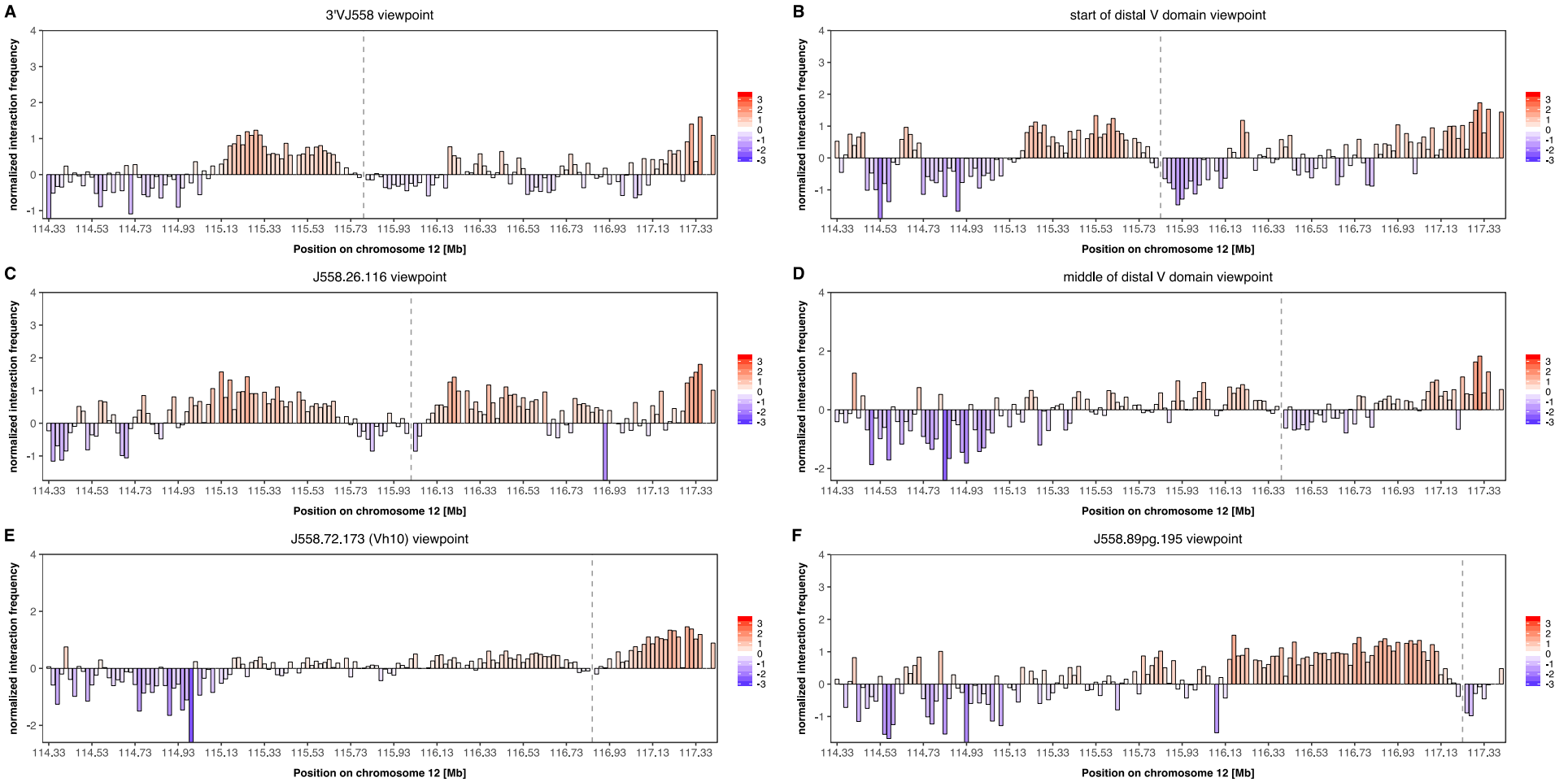

Figure 34. Virtual 4C interaction tracks for selected viewpoints extracted from the thymus coverage corrected and distance corrected interaction matrix in Figure 30B. Continued from Figure 33. Reads quantified as described in figure 30. Normalised interaction frequency corresponds to the log2(obs/exp) values and is depicted using the same colour scheme. The 20kb bin containing the viewpoint has been omitted for clarity. **A**. Interaction profile from the 3'VJ558 viewpoint (115.79-115.81Mb). **B**. Interaction profile from the Start of distal V domain viewpoint (115.83-115.85Mb). **C**. Interaction profile from the J558.26.116 viewpoint (116.01-116.03Mb). **D**. Interaction profile from the Middle of distal V domain viewpoint (116.39-116.41Mb). **E.** Interaction profile from the J558.72.173 (Vh10) viewpoint (116.85-116.87Mb). **F**. Interaction profile from the J558.89pg.195 viewpoint (117.23-117.25Mb).

Lack of long-range interactions in non-B cells

In thymocytes, the Igh locus was in an uncontracted conformation. It was depleted for very long-range interactions throughout the locus, particularly the CTCF anchors at the 3'CBEs/HS4-8 and the IGCR1 did not contact all V genes (**Figure 25**B, **Figure 28** A and C). On the other hand, I detected very frequent interactions along the matrix diagonal, which represent short-range contacts (**Figure 25**B). This spatial arrangement can be compared to an accordion shape with local contacts forming along the linear sequence, potentially reflecting a nucleosome-rich environment. As thymocytes also express the RAG recombinase to rearrange their TCR genes, D-J recombination of the Igh has been observed in a proportion of T cells (Born et al. 1988). Accordingly, I observed that the 3' end of the Igh locus is looped in the thymus, which is clearly observed in the distance corrected heatmap (**Figure 30**B). This has been previously suggested by 3C experiments (Guo et al. 2011a). The 3'CBEs/HS4-8 bin interacts very frequently with the IGCR1, and interactions of features in between, including the Eμ, J and D genes, are less enriched in distance corrected data (**Figure 30**B, **Figure 33**A-C). Interestingly, the 3'CBEs/HS4-8 seems to frequently interact with the proximal V genes up to 114.99Mb where the interactions decrease, to completely drop at 115.15Mb (**Figure 28**A, D and E, **Figure 33**A, D and E). Nonetheless, no V-DJ recombination, even with these proximal V genes, has been observed in the thymus (Born et al. 1988). This corroborates the observation that the D-J region including the IGCR1 (114.63-114.69Mb) is depleted for interactions with the V genes (**Figure 33**C). This suggests that the sequence between the Eμ and the IGCR1 is sequestered away to avoid contacts with proximal V genes (**Figure 30**B and **Figure 33** B-C), which indicates that the interaction of the 3'CBEs/HS4-8 with the proximal V genes might not be simultaneous with its interaction with the IGCR1.

Collectively, these findings establish the 3'CBEs/HS4-8 as an anchor contacting all V genes to facilitate their chance for recombination in pro-B cells, most probably via its CTCF-binding elements that are in convergent orientation to those in the V region. The data indicates that the IGCR1 might have a very similar anchor role in pro-B cells, interacting with all V genes most probably through its 5' CTCF element, which is in convergent orientation to the CTCF elements in the V region. Both anchors are absent in thymocytes. The 3'CBEs/HS4-8 and the IGCR1 form a highly looped 3' end subdomain presumably involving the 3' CTCF element of the IGCR1, which is in convergent orientation to seven 3'CBEs. This configuration would facilitate V gene interactions with D genes just downstream of the IGCR1. This subdomain is a part of a bigger 3' domain encompassing the proximal Vs and it persists in the thymus. Interestingly, the data shows that the bin containing the Eμ is looping out of this 3' domain in pro-B cells, which might indicate its high accessibility. In the thymus, where V-DJ recombination is inappropriate, the 3'CBEs/HS4-8 interaction with the IGCR1 might sequester the Eμ, J and D genes away from the V genes.

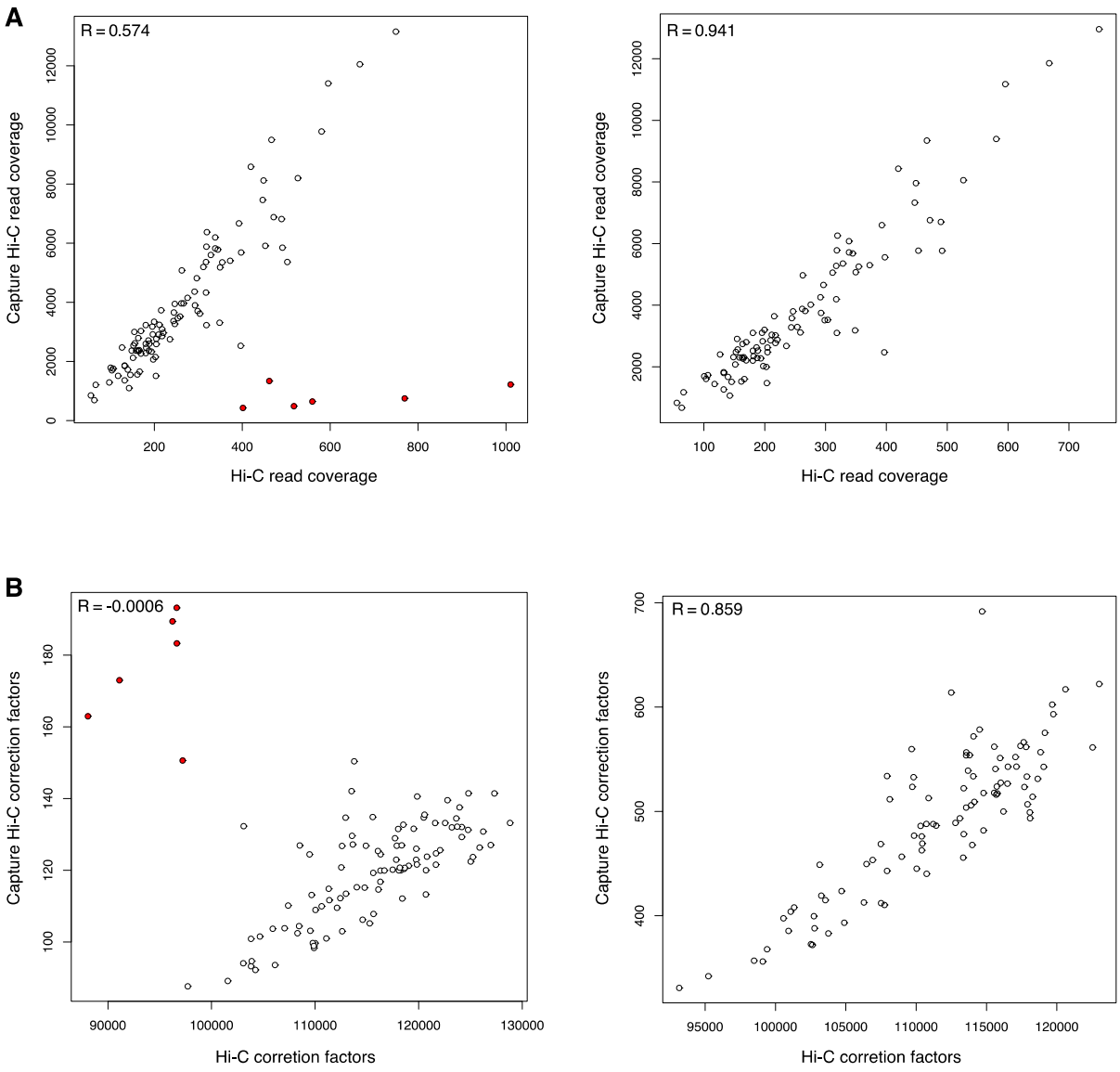

Figure 35. Read coverage patterns in Capture Hi-C and Hi-C are well correlated after removal of 6 unusually lowly covered outlier bins at the 5' end of the Igh baited region. Reads were quantified in 30kb bins in the Igh baited region chr12:114,330,000-117,450,000bp. Each circle corresponds to a 30kb bin. The outliers highlighted in red are the last 6 bins of the baited region (chr12:117,270,000-117,450,000bp) and they fall outside of the Igh TAD. Coverage outliers and correction factor outliers are the same bins. **A**. Correlation between the total number of reads in 30kb bins in Hi-C and Capture Hi-C libraries (left) and correlation after outlier removal (right). **B**. Correlation between HOMER correction factors for 30kb bins in Hi-C and Capture Hi-C (left) and correlation after outlier removal (right). For Capture Hi-C, the custom genome dataset was used. Data shown is for Rag1$^{-/-Bal}$ pro-B replicate 3 from sequencing run 1. R - Pearson's correlation coefficient.

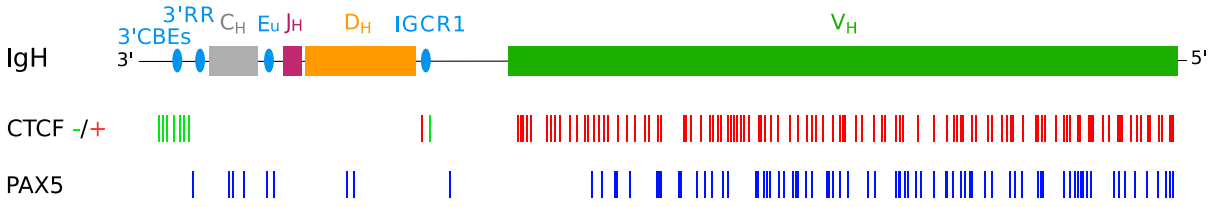

Figure 36. CTCF and PAX5 binding in the Igh locus in Rag$^{-/-}$ pro-B cells. See methods for information about the ChIP-seq datasets used. CTCF-bound sites are shown as red and green vertical

lines and the orientation is indicated. PAX5-bound sites are shown as blue vertical lines. Elements of the Igh locus are indicated above the data tracks. Figure not to scale.

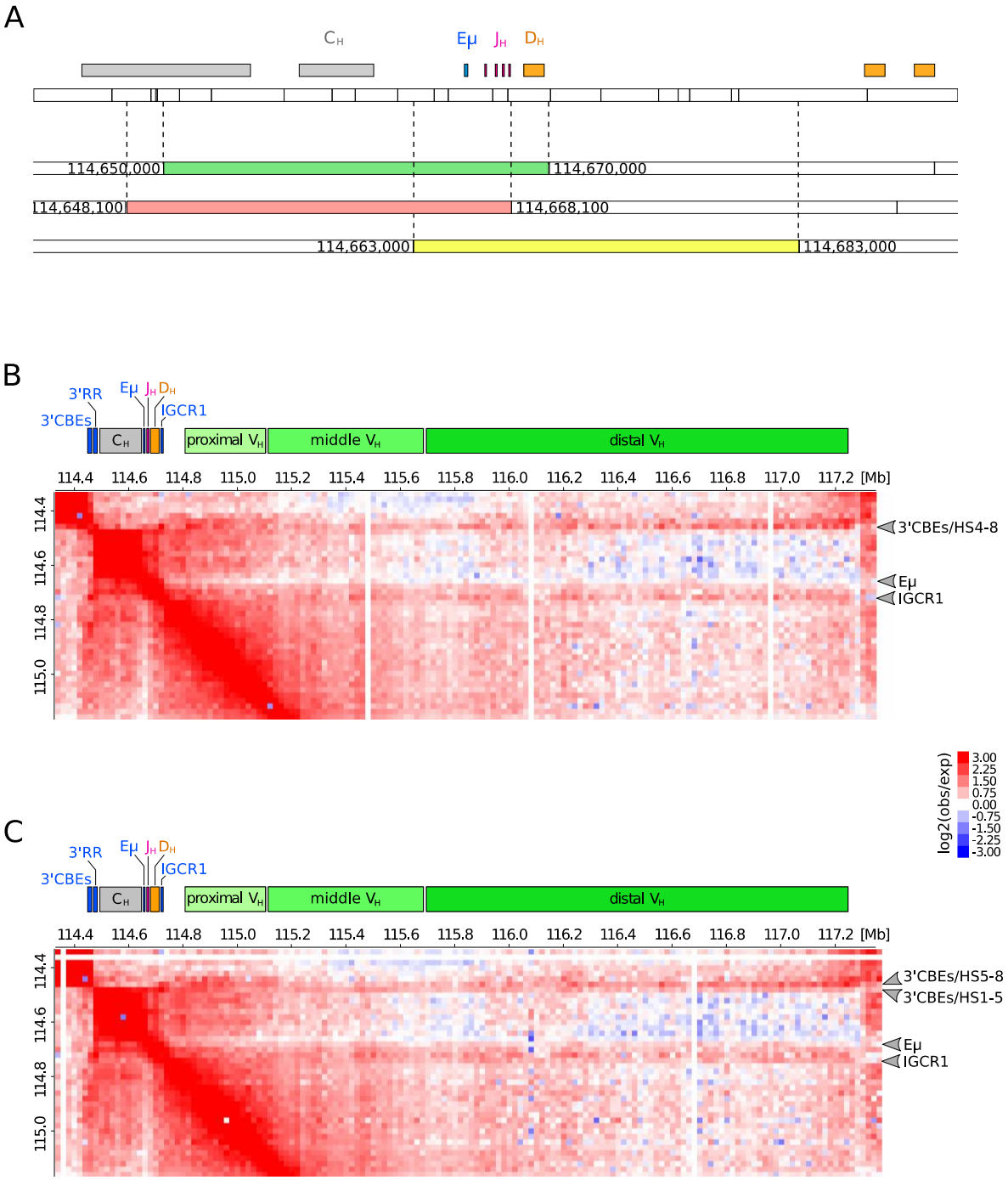

Figure 37. The bin containing the Eμ loops out of the 3' domain regardless of its position towards the D region or towards the constant region. Capture Hi-C data was re-analysed using HOMER function *analyzeHiC* with *–simpleNorm* option to correct for coverage. The re-analysis was done twice with different binning strategies. **A.** The alternative binning strategies of the Igh baited region. The green horizontal bar shows the original position of the Eμ-containing bin as well as neighbouring bins as per figure 15. The red horizontal bar shows the position of the Eμ-containing bin shifted 1.9kb downstream to exclude D genes. The yellow horizontal bar shows the position of the Eμ-containing bin shifted 7kb upstream to exclude C genes. The coordinates of each Eμ-containing bin are indicated on both sides of the horizontal bars. The annotation of white bars above shows all HindIII fragments in this region. **B.** The interaction matrix generated in HOMER using the binning strategy where the Eμ resides in a bin with the constant genes (red bar in A). The matrix layout is as

described is figure 15. **C.** The interaction matrix generated in HOMER using the binning strategy where the Eμ resides in a bin with the D genes (yellow bar in A).

3.3.5. Distal V genes form a tightly looped subdomain

Another distinct feature of the Igh spatial organisation in pro-B cells that emerged from Capture Hi-C data is a large domain in the 5' half of the locus encompassing most of the distal V genes (**Figure 25**A). This domain starts at 115.83Mb (arrow 8) just upstream of the J606 and Vh10 gene families and ends after the last V gene at 117.25Mb (arrow 9). It is also clearly enriched in the distance corrected matrix in pro-B cells, showing that these loops are very frequent despite being very long-range (**Figure 30**A). The enrichment for intra-distal V domain interactions escalates after the J558.26.116 (**Figure 27**C), which is the third most frequently used V gene in V(D)J recombination (Bolland et al. 2016). This distal V domain is less clearly defined in the thymus, but there is still enrichment for longer-range interactions as well as very frequent shorter-range interactions. Also, in the thymus, I noted a domain in the middle of the locus from 115.27Mb to 115.91Mb, encompassing middle Vs and the first distal Vs, that is characterised by a classic long-range DNA loop in the form of a radiating point (**Figure 25**B and **Figure 30**B). This is completely absent in pro-B cells and replaced by a more uniform continuum of interactions between the middle Vs and the 3' anchors. Both this large mid-locus loop and the lack of fully enriched distal V domain exemplify a lack of continuity in the looping of the Igh TAD, and therefore lack of locus contraction, in the thymus.

In pro-B cells, the middle of the locus (between the proximal V and the distal V domains) does not seem to have strong subdomains, but one could consider putative subdomains characterised by slightly less frequent interactions. A subdomain larger than the 3'CBEs-proximal V genes domain can be discerned stretching from the D genes at 114.67Mb to the last S107 gene (S107.4.66) at 115.45Mb (**Figure 25**A arrow 6). This subdomain might even extend all the way to the end of the middle Vs at 115.61Mb, where J606 genes start (arrow 7). Another possible small subdomain might start over the last middle V gene near SM7.4.63 at 115.41Mb, slightly overlapping with the previous subdomain (2 bins above arrow 6), and end at the beginning of distal V genes at 115.89Mb, a couple of bins into the distal V domain (below arrow 8). These subdomains however blend into the overall structure of a contracted, highly looped locus (**Figure 26**F and **Figure 27**A). The proximal and middle Vs contact the distal V domain as frequently as they contact each other.

These findings suggest that a tightly looped distal V domain might be a more rigid structure that moves as a unit to contact the 3' end of the locus. This could provide distal Vs with an architectural advantage and contribute to the fact that the distal Vs interact with the D gene region with the same frequency as the proximal and middle V genes do. This would give all distal V genes a similar opportunity to recombine. Taking into account the considerable frequency of interactions already present in the distal Vs in the thymus, this domain might be a largely pre-defined structure, that only 'closes up' in pro-B cells.

3.4. Polymer modelling gives all possible single structures of the Igh locus

Capture Hi-C was performed using millions of cells, and detected only interactions taking place in the nuclei at the time of cross-linking. It is therefore an ensemble of snapshots of chromatin conformations that provides valuable insights into the most frequent interactions in the genome. This gives a reliable picture of overall genome organisation and for many loci it provides exact information about interacting regions, as the most frequent interactions often directly translate to the functionality of given genomic elements in particular cell types. For example, the well studied interactions between the β-globin genes and multiple clustered HS sites in the haemoglobin beta (Hbb) locus are erythrocyte-specific, very frequent and reflect the transcriptional state of the haemoglobin beta gene in these cells (Tolhuis et al. 2002; Palstra et al. 2003). In pro-B cells however, one expects a much more heterogeneous landscape of DNA interactions precisely because the functional outcome of these interactions, a recombined V(D)J product, involves different genes in different pro-B cells. Therefore, the spatial organisation of the Igh locus most likely differs from cell to cell. It is possible to do Hi-C in single cells (Nagano et al. 2013), but so far the resolution obtained from single cell Hi-C experiments allowed only for re-constructing the shape of a whole chromosome (1Mb bins) and TADs (100kb bins) (Nagano et al. 2017; Stevens et al. 2017). Theoretically, single cell Hi-C can give rise to two proximity ligation products per restriction fragment (one for each end) per chromosome (allele). In practice, after filtering out spurious uninformative read pairs inherent to Hi-C methods, single cell Hi-C to date was only able to detect ~2% of all possible genomic interactions in a cell. For the 887 HindIII fragments in a single Igh locus, that would give just 35 contacts per cell. Moreover, it would likely be much fewer than that, because the mappability of the Igh is poor compared to the rest of the genome. The additional challenge is posed by the lack of full Igh locus sequence assembly in a mouse strain other than C57BL/6, which is essential for reconstructing single loci in single cells using F1 hybrids.

To gain an insight into potential single Igh structures, I collaborated with Luca Giorgetti and Yinxiu Zhan at the Friedrich Miescher Institute for Biomedical Research who performed polymer modelling simulations on Capture Hi-C matrices. Modelling of chromatin structure using models from polymer physics has recently been successfully applied to gain more in-depth information from ensemble chromosome conformation capture experiments (Giorgetti et al. 2014; Chiariello et al. 2016; Beagrie et al. 2017; Stevens et al. 2017; Nagano et al. 2017; Barbieri et al. 2017). Yinxiu Zhan applied a polymer modelling algorithm previously developed by Luca Giorgetti to elucidate the structure of the X chromosome inactivation centre (Giorgetti et al. 2014), to the coverage corrected interaction matrices from pro-B cells and thymocytes (**Figure 25**A and B). The model simulated all possible single structures of the Igh locus that might be present in single cells. While the two Igh alleles may have differing conformations in wild type pro-B cells undergoing recombination (Roldán et al. 2004), the

two loci might be more similar in $Rag^{-/-}$ pro-B cells as they are both poised for recombination (Sayegh 2005).

Using this method, together with the high depth of sequencing of the Capture Hi-C libraries, it was possible to model the Igh locus at 20kb resolution. Out of all 156 20kb bins in the Igh baited region only the bins exactly over the Igh locus elements were used in modelling. These are bins from the HS8 to the last V gene (114.45-117.27Mb) and have been assigned numbers from 0 to 139 (**Table 11** first column). Hereafter, these 140 20kb bins are referred to as beads, as the polymer model describes the DNA strand as a chain of beads.

The polymer model

The chromatin fibre was described as a self-avoiding polymer and Capture Hi-C interaction frequency data was used to define the interaction energies of each of the 140 beads. The distance between the beads was $a=20kb$ (distance between the centres of the beads). The polymer model has very few rules: (1) the beads comprising the polymer fibre are continuous, (2) the beads cannot be superimposed (two DNA fragments cannot be in exactly the same place at the same time) and (3) there are no spatial constraints for the overall structures. The first rule is met by the fact that the baits covered all HindIII fragments in the Igh locus. For the second rule, a hard core repulsion energy has been determined experimentally to be equal to $0.6a$ (Giorgetti et al. 2014) and beads cannot be closer than $0.6a$ to one another. Incorporating these rules and taking Capture Hi-C interaction frequencies of all beads, each bead was described by a potential (energy) that has two contributions: (1) the hard core repulsion of $0.6a$ and (2) the interaction between two beads is considered specific only if they are $1.5a$ away or closer and they interact with a specific energy Ef.

A set of possible single conformations that reflects the Capture Hi-C contact map can be obtained by finding Ef values for all pairs of beads. The model extracts the interaction probabilities of all bead pairs, which is the fraction of single conformations where a given bead pair interacts significantly. The interaction probabilities are proportional to the Capture Hi-C interaction counts and a good estimation of the proportional constant is the median of Capture Hi-C interaction counts between adjacent beads, because they are likely to be always in contact. Therefore, the contact probability for adjacent bins is $p=1$. To get all Ef values for each bead pair (i.e. all single conformations, as every conformation is composed of Efs between every bead pairs) the model starts with random values to generate a set of single conformations that it compares to the Capture Hi-C contact map. The Ef energies are iteratively optimised until the single conformations, when pooled together, resemble the ensemble Capture Hi-C interaction map (**Figure 38**). In every single conformation one can identify significant interaction partners (bead-to-bead distance $<1.5a$) of each bead. Due to the large size of the Igh locus the optimisation was performed separately on two 1.4Mb halves of the contact matrix and merged for final optimisation of the whole dataset until the full simulated matrix reached convergence with the experimental matrix (**Figure 39**).

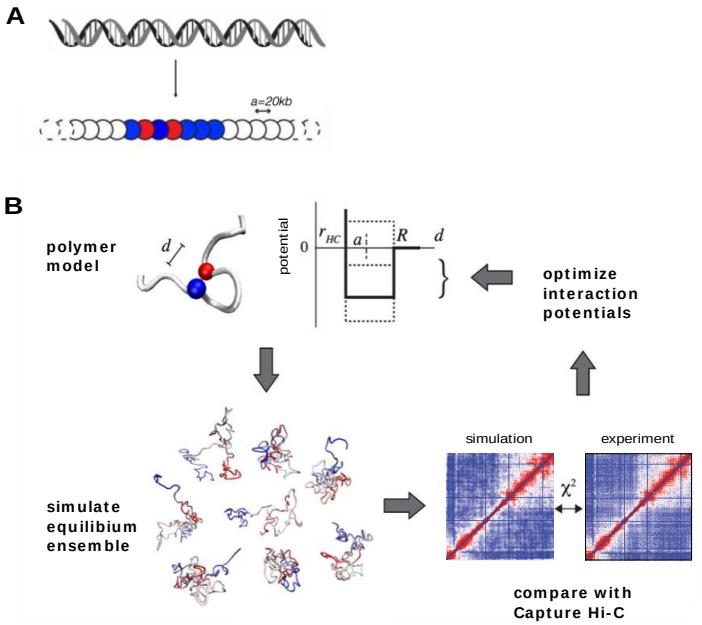

Figure 38. Overview of the polymer modelling method. A. Chromatin fibre is treated as a string of beads, where adjacent beads correspond to consecutive 20kb of DNA sequence. There is no separation between beads. **B**. Structural deconvolution of Capture Hi-C interaction frequencies by the polymer model. Pairs of beads interact via short-range interaction potential (thick line). The model is constrained by the fixed distance between adjacent bead centres ($a=20kb$). Each model gives a measure of the pairwise distances between beads (d). $R=1.5a$ is a radius of a physical interaction (attraction), whereas $r_{HC}=0.6a$ is a hard-core repulsion radius (repulsion). Monte Carlo sampling simulates the equilibrium ensemble of conformations and contact probabilities are compared to experimental Capture Hi-C interaction frequency map using chi^2 (χ^2) as a dissimilarity score. Interaction potentials are iteratively optimised by further sampling (dotted lines) until simulated equilibrium ensemble converges with the experimental data. (Adapted from Giorgetti et al. 2014).

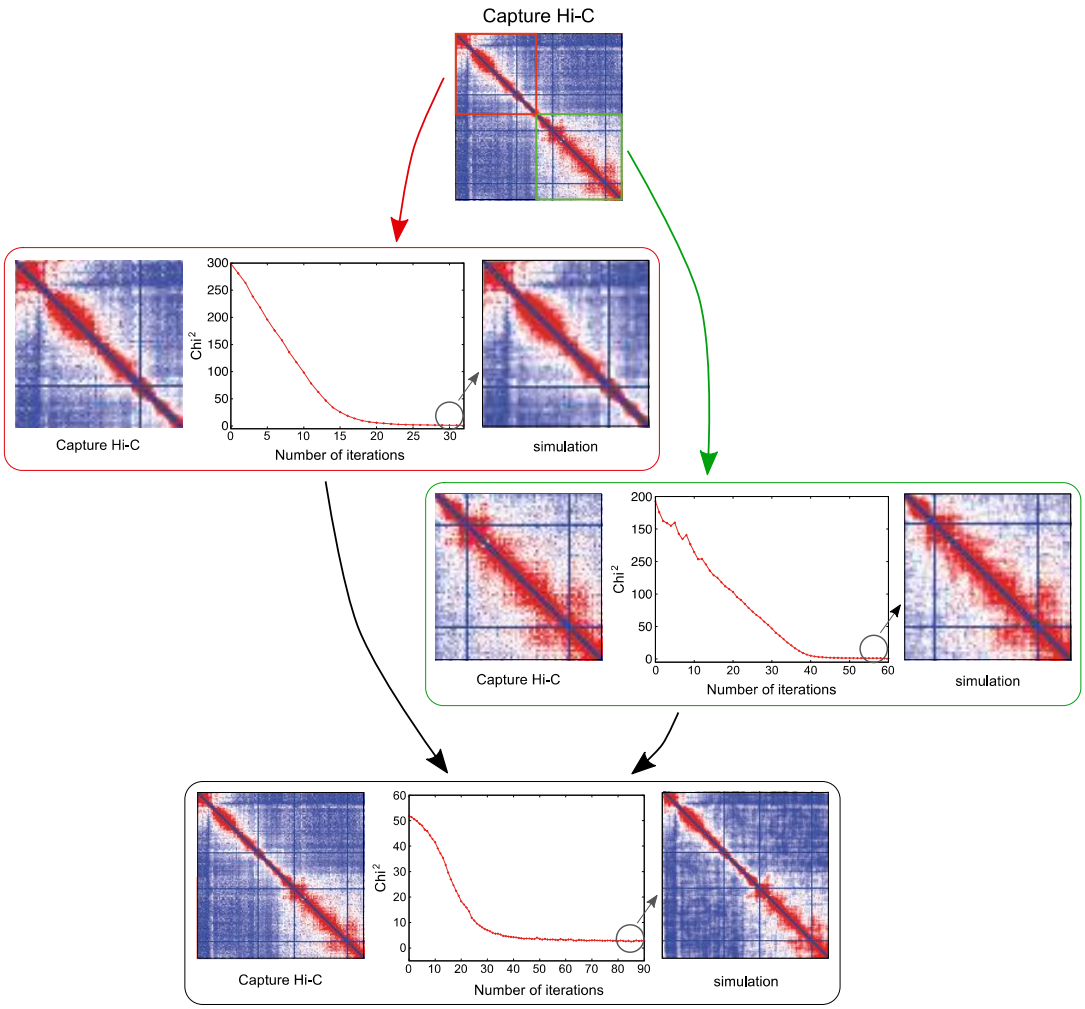

Figure 39. Convergence of Capture Hi-C maps and polymer models was performed in two steps. Capture Hi-C contact map was split into halves (green and red squares) and each of the smaller maps was simulated separately until convergence between Capture Hi-C and modelling was achieved using chi^2 as a measure of dissimilarity (middle graphs, grey arrows). The two converged parts were put back together and run to achieve final overall convergence (bottom panel). Each iteration corresponds to one full Monte Carlo sampling of fibre conformation after 1000 modifications to interaction potentials.

3.4.1. There is no single dominant structure of the Igh locus

The simulations of single structures revealed that the Igh locus conformations are a heterogenous ensemble and there is no one dominant structure favoured in the majority of cells. Two measures of structure similarity have been applied: (1) the root mean squared difference in bead-to-bead distance for all beads and (2) overlap of significant (<1.5a) bead-to-bead interactions between any two conformations (**Figure 40**). All 5001 single structures produced by the polymer model were sufficiently different to form multiple arches in the clustering dendrogram and not to form distinct privileged conformations either in pro-B cells or in thymocytes.

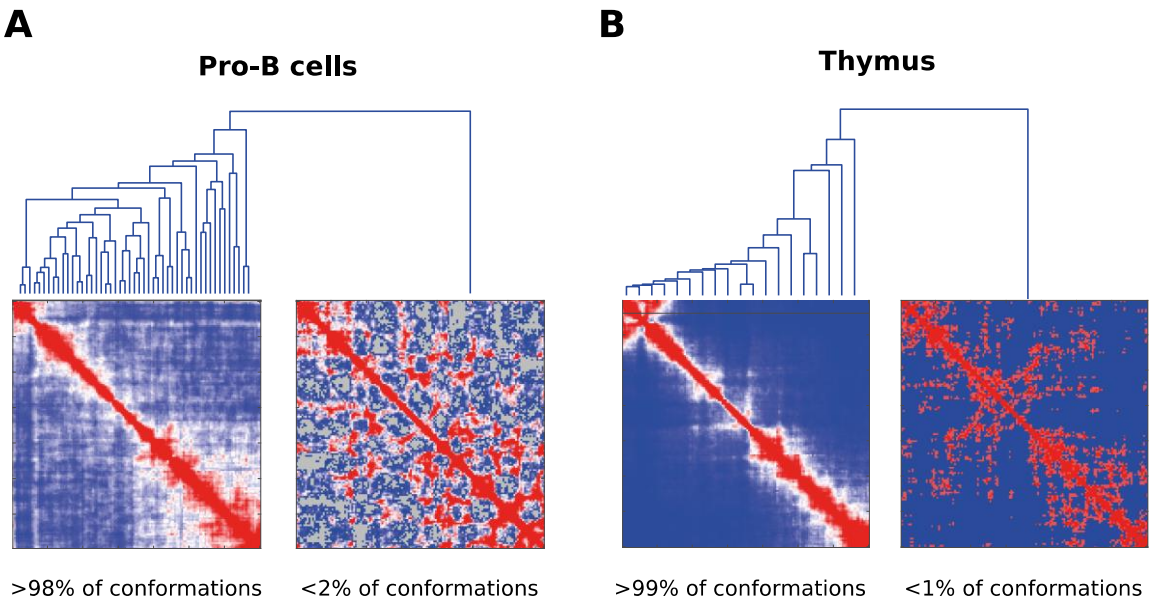

Figure 40. There is no one dominant structure describing the Igh locus either in pro-B cells (A) or in thymocytes (B). 5001 single structures have been generated by the polymer model and clustered using the root mean square distance between bead pairs as a dissimilarity score. ~99% of conformations clustered into one cluster of multiple very similar structures and there is no clear separation into groups of distinct conformations.

The simulations show that each 20kb bead contacts (bead-to-bead distance <1.5a) on average ~20 other beads in each single conformation (**Figure 41**). Beads 3-10, containing the constant genes C_H and the Eμ, contact fewer beads than an average bead. The same was observed for beads 44-46 in the middle of the locus (115.33-115.39Mb), beads 58-64 (115.61-115.75Mb), bead 15 containing the DFL16.2 and bead 120. On the other hand, the 3'CBEs/HS4-8 (bead 0) and the IGCR1 (bead 13) make more contacts than an average bead (**Figure 41**). Some beads in the distal V region make more contacts than average, but most are involved in an average number of contacts as they interact highly only within the distal V domain and with beads 0 and 13, but with low frequency with all other beads. In the single conformations generated for thymus data, each bead contacts on average ~10 other beads, with the Eμ and the constant region C still contacting fewer beads than average. These observations confirm that the simulated single structures recapitulate well the experimental interaction maps.

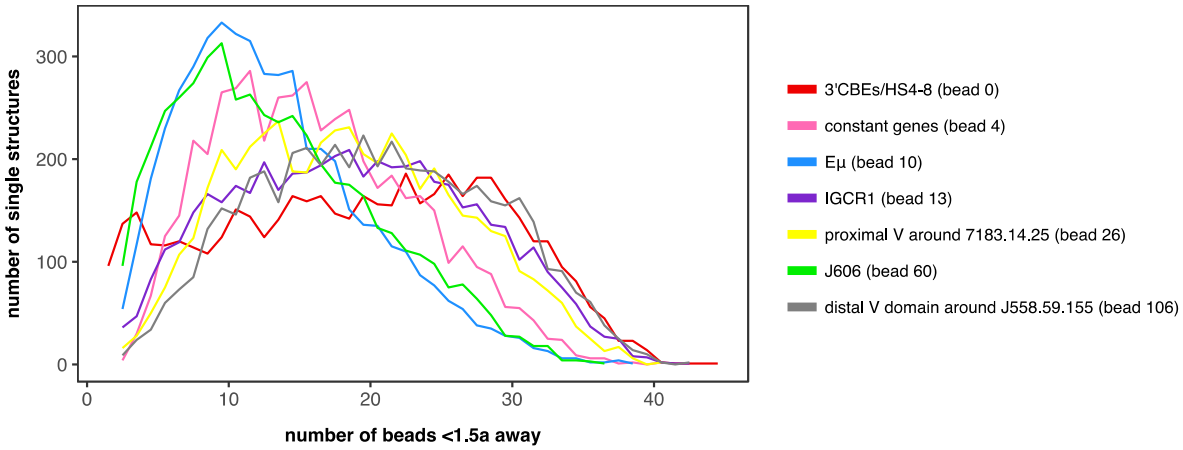

Figure 41. The number of contacted beads in single structures varies between the Igh elements. The distribution of the number of interactions (distance between bead pairs *<1.5a*) made by every bead in all 5001 single structures was calculated and plotted for selected beads. Bead reference is in table 11.

Next, the number of V beads contacted by each bead in the Igh polymer was determined to further show the overall more compacted Igh conformation in pro-B cells compared to the thymus. A significant interaction with a V bead was defined as 1.5a bead-to-V bead distance. Contacts with V beads were summed for each bead in all single structures and divided by the 5001 simulated single structures to obtain a fraction of contacted V beads (**Figure 42**). Interestingly, the V beads exhibit largely the same pattern of contacts with other V beads in both pro-B cells and thymus, albeit with decreased frequency in the thymus. Conversely, the 3'CBEs and the IGCR1 beads had a markedly different pattern of interactions with Vs in pro-B cells and in thymocytes. The 3'CBEs and the IGCR1 beads showed 4 times smaller differences in the number in contacted V beads in the thymus than in pro-B cells relative to the number of Vs contacted by the Eμ bead. This illustrates, in a different manner compared to previous studies, the overall compaction of the Igh locus in pro-B cells compared to thymocytes and that the D region and the 3'CBEs superanchor position themselves closer to the V genes in pro-B cells. A novel observation demonstrates that the V region makes largely the same contacts in both cell types but with markedly different frequencies, suggesting a residual pre-existing folding of the V genes.

Similarly, polymer modelling allowed for the investigation of the probability of a V bead (18-120) contacting any D bead (11-13) as a proxy of V-D recombination probability. Beads 11, 12 and 13 were defined as 'D beads' and bead 10 was not, as it contains constant genes and the Eμ. Although it does contain DQ52, I've shown that the interaction pattern of an Eμ-containing bin is markedly different from D-containing bins (**Figure 37**). The probability of a V-D interaction has been expressed as a frequency of a V bead contacting (<1.5a) any of the three D beads in all single structures. This was only possible thanks to simulated single conformations and could not be extracted directly from Capture Hi-C matrices.

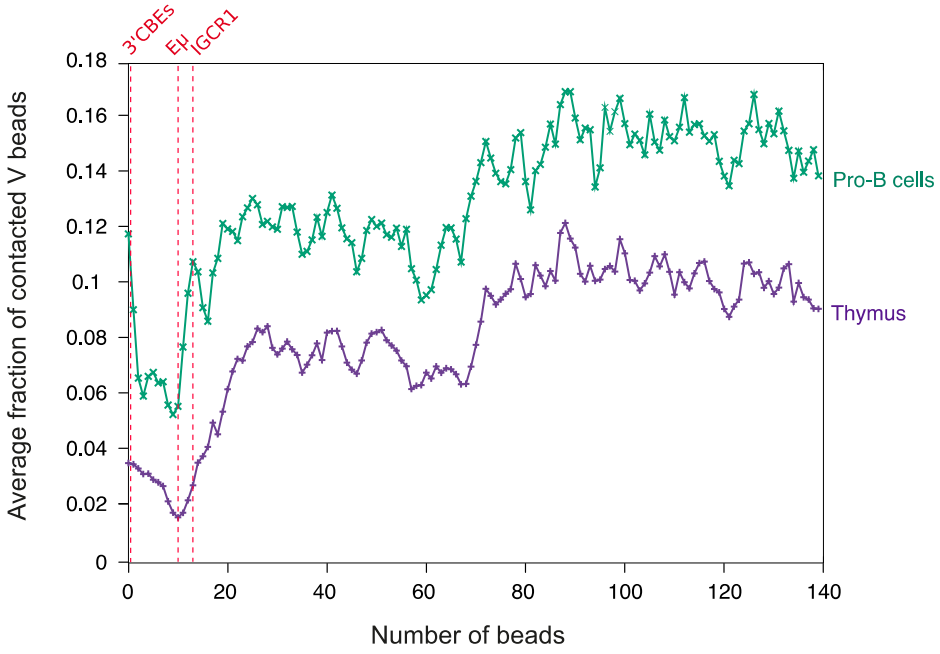

Figure 42. The pattern of interactions with V beads is similar in pro-B cells and in thymocytes. For each bead 0-139 in the modelled Igh region (Table 11), the number of contacted (*<1.5a*) V beads was calculated in each single structure and was expressed as a fraction of all V beads. A average of all single structures in shown. Vertical dashed red lines denote the position of 3' regulatory elements.

First, the V gene-containing beads were shown to make an overall similar number of significant interactions with the D beads when summed for all single structures (**Figure 43**A). This can also be observed in the interactions matrix as all Vs interact with similar frequencies with the IGCR1 and downstream D bins (**Figure 25**A). Second, the interactions were also largely equally shared between the three D beads (11-13), showing a slight increase towards the IGCR1 bead 13 (**Figure 43**B). Third, there were on average ~30 V-D interactions in each single Igh structure (**Figure 44**), which shows that the 60kb D region contacts multiple V genes simultaneously.

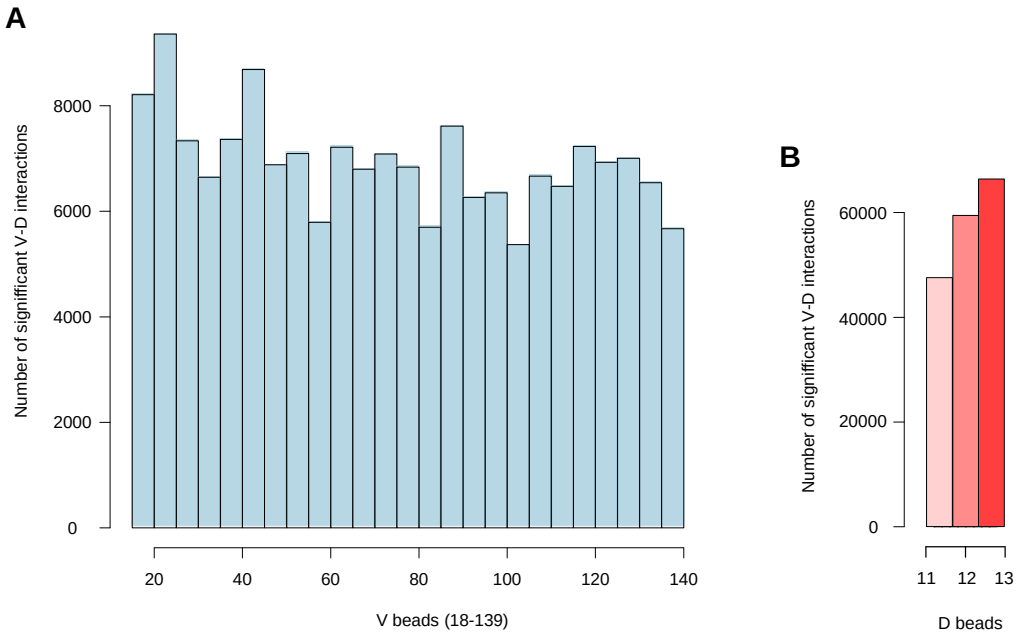

Figure 43. V beads are involved in a similar number of V-D interactions. For each V bead (18-139) (A) and each D bead (11-13) (B) the number of V-D interactions (<*1.5a*) in all 5001 simulated single structures was calculated and plotted as a total.

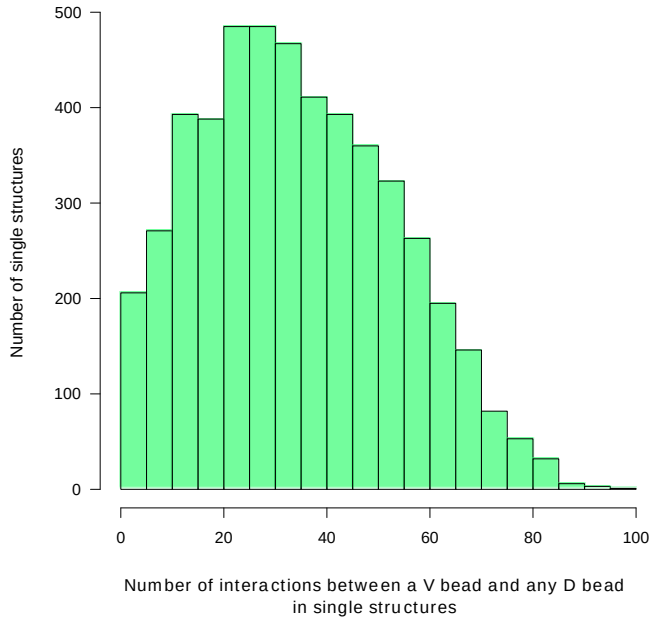

Figure 44. The D beads contact around 30 V beads at a time in every Igh structure. The frequency distribution shows the number simulated single structures that contain a given number of V-D interactions (<*1.5a*).

These findings give a first glimpse into potential single conformations of the Igh locus that might be present in single cells. Ensemble Hi-C does not allow for elucidating simultaneous or mutually exclusive interactions, whereas simulations are able to optimise the interaction parameters using contact frequency information and to re-construct a pool of possible individual structures. I have shown that the Igh locus assumes a slightly different

conformation in every cell (single cells being synonymous with single simulated structures, with the caveat that they represent an average of two Igh alleles in each cell), but the V genes contact the D genes with similar frequencies. This equally high interactivity of V genes reflects the purpose of V(D)J recombination to provide a large diversity of immunoglobulins thanks to recombining ~200 genes in different combinations. Indeed, one current model proposes an 'equal opportunity for all' V genes to have a spatial possibility to recombine (Medvedovic et al. 2013; Lucas et al. 2014; Benner et al. 2015). Other models favour the idea of major predominant interactions that define the structure of the Igh locus (Gerasimova et al. 2015, Montefiori et al. 2016). However, these models might not be mutually exclusive as I discuss in section 3.5.

3.4.2. 'Equal opportunity for all'

To further investigate the relationship between V-D interactions and V(D)J recombination, published datasets for V gene usage frequency and CTCF binding to the Igh locus were utilised.

First, we used the recombination levels of V genes in the primary antibody repertoire in pro-B cells as measured by VDJ-seq (Bolland et al. 2016). The recombination frequency of a V bead, referred to here as recombination score, was determined by taking the average of recombination frequencies of all active V genes in that bead. Active V genes were identified by a binomial test on their primary recombination read counts and then used as a binary attribute (Bolland et al. 2016). There was a positive correlation between the V-D interaction probability and V bead recombination score (**Figure 45**A). It must be borne in mind that often V genes next to each other have vastly different recombination frequencies and therefore an average is a broad approximation. When a subset of beads containing only a single V gene (62 beads out of 94) was analysed, there was no correlation between the V-D interaction probability and V gene recombination score (**Figure 45**B). The correlation in the average dataset was not very strong and could be due to highly recombining V genes 7183.2.3(81X) and Q52.2.4 in the first V bead. Nevertheless, the beads in the orange and red boxplots, which correspond to higher recombining genes, do seem to have overall more frequent interactions than the beads in green and yellow boxplots containing lower recombining genes (**Figure 45**B). This indicates that there might be a group effect, rather than a linear correlation. In conclusion, there is not a strong correlation between V-D interactions and recombination, and further experiments are needed at single V gene resolution to determine the advantage of frequently interacting V genes.

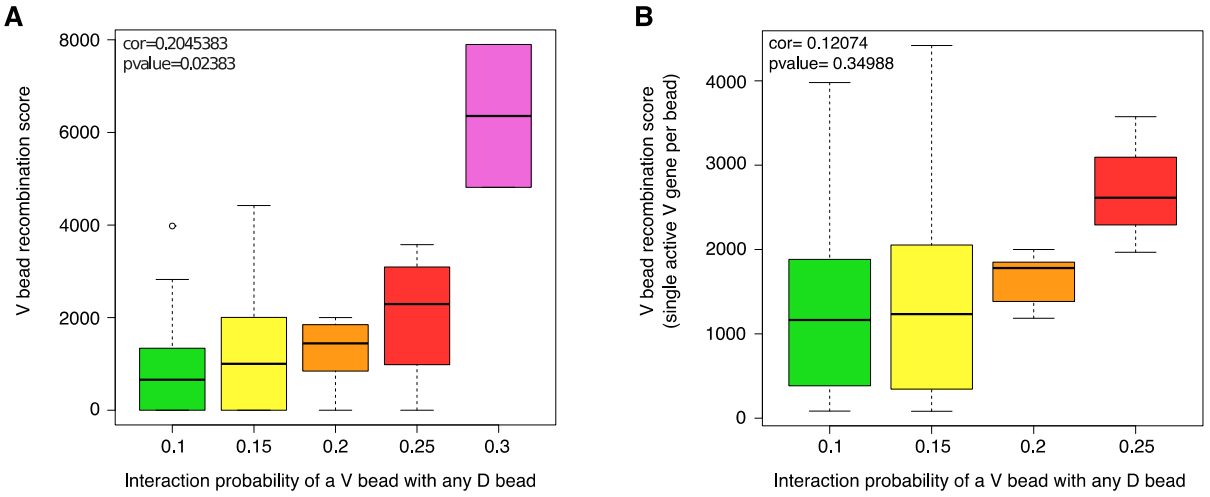

Figure 45. Correlation between V-D interaction frequency and V recombination levels. The probabilities of V-D interactions were calculated as a fraction of single simulated structures in which a given V bead contacts (*<1.5a*) at least one D bead (11-13). The X axis shows the V-D interaction probabilities split into groups of V genes with increasing contact probability. The Y axis shows the V bead recombination scores calculated as an average of recombination levels of all V genes in the 20kb beads as measured by VDJ-seq in Bolland *et al.* 2016. **A.** Correlation between V-D interaction frequency of all V beads and the V bead average recombination score. **B.** Correlation between V-D interaction frequency of V beads containing one active V gene only and the recombination level of that V gene. Pearson's correlation coefficient and p-value are indicated in the top left corner of the graphs.

Second, many regulatory mechanisms have been linked to V gene usage in V(D)J recombination, including the quality of the RSSs and chromatin states characterised by particular signatures of protein binding and histone modifications at the RSSs (Bolland et al. 2016). The proximal and middle V genes have CTCF-binding sites precisely at their RSSs, whereas in the distal V region the CTCF sites are largely intergenic. CTCF binding levels in the V beads were determined as an average of ChIP-seq peak summits called by Hashem Koohy using a published dataset (Ebert et al. 2011). I was interested in a relationship between the CTCF binding levels and V bead interaction probability with D beads. Encouraged by the anchor-like profile of the IGCR1 interacting with all V genes, I hypothesised that CTCF-binding in the V region may act as an architectural enabler for the V genes to contact D genes as well as a more precise qualifier for active recombination for the proximal and middle V genes (Bolland et al. 2016). There was a positive correlation between CTCF signal intensity in the V beads and the V bead recombination score (**Figure 46**A), but there was no correlation between CTCF signal intensity and V-D interaction frequency (**Figure 46**B). This shows that CTCF-binding levels increase the chances of V gene usage in V(D)J recombination but do not contribute to interaction frequency.

Overall, these data support the 'equal opportunity for all' model by demonstrating that recombination frequency does not depend on interaction frequency and that all V beads interact with D beads with very similar frequencies. Additionally, CTCF-binding correlates

with recombination levels supporting local CTCF role in V gene usage, but not influencing V-D contacts.

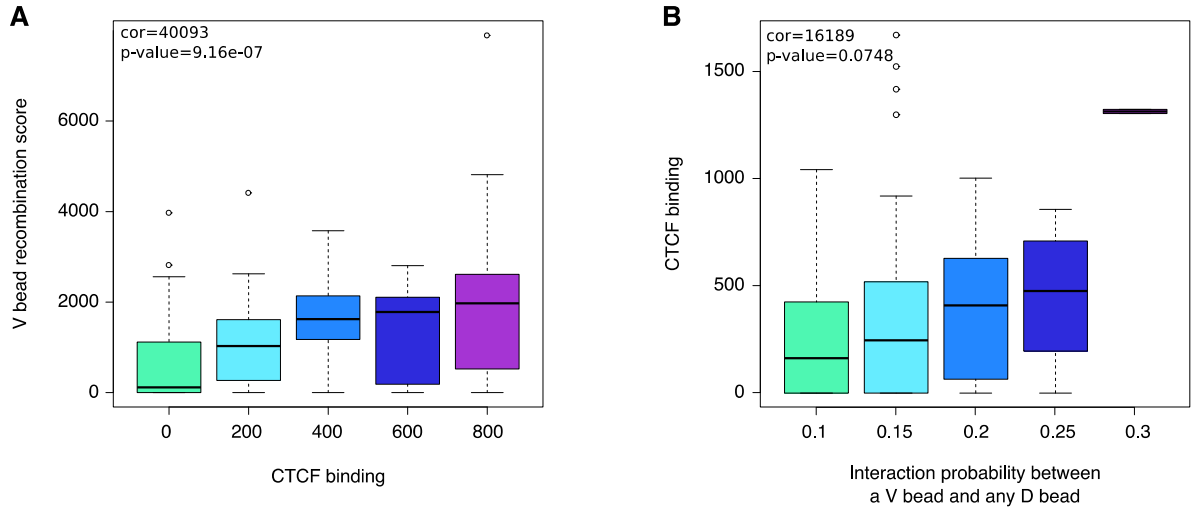

Figure 46. Recombination levels but not interaction frequencies positively correlate with CTCF binding. The V bead recombination scores were calculated as an average of recombination levels of V genes in the 20kb beads as measured by VDJ-seq in Bolland *et al.* 2016. The probabilities of V-D interactions were calculated as a fraction of single simulated structures in which a given V bead contacts (*<1.5a*) at least one D bead (11-13). The CTCF binding levels in the V beads were determined as an average of ChIP-seq peak summits in each V bead. See methods section 2.11 for peak calling and the dataset used. **A.** Correlation between the recombination score and CTCF binding levels for all V beads. **B.** Correlation between the V-D interaction frequency and CTCF binding levels for all V beads. Pearson's correlation coefficient and p-value are indicated in the top left corners.

3.4.3. New concept: centre of mass is over distal V genes and interactions preferentially occur on the periphery of the V region

Another advantage of the application of polymer modelling is that we could investigate where physically in the single structures the V-D contacts take place. To this end, we determined that the centre of mass (CM) of the Igh structures in pro-B cells is over the distal V domain (**Figure 47**A). This is largely preserved in thymocytes, albeit not for the most distal V beads (**Figure 47**B) The centre of mass is a physical property of the chromatin fibre and is defined as an average of all bead coordinates (avg x, avg y, avg z) in a given single structure and then averaged over all structures. The distal V domain is very large and frequently interacts within itself, which greatly contributes to the average bead position. Overall, the distances from the CM were much shorter in pro-B cells compared to thymocytes, which further corroborates the compacted or extended locus structures in these cells, respectively. In pro-B cells, out of all 3' elements the 3'CBEs/HS4-8 and the IGCR1 were the closest to the centre of mass (**Figure 47**A). The proximal V beads 18-33 also tend to be closer to the centre of mass. On the other hand, beads 2-10 containing the constant genes, the Eμ and J genes, were positioned further from the centre of mass in most conformations, as determined by an empirical distance cut off of *2.2a*. Also, among the V genes, beads 57-62 containing the J606 gene family, as well as several other beads (35-36, 46-47 and 67) were positioned further from the centre of mass.

Next, we considered V-containing beads only (18-139) and determined the centre of mass of the V beads (CM_V) by calculating the gyration radius (Rg) of a sphere that encompasses V beads. Next, we determined the distance (d) of D beads from the CM_V. Therefore, a V-D interaction can be described as occurring near the periphery of the V beads when d/Rg=~1 and near the centre of the V beads when d/Rg=~0. For each V bead, the median d/Rg revealed that V-D interactions preferentially occur near the periphery of the V gene 'sphere' as shown by the distances in the range of 0.75-1 Rg (**Figure 48**A). Additionally, the distance from the CM_V was positively correlated with V bead recombination scores (**Figure 48**B), further supporting the result that V-D recombination takes place on the periphery of V beads, and the D region in not buried within the V region.

These results have shown that the centre of mass of the entire Igh locus is over the V region, and the centre of mass of V genes only was used to demonstrate that V-D interactions are more likely to occur at the periphery of the V region. This analysis was only possible thanks to polymer modelling of single Igh conformations and is unattainable from ensemble Hi-C matrices.

In the light of the presented data, the recombination centre (i.e. where the RAG complex binds and the rearrangement takes place) is not synonymous with the centre of mass (neither the CM nor the CM_V). Previous studies speculated that Eμ, D and J genes reside in a viscoelastic cavity surrounded by equidistant V genes that bounce back and forth until a synapse is formed. Indeed, I have shown that the D beads simultaneously interact with ~30 V beads in each simulated Igh structure. However, a V-D interaction is more likely to occur near the periphery of the V gene region. The D beads may be surrounded by multiple V genes, but are not embedded near CM_V.

I propose that different V genes have different strategies for gaining access to D genes. The proximal V genes belong to a small subdomain encompassing the 3' end of the Igh locus and therefore have to be insulated by the IGCR1 to prevent them from dominating the recombination events. The middle V genes loop more flexibly to the D region and the distal V genes are organised in a domain that might be more rigid and move as a unit towards the D genes to give all distal Vs the opportunity to recombine. Of course it is equally likely that the D region moves towards the distal V domain as we cannot elucidate the actual direction of the movement. Lastly, remarkably, the regions of the locus that are away from centre of mass are the exact regions that are highly enriched for contacting other genes genome-wide (in *trans*) (discussed in chapter 4) (**Figure 47**A red and **Figure 69**).

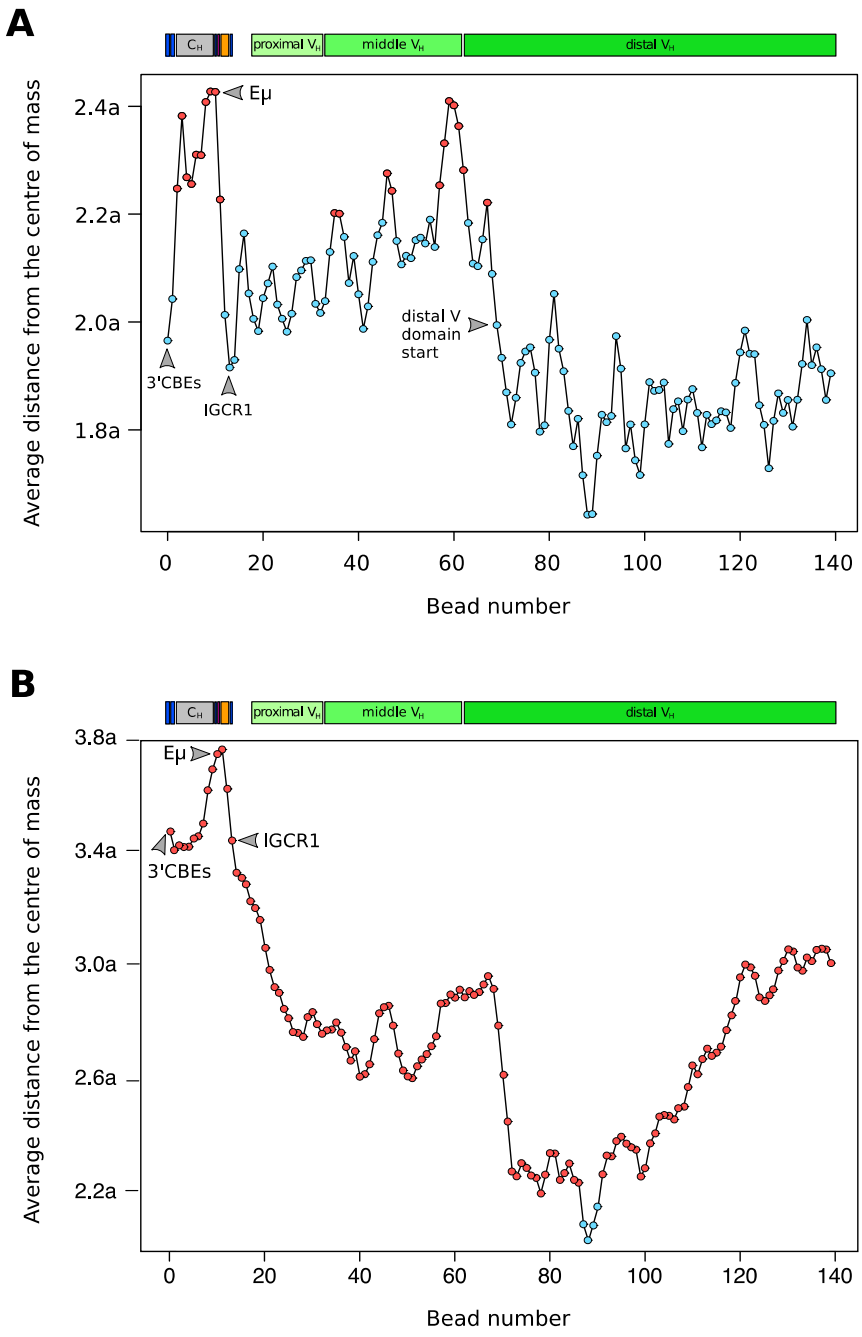

Figure 47. Relationship between 20kb beads and the centre of mass in single structures. The centre of mass (CM) of each simulated single structure was determined as an average of coordinates of all beads in the structure. The distance from the CM was measured in multiplications of bead size *a* (*0-2.4a*) and averaged for 5001 simulated single structures for every bead. The distance of *2.2a* was chosen to identify outlier beads far from the CM. Grey arrows indicate beads of interest. **A.** The distance from the CM of all beads in pro-B cells. Beads far from the centre of mass are depicted in red and the rest of the beads in blue. **B.** The distance from the CM of all beads in thymocytes. The cut-off for the red and blue annotation (*2.2a*) is the same as in (A) for comparison purposes only, and not actual outliers from the CM in thymocyte structures.

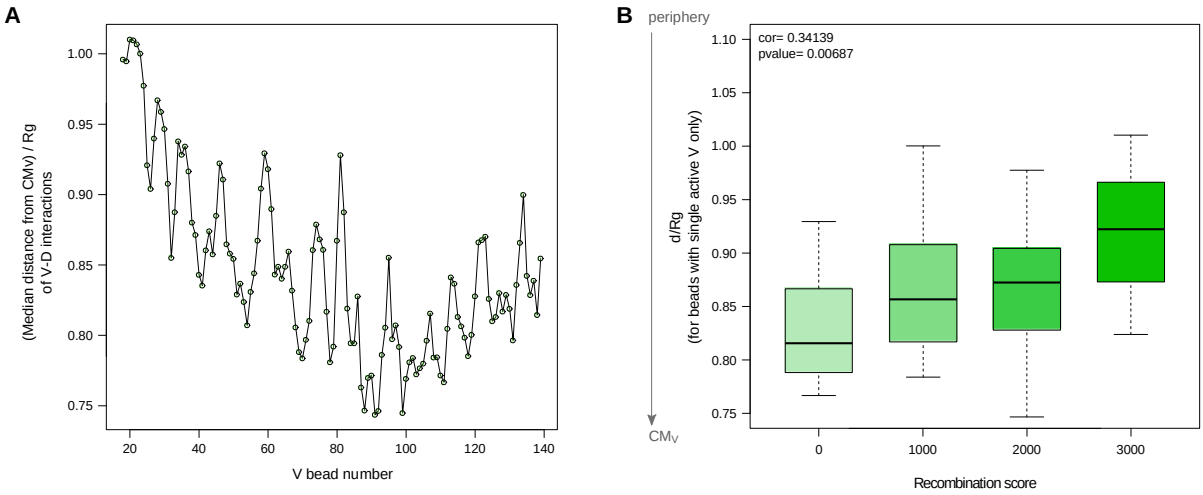

Figure 48. V-D interactions preferentially occur on the periphery of V genes. The centre of mass of the V beads only (CM_V) was determined using a gyration radius of a sphere that encompasses V beads. **A.** The Y axis shows the measure of distance from the periphery of V beads: when the V-D interaction occurs close to the V bead periphery the measure (distance/Rg) is ~1, whereas when the V-D interaction occurs far from the V bead periphery (close to the CM_V) the measure (distance/Rg) is ~0. **B.** Recombination frequency positively correlates with V-D interaction's distance from CM_V for beads containing a single active V gene. Pearson's correlation coefficient and p-value are indicated in the top left corner of the graph.

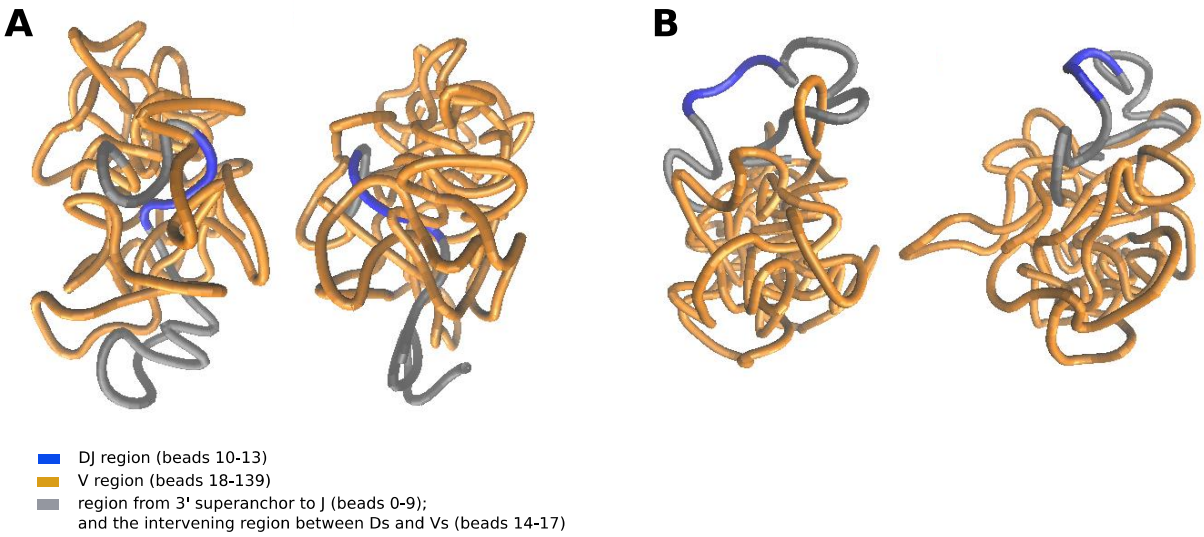

Figure 49. Example simulated Igh structures. Two structures with the DJ region most internal (A) and most external (B) out of all 5001 simulated conformations. The structures were generated in VMD software.

3.5. Discussion

First unbiased all-to-all contact frequency map of the Igh locus

The work presented in this chapter has elucidated the 3D spatial conformation of the Igh locus and thereby achieved aims 1, 2 and 3 of this thesis (section 1.6). This is the highest resolution study of the spatial organisation of the Igh to date and provides the first truly unbiased all-to-all interaction frequency map. Capture Hi-C possesses key advantages over other 'C' methods, such as an unbiased bait enrichment system compared to inefficient primer design for 5C, an enormous benefit of enriching for all restriction fragments in the locus compared to several hand-picked viewpoints in 4C, and achieves a similar or greater resolution. This is the first Hi-C-based study of the Igh locus to apply bias correction, which overcomes uneven mappability and therefore read coverage of the locus, which may have influenced previous studies.

I utilised the potential of selective enrichment of Hi-C libraries to obtain a deeper sequencing read coverage over the repetitive and therefore poorly mappable 2.8Mb Igh locus. At the time of my experiments, this was by far the largest locus to be baited for using a tiled bait system for every restriction fragment end. Since then, two studies have reported enriching for ~3Mb loci (Franke et al. 2016; Kolovos et al. 2016) and one study for 14 loci of combined size ~14.5Mb (Jäger et al. 2015). These studies used the commercially designed NibleGen Sequence Capture microarray or the Agilent SureSelect beads to pull-down the regions of interest. Here, I have presented another method for sequence capture: home-made short biotinylated RNA baits made from BAC DNA. I achieved a 45-fold enrichment of read coverage over baited regions compared to Hi-C datasets. This is comparable to previous studies utilising various forms of Capture Hi-C, which obtained between 10-fold and 150-fold enrichment (Franke et al. 2016; Kolovos et al. 2016; Mifsud et al. 2015; Schoenfelder et al. 2015a; Jäger et al. 2015; Javierre et al. 2016; Wilson et al. 2016; Dryden et al. 2014). I showed that the bait pull-down was reliably uniform across the whole region and read coverage pattern showed good correlation with pre-capture libraries. Nevertheless, there is room for improvement in this method, such as on-target efficiency, which here was ~12% whereas in studies utilising commercial bait systems this efficiency is 40-80%. This however also depends on the proportion of the genome that is being enriched for.

The interaction landscape of the Igh locus was examined here at 20kb resolution, which was the smallest fixed-width bin possible for the HindIII restriction enzyme. Of note, every single restriction fragment had reads mapping to its ends, which opens the possibility of analysis at single fragment resolution. However, for the purpose of the interaction maps being directly comparable with the polymer modelling, I chose fixed-width bins. My data recapitulated the fact that the Igh is highly enriched for intra-locus interactions when poised for recombination in $Rag^{-/-}$ pro-B cells. Accordingly, a higher frequency of interactions between the Igh and its neighbouring sequences on chromosome 12 was detected in thymocytes. In pro-B cells, the interaction map was highly enriched for long-range

interactions connecting elements far from each other in linear sequence, in particular, the 3' regulatory elements and the distal V genes. On the contrary, in the thymus, the majority of interactions were closer to the diagonal of the heatmap and there was depletion of very long-range contacts. These two observations illustrate previously established locus contraction in pro-B cells and a lack of contraction in thymocytes (Kosak et al. 2002; Fuxa et al. 2004; Hewitt et al. 2008; Rother et al. 2016).

The interaction frequency matrix in pro-B cells revealed a CTCF-mediated pattern of DNA contacts. Although other factors including Pax5, Ikzf1 and Yy1 are essential for locus contraction (Fuxa et al. 2004; Reynaud et al. 2008; Liu et al. 2007), I propose that when the locus is contracted it is CTCF that mediates direct interactions between the 3' elements and the V genes. The pattern of CTCF-binding sites in the Igh locus is suggestive of their functionality, namely, the 7 CTCF sites at the 3'CBEs/HS4-8 are in convergent orientation with the CBEs in the V region and have been proposed to act as an anchor (Benner et al. 2015), whereas the IGCR1 harbours 2 divergent CBEs, one of which is convergent with the CTCF sites in the V region and the second one is convergent with the 3'CBEs/HS4-8. This presents an ideal layout for bringing the V genes towards the D genes or vice versa. This study has confirmed and refined the superanchor at the 3' end of the locus by showing that the 20kb bin containing HS4-8 and 7 CTCF-binding sites contacts all V genes most frequently. Other studies refer to 10 3' CTCF sites (Benner et al. 2015), and the discord might be due to different CTCF ChIP-seq datasets analysed or differences in CTCF peak calling and/or the inclusion of more downstream CTCF sites. Additionally, I showed that the bin downstream rather than upstream of the superanchor is the second highest interacting point adjacent to the anchor. Although this falls outside the putative Igh locus boundary, as defined by HS8, it contains a further CTCF-binding element and there are several more CTCF sites downstream. Unsurprisingly, the 3'RR/HS1-3 does not take part in long-range interactions and it has been shown to be dispensable for V(D)J recombination (Morvan 2003; Vincent-Fabert et al. 2010). In pro-B cells, HS4-8 are associated with active chromatin marks, while HS1-3 are not (Garrett et al. 2005). The deletion of HS5-7 and most of 3'CBEs results in the distal V genes being further away from proximal V genes indicating a reduction in locus contraction (Volpi et al. 2012). A more comprehensive examination of the effect of the 3'CBEs deletion on the Igh locus architecture is required.

The analysis by Benner *et al*. 2015 using Hi-C, identified the 3'CBEs/HS4-8 as a superanchor, and not the IGCR1, presumably due to its lack of many clustered CTCF sites. My data shows that these two regions behave very similarly by frequently contacting all V genes. IGCR1 could either directly contact all V genes via its convergent CBE1 or simply because it frequently interacts with the 3'CBEs/HS4-8. It would be interesting to examine IGCR1 interactions in pro-B cells lacking the 3'CBEs. The deletion of the 3'CBEs did not show any decrease in distal V usage, but it is not certain that all superanchor CBEs have been deleted in that model (Volpi et al. 2012). This study did not examine chromatin contacts at the 3' end of the locus. A study that interrogated the impact of the IGCR1 deletion on V(D)J

recombination proposed that the IGCR1 promotes the usage of distal Vs indirectly, by suppressing the recombination of proximal Vs (Guo et al. 2011b). Locus contraction and long-range interactions with the V region have not been assessed in this study. It still remains to be experimentally confirmed that IGCR1 CBE2 interacts only downstream and the CBE1 interacts only upstream, but given their proximity of just 2.5kb this might be difficult to assess even using a more frequently cutting enzyme. A possibility remains that in $Rag^{-/-}$ pro-B cells the interactions involving the IGCR1 are slightly different to those in wild type pro-B cells that have undergone D-J recombination. Nevertheless, it has been proposed that the insulation properties of the IGCR1 are not present in $Rag^{-/-}$ pro-B cells as the IGCR1 is away from the V genes in $E2A^{-/-}$ pre-pro-B cells and repositions close to distal V genes in $Rag^{-/-}$ pro-B cells (Jhunjhunwala et al. 2008). IGCR1 sole role as an insulator rather than active mediator of interactions might explain the lack of conformational changes observed by 4C-seq in $IGCR1^{-/-}$ cell line (Medvedovic et al. 2013). I demonstrated that IGCR1 interactions stretch both downstream and upstream, and while it has an anchor-like interaction pattern with V genes, it remains to be determined how its insulator and interaction-mediating properties differ and what exactly exerts its insulation ability.

Capture Hi-C data showed that the Eμ does not participate in long-range interactions and is generally not enriched for contacts. It was not as depleted for interactions with distal Vs as the constant region was, but it was less enriched for contacts with the proximal V genes than the constant region was. Eμ is a very small element and assessing its spatial behaviour is challenging using a fixed binning approach. Nevertheless, three different binning strategies showed that the bin containing the Eμ does not make frequent contacts along the locus regardless of being in a bin with D genes or C genes. This evidence is suggestive of the Eμ looping out of the Igh structure, which was confirmed by polymer modelling. Previous 4C-seq data also hinted that the Eμ might be less interactive than other 3' elements (Medvedovic et al. 2013). The Eμ is not essential for the V(D)J recombination process *per se* as Eμ deletion does not completely abolish recombination and the formation of B cells (Perlot et al. 2005). Nevertheless, as a key enhancer driving the transcription of a recombined heavy chain, it has been the primary focus of early studies. 3C and 4C probes were often designed over the Eμ and many interactions have been reported from this viewpoint, including with the 3'CBEs/HS4-8, the 3'RR, the IGCR1 and with proximal and middle V genes (Guo et al. 2011b; 2011a; Verma-Gaur et al. 2012; Medvedovic et al. 2013). However, the interaction between the 3'CBEs/HS4-8 and the IGCR1 has always been observed to be much stronger than interactions between either of those elements and the Eμ (Guo et al. 2011b; Medvedovic et al. 2013). It is disputed to what extent the deletion of the Eμ causes lack of locus contraction (Chakraborty et al. 2009b; Guo et al. 2011b; Gerasimova et al. 2015; Medvedovic et al. 2013). Capture Hi-C showed frequent involvement of the IGCR1 and the 3'CBEs in interactions with each other and locus-wide, whereas the Eμ demonstrates fewer contacts and does not follow the interaction pattern of either the D region or the constant region.

I observed that the IGCR1 interacts very frequently with the 3'CBEs/HS4-8 and with the 3'RR forming a small 3' subdomain in both $Rag^{-/-}$ pro-B cells as well as in the thymus, which is consistent with a previous 3C study (Degner et al. 2011) and a 4C and CTCF ChIP-loop 4C study (Guo et al. 2011a). These interactions likely have a D-J recombination-promoting and V-insulating purpose and they are more frequent in the thymus, most probably due to a lack of long-range interactions in these cells. The structure of the 3' end of the Igh locus presumably has little variability in single B cells. A study that collectively examined the impact of the deletions of regulatory elements (3'RR, Eμ and IGCR1) on long-range interactions in pro-B cells did not observe any changes in locus architecture (Medvedovic et al. 2013). It suggests that no individual element is solely responsible for long-range interactions. Nevertheless, there is a difficulty in reliably assessing the deletions of regulatory elements by NGS methods, because most mutant models are on the 129Sv background, for which the Igh sequence is not fully assembled. I detected a proximal V subdomain between the IGCR1 and the first S107 V gene, which is not hugely dissimilar to a domain proposed by a recent 5C study between the Eμ and a region around the first S107 gene, albeit with 140kb resolution (Montefiori et al. 2016). An earlier 4C study also suggested a proximal V subdomain centred around 114.97Mb, which is exactly in the middle of proximal V genes (Medvedovic et al. 2013). My 20kb resolution provides a much more refined picture of this 3' domain and shows that the 3' regulatory elements also belong to it, albeit with Eμ looping out. This domain might encompass a region as large as from the 3' end of the locus to half way into the middle V genes. I showed that the middle V genes and the first ~200kb of distal V genes are not organised in any subdomains. This is in fair agreement with the 4C and 5C studies (Medvedovic et al. 2013; Montefiori et al. 2016). Interestingly, I noted that precisely this middle region forms a very long-range DNA loop in thymocytes, which is absent in pro-B cells. To sum up, Capture Hi-C fully visualised and established the extent of the 3' domain and the less looped middle V region.

I determined that in pro-B cells the distal V genes form a large highly looped domain that starts 100kb upstream of the J606 genes and ends after the last V gene, marking the end of the Igh locus and its TAD. This is the first high resolution visualisation of this domain in an all-to-all manner. I also showed a substantial frequency of interactions in the distal V domain in the thymus, however the domain is slightly less structured and lacking the most long-range contacts between the domain ends. This domain has been hinted at by a 4C-on-ChIP study that observed frequent interactions downstream of a single viewpoint at J558.72.173, which persisted even when locus contraction was reduced (Guo et al. 2011a). It was also detected by the later 4C-seq study from multiple viewpoints, however the authors did not incorporate this domain in their final model of Igh organization (Medvedovic et al. 2013). A smaller distal V domain was also proposed by the 5C study, starting 300kb into the distal Vs and ending around J558.73.173. The authors do not discuss the organisation of the last 20 V genes (Montefiori et al. 2016). By applying Capture Hi-C and coverage bias

correction I was able to fully visualise and confirm the extent of the large distal V domain in pro-B cells and its partial presence in thymocytes.

I visualised the hallmarks of absence of locus contraction in the thymus, namely the lack of interactions of the middle and distal V genes with the 3'CBEs and IGCR1. Importantly, in agreement with previous reports, the interactions between the 3'CBEs and IGCR1 were readily visualised in the thymus, where RAG complex is expressed and a proportion of Igh alleles undergo D-J recombination (Born et al. 1988). I proposed that in the thymus the Igh locus is highly looped along the diagonal, resembling an accordion shape. This reflects a non-contracted locus, lacking very long-range interactions, with chromatin quite tightly packed along the linear sequence. In the thymus, the 5' part of the Igh locus is tethered to the lamina and resides in a heterochromatic environment with V genes marked by suppressive histone marks (Kosak et al. 2002; Johnson et al. 2003; Chakraborty et al. 2009b).

The long-range interactions involving the CTCF-binding anchors visualised by Capture Hi-C are not the only mechanism shaping the 3D topology of the Igh locus. Deletion of genes including Pax5 and Yy1 results in a lack of overall locus contraction in pro-B cells (Hesslein 2002; Liu et al. 2007) (reviewed in Hewitt et al. 2010; Bossen et al. 2012), arguably to a much larger extent than mutations in any of the Igh regulatory elements. These two DNA-binding factors have binding sites throughout the Igh locus, although fewer and less strategically placed than CTCF. On one hand, the Capture Hi-C interaction frequency map clearly shows that all V genes interact very frequently with the 3'CBEs/HS4-8 and with the IGCR1. On the other hand, the frequent looping in the distal V domain cannot be fully explained by CTCF-binding, if at all, as the CTCF sites in the Vs are unidirectional. Additionally, the fact that CTCF remains bound to the Igh throughout B cell development (Degner et al. 2009) and that the 3' superanchor, as a functional genomic feature, is already present in pre-pro-B cells and remains invariant in pro-B cells (Benner et al. 2015), further support the need for involvement of other factors in locus contraction. In contrast to $Il7ra^{-/-}$ mice (Corcoran et al. 1998; Chowdhury and Sen 2001), Pax5 deficiency does not cause depletion in active histone marks and germline transcription over the distal V genes. So there is no defect in locus accessibility in $Pax5^{-/-}$ despite the lack of locus contraction and reduction in distal V usage in recombination. This points to a direct structural role of PAX5 or a signalling role that directly affects the Igh structure formation. Perplexingly, ectopic expression of Pax5 in T cells showed that it induced proximal but not distal V-DJ recombination, which recapitulated the $Pax5^{-/-}$ phenotype in pro-B cells (Fuxa et al. 2004). This indicates that in pro-B cells there is an unknown factor that promotes locus contraction and distal V rearrangement in addition to PAX5. Curiously, 30-75kb downstream of the HS8, there are 4 CTCF-binding sites in pro-B cells that overlap with PAX5 binding sites and although the interaction frequency map does not show high enrichment for interactions of this region with distal Vs, the detection might be affected by the bait boundary issue. There are many PAX5 and a few YY1 binding sites in the distal Vs, so it is possible that the observed lack of locus contraction and reduction of distal V usage is caused by disintegration of the distal V domain in the mutants. Elucidating this

would require mutating particular protein-binding sites in the distal Vs, which would undoubtedly be challenging due to the repetitiveness on this region. Also, YY1 is a ubiquitously expressed protein and likely has an overarching or indirect role in pro-B-specific locus contraction. The 5C study reported that the formation of the distal V domain is PAX5-dependent (Montefiori et al. 2016), whereas the 4C study detected interactions within distal Vs in $Pax5^{-/-}$ mice (Medvedovic et al. 2013). CTCF has been shown to directly associate with PAX5 (Ebert et al. 2011) and YY1 (Donohoe et al. 2007) in vitro, but it remains to be determined if they interact whilst bound to the Igh locus.

The Capture Hi-C interaction frequency map presented in this chapter is the first high resolution visualisation of interactions between all elements of the Igh locus in pro-B cells and in thymocytes. I showed that in pro-B cells the Igh locus in highly enriched for very long interactions underpinning locus contraction. These intra-locus contacts bear patterns of interactions between convergent CTCF sites. I also visualised the extent of the distal V domain. The model of three sub-regions, all interacting with CTCF sites at the 3' of the locus broadly agrees with previously proposed structures. It brings together two current models: the hierarchical 3-domain configuration (Guo et al. 2011a; Gerasimova et al. 2015; Montefiori et al. 2016) and the flexible interactions of all V genes with the D-J region (Medvedovic et al. 2013) via the superanchor (Benner et al. 2015). I speculate that PAX5 and YY1 binding or a PAX5- and YY1-dependent mechanism initiates large-scale locus contraction, which when established utilises the CTCF sites at the 3'CBEs/HS4-8 and the IGCR1 to provide an equal opportunity for all V genes to recombine. Finally, protein binding and histone marks at single V genes ultimately micro-manage their recombination frequency (Bolland et al. 2016). More research is needed to elucidate what mediates looping in the distal V domain as well as what exerts IGCR1's insulation ability and whether this is reflected in interactions.

Multiple possible single 3D conformations of the Igh revealed by polymer modelling

This is the first study to elucidate all possible single conformations of the Igh locus from enriched Hi-C data. In collaboration with Luca Giorgetti and Yinxiu Zhan, we utilised a polymer modelling approach to resolve simultaneous and mutually exclusive interactions from ensemble Hi-C. This showed that there is no one dominant structure of the Igh locus in pro-B cells. All 5001 generated structures were sufficiently different to not put forward a prevailing conformation or a set of a few most common conformations. This recapitulates the very purpose of the Igh locus to recombine an array of V genes encoded over 2.5Mb that all must travel over long distances to the D-J region or vice versa. Previous FISH and chromosome conformation capture studies often gave an impression of striving to find a static defined overarching structure of the Igh locus, whereas the Igh spatial organisation must be dynamic or at least different in every pro-B cell, in order to produce different immunoglobulin heavy chains.

The simulations revealed that the V region beads are involved in very similar interactions in pro-B cells and well as in non-B cells, albeit with much reduced frequency,

suggesting a level or pre-established chromatin organisation. On the other hand, the regulatory elements 3'CBEs/HS4-8 and the IGCR1 were involved in dramatically fewer interactions with the V beads in T cells compared to pro-B cells, showing the change in their physical position in single structures.

Polymer modelling of single structures allowed us to identify significantly close contacts in every conformation, that described two beads as physically interacting, which is not possible to elucidate from Capture Hi-C matrices. Thanks to the modelling we could calculate the probability of each V bead contacting any D bead as a number of single structures in which a V-D interaction was significant. The results revealed that the D region contacts ~30 V beads (~37 V genes) in every single Igh locus structure. These results also showed that the V beads make approximately the same number of contacts with the Ds across all 5001 simulated conformations. This supports the 'equal opportunity for all' model. Accordingly, V-D interaction frequencies were not correlated with the V bead recombination scores or with the CTCF-binding levels, further strengthening this model. Of note, the correlation analysis did give a slightly significant results for average V bead recombination score but insignificant for beads with a single active V gene. However, the V bead recombination scores were positively correlated with CTCF binding levels in the V beads. This suggests a role for interactions in providing equal opportunity for V genes to contact D genes. Because there are so many CTCF-binding sites in the V region, CTCF-mediated interactions might contribute to equal opportunity of all V genes to contact D genes, but higher levels of CTCF binding might give nearby genes a local advantage in recombination. Given that V genes do not cluster by their level of usage in V(D)J recombination and even adjacent V genes can recombine with dramatically different frequencies (Bolland et al. 2016), ideally I would like to correlate the interactions of all single V genes with their recombination levels and protein binding. This, however, would require using a more frequently cutting enzyme to prepare Capture Hi-C libraries to ensure that restriction fragments contain only one V gene.

Another advantage provided by the modelling allowed us to establish that V-D interactions preferentially take place on the periphery of the V gene region as defined by a sphere encompassing the V beads. Models of Igh spatial organisation often depict the D-J region residing in a cavity surrounded by equidistant V genes (Lucas et al. 2011; Outters et al. 2015). My study shows that indeed, the D region contacts multiple V genes simultaneously, but it approaches them from the outside rather than embedding itself in the middle of the V gene 'cloud'. A study that modelled first-passage times of the D-J region encountering a V gene proposed that the movement of Igh elements follows fractional Langevin motion due to observed negative velocities, which suggest that the elements bounce back and forth in a viscoelastic environment (Lucas et al. 2014). This study used Tet operators near the Eμ and in the middle of the V region, and obtained an average locus radius of 1μm, which corresponds to an average first-passage time for a V-D interaction of 12s. However, taking the locus radius of 0.5μm as determined previously by FISH (Jhunjhunwala et al. 2008) it would take only

0.8s on average for a V gene to pair with a D gene. A longer time might mean more bouncing back and forth prior to recombination. It still remains to be determined which scenario better recapitulates the interactions in the Igh locus.

In light of the presented data, the ‘equal opportunity for all’ model best describes the overall purpose of the Igh locus, which is reflected in its heterogeneous landscape of interactions and locus conformations. New insights provided here demonstrate that the D region contacts multiple V genes simultaneously in single Igh loci, but favour a lack of a previously predicted cavity or centre harbouring the D-J region on which the V genes converge. Instead, the D region comes into contact with multiple V genes on the periphery of the highly looped V region. Further biophysical and imaging studies are needed to determine the direction of V-D interactions, the extent of V gene 'bouncing' and the speed of synapse formation.

4

4. A novel network of inter-chromosomal interactions involving immunoglobulin heavy and light chain loci

4.1. Introduction

Chromosomes in the nucleus are arranged in a non-random fashion in the three-dimensional space in the nucleus (Chandra et al. 2015; Nagano et al. 2017; Stevens et al. 2017; Meaburn 2016; Fraser and Bickmore 2007). Chromosomes occupy discrete chromosome territories (Koss 1998; Nagele et al. 1999; Bolzer et al. 2005; Roix et al. 2003; Cremer and Cremer 2001) in which the active gene-rich regions preferentially reside towards the periphery of the chromosome and inactive regions localise internally (Nagano et al. 2013; Xie et al. 2017).

Inter-chromosomal interactions have been significantly less studied using chromosome conformation capture methods than intra-chromosomal interactions due to the very low proportion of trans-chromosomal di-tags in the datasets. One of the first trans-chromosomal interactions reported using the 3C method was between the promoter of the IFN-gamma gene on chromosome 10 and the regulatory regions of the Th2 cytokine locus on chromosome 11 (Spilianakis et al. 2005). The original 4C study detected a very frequent interaction between the Igf-H19 domain on chromosome 7 and the Abcg2 gene on chromosome 6 as well as the Osbpl1a gene on chromosome 18 in the mouse neonatal liver (Zhao et al. 2006). 4C including an RNA Pol II chromatin enrichment step followed by validation by FISH was used to show that genes co-regulated by the transcription factor KLF1 frequently co-localise when active in a shared transcription factory in erythroid cells (Schoenfelder et al. 2010). 4C and FISH also demonstrated an interaction between Klf4 on chromosome 4 and Oct4 (Pou5f1) on chromosome 17 (Wei et al. 2013). The original Capture Hi-C study reported trans interactions between chromosomes 16 and 22 as well as between chromosome 18 and several other chromosomes in a breast cell line MCF10 (Dryden et al. 2014). Capture Hi-C also readily detected interactions between Hox gene clusters on several different chromosomes. HoxC on chr15 interacted with HoxB on chr11 and with HoxD on chr2, whereas HoxB also interacted with HoxD and HoxA on chr6 (Schoenfelder et al. 2015b). Re-analysis of Hi-C data from

Dixon *et al*. 2012 in ESCs identified a plethora of inter-chromosomal contacts, but was unable to detect the interaction between HoxB and HoxC (Kaufmann et al. 2015). The multiplex 4C method called Capture-C detected many trans interactions but all at similarly low levels (Davies et al. 2016). Recently, an integrative study used Capture Hi-C to show contacts between eQTL (expression quantitative trait loci) and putative target genes (Javierre et al. 2016). Another recent work examined promoter interactions in a hematopoietic progenitor cell line, which led to the identification of novel protein-protein interactions co-localising at the bases of chromatin loops (Wilson et al. 2016). Most recently, an iChIP (indexed chromatin immunoprecipitation) study in a chicken B cell line reported trans interactions between the Pax5 gene and regions on chromosome 11, which when mutated caused a decrease in Pax5 expression (Fujita et al. 2017).

As for the immunoglobulin loci, their trans-chromosomal contacts were investigated to date only in mature B-cells in the context of translocations in B cell malignancies. FISH studies demonstrated that the Igh and myc loci co-localize in later stage B cells and their corresponding mouse chromosomes 12 and 15, respectively, are often positioned next to each other (Roix et al. 2003). The Myc gene is often recruited to the same transcription factory as the Igh upon B cell activation (Osborne et al. 2007; Robbiani et al. 2008) and MYC protein has recently been shown to induce global chromatin decompaction (Kieffer-Kwon et al. 2017). Several 4C-based studies carried out comprehensive analyses to study the co-occurrence of Igh locus interactions, malignant chromosomal translocations and double strand break (DSB) frequency genome-wide in later stage B cells (Chiarle et al. 2011; Klein et al. 2011; Hakim et al. 2012; Rocha et al. 2012). Although these disagreed on whether the interactions correlate with translocations, all detected multiple inter-chromosomal contact partners of the Igh. The Igh, Igk and Igl have also been shown by FISH to co-localise in transcription factories in plasma cells during production of high levels of immunoglobulin transcripts (Park et al. 2014), and to co-localise in chromosomal translocation models in splenic B cells (Wang et al. 2009). The Igh and Igk pairing in pre-B cells during allelic exclusion is the only inter-chromosomal interaction of the Ig loci in early B cells reported to date (Hewitt et al. 2008), and no studies have investigated the inter-chromosomal interactions of the Ig loci with the rest of the genome.

Investigating the Igk and Igl immunoglobulin light chain loci in wild type mice poses the same challenges as analysis of the Igh locus in wild type pro-B cells. To this end, I used Rag/81X mice (described in section 3.2), which lack the RAG recombinase and express a transgene of a pre-assembled recombined Igh product of the V gene 81X (V7183.2.3), which allows pro-B cells to progress to the pre-B cell stage whilst maintaining an intact germline sequence of all immunoglobulin loci.

In this chapter, I use Capture Hi-C to investigate the interactions of the Ig loci with each other, and I also utilise several other baited regions included in the Capture Hi-C experimental design to interrogate their contacts with the Ig loci and rest of the genome. I show that the Igh interacts with multiple regions genome-wide in $Rag^{-/-}$ pro-B cells and Rag/81X pre-B cells,

whereas the light chain loci only make trans contacts in Rag/81X pre-B cells. Further, I show that other baited genes required for B cell development share trans interaction targets with the Ig loci. I discuss the discovery of a potential co-regulatory network involving the Ig loci and their long-range interaction partners encoding essential B cell genes.

4.2. Capture Hi-C reveals a genome-wide network of inter-chromosomal interactions involving the Ig loci and genes driving B cell development

Capture Hi-C is an enriched Hi-C dataset containing interaction sequences (di-tags) that have been pulled down from a Hi-C library using baits for every restriction fragment end in the regions of interest. This allows not only for investigation of interactions within the baited regions using di-tags for which both ends map to the baits (as discussed in chapter 3), but also genome-wide interactions of the baited regions by pulling down all read pairs where at least one end maps to the bait and the other ends may map anywhere in the genome (many-to-all).

4.2.1. Calling statistically significant inter-chromosomal interactions

I was interested in examining the inter-chromosomal (trans) interaction landscape of the Ig loci and other baited genes to identify regions in the genome with which they frequently come into contact. To quantitatively score the inter-chromosomal interactions genome-wide, I performed virtual 4Cs by taking each whole baited region as a viewpoint and quantifying other ends in 0.5Mb bins genome-wide (as described in section 2.8.2). The sizes of the baited viewpoints varied from 150kb to 3.5Mb (BACs listed in section 2.5.2).

Visual inspection of the virtual 4C raw data from the Igh and Igk viewpoints showed that the Igh locus made trans contacts in both $Rag^{-/-}$ pro-B cells and Rag/81X pre-B cells (**Figure 50**). Interaction peaks were also observed in thymocytes, albeit fewer and of lower frequency than in B cells. The Igk locus showed peaks in trans only in Rag/81X pre-B cells and not in $Rag^{-/-}$ pro-B cells or thymocytes. Importantly, the interaction peaks observed in the raw data were sharp and narrow, with a high signal to background ratio. This indicated good quality data with a sufficient number of trans reads to reliably allow interaction calling. For the Igh or Igk viewpoints I obtained around 200-500 reads in the highest interacting 0.5Mb bins and for the smaller viewpoints covered by just one BAC the read count was in the range of 20-100 reads per trans-interacting 0.5Mb bin.

Notably, the strongest interaction peaks from both the Igh and Igk viewpoints were over bins containing B cell-specific genes or genes driving B cell development. Examples include all three Ig loci, Ebf1, Pax5, Foxo1, Runx1, Hmgb1, Bach2, Cux1 and Aff3. Crucially, among these only Pax5, Foxo1 and the Ig loci were covered by Capture Hi-C baits and all other interactions were with non-baited bins. Of note, other baited regions such as Hbb or Hist1 did

not interact with the Ig loci, indicating that preferential bait-to-bait interactions are not observed in Capture Hi-C datasets.

Out of the 5322 0.5Mb bins in the genome, the interactions of interest were the bins with the highest number of other end reads in each virtual 4C, i.e. the extreme high outliers. Significant contacts were identified in consultation with the Babraham statistician Anne Segonds-Pichon using the modified z-score $M_i = \frac{0.6745*([number\ of\ reads\ in\ 0.5Mb\ bin]-median)}{MAD}$, where MAD is the median of all absolute deviation values of *[number of reads in 0.5Mb bin]-median*. Z-score values above 3.5 were deemed significant. This analysis was done for each biological replicate separately (three for $Rag^{-/-}$ pro-B cells, two for Rag/81X pre-B cells and two for thymocytes) and only those 0.5Mb bins fulfilling the condition of z-score > 3.5 in every biological replicate were kept (**Table 12**). Other ends mapping to the same chromosome as the viewpoint were discarded prior to z-score analysis. No further correction was necessary, because read coverage differences do not have a big impact when quantifying in such large bins and there is no linear distance linkage for interactions between different chromosomes. A complete list of 0.5Mb bins significantly interacting with each viewpoint in each cell type, including all genes present in these bins, can be found in appendix A. A table showing how many viewpoints contact a given 0.5Mb bin can be found in Appendix B (described further in 4.2.4). The Ikzf1 (Ikaros) and Tcf3 (E2A) baited regions would also be of interest for this analysis, however these baits did not give satisfactory enrichment levels. The Ikzf1 baits failed to hybridise or were unintentionally omitted from the bait mix, whereas the Tcf3 baits enriched with lower efficiency than other baits. I performed a virtual 4C from the Tcf3 viewpoint, but there was a low signal to background ratio and many 0.5Mb bins had zero reads. This resulted in MAD=0, which precluded z-score calculation. The described z-score approach was more stringent and gave fewer significant interactions than a binomial test approach that I also performed (not shown). An average of 150 statistically significant trans interactions per viewpoint (**Table 12**) might seem high, but it is in fact only ~3% of all 5322 possible contacts. Throughout this chapter a trans interaction refers to a 0.5Mb bin that significantly interacts with a given baited viewpoint defined by the BACs used to make the baits.

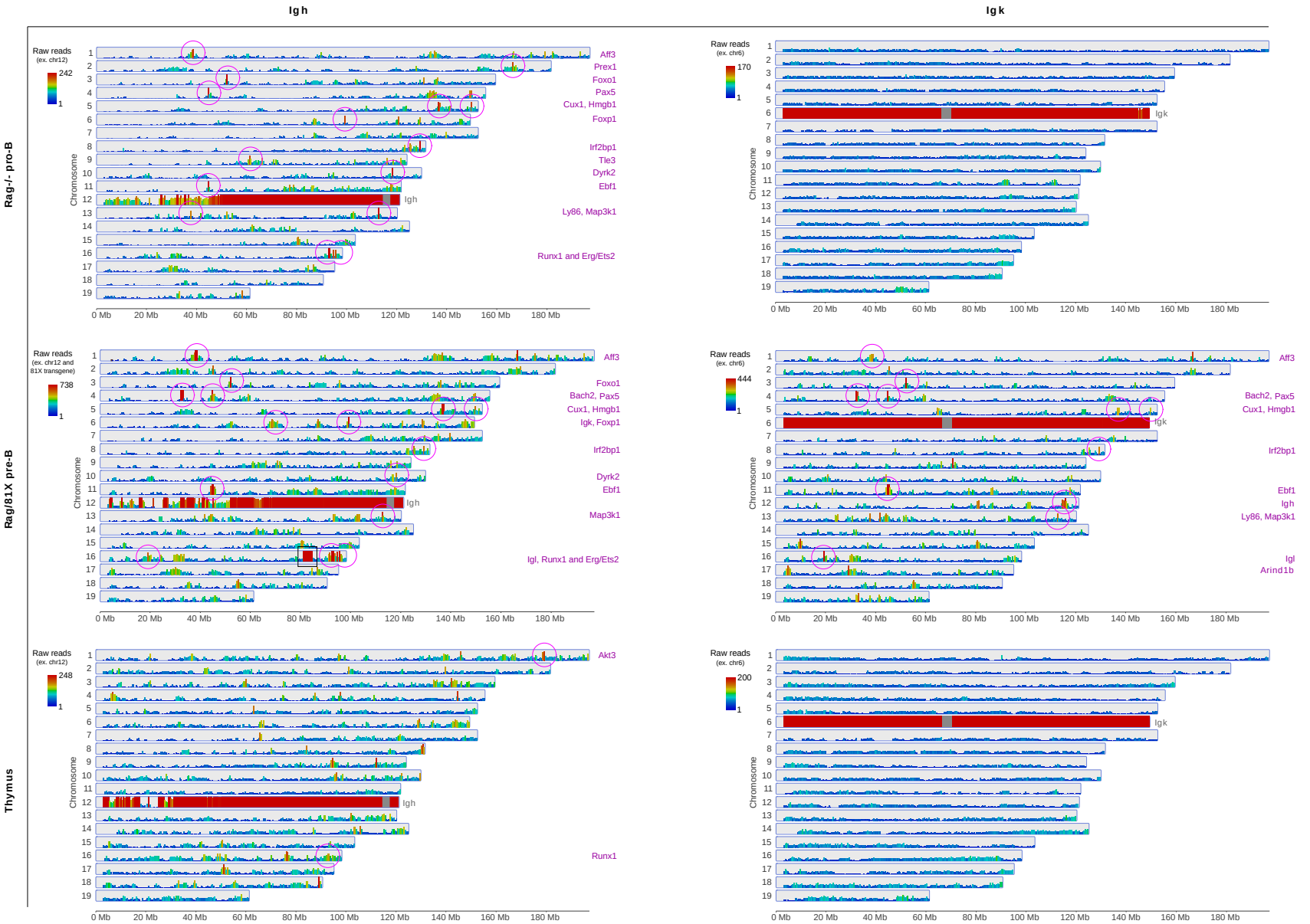
Igh
Igk
Rag-/- pro-B
Rag/81X pre-B
Thymus
Raw reads
(ex. chr12)
(ex. chr12 and 81X transgene)
(ex. chr6)
242
738
248
170
444
200
Chromosome
Aff3
Prex1
Foxo1
Pax5
Cux1, Hmgb1
Foxp1
Irf2bp1
Tle3
Dyrk2
Ebf1
Ly86, Map3k1
Runx1 and Erg/Ets2
Bach2, Pax5
Igk, Foxp1
Igl, Runx1 and Erg/Ets2
Akt3
Runx1
Igl
Arind1b
0 Mb
20 Mb
40 Mb
60 Mb
80 Mb
100 Mb
120 Mb
140 Mb
160 Mb
180 Mb

Figure 50. The Igh and Igk loci make specific inter-chromosomal contacts. Virtual 4C were performed in Seqmonk using the baited Igh locus (2.8Mb) and the baited Igk locus (3.2Mb) denoted by grey rectangles on chr12 and chr6, respectively. All other ends of reads mapping to the viewpoint were quantified in 0.5Mb bins genome-wide and plotted as raw read counts. Each karyogram is an average of biological replicates. The number of reads in 0.5Mb bins is represented by the height and the colour of the bars along the chromosomes and bars on the same chromosome as the viewpoint are saturated. 0.5Mb bins containing potential genes of interest and showing clear sharp peaks of high read counts are denoted by purple circles and labelled to the right of each karyogram.

Table 12. Statistically significant trans interactions per viewpoint per cell type.

Viewpoint	$Rag^{-/-}$ pro-B	Rag/81X pre-B	Thymus
Igh	106	132	34
Igk	5	169	1
Igl	0	146	31
Pax5	35	505	15
Foxo1	85	322	171
Il7r	61	244	34
Rag1Rag2	3	53	38

Identification of the Vh81X transgene location

It was previously unknown where in the genome of the Rag/81X mouse the Vh81X transgene was integrated. Thanks to Capture Hi-C, I identified the integration site on chromosome 16 at around 82,900,000-83,000,000. The virtual 4C from the Igh locus showed a strong peak on chr16 around 83,000,000Mb, which was not present in $Rag^{-/-}$ pro-B datasets or virtual 4Cs from other viewpoints (**Figure 50** left middle, chr16, black square). The transgene was absent from the genome assembly, therefore all reads experimentally coming from the transgene were mapped to the endogenous Igh locus, whereas their other ends interacting closely in cis with the transgene were mapped to the transgene's surrounding sequences on chromosome 16, which ultimately allowed for its identification. The interactions being in fact in cis gave a falsely high readout in virtual 4C in trans. A small level of uncertainty remains as it is not clear how many HindIII sites from the endogenous Igh there are in the Vh81X transgene, however a reciprocal virtual 4C from the integration region on ch16 gives enrichment over 8 HindIII fragments around the Eμ. If there were no Igh HindIII sites in the transgene, then a trans interaction between the transgene and the endogenous Igh locus would be the only explanation for the observed peak on chr16. However, the read count in trans would be expected to be lower than observed. Nonetheless, the lack of signal around the transgene from other viewpoints virtual 4Cs disfavours this scenario. 4Mb around the transgene (chr16:81,000,000-85,000,000) were excluded from the z-score analysis and the transgene bins are not listed in Appendix A and Appendix B.

4.2.2. Genomic regions contacting the Ig loci contain genes driving B cell development and function.

To address the third part of my hypothesis and achieve aim 4 (sections 1.5 and 1.6), I set out to identify the potential candidate genes responsible for the inter-chromosomal interactions. While I was not able to discern with absolute certainty which gene in a particular significant 0.5Mb bin is responsible for making a meaningful contact with the viewpoint, I attempted to identify relevant and interesting genes. This was a qualitative analysis based on the genes' reported or putative function in B cell development, B cell function or lymphocyte development or function. Markedly, this identification of putative genes of interest revealed that the bins interacting most frequently with the viewpoints contained genes crucial for B cell development. For top interacting bins the assignment of genes such as Foxo1, Ebf1 or Runx1 was unambiguous as they were the only genes in their 0.5Mb bin. For others, I gathered information about all genes in the bin and either assigned one or more potentially relevant genes as the bin name, or did not assign any genes when the bin contained only housekeeping genes, genes with likely irrelevant functions or no genes. For example Cux1, Aff3, Hmgb1 and Lef1 shared their 0.5Mb bins with many other genes but were picked as genes of interest due to their reported roles in B cells. Some large genes, such as Ebf1, Aff3 or Bach2 spanned two 0.5Mb bins and often both of those bins were identified as significant contacts in the z-score analysis. Also, all virtual 4Cs identified multiple 0.5Mb bins over the Ig loci as significant interactions. Therefore, some figures in this chapter contain two or more identically named interactions, which correspond to adjacent 0.5Mb bins. Importantly, some genes of interest were much smaller than the 0.5Mb bin, including Foxo1, Hmgb1, Irf8, Zfp36l2 and Lef1 and therefore I examined raw read counts within those bins at 100kb resolution to determine that the majority of interaction reads accumulated over the 100kb bin containing the gene of interest (**Figure 51**). The overall read coverage of Capture Hi-C precluded genome-wide statistical analysis in trans at such high resolution, but these examples give more confidence that indeed it is the genes with functions in B cell development that are the interaction partners.

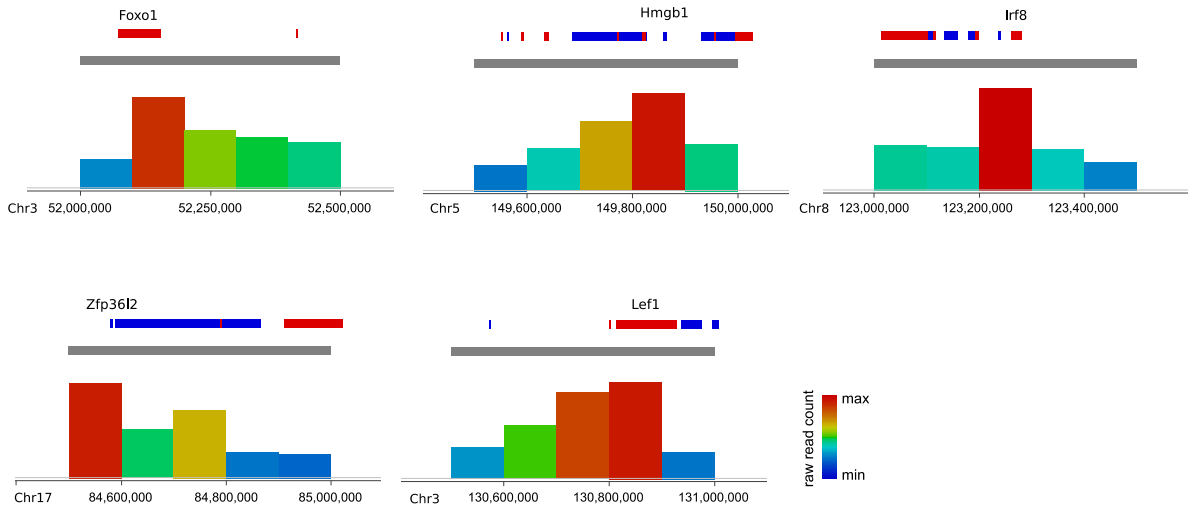

Figure 51. Reads accumulate over the genes of interest. Examples of selected 0.5Mb trans interacting bins dissected into 100kb bins. The 0.5Mb bins are denoted by grey rectangles. Ensembl genes are indicated in red (sense) and blue (antisense) and the gene of interest is labelled above. Raw reads were calculated in Seqmonk as an average of biological replicates. The height and the colour of the bars indicate read count.

Inter-chromosomal contacts in pro-B cells

In Rag$^{-/-}$ pro-B cells, the top 20 interactions of the Igh locus included bins containing Pax5, Ebf1, Runx1, Irf2bp2, Foxo1, Map3k1, Cux1, Dyrk2, Aff3, Foxp1, Hmgb1, Dyrk1a and Erg (Appendix A, Appendix B). Importantly, Igh did not contact the Igk and Igl in pro-B cells, which agrees with the light chain loci not being active at the pro-B stage. Interactions below the top 20 included Ly86, Lef1, Lgals9, Irf4, Pik3r1, Akt3 and Stat5. The Pax5 viewpoint showed a reciprocal interaction with the Igh locus and had the Foxo1, Runx1 and Irf2bp2 interactions in common with the Igh. It did not, however, share any of the other Igh top contacts. The Foxo1 viewpoint also showed a reciprocal interaction with the Igh and the two viewpoints had Pax5, Map3k1, Ebf1, Runx1 and Aff3 interactions in common. Pax5 and Foxo1 viewpoints, but not the Igh viewpoint, interacted with Rad51l1, Egr1 and Zfp36l1 which is on the same chromosome as the Igh. The Foxo1 viewpoint also contacted Myo16, Myb, Il7r, Blnk, and, surprisingly, the Igl, which were not shared with the Igh and Pax5 viewpoints. The Il7r viewpoint showed contacts with Bcl11a, Myo16, Myb, Pax5, Arid1b, Igl, Ebf1, Foxo1, Ikzf1, Zfp608 and Igh. Its interaction profile therefore resembles most closely that of the Foxo1 viewpoint. The interaction of the Il7r viewpoint with the Igh was 57th out of 61 significant interactions, which might explain why a reciprocal interaction from the Igh to Il7r was not detected. The Igh is engaged in a larger number of contacts than the Il7r is and the less frequent Igh-Il7r interaction was not significant in the Igh virtual 4C, but was significant in the Il7r virtual 4C as the Il7r viewpoint has much fewer frequent contacts. The Rag1Rag2 viewpoint interacted only with the Igh and Hmgb1 in pro-B cells as well as with a region on chromosome X with a high frequency.

Many of these interacting regions are key genes driving B cell development and their protein products have been implicated in the regulation of V(D)J recombination. However,

physical associations between those genes in the nucleus have not been studied before. Pax5 is a B cell-specific transcription factor responsible for B lineage commitment. It is essential but not sufficient for Igh locus contraction (Hesslein et al. 2003; Fuxa et al. 2004) and promotes expression (Yu et al. 1999; Hsu et al. 2003) and recruitment of the RAG complex to the Igh locus (Zhang et al. 2006b). Its deletion causes an arrest at the pro-B cell stage (Urbanek et al. 1994; Nutt et al. 1997) and reduces distal V gene usage (Fuxa et al. 2004). Ebf1 is an early specification factor (Hagman et al. 1993) that instructs lymphocyte differentiation towards the B lineage by establishing a transcriptional programme for B cell specification and commitment beyond the CLPs (Nechanitzky et al. 2013). Pax5 and Ebf1 are expressed only in B cells and not in T cells and they are involved in a positive feedback loop binding each other's promoters (Roessler et al. 2007; Treiber et al. 2010). Ebf1 also binds to promoters occupied by E2A, Pax5, Runx1 and Ets1 (Maier et al. 2004). Foxo1 is a pioneer transcription factor that activates Ebf1 expression and Ebf1 and Foxo1 share many target genes, including Pax5, to orchestrate B cell development (Mansson et al. 2012). Ebf1, which also has pioneering ability (Boller et al. 2016), upregulates Foxo1 expression (Zandi et al. 2008), which in turn activates Il7r, Rag1 and Rag2 expression (Amin and Schlissel 2008). Runx1 is an early factor in lymphocyte development and is expressed in both B and T cells. It is involved in B-lineage priming (Lukin et al. 2010) and is essential for the activation of Ebf1 expression (Yu et al. 2012). Il7r expression is upregulated in CLPs and its signalling is important in B-lineage specification and later for B cell differentiation, proliferation and survival (Corcoran et al. 1996; 1998). It activates Ebf1 indirectly via binding to the Stat5 gene (Roessler et al. 2007). These crucial transcription factors drive early B cell development by co-activating each other in multiple feedback loops and their physical genomic interactions may be an implication of specialised co-regulatory transcription factories.

Further, many other genes in the significant trans bins encode proteins essential for B cell development. Foxp1 deletion causes a developmental block at the pro-B stage and reduces the expression of B-lineage genes including Pax5, Rag1 and Rag2 (Hu et al. 2006). Hmgb1 acts as a cofactor in stabilising the conformational changes at the 12RSS and increasing RAG binding affinity for the 23RSS (Swanson 2004; Zagelbaum et al. 2016). Blnk bridges B cell receptor-associated kinase activation with downstream signalling pathways (Fu et al. 1998) and its deletion causes a pro-B to pre-B developmental block (Pappu et al. 1999). Zfp36l1 encodes a lymphocyte-specific RNA-binding protein essential for maintaining quiescence before pre-BCR expression and for reestablishing quiescence after pre-BCR-induced expansion (Hodson et al. 2010; Galloway et al. 2016). Cux1 is a tumour suppressor that directly promotes the expression of a PI3K inhibitor to control PI3K levels (Wong et al. 2014). It also binds to the matrix attachment regions (MARs) in the Igh intronic enhancer (Wang et al. 1999). Bcl11a is expressed early in lymphocyte development and its deletion results in a lack of B cells beyond the pre-pro-B stage (Liu et al. 2003). Ikaros (Ikzf1) is another very early factor vital for lymphoid lineage priming and for suppressing the myeloid program (Georgopoulos et al. 1994; Kim et al. 1999). Ikaros is required for RAG expression,

DJ recombination and Igh locus contraction (Reynaud et al. 2008). Lef1 is a member of the Wnt signalling pathway that is specifically expressed in early stages of B cell development and contributes to survival and proliferation (Reya et al. 2000). Stat5 is an Il7R target that activates Ebf1 expression (Roessler et al. 2007) and together with Oct-1 activates distal V genes for recombination (Bertolino et al. 2005). Whereas in pro-B to pre-B transition it represses premature Igk recombination (Mandal et al. 2011). Pik3r1 encodes the p85α regulatory subunit of PI3K and is necessary for the pro-B to pre-B transition (Fruman et al. 1999). Akt3 plays a role in B cell proliferation and survival and acts in a PI3K-dependent manner (So and Fruman 2012). Cebpb is also an essential factor for B cell proliferation and survival (Pal et al. 2009).

Other significantly interacting regions have less conspicuous roles in pro-B cells and V(D)J recombination but have been reported to contribute to lymphocyte development and function. Irf2bp2 is a pro-survival factor that plays a role in early T cell development (Secca et al. 2016) and its translocations have been observed in leukaemia (Jovanovic et al. 2017). Map3k1 is involved in the NFkB pathway and its deletion reduces B cell proliferation (Gallagher et al. 2007). Dyrk2 is involved in Myc degradation, cell proliferation and cell cycle progression (Taira et al. 2012). Arid1b is a component of the SWI/SNF chromatin remodelling complex and associates with BRG1. It is important in cell cycle control and tumour suppression and its mutations have been reported in B cell lymphomas (Shain and Pollack 2013). Aff3 is highly expressed in lymphocytes and its fusions to Bcl2, with which Igh also translocates, have been reported in lymphoma (Impera et al. 2008). Ly86 (MD-1) cooperates with CD180 and TLR4 in responses to bacterial lipopolysaccharide (Lee et al. 2012). Dyrk1a promotes quiescence during the large-to-small pre-B cell transition (Thompson et al. 2015). Erg acts very early in hematopoietic differentiation (Kruse et al. 2009) and its deletion or dysregulation has been reported in acute lymphoblastic leukaemia (Zhang et al. 2016). Lgals9 regulates T cell-mediated immunity by promoting expansion of T_{regs} (Mengshol et al. 2010).

Inter-chromosomal contacts in pre-B cells

In Rag/81X pre-B cells, the Igh locus retained the top 25 most frequent interactions it exhibited in pro-B cells including bins containing Pax5, Ebf1, Aff3, Foxo1 and Runx1 and gained a very frequent interaction with Bach2 (Appendix A, Appendix B), which was the highest hit in the dataset. Notably, the Igh viewpoint also gained frequent interactions with the Igk and Igl loci as they became active at the pre-B cell stage. Igh contacted both bins over the 240kb Igl locus and three bins over the 3.2Mb Igk locus. Other newly gained interactions by the Igh viewpoint in pre-B cells included bins containing Rngtt and Zfp608, Adam10 as well as two additional bins over the Ebf1 gene (chr11:44000001-44500000 and chr11:45000001-45500000). The Igk shared most of the top interactions of Igh including Ebf1, Foxo1, Pax5 and Bach2, and contacted the Igh and Igl loci. Igk also interacted with Ly86, whereas the Igh viewpoint lost that interaction in pre-B cells compared to pro-B cells. Moreover, the Igk

viewpoint interacted with Il7r, Zfp36l1, Rad51l1, Myb, Prdm1 (Blimp1), Dntt and Blnk whereas the Igh viewpoint did not. The Igl viewpoint showed reciprocal interactions with the Igh and Igk bins, involving all 7 bins over the Igk locus. The three Ig loci had in common several of the most frequent interactions including Pax5, Ebf1 and Foxo1 (Appendix B). The Igl viewpoint also contacted Bach2, albeit not as frequently as the Igh and Igk did. The three Ig loci also shared contacts with Cux1, Zfp608, Aff3, Dyrk2, Arid1b, Map3k1, Adam10 and PolII. The Igl viewpoint interacted with Irs2, Smarcd1 and Stat5, whereas the other Ig loci did not. Igl and Igk, but not Igh, interacted with Irf4, Myb, Il7r, Rad51l1, Prdm1 and Zfp36l1. In contrast to the Igh and Igk viewpoints, the Igl viewpoint did not interact with Runx1, Hmgb1, Irf8, Pik3r1 and Erg. The Pax5 viewpoint retained all interactions it made in pro-B cells and gained 470 new interactions in pre-B cells including Aff3, Cux1, Dyrk2, Hmgb1, Foxp1, Adam10, Prdm1 and Map3k1. However, the Pax5 viewpoint interaction landscape deviated from that of the Ig loci in that it did not interact with Bach2 and Ebf1. It only contacted a bin adjacent to Ebf1 (chr11:45000001-45500000) as its 228th interaction. The Foxo1 viewpoint lost 19, retained 66 and gained 256 interactions compared to pro-B cells and made contacts with most factors that the Ig loci interacted with. Its most frequent interactions were Pax5, Ebf1, Bach2, Igh, Igk, Igl, Foxp1, Ly68, Cux1, Rad51l1, Adam10, Prdm1 and Aff3. The Il7r viewpoint lost 19, retained 42 and gained 202 interactions compared to pro-B cells and it interacted with all 3 Ig loci as well as with the top hits Pax5, Foxo1, Bach2 and Ebf1. It did not interact with Runx1 and Cux1. Igk, Foxo1 and Il7r were the only viewpoints contacting Ikaros (Ikzf1), whereas only Foxo1 and Pax5 interacted with E2A (Tcf3). The Rag1Rag2 viewpoint gained 50 interactions in pre-B cells, which included Irf2bp2, Igk and Foxp1, but not Pax5, Foxo1, Ebf1 and Bach2.

Overall, the main interactions of the Ig viewpoints that were largely not present in pro-B cells and were gained in pre-B cells were with Bach2, Prdm1, Zfp608, Irf4, Adam10 and Arid1b. Bach2 was by far the most frequent new interaction in pre-B cells. It is expressed early in B cell development, binds to Rag1/2 promoters and is itself upregulated by Pax5 at the onset of V-DJ recombination. Bach2 has a crucial function in pre-B cells to ensure negative selection of cells producing auto-reactive BCRs via p53-mediated apoptosis (Swaminathan et al. 2013), and it is necessary for class switch recombination and somatic hypermutation (Muto et al. 2004) by delaying plasma cell differentiation (Igarashi et al. 2014). Prdm1 (Blimp1) is essential for plasma cell differentiation, it represses Pax5 and is itself repressed by Bach2 (Tanaka et al. 2016). Zfp608 has been shown to repress Rag1 and Rag2 expression in neonatal T cells (Zhang et al. 2006a). It has not been implicated in later lymphocyte development. Irf4 is important in the downregulation of pre-BCR, pre-B cell transition and light chain recombination (Lu et al. 2003). Irf4 is also essential for germinal centre B cells and plasma cells (Willis et al. 2014). Adam10 is expressed early in lymphocyte development and is required for marginal zone B cell formation (Gibb et al. 2010). Myb (c-Myb) is required for $CD19^{+}$ B cell formation and its deletion causes a developmental block at pre-pro-B cell stage (Fahl et al. 2009).

Inter-chromosomal contacts in thymocytes

Although the Ig loci are not considered to be active in the thymus, the Igh locus does undergo D-J recombination on a subset of alleles. The RAG complex is expressed in thymocytes and the Igh is anchored to the lamina by its 5' end with the 3' end facing the nuclear interior being more accessible (Stanhope-Baker et al. 1996; Afshar et al. 2006; Bolland et al. 2007). Capture Hi-C data showed that the Igh viewpoint did not interact with most of the genes that it contacted in B cells, but it did interact with Runx1, Pik3r1 and Akt3, which are expressed in both B cells and T cells (Lorsbach et al. 2004; Deau et al. 2014; Juntilla et al. 2007). The Igk and Igl viewpoints did not contact in thymus any of the regions that they contacted in B cell datasets. Igl did have 31 significant trans hits in thymocytes, but they did not contain genes with a role in B cell development and the vast majority of them mapped to chromosome 19, which suggests that in T cells Igl is surrounded by chromosome 19 possibly in repressive chromatin environment. The Pax5 viewpoint showed significant interactions with Igh and Arid1b in the thymus, but reciprocal interaction from the Igh to Pax5 was not detected. Similarly, the Il7r and Rag1Rag2 viewpoints contacted the Ig loci in thymocytes, but reciprocal interactions were not detected. This suggests that Pax5, Il7r and Rag1Rag2 interact with very few regions in thymocytes and the reads connecting them with the Ig loci are sufficient to be called significant. On the other hand, the Foxo1 viewpoint exhibited many significant interactions including Arid1b, Foxp1, Runx1, Myb, Igh, Ly86, Cux1, Aff3, Zfp36l2, Erg and Bach2. This suggests that the genomic environment of Foxo1 may not differ in thymocytes and B cells, as Foxo1 also functions as a transcription factor in T cell development.

Gene Ontology analysis showed enrichment for adaptive immune response genes

To characterise the genes in trans-interacting 0.5Mb bins I performed gene ontology (GO) analysis for Biological Process and Molecular Function terms using GOrilla (Eden et al. 2009) (http://cbl-gorilla.cs.technion.ac.il/). I combined all genes within the 0.5Mb bins that significantly interacted with the Igh, Igk or Igl in Rag/81X pre-B cells and they were run as the target list, against a background list of all mouse genes. GO terms significantly enriched ($P < 0.01$) in the target genes compared with the background list were returned (**Figure 52**). Of note, most probably only one gene in each significant 0.5Mb bin is responsible for mediating the interaction and while I can infer the potential gene of interest for a proportion of bins, this cannot be done systematically with a high level of confidence for all bins. Therefore, the input target list for GOrilla needed to contain every gene in significant 0.5Mb bins, creating a dataset with a high degree of noise. It is also possible that in some 0.5Mb bins an intergenic region encoding a regulatory element is responsible for the interaction and none of the genes. Remarkably, despite the noise in the data, among the top GO terms for Biological Process and Molecular Function were terms associated with immune response, adaptive immunity, B cell activation and B cell receptor binding and signalling (**Figure 52**).

This demonstrates that some of the interacting bins are highly enriched for genes involved in B cell-mediated immune response.

A

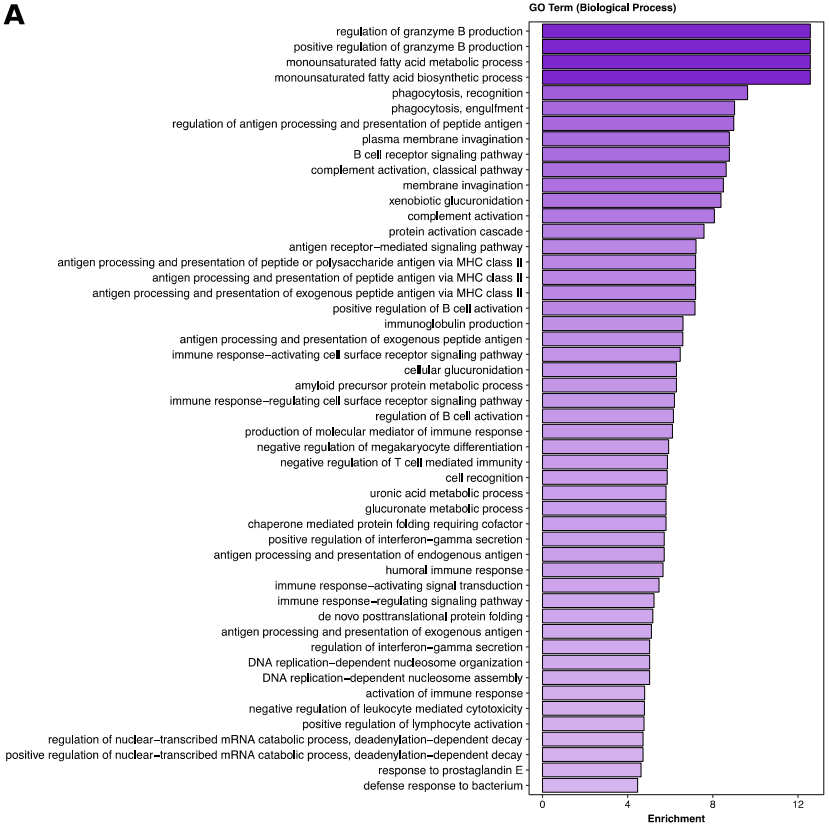
GO Term (Biological Process)
regulation of granzyme B production
positive regulation of granzyme B production
monounsaturated fatty acid metabolic process
monounsaturated fatty acid biosynthetic process
phagocytosis, recognition
phagocytosis, engulfment
regulation of antigen processing and presentation of peptide antigen
plasma membrane invagination
B cell receptor signaling pathway
complement activation, classical pathway
membrane invagination
xenobiotic glucuronidation
complement activation
protein activation cascade
antigen receptor–mediated signaling pathway
antigen processing and presentation of peptide or polysaccharide antigen via MHC class II
antigen processing and presentation of peptide antigen via MHC class II
antigen processing and presentation of exogenous peptide antigen via MHC class II
positive regulation of B cell activation
immunoglobulin production
antigen processing and presentation of exogenous peptide antigen
immune response–activating cell surface receptor signaling pathway
cellular glucuronidation
amyloid precursor protein metabolic process
immune response–regulating cell surface receptor signaling pathway
regulation of B cell activation
production of molecular mediator of immune response
negative regulation of megakaryocyte differentiation
negative regulation of T cell mediated immunity
cell recognition
uronic acid metabolic process
glucuronate metabolic process
chaperone mediated protein folding requiring cofactor
positive regulation of interferon–gamma secretion
antigen processing and presentation of endogenous antigen
humoral immune response
immune response–activating signal transduction
immune response–regulating signaling pathway
de novo posttranslational protein folding
antigen processing and presentation of exogenous antigen
regulation of interferon–gamma secretion
DNA replication–dependent nucleosome organization
DNA replication–dependent nucleosome assembly
activation of immune response
negative regulation of leukocyte mediated cytotoxicity
positive regulation of lymphocyte activation
regulation of nuclear–transcribed mRNA catabolic process, deadenylation–dependent decay
positive regulation of nuclear–transcribed mRNA catabolic process, deadenylation–dependent decay
response to prostaglandin E
defense response to bacterium
0
4
8
12
Enrichment

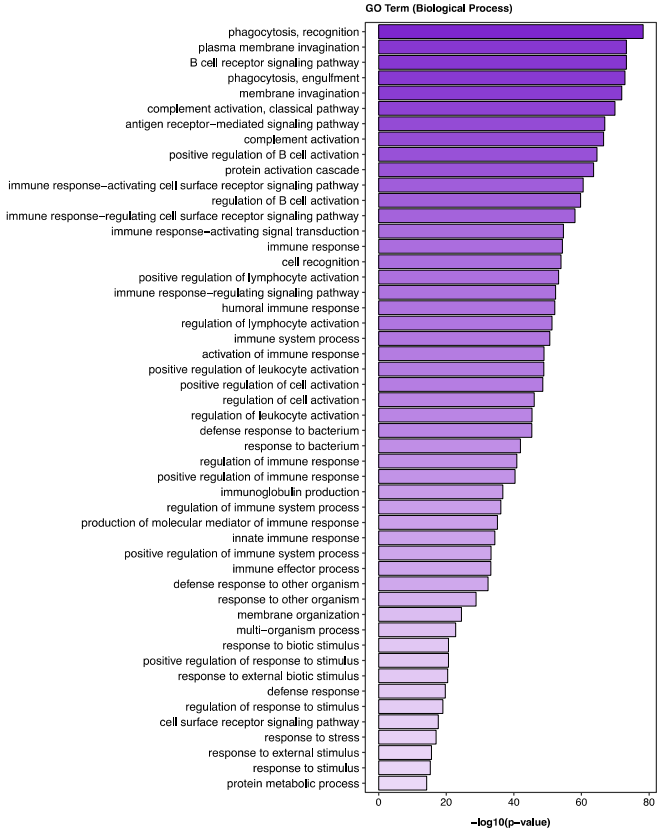
GO Term (Biological Process)
phagocytosis, recognition
plasma membrane invagination
B cell receptor signaling pathway
phagocytosis, engulfment
membrane invagination
complement activation, classical pathway
antigen receptor–mediated signaling pathway
complement activation
positive regulation of B cell activation
protein activation cascade
immune response–activating cell surface receptor signaling pathway
regulation of B cell activation
immune response–regulating cell surface receptor signaling pathway
immune response–activating signal transduction
immune response
cell recognition
positive regulation of lymphocyte activation
immune response–regulating signaling pathway
humoral immune response
regulation of lymphocyte activation
immune system process
activation of immune response
positive regulation of leukocyte activation
positive regulation of cell activation
regulation of cell activation
regulation of leukocyte activation
defense response to bacterium
response to bacterium
regulation of immune response
positive regulation of immune response
immunoglobulin production
regulation of immune system process
production of molecular mediator of immune response
innate immune response
positive regulation of immune system process
immune effector process
defense response to other organism
response to other organism
membrane organization
multi–organism process
response to biotic stimulus
positive regulation of response to stimulus
response to external biotic stimulus
defense response
regulation of response to stimulus
cell surface receptor signaling pathway
response to stress
response to external stimulus
response to stimulus
protein metabolic process
0
20
40
60
80
–log10(p–value)

B

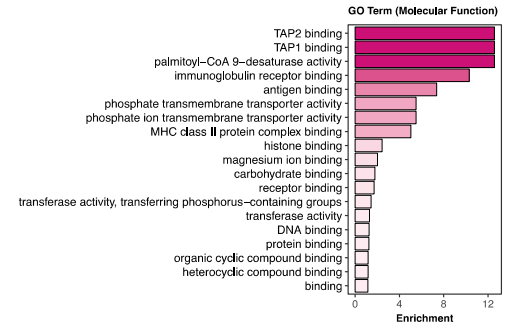
GO Term (Molecular Function)
TAP2 binding
TAP1 binding
palmitoyl–CoA 9–desaturase activity
immunoglobulin receptor binding
antigen binding
phosphate transmembrane transporter activity
phosphate ion transmembrane transporter activity
MHC class II protein complex binding
histone binding
magnesium ion binding
carbohydrate binding
receptor binding
transferase activity, transferring phosphorus–containing groups
transferase activity
DNA binding
protein binding
organic cyclic compound binding
heterocyclic compound binding
binding
0
4
8
12
Enrichment

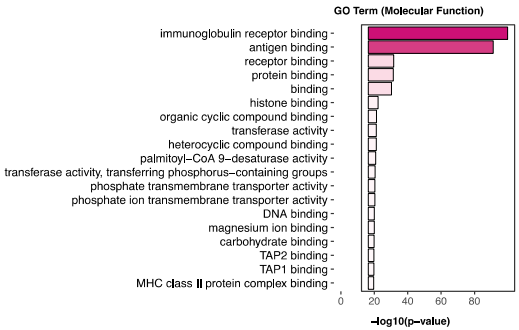
GO Term (Molecular Function)
immunoglobulin receptor binding
antigen binding
receptor binding
protein binding
binding
histone binding
organic cyclic compound binding
transferase activity
heterocyclic compound binding
palmitoyl–CoA 9–desaturase activity
transferase activity, transferring phosphorus–containing groups
phosphate transmembrane transporter activity
phosphate ion transmembrane transporter activity
DNA binding
magnesium ion binding
carbohydrate binding
TAP2 binding
TAP1 binding
MHC class II protein complex binding
0
20
40
60
80
–log10(p–value)

Figure 52. Gene Ontology terms associated with Ig loci trans interactions are enriched for terms related to B cell function. GO terms analysis was performed in GOrilla (Eden 2009). All genes in statistically significant 0.5Mb bins interacting with Igh, Igk and Igl in Rag/81X pre-B cells were pooled and served as an input to GOrilla. **A.** Top 50 enriched terms for Biological Process sorted by enrichment level (left) or p-value (right). **B.** All terms for Molecular Function sorted by enrichment level (left) or p-value (right).

Inter-chromosomal interactions overlap with several regions implicated in malignant translocations

Among previous studies that assessed the connection between the genes residing in close proximity to the Igh locus and their involvement in malignant translocations, one study observed a correlation between physical proximity and frequency of translocations (Rocha et al. 2012) whereas another one did not, attributing the frequency of translocations to the levels of AID-mediated DNA damage (Hakim et al. 2012). To examine whether significant inter-chromosomal interactions detected in Capture Hi-C contain genes implicated in malignant translocations in B cells, I compared them with genes translocating in human cancers reported in the literature. Only around half of the genes reported to translocate in early B cell lymphomas or leukaemias interacted with Capture Hi-C viewpoints. The Igh locus has been reported to translocate with several genes present in significant trans hit bins: Pax5, Ebf1, Aff3, Cd79b, Irf2bp2, Clec2d, Irf8, Nfkb2 and Foxp1 (reviewed in Somasundaram et al. 2015). On the other hand, many other translocations have been reported that involved genes not interacting significantly with the Igh locus: myc, Irf4, Ly6e, Dusp4, Cd19, Mir-155, Aicda, Bcl2l11, Bcl2, Bcl1, Bcl10, April, Ccnd1, Malt1, Crlf2 and Epor. Interestingly though, Irf4 does interact significantly with Igk, IgL, Pax5 and Il7r in pre-B cells. Notably, translocations between the Igh and Malat1, Bcl2, Bcl1, Ccnd1 and Crlf2 are most likely RAG-mediated on the Igh end rather than AID-mediated (Lieber 2016). The Igk has been reported to translocate with Bcl6, but they do not interact by Capture Hi-C. Pax5 translocates with significant trans hits such as Klf3, Jake, Taok1, Asxl1 and Igh (reviewed in Coyaud et al. 2010) but also with several non-trans hit genes: Foxp1, Ncor1, Dach2, Golga6, Etv6, Enl, Pml and Pom121. Notably, Foxp1 interacts with the Ig loci in pre-B cells, but not with Pax5. Additionally, Ebf1 has been reported to translocate with Pdgfrb and although Ebf1 has not been baited and cannot serve as a viewpoint in Capture Hi-C, interestingly, the Foxo1 viewpoint did interact with Pdgfrb. FOXO1 and EBF1 transcription factors have been shown to work cooperatively by binding the same targets (Lin et al. 2010), including each other and therefore this observation suggests that Foxo1 and Ebf1 genes may both interact with Pdgfrb. Overall, I observed that around a third of genes implicated in translocations in early B cells was among the genes in bins involved in significant trans interactions with the viewpoints. This suggests that some genes may be more prone to translocations because of frequent proximity, but the majority of translocation partners did not show frequent interactions. The comparison done here however has the caveat of using translocations reported in human cells, which might have different chromatin organisation to the mouse genome and some genes might be on different chromosomes in the mouse. Overall, trans interaction analysis opens

new avenues for discovering unreported to date translocation partners among frequently contacted regions.

Lack of interactions with many very early lymphocyte development genes

I did not detect interactions with very early lymphoid lineage factors including PU.1 (Sfp1), Oct1, Oct2, Lyl1, Tal1, Elmo2, Gata2 and Flt3. Interactions with other early factors such as Ikaros, E2A (Tcf3) and Bcl11a were detected with only a few viewpoints, not including the Igh locus. Some of these early factors are dispensable at stages later than CLPs, which might explain the lack of interactions. Overall, Capture Hi-C data suggests that in pro-B and pre-B cells the Ig loci make contacts with genes particularly responsible for B cell commitment and pro-B to pre-B cell transition.

4.2.3. Igh, Igk and Igl gain interactions in a developmental stage-specific manner

The immunoglobulin loci are activated for recombination in a stage-specific manner. The Igh locus is activated in pre-pro-B cells and pro-B cells to undergo V(D)J recombination and the light chain loci Igk and Igl are activated at the pre-B cell stage to undergo V-J recombination. Accordingly, a clear developmental stage-specific pattern emerged for significant trans interactions obtained from the z-score analysis (**Figure 53**). The Igh locus made 106 significant contacts in $Rag^{-/-}$ pro-B cells. This number increased to 132 in Rag/81X pre-B cells and it also made 34 significant contacts in thymocytes (**Table 12** and **Figure 53**). The interactions in thymocytes may be attributed to the fact that although he Igh is tethered to the lamina by its 5' end, the 3' end of the locus is active potentially able to make chromatin contacts with other loci. Interestingly, the high number of significant contacts in Rag/81X pre-B cells suggests that the expression of the Vh81X transgene does not inactivate the endogenous Igh alleles, although it is not possible to be sure that the interactions are not altered by the presence of the transgene or the V regions of the endogenous loci are not inactive. The Igk and Igl light chain loci are inactive in pro-B cells, which was reflected in the lack of trans contacts: the Igl had no interactions and Igk had five with rather low z-scores (Appendix A) (**Figure 53**). In pre-B cells, however, both light chain loci gained a large number of significant trans contacts: 169 for Igk and 146 for Igl. In contrast to the Igh, the Igk and Igl did not show many interactions in thymocytes, the Igk had one contact and the Igl had 31 contacts, 24 of which were with chromosome 19. These observations demonstrate that inter-chromosomal contacts coincide with Ig loci activation in a developmental stage-specific manner. This gives confidence that the trans contacts identified by Capture Hi-C likely reflect the genomic contacts the Ig loci make in wild type B cells.

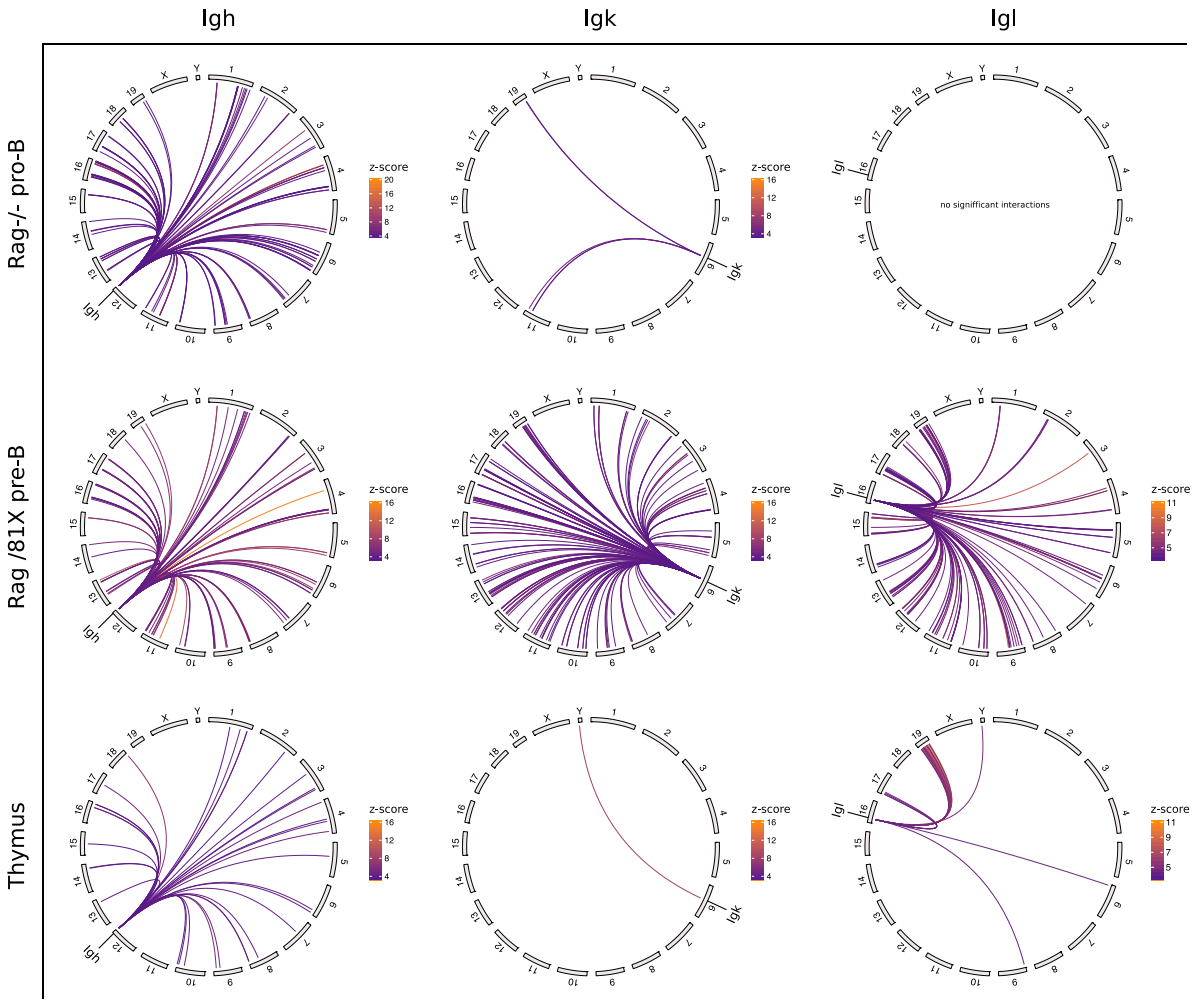

Figure 53. Trans interaction from the Ig viewpoints are developmental stage-specific. Statistically significant trans interactions from Table 12 were visualised as circular plots using the ggbio Bioconductor package (Yin 2012). Grey rectangles denote chromosomes and purple-to-orange arcs denote trans interactions. Z-score values are indicated by the colour of the arcs. The Igh and Igk viewpoints are marked on chr12 and ch6, respectively.

Second, I determined whether the same interactions persist at pre-B and pro-B stages (**Figure 54**). Out of the 106 contacts in pro-B cells, the Igh lost 39 in pre-B cells and gained 65 new ones. This shows that more than half of Igh contacts were present at both stages. Of note, the interactions that were lost still had high z-score just under 3.5 (Appendix B), further strengthening the persistence of Igh interactions in pro-B and pre-B cells. The 5 Igk interactions in pro-B cells were not among the 169 interactions acquired in pre-B cells. Conversely, all of Pax5 and Rag1Rag2 contacts present in pro-B cells were among their contacts in pre-B cells. The Foxo1 and Il7r viewpoints exhibited a pattern similar to the Igh, retaining 30-50% of their interactions and gaining a large number of new ones in pre-B cells compared to pro-B cells.

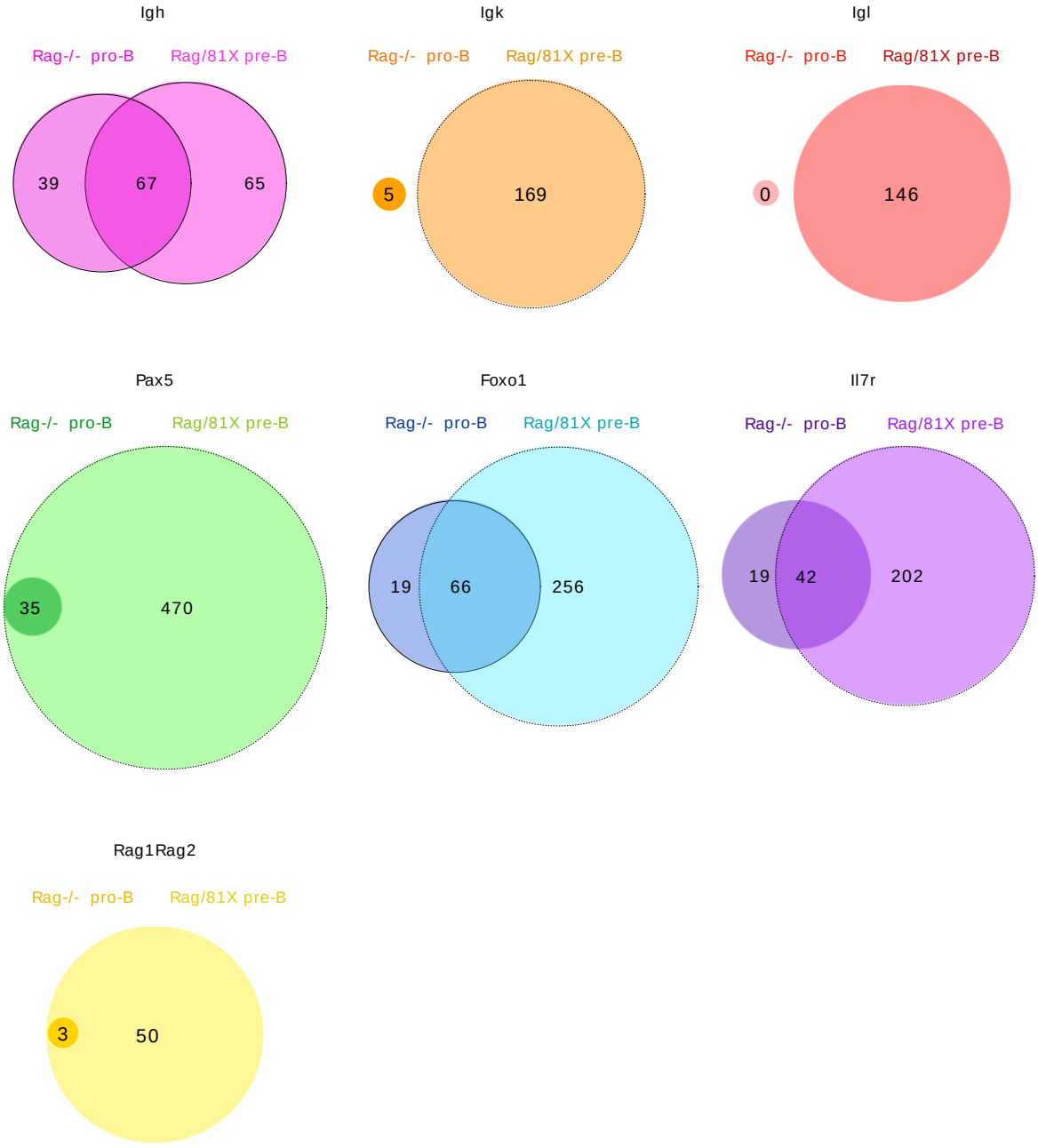

Figure 54. Overview of the number of trans interactions for each Capture Hi-C viewpoint. Venn diagrams show overlap of statistically significant trans interactions in Rag$^{-/-}$ pro-B cells and Rag/81X pre-B cells for each Capture Hi-C viewpoint.

Third, I examined the correlation between the overall trans contacts from the Igh and Igk viewpoints in Rag$^{-/-}$ pro-B cells and Rag/81X pre-B cells by plotting the virtual 4C raw data from the two viewpoints against each other (**Figure 55**). The genome-wide interaction profiles involving the Igh and the Igk loci showed very high positive correlation in Rag/81X pre-B cells but not in Rag$^{-/-}$ pro-B cells. This demonstrates that the trans interaction pattern of the Igk locus becomes similar to that of the Igh locus in pre-B cells. Overall, the profiles of significant interactions from the Ig viewpoints in all datasets clustered according to whether the Ig loci are active or inactive in a given cell type, re-iterating the similarities between active loci (**Figure 56**).

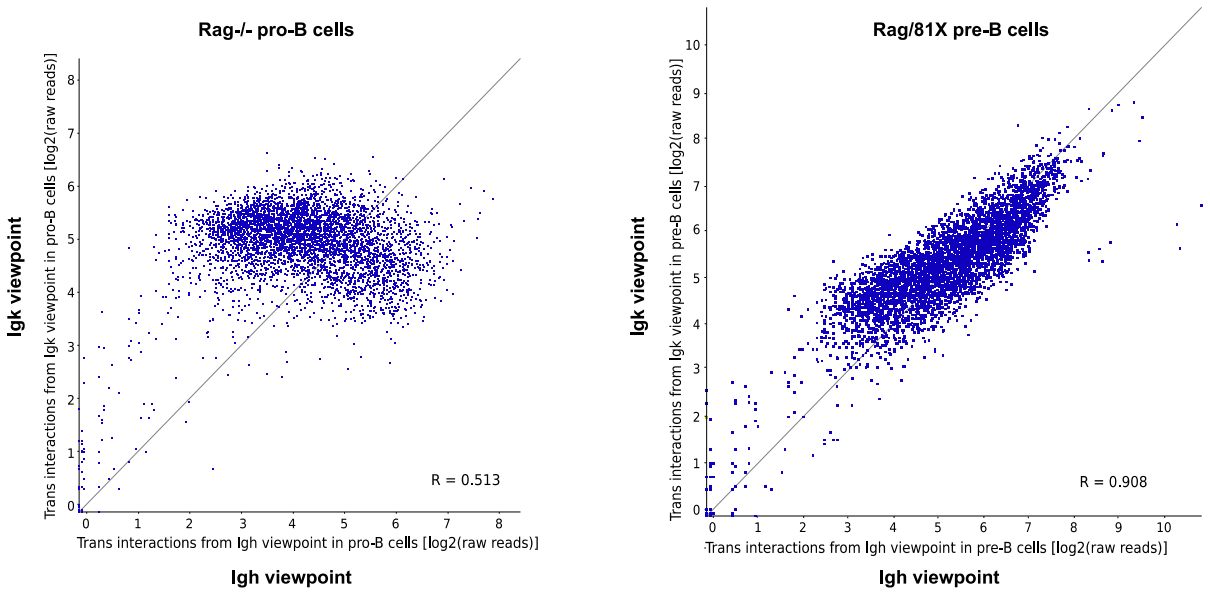

Figure 55. In pre-B cells, the Igk locus becomes engaged in similar trans interactions as the Igh. All other ends from the Igh and Igk virtual 4C were quantified in 0.5Mb bins genome-wide and plotted against each other as log2(raw reads). An average of biological replicates. R - Pearson's correlation coefficient.

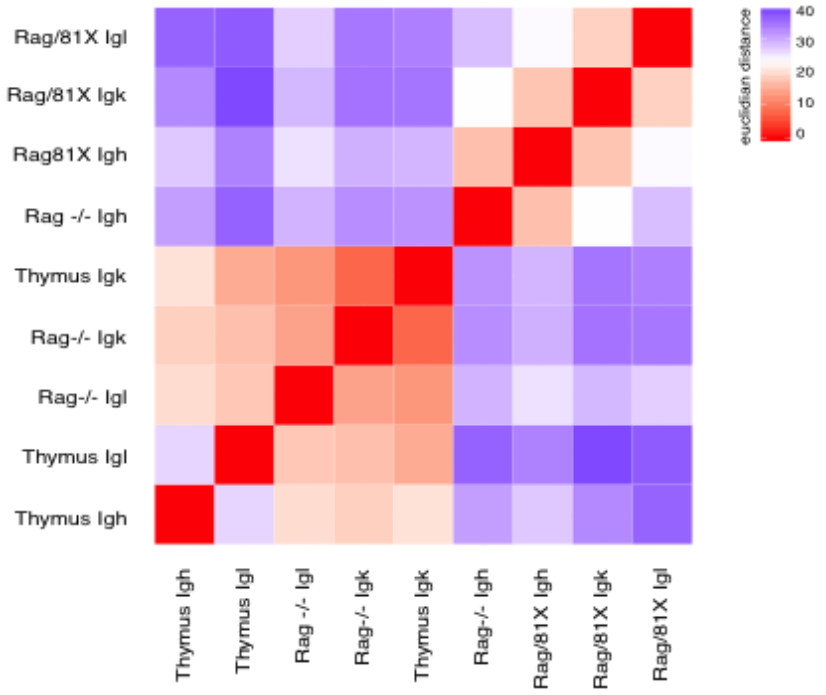

Figure 56. Inter-chromosomal interactions cluster based on the activity of the Ig viewpoint. Hierarchical clustering of statistically significant trans interaction profiles from the Ig viewpoints was performed using the Cluster and Factoextra R packages. Clustered by euclidean distance. Low distance values correspond to high similarity.

Ig loci share many trans contacts in pre-B cells

To further investigate the extent of contact overlaps I examined how many interactions the Ig loci had in common (**Figure 57**) as well as how many of those contacts were also shared by other baited viewpoints (**Figure 58**). The term 'shared' describes bins identified as interaction partners of two or more viewpoints and does not imply simultaneous 3-way interactions as it is not possible to discern from Capture Hi-C data whether interactions involving more than two genomic regions are simultaneous or mutually exclusive (discussed further in section 4.3). In $Rag^{-/-}$ pro-B cells, the 106 interactions of the Igh locus were different to the 5 contacts the Igk made and to the 31 contacts the Igl made (**Figure 57**). 5 of the Igh interactions in pro-B cells overlapped with those in the thymus, whereas the 5 Igk contacts in pro-B cells did not overlap with its single contact in the thymus. In Rag/81X pre-B cells on the other hand, the Ig loci showed a large overlap of interactions, with all three loci having 29 interactions in common. The Igh and Igk shared 79 contacts, Igh and Igl shared 39 and Igk and Igl shared 75.

The Pax5 viewpoint shared most of its trans contacts with the Foxo1 viewpoint in pro-B cells and both of these viewpoints shared several contacts with the Igh (**Figure 58**). In pre-B cells, a vast overlap of interactions was observed between all five viewpoints. 23 interactions were shared by the Ig loci, Foxo1 and Pax5 viewpoints, which accounts for the majority of contacts shared by the three Ig loci. These observations provide evidence that the trans interactions involving the Ig loci in pro-B and pre-B cells are not random, as they reflect the developmental stage-specific aspect of Ig loci activation, are B cell-specific and are characteristic for more than one Ig locus. This suggests that the Ig loci are frequently present in similar chromatin environments and in physical proximity. Indeed, among the significant interactions for each Ig viewpoint there are bins mapping to the other two Ig loci (Appendix A) (discussed in 4.2.3).

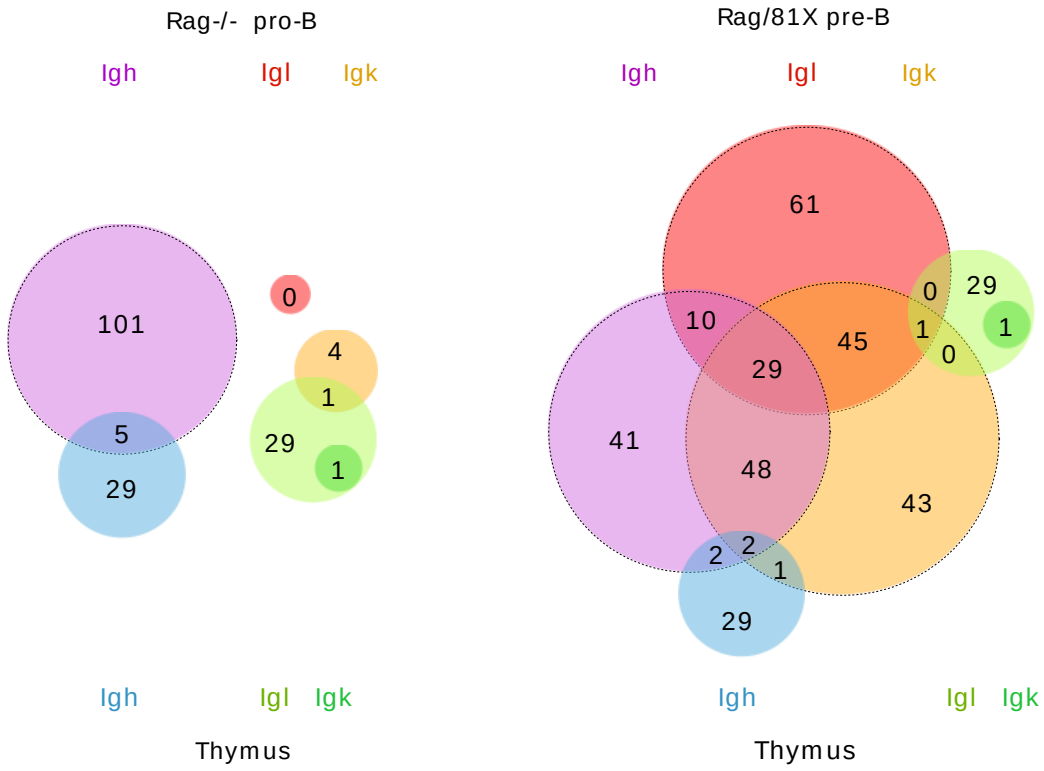

Figure 57. The Ig loci share over half of trans interaction partners. Venn diagrams show overlaps of statistically significant trans contacts from the Ig viewpoints in Rag$^{-/-}$ pro-B cells (top left, warm colours), Rag/81X pre-B cells (top right, warm colours) and thymus (bottom left and right, cold colours).

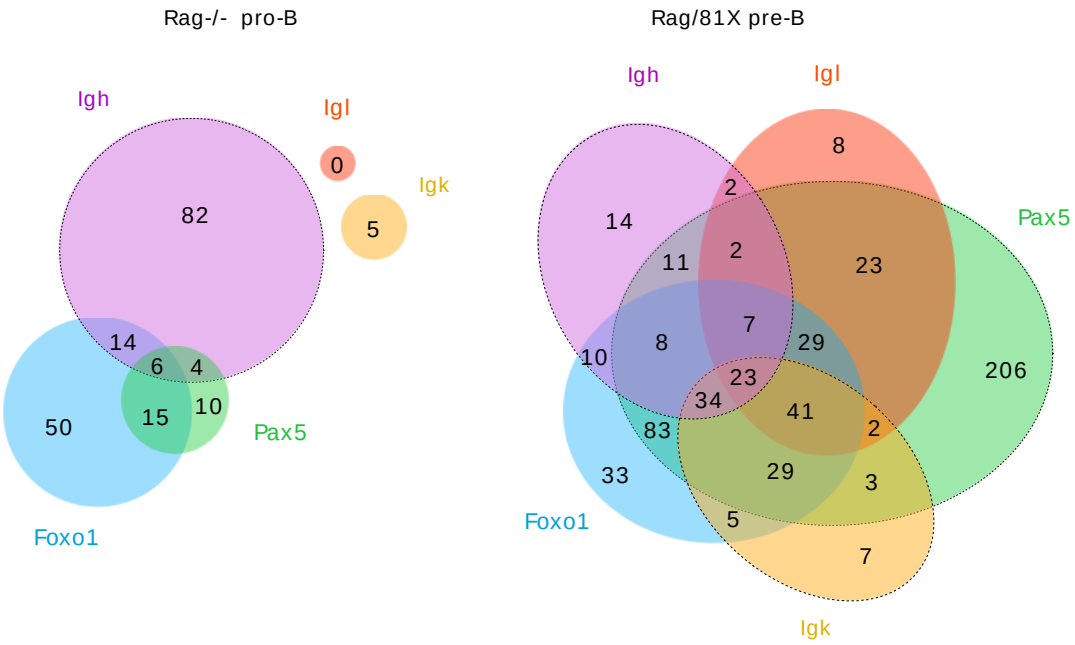

Figure 58. The Ig loci share many trans interactions with Pax5 and Foxo1 viewpoint. Venn diagrams show overlaps of statistically significant trans contacts from five Capture Hi-C viewpoints in Rag$^{-/-}$ pro-B cells and Rag/81X pre-B cells. Additional interactions in pre-B cells that are not shown: Foxo1 and Igl share 1 contact; Igk and Igl share 1 contact; Foxo1, Igk and Igl share 2 contacts; Foxo1, Igh and Igl share 1 contact; Foxo1, Igh and Igk share 11 contacts; Igh, Igk and Pax5 share 3 contacts; Foxo1, Igh, Igk and Igl share 5 contacts; and Igh, Igk, Igl and Pax5 share 1 contact.

4.2.4. Inter-chromosomal interactions cluster by viewpoint and developmental stage

To gain insight into the similarities that define the inter-chromosomal interaction profiles of the Igh, Igk, Igl, Pax5, Foxo1, Il7r and Rag1Rag2 viewpoints I performed hierarchical clustering of significant trans hits including all interactions significant for at least one viewpoint. To follow the established stringency of significant interaction calling (described in 4.2.1), for those bins that were deemed insignificant for a particular viewpoint due to one biological replicate's z-score being below 3.5, despite the average being above 3.5, I reported the minimum z-score value. Therefore, in hierarchical clustering analysis in this section, an average z-score was used for bins that were significant or insignificant in all biological replicates, but the minimum z-score was used for bins, which although they had an average z-score above 3.5, one of the biological replicates was below 3.5. The summary of all z-scores used as an input to hierarchical clustering can be found in Appendix B.

Clustering for 3 viewpoints - Igh, Igk and Igl

First, I performed hierarchical clustering of 0.5Mb bins significantly interacting with at least one Ig viewpoint in $Rag^{-/-}$ pro-B and Rag/81X pre-B cells. This revealed clustering of the datasets corresponding to active or inactive Ig loci in given cell types, as indicated by the dendrogram on the left of the heatmap in **Figure 59**A. The upper group of four clustered datasets contains interactions of all Ig loci in pre-B cells and interactions of the Igh in pro-B cells, whereas the bottom cluster of five datasets contains interactions of the Ig loci in the thymus as well as the Igk and Igl interactions in pro-B cells.

Subsequently, I performed hierarchical clustering again on the active datasets only (**Figure 59**B). This analysis identified a top cluster of 0.5Mb bins containing Ebf1, Bach2, Foxo1 and Pax5, followed by pre-B cell-specific interactions between the Ig loci themselves as well as with Zfp608, Zfp36l1, Arid1b, Adam10, Myb and Il7r. Further, Runx1, Irf2bp2, Map3k1, Cux1, Erg and Aff3 characterise mainly the Igh and Igk viewpoints. To sum up, this clustering analysis identified the top inter-chromosomal interaction partners shared by the Ig loci and showed clusters of pro-B and pre-B cell specific contacts.

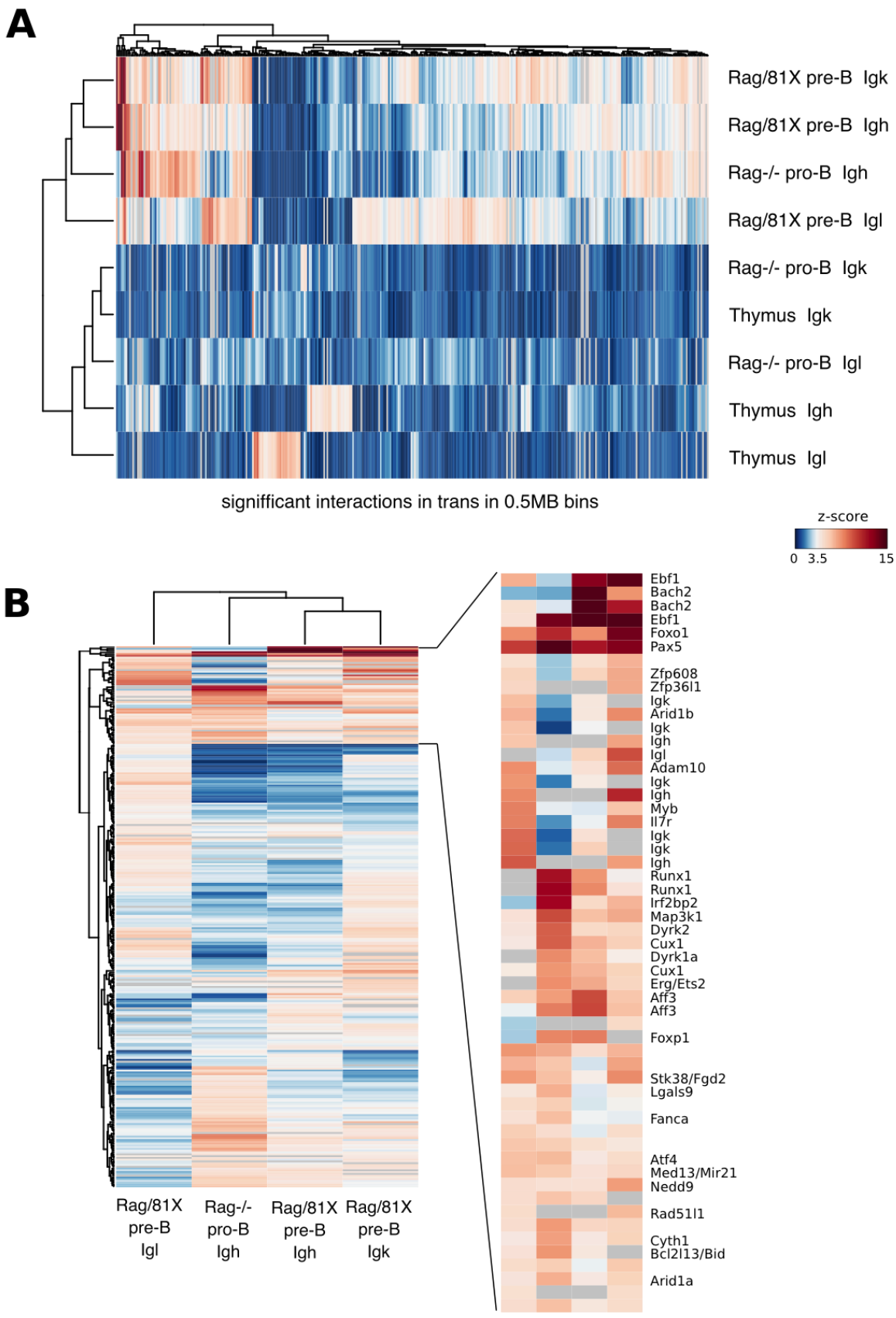

Figure 59. The Ig loci have similar trans interaction pattern when they are active. All interactions in 0.5Mb bins from the Ig viewpoints, statistically significant in at least one cell type, were clustered using heatmap.2 in R with default distance function ('Euclidean'), default clustering function ('complete') and dendrogram clustering was applied to both columns and rows. White-to-red bins have z-scores > 3.5 and white-to-blue bins have z-scores < 3.5. **A.** Clustering of trans interactions from

three Ig viewpoints in three cell types. **B.** Clustering of trans interactions in 'active' datasets (left) and a zoom in on the top cluster of bins (right). Genes of interest are listed next to selected 0.5Mb bins.

Clustering for 7 viewpoints - Ig loci, Pax5, Foxo1, Il7r and Rag1Rag1

Next, I performed hierarchical clustering on all 7 viewpoints in 3 cell types (**Figure 60**A). The dendrogram on the left of the heatmap shows that the bins contacting the three Ig loci in Rag/81X pre-B cells cluster together with datasets from the Igh, Pax5 and Foxo1 viewpoints in $Rag^{-/-}$ pro-B cells as well as Foxo1 in the thymus, establishing one active cluster (top 7 datasets in **Figure 60**A). Notably, a second active cluster was formed by bins interacting with the Pax5, Foxo1 and Il7r viewpoints in Rag/81X pre-B cells. The negative cluster contained most thymus datasets and $Rag^{-/-}$ pro-B datasets for Igk, Igl and Il7r viewpoints. The interactions of the Rag1Rag2 viewpoint in both pro-B and pre-B cells occupied a separate cluster.

Further, I performed hierarchical clustering again on the two active clusters (**Figure 60**B and **Figure 61**). As a result of including Pax5 and Foxo1 viewpoints in pro-B cells in the active cluster identified in **Figure 59**, the bins containing the Igh locus genes became the top contacts defining this cluster, followed by the top bins from **Figure 59**B: Pax5, Foxo1, Ebf1 and Bach2 (**Figure 60**B). The second active cluster (**Figure 61**) showed similar top interacting bins as well as multiple Igk bins. Overall, this 7 viewpoint clustering analysis revealed similar patterns to the 3 viewpoint analysis, which shows that the non-Ig viewpoints share the interaction pattern of the Ig loci.

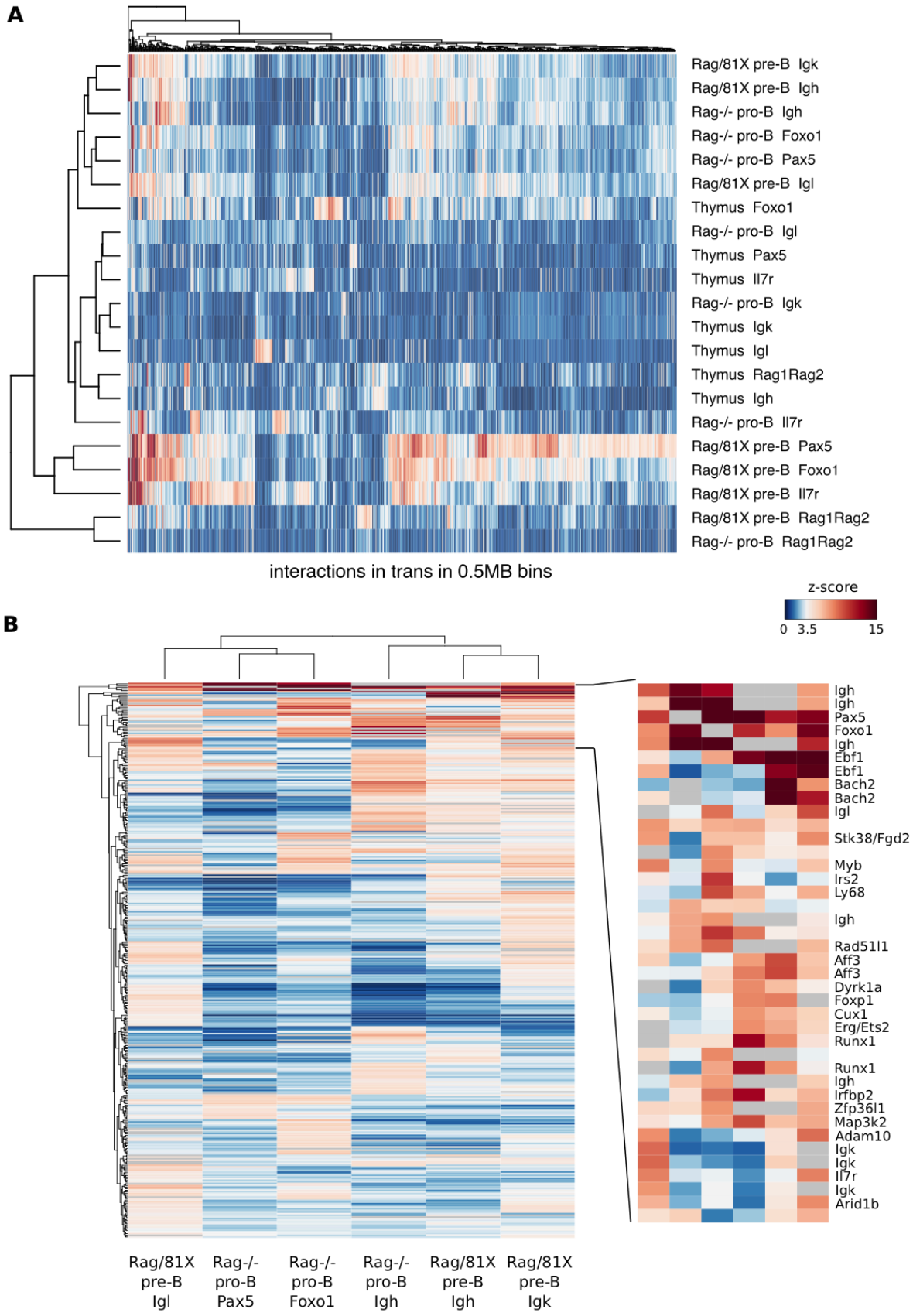

Figure 60. Seven Capture Hi-C viewpoints have similar trans interactions. All interactions in 0.5Mb bins from the Igh, Igk, Igl, Pax5, Foxo1, Il7r and Rag1Rag2 viewpoints, statistically significant in at least one cell type, were clustered using heatmap.2 in R with default distance function ('Euclidean'), default clustering function ('complete') and dendrogram clustering was applied to both columns and rows. White-to-red bins have z-scores > 3.5 and white-to-blue bins have z-scores < 3.5. **A.** Clustering of trans interactions from seven viewpoints in three cell types. **B.** Clustering of trans

interactions in six ‘active’ datasets (left) as determined by the top part of the row dendrogram in (A) and a zoom in on the top cluster of bins (right). Genes of interest are listed next to selected 0.5Mb bins
.

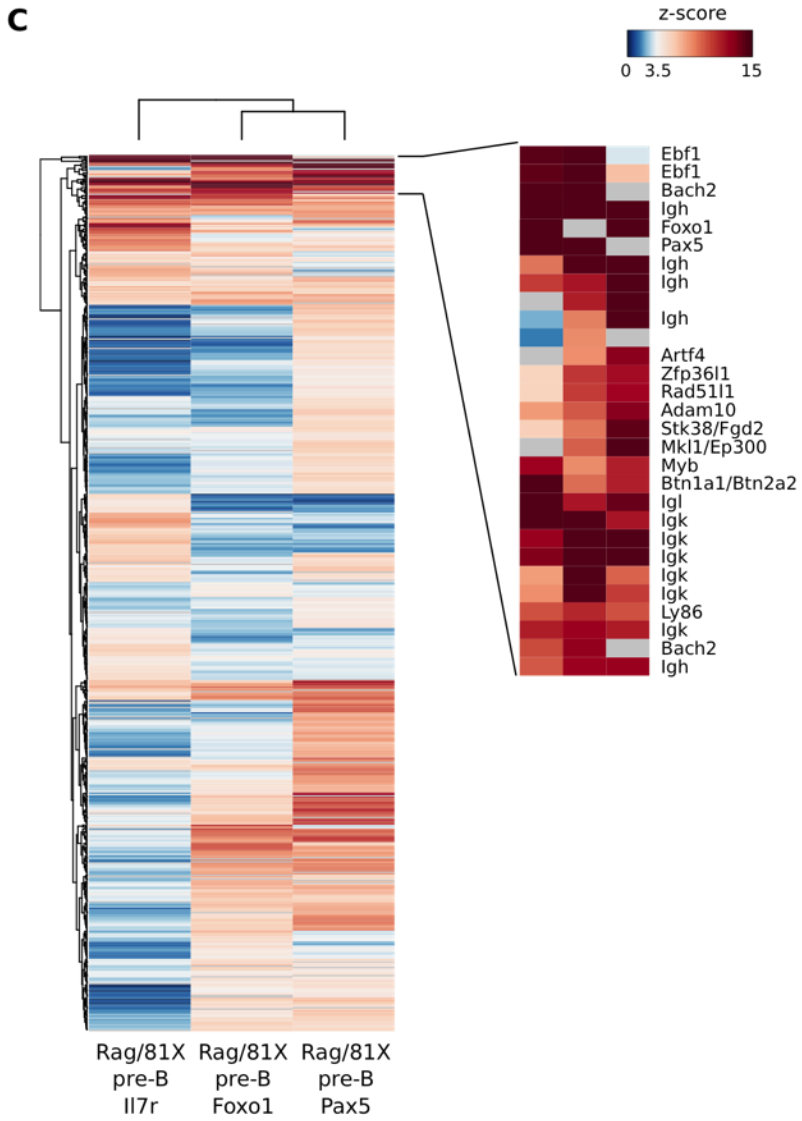

Figure 61. Clustering of trans interactions in three ‘active’ datasets (left) as determined by the bottom part of the row dendrogram in Figure 50A. Zoom in on the top cluster of bins (right). Genes of interest are listed next to selected 0.5Mb bins.

4.2.5. Inter-chromosomal interactions segregate to A and B compartments depending on the activity of the viewpoint

To further characterise the 0.5Mb bins interacting with the Capture Hi-C viewpoints and the chromatin environment of the viewpoints in different cell types I performed an A/B compartment analysis. Hi-C analyses to date have shown that genome-wide interactions segregate into an alternating pattern of two types of large multi-megabase genomic domains: A compartments containing gene-rich euchromatic regions and B compartments containing gene-poor heterochromatic regions (Lieberman-Aiden et al. 2009; Yaffe and Tanay 2011; Nagano et al. 2017; Belaghzal et al. 2017). A and B compartments display increased interaction frequencies with the same compartment type. A and B compartments emerged as

the dominant quality in discrimination between active and inactive chromatin as established by the principal component analysis (PCA), which identifies the major contributor to the variance in Hi-C data.

I used the genome-wide A and B compartments identified in Hi-C datasets (described in section 2.8.2.) to examine which compartments the significant trans hits fall into. First, I pooled all significant 0.5Mb trans hits from the Ig viewpoints in the 'active' datasets (i.e. Igh hits in pro-B and pre-B cells, Igk hits in pre-B cells and Igl hits in pre-B cells), and measured what compartments these bins fall into in each cell type (**Figure 62**A). A vast majority of these bins resided in A compartments in all 3 cell types, even in thymocytes when not contacted by the Ig loci. This pattern suggests that the Ig loci interaction partners tend to reside in active chromatin domains regardless of the presence of an interaction. Second, I examined the compartments of the trans hits in the 'inactive' datasets (**Figure 62**B). I observed that the bins interacting with the Igh locus in the thymus reside in A compartments (and the same bins also reside in A compartment in pro-B and pre-B cells, not plotted). On the other hand, the bins contacting the Igk in pro-B cells as well as the bins contacting the Igl in the thymus reside in B compartments (and the same bins also reside in B compartments in pro-B and pre-B cells, not plotted). The Igk viewpoint did not have any significant interactions in the thymus and the Igl did not have any significant contacts in pro-B cells. These observations suggest that the Igh and its contacts reside in an active chromatin environment in all three cell types, whereas the Igk and Igl and their contacts reside in repressive chromatin in cells other than pre-B cells.

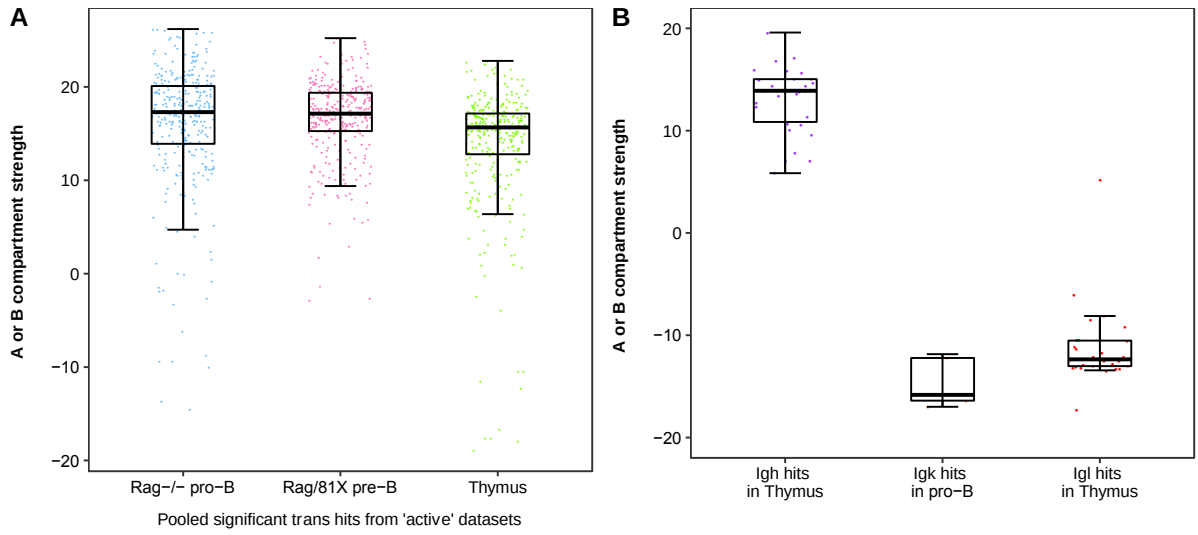

Figure 62. Trans hits in active datasets as well as Igh hits in thymocytes tend to reside in A compartments. A/B compartment analysis was performed in HOMER on 0.5Mb bins using non-enriched Hi-C datasets. Values > 0 indicate A compartments and the higher the positive number the stronger the A compartment, whereas values < 0 indicate B compartments and the lower the negative number the stronger the B compartment. **A**. Trans hits from the 'active' datasets (Igh viewpoint in $Rag^{-/-}$ pro-B cells and Rag/81X pre-B cells, Igk viewpoint in Rag/81X pre-B cell and Igl viewpoint in Rag/81X pre-B cells) were pooled and their A/B compartments plotted in each cell type. **B**. Trans hits from the 'inactive' datasets are plotted separately.

To examine this further, I inspected selected 0.5Mb bins to explore whether there are any deviations from the general rules described in the previous paragraph. The Igh locus (six 0.5Mb bins), despite having low read coverage in Hi-C to reliably call A/B compartments on each 0.5Mb bin, can be generally attributed an A compartment in all three cell types (**Figure 63**A). On the contrary, the Igk locus (seven 0.5Mb bins) resides in a B compartment when inactive in pro-B cells and thymocytes and its environment changes to an A compartment in pre-B cells (**Figure 63**B). Similarly, the Igl locus resides in a B compartment in thymocytes, in an A compartment in pre-B cells and in an ambivalent compartment in pro-B cells (**Figure 63**C). Genes that always reside in A compartments include Pax5, Runx1, Il7r, Arid1b, Cux1, Irf2bp2, Irf4, Zfp608 and Zfp36l1 (**Figure 63**D, F, H, **Figure 64**). Interestingly, Ebf1 resides in an A compartment in pro-B and pre-B cells, but in a B compartment in thymocytes. Bins around the Ebf1 bin become more enriched for A compartments in pre-B cells compared to pro-B cells, concomitantly with many Capture Hi-C viewpoints showing more frequent interactions with Ebf1 and surrounding bins in pre-B cells. Lin *et al*. 2012 have previously shown that Ebf1 switches from a B compartment in pre-pro-B cells to an A compartment in pro-B cells (Lin et al. 2012). Bach2 spans two 0.5Mb bins and the downstream bin always resides in an A compartment, whereas the upstream bin has a very weak enrichment for A compartment in pre-B cells and for B compartment in pro-B cells.

I then inspected the A/B compartment status of several 0.5Mb bins that were called significant in the 'inactive' datasets (**Figure 65**). For example, the Akt3 bin, similarly to Runx1, interacts with the Igh viewpoint in all three cell types and in each of them it resides in an A compartment. The 9_112000000 (chr9:112000000-112500000) bin and the 2_139500000 (chr2:139500000-140000000) bin, which did not contain any obvious genes of interest, are examples of bins that interact with the Igh viewpoint in the thymus, but not in B cells, and reside in A compartments only in thymocytes. On the other hand, other bins including 11_92500000 (chr11:92500000-93000000) and 19_50500000 (ch19:50500000-51000000) interact with the Igk viewpoint only in the thymus but they reside in large B compartments in all three cell types. Similarly, the 19_43000001 (chr19:43000000-43500000) bin contacts the Igl viewpoint in thymocytes and resides in a distinct B compartment between two larger A compartments in all cell types.

Overall, most trans hit bins reside in either an A or a B compartment in all three cell types, suggesting that their chromatin environment does not change dramatically in a developmental stage-specific manner. A compartments might poise genomic regions for functional interactions with the Ig loci at appropriate developmental stages. For a minority of bins, the compartment type changes in different cells and according to the presence or absence of an interaction.

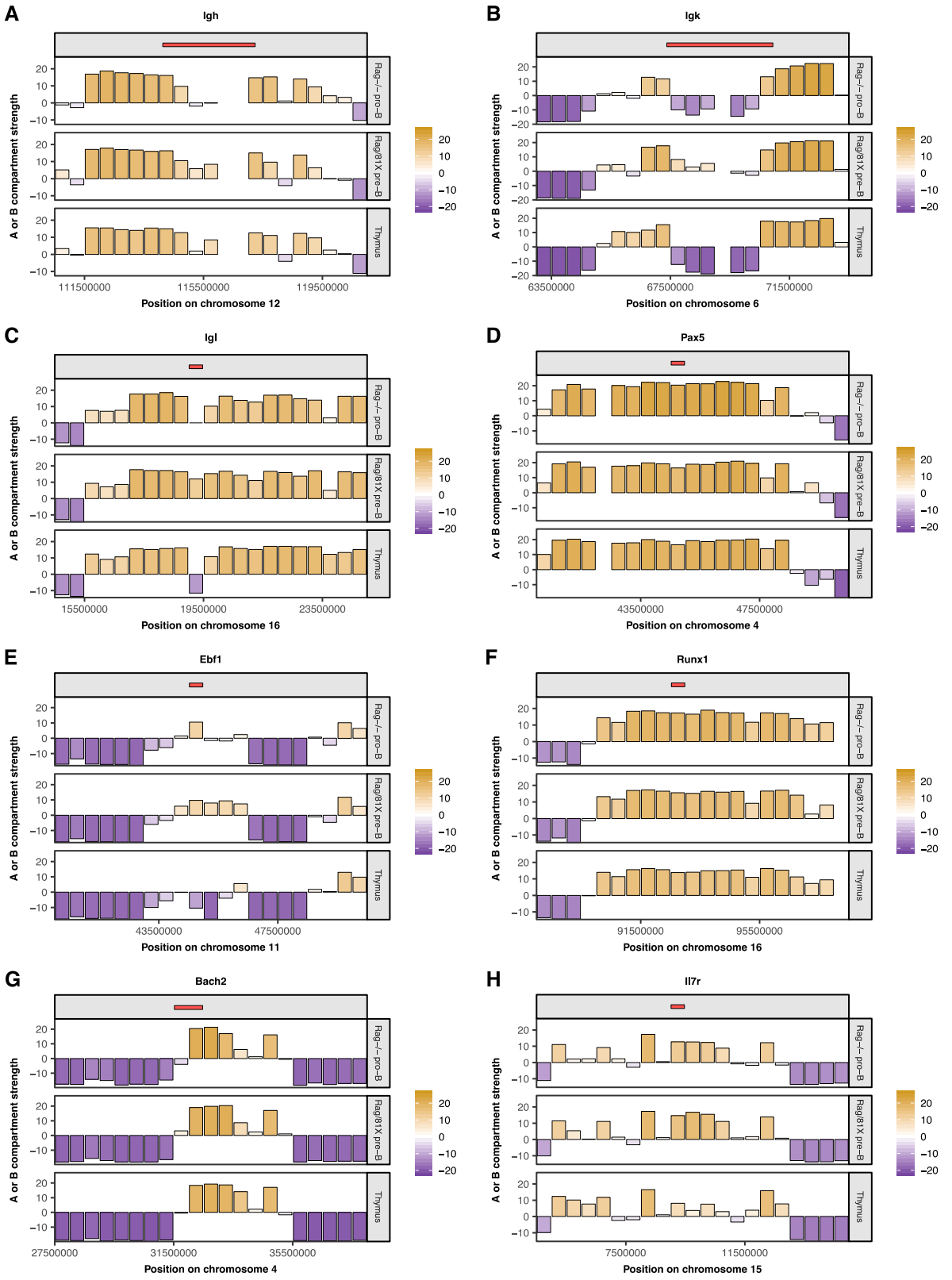

Figure 63. Top interaction partners of Ig loci reside in A compartments. Each panel A-H displays a 10Mb region around a statistically significant trans hit bin. Genes of interest are indicated by red rectangles. White-to-yellow bars represent A compartments and white-to-purple bars represent B compartments. The higher the positive value the stronger the A compartment, whereas the lower the negative value the stronger the B compartment. Empty spaces between bars indicate low read coverage preventing HOMER from calling the compartment.

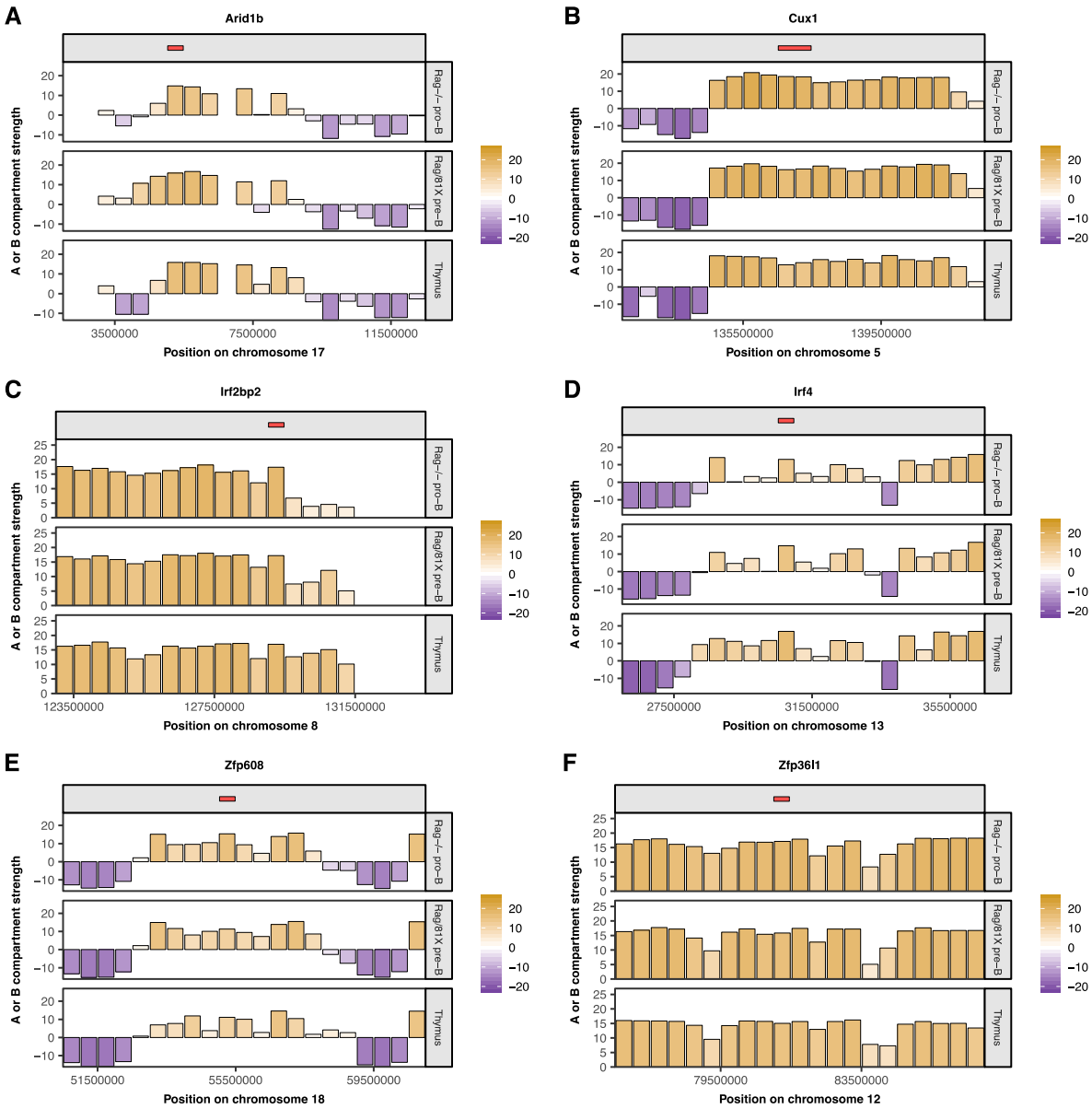

Figure 64. Continued from Figure 63.

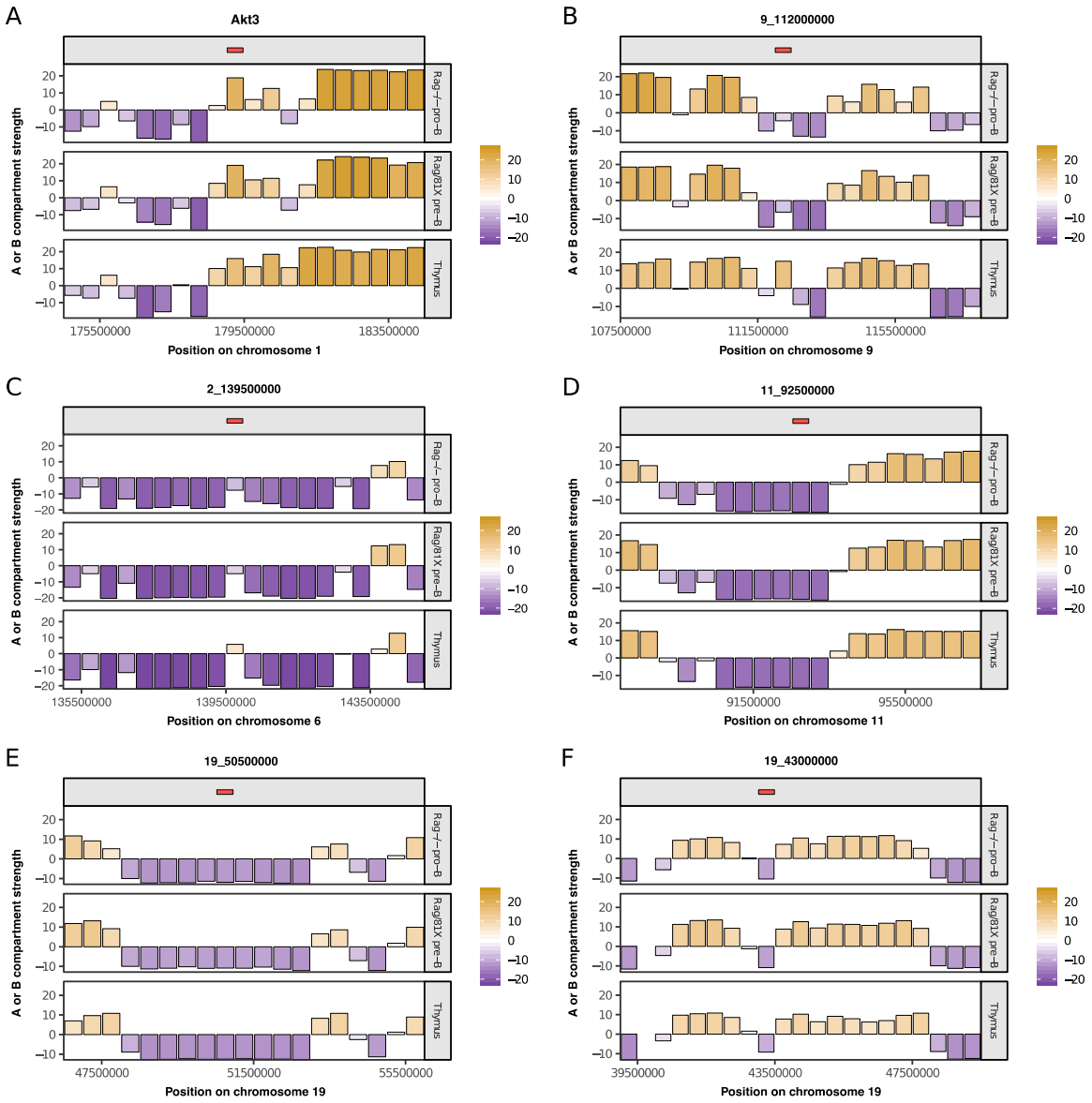

Figure 65. Interaction partners of heavy and light chain loci in 'inactive' datasets reside in opposite compartments. Each panel A-F displays a 10Mb region around a statistically significant trans hit bin. Genes of interest are indicated by red rectangles. White-to-yellow bars represent A compartments and white-to-purple bars represent B compartments. The higher the positive value the stronger the A compartment, whereas the lower the negative value the stronger the B compartment.

4.2.6. High expression contributes to but is not sufficient for interactions

To gain further insight into the observed inter-chromosomal interactions, I examined the expression status of the regions involved in trans contacts. To this end, I analysed nuclear RNA-seq datasets for $Rag^{-/-}$ pro-B cells and Rag/81X pre-B cells produced by Louise Matheson in the lab and compared them with the interaction frequencies of all 0.5Mb bins genome-wide from the Igh viewpoint virtual 4C dataset (**Figure 66**A). It became clear that the statistically significant interaction partners of the Igh viewpoint do not exclusively contain the most highly expressed genes and there are many insignificant bins with the same or higher expression levels. Indeed, no interaction was detected with bins containing the highest

expressed genes in pro-B and pre-B cells, for example Malat1, Hist1h4d, Cdk8, Actb, Cd19, Cd93 and Sox4. The expression of these genes was only matched by that of the Igh Iμ/μ_0 transcripts and Jarid2 transcript among the significant trans hits. Jarid2 is an example of a gene that is expressed at higher levels in pro-B cells, but it interacts with Ig loci only in pre-B cells. The most highly interacting regions in pro-B and pre-B cells such as Pax5 and Ebf1 had slightly lower transcript counts than the top transcribed genes. Nevertheless, the majority of frequently interacting bins contain relatively highly expressed genes (**Figure 66**B) as expected, since these are genes driving B cell development that perform crucial functions at these developmental stages. Overall, the Ig loci only interact with specific regions that form a small subset of highly expressed genes.

As discussed in section 4.2.2, the Igh viewpoint lost 39 but gained 65 interactions in Rag/81X pre-B cells compared $Rag^{-/-}$ pro-B cells. I was interested to see if these changes were accompanied by changes in expression levels. I plotted the RNA-seq read counts in bins significantly contacted by the Igh in pro-B cells and pre-B cells in three categories: 'lost pro-B → pre-B', 'retained pro-B → pre-B', and 'gained pro-B → pre-B', flanked by 'all hits' in the corresponding cell type (**Figure 66**C). For bins in each of these four categories I reported RNA-seq read counts from both the pro-B and the pre-B cell RNA-seq datasets. In other words, the 'lost', 'retained' and 'gained' labels refer to Capture Hi-C trans interactions, whereas the '$Rag^{-/-}$ pro-B cells' and 'Rag/81X pre-B cells' labels refer to RNA-seq datasets. I first compared the differences in expression between paired datasets (green vs green, purple vs purple and blue vs blue). Bins in the 'lost' category showed no change in expression between pro-B and pre-B cells, which indicates that the interactions that were lost did not decrease their expression levels (**Figure 66**C green). On the other hand, bins in the 'retained' category increased their expression levels between pro-B cells and pre-B cells, showing that the bins remaining in contact with the Igh in pre-B cells increase their expression (**Figure 66**C purple). Examples of retained interactions where genes increased their expression include Pax5, Foxo1 and Map3k1 (**Figure 67**). Bins in the 'gained' category also increased their expression while gaining significant interactions with the Igh in pre-B cells (**Figure 66**C blue). Examples of pre-B cell-specific interactions in which the genes of interest increased their expression were Bach2, Arid1b and Adam10 (**Figure 68**). The overall expression level of 'gained' bins in pre-B cells was comparable to the expression of 'lost' and 'retained' bins in pre-B cells. However, the 'gained' bins had lower expression in pro-B cells, which indicates that the biggest change in expression vs interactions characterises bins gaining interactions between pro-B and pre-B stages.

Further, I examined the expression levels of selected putative genes of interest, as the analysis in the previous paragraphs referred to the sum of RNA-seq reads in 0.5Mb bins. The number of interacting 0.5Mb bins around genes such as Pax5, Ebf1, Aff3 and Map3k1 increased in pre-B cells compared to pro-B cells, as did the transcription levels of these genes (**Figure 67**). This might suggest that the chromatin environment becomes increasingly more accessible around these regions in pre-B cells. For Runx1, the number of contacted bins

around the gene increased in pre-B cells only for the Igh viewpoint, and the expression level remained unchanged. Foxo1 transcription increased substantially in pre-B cells, but the number of contacted bins around the gene remained similar to pro-B cells. Genes such as Bach2, Arid1b, Adam10 and Zfp36l1 were much more highly expressed in pre-B cells than in pro-B cells and this coincided with a gain of interactions with the Ig viewpoints (**Figure 68**). On the other hand, Zfp608 was highly expressed in both pro-B and pre-B cells, but it only interacts with the Ig loci in pre-B cells. Il7r, Myb and Irf4 were also more highly expressed in pre-B cells but despite contacting the Igk and Igl, they do not contact the Igh. Dyrk2 and Irf2bp2 interactions with the Igh remained unchanged between pre-B and pro-B cells but their expression increased in pre-B cells. Akt3 was quite lowly expressed and it interacts only with the Igh viewpoint. Itpkb and Nktr are examples of genes that only interacted with the Igh in pro-B cells and their expression decreased in pre-B cells compared to pro-B cells. Overall, this data shows that there is a tendency for genes of interest to show an increase in transcription levels as the bin gains interactions with the Ig viewpoints. However, this is not a ubiquitous rule, and foremost, not all highest transcribed genes contact the Ig loci.

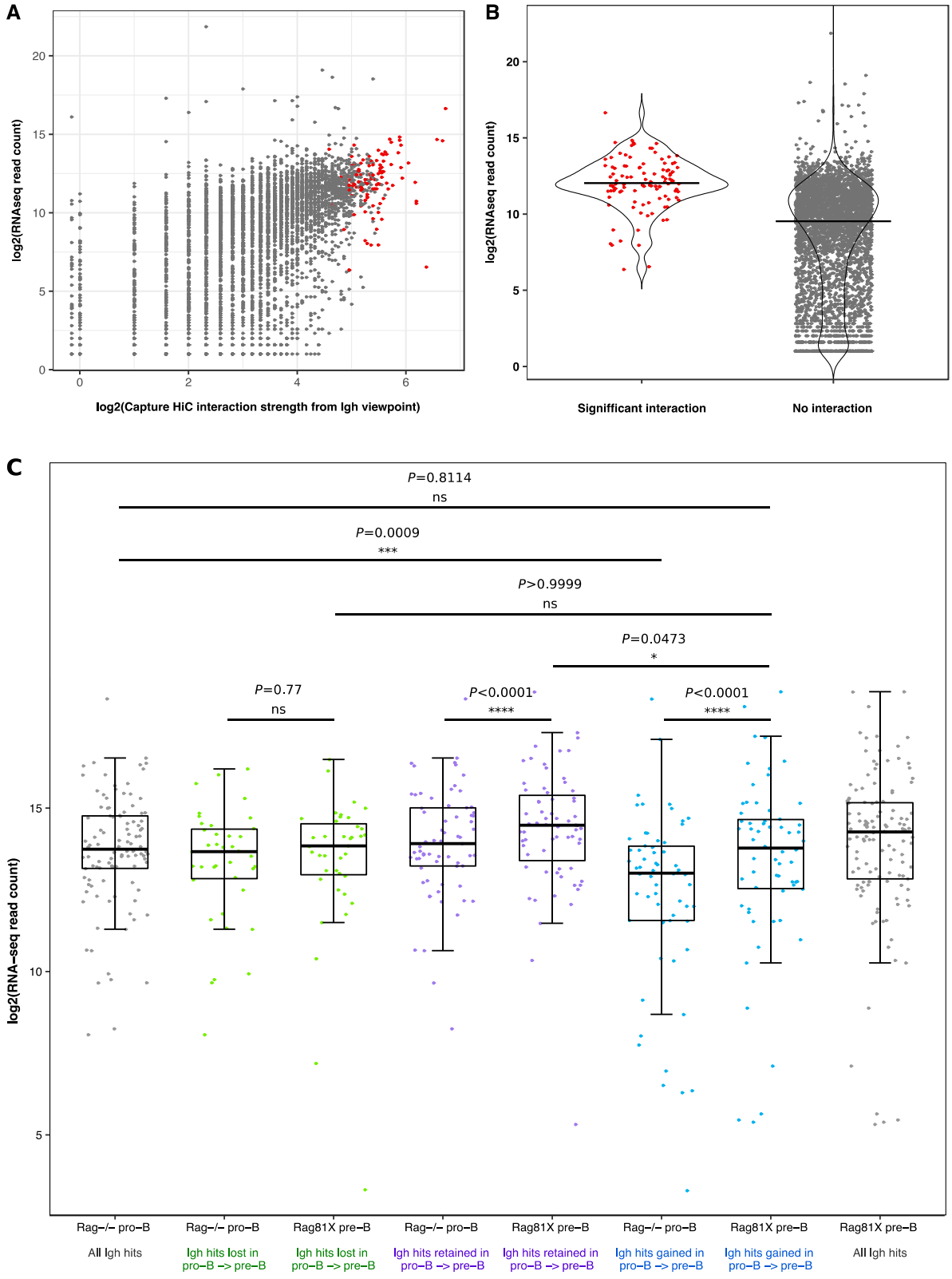

Figure 66. Significant trans interactions are not all highly transcribed. A. All other ends from the Igh virtual 4C in Rag$^{-/-}$ pro-B cells were quantified in 0.5Mb bins genome-wide and plotted against nucRNA-seq read counts in the same bins as log2(raw reads) (grey circles). Statistically significant interactions with z-score > 3.5 are shown as red circles. **B.** Bean plots showing nucRNA-seq count for significant and insignificant 0.5Mb trans bins. **C.** nucRNA-seq read counts were calculated in significant 0.5Mb trans bins and corrected for library size. The green, purple and blue categories correspond to 39 lost, 67 retained and 65 gained interaction shown in Figure 40 for the Igh viewpoint.

nucRNA-seq read values correspond to the cell type indicated below each boxplot. The grey category contains all trans hits in either Rag$^{-/-}$ pro-B cells or Rag/81X pre-B cells (thus, green+purple pro-B = grey pro-B and purple+blue pre-B = grey pre-B). P-values within groups (lost pro-B vs lost pre-B, retained pro-B vs retained pre-B and gained pro-B vs gained pre-B) were calculated using a paired t-test with Bonferroni correction for multiple testing. P-values between groups (retained pre-B vs gained pre-B, lost pre-B vs gained pre-B and all pro-B vs gained pre-B) were calculated using one-way ANOVA with Sidak's multiple comparisons test.

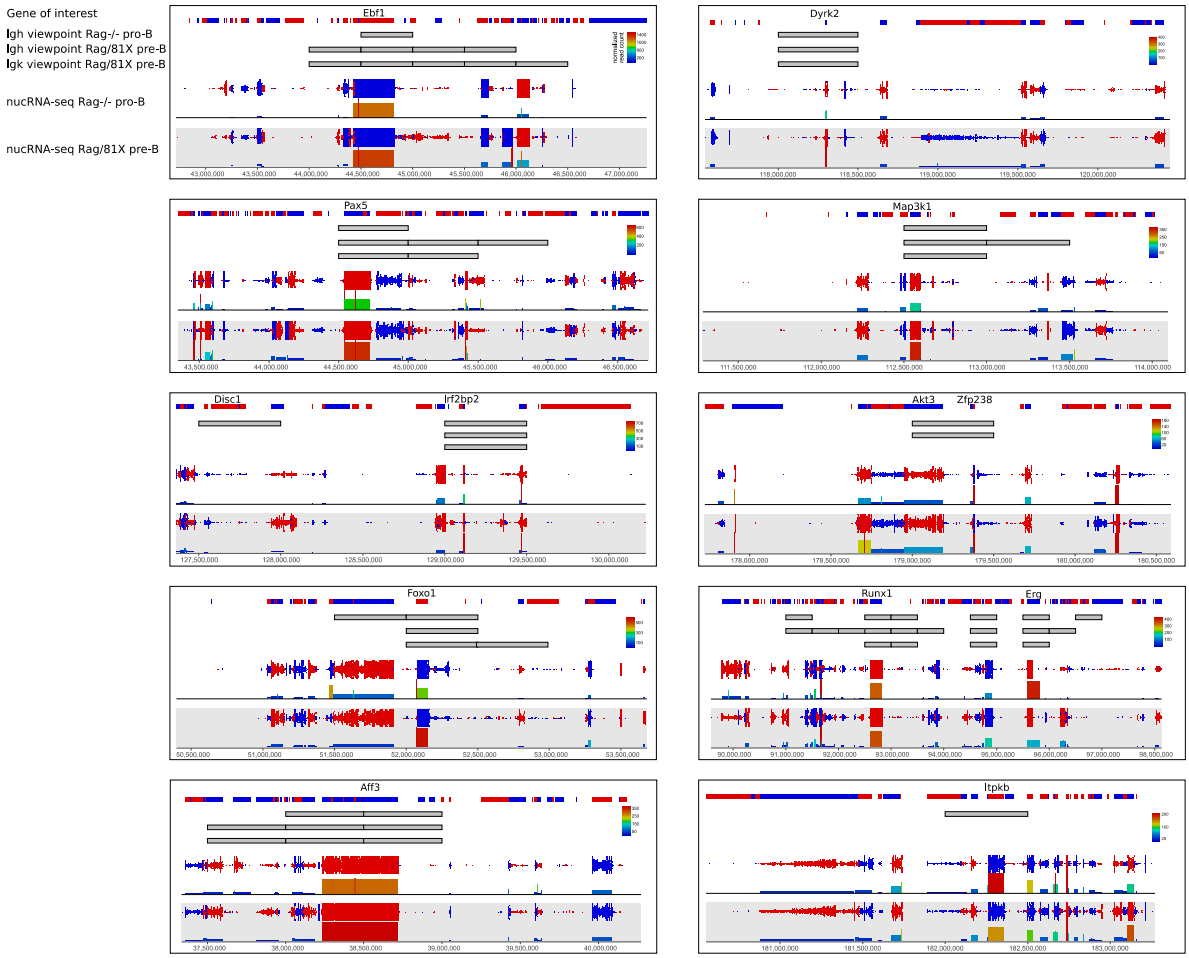

Figure 67. nucRNA-seq over the genes of interest. Seqmonk browser shots. nucRNA-seq reads were quantified over the genes of interest and normalised for gene length and per million reads in the dataset, which is represented by the height and colour of the bars depicted below the reads. Red and blue reads indicate read directionality and correspond to the Ensembl genes at the top of each figure (blue genes have red reads, red genes have blue reads). Genes of interest are labelled above Ensembl gene track. Grey rectangles indicate statistically significant 0.5Mb bins in a given dataset.

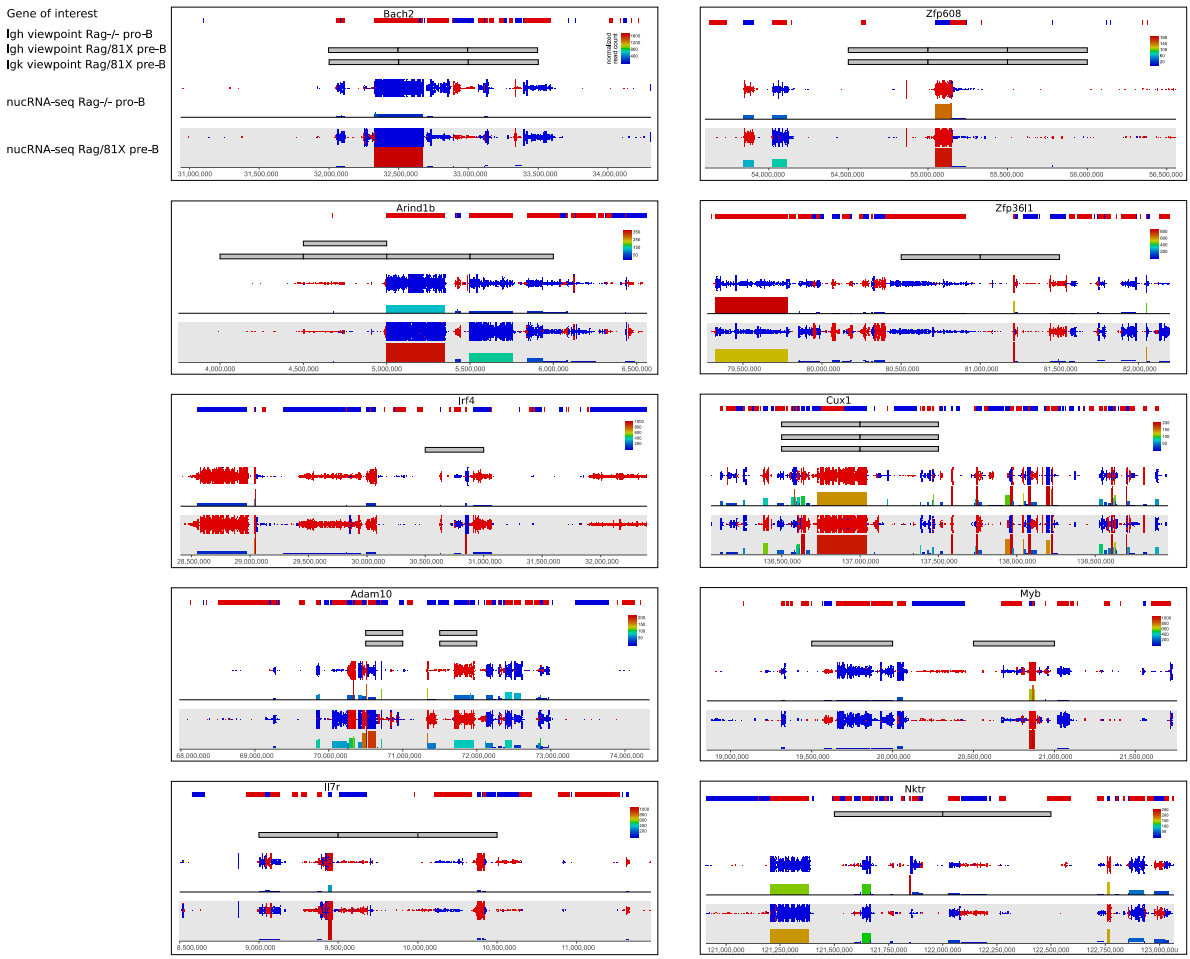

Figure 68. Continued from Figure 67.

4.2.7. Regions that are further from the Igh locus centre of mass are contacted in trans more often

To examine the relationship between the highly looped and contracted Igh locus TAD and the inter-chromosomal contacts in pro-B cells, I carried out a reciprocal analysis of the top 14 Igh trans hits (Appendix B) and performed virtual 4Cs from these 14 0.5Mb viewpoints (**Figure 69**). Apart from Pax5 and Foxo1 these regions were not baited, but they can serve as viewpoints for detecting reciprocal interactions with baited regions such as the Igh (other end-to-bait). The other ends from the top 14 trans hits were quantified in 40kb bins over the Igh locus, which revealed that the 20kb bins that were most peripheral in the polymer models, i.e. the ones furthest from the centre of mass, are precisely the regions that are the most frequently contacted in trans (**Figure 69** and **Figure 47**A). Beads (bins) 8-11 (144.61-114.68Mb) and 44-47 (115.33-115.41Mb) showed the highest enrichment for trans contacts (**Figure 69** the D-J region and the middle Vs). These peripheral bins are looping out of the Igh locus structures and might be more accessible to trans interactions. Also, for most trans hits, beads 58-63 (115.61-115.73) showed moderate enrichment, as did a region over PAIR10 (at 116.89Mb) in the distal V domain. Interestingly, although PAIR10 is not peripheral it is the most highly transcribed region in the Vs (Ebert et al. 2011). The mechanism of these

contacts needs to be investigated further, but it is possible that the trans hit genes are engaged in functional contacts with the Eμ-J region and the middle V bins are contacted by sterical proximity. It is also possible that the contacts between the Eμ, middle Vs and the trans hits are simply a reflection of Igh structure in 3D.

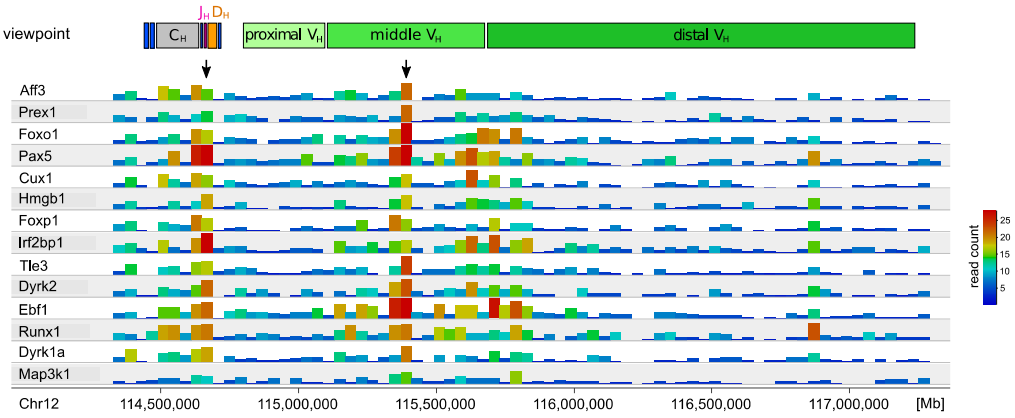

Figure 69. Regions of the Igh locus residing near the periphery of the locus 3D structure are most frequently contacted in trans. Seqmonk browser shot of virtual 4C tracks from 14 viewpoints in trans in $Rag^{-/-}$ pro-B cells. Average of 3 biological replicates. Raw read counts are displayed in 40kb bins. The top panel shows the elements of the Igh locus. Arrows indicate the regions of the Igh most frequently contacted by the 14 trans hits.

4.3. 3D DNA FISH validates genome-wide interactions identified by Capture Hi-C

To achieve aim 5 of this thesis (section 1.6) I performed 3D DNA Fluorescence In-Situ Hybridisation (FISH) to validate *in vivo* the most significant inter-chromosomal interactions discovered by Capture Hi-C.

4.3.1. Experimental design

For FISH experiments, I used FACS sorted $Rag^{-/-}$ pro-B cells ($B220^+$, $CD19^+$, $CD43^+$) (**Figure 70**), Rag/81X pre-B cells ($B220^+$, $CD19^+$, $CD43^-$, $CD25^+$) (**Figure 71**), double-positive thymocytes ($CD4^+$, $CD8^+$) (**Figure 72**) and $E\mu^{-/-}$ $Rag^{-/-}$ pro-B cells ($B220^+$, $CD19^+$, $CD43^+$). Fluorescently-labelled BACs listed in section 2.5.2 were used as FISH probes. For the Igh locus, I used a BAC probe RP23-109B20 over the D-J region (referred to as 'Igh(DJ)') for experiments in $Rag^{-/-}$ pro-B cells and thymocytes (**Figure 14**). For experiments in Rag/81X pre-B cells I used a BAC probe RP23-70F21 in the V region (referred to as 'Igh(V)'), because the Igh(DJ) probe was detecting the Vh81X transgene on chromosome 16 giving three fluorescent signals per cell. I imaged a large number of cells on each slide (~1000) in order to sufficiently cover the small distance fraction (<1μm) of the cumulative distribution and to be able to accurately detect the occurrence of rare interaction events. A

distance of 1µm was chosen based on the literature (Osborne et al. 2004; Schoenfelder et al. 2010; Park et al. 2014) as a cut off for a significant inter-chromosomal contact.

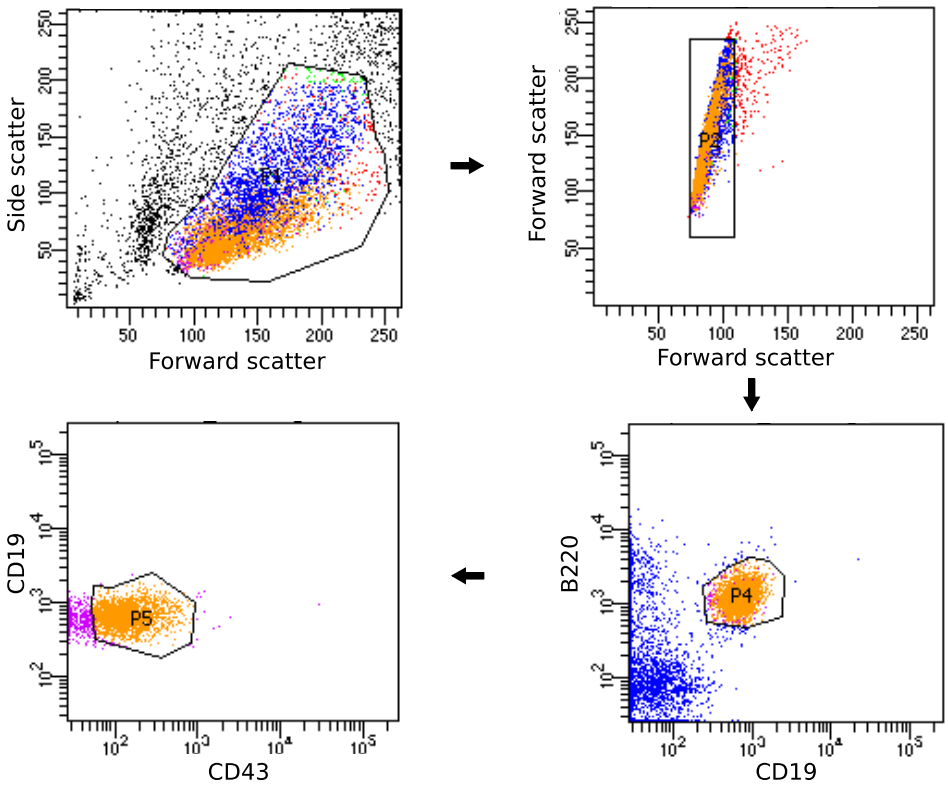

Figure 70. Representative fluorescence-activated cell sorting (FACS) plots for Rag$^{-/-}$ pro-B cells. Forward scatter and side scatter were used to draw a gate representing the lymphocyte population (top left), and to distinguish single cells (top right). Pro-B cells were then sorted by B220^{+}, CD19^{+} (bottom right) and CD43^{+} (bottom left).

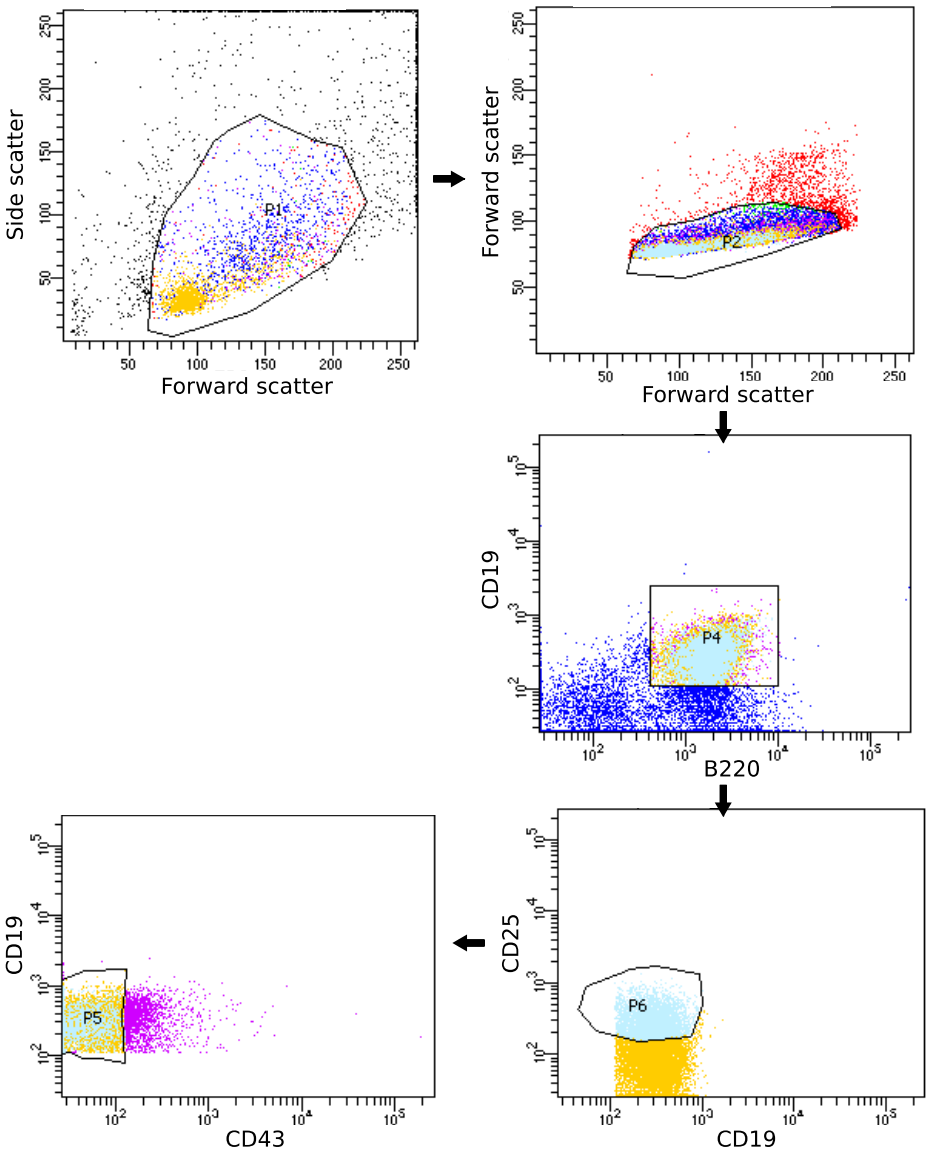

Figure 71. Representative fluorescence-activated cell sorting (FACS) plots for Rag/81X pre-B cells. Forward scatter and side scatter were used to draw a gate representing the lymphocyte population (top left), and to distinguish single cells (top right). Pre-B cells were then sorted by $B220^{+}$, $CD19^{+}$ (middle), $CD25^{+}$ (bottom right) and $CD43^{-}$ (bottom left).

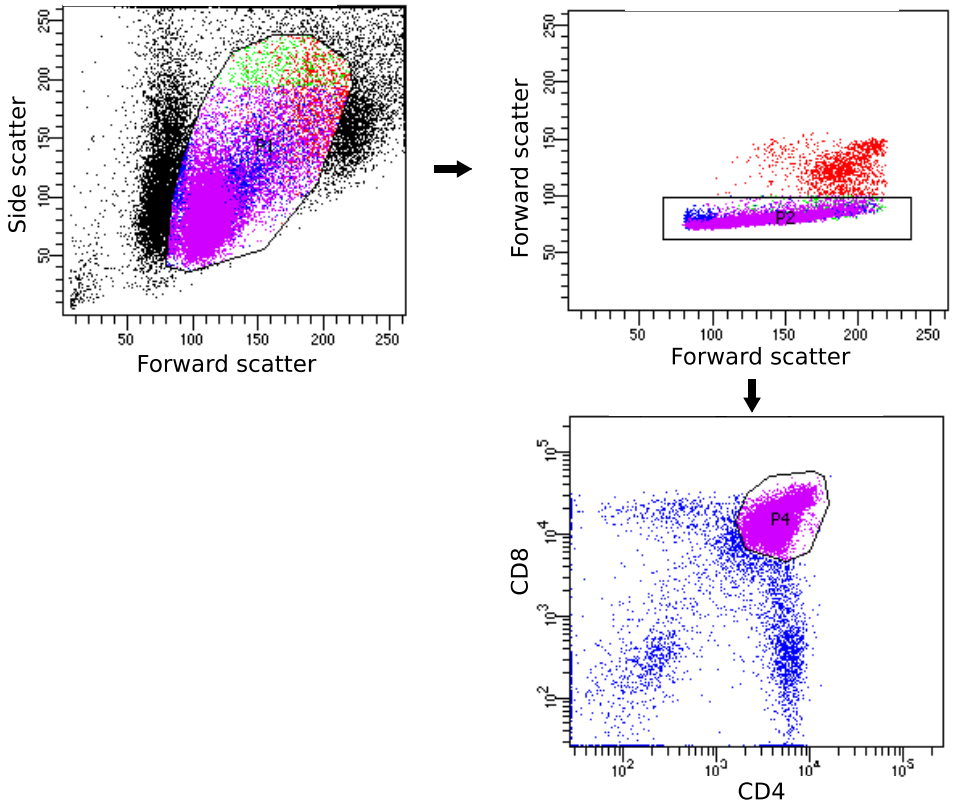

Figure 72. Representative fluorescence-activated cell sorting (FACS) plots for double positive (DP) thymocytes. Forward scatter and side scatter were used to draw a gate representing the lymphocyte population (top left), and to distinguish single cells (top right). DP thymocytes were then sorted by $CD4^+$, $CD8^+$ (bottom).

Nuclear volume adjustment

Overall, more than 20,000 cells for each $Rag^{-/-}$ pro-B, Rag/81X pre-B and thymus and over 10,000 cells for $E\mu^{-/-}$pro-B cells were imaged on the Metacyte and the average nuclear volume per slide was calculated. Whereas there was no difference between the $Rag^{-/-}$ pro-B, Rag/81X pre-B and $E\mu^{-/-}$ pro-B nuclei, the thymocyte nuclei were significantly smaller (**Figure 73**). To adjust for this, I calculated the average nuclear volume per genotype (50.61μm^3 for the thymus and 60.31μm^3 for $Rag^{-/-}$ pro-B and Rag/81X pre-B taken together) and, assuming nuclei are spheres, I determined that on average the ratio of the B cell radius to the thymocyte radius is $\frac{r_{Rag}}{r_{Thy}} = \sqrt[3]{\frac{V_{Rag}}{V_{Thy}}} = \sqrt[3]{\frac{60.31}{50.61}}$ =1.0601699. Therefore, all distances between fluorescent signals measured in the thymus were multiplied by 1.0601699 to normalise for nuclear volume difference between B cells and thymocytes.

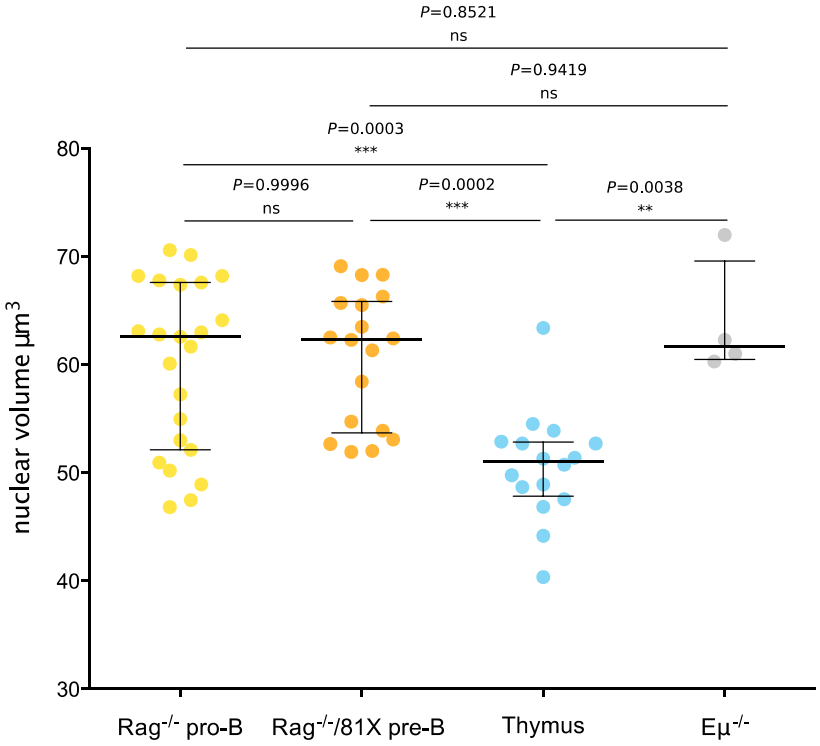

Figure 73. B cells have larger nuclei than thymocytes. Nuclear volumes were measured using Metacyte and Metafer automatic imaging software. Each data point represents an average of nuclear volumes of hundreds of cells measured on one slide. P-values were calculated using Kruskal-Wallis test with Dunn's correction for multiple comparisons.

Random association of loci

It must be noted that inter-chromosomal interactions are rare events and there is a scarcity of published data to be able to establish *a priori* the frequency of significant interactions. To assess whether the proportion of detected distances below 1µm is non-random, I determined that the probability of a random association of two loci from either allele within 1µm radius in an average spherical nucleus of volume 60.31µm^3 is p= $\frac{\frac{4}{3}\times\pi\times1^3}{60.31}$= 0.069. Therefore, if two loci associate within 1µm radius in fewer than 6.9% of cells, this association could be random. For 3 loci to simultaneously associate at random the probability is 6.9% x 6.9% = 0.48%. Previous FISH experiments showed that the frequency of overlap (<1µm) in later B cells between the Igh and a typical active gene is 3-5%, whereas the frequency of overlap between Igh and a silent gene is 1-2% (Hakim et al. 2012). A study in erythrocytes showed that Hba and Hbb genes make functional contacts with their targets in 7-8% of cells (Schoenfelder et al. 2010).

4.3.2. 3D DNA FISH validates Ig loci interaction partners identified by Capture Hi-C

Representative images of single cells and a field of view in **Figure 74** show that FISH signals were strong and clean and present in a majority of cells. I have represented FISH data as cumulative distributions, bar plots and boxplots to give a full picture of measured distances. This should facilitate the ease of comparison with Capture Hi-C (reviewed in Giorgetti and Heard 2016).

I validated the trans interactions of the Igh and Igk loci with Pax5, Ebf1, Foxo1, Runx1 and Bach2 genes as well as with each other. I used myc and Rag1/2 probes as negative controls. Although myc does interact with the Igh in splenic B cells (Osborne et al. 2007; Robbiani et al. 2008), it does not interact in pro-B cells (Lin et al. 2012; Zhang et al. 2012; Gerasimova et al. 2015). Whereas Rag1/2 was identified here by Capture Hi-C as not interacting with the Ig loci viewpoints in B cells, however it was interacting significantly in thymocytes. The cumulative distributions of distances between the Igh and the genes of interest show a higher percentage of cells with shorter distances (<1μm) in $Rag^{-/-}$ pro-B cells and Rag/81X pre-B cells than in thymocytes (**Figure 75**). For the interactions between the Igh locus and Pax5 or Foxo1, the distributions of distances below 1μm were similar in pro-B and pre-B cells (**Figure 75**A an C). For the Ebf1 interaction with the Igh there was a larger number of shorter distances in pre-B cells than in pro-B cells consistent with higher z-scores of Ebf1-containing bins in pre-B cell Capture Hi-C (**Figure 75**B). For the Runx1 interaction with the Igh locus there was a larger number of shorter distances in pro-B cells compared to thymocytes, and the distribution of distances in pre-B cells was intermediate, converging with thymocyte values at the 1μm cut off (**Figure 75**D). Notably, this is due to an increase in the number of short distances in thymocytes and not a decrease in short distances in pre-B cells, which is in agreement with Runx1 interacting significantly with the Igh in thymocytes by Capture Hi-C. Bach2 and Igk interact with the Igh locus only pre-B cells, which was confirmed by a larger number of short distances in pre-B cells compared to pro-B cells and thymocytes (**Figure 75**E and F). Ebf1+Igh and Bach2+Igh interactions exhibited the steepest cumulative distribution profiles in pre-B cells out of all pairwise contacts tested, which confirms their top two highest z-scores in Capture Hi-C analysis. The negative control myc+Igh and Rag1/2+Igh, which showed low number of distances below 1μm in all three cell types, albeit the interaction with Rag1/2 was significant in thymocytes(**Figure 75**G).

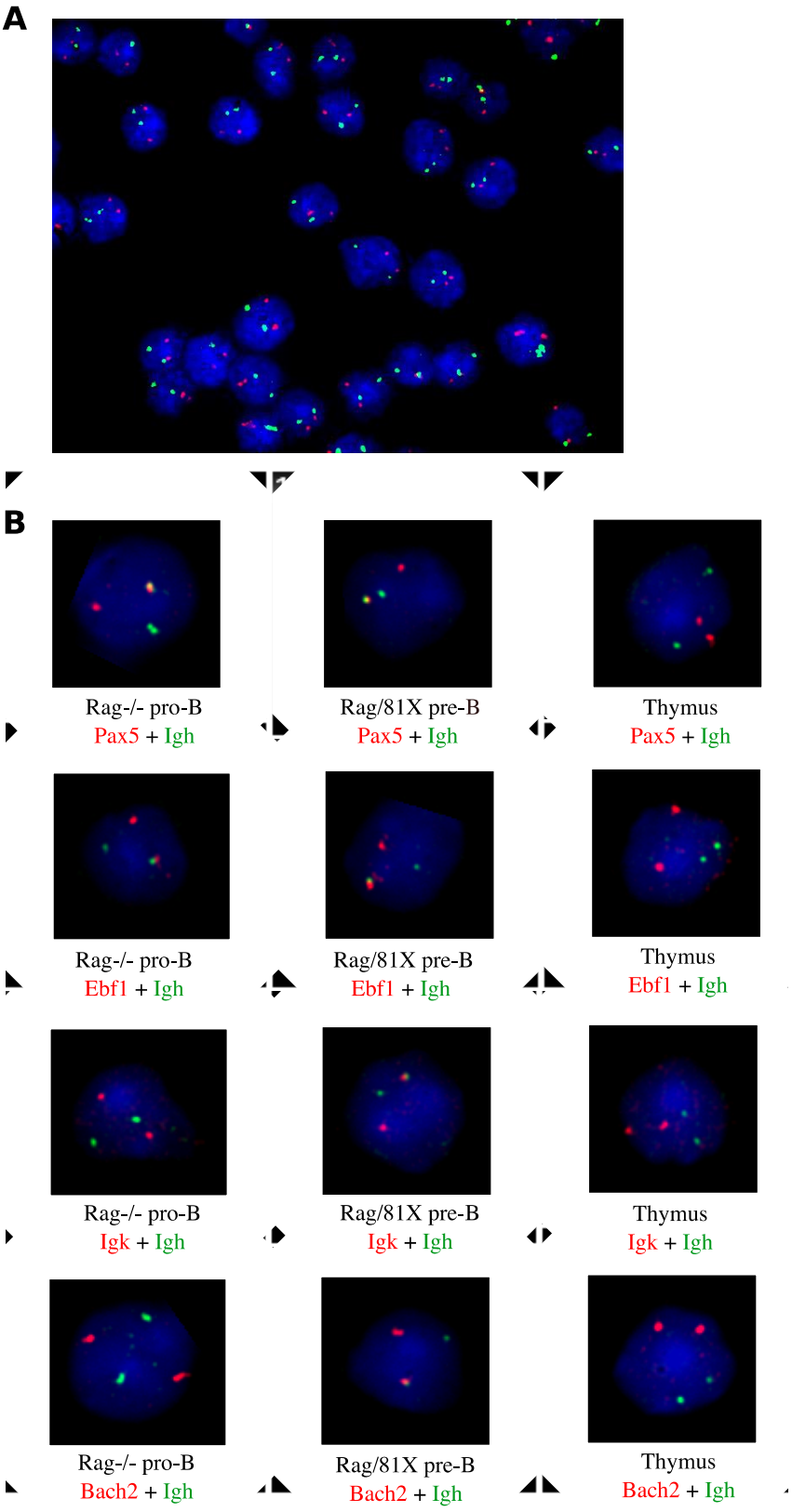

Figure 74. Representative images of single nuclei. The probes used for the Igh were Igh(DJ) (RP23-109B20) in Rag$^{-/-}$ pro-B cells and thymus, and Igh(V) (RP23-70F21) in Rag/81X pre-B cells. The Igh probes were labeled with Alexa Fluor 488 (green), the probes for genes of interest were labeled with Alexa Fluor 555 (red) and hybridized to fixed pro-B, pre-B and DP T cells. The nuclear area was stained with DAPI. Fluorescent signals were acquired using the Metacyte software.

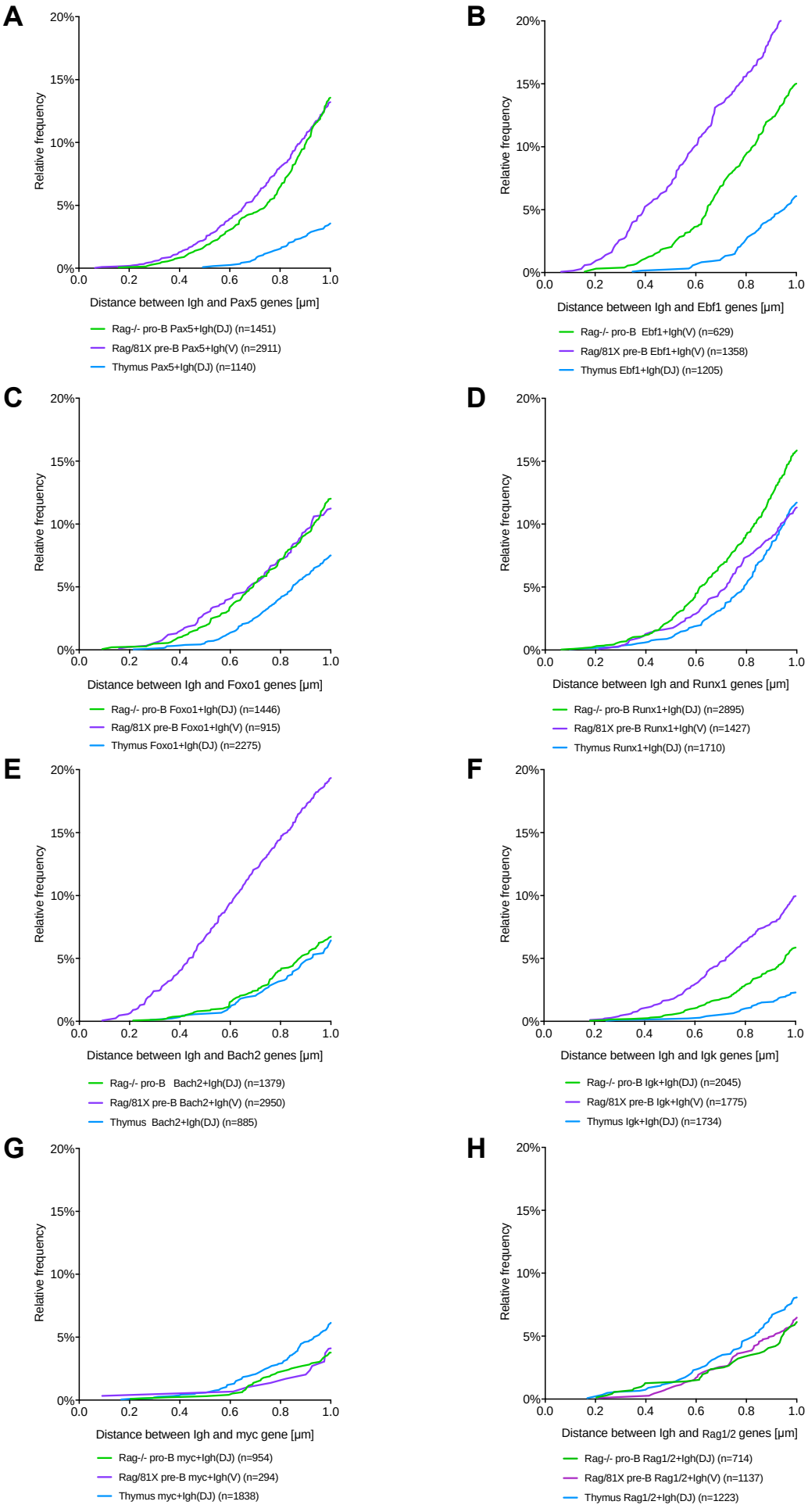
A
Relative frequency
20%
15%
10%
5%
0%
0.0
0.2
0.4
0.6
0.8
1.0
Distance between Igh and Pax5 genes [µm]
Rag-/- pro-B Pax5+Igh(DJ) (n=1451)
Rag/81X pre-B Pax5+Igh(V) (n=2911)
Thymus Pax5+Igh(DJ) (n=1140)
B
Relative frequency
Distance between Igh and Ebf1 genes [µm]
Rag-/- pro-B Ebf1+Igh(V) (n=629)
Rag/81X pre-B Ebf1+Igh(V) (n=1358)
Thymus Ebf1+Igh(DJ) (n=1205)
C
Relative frequency
Distance between Igh and Foxo1 genes [µm]
Rag-/- pro-B Foxo1+Igh(DJ) (n=1446)
Rag/81X pre-B Foxo1+Igh(V) (n=915)
Thymus Foxo1+Igh(DJ) (n=2275)
D
Relative frequency
Distance between Igh and Runx1 genes [µm]
Rag-/- pro-B Runx1+Igh(DJ) (n=2895)
Rag/81X pre-B Runx1+Igh(V) (n=1427)
Thymus Runx1+Igh(DJ) (n=1710)
E
Relative frequency
Distance between Igh and Bach2 genes [µm]
Rag-/- pro-B Bach2+Igh(DJ) (n=1379)
Rag/81X pre-B Bach2+Igh(V) (n=2950)
Thymus Bach2+Igh(DJ) (n=885)
F
Relative frequency
Distance between Igh and Igk genes [µm]
Rag-/- pro-B Igk+Igh(DJ) (n=2045)
Rag/81X pre-B Igk+Igh(V) (n=1775)
Thymus Igk+Igh(DJ) (n=1734)
G
Relative frequency
Distance between Igh and myc gene [µm]
Rag-/- pro-B myc+Igh(DJ) (n=954)
Rag/81X pre-B myc+Igh(V) (n=294)
Thymus myc+Igh(DJ) (n=1838)
H
Relative frequency
Distance between Igh and Rag1/2 genes [µm]
Rag-/- pro-B Rag1/2+Igh(DJ) (n=714)
Rag/81X pre-B Rag1/2+Igh(V) (n=1137)
Thymus Rag1/2+Igh(DJ) (n=1223)

Figure 75. Cumulative distributions of distances <1µm between the Igh locus and genes of interest. The closest green and red signal pairs in each cell were used. n = number of cells analysed per slide. Igh(DJ) refers to a FISH probe made from BAC RP23-109B20 over the D-J region. Igh(V) refers to a FISH probe from BAC RP23-70F21 in the V region.

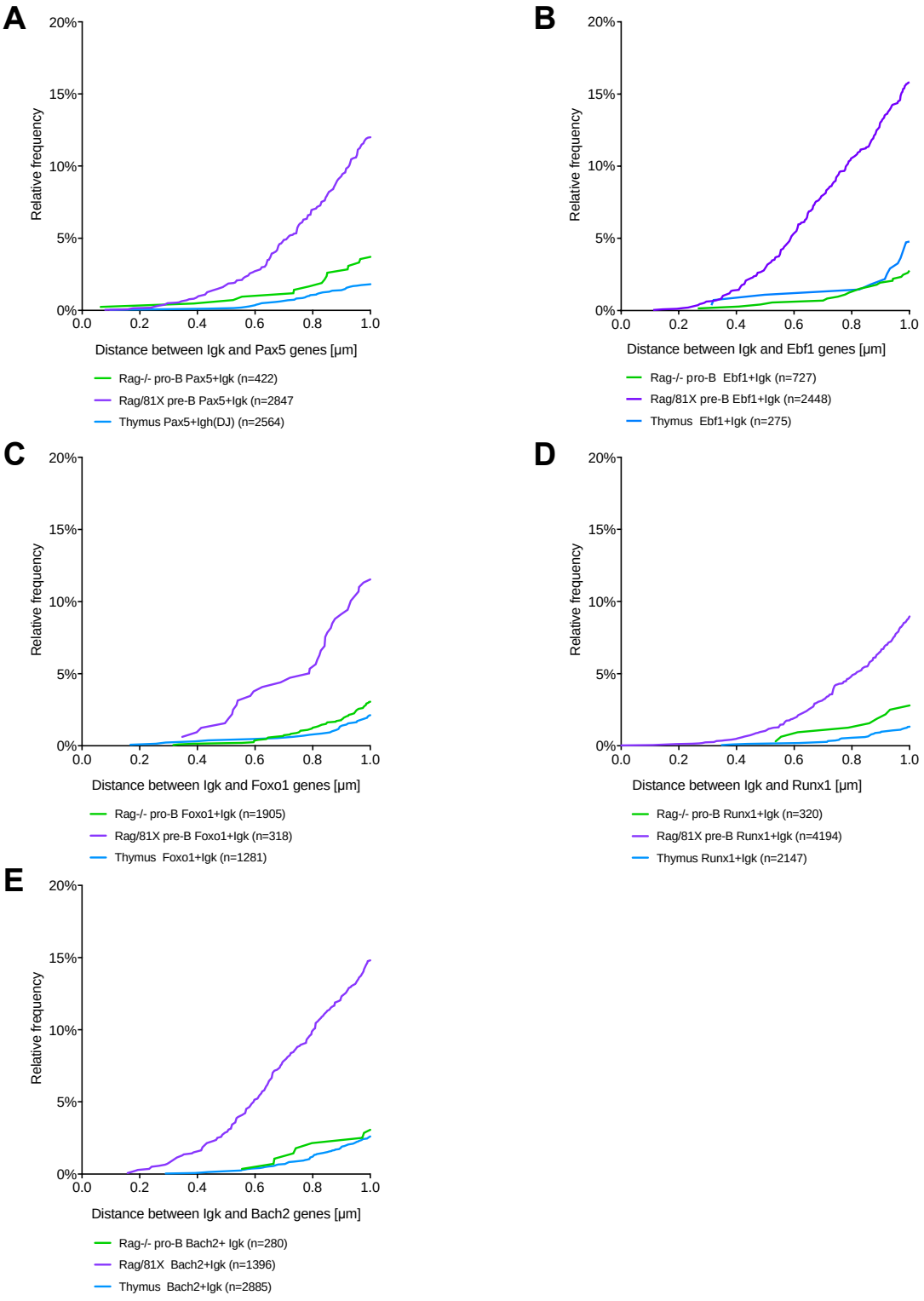

Figure 76. Cumulative distributions of distances <1µm between the Igk locus and genes of interest. The closest green and red signal pairs in each cell were used. n = number of cells analysed per slide. Igh probes described in Figure 75.

The interactions between the Igk locus and the genes of interest all show similar cumulative distributions of distances below 1μm, characterised by very low numbers of short distances in $Rag^{-/-}$ pro-B cells and in thymocytes and high numbers of short distances in Rag/81X pre-B cells (**Figure 76**). The interactions of the Igk with Ebf1 and Bach2 showed the largest number of short distances, in agreement with the most frequent interactions by Capture Hi-C.

To assess the reproducibility of FISH experiments, I carried out two separate experiments for Ebf1+Igh and for Foxo1+Igh using different mice on different days. In both cases the results from two biological replicates were very similar confirming a high level of consistency and that the method is well optimised for lymphocytes (**Figure 77**).

Full cumulative distributions for Pax5+Igh, Bach2+Igh and myc+Igh show the full range of distances measured in each experiment (**Figure 78**). The distances between Pax5 and Igh are consistently shorter in pro-B and pre-B cells than in thymocytes. For Bach2 and Igh the distances are shorter in pre-B cells up to~2.5μm, which is well beyond the region of 1μm set as distance of significant interaction. Myc and Igh showed very similar distance distribution in all three cell types, with distances in thymocytes being marginally shorter.

To determine whether the observed high frequencies of short distances reflect non-random contact probabilities and are statistically significant, I plotted the data as bar graphs highlighting the 6.9% probability of a random interaction (**Figure 79** and **Figure 80**). I also delineated the distances below 1μm in three distance brackets to show the increase in very short distances (<0.5μm) in Rag/81X pre-B cells. For the Igh interactions with Pax5, Ebf1, Foxo1 and Runx1 in pro-B and pre-B cells the frequency of short distances (<1μm) was 10%-20%, well above the 6.9% of random probability (**Figure 79**A, B, C and D). The Igh interactions with Igk and Bach2 in pre-B cells showed 10% and 19% of distances below 1μm, respectively, whereas they were below 6.9% in pro-B cells (**Figure 79**E and F). Most of these six pairwise contacts were below 6.9% in thymocytes, apart from Runx1+Igh which indeed was identified as a significant interaction by Capture Hi-C. Foxo1+Igh was marginally above 6.9%, but it was not called as significant by Capture Hi-C. Myc+Igh had less than 6.9% of distances below 1μm in all three cell types (**Figure 79**G), whereas Rag1/2 was borderline above 6.9% in thymocytes (**Figure 79**H), in agreement with Capture Hi-C data.. The Igk showed 12%-16% of short distances for all pairwise interactions in pre-B cells and less than 6.9% in pro-B cells and thymocytes (**Figure 80**). In summary, FISH experiments showed that trans interactions in the 'active' datasets occur at a frequency higher than expected at random and very short distances (<0.5μm) between probes prevail in B cells compared to thymocytes. All comparisons between active and inactive datasets were statistically significant as determined by the Fisher's exact test with Bonferroni correction for multiple testing. Collectively, this data confirms the top inter-chromosomal contacts of the Igh and Igk loci identified by Capture Hi-C.

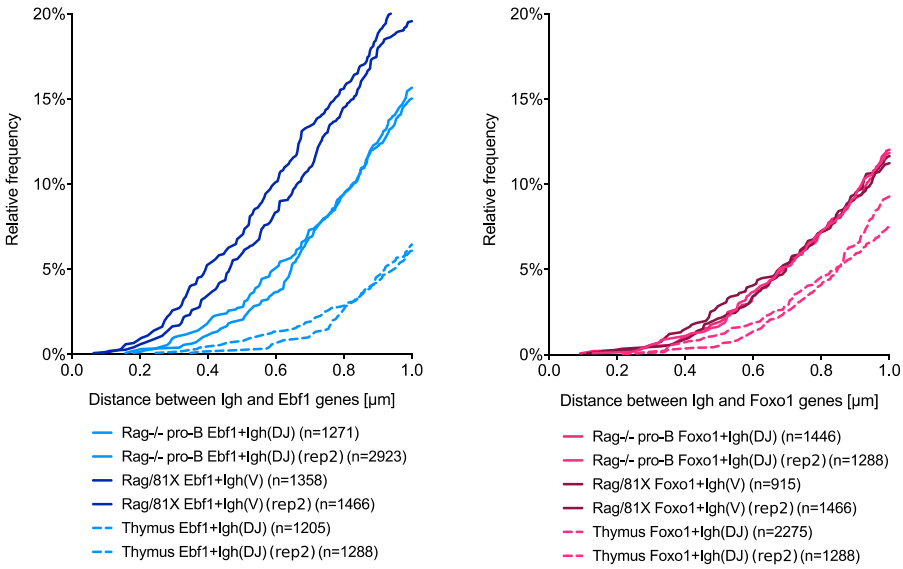

Figure 77. Biological replicates of FISH experiments are highly reproducible. Replicate experiments were performed in separate batches on separate days using separate animals and are indicated by the same line colour and style. The closest green and red signal pairs in each cell were used. n = number of cells analysed per slide. Igh probes described in Figure 75.

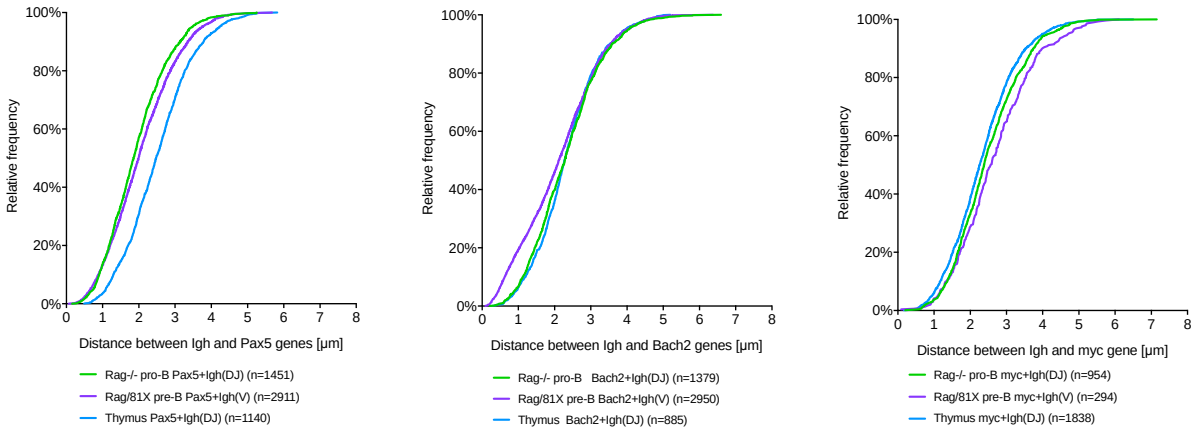

Figure 78. Cumulative distributions of all distances measured between the Igh locus and genes of interest. The closest green and red signal pairs in each cell were used. n = number of cells analysed per slide. Igh probes described in Figure 75.

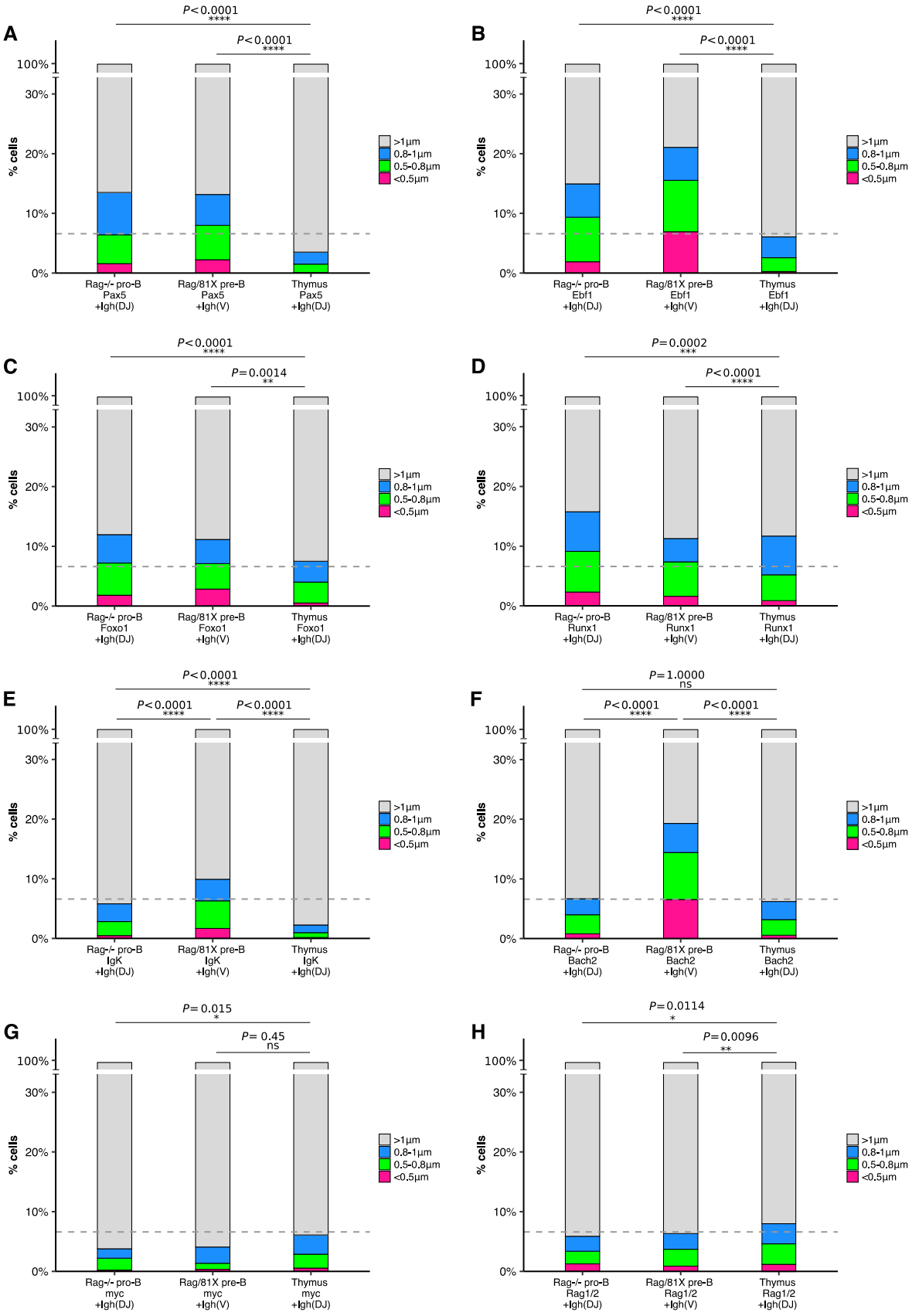

Figure 79. The Igh locus interacts with genes of interest with higher frequency in B cells than in thymocytes and more frequently than random contacts. The distances measured are as in Figure 75 but including distances >1µm. The distances <1µm are plotted as coloured stacked bar charts in three categories: <0.5µm, 0.5-0.8µm and 0.8-1µm; The distances >1µm are in grey. Dashed line denotes the probability of a random interaction at 6.9%. Igh probes described in Figure 75. P-values were calculated using the Fisher's exact test with Bonferroni correction for multiple comparisons.

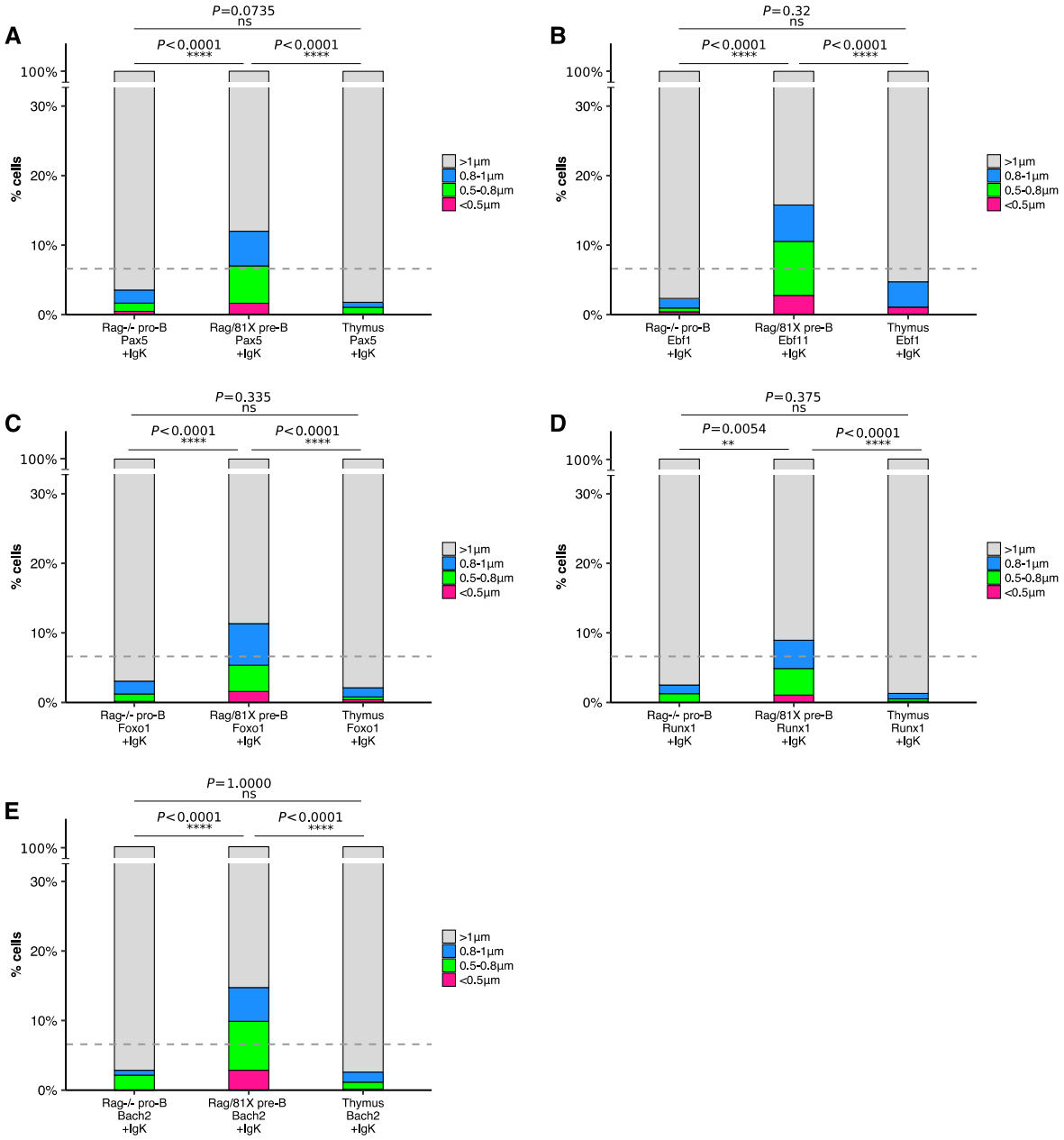

Figure 80. The Igk locus interacts with genes of interest with higher frequency in B cells than in thymocytes and more frequently than random contacts. The distances measured are as in Figure 76 but including distances >1µm. The distances <1µm are plotted as coloured stacked bar charts in three categories: <0.5µm, 0.5-0.8µm and 0.8-1µm; The distances >1µm are in grey. Dashed line denotes the probability of a random interaction at 6.9%. Igh probes described in Figure 75. P-values were calculated using the Fisher's exact test with Bonferroni correction for multiple comparisons.

Hi-C and FISH give different measures of spatial relationship between two genomic locations. Hi-C-based methods determine how often two given regions are within cross-linking proximity, whereas FISH measures the absolute distance between them. Both of these approaches capture only one time point per cell, and large numbers of cells are used to elucidate the contact frequency (Hi-C) or the distribution of distances (FISH) in a given cell type. Nevertheless, it is not always possible to distinguish between a population in which the regions of interest come into contact in a proportion of cells and do not in the rest of the cells,

and a dynamic interaction that is formed and released sequentially due to dynamic regulation of these regions. This is somewhat easier to elucidate from Hi-C, as regions that interact frequently with multiple other regions are likely involved in more dynamic contacts. Similarly to full cumulative distributions, box whisker plots show the full range of measured distances and demonstrate that the differences described above largely persist throughout the whole datasets, and not only for the distances below 1μm (**Figure 81** and **Figure 82**). Although comparing just the median distances might be misleading and arguably the datapoints above 1μm introduce noise, statistical tests on the full range of distances still gave significant differences between cell types, overall strengthening the findings. The significance was assessed using the Kruskal-Wallis test with Dunn's correction for multiple testing. All distances measured for Pax5+Igh, Ebf1+Igh and Igk+Igh were consistently shorter in all measured pro-B and pre-B cells compared to thymocytes (**Figure 81**A, B and E). Foxo1+Igh showed a significant difference between pro-B and thymocytes, but not pre-B and thymocytes, demonstrating that the distances above 1μm mask the differences seen for short distances (**Figure 81**C and **Figure 75**C). For Runx1+Igh the distances in pro-B cells were not significantly different from thymocytes, although they was a slight distance below 1μm, whereas in pre-B cells the longer distances are larger than the distances in thymocytes masking the fact that they were equal at 1μm (**Figure 81**D and **Figure 75**D). For Bach2+Igh all distances were significantly shorter in pre-B cells than in pro-B cells and thymocytes (**Figure 81**F). In contrast, myc+Igh and Rag1/2+Igh all distances were significantly longer in pro-B and pre-B cells compared to thymocytes (**Figure 81**G and H). All distances measured for Pax5+Igk, Ebf1+Igk, Foxo1+Igk, Runx1+Igk and Bach2+Igk were consistently shorter in all measured pre-B cells compared to pro-B cells and thymocytes (**Figure 82**). In summary, this data shows that in most cases the full distribution of interaction distances follows the pattern observed for values <1 μm, which suggests that trans interaction are dynamic and overall more frequent for the Igh in pro-B cells and pre-B cells and for the Igk in pre-B cells compared to thfie thymus.

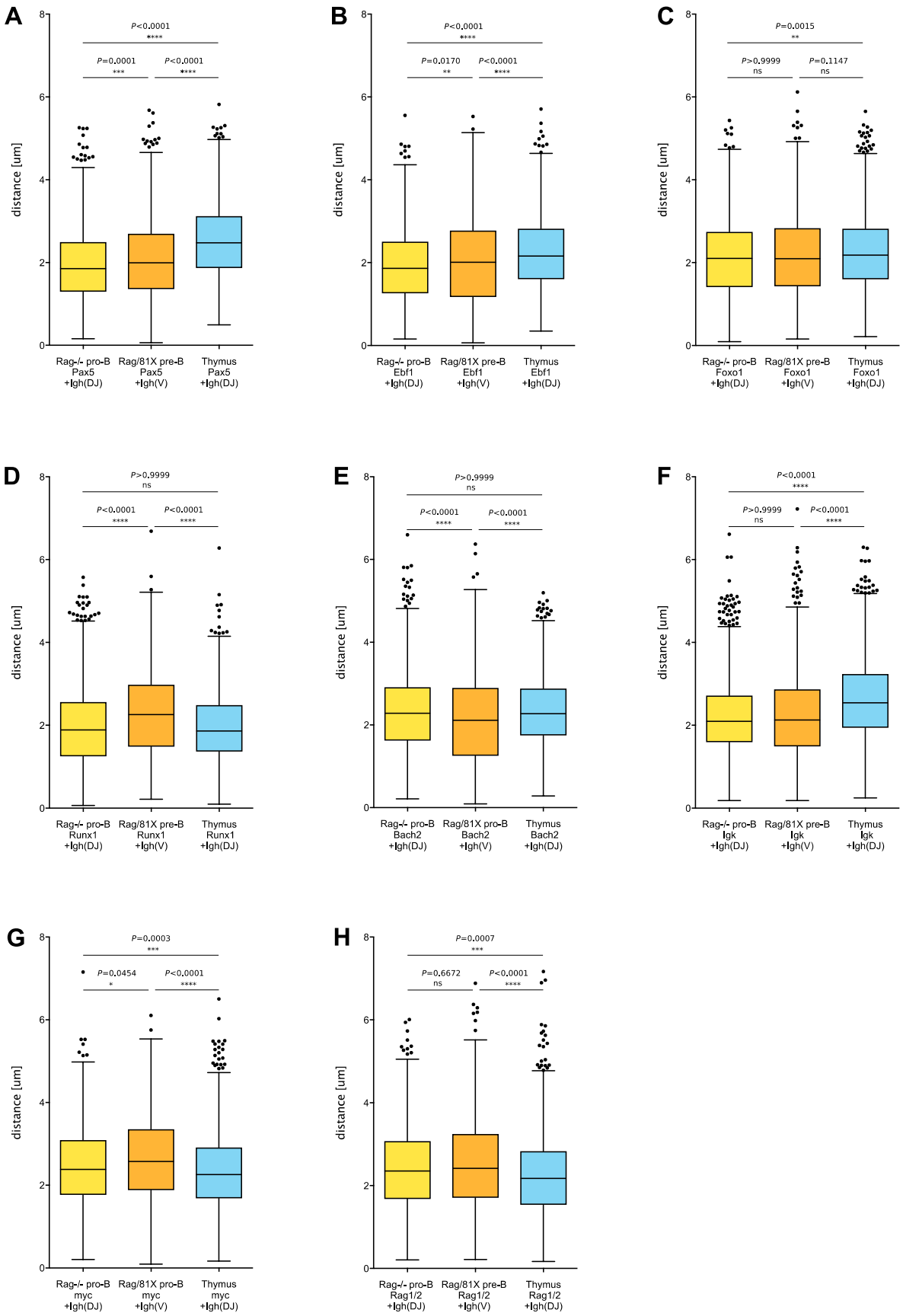

Figure 81. Distances between the Igh locus and the genes of interest are shorter in B cells than in thymocytes. All distances measured are plotted. The closest green and red signal pairs in each cell were used. Boxplots indicate the first and third quartiles, and the band inside the box is the median distance between the signals. The whiskers indicate 1.5 interquartile range and the dots indicate

outliers. Igh probes described in Figure 75. P-values were calculated using the Kruskal-Wallis test with Dunn's correction for multiple comparisons.

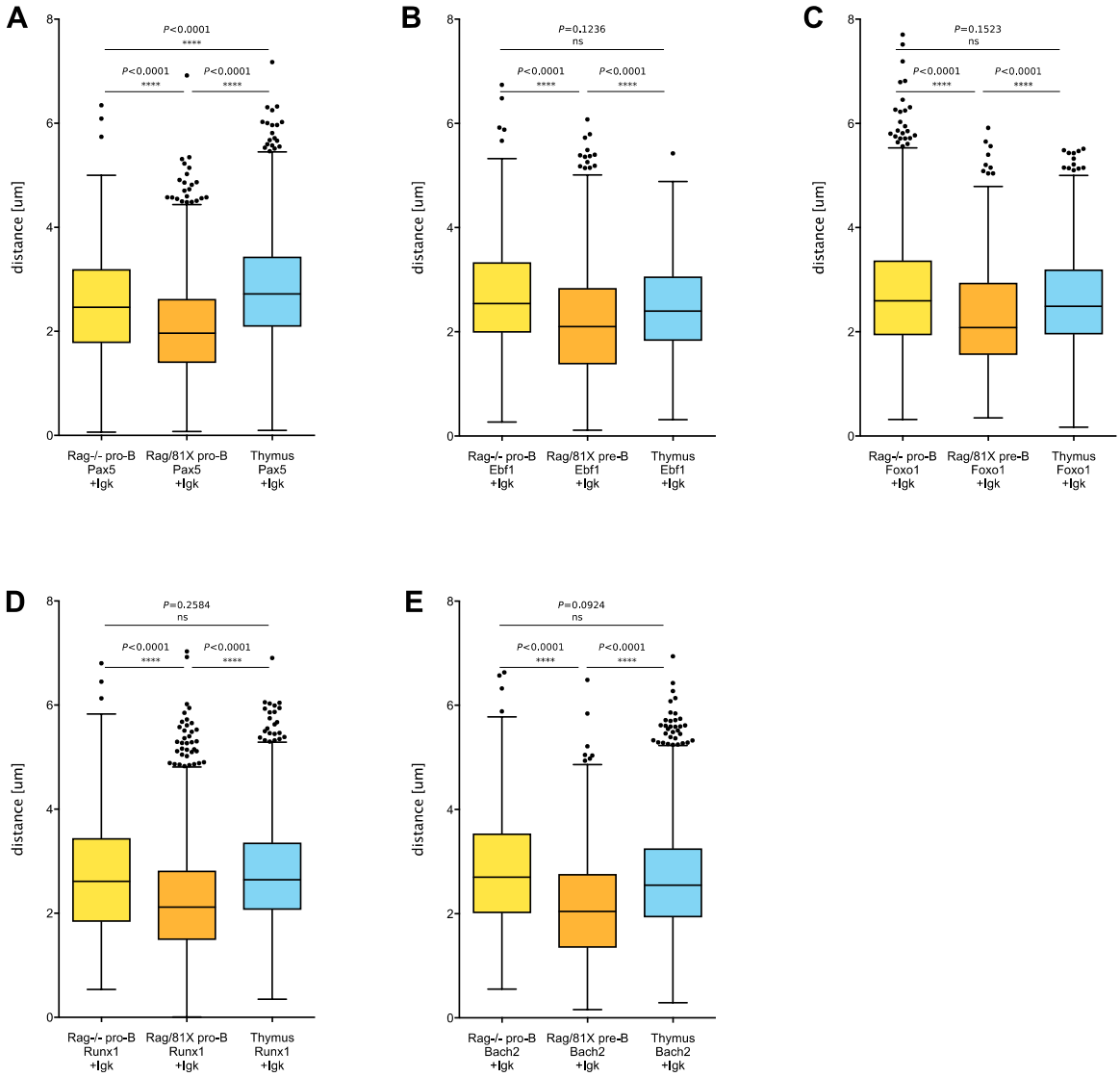

Figure 82. Distances between the Igk locus and the genes of interest are shorter in pre-B cells than in pro-B cells and thymocytes. All distances measured are plotted. The closest green and red signal pairs in each cell were used. Boxplots indicate the first and third quartiles, and the band inside the box is the median distance between the signals. The whiskers indicate 1.5 interquartile range and the dots indicate outliers. Igh probes described in Figure 75. P-values were calculated using the Kruskal-Wallis test with Dunn's correction for multiple comparisons.

Since two different BAC probes were used to image the Igh locus in $Rag^{-/-}$ pro-B cells and Rag/81X pre-B cells (Igh(DJ) and Igh(V), respectively), I tested the difference in distances between the Igh and Ebf1, Foxo1 and Runx1 using the Igh(V) probe in $Rag^{-/-}$ pro-B cells (**Figure 83**). In section 4.2.7 I showed that the trans hits contact the Igh predominantly around the Eμ-D-J region and around 115.3-115.7Mb in the V region. However, the Igh(V) probe detects sequences at 115.95-116.05Mb and as might be expected, the comparison showed increased distances in pro-B cells for Igh(V)+Foxo1 and Igh(V)+Runx1. This means

that the distances between the Eμ-J-D region and Foxo1 as well as Runx1 might in fact be slightly shorter than the measurements detected using the Igh(V) probe in pre-B cells, which would further strengthen the significance of the findings. Interestingly, for Igh(V)+Ebf1 there was an increase in very short distances (below 0.5μm) and indeed, the Ebf1 appears to preferentially interact with the Igh in the V region (**Figure 83**B and **Figure 69**). However, the overall number of distances shorter than 1μm was equal for the Igh(DJ) and the Igh(V) probes.

In summary, I found that the distances between the Igh and the genes of interest were shorter in both pro-B cells using the Igh(DJ) probe and pre-B cells using the Igh(V), compared to thymocytes and using the Igh(DJ) probe in pre-B cells would most probably produce an even higher number of short distances.

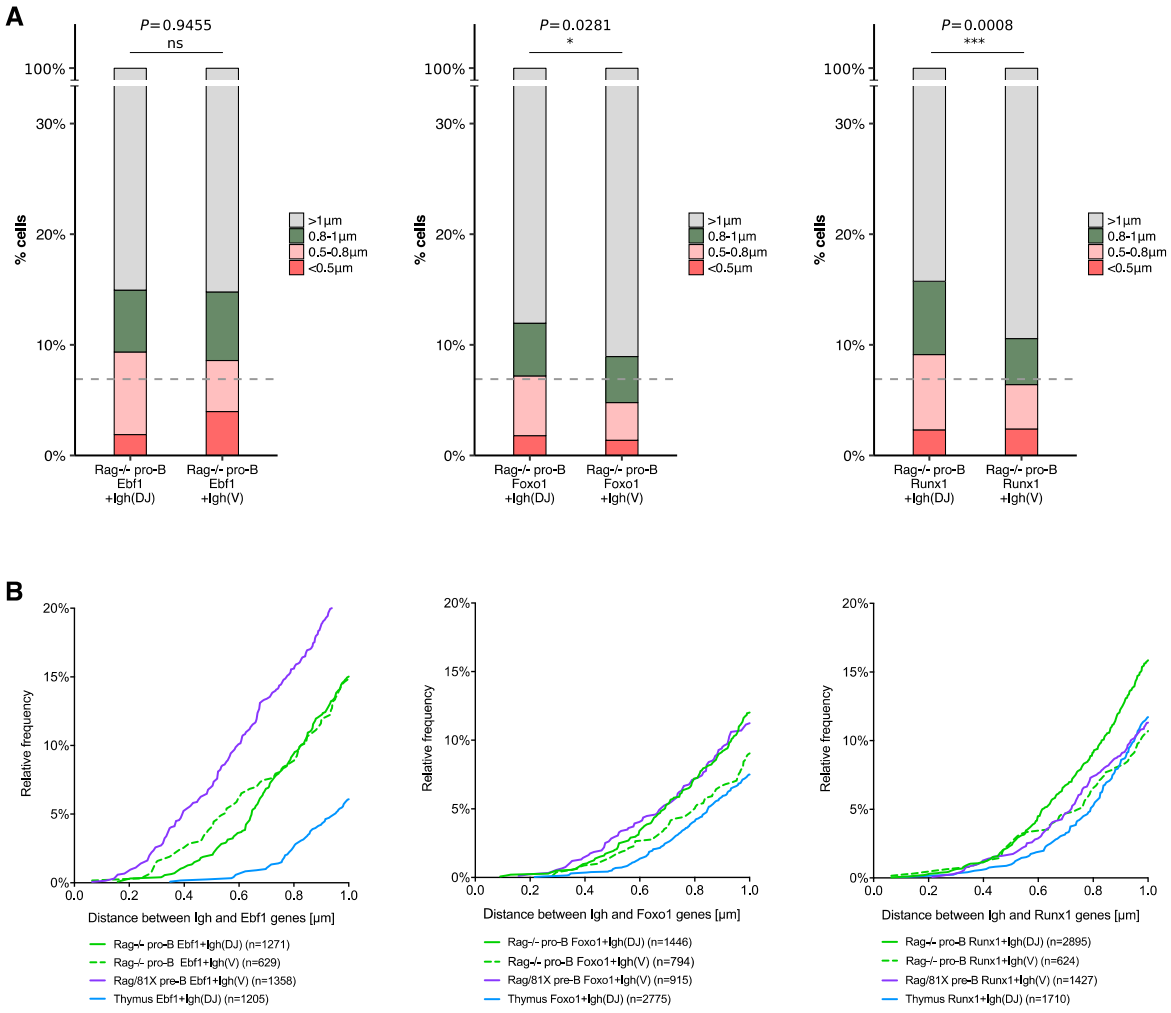

Figure 83. The D-J region of the Igh participates in trans interactions more frequently than the distal V region. A. Distances using the Igh(V) probe in Rag$^{-/-}$ pro-B cells are compared to distances using the Igh(DJ) probe from Figure 79. The distances <1μm are plotted as coloured stacked bar charts in three categories: <0.5μm, 0.5-0.8μm and 0.8-1μm; The distances >1μm are in grey. Dashed line denotes the probability of a random interaction at 6.9%. Igh probes described in Figure 75. P-values were calculated using the Mann-Whitney test. **B.** Distances <1μ for the Igh(V) probe in Rag$^{-/-}$ pro-B cells were plotted onto the cumulative distribution plots from Figure 75.

4.3.3. Eμ deletion moderately reduced inter-chromosomal interactions

To investigate the role of the Eμ enhancer in inter-chromosomal interactions, I performed FISH in pro-B cells from $E\mu^{-/-}$ $Rag^{-/-}$ mice. These pro-B cells had reduced locus contraction in a previous FISH study (Perlot et al. 2005) but not in a recent 4C-seq study (Medvedovic et al. 2013). Eμ mutation causes a reduction in V(D)J recombination levels and diversity (Perlot et al. 2005; Afshar et al. 2006; Bolland et al. 2007). Here, I observed a statistically significant albeit moderate reduction in Igh contacts with Pax5, Ebf1, Foxo1 and Runx1 in $E\mu^{-/-}$ $Rag^{-/-}$ pro-B cells compared to $Rag^{-/-}$ pro-B cells (**Figure 84**). The most pronounced difference was for Foxo1+Igh. Overall, this moderate reduction suggests that Eμ deletion perturbs the Igh locus structure and its ability to make contacts in trans. However, except for Foxo1, the reduced number of short distances was not as low as in thymocytes and was still above the 6.9% probability of a random contact.

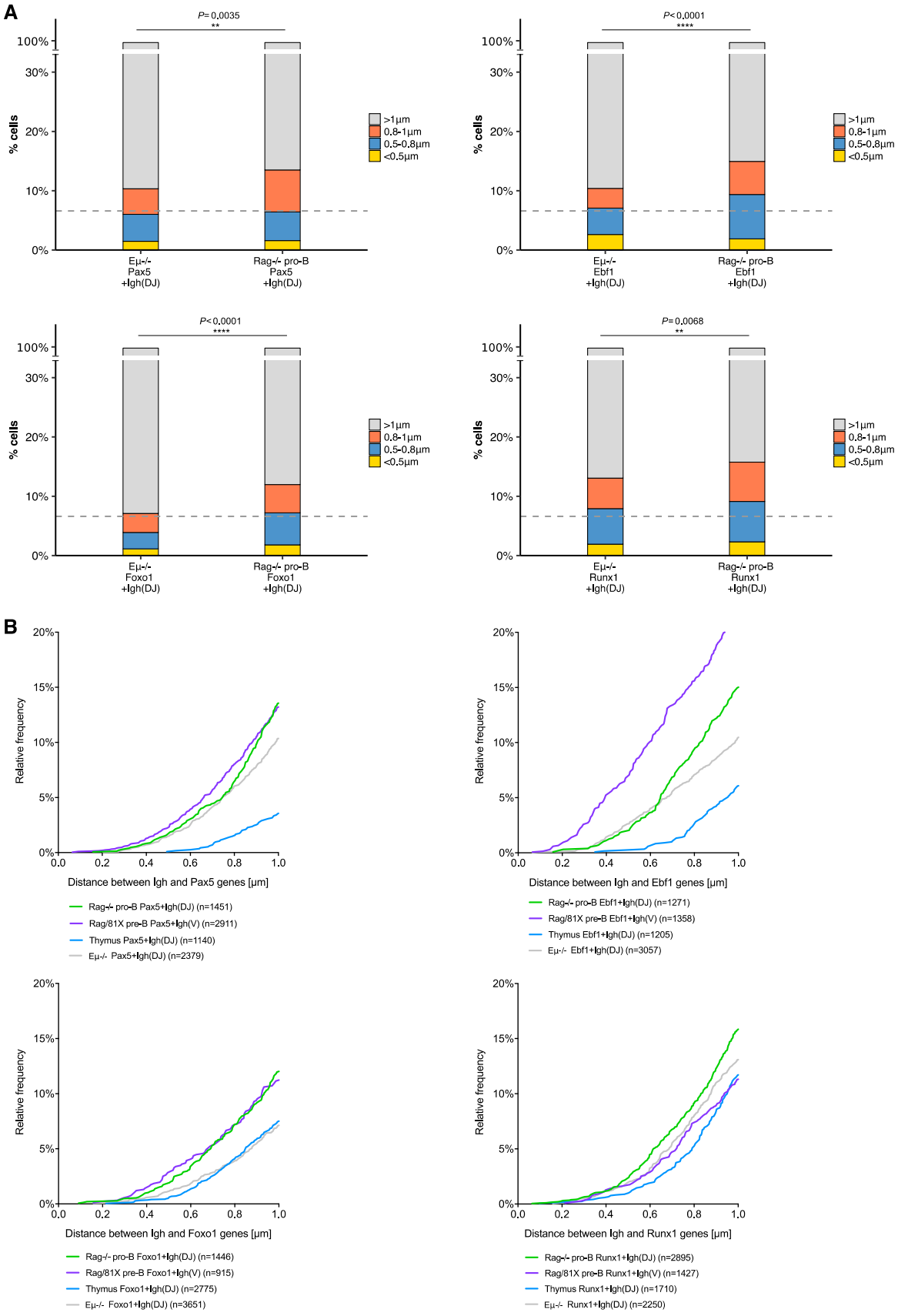

Figure 84. Deletion of the Igh Eμ enhancer causes decrease in trans interaction frequency. A. Distances between the Igh and the genes of interest in Rag$^{-/-}$ Eμ$^{-/-}$ pro-B cells are compared to distances Rag$^{-/-}$ pro-B cells from Figure 79. The distances <1μm are plotted as coloured stacked bar charts in three categories: <0.5μm, 0.5-0.8μm and 0.8-1μm; The distances >1μm are in grey. Dashed line denotes the probability of a random interaction at 6.9%. Igh probes described in Figure 75. P-

values were calculated using the Mann-Whitney test. **B.** Distances <1μ in Rag$^{-/-}$ Eμ$^{-/-}$ pro-B cells were plotted onto the cumulative distribution plots from Figure 75.

4.3.4. Simultaneous interaction between the Igh, Foxo1 and Ebf1

Hi-C does not generally provide information about simultaneous interactions between more than two loci. Given that the Igh interacts with Foxo1 and Ebf1, and Foxo1 interacts with Ebf1, by Capture Hi-C, I wanted to determine whether the Igh locus interacts with multiple trans hits at the same time. I performed 3 colour FISH and demonstrated that Ebf1 and Foxo1 co-localise with the Igh locus simultaneously in 1.52% of Rag$^{-/-}$ pro-B cells and in 2.86% of Rag/81X pre-B cells, which is more frequently than the 0.48% probability of a random interaction involving three loci (**Figure 85**A). The three probes co-localized in 0.46% of thymocytes. I also examined the pairwise interactions in this experiment, which showed that the contacts involving Ebf1 are more frequent in both pro-B and pre-B cells, suggesting that Ebf1 contacts the Igh simultaneously with Foxo1 but also without Foxo1 proximity. Similarly, Ebf1 and Foxo1 also interact without proximity to Igh (**Figure 85**B).

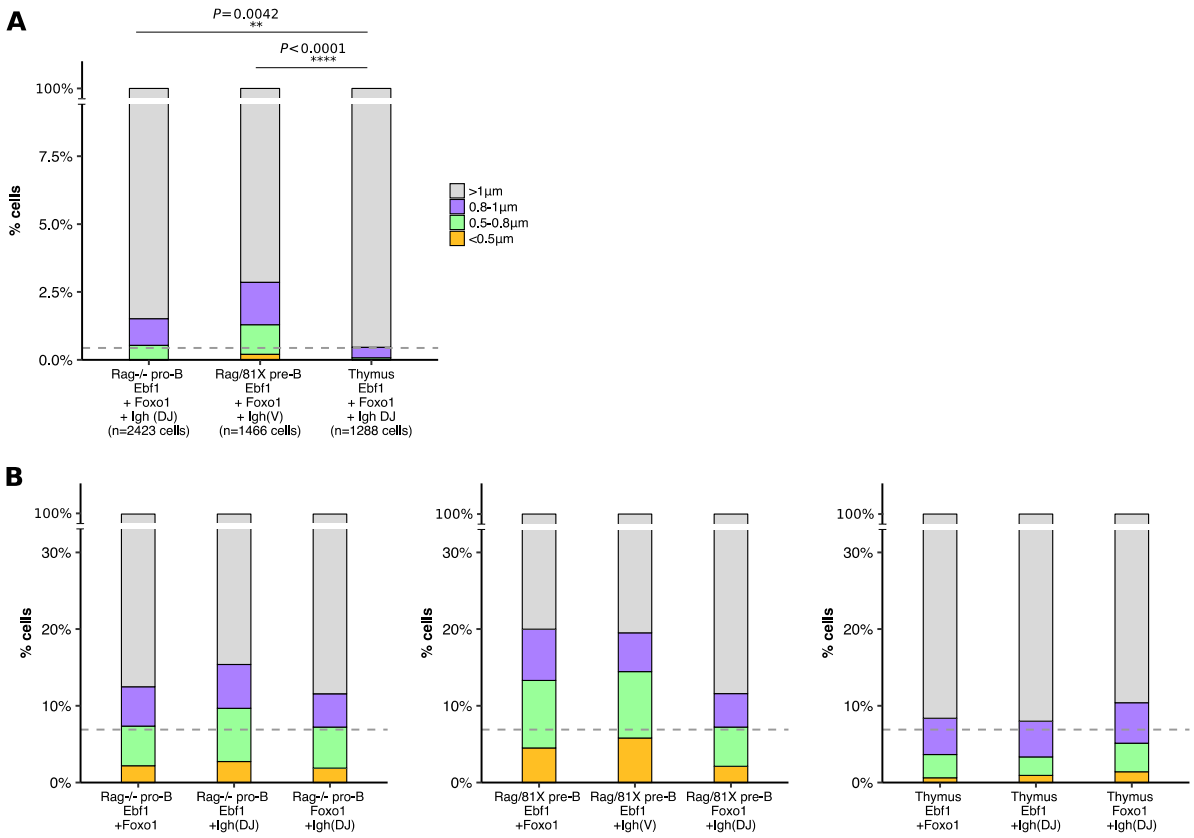

Figure 85. The Igh locus interacts simultaneously with Ebf1 and Foxo1. The distances <1μm are plotted as coloured stacked bar charts in three categories: <0.5μm, 0.5-0.8μm and 0.8-1μm; The distances >1μm are in grey. Igh probes described in Figure 75. **A.** Three loci co-localise within 1μm. Pairwise distances computed by Metafer were filtered to retain only cells with all three fluorescent signals within 1μm from each other. P-values were calculated using the Fisher's exact test with Bonferroni correction for multiple comparisons. Dashed line denotes the probability of a random bipartite interaction at 6.9%. **B.** Three pairwise interactions are plotted in one cell type per graph. Dashed line denotes the probability of a random tripartite interaction at 0.48%.

4.4. Ig loci and their interaction partners form a putative co-regulatory network

In the previous sections I have shown that the three Ig loci contact a very similar subset of genomic regions when they are active in pre-B cells. I visualised this putative network of inter-chromosomal interactions using Cytoscape software (**Figure 86**). As described in section 4.2.3, some genes of interest span more than one 0.5Mb bin and trans contacts also often include multiple consecutive 0.5Mb bins adjacent to each other in genomic sequence. To illustrate the interaction relationships more concisely, consecutive 0.5Mb bins were treated as one contacted region and interesting genes present in these bins were combined to give the node a common name. Therefore, the number of interacting nodes for each viewpoint in the network visualisation in **Figure 86** is lower than the original number of significant 0.5Mb bins. For example, the Igk node has 115 interacting nodes as opposed to 169 statistically significant 0.5Mb bins. For example, the five consecutive 0.5Mb bins over and near the Ebf1 gene were treated as one interacting region named 'Ebf1'. A heavily contacted region on chromosome 17 (4-9 0.5Mb bins depending on the Ig viewpoint) contained multiple interesting genes and was named 'Stk38/Fgd2/Pim1/Rnf8/Brd4'. Other examples include three bins around Pax5, Foxo1, Bach2 (named 'Bach2/Rngtt'), Zfp608 and Zfp36l1 (named 'Rad51l1/Zfp36l1'), four bins around Arid1b and six bins around Runx1 (named 'Runx1/Synj1/Il1rb'). Some regions did not contain any obvious genes of interest and their corresponding nodes are unlabelled.

It is not clear why these interactions take place and what mechanisms govern them, but their much higher than random frequency suggests that they have a functional role. Many of the genes in the trans contact network co-regulate each other and so might benefit from spatial proximity. Although transcription, translation and protein binding to the DNA are not coupled in space and time, co-localisation of multiple genes requiring binding of the same transcription factors may be a highly efficient and favoured chromatin arrangement. Indeed, there are several examples of co-regulated genes associating spatially in the nucleus (Schoenfelder et al. 2010; Apostolou and Thanos 2008; Spilianakis et al. 2005; Ben-Elazar et al. 2013). It is also possible that these frequently interacting genes encoding factors driving B cell development take advantage of the transcription factories formed at the Ig loci (Bolland et al. 2004; Osborne et al. 2004; Park et al. 2014). Further experiments are needed to elucidate the functions and mechanisms of these inter-chromosomal contacts.

Nevertheless, there is already substantial published evidence that the protein products of the genes found here to be interacting with the Ig loci bind each other's promoters and bind to the Ig loci. The Igh and Igk loci have multiple binding sites for several proteins encoded by the trans interacting genes, for example Pax5 (Revilla-i-Domingo et al. 2012), Ebf1 (Vilagos et al. 2012) and Irf4 (Schwickert et al. 2014). Furthermore, Pax5 has been shown to bind to the promoters or gene bodies of Ebf1 (Roessler et al. 2007), Rag2, Nedd9, Runx1, Pax5, Foxo1, Irf4, Irf8, Ikzf3 (McManus et al. 2011), Blnk (Schebesta et al. 2002), Cd19

(Kozmik et al. 1992), Rag1 and Bach2 (Schebesta et al. 2007). Reciprocally, Irf4 and Irf8 bind to the Pax5 gene and its intronic enhancer (Decker et al. 2009). Ebf1 binds and activates the expression of Pax5 (Zandi et al. 2008), Foxo1 and its own promoter (Lin et al. 2010; Roessler et al. 2007), and it also binds to Ets1, Il7r, Myb and Bach2 (Kong et al. 2016). Foxo1 binds and activates Pax5, Ebf1, Il7r, Erg, Dntt, Foxp1, Ets1, Lef1, Cd19 (Lin et al. 2012), Rag1 and Rag2 (Amin and Schlissel 2008). Runx1 binds to the Ebf1 promoter and is essential for its activation (Seo et al. 2012) and also regulates its own promoter (Martinez et al. 2016). Ets1 binds to the Ebf1 promoter (Roessler et al. 2007). Cux1 binds to the matrix attachment regions (MARs) in the Igh locus (Sansregret and Nepveu 2008). Additionally, E2A binds and activates Ebf1, Foxo1, Pax5, Rag1 and Il7r and although no interactions between E2A and the Ig loci were identified here, E2A protein could be a co-regulatory factor benefitting from all its targets being in close proximity without the need for the E2A gene to be in physical proximity.

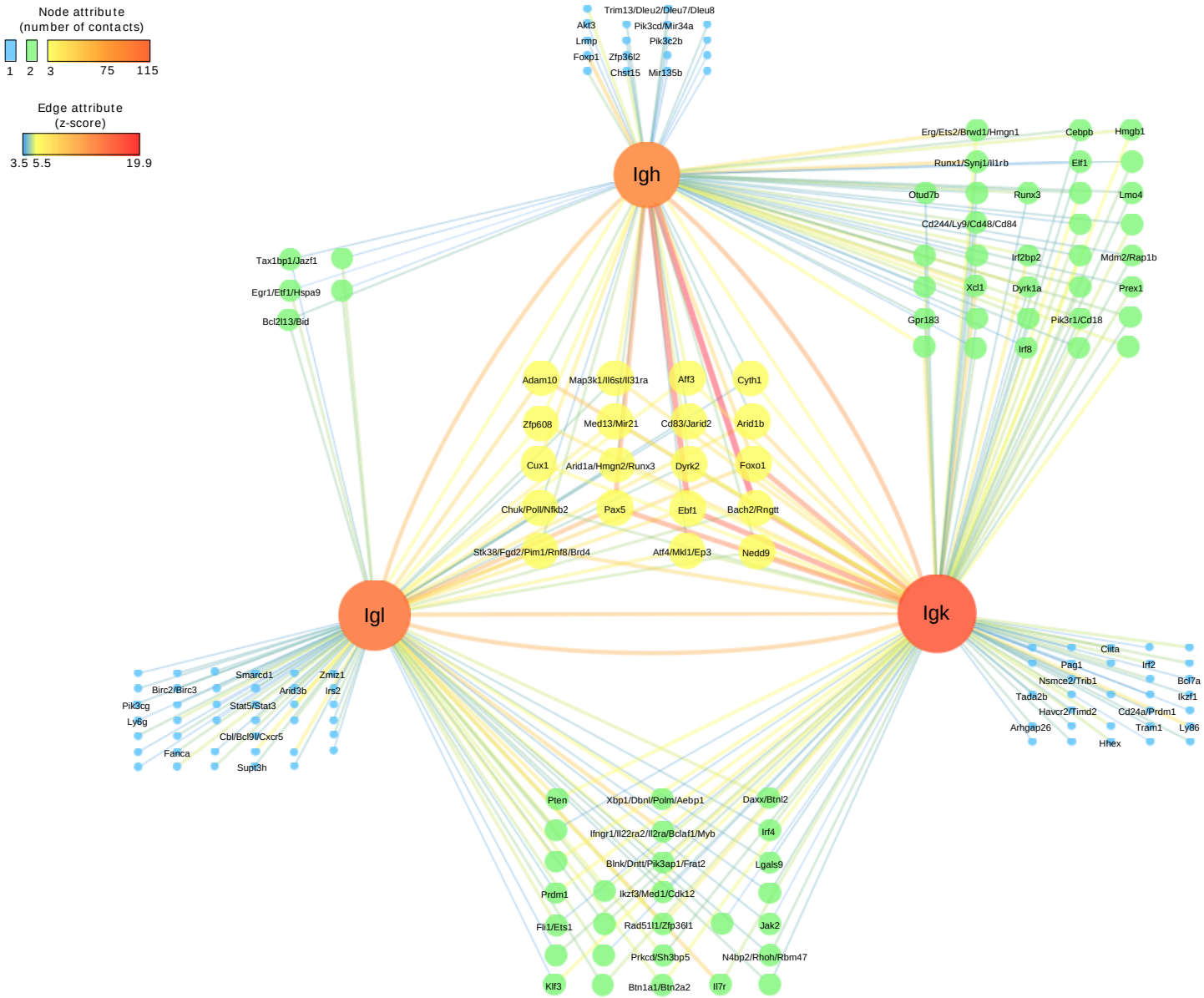
Node attribute
(number of contacts)
1 2 3 75 115
Edge attribute
(z-score)
3.5 5.5 19.9
Trim13/Dleu2/Dleu7/Dleu8
Akt3
Pik3cd/Mir34a
Lrmp
Pik3c2b
Foxp1
Zfp36l2
Chst15
Mir135b
Igh
Erg/Ets2/Brwd1/Hmgn1
Cebpb
Hmgb1
Runx1/Synj1/Il1rb
Elf1
Otud7b
Runx3
Lmo4
Cd244/Ly9/Cd48/Cd84
Irf2bp2
Mdm2/Rap1b
Xcl1
Dyrk1a
Prex1
Gpr183
Pik3r1/Cd18
Irf8
Tax1bp1/Jazf1
Egr1/Etf1/Hspa9
Bcl2l13/Bid
Adam10
Map3k1/Il6st/Il31ra
Aff3
Cyth1
Zfp608
Med13/Mir21
Cd83/Jarid2
Arid1b
Cux1
Arid1a/Hmgn2/Runx3
Dyrk2
Foxo1
Chuk/Poll/Nfkb2
Pax5
Ebf1
Bach2/Rngtt
Stk38/Fgd2/Pim1/Rnf8/Brd4
Atf4/Mkl1/Ep3
Nedd9
Igl
Igk
Smarcd1
Zmiz1
Birc2/Birc3
Arid3b
Irs2
Pik3cg
Stat5/Stat3
Ly6g
Cbl/Bcl9l/Cxcr5
Fanca
Supt3h
Ciita
Irf2
Pag1
Bcl7a
Nsmce2/Trib1
Ikzf1
Tada2b
Havcr2/Timd2
Cd24a/Prdm1
Arhgap26
Tram1
Ly86
Hhex
Pten
Xbp1/Dbnl/Polm/Aebp1
Daxx/Btnl2
Ifngr1/Il22ra2/Il2ra/Bclaf1/Myb
Irf4
Blnk/Dntt/Pik3ap1/Frat2
Lgals9
Prdm1
Ikzf3/Med1/Cdk12
Fli1/Ets1
Rad51l1/Zfp36l1
Jak2
Prkcd/Sh3bp5
N4bp2/Rhoh/Rbm47
Klf3
Btn1a1/Btn2a2
Il7r

Figure 86. The trans interaction network of the Ig loci in Rag/81X pre-B cells. Regions contacted by all three Ig loci are in the middle of the triangle (yellow circles), regions contacted by two Ig loci are outside of the triangle between two contacted Ig nodes (green circles) and the regions contacted by only one Ig locus are next to the corresponding Ig node (blue circles). The size and the colour of the nodes (circles) represent the number of interactions the nodes are involved in (node attribute = the number of edges connecting it). The thickness and the colour of the edges represent the frequency of the interaction (z-score value). The network was visualized using Cytoscape software.

To gain a systematic insight into potential co-regulatory mechanisms driving the inter-chromosomal contacts I used iREGULON - an analysis tool compatible with Cytoscape that identifies putative transcription factor binding targets based on DNA motifs. Similarly to the GO terms analysis in 4.2.2, iREGULON requires a list of gene names as input and so all genes in the significant 0.5Mb bins for each Ig viewpoint were used. This meant that only a fraction of these genes were truly genes of interest responsible for the trans interactions, however, this approach might reveal regulatory patterns not previously appreciated by qualitative identification of genes of interest. iREGULON identifies TF binding motifs 10kb upstream and 10kb downstream of the TSS and reports motif enrichment in the input gene list. To visualise the results, I constructed networks composed of transcription factors enriched in iREGULON analysis that were also trans hits in Capture Hi-C datasets (**Figure 87**). Each rectangle belongs to a single gene in the input data (not to a 0.5Mb bin). Genes that were not predicted to bind any of the transcription factors shown were not depicted. Among the enriched TF binding motifs were several trans hits including Pax5, Runx1, Foxo1, Irf4, Irf8, Ebf1, Cux1, Ikaros and Ets1. Out of these, Pax5, Runx1 and Ikaros were enriched in all datasets. Interestingly, the Ikaros gene only interacted with the Igk viewpoint in Capture Hi-C but its binding was predicted at numerous trans hit genes of all three Ig viewpoints. The Ikaros protein might be co-regulating its putative co-localising targets without the Ikaros gene contacting the Ig. Of note, Ikaros has at least 4 isoforms with specialised functions and they bind similar motifs (Schjerven et al. 2013), which are very short (GGAA) and share sequence similarity with Ets motifs (Ferreiros-Vidal et al. 2013, Zhang et al. 2011), and so the iREGULON analysis might have overestimated Ikaros motifs. On the other hand, Ikaros has been experimentally shown to bind ~30% of GGAA motifs in a pre-B cell line and to co-localise with the binding of E2A, EBF1 and FOXO1 (Ferreiros-Vidal et al. 2013). Perplexingly, the E2A motif was not enriched in any dataset, despite directly regulating many genes driving B cell development. Interestingly, YY1 motif was enriched in all pre-B datasets, but the Yy1 gene did not interact with Capture Hi-C viewpoints (Yy1 gene is located on chr12 and so was excluded from the virtual 4C from the Igh viewpoint). This analysis indicates that indeed co-regulatory dependencies might be the mechanism underlying the novel inter-chromosomal contact network in pro-B and pre-B cells presented in this chapter. Experimental validation of these relationships will be an important next step.

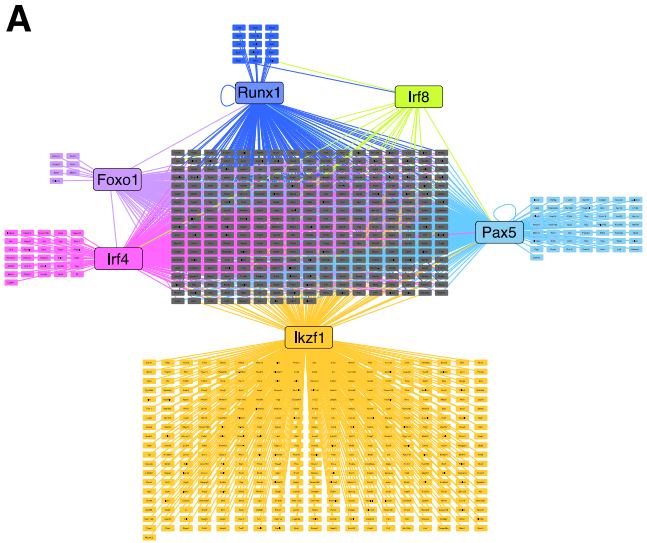
A
Runx1
Irf8
Foxo1
Pax5
Irf4
Ikzf1

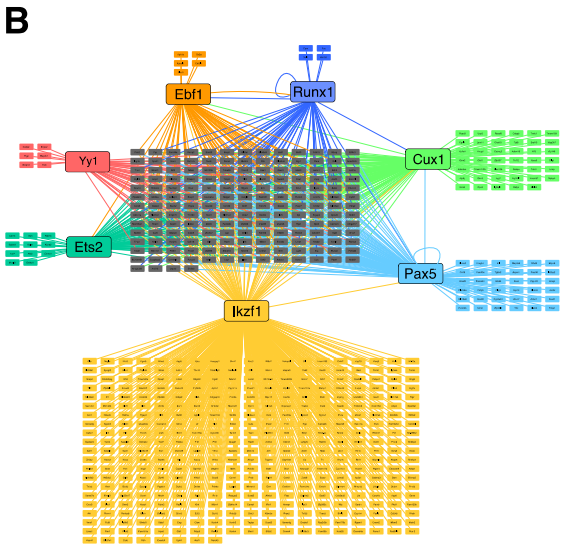
B
Ebf1
Runx1
Yy1
Cux1
Ets2
Pax5
Ikzf1

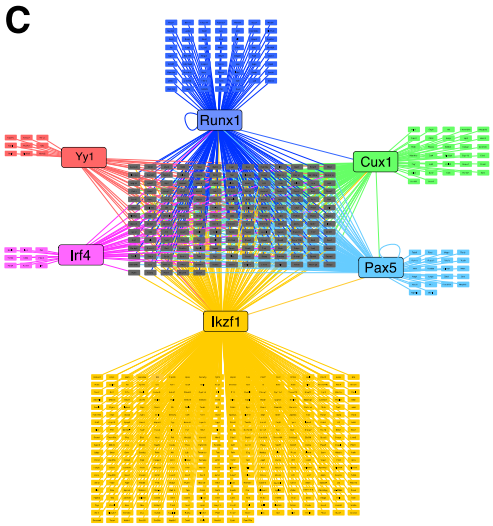
C
Runx1
Yy1
Cux1
Irf4
Pax5
Ikzf1

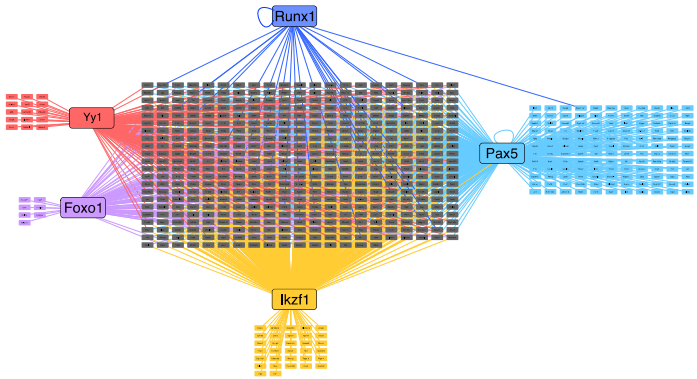
D
Runx1
Yy1
Pax5
Foxo1
Ikzf1

Figure 87. Genes interacting with the Ig loci might be co-regulated by shared transcription factors. Significant trans hits from the Ig virtual 4Cs were searched for transcription factor (TF) binding motifs using iREGULON in Cytoscape. Each rectangle represents a gene in significantly interacting 0.5Mb bins. TFs found to be enriched among the trans hits are labelled. Genes predicted to contain a motif for a given TF are connected to that TF with a coloured edge. Grey rectangles represent genes regulated by more than one TF. Genes not having a motif for any of the enriched TFs are not shown. **A.** Igh hits in $Rag^{-/-}$ pro-B cells. **B.** Igh hits in Rag/81X pre-B cells. **C.** Igk hits in Rag/81X pre-B cells. **D.** Igl hits in Rag/81X pre-B cells.

4.5. Discussion

In this chapter I have shown that Capture Hi-C is capable of detecting inter-chromosomal interactions between multiple baited viewpoints and the rest of the genome. Trans interactions involving the Ig loci have not been studied in the past, except for co-localisation of the Igh and Igk. Here, I performed multiple 4C-like experiments from baited viewpoints of Igh, Igk, Igl, Pax5, Foxo1, Il7r and Rag1/2 and obtained clear sharp peaks genome-wide with a high signal to background ratio. I carried out genome-wide analysis in 0.5Mb bins, but dissected several bins containing short genes of interest into 100kb bins and showed that the 100kb region with the highest number of reads contained the gene of interest. I applied stringent statistical analysis to call significant trans interactions and found that all viewpoints except Rag1/2 interact frequently with the same genomic regions. The top interactions involved B cell-specific genes and genes driving B cell development such as Ebf1, Pax5, Foxo1, Runx1, Bach2, Igh, Igk and Igl. Furthermore, I demonstrated that the Ig viewpoints make trans contacts in a developmental stage-specific manner. In pre-B cells, the Igk and Igl largely adopt the interaction profile of the Igh in pro-B cells. The interaction profile of the Pax5 viewpoint differed slightly from other viewpoints as it did not interact with Ebf1 and Bach2. Together, this data shows that inter-chromosomal contacts between the Ig loci and genes driving B cell development are non-random and may have a functional role.

In my efforts to elucidate the general characteristics of the chromatin environment of the trans interactions I have shown that the regions contacted by active Ig loci reside in active, gene-rich A compartments. Trans hits of the Igh locus in pro-B and pre-B cells as well trans hits of the Igk and Igl in pre-B cells map to A compartments, whereas trans hits of the Igk and Igl in pro-B cells and thymocytes map to silent B compartments. Interestingly, the Igh interacted with A compartments in thymocytes, which suggests that the Igh locus is partially active in all lymphocytes and might reside in a poised chromatin environment even when sequestered at the lamina in T cells. On the other hand, because the recombination of the light chain loci does not commence until recombination of the Igh is complete, these loci may be heavily repressed prior to the pre-B cell stage, as suggested by Rother *et al.* 2016 (Rother et al. 2016). This is corroborated by the fact that the Igk and Igl themselves resided in A compartments only in pre-B cells. Secondly, I showed that although the trans interacting regions contained highly transcribed B cell-specific genes, there was a plethora of other highly transcribed regions that were not interacting with the Capture Hi-C viewpoints,

strongly suggesting that the trans contacts are specific and do not simply reflect co-localisation of active regions.

Validation of the top inter-chromosomal contacts by FISH confirmed that these interactions occur at frequencies exceeding that of a random contact between any two loci in the nucleus. I showed that trans interactions were reduced in the absence of the Eμ enhancer, however, not to the level of random interaction frequency as seen in the thymus. This suggests that the presence of functional Eμ is not absolutely required for inter-chromosomal interactions involving the Igh locus, but its absence might slightly change the locus conformation into one less favourable for frequent trans contacts. The main focal points of interactions with the Eμ region covered by the FISH probe may be the MARS regions either side of the Eμ. On the other hand, Pol II binding is reduced in $E\mu^{-/-}$ pro-B cells (Chakraborty et al. 2009b) and if interactions preferentially occur in a transcription factory into which the Eμ recruits the Igh locus, I would expect a larger reduction in interactions than observed here. Further experiments are needed to investigate the role of the Eμ and Pol II in mediating trans interactions. First, immuno-FISH could be used to show whether the Ig loci are in close proximity to their trans interaction partners only when they are bound by Pol II. Second, RNA-DNA FISH could assess whether the trans hit genes are being transcribed while co-localising with the Ig loci or with each other. Third, not all Ig loci are contracted at the developmental stage at which they are active and it needs to be established whether the trans contacts preferentially occur with a contracted Ig allele.

I have shown that the Igh interacts simultaneously with Ebf1 and Foxo1 with a frequency higher than expected from a random association. Simultaneous interactions between the Igh, Ebf1 and Pax5 would be interesting to assess since Capture Hi-C data indicates that Pax5 and Ebf1 do not interact frequently and therefore might contact the Ig loci at different times. Reports suggest that Ebf1 and Foxo1 work in synergy and bind to the same targets (Lin et al. 2010; Mansson et al. 2012), and also Pax5, Ebf1 and Runx1 have been proposed to work in synergy (Maier et al. 2004). Traditionally, Hi-C does not provide information about simultaneous interactions between more than two loci, however this could be deciphered by extracting reads from the raw Capture Hi-C data that contain more than one ligation junction. These reads represent ligation between several restriction fragments within cross-linking proximity and could reveal groups of genes that often reside together. This is a very inefficient approach as only less than 1% of reads in a 4C-seq or Capture Hi-C dataset comprise such 3-way reads, nevertheless an analysis of this type has been performed using a 4-cutter restriction enzyme to show simultaneous interaction of three regulatory elements in the Igk locus (Proudhon et al. 2016). Inter-chromosomal interactions involving 3 loci have been demonstrated between circadian clock genes and were mediated by CTCF (Zhao et al. 2015). Interestingly, a recent chromosomal walks method (C-walks) analysed thousands of multi-loci interactions and concluded that in fact nested pair-wise interactions are a dominant feature of genomic contacts and multi-loci inter-TAD interactions reflect stochastic associations of transcribing and early replication genes, with the exception of Hox-mediated

interaction hub (Olivares-Chauvet et al. 2016). It is therefore essential to determine whether the immunoglobulin genes indeed participate in a multi-loci synergistic interaction hub or their pairwise trans contacts are separated in time. Additionally, it remains to be determined whether the Ig loci contact B cell-specific genes while interacting with each other.

The observation that the regions preferentially residing nearer the periphery of the Igh locus structures are more frequently contacted by other genomic regions in trans could be validated by FISH. I have already shown that the 3' end of the locus (the DJ region) interacts in trans more frequently than the distal V region (BAC probe 115.95-116.05Mb). It remains to be tested whether the more peripheral beads at 115.3-115.7Mb in the V region interact with trans hits at frequencies similar to that of the DJ region.

The Capture Hi-C results obtained here using $Rag^{-/-}$ and Rag/81X mouse models should be confirmed in wild type pro-B and pre-B cells. Firstly, all Ig loci were in germline configuration, whereas it will be important to determine how trans interactions differ for the recombined and the silenced alleles. Secondly, the Igh locus has not been extensively studied in the Rag/81X mouse and it is not known whether, given the presence of the 81X transgene, the trans contacts of the endogenous Igh locus in these cells fully recapitulate the contacts of the recombined Igh locus in wild type pre-B cells. It will be challenging to determine which interactions involve the recombining Igh allele, but FISH could provide an insight into whether trans contacts preferentially involve the recombining Igh allele. Another outstanding question is whether trans interactions detected here also take place in later stage B cells, but involving only the expressed allele. If this were the case, it might suggest a relationship between trans interactions and immunoglobulin transcription. If there is a co-regulatory and/or transcription factory-mediated mechanism for trans contacts then it would be reasonable to expect that these interactions persist in later B cells as many genes important in early B cell development continue to be expressed and indeed have roles in later B cells.

The putative co-regulatory mechanisms that bring multiple genes together in trans and the functional role of these interactions remains to be determined experimentally. Here, the *in silico* motif analysis suggests that many of the trans hits are bound by the same transcription factors and so they might be co-regulated in a transcription factory. Mutant models carrying deletions of the top trans hits will be crucial in elucidating the putative co-regulatory network of interactions. Using perturbed systems to elucidate precise direct mechanisms will be challenging, because the top interacting genes encode crucial transcription factors driving B cell development and their depletion causes pleiotropic effects that might mask direct effects on gene interactions. Also, precise roles of many B cell-specific factors in V(D)J recombination are still unknown. For example, deletion of Pax5 causes a lack of Igh locus contraction and prevents B cell commitment, but expression of Pax5 in non-B cells is not sufficient to induce locus contraction (Hesslein et al. 2003; Fuxa et al. 2004). Ebf1 deletion results in a developmental block at the pre-pro-B cell stage precluding assessing its precise involvement in the trans network in pro-B and pre-B cells (Gyory et al. 2012; Vilagos et al. 2012). To alleviate these problems, mouse models bearing genes with flox sites (fl/fl) could

be used to delete the genes of interest at appropriate developmental stages by introducing Cre under the regulation of a pro-B cell or pre-B cell-specific promoter. Also, pro-B and pre-B cell lines might be used to introduce mutations of genes of interest. Rag KO cell lines or line carrying an inducible Rag transgene may be utilised for this purpose. First, FISH could assess whether depletion of TFs perturbs trans interactions; Capture Hi-C in the promising mutants would then provide a comprehensive picture of perturbed interactions in the absence of a particular factor. If a knockout model, even conditional, has too broad effect, then an approach of shRNA knockdown in short-term cultured ex vivo pro-B and pre-B cells might be more useful to asses the immediate effect of mRNA and protein depletion on trans interactions. Another strategy for studying depletion of genes with pleiotropic effects is crossing fl/fl mice with ERt-Cre, which enables controlled activation of Cre upon administration of tamoxifen. This and shRNA approach however might be burdened by an incomplete depletion of the factors of interest and a possibility that factors already bound to DNA will obscure the analysis. A challenge in using mutants might lie in discerning whether the interactions of the mutated gene of interest are diminished due to the lack of functional transcription factor protein or due to the mutation itself. A gene with a mutated promoter or exon might not contact other genes due to a lack of regulatory elements or a lack of receiving upstream signals. This would not be an issue in an shRNA approach and a comparison of these two might discern the roles of the gene and the protein product. Last, it might also be useful to use CRISPR-Cas9 to mutate single TF binding sites in the promoters of genes involved in the trans interaction network to determine if co-regulation by the same TFs is responsible for their co-localisation. For example, one might mutate the Pax5-, Ebf1- or Foxo1- binding sites in the Ebf1 promoter and examine whether the Ebf1 gene still participates in trans contacts. This will be a challenging and laborious approach, but possibly the most precise way to interrogate the TF binding role in inter-chromosomal interactions.

Collectively, in this chapter I explored a novel aspect of early B cell development and discovered a network of long-range genomic contacts bringing together genes from different chromosomes into physical proximity in the nucleus. I investigated genome-wide interactions of the immunoglobulin loci and found that they largely contact the same genes and that those interactions take place in a developmental stage specific manner. In pro-B cells, only the Igh locus is active and engaged in trans interactions, whereas in pre-B cells all three Ig loci are active and make genome-wide contacts. These interactions were probed using a new Hi-C enrichment method, Capture Hi-C, which allowed baiting of several viewpoints in one experiment to obtain a many-to-all interaction landscape of B cell-specific genes. Stringent statistical analysis revealed a pool of the top most frequent contacts involving the Ig loci and genes such as Ebf1, Pax5, Foxo1, Runx1 and Bach2. I validated these by FISH to confirm they occur more frequently than random contacts. Some of these contacts involve three loci simultaneously, whereas others might be mutually exclusive, which requires further investigation. Transcription factor motif enrichment suggests that this interaction network might be governed by co-regulatory relationships. I propose that the Ig loci, when active,

reside in accessible chromatin and make specific frequent inter-chromosomal contacts with genes orchestrating B cell development.

5

5. General discussion

The work presented in this thesis has resolved the spatial organisation of the Igh locus in pro-B cells and provided evidence for genome-wide inter-chromosomal interactions involving the immunoglobulin loci. Firstly, I used an enriched Hi-C method to produce an all-to-all map of interactions between the Igh elements at highest resolution to date and applied polymer modelling to gain insight into single Igh structures. Secondly, I discovered a network of physical contacts involving all three Ig loci and genes essential for B cell development.

5.1. Novel insights into the Igh locus architecture

The spatial positioning of the coding and regulatory elements in the Igh locus has been studied extensively, however assays to date struggled to provide contact frequencies between all Igh elements at high resolution. The limiting factors are sequencing depth required for highly complex Hi-C libraries and the Igh locus being less readily mappable compared to the rest of the genome. 4C-seq studies provided high resolution interaction data from a handful of viewpoints, whereas Hi-C and 5C provided all-to-all interactions at lower resolution (Guo et al. 2011a; Medvedovic et al. 2013; Montefiori et al. 2016; Benner et al. 2015). Here I applied an unbiased enrichment step to a Hi-C library, Capture Hi-C, to pull-down all interactions involving the Igh locus, which gave 45-fold enrichment in read coverage over Hi-C datasets. Further improvement of Capture Hi-C read coverage over baited region could involve two sequential capture steps for more efficient pull-down of interactions of interest.

I resolved the average spatial conformation of the Igh locus in pro-B cells at 20kb resolution. The contact frequency map revealed that the CTCF-binding elements at the 3' of the locus and the insulator IGCR1 5' of D genes act as superanchors by contacting all V genes with similar frequencies. These CBEs clearly form focal points for V interactions and suggest that direct contacts are mediated by CTCF binding. This is in agreement with recent findings that convergent CTCF sites interact preferentially (Rao et al. 2014a; Sanborn et al. 2015; de Wit et al. 2015b; Gómez-Marín et al. 2015) as indeed the CBEs in these two elements are in convergent orientation to the CBEs in the V region. My data also shows the 20kb region containing the Eμ seems to be one of the least interacting regions of the locus, suggesting that

it may ‘loop out’ of the contracted Igh structure. This might be due to the fact that the Eμ resides in very active and open chromatin, and the region over the Eμ and J genes binds large protein complexes including RAG2, BRG1 and RNA Pol II and is anchored in a transcription factory. Frequent interactions of the V genes with the IGCR1 region and the two 20kb D gene bins downstream show that V interactions are precisely concentrated over genes with which they are poised for recombination. Similar interaction pattern can be deduced from previous 4C-seq data, that also showed more frequent interaction involving the 3’CBEs and the IGCR1 than the Eμ, however the authors did not draw attention to this finding (Medvedovic et al. 2013). My observations of similar interaction frequencies between the Vs and the two regulatory elements at the 3’ end are in agreement with the 'flexible looping' model (Medvedovic et al. 2013) and the recently identified 3’ superanchor (Benner et al. 2015).

The comprehensive map of Igh interactions revealed that the distal V genes are organised into a highly looped subdomain, which is also present to a large extent in T cells. This validates and expands the 4C-seq study, which observed the presence of local V interactions in uncontracted Igh locus in $Pax5^{-/-}$ pro-B cells (Medvedovic et al. 2013), and the 5C study (Montefiori et al. 2016), which identified two interaction focal points approximately around the boundaries of the distal V domain. My data also confirmed the previously proposed 3’ subdomain encompassing the 3’ end of the locus and the proximal V genes (Guo et al. 2011a; Medvedovic et al. 2013; Montefiori et al. 2016). Ultimately, my findings have reconciled the ‘flexible looping’ model (Medvedovic et al. 2013) and the '3 domain model' (Montefiori et al. 2016) by providing the entire all-to-all interaction landscape on the Igh locus. It has readily illustrated both the uniform looping of the V genes to the 3’CBEs and the IGCR1 as well as the presence of the proximal and distal V subdomains.

My collaboration with Luca Giorgetti's lab to apply polymer modelling and simulate all possible single structures from the ensemble data has provided the first quantitative insights into multi-way interactions between the Igh elements. The deconvolution of putative individual conformations showed that they are highly variable and there is not one prevalent favoured conformation that the Igh assumes when contracted. This approach cannot distinguish between the alleles as it was not possible to use single nucleotide polymorphisms, but the modeling provided the best possible estimation of single structures. Ultimately, single-cell Hi-C in F1 hybrids could give an unambiguous picture of the heterogeneity of single Igh structures, although at present this method achieves much lower resolution that ensemble Hi-C. Efforts to assemble the sequence of the Igh locus in the 129Sv mouse strain are under way in our lab. The simulated single structures suggest that the D gene region contacts a large number V genes at a time, but is not embedded centrally between them. Rather, the V genes form the centre of mass, which is contacted by the D genes. It must be borne in mind that these experiment were carried out in $Rag^{-/-}$ pro-B cells, which do not have a recombined DJ focal point, with which V genes would normally interact in wild type pro-B cells. The interaction frequency between the V and the D elements did not exhibit a strong positive linear correlation with V gene recombination frequency, similar to the Tcrb locus

(Gopalakrishnan et al. 2013). However, there may be multiple layers to this relationship and there might be a group effect as overall higher interaction frequencies were observed for the most frequently recombining V genes. Additionally, the level of CTCF binding in the V region correlated with V gene usage. Data presented in this thesis largely supports the 'equal opportunity for all' model postulating that V genes contact the DJ region at similar frequencies to facilitate the generation of a diverse antibody repertoire. However, this model was proposed some time ago to draw attention to the fact that the distal V genes, although positioned far away in the linear sequence from the recombination centre, are used in V(D)J recombination with frequency comparable to that of the proximal V genes. It is now clear that V genes recombine with vastly different frequencies which is not dictated by their linear position, i.e. V genes very close to each other can recombine with markedly different frequencies, the mechanism of which was recently characterized in our lab by identifying local chromatin states that govern V gene usage. The 'equal opportunity for all' model might be too simplified and further research is needed to elucidate the relationships between recombination frequencies, local chromatin determinants and interactions frequencies. Future work should entail quantitative analysis of chromatin states of single V genes to create a score similar to that of RSSs quality score, which could bridge the comparison between recombination and interaction frequencies at single V gene resolution.

To definitively determine the relationship between the epigenetic factors, chromatin interactions and V(D)J recombination, chromosome conformation data at single V gene resolution will be required and could be achieved by using a 4-cutter restriction enzyme. Higher resolution would provide more precision for overlaying information from ChIP-seq datasets for key histone modifications and factors including YY1 and Pax5. This would enable random forest classification and chromatin HMM (Hidden Markov Model) to model chromatin states to gain more insight into the contribution of these features to V-D interactions, similarly to that performed for V gene recombination levels (Bolland et al. 2016). Higher resolution would also aid the dissection of the individual interaction profiles of the two CBEs in the IGCR1.

Hi-C and FISH experiments provide only a static view of chromatin interactions at one time point. Only the application of single-cell live imaging will ultimately elucidate the spatiotemporal dynamics of the recombination synapse formation. Super-resolution microscopy and new labeling methods utilizing CRISPR/Cas or TALENs may be a better alternative to the previously used Tet operator system. It will be important to determine whether the first interaction results in a recombination synapse or there is indeed dynamic bouncing of V and DJ regions. The direction of interactions is also unknown. The DJ region might move towards the centre of mass containing highly looped distal V genes, encountering proximal and middle Vs on its way. Alternatively, the distal V domain might 1move like a ball on a hinge towards the DJ region to present V genes for recombination. The movement might also be bilateral with a major contribution from locus contraction and a minor

contribution from current V genes' positions in a given pro-B cell, in which case contacts could happen very rapidly between the DJ and the first encountered V gene.

5.2. A putative B cell-specific inter-chromosomal interaction network

I utilised the fact that Capture Hi-C baits detect interactions between the baited regions and the rest of the genome and discovered that the immunoglobulin loci frequently contact other genes driving B cell development, such as Pax5, Ebf1 and Foxo1. These interactions are cell type- and developmental stage-specific. In pro-B cells, only the heavy chain locus, and not the light chain loci, is involved in inter-chromosomal interactions, whereas in pre-B cells all three immunoglobulin loci interact with each other, and make similar contacts genome-wide. I validated the top most frequent interactions by FISH as an independent imaging method and detected consistently shorter distances between the Ig loci and the most frequently contacted genes identified by Capture Hi-C. I also detected a simultaneous interaction between the Igh, Ebf1 and Foxo1. This is the first insight into genome-wide interactions of the Ig loci in early B cells and opens new avenues for investigating multigene contact hubs involving the Ig loci.

I related the inter-chromosomal contacts back to the Igh structure and observed that the Igh elements that tend to reside at the periphery of the locus are most frequently contacted in trans. It remains to be elucidated whether this is a cause or effect of the Igh locus 3D structure.

Thanks to Capture Hi-C I also identified the previously unknown integration site of the 81X transgene on chromosome 16. Additional experiments in wild type pre-B cells with conditional Rag knockout could determine whether and to what extent the presence of the transgene alters the inter-chromosomal contacts of the endogenous loci identified here. More importantly, this would provide an overall better system to study interactions in pre-B cells. Additionally, if F1 hybrid experiments were possible, baits designed for the allele carrying the transgene could directly show what interactions the transgene itself is involved in.

There is scope for technical improvement in detection of trans interactions. The main one being greater sequencing depth to allow for statistical analysis at higher than 0.5Mb resolution. The double capture proposed above would also ensure greater read coverage of trans interactions. This would ameliorate the current conundrum that virtual 4Cs from the smaller viewpoints such as Il7r and Rag1Rag2 identified an interaction with the Igh, but reciprocal 4C from the Igh viewpoint did not call these interactions as significant.

The identification of the genome-wide trans contact network centralised on the Ig loci opens up new avenues for identification of mechanisms driving these interactions. Co-regulatory and co-transcriptional dependencies are potential reasons for spatial proximity of B-cell specific genes and will be elucidated by a new member of our lab. The use of conditional or short-term knockouts will be essential, as many of the interaction partners

encode factors with pleiotropic effects on B cell development. Further precise mutations of particular TF binding sites using CRISPR/Cas9 could determine whether binding of a transcription factor contributes to spatial proximity of co-regulated genes. These could include for example the EBF1-binding sites in the Pax5 and Foxo1 promoters or the FOXO1-binding sites in the promoters of Pax5 and Ebf1. Another approach could involve knocking out a gene of interest such as Pax5 while simultaneously overexpressing PAX5 protein in order to separate the participation of the gene in the interaction network and the role of the protein in mediating interactions.

5.3. Summary

In summary, during my PhD I have shown that a novel Hi-C enrichment method enables to probe the 3D organisation of the repetitive immunoglobulin heavy chain locus. I produced the first all-to-all contact map of the Igh at unprecedented resolution. The interaction landscape showed that the 3' end of the locus in organised into a subdomain, the distal V genes form another large subdomain and two superanchors mediate frequently interactions between the D and the V genes. This provides a link between two current models of the Igh structure, one favouring 3 large domains and the other flexible interactions of similar frequencies to provide all V genes a chance for recombination and generation of a diverse antibody repertoire. Furthermore, polymer modelling provided a first ever glimpse at putative single structures of the Igh locus and suggests that recombination frequency correlates slightly with interactions, but both central and peripheral V genes have equal chance to recombine. Capture Hi-C also revealed a previously undiscovered network of inter-chromosomal interactions between the Ig loci and genes driving B cell development. Collectively, data presented in this thesis provide a comprehensive analysis of genomic organisation of the immunoglobulin loci.

References

Adolfsson J, Borge OJ, Bryder D, Theilgaard-Monch K, Astrand-Grundstrom I, Sitnicka E, Sasaki Y, Jacobsen SE. 2001. Upregulation of Flt3 expression within the bone marrow Lin(-)Sca1(+)c-kit(+) stem cell compartment is accompanied by loss of self-renewal capacity. *Immunity* **15**: 659–669.

Adolfsson J, Mansson R, Buza-Vidas N, Hultquist A, Liuba K, Jensen CT, Bryder D, Yang L, Borge O-J, Thoren LAM, et al. 2005. Identification of Flt3+ Lympho-Myeloid Stem Cells Lacking Erythro-Megakaryocytic Potential: A Revised Road Map for Adult Blood Lineage Commitment. *Cell* **121**: 295–306.

Afshar R, Pierce S, Bolland DJ, Corcoran A, Oltz EM. 2006. Regulation of IgH gene assembly: role of the intronic enhancer and 5'DQ52 region in targeting DHJH recombination. *The Journal of Immunology* **176**: 2439–2447.

Allman D, Lindsley RC, DeMuth W, Rudd K, Shinton SA, Hardy RR. 2001. Resolution of three nonproliferative immature splenic B cell subsets reveals multiple selection points during peripheral B cell maturation. *The Journal of Immunology* **167**: 6834–6840.

Alt FW, Baltimore D. 1982. Joining of immunoglobulin heavy chain gene segments: implications from a chromosome with evidence of three D-JH fusions. *Proc Natl Acad Sci USA* **79**: 4118–4122.

Amano T, Sagai T, Tanabe H, Mizushina Y, Nakazawa H, Shiroishi T. 2009. Chromosomal Dynamics at the Shh Locus: Limb Bud-Specific Differential Regulation of Competence and Active Transcription. *Developmental Cell* **16**: 47–57.

Amin RH, Schlissel MS. 2008. Foxo1 directly regulates the transcription of recombination-activating genes during B cell development. *Nat Immunol* **9**: 613–622.

Apostolou E, Thanos D. 2008. Virus Infection Induces NF-kappaB-dependent interchromosomal associations mediating monoallelic IFN-beta gene expression. *Cell* **134**: 85–96.

Arnaout R, Lee W, Cahill P, Honan T, Sparrow T, Weiand M, Nusbaum C, Rajewsky K, Koralov SB. 2011. High-Resolution Description of Antibody Heavy-Chain Repertoires in Humans ed. M. Reindl. *PLoS ONE* **6**: e22365.

Ay, F., & Noble, W. S. 2015. Analysis methods for studying the 3D architecture of the genome. *Genome Biology*, **16**(1), 1306. http://doi.org/10.1186/s13059-015-0745-7

Bain G. 1994. E2A proteins are required for proper B cell development and initiation of immunoglobulin gene rearrangements. *Cell* **79**: 885–892.

Banerji J, Olson L, Schaffner W. 1983. A lymphocyte-specific cellular enhancer is located downstream of the joining region in immunoglobulin heavy chain genes. *Cell* **33**: 729–740.

Barbieri M, Chotalia M, Fraser J, Lavitas LM, Dostie J, Pombo A, Nicodemi M. 2012. Complexity of chromatin folding is captured by the strings and binders switch model. *Proc Nat Acad Sci USA* **109**.

Barbieri M, Xie SQ, Torlai Triglia E, Chiariello AM, Bianco S, de Santiago I, Branco MR, Rueda D, Nicodemi M, Pombo A. 2017. Active and poised promoter states drive folding of the extended HoxB locus in mouse embryonic stem cells. *Nature Structural & Molecular Biology* **24**: 515–524.

Bassing CH, Swat W, Alt FW. 2002. The mechanism and regulation of chromosomal V(D)J recombination. *Cell* **109 Suppl**: S45–55.

Beagan JA, Duong MT, Titus KR, Zhou L, Cao Z, Ma J, Lachanski CV, Gillis DR, Phillips-Cremins JE. 2017. YY1 and CTCF orchestrate a 3D chromatin looping switch during early neural lineage commitment. *Genome Res* **27**: 1139–1152.

Beagrie RA, Scialdone A, Schueler M, Kraemer DCA, Chotalia M, Xie SQ, Barbieri M, de Santiago I, Lavitas

L-M, Branco MR, et al. 2017. Complex multi-enhancer contacts captured by genome architecture mapping. *Nature Publishing Group* 1–25.

Belaghzal H, Dekker J, Gibcus JH. 2017. Hi-C 2.0: An optimized Hi-C procedure for high-resolution genome-wide mapping of chromosome conformation. *Methods* **123**: 56–65.

Bell AC, West AG, Felsenfeld G. 1999. The protein CTCF is required for the enhancer blocking activity of vertebrate insulators. *Cell* **98**: 387–396.

Belton J-M, McCord RP, Gibcus JH, Naumova N, Zhan Y, Dekker J. 2012. Hi–C: A comprehensive technique to capture the conformation of genomes. *Methods* **58**: 268–276.

Ben-Elazar S, Yakhini Z, Yanai I. 2013. Spatial localization of co-regulated genes exceeds genomic gene clustering in the Saccharomyces cerevisiae genome. *Nucleic Acids Res* **41**: 2191–2201.

Benedict CL, Gilfillan S, Thai TH, Kearney JF. 2000. Terminal deoxynucleotidyl transferase and repertoire development. *Immunol Rev* **175**: 150–157.

Benner C, Isoda T, Murre C. 2015. New roles for DNA cytosine modification, eRNA, anchors, and superanchors in developing B cell progenitors. *Proc Natl Acad Sci USA* **112**: 12776–12781.

Bergeron S, Madathiparambil T, Swanson PC. 2005. Both high mobility group (HMG)-boxes and the acidic tail of HMGB1 regulate recombination-activating gene (RAG)-mediated recombination signal synapsis and cleavage in vitro. *Journal of Biological Chemistry* **280**: 31314–31324.

Bertolino E, Reddy K, Medina KL, Parganas E, Ihle J, Singh H. 2005. Regulation of interleukin 7–dependent immunoglobulin heavy-chain variable gene rearrangements by transcription factor STAT5. *Nat Immunol* **6**: 836–843.

Bickmore WA, van Steensel B. 2013. Genome Architecture: Domain Organization of Interphase Chromosomes. *Cell* **152**: 1270–1284.

Boehm T. 2011. Design principles of adaptive immune systems. *Nat Rev Immunol* **11**: 307–317.

Bolland DJ, King MR, Reik W, Corcoran AE, Krueger C. 2013. Robust 3D DNA FISH Using Directly Labeled Probes. *JoVE* 1–9.

Bolland DJ, Koohy H, Wood AL, Matheson LS, Krueger F, Stubbington MJT, Baizan-Edge A, Chovanec P, Stubbs BA, Tabbada K, et al. 2016. Two Mutually Exclusive Local Chromatin States Drive Efficient V(D)J Recombination. *Cell Reports* **15**: 1–28.

Bolland DJ, Wood AL, Afshar R, Featherstone K, Oltz EM, Corcoran AE. 2007. Antisense Intergenic Transcription Precedes Igh D-to-J Recombination and Is Controlled by the Intronic Enhancer E. *Molecular and Cellular Biology* **27**: 5523–5533.

Bolland DJ, Wood AL, Johnston CM, Bunting SF, Morgan G, Chakalova L, Fraser PJ, Corcoran AE. 2004. Antisense intergenic transcription in V(D)J recombination. *Nat Immunol* **5**: 630–637.

Boller S, Ramamoorthy S, Akbas D, Nechanitzky R, Burger L, Murr R, Schübeler D, Grosschedl R. 2016. Pioneering Activity of the C-Terminal Domain of EBF1 Shapes the Chromatin Landscape for B Cell Programming. *Immunity* **44**: 1–32.

Bolzer A, Kreth G, Solovei I, Koehler D, Saracoglu K, Fauth C, Muller S, Eils R, Cremer C, Speicher MR, et al. 2005. Three-dimensional maps of all chromosomes in human male fibroblast nuclei and prometaphase rosettes. *PLoS Biol* **3**: e157.

Born W, White J, Kappler J, Marrack P. 1988. Rearrangement of IgH genes in normal thymocyte development. *J Immunol* **140**: 3228.

Bossen C, Mansson R, Murre C. 2012. Chromatin topology and the regulation of antigen receptor assembly. *Annu Rev Immunol* **30**: 337–356.

Brackley CA, Brown JM, Waithe D, Babbs C, Davies J, Hughes JR, Buckle VJ, Marenduzzo D. 2016. Predicting the three-dimensional folding of cis-regulatory regions in mammalian genomes using bioinformatic data and polymer models. **17**: 1306.

Branco MR, Pombo A. 2006. Intermingling of Chromosome Territories in Interphase Suggests Role in Translocations and Transcription-Dependent Associations ed. P. Becker. *PLoS Biol* **4**: e138.

Brodeur PH, Riblet R. 1984. The immunoglobulin heavy chain variable region (Igh-V) locus in the mouse. I. One hundred Igh-V genes comprise seven families of homologous genes. *Eur J Immunol* **14**: 922–930.

Cairns J, Freire-Pritchett P, Wingett SW, Várnai C, Dimond A, Plagnol V, Zerbino D, Schoenfelder S, Javierre BM, Osborne C, et al. 2016. CHiCAGO: robust detection of DNA looping interactions in Capture Hi-C data. **17**: 127.

Capra JD, Kehoe JM. 1975. Hypervariable regions, idiotypy, and the antibody-combining site. *Adv Immunol* **20**: 1–40.

Chakraborty T, Chowdhury D, Keyes A, Jani A, Subrahmanyam R, Ivanova I, Sen R. 2007. Repeat Organization and Epigenetic Regulation of the DH-Cμ Domain of the Immunoglobulin Heavy-Chain Gene Locus. *Molecular Cell* **27**: 842–850.

Chakraborty T, Perlot T, Subrahmanyam R, Jani A, Goff PH, Zhang Y, Ivanova I, Alt FW, Sen R. 2009a. A 220-nucleotide deletion of the intronic enhancer reveals an epigenetic hierarchy in immunoglobulin heavy chain locus activation. *J Exp Med* **206**: 1019–1027.

Chakraborty T, Perlot T, Subrahmanyam R, Jani A, Goff PH, Zhang Y, Ivanova I, Alt FW, Sen R. 2009b. A 220-nucleotide deletion of the intronic enhancer reveals an epigenetic hierarchy in immunoglobulin heavy chain locus activation. *J Exp Med* **206**: 1019–1027.

Chambeyron S, Bickmore WA. 2004. Chromatin decondensation and nuclear reorganization of the HoxB locus upon induction of transcription. *Genes Dev* **18**: 1119–1130.

Chandra T, Ewels PA, Schoenfelder S, Furlan-Magaril M, Wingett SW, Kirschner K, Thuret J-Y, Andrews S, Fraser P, Reik W. 2015. Global Reorganization of the Nuclear Landscape in Senescent Cells. *CellReports* **10**: 471–483.

Chen Z, Xiao Y, Zhang J, Li J, Liu Y, Zhao Y, Ma C, Luo J, Qiu Y, Huang G, et al. 2011. Transcription factors E2A, FOXO1 and FOXP1 regulate recombination activating gene expression in cancer cells. *PLoS ONE* **6**: e20475.

Chiariello AM, Annunziatella C, Bianco S, Esposito A, Nicodemi M. 2016. Polymer physics of chromosome large-scale 3D organisation. *Nature Publishing Group* **6**: 787.

Chiarle R, Zhang Y, Frock RL, Lewis SM, Molinie B, Ho Y-J, Myers DR, Choi VW, Compagno M, Malkin DJ, et al. 2011. Genome-wide translocation sequencing reveals mechanisms of chromosome breaks and rearrangements in B cells. *Cell* **147**: 107–119.

Chien R, Zeng W, Kawauchi S, Bender MA, Santos R, Gregson HC, Schmiesing JA, Newkirk DA, Kong X, Ball ARJ, et al. 2011. Cohesin mediates chromatin interactions that regulate mammalian beta-globin expression. *Journal of Biological Chemistry* **286**: 17870–17878.

Choi NM, Loguercio S, Verma-Gaur J, Degner SC, Torkamani A, Su AI, Oltz EM, Artyomov M, Feeney AJ. 2013. Deep Sequencing of the Murine Igh Repertoire Reveals Complex Regulation of Nonrandom V Gene Rearrangement Frequencies. *The Journal of Immunology* **191**: 2393–2402.

Chowdhury D, Sen R. 2001. Stepwise activation of the immunoglobulin mu heavy chain gene locus. *The EMBO Journal* **20**: 6394–6403.

Church GM, Ephrussi A, Gilbert W, Tonegawa S. 1985. Cell-type-specific contacts to immunoglobulin enhancers in nuclei. *Nature* **313**: 798–801.

Ciubotaru M, Ptaszek LM, Baker GA, Baker SN, Bright FV, Schatz DG. 2003. RAG1-DNA binding in V(D)J

recombination. Specificity and DNA-induced conformational changes revealed by fluorescence and CD spectroscopy. *Journal of Biological Chemistry* **278**: 5584–5596.

Cobb RM, Oestreich KJ, Osipovich OA, Oltz EM. 2006. Accessibility control of V(D)J recombination. *Adv Immunol* **91**: 45–109.

Cockerill PN, Yuen MH, Garrard WT. 1987. The enhancer of the immunoglobulin heavy chain locus is flanked by presumptive chromosomal loop anchorage elements. *Journal of Biological Chemistry* **262**: 5394–5397.

Corcoran AE. 2005. Immunoglobulin locus silencing and allelic exclusion. *Seminars in Immunology* **17**: 141–154.

Corcoran AE, Riddell A, Krooshoop D, Venkitaraman AR. 1998. Impaired immunoglobulin gene rearrangement in mice lacking the IL-7 receptor. *Nature* **391**: 904–907.

Corcoran AE, Smart FM, Cowling RJ, Crompton T, Owen MJ, Venkitaraman AR. 1996. The interleukin-7 receptor alpha chain transmits distinct signals for proliferation and differentiation during B lymphopoiesis. *The EMBO Journal* **15**: 1924–1932.

Cowell LG, Davila M, Kepler TB, Kelsoe G. 2002. Identification and utilization of arbitrary correlations in models of recombination signal sequences. **3**: RESEARCH0072.

Coyaud E, Struski S, Prade N, Familiades J, Eichner R, Quelen C, Bousquet M, Mugneret F, Talmant P, Pages M-P, et al. 2010. Wide diversity of PAX5 alterations in B-ALL: a Groupe Francophone de Cytogenetique Hematologique study. *Blood* **115**: 3089–3097.

Cremer T, Cremer C. 2001. Chromosome territories, nuclear architecture and gene regulation in mammalian cells. *Nat Rev Genet* **2**: 292–301.

Cremer T, Cremer M. 2010. Chromosome Territories. *Cold Spring Harb Perspect Biol* **2**: a003889–a003889.

Dariavach P, Williams GT, Campbell K, Pettersson S, Neuberger MS. 1991. The mouse IgH 3′-enhancer. *Eur J Immunol* **21**: 1499–1504.

Davies JOJ, Oudelaar AM, Higgs DR, Hughes JR. 2017. How best to identify chromosomal interactions: a comparison of approaches. *Nature Methods* **14**: 125–134.

Davies JOJ, Telenius JM, McGowan SJ, Roberts NA, Taylor S, Higgs DR, Hughes JR. 2016. Multiplexed analysis of chromosome conformation at vastly improved sensitivity. *Nat Meth* **13**: 74–80.

de Wit E, de Laat W. 2012. A decade of 3C technologies: insights into nuclear organization. *Genes Dev* **26**: 11–24.

de Wit E, Vos ESM, Holwerda SJB, Valdes-Quezada C, Verstegen MJAM, Teunissen H, Splinter E, Wijchers PJ, Krijger PHL, de Laat W. 2015a. CTCF Binding Polarity Determines Chromatin Looping. *Molecular Cell* **60**: 1–29.

de Wit E, Vos ESM, Holwerda SJB, Valdes-Quezada C, Verstegen MJAM, Teunissen H, Splinter E, Wijchers PJ, Krijger PHL, de Laat W. 2015b. CTCF Binding Polarity Determines Chromatin Looping. 1–29.

Deau M-C, Heurtier L, Frange P, Suarez F, Bole-Feysot C, Nitschke P, Cavazzana M, Picard C, Durandy A, Fischer A, et al. 2014. A human immunodeficiency caused by mutations in the PIK3R1 gene. *J Clin Invest* **124**: 3923–3928.

Decker T, Pasca di Magliano M, McManus S, Sun Q, Bonifer C, Tagoh H, Busslinger M. 2009. Stepwise activation of enhancer and promoter regions of the B cell commitment gene Pax5 in early lymphopoiesis. *Immunity* **30**: 508–520.

Degner SC, Verma-Gaur J, Wong TP, Bossen C, Iverson GM, Torkamani A, Vettermann C, Lin YC, Ju Z, Schulz D, et al. 2011. CCCTC-binding factor (CTCF) and cohesin influence the genomic architecture of the Igh locus and antisense transcription in pro-B cells. *Proc Natl Acad Sci USA* **108**: 9566–9571.

Degner SC, Wong TP, Jankevicius G, Feeney AJ. 2009. Cutting edge: developmental stage-specific recruitment of cohesin to CTCF sites throughout immunoglobulin loci during B lymphocyte development. *J Immunol* **182**: 44–48.

Dekker J. 2002. Capturing Chromosome Conformation. *Science* **295**: 1306–1311.

DeKoter RP, Singh H. 2000. Regulation of B Lymphocyte and Macrophage Development by Graded Expression of PU.1. *Science* **288**: 1439–1441.

Deng W, Shi X, Tjian R, Lionnet T, Singer RH. 2015. CASFISH: CRISPR/Cas9-mediated in situ labeling of genomic loci in fixed cells. *Proc Natl Acad Sci USA* **112**: 11870–11875.

Dias S, Mansson R, Gurbuxani S, Sigvardsson M, Kee BL. 2008a. E2A Proteins Promote Development of Lymphoid-Primed Multipotent Progenitors. *Immunity* **29**: 217–227.

Dias S, Mansson R, Gurbuxani S, Sigvardsson M, Kee BL. 2008b. E2A proteins promote development of lymphoid-primed multipotent progenitors. *Immunity* **29**: 217–227.

Dixon JR, Jung I, Selvaraj S, Shen Y, Antosiewicz-Bourget JE, Lee AY, Ye Z, Kim A, Rajagopal N, Xie W, et al. 2015. Chromatin architecture reorganization during stem cell differentiation. *Nature* **518**: 331–336.

Dixon JR, Selvaraj S, Yue F, Kim A, Li Y, Shen Y, Hu M, Liu JS, Ren B. 2012. Topological domains in mammalian genomes identified by analysis of chromatin interactions. *Nature* **485**: 376–380.

Dolence JJ, Gwin KA, Shapiro MB, Medina KL. 2014. Flt3 signaling regulates the proliferation, survival, and maintenance of multipotent hematopoietic progenitors that generate B cell precursors. *Exp Hematol* **42**: 380–393.e3.

Donohoe ME, Zhang L-F, Xu N, Shi Y, Lee JT. 2007. Identification of a Ctcf cofactor, Yy1, for the X chromosome binary switch. *Molecular Cell* **25**: 43–56.

Dostie J, Dekker J. 2007. Mapping networks of physical interactions between genomic elements using 5C technology. *Nature Protocols* **2**: 988–1002.

Dostie J, Richmond TA, Arnaout RA, Selzer RR, Lee WL, Honan TA, Rubio ED, Krumm A, Lamb J, Nusbaum C, et al. 2006. Chromosome Conformation Capture Carbon Copy (5C): A massively parallel solution for mapping interactions between genomic elements. *Genome Res* **16**: 1299–1309.

Dryden NH, Broome LR, Dudbridge F, Johnson N, Orr N, Schoenfelder S, Nagano T, Andrews S, Wingett S, Kozarewa I, et al. 2014. Unbiased analysis of potential targets of breast cancer susceptibility loci by Capture Hi-C. *Genome Res* **24**: 1854–1868.

Dunnick WA, Collins JT, Shi J, Westfield G, Fontaine C, Hakimpour P, Papavasiliou FN. 2009. Switch recombination and somatic hypermutation are controlled by the heavy chain 3′ enhancer region. *J Exp Med* **206**: 2613–2623.

Ebert A, McManus S, Tagoh H, Medvedovic J, Salvagiotto G, Novatchkova M, Tamir I, Sommer A, Jaritz M, Busslinger M. 2011. The Distal VH Gene Cluster of the Igh Locus Contains Distinct Regulatory Elements with Pax5 Transcription Factor-Dependent Activity in Pro-B Cells. *Immunity* **34**: 175–187.

Ebert A, Medvedovic J, Tagoh H, Schwickert TA, Busslinger M. 2013. Control of antigen receptor diversity through spatial regulation of V(D)J recombination. *Cold Spring Harbor Symposia on Quantitative Biology* **78**: 11–21.

Eden E, Navon R, Steinfeld I, Lipson D, Yakhini Z. 2009. GOrilla: a tool for discovery and visualization of enriched GO terms in ranked gene lists. *BMC Bioinformatics* **10**: 48.

Ephrussi A, Church GM, Tonegawa S, Gilbert W. 1985. B lineage--specific interactions of an immunoglobulin enhancer with cellular factors in vivo. *Science* **227**: 134–140.

Espinoza CR, Feeney AJ. 2005. The extent of histone acetylation correlates with the differential rearrangement frequency of individual VH genes in pro-B cells. *The Journal of Immunology* **175**: 6668–6675.

Fahl SP, Crittenden RB, Allman D, Bender TP. 2009. c-Myb is required for pro-B cell differentiation. *The Journal of Immunology* **183**: 5582–5592.

Featherstone K, Wood AL, Bowen AJ, Corcoran AE. 2010. The Mouse Immunoglobulin Heavy Chain V-D Intergenic Sequence Contains Insulators That May Regulate Ordered V(D)J Recombination. *Journal of Biological Chemistry* **285**: 9327–9338.

Feng S, Cokus SJ, Schubert V, Zhai J, Pellegrini M, Jacobsen SE. 2014. Genome-wide Hi-C Analyses in Wild-Type and Mutants Reveal High-Resolution Chromatin Interactions in Arabidopsis. *Molecular Cell* **55**: 694–707.

Fitzsimmons SP, Bernstein RM, Max EE, Skok JA, Shapiro MA. 2007. Dynamic Changes in Accessibility, Nuclear Positioning, Recombination, and Transcription at the Igκ Locus. *The Journal of Immunology* **179**: 5264–5273.

Flajnik MF, Kasahara M. 2010. Origin and evolution of the adaptive immune system: genetic events and selective pressures. *Nat Rev Genet* **11**: 47–59.

Franke M, Ibrahim DM, Andrey G, Schwarzer W, Heinrich V, Schöpflin R, Kraft K, Kempfer R, Jerković I, Chan W-L, et al. 2016. Formation of new chromatin domains determines pathogenicity of genomic duplications. *Nature Publishing Group* **538**: 265–269.

Fraser P, Bickmore W. 2007. Nuclear organization of the genome and the potential for gene regulation. *Nature* **447**: 413–417.

Freire-Pritchett P, Schoenfelder S, Várnai C, Wingett SW, Cairns J, Collier AJ, Garcia-Vilchez R, Furlan-Magaril M, Osborne CS, Fraser P, et al. 2017. Global reorganisation of cis-regulatory units upon lineage commitment of human embryonic stem cells. *Elife* **6**.

Fruman DA, Snapper SB, Yballe CM, Davidson L, Yu JY, Alt FW, Cantley LC. 1999. Impaired B cell development and proliferation in absence of phosphoinositide 3-kinase p85alpha. *Science* **283**: 393–397.

Fu C, Turck CW, Kurosaki T, Chan AC. 1998. BLNK: a central linker protein in B cell activation. *Immunity* **9**: 93–103.

Fudenberg G, Imakaev M, Lu C, Goloborodko A, Abdennur N, Mirny LA. 2016. Formation of Chromosomal Domains by Loop Extrusion. *Cell Reports* **15**: 1–13.

Fujita T, Kitaura F, Yuno M, Suzuki Y, Sugano S, Fujii H. 2017. Locus-specific ChIP combined with NGS analysis reveals genomic regulatory regions that physically interact with the Pax5 promoter in a chicken B cell line. *DNA Research*.

Fuxa M. 2004. Pax5 induces V-to-DJ rearrangements and locus contraction of the immunoglobulin heavy-chain gene. *Genes Dev* **18**: 411–422.

Fuxa M, Busslinger M. 2007. Reporter gene insertions reveal a strictly B lymphoid-specific expression pattern of Pax5 in support of its B cell identity function. *The Journal of Immunology* **178**: 8221–8221.

Gallagher E, Enzler T, Matsuzawa A, Anzelon-Mills A, Otero D, Holzer R, Janssen E, Gao M, Karin M. 2007. Kinase MEKK1 is required for CD40-dependent activation of the kinases Jnk and p38, germinal center formation, B cell proliferation and antibody production. *Nat Immunol* **8**: 57–63.

Galloway A, Saveliev A, Lukasiak S, Hodson DJ, Bolland D, Balmanno K, Ahlfors H, Monzon-Casanova E, Mannurita SC, Bell LS, et al. 2016. RNA-binding proteins ZFP36L1 and ZFP36L2 promote cell quiescence. *Science* **352**: 453–459.

Garrett FE, Emelyanov AV, Sepulveda MA, Flanagan P, Volpi S, Li F, Loukinov D, Eckhardt LA, Lobanenkov VV, Birshtein BK. 2005. Chromatin architecture near a potential 3' end of the igh locus involves modular regulation of histone modifications during B-Cell development and in vivo occupancy at CTCF sites. *Molecular and Cellular Biology* **25**: 1511–1525.

Georgiou G, Ippolito GC, Beausang J, Busse CE, Wardemann H, Quake SR. 2014. The promise and challenge of

high-throughput sequencing of the antibody repertoire. *Nat Biotechnol* **32**: 158–168.

Georgopoulos K, Bigby M, Wang JH, Molnar A, Wu P, Winandy S, Sharpe A. 1994. The Ikaros gene is required for the development of all lymphoid lineages. *Cell* **79**: 143–156.

Gerasimova T, Guo C, Ghosh A, Qiu X, Montefiori L, Verma-Gaur J, Choi NM, Feeney AJ, Sen R. 2015. A structural hierarchy mediated by multiple nuclear factors establishes IgH locus conformation. *Genes Dev* **29**: 1683–1695.

Giambra V, Volpi S, Emelyanov AV, Pflugh D, Bothwell ALM, Norio P, Fan Y, Ju Z, Skoultchi AI, Hardy RR, et al. 2008. Pax5 and linker histone H1 coordinate DNA methylation and histone modifications in the 3' regulatory region of the immunoglobulin heavy chain locus. *Molecular and Cellular Biology* **28**: 6123–6133.

Gibb DR, Shikh El M, Kang D-J, Rowe WJ, Sayed El R, Cichy J, Yagita H, Tew JG, Dempsey PJ, Crawford HC, et al. 2010. ADAM10 is essential for Notch2-dependent marginal zone B cell development and CD23 cleavage in vivo. *J Exp Med* **207**: 623–635.

Gillies SD, Morrison SL, Oi VT, Tonegawa S. 1983. A tissue-specific transcription enhancer element is located in the major intron of a rearranged immunoglobulin heavy chain gene. *Cell* **33**: 717–728.

Giorgetti L, Galupa R, Nora EP, Piolot T, Lam F, Dekker J, Tiana G, Heard E. 2014. Predictive Polymer Modeling Reveals Coupled Fluctuations in Chromosome Conformation and Transcription. *Cell* **157**: 950–963.

Giorgetti L, Heard E. 2016. Closing the loop: 3C versus DNA FISH. **17**: 154.

Gopalakrishnan S, Majumder K, Predeus A, Huang Y, Koues OI, Verma-Gaur J, Loguercio S, Su AI, Feeney AJ, Artyomov MN, et al. 2013. Unifying model for molecular determinants of the preselection Vbeta repertoire. *Proc Natl Acad Sci USA* **110**: E3206–15.

Gómez-Marín C, Tena JJ, Acemel RD, López-Mayorga M, Naranjo S, la Calle-Mustienes de E, Maeso I, Beccari L, Aneas I, Vielmas E, et al. 2015. Evolutionary comparison reveals that diverging CTCF sites are signatures of ancestral topological associating domains borders. *Proc Natl Acad Sci USA* **112**: 7542–7547.

Greenbaum S, Lazorchak AS, Zhuang Y. 2004. Differential Functions for the Transcription Factor E2A in Positive and Negative Gene Regulation in Pre-B Lymphocytes. *Journal of Biological Chemistry* **279**: 45028–45035.

Greig KT, de Graaf CA, Murphy JM, Carpinelli MR, Pang SHM, Frampton J, Kile BT, Hilton DJ, Nutt SL. 2010. Critical roles for c-Myb in lymphoid priming and early B-cell development. *Blood* **115**: 2796–2805.

Guo C, Gerasimova T, Hao H, Ivanova I, Chakraborty T, Selimyan R, Oltz EM, Sen R. 2011a. Two Forms of Loops Generate the Chromatin Conformation of the Immunoglobulin Heavy-Chain Gene Locus. *Cell* **147**: 332–343.

Guo C, Yoon HS, Franklin A, Jain S, Ebert A, Cheng H-L, Hansen E, Despo O, Bossen C, Vettermann C, et al. 2011b. CTCF-binding elements mediate control of V(D)J recombination. *Nature* **477**: 424–430.

Gyory I, Boller S, Nechanitzky R, Mandel E, Pott S, Liu E, Grosschedl R. 2012. Transcription factor Ebf1 regulates differentiation stage-specific signaling, proliferation, and survival of B cells. *Genes Dev* **26**: 668–682.

Hadjur S, Williams LM, Ryan NK, Cobb BS, Sexton T, Fraser P, Fisher AG, Merkenschlager M. 2009. Cohesins form chromosomal cis-interactions at the developmentally regulated IFNG locus. *Nature* **460**: 410–413.

Hagege H, Klous P, Braem C, Splinter E, Dekker J, Cathala G, de Laat W, Forne T. 2007. Quantitative analysis of chromosome conformation capture assays (3C-qPCR). *Nature Protocols* **2**: 1722–1733.

Hagman J, Belanger C, Travis A, Turck CW, Grosschedl R. 1993. Cloning and functional characterization of early B-cell factor, a regulator of lymphocyte-specific gene expression. *Genes Dev* **7**: 760–773.

Hakim O, Resch W, Yamane A, Klein I, Kieffer-Kwon K-R, Jankovic M, Oliveira T, Bothmer A, Voss TC, Ansarah-Sobrinho C, et al. 2012. DNA damage defines sites of recurrent chromosomal translocations in B lymphocytes. *Nature* **7**: 233–555.

Hardy RR, Hayakawa K. 2001. B cell development pathways. *Annu Rev Immunol* **19**: 595–621.

Hardy RR, Kincade PW, Dorshkind K. 2007. The protean nature of cells in the B lymphocyte lineage. *Immunity* **26**: 703–714.

Heath H, de Almeida CR, Sleutels F, Dingjan G, van de Nobelen S, Jonkers I, Ling K-W, Gribnau J, Renkawitz R, Grosveld F, et al. 2008. CTCF regulates cell cycle progression of αβ T cells in the thymus. *The EMBO Journal* **27**: 2839–2850.

Heinz S, Benner C, Spann N, Bertolino E, Lin YC, Laslo P, Cheng JX, Murre C, Singh H, Glass CK. 2010. Simple combinations of lineage-determining transcription factors prime cis-regulatory elements required for macrophage and B cell identities. *Molecular Cell* **38**: 576–589.

Hesslein. 2002. Pax5 is required for recombination of transcribed, acetylated, 5. 1–7.

Hesslein DGT, Pflugh DL, Chowdhury D, Bothwell ALM, Sen R, Schatz DG. 2003. Pax5 is required for recombination of transcribed, acetylated, 5' IgH V gene segments. *Genes Dev* **17**: 37–42.

Hewitt SL, Chaumeil J, Skok JA. 2010. Chromosome dynamics and the regulation of V(D)J recombination. *Immunol Rev* **237**: 43–54.

Hewitt SL, Farmer D, Marszalek K, Cadera E, Liang H-E, Xu Y, Schlissel MS, Skok JA. 2008. Association between the Igk and Igh immunoglobulin loci mediated by the 3' Igk enhancer induces 'decontraction' of the Igh locus in pre-B cells. *Nat Immunol* **9**: 396–404.

Hnisz D, Weintraub AS, Day DS, Valton A-L, Bak RO, Li CH, Goldmann J, Lajoie BR, Fan ZP, Sigova AA, et al. 2016. Activation of proto-oncogenes by disruption of chromosome neighborhoods. *Science (New York, NY)* **351**: 1454–1458.

Hodson DJ, Janas ML, Galloway A, Bell SE, Andrews S, Li CM, Pannell R, Siebel CW, MacDonald HR, De Keersmaecker K, et al. 2010. Deletion of the RNA-binding proteins ZFP36L1 and ZFP36L2 leads to perturbed thymic development and T lymphoblastic leukemia. *Nat Immunol* **11**: 717–724.

Holwerda SJB, de Laat W. 2013. CTCF: the protein, the binding partners, the binding sites and their chromatin loops. *Phil Trans R Soc Lond B* **368**.

Horike S-I, Cai S, Miyano M, Cheng J-F, Kohwi-Shigematsu T. 2005. Loss of silent-chromatin looping and impaired imprinting of DLX5 in Rett syndrome. *Nat Genet* **37**: 31–40.

Hsieh T-HS, Weiner A, Lajoie B, Dekker J, Friedman N, Rando OJ. 2015. Mapping Nucleosome Resolution Chromosome Folding in Yeast by Micro-C. *Cell* **162**: 108–119.

Hsu L-Y, Lauring J, Liang H-E, Greenbaum S, Cado D, Zhuang Y, Schlissel MS. 2003. A conserved transcriptional enhancer regulates RAG gene expression in developing B cells. *Immunity* **19**: 105–117.

Hu H, Wang B, Borde M, Nardone J, Maika S, Allred L, Tucker PW, Rao A. 2006. Foxp1 is an essential transcriptional regulator of B cell development. *Nat Immunol* **7**: 819–826.

Hu J, Zhang Y, Zhao L, Frock RL, Du Z, Meyers RM, Meng F-L, Schatz DG, Alt FW. 2015. Chromosomal Loop Domains Direct the Recombination of Antigen Receptor Genes. *Cell* **163**: 947–959.

Huang G, Zhang P, Hirai H, Elf S, Yan X, Chen Z, Koschmieder S, Okuno Y, Dayaram T, Growney JD, et al. 2008. PU.1 is a major downstream target of AML1 (RUNX1) in adult mouse hematopoiesis. *Nat Genet* **40**: 51–60.

Hughes JR, Roberts N, McGowan S, Hay D, Giannoulatou E, Lynch M, De Gobbi M, Taylor S, Gibbons R, Higgs DR. 2014. Analysis of hundreds of cis-regulatory landscapes at high resolution in a single, high-throughput experiment. *Nature Genetics* **46**: 1–10.

Iborra FJ, Pombo A, Jackson DA, Cook PR. 1996. Active RNA polymerases are localized within discrete transcription "factories' in human nuclei. *Journal of Cell Science* **109 (Pt 6)**: 1427–1436.

Igarashi H, Gregory SC, Yokota T, Sakaguchi N, Kincade PW. 2002. Transcription from the RAG1 locus marks the earliest lymphocyte progenitors in bone marrow. *Immunity* **17**: 117–130.

Igarashi K, Ochiai K, Itoh-Nakadai A, Muto A. 2014. Orchestration of plasma cell differentiation by Bach2 and its gene regulatory network. *Immunol Rev* **261**: 116–125.

Imakaev M, Fudenberg G, McCord RP, Naumova N, Goloborodko A, Lajoie BR, Dekker J, Mirny LA. 2012. Iterative correction of Hi-C data reveals hallmarks of chromosome organization. *Nature Methods* **9**: 999–1003.

Impera L, Albano F, Cunsolo Lo C, Funes S, Iuzzolino P, Laveder F, Panagopoulos I, Rocchi M, Storlazzi CT. 2008. A novel fusion 5"AFF3/3"BCL2 originated from a t(2;18)(q11.2;q21.33) translocation in follicular lymphoma. *Oncogene* **27**: 6187–6190.

Inlay MA, Bhattacharya D, Sahoo D, Serwold T, Seita J, Karsunky H, Plevritis SK, Dill DL, Weissman IL. 2009. Ly6d marks the earliest stage of B-cell specification and identifies the branchpoint between B-cell and T-cell development. *Genes Dev* **23**: 2376–2381.

Iwasaki H, Somoza C, Shigematsu H, Duprez EA, Iwasaki-Arai J, Mizuno S-I, Arinobu Y, Geary K, Zhang P, Dayaram T, et al. 2005. Distinctive and indispensable roles of PU.1 in maintenance of hematopoietic stem cells and their differentiation. *Blood* **106**: 1590–1600.

Jackson DA, Hassan AB, Errington RJ, Cook PR. 1993. Visualization of focal sites of transcription within human nuclei. *The EMBO Journal* **12**: 1059–1065.

Javierre BM, Burren OS, Wilder SP, Kreuzhuber R, Hill SM, Sewitz S, Cairns J, Wingett SW, Várnai C, Thiecke MJ, et al. 2016. Lineage-Specific Genome Architecture Links Enhancers and Non-coding Disease Variants to Target Gene Promoters. *Cell* **167**: 1369–1384.e19.

Jäger R, Migliorini G, Henrion M, Kandaswamy R, Speedy HE, Heindl A, Whiffin N, Carnicer MJ, Broome L, Dryden N, et al. 2015. Capture Hi-C identifies the chromatin interactome of colorectal cancer risk loci. *Nature Communications* **6**: 6178.

Jhunjhunwala S, Van Zelm MC, Peak MM, Cutchin S, Riblet R, van Dongen JJM, Grosveld FG, Knoch TA, Murre C. 2008. The 3D Structure of the Immunoglobulin Heavy-Chain Locus: Implications for Long-Range Genomic Interactions. *Cell* **133**: 265–279.

Ji Y, Resch W, Corbett E, Yamane A, Casellas R, Schatz DG. 2010. The in vivo pattern of binding of RAG1 and RAG2 to antigen receptor loci. *Cell* **141**: 419–431.

Jiang H, Chang F-C, Ross AE, Lee J, Nakayama K, Nakayama K, Desiderio S. 2005. Ubiquitylation of RAG-2 by Skp2-SCF links destruction of the V(D)J recombinase to the cell cycle. *Molecular Cell* **18**: 699–709.

Johnson K, Angelin-Duclos C, Park S, Calame KL. 2003. Changes in Histone Acetylation Are Associated with Differences in Accessibility of VH Gene Segments to V-DJ Recombination during B-Cell Ontogeny and Development. *Molecular and Cellular Biology* **23**: 2438–2450.

Johnson K, Hashimshony T, Sawai CM, Pongubala JMR, Skok JA, Aifantis I, Singh H. 2008. Regulation of Immunoglobulin Light-Chain Recombination by the Transcription Factor IRF-4 and the Attenuation of Interleukin-7 Signaling. *Immunity* **28**: 335–345.

Johnson K, Pflugh DL, Yu D, Hesslein DGT, Lin K-I, Bothwell ALM, Thomas-Tikhonenko A, Schatz DG, Calame K. 2004. B cell-specific loss of histone 3 lysine 9 methylation in the V(H) locus depends on Pax5. *Nat Immunol* **5**: 853–861.

Johnston CM, Wood AL, Bolland DJ, Corcoran AE. 2006. Complete sequence assembly and characterization of the C57BL/6 mouse Ig heavy chain V region. *The Journal of Immunology* **176**: 4221–4234.

Jovanovic JV, Chillon MC, Vincent-Fabert C, Dillon R, Voisset E, Gutierrez NC, Sanz RG, Lopez AAM,

Morgan YG, Lok J, et al. 2017. The cryptic IRF2BP2-RARA fusion transforms hematopoietic stem/progenitor cells and induces retinoid-sensitive acute promyelocytic leukemia. *Leukemia* **31**: 747–751.

Juntilla MM, Wofford JA, Birnbaum MJ, Rathmell JC, Koretzky GA. 2007. Akt1 and Akt2 are required for αβ thymocyte survival and differentiation. *Proc Natl Acad Sci USA* **104**: 12105–12110.

Kagey MH, Newman JJ, Bilodeau S, Zhan Y, Orlando DA, van Berkum NL, Ebmeier CC, Goossens J, Rahl PB, Levine SS, et al. 2010. Mediator and cohesin connect gene expression and chromatin architecture. *Nature* **467**: 430–435.

Kaikkonen MU, Niskanen H, Romanoski CE, Kansanen E, Kivela AM, Laitalainen J, Heinz S, Benner C, Glass CK, Yla-Herttuala S. 2014. Control of VEGF-A transcriptional programs by pausing and genomic compartmentalization. *Nucleic Acids Res* **42**: 12570–12584.

Karathia H, Kingsford C, Girvan M, Hannenhalli S. 2016. A pathway-centric view of spatial proximity in the 3D nucleome across cell lines. *Nature Publishing Group* **6**: 39279.

Kaufmann S, Fuchs C, Gonik M, Khrameeva EE, Mironov AA, Frishman D. 2015. Inter-Chromosomal Contact Networks Provide Insights into Mammalian Chromatin Organization ed. B.P. Chadwick. *PLoS ONE* **10**: e0126125.

Kieffer-Kwon K-R, Nimura K, Rao SSP, Xu J, Jung S, Pekowska A, Dose M, Stevens E, Mathe E, Dong P, et al. 2017. Myc Regulates Chromatin Decompaction and Nuclear Architecture during B Cell Activation. *Molecular Cell* **67**: 566–578.e10.

Kim J, Sif S, Jones B, Jackson A, Koipally J, Heller E, Winandy S, Viel A, Sawyer A, Ikeda T, et al. 1999. Ikaros DNA-binding proteins direct formation of chromatin remodeling complexes in lymphocytes. *Immunity* **10**: 345–355.

Kim M, Cooper DD, Hayes SF, Spangrude GJ. 1998. Rhodamine-123 staining in hematopoietic stem cells of young mice indicates mitochondrial activation rather than dye efflux. *Blood* **91**: 4106–4117.

Kim SU. 1990. Neurobiology of human oligodendrocytes in culture. *J Neurosci Res* **27**: 712–728.

Kleiman E, Jia H, Loguercio S, Su AI, Feeney AJ. 2016. YY1 plays an essential role at all stages of B-cell differentiation. *Proc Natl Acad Sci USA* **113**: E3911–E3920.

Klein IA, Resch W, Jankovic M, Oliveira T, Yamane A, Nakahashi H, Di Virgilio M, Bothmer A, Nussenzweig A, Robbiani DF, et al. 2011. Translocation-Capture Sequencing Reveals the Extent and Nature of Chromosomal Rearrangements in B Lymphocytes. *Cell* **147**: 1–12.

Kolovos P, Georgomanolis T, Koeferle A, Larkin JD, Brant L, Nikolićć M, Gusmao EG, Zirkel A, Knoch TA, van Ijcken WF, et al. 2016. Binding of nuclear factor κB to noncanonical consensus sites reveals its multimodal role during the early inflammatory response. *Genome Res* **26**: 1478–1489.

Kolovos P, van de Werken HJ, Kepper N, Zuin J, Brouwer RW, Kockx CE, Wendt KS, van IJcken WF, Grosveld F, Knoch TA. 2014. Targeted Chromatin Capture (T2C): a novel high resolution high throughput method to detect genomic interactions and regulatory elements. *Epigenetics & Chromatin* **7**: 1–17.

Kondo M, Weissman IL, Akashi K. 1997. Identification of clonogenic common lymphoid progenitors in mouse bone marrow. *Cell* **91**: 661–672.

Kong NR, Davis M, Chai L, Winoto A, Tjian R. 2016. MEF2C and EBF1 Co-regulate B Cell-Specific Transcription ed. H.L. Grimes. *PLoS Genet* **12**: e1005845.

Kosak ST, Skok JA, Medina KL, Riblet R, Le Beau MM, Fisher AG, Singh H. 2002. Subnuclear compartmentalization of immunoglobulin loci during lymphocyte development. *Science* **296**: 158–162.

Koss LG. 1998. Characteristics of chromosomes in polarized normal human bronchial cells provide a blueprint for nuclear organization. *Cytogenet Cell Genet* **82**: 230–237.

Kozmik Z, Wang S, Dorfler P, Adams B, Busslinger M. 1992. The promoter of the CD19 gene is a target for the

B-cell-specific transcription factor BSAP. *Molecular and Cellular Biology* **12**: 2662–2672.

Krantz ID, McCallum J, DeScipio C, Kaur M, Gillis LA, Yaeger D, Jukofsky L, Wasserman N, Bottani A, Morris CA, et al. 2004. Cornelia de Lange syndrome is caused by mutations in NIPBL, the human homolog of Drosophila melanogaster Nipped-B. *Nat Genet* **36**: 631–635.

Kruse EA, Loughran SJ, Baldwin TM, Josefsson EC, Ellis S, Watson DK, Nurden P, Metcalf D, Hilton DJ, Alexander WS, et al. 2009. Dual requirement for the ETS transcription factors Fli-1 and Erg in hematopoietic stem cells and the megakaryocyte lineage. *Proc Natl Acad Sci USA* **106**: 13814–13819.

Kubo N, Ishii H, Gorkin D, Meitinger F, Xiong X, Fang R, Liu T, Ye Z, Li B, Dixon J, et al. 2017. Preservation of Chromatin Organization after Acute Loss of CTCF in Mouse Embryonic Stem Cells. *bioRxiv* 1–52.

Kumar S, Wuerffel R, Achour I, Lajoie B, Sen R, Dekker J, Feeney AJ, Kenter AL. 2013. Flexible ordering of antibody class switch and V(D)J joining during B-cell ontogeny. *Genes Dev* **27**: 2439–2444.

Lauring J, Schlissel MS. 1999. Distinct factors regulate the murine RAG-2 promoter in B- and T-cell lines. *Molecular and Cellular Biology* **19**: 2601–2612.

Le Dily F, Baù D, Pohl A, Vicent GP, Serra F, Soronellas D, Castellano G, Wright RHG, Ballare C, Filion G, et al. 2014. Distinct structural transitions of chromatin topological domains correlate with coordinated hormone-induced gene regulation. *Genes Dev* **28**: 2151–2162.

Lee CC, Avalos AM, Ploegh HL. 2012. Accessory molecules for Toll-like receptors and their function. *Nat Rev Immunol* **12**: 168–179.

Lennon GG, Perry RP. 1985. C mu-containing transcripts initiate heterogeneously within the IgH enhancer region and contain a novel 5'-nontranslatable exon. *Nature* **318**: 475–478.

Lettice LA, Horikoshi T, Heaney SJH, van Baren MJ, van der Linde HC, Breedveld GJ, Joosse M, Akarsu N, Oostra BA, Endo N, et al. 2002. Disruption of a long-range cis-acting regulator for Shh causes preaxial polydactyly. *Proc Natl Acad Sci USA* **99**: 7548–7553.

Li F, Eckhardt LA. 2009. A role for the IgH intronic enhancer Eμ in enforcing allelic exclusion. *J Exp Med* **206**: 153–167.

Li YS, Wasserman R, Hayakawa K, Hardy RR. 1996. Identification of the earliest B lineage stage in mouse bone marrow. *Immunity* **5**: 527–535.

Lieber MR. 2016. Mechanisms of Human Lymphoid Chromosomal Translocations. *Nat Rev Cancer* **16**: 387–398.

Lieberman-Aiden E, van Berkum NL, Williams L, Imakaev M, Ragoczy T, Telling A, Amit I, Lajoie BR, Sabo PJ, Dorschner MO, et al. 2009. Comprehensive mapping of long-range interactions reveals folding principles of the human genome. *Science* **326**: 289–293.

Lin SG, Ba Z, Du Z, Zhang Y, Hu J, Alt FW. 2016. Highly sensitive and unbiased approach for elucidating antibody repertoires. *Proc Natl Acad Sci USA* **113**: 7846–7851.

Lin SG, Guo C, Su A, Zhang Y, Alt FW. 2015. CTCF-binding elements 1 and 2 in the Ighintergenic control region cooperatively regulate V(D)J recombination. *Proc Natl Acad Sci USA* **112**: 1815–1820.

Lin YC, Benner C, Mansson R, Heinz S, Miyazaki K, Miyazaki M, Chandra V, Bossen C, Glass CK, Murre C. 2012. Global changes in the nuclear positioning of genes and intra- and interdomain genomic interactions that orchestrate B cell fate. *Nat Immunol* **13**: 1196–1204.

Lin YC, Jhunjhunwala S, Benner C, Heinz S, Welinder E, Mansson R, Sigvardsson M, Hagman J, Espinoza CA, Dutkowski J, et al. 2010. A global network of transcription factors, involving E2A, EBF1 and Foxo1, that orchestrates B cell fate. *Nature Publishing Group* **11**: 635–643.

Liu C, Cheng Y-J, Wang J-W, Weigel D. 2017. Prominent topologically associated domains differentiate global chromatin packing in rice from Arabidopsis. *Nat Plants*.

Liu H, Schmidt-Supprian M, Shi Y, Hobeika E, Barteneva N, Jumaa H, Pelanda R, Reth M, Skok J, Rajewsky K, et al. 2007. Yin Yang 1 is a critical regulator of B-cell development. *Genes Dev* **21**: 1179–1189.

Liu P, Keller JR, Ortiz M, Tessarollo L, Rachel RA, Nakamura T, Jenkins NA, Copeland NG. 2003. Bcl11a is essential for normal lymphoid development. *Nat Immunol* **4**: 525–532.

Lorsbach RB, Moore J, Ang SO, Sun W, Lenny N, Downing JR. 2004. Role of RUNX1 in adult hematopoiesis: analysis of RUNX1-IRES-GFP knock-in mice reveals differential lineage expression. *Blood* **103**: 2522–2529.

Lu R, Medina KL, Lancki DW, Singh H. 2003. IRF-4,8 orchestrate the pre-B-to-B transition in lymphocyte development. *Genes Dev* **17**: 1703–1708.

Lucas JS, Bossen C, Murre C. 2011. Transcription and recombination factories: common features? *Current Opinion in Cell Biology* **23**: 318–324.

Lucas JS, Zhang Y, Dudko OK, Murre C. 2014. 3D Trajectories Adopted by Coding and Regulatory DNA Elements: First-Passage Times for Genomic Interactions. *Cell* **158**: 339–352.

Lukin K, Fields S, Lopez D, Cherrier M, Ternyak K, Ramirez J, Feeney AJ, Hagman J. 2010. Compound haploinsufficiencies of Ebf1 and Runx1 genes impede B cell lineage progression. *Proc Natl Acad Sci USA* **107**: 7869–7874.

Maes J, Chappaz S, Cavelier P, O'Neill L, Turner B, Rougeon F, Goodhardt M. 2006. Activation of V(D)J recombination at the IgH chain JH locus occurs within a 6-kilobase chromatin domain and is associated with nucleosomal remodeling. *The Journal of Immunology* **176**: 5409–5417.

Maes J, O'Neill LP, Cavelier P, Turner BM, Rougeon F, Goodhardt M. 2001. Chromatin remodeling at the Ig loci prior to V(D)J recombination. *The Journal of Immunology* **167**: 866–874.

Maier H, Ostraat R, Gao H, Fields S, Shinton SA, Medina KL, Ikawa T, Murre C, Singh H, Hardy RR, et al. 2004. Early B cell factor cooperates with Runx1 and mediates epigenetic changes associated with mb-1 transcription. *Nat Immunol* **5**: 1069–1077.

Majumder P, Gomez JA, Chadwick BP, Boss JM. 2008. The insulator factor CTCF controls MHC class II gene expression and is required for the formation of long-distance chromatin interactions. *J Exp Med* **205**: 785–798.

Malin S, McManus S, Cobaleda C, Novatchkova M, Delogu A, Bouillet P, Strasser A, Busslinger M. 2010. Role of STAT5 in controlling cell survival and immunoglobulin gene recombination during pro-B cell development. *Nat Immunol* **11**: 171–179.

Mandal M, Powers SE, Maienschein-Cline M, Bartom ET, Hamel KM, Kee BL, Dinner AR, Clark MR. 2011. Epigenetic repression of the Igk locus by STAT5-mediated recruitment of the histone methyltransferase Ezh2. *Nat Immunol* **12**: 1212–1220.

Mansson R, Welinder E, Ahsberg J, Lin YC, Benner C, Glass CK, Lucas JS, Sigvardsson M, Murre C. 2012. Positive intergenic feedback circuitry, involving EBF1 and FOXO1, orchestrates B-cell fate. *Proc Natl Acad Sci USA* **109**: 21028–21033.

Martin F, Chen X, Kearney JF. 1997. Development of VH81X transgene-bearing B cells in fetus and adult: sites for expansion and deletion in conventional and CD5/B1 cells. *International Immunology* **9**: 493–505.

Martin P, McGovern A, Orozco G, Duffus K, Yarwood A, Schoenfelder S, Cooper NJ, Barton A, Wallace C, Fraser P, et al. 2015. Capture Hi-C reveals novel candidate genes and complex long-range interactions with related autoimmune risk loci. *Nature Communications* **6**: 10069.

Martinez M, Hinojosa M, Trombly D, Morin V, Stein J, Stein G, Javed A, Gutierrez SE. 2016. Transcriptional Auto-Regulation of RUNX1 P1 Promoter. *PLoS ONE* **11**: e0149119.

Matthews AGW, Kuo AJ, Ramon-Maiques S, Han S, Champagne KS, Ivanov D, Gallardo M, Carney D, Cheung P, Ciccone DN, et al. 2007. RAG2 PHD finger couples histone H3 lysine 4 trimethylation with V(D)J

recombination. *Nature* **450**: 1106–1110.

Matthias P, Baltimore D. 1993. The immunoglobulin heavy chain locus contains another B-cell-specific 3' enhancer close to the alpha constant region. *Molecular and Cellular Biology* **13**: 1547–1553.

Maul RW, Gearhart PJ. 2010. Controlling somatic hypermutation in immunoglobulin variable and switch regions. *Immunologic research* **47**: 113–122.

Mårtensson I-L, Ceredig R. 2000. Role of the surrogate light chain and the pre-B-cell receptor in mouse B-cell development. *Immunology* **101**: 435–441.

McBlane JF, van Gent DC, Ramsden DA, Romeo C, Cuomo CA, Gellert M, Oettinger MA. 1995. Cleavage at a V(D)J recombination signal requires only RAG1 and RAG2 proteins and occurs in two steps. *Cell* **83**: 387–395.

McManus S, Ebert A, Salvagiotto G, Medvedovic J, Sun Q, Tamir I, Jaritz M, Tagoh H, Busslinger M. 2011. The transcription factor Pax5 regulates its target genes by recruiting chromatin-modifying proteins in committed B cells. *The EMBO Journal* **30**: 2388–2404.

Meaburn KJ. 2016. Spatial Genome Organization and Its Emerging Role as a Potential Diagnosis Tool. *Front Gene* **7**: 134.

Meaburn KJ, Misteli T. 2007. Cell biology: Chromosome territories. *Nature* **445**: 379–781.

Medvedovic J, Ebert A, Tagoh H, Tamir IM, Schwickert TA, Novatchkova M, Sun Q, Veld PJHIT, Guo C, Yoon HS, et al. 2013. Flexible Long-Range Loops in the VH Gene Region of the Igh Locus Facilitate the Generation of a Diverse Antibody Repertoire. *Immunity* **39**: 229–244.

Meier JT, Lewis SM. 1993. P nucleotides in V(D)J recombination: a fine-structure analysis. *Molecular and Cellular Biology* **13**: 1078–1092.

Mengshol JA, Golden-Mason L, Arikawa T, Smith M, Niki T, McWilliams R, Randall JA, McMahan R, Zimmerman MA, Rangachari M, et al. 2010. A crucial role for Kupffer cell-derived galectin-9 in regulation of T cell immunity in hepatitis C infection. *PLoS ONE* **5**: e9504.

Merkenschlager M. 2010. Ikaros in immune receptor signaling, lymphocyte differentiation, and function. *Signalling by Immunoreceptors* **584**: 4910–4914.

Miele A, Gheldof N, Tabuchi TM, Dostie J, Dekker J. 2006. Mapping chromatin interactions by chromosome conformation capture. *Curr Protoc Mol Biol* **Chapter 21**: Unit 21.11.

Mifsud B, Martincorena I, Darbo E, Sugar R, Schoenfelder S, Fraser P, Luscombe NM. 2017. GOTHiC, a probabilistic model to resolve complex biases and to identify real interactions in Hi-C data. ed. M. Isalan. *PLoS ONE* **12**: e0174744.

Mifsud B, Tavares-Cadete F, Young AN, Sugar R, Schoenfelder S, Ferreira L, Wingett SW, Andrews S, Grey W, Ewels PA, et al. 2015. Mapping long-range promoter contacts in human cells with high-resolution capture Hi-C. *Nature Genetics* **47**: 1–12.

Mitchell JA, Fraser P. 2008. Transcription factories are nuclear subcompartments that remain in the absence of transcription. *Genes Dev* **22**: 20–25.

Mombaerts P, Iacomini J, Johnson RS, Herrup K, Tonegawa S, Papaioannou VE. 1992. RAG-1-deficient mice have no mature B and T lymphocytes. *Cell* **68**: 869–877.

Montefiori L, Wuerffel R, Roqueiro D, Lajoie B, Guo C, Gerasimova T, De S, Wood W, Becker KG, Dekker J, et al. 2016. Extremely Long-Range Chromatin Loops Link Topological Domains to Facilitate a Diverse Antibody Repertoire. *CellReports* **14**: 1–31.

Morshead KB, Ciccone DN, Taverna SD, Allis CD, Oettinger MA. 2003. Antigen receptor loci poised for V(D)J rearrangement are broadly associated with BRG1 and flanked by peaks of histone H3 dimethylated at lysine 4. *Proc Natl Acad Sci USA* **100**: 11577–11582.

Morvan CL. 2003. The immunoglobulin heavy-chain locus hs3b and hs4 3' enhancers are dispensable for VDJ assembly and somatic hypermutation. *Blood* **102**: 1421–1427.

Mullen AC, Orlando DA, Newman JJ, Lovén J, Kumar RM, Bilodeau S, Reddy J, Guenther MG, DeKoter RP, Young RA. 2011. Master Transcription Factors Determine Cell-Type-Specific Responses to TGF-β Signaling. *Cell* **147**: 565–576.

Muto A, Tashiro S, Nakajima O, Hoshino H, Takahashi S, Sakoda E, Ikebe D, Yamamoto M, Igarashi K. 2004. The transcriptional programme of antibody class switching involves the repressor Bach2. *Nature* **429**: 566–571.

Nagano T, Lubling Y, Stevens TJ, Schoenfelder S, Yaffe E, Dean W, Laue ED, Tanay A, Fraser P. 2013. Single-cell Hi-C reveals cell-to-cell variability in chromosome structure. *Nature* **502**: 59–64.

Nagano T, Lubling Y, Várnai C, Dudley C, Leung W, Baran Y, Mendelson Cohen N, Wingett S, Fraser P, Tanay A. 2017. Cell-cycle dynamics of chromosomal organization at single-cell resolution. *Nature* **547**: 61–67.

Nagano T, Várnai C, Schoenfelder S, Javierre BM, Wingett SW, Fraser P. 2015. Comparison of Hi-C results using in-solution versus in-nucleus ligation. **16**: 1068.

Nagele RG, Freeman T, McMorrow L, Thomson Z, Kitson-Wind K, Lee HY. 1999. Chromosomes exhibit preferential positioning in nuclei of quiescent human cells. *Journal of Cell Science* **112 (Pt 4)**: 525–535.

Nasmyth K, Haering CH. 2009. Cohesin: Its Roles and Mechanisms. *Annu Rev Genet* **43**: 525–558.

Naumova N, Imakaev M, Fudenberg G, Zhan Y, Lajoie BR, Mirny LA, Dekker J. 2013. Organization of the Mitotic Chromosome. *Science* **342**: 948–953.

Nechanitzky R, Akbas D, Scherer S, Gyory I, Hoyler T, Ramamoorthy S, Diefenbach A, Grosschedl R. 2013. Transcription factor EBF1 is essential for the maintenance of B cell identity and prevention of alternative fates in committed cells. *Nat Immunol* **14**: 867–875.

Nemazee D. 2006. Receptor editing in lymphocyte development and central tolerance. *Nat Rev Immunol* **6**: 728–740.

Ng SY-M, Yoshida T, Zhang J, Georgopoulos K. 2009. Genome-wide lineage-specific transcriptional networks underscore Ikaros-dependent lymphoid priming in hematopoietic stem cells. *Immunity* **30**: 493–507.

Nikolajczyk BS, Sanchez JA, Sen R. 1999. ETS Protein–Dependent Accessibility Changes at the Immunoglobulin μ Heavy Chain Enhancer. *Immunity* **11**: 11–20.

Noordermeer D, Leleu M, Splinter E, Rougemont J, de Laat W, Duboule D. 2011. The dynamic architecture of Hox gene clusters. *Science* **334**: 222–225.

Nora EP, Goloborodko A, Valton A-L, Gibcus JH, Uebersohn A, Abdennur N, Dekker J, Mirny LA, Bruneau BG. 2017. Targeted Degradation of CTCF Decouples Local Insulation of Chromosome Domains from Genomic Compartmentalization. *Cell* **169**: 930–933.e22.

Nora EP, Lajoie BR, Schulz EG, Giorgetti L, Okamoto I, Servant N, Piolot T, van Berkum NL, Meisig J, Sedat J, et al. 2012. Spatial partitioning of the regulatory landscape of the X-inactivation centre. *Nature* **485**: 381–385.

Nutt SL, Urbanek P, Rolink A, Busslinger M. 1997. Essential functions of Pax5 (BSAP) in pro-B cell development: difference between fetal and adult B lymphopoiesis and reduced V-to-DJ recombination at the IgH locus. *Genes Dev* **11**: 476–491.

Olivares-Chauvet P, Mukamel Z, Lifshitz A, Schwartzman O, Elkayam NO, Lubling Y, Deikus G, Sebra RP, Tanay A. 2016. Capturing pairwise and multi-way chromosomal conformations using chromosomal walks. *Nature* **540**: 296–300.

Ong C-T, Corces VG. 2014. CTCF: an architectural protein bridging genome topology and function. *Nat Rev Genet* **15**: 1–13.

Orlanski S, Labi V, Reizel Y, Spiro A, Lichtenstein M, Levin-Klein R, Koralov SB, Skversky Y, Rajewsky K, Cedar H, et al. 2016. Tissue-specific DNA demethylation is required for proper B-cell differentiation and function. *Proc Natl Acad Sci USA* **113**: 5018–5023.

Osborne CS, Chakalova L, Brown KE, Carter D, Horton A, Debrand E, Goyenechea B, Mitchell JA, Lopes S, Reik W, et al. 2004. Active genes dynamically colocalize to shared sites of ongoing transcription. *Nat Genet* **36**: 1065–1071.

Osborne CS, Chakalova L, Mitchell JA, Horton A, Wood AL, Bolland DJ, Corcoran AE, Fraser P. 2007. Myc Dynamically and Preferentially Relocates to a Transcription Factory Occupied by Igh ed. Susan M Gasser. *PLoS Biol* **5**: e192–10.

Outters P, Jaeger S, Zaarour N, Ferrier P. 2015. Long-Range Control of V(D)J Recombination & Allelic Exclusion: Modeling Views. *Adv Immunol* **128**: 363–413.

Pal R, Janz M, Galson DL, Gries M, Li S, Johrens K, Anagnostopoulos I, Dorken B, Mapara MY, Borghesi L, et al. 2009. C/EBPbeta regulates transcription factors critical for proliferation and survival of multiple myeloma cells. *Blood* **114**: 3890–3898.

Palstra R-J, Tolhuis B, Splinter E, Nijmeijer R, Grosveld F, de Laat W. 2003. The |[beta]|-globin nuclear compartment in development and erythroid differentiation. *Nat Genet* **35**: 190–194.

Pan X, Papasani M, Hao Y, Calamito M, Wei F, Quinn WJ III, Basu A, Wang J, Hodawadekar S, Zaprazna K, et al. 2013. YY1 controls Igκ repertoire and B-cell development, and localizes with condensin on the Igκ locus. *The EMBO Journal* **32**: 1168–1182.

Pappu R, Cheng AM, Li B, Gong Q, Chiu C, Griffin N, White M, Sleckman BP, Chan AC. 1999. Requirement for B cell linker protein (BLNK) in B cell development. *Science* **286**: 1949–1954.

Parada LA, McQueen PG, Munson PJ, Misteli T. 2002. Conservation of relative chromosome positioning in normal and cancer cells. *Curr Biol* **12**: 1692–1697.

Parelho V, Hadjur S, Spivakov M, Leleu M, Sauer S, Gregson HC, Jarmuz A, Canzonetta C, Webster Z, Nesterova T, et al. 2008. Cohesins functionally associate with CTCF on mammalian chromosome arms. *Cell* **132**: 422–433.

Park SK, Xiang Y, Feng X, Garrard WT. 2014. Pronounced cohabitation of active immunoglobulin genes from three different chromosomes in transcription factories during maximal antibody synthesis. *Genes Dev* **28**: 1159–1164.

Paulson JR, Laemmli UK. 1977. The structure of histone-depleted metaphase chromosomes. *Cell* **12**: 817–828.

Perlot T, Alt FW, Bassing CH, Suh H, Pinaud E. 2005. Elucidation of IgH intronic enhancer functions via germ-line deletion. *Proc Natl Acad Sci USA* **102**: 14362–14367.

Perlot T, Pawlitzky I, Manis JP, Zarrin AA, Brodeur PH, Alt FW. 2010. Analysis of Mice Lacking DNaseI Hypersensitive Sites at the 5′ End of the IgH Locus ed. S.D. Fugmann. *PLoS ONE* **5**: e13992.

Phillips JE, Corces VG. 2009. CTCF: Master Weaver of the Genome. *Cell* **137**: 1194–1211.

Phillips-Cremins JE, Sauria MEG, Sanyal A, Gerasimova TI, Lajoie BR, Bell JSK, Ong C-T, Hookway TA, Guo C, Sun Y, et al. 2013. Architectural protein subclasses shape 3D organization of genomes during lineage commitment. *Cell* **153**: 1281–1295.

Pinaud E, Khamlichi AA, Le Morvan C, Drouet M, Nalesso V, Le Bert M, Cogne M. 2001. Localization of the 3' IgH locus elements that effect long-distance regulation of class switch recombination. *Immunity* **15**: 187–199.

Pope BD, Ryba T, Dileep V, Yue F, Wu W, Denas O, Vera DL, Wang Y, Hansen RS, Canfield TK, et al. 2014. Topologically associating domains are stable units of replication-timing regulation. *Nature* **515**: 402–405.

Predeus AV, Gopalakrishnan S, Huang Y, Tang J, Feeney AJ, Oltz EM, Artyomov MN. 2014. Targeted

Chromatin Profiling Reveals Novel Enhancers in Immunoglobulin Heavy and Light Chain Loci. *J Immunol* **192**: 1064–1070.

Proudhon C, Snetkova V, Raviram R, Lobry C, Badri S, Jiang T, Hao B, Trimarchi T, Kluger Y, Aifantis I, et al. 2016. Active and Inactive Enhancers Cooperate to Exert Localized and Long-Range Control of Gene Regulation. *CellReports* **15**: 2159–2169.

Qian J, Wang Q, Dose M, Pruett N, Kieffer-Kwon K-R, Resch W, Liang G, Tang Z, Mathe E, Benner C, et al. 2014. B Cell Super-Enhancers and Regulatory Clusters Recruit AID Tumorigenic Activity. *Cell* **159**: 1524–1537.

Ragoczy T, Bender MA, Telling A, Byron R, Groudine M. 2006. The locus control region is required for association of the murine beta-globin locus with engaged transcription factories during erythroid maturation. *Genes Dev* **20**: 1447–1457.

Rankin S, Dawson DS. 2016. Recent advances in cohesin biology [version 1; referees: 4 approved]. *F1000Res* **5**.

Rao S, Huang S-C, Glenn St Hilaire B, Engreitz JM, Perez EM, Kieffer-Kwon K-R, Sanborn AL, Johnstone SE, Bochkov ID, Huang X, et al. 2017. Cohesin Loss Eliminates All Loop Domains, Leading To Links Among Superenhancers And Downregulation Of Nearby Genes. *bioRxiv*.

Rao SSP, Huntley MH, Durand NC, Stamenova EK, Bochkov ID, Robinson JT, Sanborn AL, Machol I, Omer AD, Lander ES, et al. 2014a. A 3D Map of the Human Genome at Kilobase Resolution Reveals Principles of Chromatin Looping. *Cell* **159**: 1665–1680.

Rao SSP, Huntley MH, Durand NC, Stamenova EK, Bochkov ID, Robinson JT, Sanborn AL, Machol I, Omer AD, Lander ES, et al. 2014b. A 3D Map of the Human Genome at Kilobase Resolution Reveals Principles of Chromatin Looping. *Cell* **159**: 1665–1680.

Rao SSP, Huntley MH, Durand NC, Stamenova EK, Bochkov ID, Robinson JT, Sanborn AL, Machol I, Omer AD, Lander ES, et al. 2014c. A 3D Map of the Human Genome at Kilobase Resolution Reveals Principles of Chromatin Looping. *Cell* **159**: 1665–1680.

Rao SSP, Huntley MH, Durand NC, Stamenova EK, Bochkov ID, Robinson JT, Sanborn AL, Machol I, Omer AD, Lander ES, et al. 2014d. A 3D map of the human genome at kilobase resolution reveals principles of chromatin looping. *Cell* **159**.

Ren L, Wang Y, Shi M, Wang X, Yang Z, Zhao Z. 2012. CTCF Mediates the Cell-Type Specific Spatial Organization of the Kcnq5 Locus and the Local Gene Regulation ed. Z. Zhou. *PLoS ONE* **7**: e31416.

Revilla-i-Domingo R, Bilic I, Vilagos B, Tagoh H, Ebert A, Tamir IM, Smeenk L, Trupke J, Sommer A, Jaritz M, et al. 2012. The B-cell identity factor Pax5 regulates distinct transcriptional programmes in early and late B lymphopoiesis. *The EMBO Journal* **31**: 3130–3146.

Reya T, O'Riordan M, Okamura R, Devaney E, Willert K, Nusse R, Grosschedl R. 2000. Wnt signaling regulates B lymphocyte proliferation through a LEF-1 dependent mechanism. *Immunity* **13**: 15–24.

Reynaud D, A Demarco I, L Reddy K, Schjerven H, Bertolino E, Chen Z, Smale ST, Winandy S, Singh H. 2008. Regulation of B cell fate commitment and immunoglobulin heavy-chain gene rearrangements by Ikaros. *Nat Immunol* **9**: 927–936.

Ribeiro de Almeida C, Stadhouders R, de Bruijn MJW, Bergen IM, Thongjuea S, Lenhard B, van IJcken W, Grosveld F, Galjart N, Soler E, et al. 2011. The DNA-binding protein CTCF limits proximal Vκ recombination and restricts κ enhancer interactions to the immunoglobulin κ light chain locus. *Immunity* **35**: 501–513.

Robbiani DF, Bothmer A, Callen E, Reina-San-Martin B, Dorsett Y, Difilippantonio S, Bolland DJ, Chen HT, Corcoran AE, Nussenzweig A, et al. 2008. AID is required for the chromosomal breaks in c-myc that lead to c-myc/IgH translocations. *Cell* **135**: 1028–1038.

Robin JD, Ludlow AT, Batten K, Gaillard M-C, Stadler G, Magdinier F, Wright WE, Shay JW. 2015. SORBS2 transcription is activated by telomere position effect-over long distance upon telomere shortening in muscle

cells from patients with facioscapulohumeral dystrophy. *Genome Res* **25**: 1781–1790.

Rocha PP, Micsinai M, Kim JR, Hewitt SL, Souza PP, Trimarchi T, Strino F, Parisi F, Kluger Y, Skok JA. 2012. Close Proximity to Igh Is a Contributing Factor to AID-Mediated Translocations. *Molecular Cell* **47**: 873–885.

Roessler S, Gyory I, Imhof S, Spivakov M, Williams RR, Busslinger M, Fisher AG, Grosschedl R. 2007. Distinct promoters mediate the regulation of Ebf1 gene expression by interleukin-7 and Pax5. *Molecular and Cellular Biology* **27**: 579–594.

Roix JJ, McQueen PG, Munson PJ, Parada LA, Misteli T. 2003. Spatial proximity of translocation-prone gene loci in human lymphomas. *Nat Genet* **34**: 287–291.

Roldán E, Fuxa M, Chong W, Martinez D, Novatchkova M, Busslinger M, Skok JA. 2004. Locus "decontraction" and centromeric recruitment contribute to allelic exclusion of the immunoglobulin heavy-chain gene. *Nat Immunol* **6**: 31–41.

Rolink AG, Andersson J, Melchers F. 2004. Molecular mechanisms guiding late stages of B-cell development. *Immunol Rev* **197**: 41–50.

Rolink AG, Winkler T, Melchers F, Andersson J. 2000. Precursor B cell receptor-dependent B cell proliferation and differentiation does not require the bone marrow or fetal liver environment. *J Exp Med* **191**: 23–32.

Rooney S, Chaudhuri J, Alt FW. 2004. The role of the non-homologous end-joining pathway in lymphocyte development. *Immunol Rev* **200**: 115–131.

Rosa A, Everaers R. 2008. Structure and dynamics of interphase chromosomes. **4**: e1000153.

Rother MB, Palstra R-J, Jhunjhunwala S, van Kester KAM, van IJcken WFJ, Hendriks RW, van Dongen JJM, Murre C, van Zelm MC. 2016. Nuclear positioning rather than contraction controls ordered rearrangements of immunoglobulin loci. *Nucleic Acids Res* **44**: 175–186.

Rubio ED, Reiss DJ, Welcsh PL, Disteche CM, Filippova GN, Baliga NS, Aebersold R, Ranish JA, Krumm A. 2008. CTCF physically links cohesin to chromatin. *Proc Natl Acad Sci USA* **105**: 8309–8314.

Rudan MV, Barrington C, Henderson S, Ernst C, Odom DT, Tanay A, Hadjur S. 2015. Comparative Hi-C Reveals that CTCF Underlies Evolution of Chromosomal Domain Architecture. *CellReports* **10**: 1297–1309.

Rumfelt LL, Zhou Y, Rowley BM, Shinton SA, Hardy RR. 2006. Lineage specification and plasticity in CD19-early B cell precursors. *J Exp Med* **203**: 675–687.

Sahlén P, Abdullayev I, Ramsköld D, Matskova L, Rilakovic N, Lötstedt B, Albert TJ, Lundeberg J, Sandberg R. 2015. Genome-wide mapping of promoter-anchored interactions with close to single-enhancer resolution. 1–13.

Sakai E, Bottaro A, Alt FW. 1999. The Ig heavy chain intronic enhancer core region is necessary and sufficient to promote efficient class switch recombination. *International Immunology* **11**: 1709–1713.

Saldanha AJ. 2004. Java Treeview--extensible visualization of microarray data. *Bioinformatics* **20**: 3246–3248.

Sanborn AL, Rao SSP, Huang S-C, Durand NC, Huntley MH, Jewett AI, Bochkov ID, Chinnappan D, Cutkosky A, Li J, et al. 2015. Chromatin extrusion explains key features of loop and domain formation in wild-type and engineered genomes. *Proc Natl Acad Sci USA* **112**: E6456–E6465.

Sansregret L, Nepveu A. 2008. The multiple roles of CUX1: Insights from mouse models and cell-based assays. *Gene* **412**: 84–94.

Sanyal A, Lajoie BR, Jain G, Dekker J. 2012. The long-range interaction landscape of gene promoters. *Nature* **489**: 109–113.

Sayegh C. 2005. Visualization of looping involving the immunoglobulin heavy-chain locus in developing B

cells. *Genes Dev* **19**: 322–327.

Sayegh CE, Quong MW, Agata Y, Murre C. 2003. E-proteins directly regulate expression of activation-induced deaminase in mature B cells. *Nat Immunol* **4**: 586–593.

Schatz DG, Ji Y. 2011. Recombination centres and the orchestration of V(D)J recombination. *Nat Rev Immunol* **11**: 251–263.

Schatz DG, Swanson PC. 2011. V(D)J recombination: mechanisms of initiation. *Annu Rev Genet* **45**: 167–202.

Schebesta A, McManus S, Salvagiotto G, Delogu A, Busslinger GA, Busslinger M. 2007. Transcription Factor Pax5 Activates the Chromatin of Key Genes Involved in B Cell Signaling, Adhesion, Migration, and Immune Function. *Immunity* **27**: 49–63.

Schebesta M, Pfeffer PL, Busslinger M. 2002. Control of pre-BCR signaling by Pax5-dependent activation of the BLNK gene. *Immunity* **17**: 473–485.

Schjerven H, McLaughlin J, Arenzana TL, Frietze S, Cheng D, Wadsworth SE, Lawson GW, Bensinger SJ, Farnham PJ, Witte ON, et al. 2013. Selective regulation of lymphopoiesis and leukemogenesis by individual zinc fingers of Ikaros. *Nat Immunol* **14**: 1073–1083.

Schmidt D, Schwalie PC, Ross-Innes CS, Hurtado A, Brown GD, Carroll JS, Flicek P, Odom DT. 2010. A CTCF-independent role for cohesin in tissue-specific transcription. *Genome Res* **20**: 578–588.

Schmitt AD, Hu M, Ren B. 2016. Genome-wide mapping and analysis of chromosome architecture. *Nature Publishing Group* 1–13.

Schoenfelder S, Furlan-Magaril M, Mifsud B, Tavares-Cadete F, Sugar R, Javierre BM, Nagano T, Katsman Y, Sakthidevi M, Wingett SW, et al. 2015a. The pluripotent regulatory circuitry connecting promoters to their long-range interacting elements. *Genome Res* **25**: 582–597.

Schoenfelder S, Sexton T, Chakalova L, Cope NF, Horton A, Andrews S. 2010. Preferential associations between co-regulated genes reveal a transcriptional interactome in erythroid cells. *Nat Genet* **42**.

Schoenfelder S, Sexton T, Chakalova L, Cope NF, Horton A, Andrews S, Kurukuti S, Mitchell JA, Umlauf D, Dimitrova DS, et al. 2009. Preferential associations between co-regulated genes reveal a transcriptional interactome in erythroid cells. *Nature Genetics* **42**: 53–61.

Schoenfelder S, Sugar R, Dimond A, Javierre BM, Armstrong H, Mifsud B, Dimitrova E, Matheson L, Tavares-Cadete F, Furlan-Magaril M, et al. 2015b. Polycomb repressive complex PRC1 spatially constrains the mouse embryonic stem cell genome. *Nature Genetics* 1–11.

Schroeder HWJ, Cavacini L. 2010. Structure and function of immunoglobulins. *J Allergy Clin Immunol* **125**: S41–52.

Schwalie PC, Ward MC, Cain CE, Faure AJ, Gilad Y, Odom DT, Flicek P. 2013. Co-binding by YY1 identifies the transcriptionally active, highly conserved set of CTCF-bound regions in primate genomes. **14**: R148.

Schwickert TA, Tagoh H, Gültekin S, Dakic A, Axelsson E, Minnich M, Ebert A, Werner B, Roth M, Cimmino L, et al. 2014. Stage-specific control of early B cell development by the transcription factor Ikaros. *Nat Immunol* **15**: 283–293.

Secca C, Faget DV, Hanschke SC, Carneiro MS, Bonamino MH, de-Araujo-Souza PS, Viola JPB. 2016. IRF2BP2 transcriptional repressor restrains naive CD4 T cell activation and clonal expansion induced by TCR triggering. *J Leukoc Biol* **100**: 1081–1091.

Seitan VC, Faure AJ, Zhan Y, McCord RP, Lajoie BR, Ing-Simmons E, Lenhard B, Giorgetti L, Heard E, Fisher AG, et al. 2013. Cohesin-based chromatin interactions enable regulated gene expression within preexisting architectural compartments. *Genome Res* **23**: 2066–2077.

Seitan VC, Hao B, Tachibana-Konwalski K, Lavagnolli T, Mira-Bontenbal H, Brown KE, Teng G, Carroll T, Terry A, Horan K, et al. 2011. A role for cohesin in T-cell-receptor rearrangement and thymocyte

differentiation. *Nature* **476**: 467–471.

Seitan VC, Krangel MS, Merkenschlager M. 2012. Cohesin, CTCF and lymphocyte antigen receptor locus rearrangement. *Trends in Immunology* **33**: 153–159.

Selimyan R, Gerstein RM, Ivanova I, Precht P, Subrahmanyam R, Perlot T, Alt FW, Sen R. 2013. Localized DNA demethylation at recombination intermediates during immunoglobulin heavy chain gene assembly. *PLoS Biol* **11**: e1001475.

Seo W, Ikawa T, Kawamoto H, Taniuchi I. 2012. Runx1–Cbfβ facilitates early B lymphocyte development by regulating expression of Ebf1. *J Exp Med* **209**: 1255–1262.

Sexton T, Yaffe E, Kenigsberg E, Bantignies F, Leblanc B, Hoichman M, Parrinello H, Tanay A, Cavalli G. 2012. Three-Dimensional Folding and Functional Organization Principles of the Drosophila Genome. *Cell* **148**: 458–472.

Shain AH, Pollack JR. 2013. The Spectrum of SWI/SNF Mutations, Ubiquitous in Human Cancers ed. F. Kashanchi. *PLoS ONE* **8**: e55119.

Shi X, Eckhardt LA. 2001. Deletional analyses reveal an essential role for the hs3b/hs4 IgH 3′ enhancer pair in an Ig-secreting but not an earlier-stage B cell line. *International Immunology* **13**: 1003–1012.

Shi Y, Seto E, Chang LS, Shenk T. 1991. Transcriptional repression by YY1, a human GLI-Kruppel-related protein, and relief of repression by adenovirus E1A protein. *Cell* **67**: 377–388.

Shimazaki N, Askary A, Swanson PC, Lieber MR. 2012. Mechanistic basis for RAG discrimination between recombination sites and the off-target sites of human lymphomas. *Molecular and Cellular Biology* **32**: 365–375.

Shinkai Y, Rathbun G, Lam KP, Oltz EM, Stewart V, Mendelsohn M, Charron J, Datta M, Young F, Stall AM. 1992. RAG-2-deficient mice lack mature lymphocytes owing to inability to initiate V(D)J rearrangement. *Cell* **68**: 855–867.

Simonis M, Klous P, Splinter E, Moshkin Y, Willemsen R, de Wit E, van Steensel B, de Laat W. 2006. Nuclear organization of active and inactive chromatin domains uncovered by chromosome conformation capture–on-chip (4C). *Nat Genet* **38**: 1348–1354.

So L, Fruman DA. 2012. PI3K Signaling in B and T Lymphocytes: New Developments and Therapeutic Advances. *The Biochemical journal* **442**: 465–481.

Sofueva S, Yaffe E, Chan W-C, Georgopoulou D, Vietri Rudan M, Mira-Bontenbal H, Pollard SM, Schroth GP, Tanay A, Hadjur S. 2013. Cohesin-mediated interactions organize chromosomal domain architecture. *The EMBO Journal* **32**: 3119–3129.

Soler E, Andrieu-Soler C, de Boer E, Bryne JC, Thongjuea S, Stadhouders R, Palstra R-J, Stevens M, Kockx C, van IJcken W, et al. 2010. The genome-wide dynamics of the binding of Ldb1 complexes during erythroid differentiation. *Genes Dev* **24**: 277–289.

Somasundaram R, Prasad MAJ, Ungerbäck J, Sigvardsson M. 2015. Transcription factor networks in B-cell differentiation link development to acute lymphoid leukemia. *Blood* **126**: 144–152.

Spilianakis CG, Lalioti MD, Town T, Lee GR, Flavell RA. 2005. Interchromosomal associations between alternatively expressed loci. *Nature* **435**: 637–645.

Splinter E, de Wit E, van de Werken HJG, Klous P, de Laat W. 2012. Determining long-range chromatin interactions for selected genomic sites using 4C-seq technology: from fixation to computation. *Methods* **58**: 221–230.

Splinter E, Grosveld F, de Laat W. 2004. 3C technology: analyzing the spatial organization of genomic loci in vivo. *Methods Enzymol* **375**: 493–507.

Splinter E, Heath H, Kooren J, Palstra RJ, Klous P, Grosveld F, Galjart N, de Laat W. 2006. CTCF mediates

long-range chromatin looping and local histone modification in the β-globin locus. *Gen Devel* **20**.

Stadhouders R, Kolovos P, Brouwer R, Zuin J, van den Heuvel A, Kockx C, Palstra R-J, Wendt KS, Grosveld F, van IJcken W, et al. 2013. Multiplexed chromosome conformation capture sequencing for rapid genome-scale high-resolution detection of long-range chromatin interactions. *Nature Protocols* **8**: 509–524.

Stadhouders R, Thongjuea S, Andrieu-Soler C, Palstra R-J, Bryne JC, van den Heuvel A, Stevens M, de Boer E, Kockx C, van der Sloot A, et al. 2012. Dynamic long-range chromatin interactions control Myb proto-oncogene transcription during erythroid development. *The EMBO Journal* **31**: 986–999.

Stanhope-Baker P, Hudson KM, Shaffer AL, Constantinescu A, Schlissel MS. 1996. Cell type-specific chromatin structure determines the targeting of V(D)J recombinase activity in vitro. *Cell* **85**: 887–897.

Stevens TJ, Lando D, Basu S, Atkinson LP, Cao Y, Lee SF, Leeb M, Wohlfahrt KJ, Boucher W, O'Shaughnessy-Kirwan A, et al. 2017. 3D structures of individual mammalian genomes studied by single-cell Hi-C. *Nature* **544**: 59–64.

Storb U, Arp B. 1983. Methylation patterns of immunoglobulin genes in lymphoid cells: correlation of expression and differentiation with undermethylation. *Proc Natl Acad Sci USA* **80**: 6642–6646.

Stubbington MJT, Corcoran AE. 2013. Non-coding transcription and large-scale nuclear organisation of immunoglobulin recombination. *Current Opinion in Genetics & Development* **23**: 81–88.

Subrahmanyam R, Du H, Ivanova I, Chakraborty T, Ji Y, Zhang Y, Alt FW, Schatz DG, Sen R. 2012. Localized epigenetic changes induced by DH recombination restricts recombinase to DJH junctions. *Nat Immunol* **13**: 1205–1212.

Subrahmanyam R, Sen R. 2010. RAGs' eye view of the immunoglobulin heavy chain gene locus. *Seminars in Immunology* **22**: 337–345.

Swaminathan S, Huang C, Geng H, Chen Z, Harvey R, Kang H, Ng C, Titz B, Hurtz C, Sadiyah MF, et al. 2013. BACH2 mediates negative selection and p53-dependent tumor suppression at the pre-B cell receptor checkpoint. *Nature Medicine* **19**: 1014–1022.

Swanson PC. 2002. A RAG-1/RAG-2 Tetramer Supports 12/23-Regulated Synapsis, Cleavage, and Transposition of V(D)J Recombination Signals. *Molecular and Cellular Biology* **22**: 7790–7801.

Swanson PC. 2004. The bounty of RAGs: recombination signal complexes and reaction outcomes. *Immunol Rev* **200**: 90–114.

Symmons O, Uslu VV, Tsujimura T, Ruf S, Nassari S, Schwarzer W, Ettwiller L, Spitz F. 2014. Functional and topological characteristics of mammalian regulatory domains. *Genome Res* **24**: 390–400.

Taira N, Mimoto R, Kurata M, Yamaguchi T, Kitagawa M, Miki Y, Yoshida K. 2012. DYRK2 priming phosphorylation of c-Jun and c-Myc modulates cell cycle progression in human cancer cells. *J Clin Invest* **122**: 859–872.

Tanaka H, Muto A, Shima H, Katoh Y, Sax N, Tajima S, Brydun A, Ikura T, Yoshizawa N, Masai H, et al. 2016. Epigenetic Regulation of the Blimp-1 Gene (Prdm1) in B Cells Involves Bach2 and Histone Deacetylase 3. *Journal of Biological Chemistry* **291**: 6316–6330.

Tang Q, Danila MI, Cui X, Parks L, Baker BJ, Reynolds RJ, Raman C, Wanseck KC, Redden DT, Johnson MR, et al. 2015a. Brief Report: Expression of Interferon-γ Receptor Genes in Peripheral Blood Mononuclear Cells Is Associated With Rheumatoid Arthritis and Its Radiographic Severity in African Americans. *Arthritis & Rheumatology* **67**: 1165–1170.

Tang Z, Luo OJ, Li X, Zheng M, Zhu JJ, Szalaj P, Trzaskoma P, Magalska A, Wlodarczyk J, Ruszczycki B, et al. 2015b. CTCF-Mediated Human 3D Genome Architecture Reveals Chromatin Topology for Transcription. *Cell* **163**: 1611–1627.

Teng G, Maman Y, Resch W, Kim M, Yamane A, Qian J, Kieffer-Kwon K-R, Mandal M, Ji Y, Meffre E, et al. 2015. RAG Represents a Widespread Threat to the Lymphocyte Genome. *Cell* **162**: 751–765.

Thompson BJ, Bhansali R, Diebold L, Cook DE, Stolzenburg L, Casagrande A-S, Besson T, Leblond B, Désiré L, Malinge S, et al. 2015. DYRK1A controls the transition from proliferation to quiescence during lymphoid development by destabilizing Cyclin D3. *J Exp Med* **212**: 953–970.

Thompson CB. 1995. New insights into V(D)J recombination and its role in the evolution of the immune system. *Immunity* **3**: 531–539.

Timblin GA, Schlissel MS. 2013. Ebf1 and c-Myb repress rag transcription downstream of Stat5 during early B cell development. *J Immunol* **191**: 4676–4687.

Tolhuis B, Palstra R-J, Splinter E, Grosveld F, de Laat W. 2002. Looping and Interaction between Hypersensitive Sites in the Active β-globin Locus. *Molecular Cell* **10**: 1453–1465.

Tonkin ET, Wang T-J, Lisgo S, Bamshad MJ, Strachan T. 2004. NIPBL, encoding a homolog of fungal Scc2-type sister chromatid cohesion proteins and fly Nipped-B, is mutated in Cornelia de Lange syndrome. *Nat Genet* **36**: 636–641.

Trask BJ. 1991. Gene mapping by in situ hybridization. *Current Opinion in Genetics & Development* **1**: 82–87.

Treiber T, Mandel EM, Pott S, Gyory I, Firner S, Liu ET, Grosschedl R. 2010. Early B cell factor 1 regulates B cell gene networks by activation, repression, and transcription- independent poising of chromatin. *Immunity* **32**: 714–725.

Urbanek P, Wang ZQ, Fetka I, Wagner EF, Busslinger M. 1994. Complete block of early B cell differentiation and altered patterning of the posterior midbrain in mice lacking Pax5/BSAP. *Cell* **79**: 901–912.

van Berkum NL, Lieberman-Aiden E, Williams L, Imakaev M, Gnirke A, Mirny LA, Dekker J, Lander ES. 2010. Hi-C: a method to study the three-dimensional architecture of genomes. *JoVE*.

Van Bortle K, Nichols MH, Li L, Ong C-T, Takenaka N, Qin ZS, Corces VG. 2014. Insulator function and topological domain border strength scale with architectural protein occupancy. **15**: R82.

van de Werken HJG, Landan G, Holwerda SJB, Hoichman M, Klous P, Chachik R, Splinter E, Valdes-Quezada C, Öz Y, Bouwman BAM, et al. 2012. Robust 4C-seq data analysis to screen for regulatory DNA interactions. *Nature Methods* **9**: 969–972.

van Gent DC, Hiom K, Paull TT, Gellert M. 1997. Stimulation of V(D)J cleavage by high mobility group proteins. *The EMBO Journal* **16**: 2665–2670.

Verma-Gaur J, Torkamani A, Schaffer L, Head SR, Schork NJ, Feeney AJ. 2012. Noncoding transcription within the Igh distal V(H) region at PAIR elements affects the 3D structure of the Igh locus in pro-B cells. *Proc Natl Acad Sci USA* **109**: 17004–17009.

Vernimmen D, Marques-Kranc F, Sharpe JA, Sloane-Stanley JA, Wood WG, Wallace HA, Smith AJ, Higgs DR. 2009. Chromosome looping at the human α-globin locus is mediated via the major upstream regulatory element (HS- 40). *Blood* **114**.

Vilagos B, Hoffmann M, Souabni A, Sun Q, Werner B, Medvedovic J, Bilic I, Minnich M, Axelsson E, Jaritz M, et al. 2012. Essential role of EBF1 in the generation and function of distinct mature B cell types. *J Exp Med* **209**: 775–792.

Vincent-Fabert C, Fiancette R, Pinaud E, Truffinet V, Cogne N, Cogne M, Denizot Y. 2010. Genomic deletion of the whole IgH 3' regulatory region (hs3a, hs1,2, hs3b, and hs4) dramatically affects class switch recombination and Ig secretion to all isotypes. *Blood* **116**: 1895–1898.

Volpi EV, Chevret E, Jones T, Vatcheva R, Williamson J, Beck S, Campbell RD, Goldsworthy M, Powis SH, Ragoussis J, et al. 2000. Large-scale chromatin organization of the major histocompatibility complex and other regions of human chromosome 6 and its response to interferon in interphase nuclei. *J Cell Sci* **113**: 1565.

Volpi SA, Verma-Gaur J, Hassan R, Ju Z, Roa S, Chatterjee S, Werling U, Hou H, Will B, Steidl U, et al. 2012. Germline Deletion of Igh 3' Regulatory Region Elements hs 5, 6, 7 (hs5-7) Affects B Cell-Specific

Regulation, Rearrangement, and Insulation of the Igh Locus. *The Journal of Immunology* **188**: 2556–2566.

Wallace JA, Felsenfeld G. 2007. We gather together: insulators and genome organization. *Current Opinion in Genetics & Development* **17**: 400–407.

Wang C, Liu C, Roqueiro D, Grimm D, Schwab R, Becker C, Lanz C, Weigel D. 2015. Genome-wide analysis of local chromatin packing in Arabidopsis thaliana. *Genome Res* **25**: 246–256.

Wang JH, Gostissa M, Yan CT, Goff P, Hickernell T, Hansen E, Difilippantonio S, Wesemann DR, Zarrin AA, Rajewsky K, et al. 2009. Mechanisms promoting translocations in editing and switching peripheral B cells. *Nature Publishing Group* **460**: 231–236.

Wang JH, Nichogiannopoulou A, Wu L, Sun L, Sharpe AH, Bigby M, Georgopoulos K. 1996. Selective defects in the development of the fetal and adult lymphoid system in mice with an Ikaros null mutation. *Immunity* **5**: 537–549.

Wang Z, Goldstein A, Zong RT, Lin D, Neufeld EJ, Scheuermann RH, Tucker PW. 1999. Cux/CDP homeoprotein is a component of NF-muNR and represses the immunoglobulin heavy chain intronic enhancer by antagonizing the bright transcription activator. *Molecular and Cellular Biology* **19**: 284–295.

Wei X-C, Dohkan J-I, Kishi H, Wu C-X, Kondo S, Muraguchi A. 2005. Characterization of the proximal enhancer element and transcriptional regulatory factors for murine recombination activating gene-2. *Eur J Immunol* **35**: 612–621.

Wei Z, Gao F, Kim S, Yang H, Lyu J, An W, Wang K, Lu W. 2013. Klf4 organizes long-range chromosomal interactions with the oct4 locus in reprogramming and pluripotency. *Cell Stem Cell* **13**: 36–47.

Wendt KS, Yoshida K, Itoh T, Bando M, Koch B, Schirghuber E, Tsutsumi S, Nagae G, Ishihara K, Mishiro T, et al. 2008. Cohesin mediates transcriptional insulation by CCCTC-binding factor. *Nature* **451**: 796–801.

Willis SN, Good-Jacobson KL, Curtis J, Light A, Tellier J, Shi W, Smyth GK, Tarlinton DM, Belz GT, Corcoran LM, et al. 2014. Transcription factor IRF4 regulates germinal center cell formation through a B cell-intrinsic mechanism. *The Journal of Immunology* **192**: 3200–3206.

Wilson NK, Schoenfelder S, Hannah R, Sanchez Castillo M, Schutte J, Ladopoulos V, Mitchelmore J, Goode DK, Calero-Nieto FJ, Moignard V, et al. 2016. Integrated genome-scale analysis of the transcriptional regulatory landscape in a blood stem/progenitor cell model. *Blood* **127**: e12–23.

Wingett S, Ewels P, Furlan-Magaril M, Nagano T, Schoenfelder S, Fraser P, Andrews S. 2015. HiCUP: pipeline for mapping and processing Hi-C data. *F1000Res* **4**: 1310.

Wong CC, Martincorena I, Rust AG, Rashid M, Alifrangis C, Alexandrov LB, Tiffen JC, Kober C, Green AR, Massie CE, et al. 2014. Inactivating CUX1 mutations promote tumorigenesis. *Nat Genet* **46**: 33–38.

Wu TT, Kabat EA. 1970. An analysis of the sequences of the variable regions of Bence Jones proteins and myeloma light chains and their implications for antibody complementarity. *J Exp Med* **132**: 211–250.

Xie WJ, Meng L, Liu S, Zhang L, Cai X, Gao YQ. 2017. Structural Modeling of Chromatin Integrates Genome Features and Reveals Chromosome Folding Principle. *Nature Publishing Group* **7**: 2818.

Yaffe E, Tanay A. 2011. Probabilistic modeling of Hi-C contact maps eliminates systematic biases to characterize global chromosomal architecture. *Nature Genetics* **43**: 1059–1065.

Yancopoulos GD, Alt FW. 1985. Developmentally controlled and tissue-specific expression of unrearranged VH gene segments. *Cell* **40**: 271–281.

Ye J. 2004. The immunoglobulin IGHD gene locus in C57BL/6 mice. *Immunogenetics* **56**: 1–6.

Yu W, Misulovin Z, Suh H, Hardy RR, Jankovic M, Yannoutsos N, Nussenzweig MC. 1999. Coordinate Regulation of RAG1 and RAG2 by Cell Type-Specific DNA Elements 5′ of RAG2. *Science* **285**: 1080–1084.

Yu Y, Wang J, Khaled W, Burke S, Li P, Chen X, Yang W, Jenkins NA, Copeland NG, Zhang S, et al. 2012. Bcl11a is essential for lymphoid development and negatively regulates p53. *J Exp Med* **209**: 2467–2483.

Zagelbaum J, Shimazaki N, Esguerra ZA, Watanabe G, Lieber MR, Rothenberg E. 2016. Real-time analysis of RAG complex activity in V(D)J recombination. *Proc Natl Acad Sci USA* **113**: 11853–11858.

Zandi S, Mansson R, Tsapogas P, Zetterblad J, Bryder D, Sigvardsson M. 2008. EBF1 Is Essential for B-Lineage Priming and Establishment of a Transcription Factor Network in Common Lymphoid Progenitors. *The Journal of Immunology* **181**: 3364–3372.

Zhan Y, Giorgetti L, Tiana G. 2017a. Modelling genome-wide topological associating domains in mouse embryonic stem cells. *Chromosome Research* 1–10.

Zhan Y, Mariani L, Barozzi I, Schulz EG, Blüthgen N, Stadler M, Tiana G, Giorgetti L. 2017b. Reciprocal insulation analysis of Hi-C data shows that TADs represent a functionally but not structurally privileged scale in the hierarchical folding of chromosomes. *Genome Res* **27**: 479–490.

Zhang F, Thomas LR, Oltz EM, Aune TM. 2006a. Control of thymocyte development and recombination-activating gene expression by the zinc finger protein Zfp608. *Nat Immunol* **7**: 1309–1316.

Zhang J, McCastlain K, Yoshihara H, Xu B, Chang Y, Churchman ML, Wu G, Li Y, Wei L, Iacobucci I, et al. 2016. Deregulation of DUX4 and ERG in acute lymphoblastic leukemia. *Nat Genet* **48**: 1481–1489.

Zhang Y, Liu T, Meyer CA, Eeckhoute J, Johnson DS, Bernstein BE, Nussbaum C, Myers RM, Brown M, Li W, et al. 2008. Model-based Analysis of ChIP-Seq (MACS). **9**: R137.

Zhang Y, McCord RP, Ho Y-J, Lajoie BR, Hildebrand DG, Simon AC, Becker MS, Alt FW, Dekker J. 2012. Spatial Organization of the Mouse Genome and Its Role in Recurrent Chromosomal Translocations. *Cell* **148**: 908–921.

Zhang Z, Espinoza CR, Yu Z, Stephan R, He T, Williams GS, Burrows PD, Hagman J, Feeney AJ, Cooper MD. 2006b. Transcription factor Pax5 (BSAP) transactivates the RAG-mediated V(H)-to-DJ(H) rearrangement of immunoglobulin genes. *Nat Immunol* **7**: 616–624.

Zhao H, Sifakis EG, Sumida N, Millán-Ariño L, Scholz BA, Svensson JP, Chen X, Ronnegren AL, de Lima CDM, Varnoosfaderani FS, et al. 2015. PARP1- and CTCF-Mediated Interactions between Active and Repressed Chromatin at the Lamina Promote Oscillating Transcription. *Molecular Cell* **59**: 984–997.

Zhao Z, Tavoosidana G, Sjölinder M, Göndör A, Mariano P, Wang S, Kanduri C, Lezcano M, Sandhu KS, Singh U, et al. 2006. Circular chromosome conformation capture (4C) uncovers extensive networks of epigenetically regulated intra- and interchromosomal interactions. *Nat Genet* **38**: 1341–1347.

Zhou J, Ermakova OV, Riblet R, Birshtein BK, Schildkraut CL. 2002. Replication and subnuclear location dynamics of the immunoglobulin heavy-chain locus in B-lineage cells. *Molecular and Cellular Biology* **22**: 4876–4889.

Zhuang Y. 1994. The helix-loop-helix gene E2A is required for B cell formation. *Cell* **79**: 875–884.

Zuin J, Dixon JR, van der Reijden MIJA, Ye Z, Kolovos P, Brouwer RWW, van de Corput, M. P. C., van de Werken HJG, Knoch TA, van IJcken WFJ, et al. 2014. Cohesin and CTCF differentially affect chromatin architecture and gene expression in human cells. *Proc Nat Acad Sci USA* **111**.

Appendix A

0.5Mb bins (column 1) significantly interacting (z-score > 3.5, column 2) with the viewpoint (green bar). All genes present in each bin are listed (column 3)

trans interactions from Igh viewpoint in Rag-/- pro-B		
bin	**z-score**	**genes in bin**
chr4:44500001-45000000	15.33	Gm19980 Pax5 AL772319.1 Gm12462 Zcchc7 AL805896.1 Gm12678 Gm12493 Gm12679 Grhpr
chr11:44500001-45000000	13.77	Ebf1 Gm12159 Gm12160
chr16:92500001-93000000	12.72	Clic6 Runx1 Gm16801
chr8:129000001-129500000	12.45	AC118255.1 Gm16983 Irf2bp2 Tomm20 SNORA14 Rbm34
chr16:93000001-93500000	12.26	Mir802
chr3:52000001-52500000	11.46	Foxo1 RP24-337A16.1 Gm10293
chr13:112500001-113000000	10.29	Mier3 Gm15287 Map3k1 Gm15327 Gm15325 Gm15324 Gm15326 Gm15322 Gm15323
chr5:136500001-137000000	9.58	Dtx2 Upk3b 2310043J07Rik Rasa4 U12 Gm15701 Polr2j Lrwd1 Alkbh4 Orai2 Prkrip1 Sh2b2 Cux1 Gm16599
chr10:118000001-118500000	9.56	Dyrk2 4932442E05Rik
chr9:61000001-61500000	8.75	Gm10655 Tle3
chr1:38500001-39000000	8.72	Aff3 Lonrf2 Chst10 Nms
chr2:166000001-166500000	8.58	5S_rRNA Gm11466 Gm11467 Gm11468 Gm14268 5031425F14Rik Gm14267 Prex1 AL732357.1
chr6:99000001-99500000	8.45	Foxp1 Eif4e3 AC152987.1
chr5:149500001-150000000	8.42	2210417A02Rik n-R5s179 4930505K14Rik Gm15407 Katnal1 Gm15410 Gm15406 8430423G03Rik 1810059H22Rik Gm15409 Gm15411 Gm15408 Hmgb1 5730422E09Rik AC122546.2 Uspl1
chr16:94500001-95000000	8.21	Hlcs Ripply3 Pigp Ttc3 U1 Dscr3 Dyrk1a Kcnj6
chr16:95500001-96000000	8.11	Kcnj15 Erg Ets2
chr5:137000001-137500000	7.87	Cux1 4731417B20Rik Myl10 Emid2 RP24-498F17.1 Rabl5 4933404O12Rik Fis1 Cldn15 Znhit1 Plod3 Mir702
chr6:120500001-121000000	7.85	Cecr2 Slc25a18 Atp6v1e1 Bcl2l13 Bid Mical3 Mical3
chr8:125000001-125500000	7.72	Gm20388 Ctu2 Fam38a U6 Cdt1 Aprt Galns Trappc2l Pabpn1l Cbfa2t3 Gm10612 Acsf3 Gm16378 Cdh15 Ankrd11
chr1:38000001-38500000	7.64	Gm15457 Lyg1 7SK Txndc9 Eif5b Rev1 Aff3 Gm16150 Gm16151 Gm16152
chr4:149500001-150000000	7.63	Slc2a5 Slc2a7 Car6 Eno1 Rere U6 Gm13091
chr11:117500001-118000000	7.55	Tnrc6c Tmc6 Tmc8 Gm11723 Gm11724 6030468B19Rik Syngr2 Afmid Tk1 Birc5 Cldn27 Tha1 Gm11725 Socs3 Pgs1 Dnahc17 Gm11738 Cyth1
chr19:58000001-58500000	7.52	Atrnl1 Gm16277 Gfra1
chr15:80500001-81000000	7.22	Fam83f Tnrc6b AC125540.1 Adsl Sgsm3 Mkl1 U4
chr4:134500001-135000000	7.21	Gm16225 Runx3 Gm16224 Clic4 Gm12984 Srrm1 A330049M08Rik Rcan3 Mir700 Gm15979
chr13:37500001-38000000	7.13	Ly86 Rreb1
chr4:149000001-149500000	7.04	Clstn1 Pik3cd Tmem201 Slc25a33 Gm13068 Gm16188 Gm13073 n-R5s193 snoZ178 Spsb1 Gm13070 H6pd Gm13067 Mir34a Gpr157 Gm13093 Slc2a5
chr3:130500001-131000000	7.02	SNORA61 AC114668.1 Lef1 Hadh Cyp2u1
chr11:77000001-77500000	7.01	Efcab5 Ssh2 SNORD86 Ssh2 Coro6 Ankrd13b 2210008F06Rik Git1 Trp53i13 Abhd15 Gm10392 Taok1 SNORA17 Nufip2
chr4:133000001-133500000	6.97	Gm13257 Fam46b Trnp1 1810019J16Rik Gm17688 Nudc Nr0b2 Gpatch3 Gpn2 Sfn Zdhhc18 BX537327.1 Pigv Arid1a U4 Gm12974 Rps6ka1 Gm17623 Gm12977 U6
chr11:78500001-79000000	6.95	Nlk Fam58b AL591376.1 U6 1810012P15Rik Nos2 Lgals9 Ksr1 Gm11201
chr17:86500001-87000000	6.92	Srbd1 Prkce Gm10309
chr3:136000001-136500000	6.75	Ppp3ca
chr15:80000001-80500000	6.60	Mgat3 Smcr7l Atf4 Rps19bp1 Cacna1i Enthd1 SNORA17 Grap2
chr9:116000001-116500000	6.56	Tgfbr2 AC131777.1 Rbms3
chr13:52000001-52500000	6.53	Gm16767
chr8:125500001-126000000	6.49	Gm20388 Ankrd11 U6 Spg7 Rpl13 Snord68 Cpne7 Sult5a1 Dpep1 Chmp1a 4732415M23Rik Cdk10 Spata2L 4933417D19Rik 1300018I17Rik Zfp276 AC155810.1 Fanca Spire2 Tcf25 AC122266.1 Mc1r Tubb3 Def8 SNORA63
chr6:129000001-129500000	6.48	Klrb1f Clec2e Klrb1-ps1 U7 Clec2d 2310001H17Rik Cd69 4922502D21Rik Clec12a Clec12b Clec1a Clec1b Clec9a Clec7a Olr1 D630042F21Rik 1700101I11Rik Gabarapl1
chr4:134000001-134500000	6.43	1700021N21Rik Stmn1 AL669982.1 Paqr7 2610002D18Rik Fam54b Sepn1 Man1c1 Ldlrap1 AL645531.1 Tmem57 Rhd Tmem50a D4Wsu53e Syf2
chr11:118000001-118500000	6.40	Cyth1 U6 Usp36 Timp2 BC100451 Lgals3bp Cant1 C1qtnf1 Gm11747 Gm11748 Engase Rbfox3
chr1:182000001-182500000	6.37	Cdc42bpa Adck3 Psen2 Gm5069 Itpkb 6330403A02Rik Parp1
chr8:123000001-123500000	6.35	Gse1 Gins2 Cox4nb Cox4i1 7SK Irf8
chr1:179000001-179500000	6.33	Akt3 Gm17407 Zfp238
chr9:66000001-66500000	6.31	Dapk2 Herc1 U6 Fbxl22 Usp3 Gm15563
chr17:29000001-29500000	6.31	Pnpla1 4930539E08Rik 1700030A11Rik Gm16191 Pxt1 Kctd20 Stk38 U2 Gm16196 Gm16195 Srsf3 Gm16197 Cdkn1a Gm16194 Rab44 Cpne5 Ppil1 BC004004 Pi16 Mtch1 Fgd2
chr6:87000001-87500000	6.21	Gfpt1 D6Ertd527e Antxr1 n-R5s164 Gkn1 Gkn2 Gkn3 Bmp10 Arhgap25
chr13:102500001-103000000	6.21	Pik3r1 7SK

chr19:33000001-33500000	6.17	7SK Rnls Gm7237
chr9:121500001-122000000	6.10	Lyzl4 4930596M17Rik Vipr1 Sec22c Deb1 Nktr E530011L22Rik Zfp651 Kbtbd5 Hhatl Ccdc13 Gm17163 Higd1a Ccbp2 Cyp8b1 1700048O20Rik Fam198a C85492
chr11:86000001-86500000	6.06	Brip1 4632419I22Rik Ints2 Med13 U3 Y_RNA 5S_rRNA U6 Rnft1 Rps6kb1 Tubd1 Vmp1 Mir21 Ptrh2
chr7:139500001-140000000	6.05	Fgfr2 Chst15 Oat Nkx1-2 Gm16764 Lhpp Gm15582 Fam53b
chr11:86500001-87000000	5.94	Ptrh2 Cltc Dhx40 AL596111.1 Ypel2 SCARNA3 Gdpd1 Gm11479 1200011M11Rik Prr11 Fam33a Mir301 Gm11491 Trim37
chr17:30000001-30500000	5.94	Mdga1 Gm16758 SNORA70 Zfand3 Btbd9 U6
chr4:135500001-136000000	5.93	Hmgcl Gale Lypla2 1110049F12Rik Tceb3 Gm13008 AL672076.1 Rpl11 BX530725.1 U6 Id3 E2f2 Asap3 Tcea3 Zfp46 Hnrnpr 2610528B01Rik 9130020K20Rik Gm17388 Htr1d
chr14:122000001-122500000	5.89	Dock9 Ubac2 Gpr18 Gpr183 Timm8a2
chr9:61500001-62000000	5.86	Rplp1 Kif23 Paqr5 7SK Glce AC123610.1
chr1:133500001-134000000	5.75	Avpr1b Ctse 5430435G22Rik Slc26a9 Pm20d1 AC161805.1 Slc41a1 Rab7l1 Nucks1 Slc45a3 Elk4 Mfsd4 Gm17288 U6
chr1:166500001-167000000	5.70	Dpt Xcl1 AC133891.1
chr11:100500001-101000000	5.69	Zfp385c Gm11547 Dhx58 Kat2a Hspb9 Rab5c Kcnh4 Hcrt Ghdc 7SK Stat5b Stat5a Stat3 Ptrf Atp6v0a1 Naglu Hsd17b1 Coasy Mlx Psmc3ip Fam134c Tubg1
chr7:108000001-108500000	5.68	Relt Arhgef17 AC150744.1 P2ry6 P2ry2 Fchsd2 Atg16l2 Stard10 RP24-126J17.2 Arap1
chr2:167500001-168000000	5.64	Tmem189 Cebpb A530013C23Rik Gm14321 9230111E07Rik 1200007C13Rik Gm14319 Ptpn1 Fam65c Gm14236 AL831766.1 Pard6b Gm14235 E130018N17Rik
chr17:84500001-85000000	5.61	Zfp36l2 Thada U6 U6 Plekhh2
chr16:24000001-24500000	5.55	1110054M08Rik Lpp U7
chr1:193000001-193500000	5.41	Atf3 7SK D730003I15Rik Nenf Tmem206 Ppp2r5a Dtl Ints7
chr6:87500001-88000000	5.34	Prokr1 Aplf E230015B07Rik 1810020O05Rik AC158626.1 Ccdc48 Gm5879 Gp9 Rab43 Isy1 Cnbp Copg Gm16723 8430410A17Rik H1fx Gm5577 Rab7
chr3:103500001-104000000	5.32	Gm16520 BC027582 Olfml3 Gm10964 Hipk1 Gm15886 Dclre1b Gm15471 Ap4b1 Bcl2l15 Ptpn22 Gm15472 Rsbn1 A130049A11Rik Phtf1 Magi3 U6
chr9:118500001-119000000	5.30	Itga9 Gm2415 Gm16295 Ctdspl Mir26a-1 Vill Plcd1
chr4:133500001-134000000	5.28	Hmgn2 Dhdds Lin28a Gm13061 Gm13060 Aim1l Cd52 Ubxn11 Sh3bgrl3 Ccdc21 Gm17345 Gm7534 Catsper4 Cnksr1 Zfp593 E130218I03Rik Grrp1 Pdik1l Trim63 Slc30a2 Extl1 Pafah2
chr16:32000001-32500000	5.28	Senp5 Pak2 SNORA17 Pigx 1500031L02Rik Gm15729 Lrrc33 Bex6 Fbxo45 SNORA79 Wdr53 Mir1946a 2310010M20Rik Rnf168 AC087556.1 Ubxn7 Tm4sf19 Tctex1d2 Pcyt1a Osta Zdhhc19
chr2:166500001-167000000	5.23	Prex1 7SK U6 Trp53rk Arfgef2 Cse1l Gm17096 Stau1 Ddx27 Znfx1 1500012F01Rik SNORD12 SNORD12 Snord12 Gm14290 Kcnb1
chr11:120000001-120500000	5.17	Slc38a10 Gm11769 2810410L24Rik Gm11770 2900052L18Rik Bahcc1 Gm11772 Actg1 AL669855.1 0610009L18Rik Fscn2 2310003H01Rik Nploc4 Tspan10 Pde6g 1810049H13Rik Ccdc137 Arl16 Hgs Mrpl12 Gm16755 Gm11788 Slc25a10 Gm11789 Gcgr Fam195b Dysfip1 P4hb Arhgdia Thoc4 Anapc11 Npb Pcyt2 Sirt7 Mafg Gm17586 Pycr1
chr1:89500001-90000000	5.15	Inpp5d Atg16l1 SCARNA6 Scarna6 5830472F04Rik Sag Dgkd Usp40 AC087801.1 Ugt1a10 RP23-324B17.1 Ugt1a9 Ugt1a8 Ugt1a7c Ugt1a6a Ugt1a6b
chr17:29500001-30000000	5.12	Fgd2 Gm16912 Pim1 Gm17657 Tmem217 Tbc1d22b Ftsjd2 AC163629.1 0610038L08Rik Rnf8 1110021J02Rik Mdga1
chr18:68000001-68500000	5.10	Cep192 D18Ertd653e 4933403F05Rik Rnmt Mc5r
chr6:145500001-146000000	5.06	Ifltd1 Tuba3b Gm15704 Rassf8 Rassf8 Bhlhe41 Sspn Gm15705
chr4:132500001-133000000	5.05	Fgr Ahdc1 Gm10151 Wasf2 7SK Gpr3 Cd164l2 Map3k6 Sytl1 Tmem222 Wdtc1 Slc9a1 AL671882.1
chr8:127500001-128000000	5.01	Tsnax Disc1 AL672234.1 Gm16237 Sipa1l2
chr7:121500001-122000000	4.96	4933406I18Rik Pde3b Cyp2r1 Calca Gm15500 Calcb Insc SNORA17
chr17:31000001-31500000	4.95	Dnahc8 Glp1r Umodl1 AC165951.1 Abcg1 5S_rRNA Tff3 Tff2 Gm15318 Tff1 Tmprss3 Ubash3a Rsph1 Slc37a1
chr1:173500001-174000000	4.93	Cd244 Ly9 Slamf7 Cd48 U6 U6 Slamf1 Cd84 Gm10521 Slamf6 Vangl2 Nhlh1 Ncstn
chr4:135000001-135500000	4.88	Nipal3 4930555I21Rik AL670720.1 Grhl3 U6 1700029M20Rik Il28ra Il22ra1 9130219A07Rik Myom3 Srsf10 Pnrc2 Cnr2 Fuca1
chr13:54000001-54500000	4.87	Drd1a Sfxn1 Hrh2 Gm16578 Cplx2
chr17:32000001-32500000	4.86	Hsf2bp 7SK Rrp1b Pdxk-ps Gm17276 Notch3 Ephx3 Brd4 Gm17549 Akap8 Akap8l Wiz
chr11:116000001-116500000	4.86	Mrpl38 Fbf1 SCARNA4 Acox1 2310004N24Rik Cdk3-ps Evpl Srp68 Galr2 Exoc7 Gm16831 n-R5s74 Foxj1 Rnf157 Fam100b Qrich2 Gm11739 Prpsap1 Sphk1 Ube2o Aanat Rhbdf2
chr3:51500001-52000000	4.83	Maml3 AC116729.1 n-R5s196
chr10:94500001-95000000	4.80	Cradd Socs2 5730420D15Rik Mrpl42 Ube2n
chr3:135500001-136000000	4.79	Slc39a8 Bank1
chr6:145000001-145500000	4.77	Bcat1 Gm15687 Lrmp Casc1 Gm15543 Lyrm5 Kras Gm15706 7SK 2010013B24Rik Ifltd1 SNORA17 1700073E17Rik Gm15499 SNORA17
chr13:41500001-42000000	4.73	Nedd9 AC154848.1 Tmem170b Gm5082 9530008L14Rik 1700061E18Rik U6
chr16:30000001-30500000	4.72	4632428C04Rik Hes1 n-R5s32 Gm17516 Cpn2 Lrrc15 Gp5 Atp13a3
chr16:33500001-34000000	4.71	Zfp148 Slc12a8 Heg1 Gm15658 Gm15657 Muc13 Itgb5 Umps Gm15829 Kalrn
chr16:32500001-33000000	4.68	Zdhhc19 Tfrc Tnk2 Gm10818 Muc4 Muc20 1700021K19Rik Fyttd1 Lrch3 Gm17106
chr6:128500001-129000000	4.67	BC048546 Klrb1a Gm5884 Clec2j Clec2h Klrb1 Klrb1c Klrb1b Gm17395 BC035044 Clec2i Clec2g Gm15987 BC064078 Klrb1f
chr17:87000001-87500000	4.66	Prkce U6 Epas1 1700090G07Rik Atp6v1e2 Rhoq Pigf Cript SNORA40
chr4:132000001-132500000	4.65	Med18 snoU13 Sesn2 Gm12981 Atpif1 Gm12999 Dnajc8 U6 Ptafr Eya3 Xkr8 Smpdl3b Rpa2 BC013712 Ppp1r8 SCARNA1 Stx12 Fam76a U6
chr13:102000001-102500000	4.59	Pik3r1 Gm11016
chr10:92500001-93000000	4.53	4930485B16Rik Cdk17 Mir1931 Elk3 Lta4h Hal Amdhd1

chr14:65000001-65500000	4.43	Msra A930011O12Rik Mir124a-1 AC134898.1 Kif13b SNORA36 Hmbox1
chr1:166000001-166500000	4.35	Sell Selp Gm16587 Gm16548 F5 Slc19a2 4930455F23Rik Blzf1 Nme7 Atp1b1 Gm16608
chr13:103000001-103500000	4.29	Cd180
chr16:96500001-97000000	4.26	B3galt5 Igsf5 Itgb2l Pcp4 Dscam
chr16:91000001-91500000	4.10	Synj1 4930404I05Rik Gcfc1 4931406G06Rik 4932438H23Rik Gm9881 Olig2 Olig1 Gm15966 U4 Ifnar2 Il10rb A930006K02Rik Ifnar1
chr16:30500001-31000000	4.09	Tmem44 Lsg1 Fam43a U6 SNORA17 AI480653 Gm15742
chr9:122000001-122500000	4.08	Snrk Ano10 Gm10606 Abhd5 9530059O14Rik
chr7:106000001-106500000	4.05	Wnt11 Uvrag SNORA17 Dgat2 Mogat2 Gm16890 Mtap6 Serpinh1
chr2:163000001-163500000	3.97	Tox2 Jph2 3230401D17Rik Gdap1l1 Fitm2 2310001K24Rik R3hdml 0610008F07Rik Hnf4a U6 Ttpal Serinc3 0610039K10Rik Pkig

trans interactions from Igh viewpoint in Rag/81X pre-B

bin	z-score	genes in bin
chr4:32000001-32500000	19.82	Map3k7 U4 Bach2 D130062J21Rik Gm11932
chr4:32500001-33000000	18.89	Bach2 7SK BC024582 Gja10 Casp8ap2 Mdn1 Lyrm2 Ankrd6
chr11:44500001-45000000	17.25	Ebf1 Gm12159 Gm12160
chr11:45000001-45500000	13.28	Gm12160 Gm12162 SNORA17
chr4:44500001-45000000	12.11	Gm19980 Pax5 AL772319.1 Gm12462 Zcchc7 AL805896.1 Gm12678 Gm12493 Gm12679 Grhpr
chr1:38500001-39000000	10.47	Aff3 Lonrf2 Chst10 Nms
chr1:38000001-38500000	10.30	Gm15457 Lyg1 7SK Txndc9 Eif5b Rev1 Aff3 Gm16150 Gm16151 Gm16152
chr6:99000001-99500000	8.68	Foxp1 Eif4e3 AC152987.1
chr16:92500001-93000000	8.29	Clic6 Runx1 Gm16801
chr3:52000001-52500000	8.07	Foxo1 RP24-337A16.1 Gm10293
chr16:93000001-93500000	7.91	Mir802
chr16:95500001-96000000	7.18	Kcnj15 Erg Ets2
chr4:33000001-33500000	7.04	Ankrd6 Rragd 4933421O10Rik Ube2j1 Gabrr2 Gabrr1 Pm20d2 Srsf12 Pnrc1 Gm11934 AL772272.1 Rngtt
chr1:166500001-167000000	6.89	Dpt Xcl1 AC133891.1
chr5:136500001-137000000	6.80	Dtx2 Upk3b 2310043J07Rik Rasa4 U12 Gm15701 Polr2j Lrwd1 Alkbh4 Orai2 Prkrip1 Sh2b2 Cux1 Gm16599
chr5:137000001-137500000	6.69	Cux1 4731417B20Rik Myl10 Emid2 RP24-498F17.1 Rabl5 4933404O12Rik Fis1 Cldn15 Znhit1 Plod3 Mir702
chr16:94500001-95000000	6.48	Hlcs Ripply3 Pigp Ttc3 U1 Dscr3 Dyrk1a Kcnj6
chr13:112500001-113000000	6.32	Mier3 Gm15287 Map3k1 Gm15327 Gm15325 Gm15324 Gm15326 Gm15322 Gm15323
chr11:44000001-44500000	5.85	Gm12154 Il12b Ublcp1 AL669944.1 Rnf145 4930597A21Rik Ebf1 Gm12158
chr6:68500001-69000000	5.74	Igkv12-98 Gm16637 Igkv10-96 Igkv10-95 Igkv10-94 Igkv19-93 Igkv4-92 Igkv4-91 Igkv4-90 Igkv12-89 Igkv1-88 Gm11145 Igkv4-86 Igkv13-84 Igkv4-81 Igkv4-80 Igkv4-79
chr2:45000001-45500000	5.67	Gm13479
chr18:55000001-55500000	5.59	Zfp608 Gm17270 Gm4221 SNORA40 U6
chr16:91500001-92000000	5.52	Ifnar1 Ifngr2 Tmem50b Gm15964 Dnajc28 Gart Son Donson Atp5o Gm10785 Cryzl1 Itsn1 U6 Gm15976 D430001F17Rik
chr16:19000001-19500000	5.51	Iglc3 Iglv1 Iglc2 Iglv3 Iglv2 Olfr164 SNORA17 AC112681.1 Olfr165 SNORA17 Olfr166
chr11:45500001-46000000	5.51	F630206G17Rik AL645948.1 Clint1 Lsm11 Thg1l Sox30 Gm12166 Adam19 Gm16033 Gm16034 Nipal4
chr1:37500001-38000000	5.36	Mgat4a 2010300C02Rik 4930556I23Rik Tsga10 Gm17715 Lipt1 Mitd1 Mrpl30 Lyg2 Gm15457
chr8:125000001-125500000	5.32	Gm20388 Ctu2 Fam38a U6 Cdt1 Aprt Galns Trappc2l Pabpn1l Cbfa2t3 Gm10612 Acsf3 Gm16378 Cdh15 Ankrd11
chr6:87000001-87500000	5.30	Gfpt1 D6Ertd527e Antxr1 n-R5s164 Gkn1 Gkn2 Gkn3 Bmp10 Arhgap25
chr6:128500001-129000000	5.28	BC048546 Klrb1a Gm5884 Clec2j Clec2h Klrb1 Klrb1c Klrb1b Gm17395 BC035044 Clec2i Clec2g Gm15987 BC064078 Klrb1f
chr5:149500001-150000000	5.23	2210417A02Rik n-R5s179 4930505K14Rik Gm15407 Katnal1 Gm15410 Gm15406 8430423G03Rik 1810059H22Rik Gm15409 Gm15411 Gm15408 Hmgb1 5730422E09Rik AC122546.2 Uspl1
chr8:129000001-129500000	5.21	AC118255.1 Gm16983 Irf2bp2 Tomm20 SNORA14 Rbm34
chr16:93500001-94000000	5.20	Setd4 Cbr1 7SK Cbr3 Dopey2 2310043M15Rik Morc3 Chaf1b Cldn14
chr7:139500001-140000000	5.19	Fgfr2 Chst15 Oat Nkx1-2 Gm16764 Lhpp Gm15582 Fam53b
chr10:118000001-118500000	5.17	Dyrk2 4932442E05Rik
chr1:136500001-137000000	5.13	Kdm5b Gm3834 Syt2 Ppp1r12b AC131591.1 Ube2t Lgr6
chr13:102500001-103000000	5.03	Pik3r1 7SK
chr17:86500001-87000000	5.01	Srbd1 Prkce Gm10309
chr4:134500001-135000000	4.97	Gm16225 Runx3 Gm16224 Clic4 Gm12984 Srrm1 A330049M08Rik Rcan3 Mir700 Gm15979
chr6:145500001-146000000	4.97	Ifltd1 Tuba3b Gm15704 Rassf8 Rassf8 Bhlhe41 Sspn Gm15705
chr15:80500001-81000000	4.92	Fam83f Tnrc6b AC125540.1 Adsl Sgsm3 Mkl1 U4
chr1:173500001-174000000	4.89	Cd244 Ly9 Slamf7 Cd48 U6 U6 Slamf1 Cd84 Gm10521 Slamf6 Vangl2 Nhlh1 Ncstn
chr17:30000001-30500000	4.83	Mdga1 Gm16758 SNORA70 Zfand3 Btbd9 U6
chr13:44000001-44500000	4.81	Gm5083
chr16:96000001-96500000	4.80	2810404F17Rik 1600002D24Rik Gm15340 Psmg1 Brwd1 Gm15342 1700093J21Rik Gm15341 Hmgn1 Wrb Gm15317 Lca5l Sh3bgr B3galt5
chr6:69000001-69500000	4.78	Igkv4-78 Igkv4-74 Igkv4-73 Igkv4-72 Igkv4-71 Igkv4-70 Igkv4-69 Igkv4-68 RNaseP_nuc Igkv4-63 Igkv4-62 Igkv4-61 Igkv4-59 Igkv4-58 AC156953.1 Igkv4-57-1
chr9:70500001-71000000	4.75	Fam63b Gm10642 Adam10 Lipc CT025701.1 Gm3436 Aqp9
chr13:103500001-104000000	4.75	Cd180 Mast4 1700099I09Rik 1700099I09Rik Gm17160
chr13:41500001-42000000	4.74	Nedd9 AC154848.1 Tmem170b Gm5082 9530008L14Rik 1700061E18Rik U6
chr3:136000001-136500000	4.73	Ppp3ca

chr13:93000001-93500000	4.73	Msh3 Dhfr C030017D09Rik Ankrd34b Fam151b Zfyve16 Spz1 Serinc5
chr4:149500001-150000000	4.69	Slc2a5 Slc2a7 Car6 Eno1 Rere U6 Gm13091
chr16:32000001-32500000	4.69	Senp5 Pak2 SNORA17 Pigx 1500031L02Rik Gm15729 Lrrc33 Bex6 Fbxo45 SNORA79 Wdr53 Mir1946a 2310010M20Rik Rnf168 AC087556.1 Ubxn7 Tm4sf19 Tctex1d2 Pcyt1a Osta Zdhhc19
chr13:103000001-103500000	4.66	Cd180
chr11:86000001-86500000	4.66	Brip1 4632419I22Rik Ints2 Med13 U3 Y_RNA 5S_rRNA U6 Rnft1 Rps6kb1 Tubd1 Vmp1 Mir21 Ptrh2
chr2:167500001-168000000	4.62	Tmem189 Cebpb A530013C23Rik Gm14321 9230111E07Rik 1200007C13Rik Gm14319 Ptpn1 Fam65c Gm14236 AL831766.1 Pard6b Gm14235 E130018N17Rik
chr4:59000001-59500000	4.56	Dnajc25 Gm20503 Gng10 AI481877 Gm12594 Ugcg Gm12596 Susd1 Rod1
chr4:45000001-45500000	4.55	Grhpr Zbtb5 1700055D18Rik Polr1e Fbxo10 Tomm5 Gm10982 Frmpd1 2900093L17Rik Rg9mtd3 Exosc3 Dcaf10 Mcart1 AL772376.2 Mcart1 Shb
chr18:54500001-55000000	4.53	9430076G02Rik
chr1:133500001-134000000	4.52	Avpr1b Ctse 5430435G22Rik Slc26a9 Pm20d1 AC161805.1 Slc41a1 Rab7l1 Nucks1 Slc45a3 Elk4 Mfsd4 Gm17288 U6
chr14:122000001-122500000	4.51	Dock9 Ubac2 Gpr18 Gpr183 Timm8a2
chr4:149000001-149500000	4.50	Clstn1 Pik3cd Tmem201 Slc25a33 Gm13068 Gm16188 Gm13073 n-R5s193 snoZ178 Spsb1 Gm13070 H6pd Gm13067 Mir34a Gpr157 Gm13093 Slc2a5
chr4:45500001-46000000	4.49	Shb AL772376.1 U6 Gm12408 Gm829 Gm12410 Gm12409 Aldh1b1 Igfbpl1 1300002K09Rik E230008N13Rik Tdrd7
chr3:143500001-144000000	4.44	Lmo4
chr6:120500001-121000000	4.43	Cecr2 Slc25a18 Atp6v1e1 Bcl2l13 Bid Mical3 Mical3
chr16:33500001-34000000	4.43	Zfp148 Slc12a8 Heg1 Gm15658 Gm15657 Muc13 Itgb5 Umps Gm15829 Kalrn
chr16:30500001-31000000	4.43	Tmem44 Lsg1 Fam43a U6 SNORA17 AI480653 Gm15742
chr1:193000001-193500000	4.42	Atf3 7SK D730003I15Rik Nenf Tmem206 Ppp2r5a Dtl Ints7
chr17:4500001-5000000	4.41	U6 Arid1b
chr2:166000001-166500000	4.38	Prex1
chr13:44500001-45000000	4.37	Jarid2 SNORA61
chr13:93500001-94000000	4.37	Thbs4 Mtx3 Cmya5 Papd4
chr6:70500001-71000000	4.36	Igkv3-10 Igkv3-9 Igkv3-7 Gm16774 Igkv3-4 Igkv3-3 Igkv3-2 Igkv3-1 Igkj1 Igkj2 Igkj3 Igkj4 Igkj5 Igkc Rpia Eif2ak3 SNORA5 1700011F03Rik Foxi3 U1
chr9:66000001-66500000	4.36	Dapk2 Herc1 U6 Fbxl22 Usp3 Gm15563
chr3:95500001-96000000	4.35	Ecm1 Tars2 Rprd2 U1 Prpf3 Gm16884 Mrps21 C920021L13Rik Gm129 BC028528 Aph1a Car14 Anp32e Plekho1 Vps45 Otud7b Mtmr11 Gm17690 Sf3b4 SNORA19 Sv2a
chr1:156500001-157000000	4.34	Cacna1e Gm9530 Ier5 Mr1
chr15:81000001-81500000	4.32	Mkl1 4930483J18Rik Mchr1 Slc25a17 St13 Xpnpep3 Dnajb7 Gm17025 Rbx1 Gm5218 Ep300 AC160528.1 U6 L3mbtl2
chr15:80000001-80500000	4.31	Mgat3 Smcr7l Atf4 Rps19bp1 Cacna1i Enthd1 SNORA17 Grap2
chr19:58000001-58500000	4.31	Atrnl1 Gm16277 Gfra1
chr16:32500001-33000000	4.31	Zdhhc19 Tfrc Tnk2 Gm10818 Muc4 Muc20 1700021K19Rik Fyttd1 Lrch3 Gm17106
chr11:117500001-118000000	4.30	Tnrc6c Tmc6 Tmc8 Gm11723 Gm11724 6030468B19Rik Syngr2 Afmid Tk1 Birc5 Cldn27 Tha1 Gm11725 Socs3 Pgs1 Dnahc17 Gm11738 Cyth1
chr14:62500001-63000000	4.29	Dleu7 Rnaseh2b
chr6:146000001-146500000	4.29	Itpr2 Gm17706 4933424B01Rik
chr4:133000001-133500000	4.27	Gm13257 Fam46b Trnp1 1810019J16Rik Gm17688 Nudc Nr0b2 Gpatch3 Gpn2 Sfn Zdhhc18 BX537327.1 Pigv Arid1a U4 Gm12974 Rps6ka1 Gm17623 Gm12977 U6
chr6:129000001-129500000	4.26	Klrb1f Clec2e Klrb1-ps1 U7 Clec2d 2310001H17Rik Cd69 4922502D21Rik Clec12a Clec12b Clec1a Clec1b Clec9a Clec7a Olr1 D630042F21Rik 1700101I11Rik Gabarapl1
chr11:77000001-77500000	4.25	Efcab5 Ssh2 SNORD86 Ssh2 Coro6 Ankrd13b 2210008F06Rik Git1 Trp53i13 Abhd15 Gm10392 Taok1 SNORA17 Nufip2
chr9:116000001-116500000	4.24	Tgfbr2 AC131777.1 Rbms3
chr7:135000001-135500000	4.24	AC149222.1 Zfp668 Zfp646 Prss53 Vkorc1 Bckdk Myst1 Prss8 Prss36 Fus Gm17468 B230325K18Rik Pycard Gm15533 Trim72 U1 Itgam Itgax Itgad Cox6a2 9130023H24Rik Armc5 Tgfb1i1 Slc5a2 BC017158 AC124566.1
chr17:84500001-85000000	4.23	Zfp36l2 Thada U6 U6 Plekhh2
chr14:77000001-77500000	4.21	9030625A04Rik Ccdc122
chr10:117000001-117500000	4.18	Cpm U6 Mdm2 Slc35e3 Nup107 Rap1b
chr16:91000001-91500000	4.16	Synj1 4930404I05Rik Gcfc1 4931406G06Rik 4932438H23Rik Gm9881 Olig2 Olig1 Gm15966 U4 Ifnar2 Il10rb A930006K02Rik Ifnar1
chr18:35500001-36000000	4.10	Sil1 Gm5239 Snhg4 SNORA74 Snora74a Matr3 Paip2 Slc23a1 2010001M09Rik Gm1614 Spata24 Dnajc18 1700066B19Rik Ecscr Tmem173 Gm16490 Ube2d2 Cxxc5
chr6:68000001-68500000	4.09	Igkv9-120 Igkv1-117 Igkv2-116 Igkv1-115 Igkv2-112 Igkv14-111 SNORA17 Igkv1-110 Igkv2-109 Igkv16-104 Igkv15-103 Igkv14-100 SNORA17 Igkv1-99
chr16:24000001-24500000	4.07	1110054M08Rik Lpp U7
chr16:30000001-30500000	4.06	4632428C04Rik Hes1 n-R5s32 Gm17516 Cpn2 Lrrc15 Gp5 Atp13a3
chr6:52500001-53000000	4.05	Hibadh SNORA32 Tax1bp1 Jazf1 SCARNA20
chr16:20000001-20500000	4.05	Klhl24 Yeats2 Map6d1 Parl Cyp2ab1 Abcc5 7SK Eif2b5
chr6:145000001-145500000	4.04	Bcat1 Gm15687 Lrmp Casc1 Gm15543 Lyrm5 Kras Gm15706 7SK 2010013B24Rik Ifltd1 SNORA17 1700073E17Rik Gm15499 SNORA17
chr4:134000001-134500000	4.04	1700021N21Rik Stmn1 AL669982.1 Paqr7 2610002D18Rik Fam54b Sepn1 Man1c1 Ldlrap1 AL645531.1 Tmem57 Rhd Tmem50a D4Wsu53e Syf2
chr7:108000001-108500000	4.03	Relt Arhgef17 AC150744.1 P2ry6 P2ry2 Fchsd2 Atg16l2 Stard10 RP24-126J17.2 Arap1
chr6:148000001-148500000	4.01	Far2 Gm16583 Ergic2 Gm17216 Tmtc1 Rps4y2
chr9:61000001-61500000	3.97	Gm10655 Tle3

chr11:118000001-118500000	3.92	Cyth1 U6 Usp36 Timp2 BC100451 Lgals3bp Cant1 C1qtnf1 Gm11747 Gm11748 Engase Rbfox3
chr1:134000001-134500000	3.91	Cdk18 Lemd1 Mir135b 1700037F24Rik Gm10188 Klhdc8a Nuak2 Tmcc2 Gm15849 Dstyk 6030442K20Rik Rbbp5 Tmem81 Cntn2 Nfasc
chr19:45500001-46000000	3.90	Btrc Gm6807 Poll Dpcd Fbxw4 Gm17018 Fgf8 Npm3 Gm15491 Mgea5 Kcnip2 9130011E15Rik
chr17:29000001-29500000	3.90	Pnpla1 4930539E08Rik 1700030A11Rik Gm16191 Pxt1 Kctd20 Stk38 U2 Gm16196 Gm16195 Srsf3 Gm16197 Cdkn1a Gm16194 Rab44 Cpne5 Ppil1 BC004004 Pi16 Mtch1 Fgd2
chr1:135000001-135500000	3.88	Pik3c2b Ppp1r15b Plekha6 Golt1a Kiss1 Ren1 Etnk2 Sox13 SNORA32
chr17:30500001-31000000	3.87	Btbd9 Gm9874 Glo1 Dnahc8 U6
chr8:123000001-123500000	3.87	Gse1 Gins2 Cox4nb Cox4i1 AC114819.1 7SK Irf8
chr4:135000001-135500000	3.86	Nipal3 4930555I21Rik AL670720.1 Grhl3 U6 1700029M20Rik Il28ra Il22ra1 9130219A07Rik Myom3 Srsf10 Pnrc2 Cnr2 Fuca1
chr6:98500001-99000000	3.85	AC158665.1 Foxp1
chr1:133000001-133500000	3.85	Dyrk3 Eif2d Rassf5 Ikbke Srgap2 AC109299.1 Fam72a Avpr1b
chr16:29500001-30000000	3.82	Atp13a4 Opa1 Gm17734 Gm16761 Gm1968
chr9:71500001-72000000	3.79	Cgnl1 Tcf12 Rpl15-ps2 U6
chr6:86500001-87000000	3.79	1600020E01Rik AC158662.1 Asprv1 Mxd1 Snrnp27 Gmcl1 Anxa4 Aak1 Nfu1 Gfpt1
chr10:116500001-117000000	3.77	Cct2 Frs2 SNORA13 Yeats4 9530003J23Rik Gm10936 Lyz2 Lyz1 Cpsf6
chr9:118500001-119000000	3.76	Itga9 Gm2415 Gm16295 Ctdspl Mir26a-1 Vill Plcd1
chr16:31000001-31500000	3.74	AI480653 Acap2 Ppp1r2 Apod Bdh1 Gm15743
chr14:79500001-80000000	3.72	1300010F03Rik Zfp957 1190002H23Rik Naa16 AC124745.1 Mtrf1 Kbtbd7 Gm5465 Wbp4 Elf1 Sugt1
chr2:30500001-31000000	3.72	9330198N18Rik Gm14486 Gm14488 AL928593.1 1700001O22Rik 4930527E20Rik Mettl11a Asb6 Prrx2 Ptges Tor1b Tor1a BC005624 Usp20 Fnbp1
chr13:113000001-113500000	3.71	Ankrd55 U2 Il6st Il31ra Ddx4 Slc38a9
chr1:179000001-179500000	3.70	Akt3 Gm17407 Zfp238
chr16:92000001-92500000	3.70	U6 Mrps6 Slc5a3 Gm16309 Gm16310 Kcne2 Fam165b Gm15980 4930563D23Rik Kcne1 Rcan1 2410124H12Rik Clic6
chr18:55500001-56000000	3.67	AC149599.1
chr7:129500001-130000000	3.67	Prkcb 7SK Cacng3
chr1:136000001-136500000	3.62	Gm8618 Chit1 Chi3l1 Mybph Adora1 U6 Myog Ppfia4 Tmem183a 4933406M09Rik Cyb5r1 Adipor1 Klhl12 Gm11092 Rabif SNORA61 4931440L10Rik Kdm5b
chr17:31500001-32000000	3.62	Pde9a Wdr4 Ndufv3 4833413E03Rik Pknox1 AC166172.1 Cbs U2af1 Cryaa Sik1
chr4:132500001-133000000	3.58	Fgr Ahdc1 Gm10151 Wasf2 7SK Gpr3 Cd164l2 Map3k6 Sytl1 Tmem222 Wdtc1 Slc9a1 AL671882.1
chr18:35000001-35500000	3.53	Reep2 Egr1 Gm17507 Etf1 Hspa9 SNORD63 SNORD63 Gm6724 Ctnna1 Lrrtm2 Sil1 AC121874.1 snoU13

trans interactions from Igh viewpoint in Thymus

bin	z-score	genes in bin
chr18:89000001-89500000	6.86	Socs6 Rttn Cd226 Dok6
chr9:112000001-112500000	5.52	Arpp21 Mir128-2 2310075C17Rik 2900079G21Rik SNORA17
chr8:130500001-131000000	5.43	Gm17350 Nrp1 Mir1903
chr17:51000001-51500000	5.23	Tbc1d5 U4
chr4:144500001-145000000	5.17	Dhrs3 Vps13d Vps13d Tnfrsf1b Tnfrsf8
chr1:179000001-179500000	5.12	Akt3 Gm17407 Zfp238
chr9:94500001-95000000	5.02	U6 Slc9a9 Gm16262
chr16:76000001-76500000	4.87	Samsn1 Gm15555 SNORA17 Nrip1 Gm9843
chr4:6500001-7000000	4.84	SNORA17 Tox Gm11802
chr16:76500001-77000000	4.84	
chr4:97500001-98000000	4.72	Nfia Y_RNA 0610025J13Rik
chr3:142000001-142500000	4.69	Pdlim5 Gbp5 Gbp7 Gbp3 Gbp1 Gbp2 Ccbl2 Gm15540 Gtf2b U6 Pkn2 SNORA17
chr6:129000001-129500000	4.63	Klrb1f Clec2e Klrb1-ps1 U7 Clec2d 2310001H17Rik Cd69 4922502D21Rik Clec12a Clec12b Clec1a Clec1b Clec9a Clec7a Olr1 D630042F21Rik 1700101I11Rik Gabarapl1
chr1:145500001-146000000	4.54	Cdc73 Glrx2 Trove2 Uchl5 snoU109 Rgs2 Rgs13
chr10:96000001-96500000	4.40	Btg1 AC152946.1
chr7:65500001-66000000	4.36	AC102205.1 Atp10a
chr8:130000001-130500000	4.35	Pard3 5S_rRNA
chr14:105500001-106000000	4.28	Rbm26 Gm17066 U6 Ndfip2 U6 4930449E01Rik 9330188P03Rik
chr5:63000001-63500000	4.27	Arap2 Gm17384
chr3:60000001-60500000	4.25	Mbnl1
chr8:84000001-84500000	4.18	Inpp4b 4930579O11Rik
chr1:178500001-179000000	4.17	U6 Cep170 Mir350 7SK Sdccag8 AC144905.1 Gm15423 Akt3
chr13:102000001-102500000	4.09	Pik3r1 Gm11016
chr10:122000001-122500000	3.88	Ppm1h Mirlet7i Mon2
chr6:143500001-144000000	3.87	1700060C16Rik Sox5 4933415D12Rik
chr16:93000001-93500000	3.86	Mir802
chr10:129500001-129993255	3.85	Olfr822 Olfr823 Olfr824 Olfr825 Olfr826 Olfr827 Neurod4 5830405N20Rik Vmn2r84 Vmn2r85 Vmn2r86 Vmn2r87
chr4:87500001-88000000	3.77	Mllt3 Gm12631 BC057079 Mir491
chr16:92500001-93000000	3.76	Clic6 Runx1 Gm16801
chr15:50500001-51000000	3.76	Trps1 mmu-mir-1907
chr2:139500001-140000000	3.75	Gm14066 Ism1 Tasp1 Esf1 Gm17374 2310003L22Rik
chr14:103500001-104000000	3.68	Mycbp2 Scel
chr3:135000001-135500000	3.68	Nhedc2 Nhedc1 Cisd2 4930539J05Rik Ube2d3 Manba Nfkb1 Gm9799 Slc39a8
chr1:97000001-97500000	3.67	Fam174a U7 St8sia4

trans interactions from Igk viewpoint in Rag-/- pro-B		
bin	z-score	genes in bin
chr19:50500001-51000000	4.94	Sorcs1 Gm16745 5S_rRNA
chr11:111500001-112000000	4.57	Gm11674 Gm11680
chr11:92500001-93000000	4.51	SNORA48 Car10
chr11:91500001-92000000	4.37	AL662785.1
chr19:48500001-49000000	3.91	Sorcs3

trans interactions from Igk viewpoint in Rag/81X pre-B		
bin	z-score	genes in bin
chr11:44500001-45000000	15.46	Ebf1 Gm12159 Gm12160
chr11:45000001-45500000	14.62	Gm12160 Gm12162 SNORA17
chr3:52000001-52500000	13.84	Foxo1 RP24-337A16.1 Gm10293
chr4:44500001-45000000	13.46	Gm19980 Pax5 AL772319.1 Gm12462 Zcchc7 AL805896.1 Gm12678 Gm12493 Gm12679 Grhpr
chr4:32000001-32500000	12.00	Map3k7 U4 Bach2 D130062J21Rik Gm11932
chr12:115500001-116000000	11.56	Ighv3-8 Ighv12-3 Ighv1-5 Ighv10-3 Ighv1-7 Ighv15-2 Ighv1-9 Ighv1-12 Gm17686 Gm16857 Gm16858 Ighv1-18 Ighv1-19 Ighv1-20 Gm16860
chr16:19000001-19500000	10.18	Iglc3 Iglv1 Iglc2 Iglv3 Iglv2 Olfr164 SNORA17 AC112681.1 Olfr165 SNORA17 Olfr166
chr9:70500001-71000000	9.16	Fam63b Gm10642 Adam10 Lipc CT025701.1 Gm3436 Aqp9
chr15:9500001-10000000	8.55	Spef2 7SK
chr1:166500001-167000000	8.34	Dpt Xcl1 AC133891.1
chr17:4500001-5000000	8.25	U6 Arid1b
chr17:29000001-29500000	8.18	Pnpla1 4930539E08Rik 1700030A11Rik Gm16191 Pxt1 Kctd20 Stk38 U2 Gm16196 Gm16195 Srsf3 Gm16197 Cdkn1a Gm16194 Rab44 Cpne5 Ppil1 BC004004 Pi16 Mtch1 Fgd2
chr4:32500001-33000000	7.97	Bach2 7SK BC024582 Gja10 Casp8ap2 Mdn1 Lyrm2 Ankrd6
chr12:114500001-115000000	7.68	Ighg2c Ighg Ighg1 Ighm Adam6b Adam6a Ighv2-4
chr13:41500001-42000000	7.67	Nedd9 AC154848.1 Tmem170b Gm5082 9530008L14Rik 1700061E18Rik U6
chr12:115000001-115500000	7.42	Ighv11-2 Ighv14-3 Ighv9-2 Ighv9-3 Ighv3-3
chr2:45000001-45500000	7.42	Gm13479
chr19:33000001-33500000	7.38	7SK Rnls Gm7237
chr13:112500001-113000000	7.14	Mier3 Gm15287 Map3k1 Gm15327 Gm15325 Gm15324 Gm15326 Gm15322 Gm15323
chr12:81000001-81500000	7.13	Zfp36l1 Gm17591 2310015A10Rik Actn1 Gm17425 Gm17373 Gm17301 Dcaf5 Scarna3b
chr18:55000001-55500000	7.12	Zfp608 Gm17270 Gm4221 SNORA40 U6
chr13:37500001-38000000	6.96	Ly86 Rreb1
chr13:44000001-44500000	6.76	Gm5083
chr17:5000001-5500000	6.76	Arid1b 5730437N04Rik AC166064.1 Zdhhc14
chr15:80500001-81000000	6.69	Fam83f Tnrc6b AC125540.1 Adsl Sgsm3 Mkl1 U4
chr8:129000001-129500000	6.66	AC118255.1 Gm16983 Irf2bp2 Tomm20 SNORA14 Rbm34
chr12:80500001-81000000	6.57	Rad51l1
chr1:38500001-39000000	6.38	Aff3 Lonrf2 Chst10 Nms
chr16:30000001-30500000	6.23	4632428C04Rik Hes1 n-R5s32 Gm17516 Cpn2 Lrrc15 Gp5 Atp13a3
chr10:20500001-21000000	6.22	Ahi1 Myb Gm16786 AC153556.1
chr1:38000001-38500000	6.10	Gm15457 Lyg1 7SK Txndc9 Eif5b Rev1 Aff3 Gm16150 Gm16151 Gm16152
chr13:24500001-25000000	6.06	Cmah U6 Fam65b Gm11346 C530050E15Rik 1700016G14Rik Gmnn BC005537 SNORA32 Acot13 Tdp2 D130043K22Rik 4932702P03Rik Aldh5a1
chr5:64500001-65000000	6.04	Pgm1 SNORA17 Tbc1d1
chr19:41000001-41500000	6.03	Blnk Dntt Opalin Tll2 Tm9sf3 Pik3ap1
chr11:86500001-87000000	6.00	Ptrh2 Cltc Dhx40 AL596111.1 Ypel2 SCARNA3 Gdpd1 Gm11479 1200011M11Rik Prr11 Fam33a Mir301 Gm11491 Trim37
chr12:116000001-116500000	5.84	Ighv1-23 Ighv1-24 Ighv1-42 Ighv1-43 Gm16966 Gm16830 Ighv8-5 Gm16829 Gm16828 AB069917 Ighv8-6 Ighv1-54 Gm16792 Gm16791
chr15:10000001-10500000	5.83	Prlr Agxt2 Dnajc21 Brix1 Rad1 Ttc23l Rai14
chr10:44000001-44500000	5.82	Atg5 Mir1929 Prdm1 U6 U6
chr5:136500001-137000000	5.76	Dtx2 Upk3b 2310043J07Rik Rasa4 U12 Gm15701 Polr2j Lrwd1 Alkbh4 Orai2 Prkrip1 Sh2b2 Cux1 Gm16599
chr16:30500001-31000000	5.75	Tmem44 Lsg1 Fam43a U6 SNORA17 AI480653 Gm15742
chr4:59000001-59500000	5.73	Dnajc25 Gm20503 Gng10 AI481877 Gm12594 Ugcg Gm12596 Susd1 Rod1
chr11:45500001-46000000	5.69	F630206G17Rik AL645948.1 Clint1 Lsm11 Thg1l Sox30 Gm12166 Adam19 Gm16033 Gm16034 Nipal4
chr19:32000001-32500000	5.69	A1cf Asah2 Sgms1 2700046G09Rik
chr4:133000001-133500000	5.62	Gm13257 Fam46b Trnp1 1810019J16Rik Gm17688 Nudc Nr0b2 Gpatch3 Gpn2 Sfn Zdhhc18 BX537327.1 Pigv Arid1a U4 Gm12974 Rps6ka1 Gm17623 Gm12977 U6
chr5:137000001-137500000	5.60	Cux1 4731417B20Rik Myl10 Emid2 RP24-498F17.1 Rabl5 4933404O12Rik Fis1 Cldn15 Znhit1 Plod3 Mir702
chr11:117500001-118000000	5.60	Tnrc6c Tmc6 Tmc8 Gm11723 Gm11724 6030468B19Rik Syngr2 Afmid Tk1 Birc5 Cldn27 Tha1 Gm11725 Socs3 Pgs1 Dnahc17 Gm11738 Cyth1
chr18:54500001-55000000	5.59	9430076G02Rik
chr19:32500001-33000000	5.56	Rpl9-ps6 Minpp1 Papss2 Atad1 Pten
chr5:149500001-150000000	5.54	2210417A02Rik n-R5s179 4930505K14Rik Gm15407 Katnal1 Gm15410 Gm15406 8430423G03Rik 1810059H22Rik Gm15409 Gm15411 Gm15408 Hmgb1 5730422E09Rik AC122546.2 Uspl1
chr17:4000001-4500000	5.53	
chr5:65000001-65500000	5.51	AC122043.1 Klf3 Tlr1 Tlr6 Fam114a1 Mir574 Tmem156 Klhl5
chr8:125000001-125500000	5.49	Gm20388 Ctu2 Fam38a U6 Cdt1 Aprt Galns Trappc2l Pabpn1l Cbfa2t3 Gm10612 Acsf3 Gm16378

		Cdh15 Ankrd11
chr11:44000001-44500000	5.47	Gm12154 Il12b Ublcp1 AL669944.1 Rnf145 4930597A21Rik Ebf1 Gm12158
chr16:95500001-96000000	5.46	Kcnj15 Erg Ets2
chr10:118000001-118500000	5.45	Dyrk2 4932442E05Rik
chr13:23500001-24000000	5.42	Abt1 C230035I16Rik Btn1a1 Btn2a2 Gm11335 Hist1h4h Hist1h2af Hist1h3g Hist1h2bh Hist1h3f Hist1h4f Hist1h1d Hist1h3e Hist1h2ae Hist1h2bg Hist1h2bf Hist1h2ad Hist1h3d Gm17658 Hist1h4d Hist1h2be Gm11398 Hist1h1e U6 Hist1h2ac 5S_rRNA Hist1h2bc Hist1h1t Hist1h4c Hfe Hist1h1c Hist1h3c Hist1h2bb Hist1h2ab Hist1h3b 4930558J22Rik Hist1h4b Hist1h4a Hist1h3a Hist1h1a Trim38 Gm11337 Slc17a2 Slc17a3 Slc17a1 Slc17a4
chr15:81000001-81500000	5.39	Mkl1 4930483J18Rik Mchr1 Slc25a17 St13 Xpnpep3 Dnajb7 Gm17025 Rbx1 Gm5218 Ep300 AC160528.1 U6 L3mbtl2
chr1:37500001-38000000	5.36	Mgat4a 2010300C02Rik 4930556I23Rik Tsga10 Gm17715 Lipt1 Mitd1 Mrpl30 Lyg2 Gm15457
chr12:101500001-102000000	5.35	Ttc7b Rps6ka5
chr11:86000001-86500000	5.35	Brip1 4632419I22Rik Ints2 Med13 U3 Y_RNA 5S_rRNA U6 Rnft1 Rps6kb1 Tubd1 Vmp1 Mir21 Ptrh2
chr7:135000001-135500000	5.33	AC149222.1 Zfp668 Zfp646 Prss53 Vkorc1 Bckdk Myst1 Prss8 Prss36 Fus Gm17468 B230325K18Rik Pycard Gm15533 Trim72 U1 Itgam Itgax Itgad Cox6a2 9130023H24Rik Armc5 Tgfb1i1 Slc5a2 BC017158 AC124566.1
chr16:29500001-30000000	5.29	Atp13a4 Opa1 Gm17734 Gm16761 Gm1968
chr17:31500001-32000000	5.22	Pde9a Wdr4 Ndufv3 4833413E03Rik Pknox1 AC166172.1 Cbs U2af1 Cryaa Sik1
chr3:60000001-60500000	5.19	Mbnl1
chr12:100500001-101000000	5.18	Foxn3 3300002A11Rik Gm16956 2610021K21Rik
chr11:77000001-77500000	5.17	Efcab5 Ssh2 SNORD86 Ssh2 Coro6 Ankrd13b 2210008F06Rik Git1 Trp53i13 Abhd15 Gm10392 Taok1 SNORA17 Nufip2
chr13:52000001-52500000	5.16	Gm16767
chr13:44500001-45000000	5.09	Jarid2 SNORA61
chr15:80000001-80500000	5.07	Mgat3 Smcr7l Atf4 Rps19bp1 Cacna1i Enthd1 SNORA17 Grap2
chr17:31000001-31500000	5.07	Dnahc8 Glp1r Umodl1 AC165951.1 Abcg1 5S_rRNA Tff3 Tff2 Gm15318 Tff1 Tmprss3 Ubash3a Rsph1 Slc37a1
chr12:101000001-101500000	5.05	2610021K21Rik Tdp1 Kcnk13 AC159243.1 Psmc1 BC002230 Gm10433 Calm1 Gm17302
chr11:22500001-23000000	5.03	Gm17335 Gm12052 Gm12055 Gm12056 Commd1 B3gnt2 RP23-242C19.6 SNORA63 RP23-242C19.5 U6 Zrsr1 Cct4 Fam161a 5S_rRNA Gm12059
chr8:47500001-48000000	5.03	Acsl1 Mlf1ip Ccdc111 Casp3 Gm16675 Irf2
chr19:37500001-38000000	5.03	Hhex U6 Exoc6 Cyp26c1 Cyp26a1 Myof
chr15:9000001-9500000	5.03	1110020G09Rik Skp2 Lmbrd2 Ugt3a1 Ugt3a2 Capsl Il7r
chr7:108000001-108500000	5.02	Relt Arhgef17 AC150744.1 P2ry6 P2ry2 Fchsd2 Atg16l2 Stard10 RP24-126J17.2 Arap1
chr9:66000001-66500000	5.02	Dapk2 Herc1 U6 Fbxl22 Usp3 Gm15563
chr2:166000001-166500000	5.01	5S_rRNA Gm11466 Gm11467 Gm11468 Gm14268 5031425F14Rik Gm14267 Prex1 AL732357.1
chr17:5500001-6000000	5.00	Zdhhc14 Snx9 Synj2
chr18:55500001-56000000	4.93	AC149599.1
chr16:10500001-11000000	4.90	Ciita Dexi Clec16a Gm15558 Socs1 Tnp2 Prm3 Prm2 Prm1 Gm10343 Gm11172 Gm17410 A630055G03Rik Litaf AC164093.1 U1
chr13:43500001-44000000	4.86	Ranbp9 U6 Ccdc90a Rnf182 Cd83 U6
chr13:30500001-31000000	4.85	Uqcrfs1 4930519D14Rik Dusp22 Irf4 Exoc2
chr7:87000001-87500000	4.83	Ap3s2 Gm17512 5430400D12Rik 2610034B18Rik AC110903.1 Zfp710 Idh2 AC164075.1 Mir1965 Sema4b Cib1 D330012F22Rik Ttll13 Ngrn Vps33b Prc1 6330403N20Rik Rccd1 Unc45a Hddc3 Man2a2
chr13:24000001-24500000	4.83	Slc17a4 Hist1h2ba Hist1h2aa Scgn Gm11339 Lrrc16a SNORA17 Cmah Gm11342 Gm11345
chr19:45500001-46000000	4.83	Btrc Gm6807 Poll Dpcd Fbxw4 Gm17018 Fgf8 Npm3 Gm15491 Mgea5 Kcnip2 9130011E15Rik
chr9:71500001-72000000	4.79	Cgnl1 Tcf12 Rpl15-ps2 U6
chr16:24000001-24500000	4.78	1110054M08Rik Lpp U7
chr17:73000001-73500000	4.78	Ypel5 Lbh U6 Lclat1
chr16:32000001-32500000	4.78	Senp5 Pak2 SNORA17 Pigx 1500031L02Rik Gm15729 Lrrc33 Bex6 Fbxo45 SNORA79 Wdr53 Mir1946a 2310010M20Rik Rnf168 AC087556.1 Ubxn7 Tm4sf19 Tctex1d2 Pcyt1a Osta Zdhhc19
chr17:29500001-30000000	4.75	Fgd2 Gm16912 Pim1 Gm17657 Tmem217 Tbc1d22b Ftsjd2 AC163629.1 0610038L08Rik Rnf8 1110021J02Rik Mdga1
chr13:51000001-51500000	4.73	Y_RNA Spin1 Nxnl2 Hist1h2al
chr4:8500001-9000000	4.72	Rab2a Chd7
chr19:41500001-42000000	4.68	U7 Lcor Gm340 AI606181 Slit1 7SK Arhgap19 Frat2 Rrp12 Pgam1 Exosc1
chr15:36500001-37000000	4.67	Pabpc1 Ywhaz AC138604.1 Gm10384 Zfp706 Gm16631
chr4:134000001-134500000	4.64	1700021N21Rik Stmn1 AL669982.1 Paqr7 2610002D18Rik Fam54b Sepn1 Man1c1 Ldlrap1 AL645531.1 Tmem57 Rhd Tmem50a D4Wsu53e Syf2
chr10:117000001-117500000	4.63	Cpm U6 Mdm2 Slc35e3 Nup107 Rap1b
chr5:66000001-66500000	4.61	Pds5a U6 1700022K14Rik N4bp2 SNORA73 Rhoh Chrna9 9130230L23Rik AC115293.1 Rbm47
chr14:32000001-32500000	4.60	Tnnc1 Nisch Tnnc1 Sema3g Phf7 Bap1 Dnahc1 Capn7 Sh3bp5 Mettl6 Eaf1 Colq 7SK Hacl1 Btd
chr3:143500001-144000000	4.59	Lmo4
chr16:92500001-93000000	4.57	Clic6 Runx1 Gm16801
chr15:58500001-59000000	4.55	Fer1l6 Tmem65 U1 Gm5959 Trmt12 Rnf139 Tatdn1 Ndufb9 Mtss1
chr18:39500001-40000000	4.54	Arhgap26 Gm15337 Nr3c1 Gm10008 Pabpc2
chr16:20000001-20500000	4.53	Klhl24 Yeats2 Map6d1 Parl Cyp2ab1 Abcc5 7SK Eif2b5
chr1:173500001-174000000	4.52	Cd244 Ly9 Slamf7 Cd48 U6 U6 Slamf1 Cd84 Gm10521 Slamf6 Vangl2 Nhlh1 Ncstn
chr12:86500001-87000000	4.52	Pgf Eif2b2 Mlh3 Acyp1 Fam164c Nek9 Tmed10 Fos Jdp2
chr13:103000001-103500000	4.52	Cd180
chr12:16000001-16500000	4.49	AC102435.1

chr2:167500001-168000000	4.48	Tmem189 Cebpb A530013C23Rik Gm14321 9230111E07Rik 1200007C13Rik Gm14319 Ptpn1 Fam65c Gm14236 AL831766.1 Pard6b Gm14235 E130018N17Rik
chr13:93000001-93500000	4.48	Msh3 Dhfr C030017D09Rik Ankrd34b Fam151b Zfyve16 Spz1 Serinc5
chr14:79500001-80000000	4.47	1300010F03Rik Zfp957 1190002H23Rik Naa16 AC124745.1 Mtrf1 Kbtbd7 Gm5465 Wbp4 Elf1 Sugt1
chr9:61000001-61500000	4.46	Gm10655 Tle3
chr19:55500001-56000000	4.46	Vti1a 4930552P12Rik Tcf7l2
chr4:59500001-60000000	4.44	Rod1 AL824704.1 Hsdl2 E130308A19Rik 1110054O05Rik Snx30 Gm12542 Slc46a2 Mup4 Mup6
chr18:35500001-36000000	4.41	Sil1 Gm5239 Snhg4 SNORA74 Snora74a Matr3 Paip2 Slc23a1 2010001M09Rik Gm1614 Spata24 Dnajc18 1700066B19Rik Ecscr Tmem173 Gm16490 Ube2d2 Cxxc5
chr11:98000001-98500000	4.40	Ikzf3 Fbxl20 Med1 Cdk12 AL591205.1 n-R5s73 Neurod2 Ppp1r1b 1700003D09Rik Stard3 Tcap Pnmt Pgap3 Erbb2 U6 1810046J19Rik Gm12352 Grb7 U2 Zpbp2 Ormdl3 Gm12 Gm12355 Gsdma3
chr14:16500001-17000000	4.39	
chr17:30000001-30500000	4.37	Mdga1 Gm16758 SNORA70 Zfand3 Btbd9 U6
chr10:94500001-95000000	4.36	Cradd Socs2 5730420D15Rik Mrpl42 Ube2n
chr1:14000001-14500000	4.34	Eya1 AC156988.1
chr8:123000001-123500000	4.34	Gse1 Gins2 Cox4nb Cox4i1 7SK Irf8
chr11:11500001-12000000	4.32	4930512M02Rik Gm11999 Ikzf1 Gm12000 Fignl1 Ddc 1700042O10Rik SCARNA4 Grb10 U1
chr12:116500001-117000000	4.32	Gm9740 Gm16633 Ighv1-59 Gm16900 Gm9232 Ighv1-62-2 Gm9235 Ighv8-9 Ighv1-63 Gm16865 Ighv8-11 Gm16901 Ighv1-67 Gm16708 Ighv8-12 Ighv1-71 Gm16709
chr1:13500001-14000000	4.30	Tram1 Lactb2 Xkr9 SNORA17 7SK
chr4:134500001-135000000	4.29	Gm16225 Runx3 Gm16224 Clic4 Gm12984 Srrm1 A330049M08Rik Rcan3 Mir700 Gm15979
chr16:32500001-33000000	4.29	Zdhhc19 Tfrc Tnk2 Gm10818 Muc4 Muc20 1700021K19Rik Fyttd1 Lrch3 Gm17106
chr16:31000001-31500000	4.26	AI480653 Acap2 Ppp1r2 Apod Bdh1 Gm15743
chr12:70500001-71000000	4.26	AC153658.1 Mettl21d Sos2 U6 L2hgdh Atp5s Cdkl1 Mir681 4930512B01Rik Map4k5 4931403G20Rik Atl1
chr17:86500001-87000000	4.26	Srbd1 Prkce Gm10309
chr4:45000001-45500000	4.25	Grhpr Zbtb5 1700055D18Rik Polr1e Fbxo10 Tomm5 Gm10982 Frmpd1 2900093L17Rik Rg9mtd3 Exosc3 Dcaf10 Mcart1 AL772376.2 Mcart1 Shb
chr14:77000001-77500000	4.24	9030625A04Rik Ccdc122
chr15:59000001-59500000	4.24	Gm5045 Sqle E430025E21Rik Nsmce2 Trib1
chr10:19500001-20000000	4.24	U6 Slc35d3 Pex7 Map3k5 Mtap7
chr10:5500001-6000000	4.20	Esr1 SNORD88 RNase_MRP Gm221 U1 1700052N19Rik Rmnd1 Gm16153 Zbtb2 Akap12
chr1:166000001-166500000	4.12	Sell Selp Gm16587 Gm16548 F5 Slc19a2 4930455F23Rik Blzf1 Nme7 Atp1b1 Gm16608
chr11:78500001-79000000	4.12	Nlk Fam58b AL591376.1 U6 1810012P15Rik Nos2 Lgals9 Ksr1 Gm11201
chr3:95500001-96000000	4.11	Ecm1 Tars2 Rprd2 U1 Prpf3 Gm16884 Mrps21 C920021L13Rik Gm129 BC028528 Aph1a Car14 Anp32e Plekho1 Vps45 Otud7b Mtmr11 Gm17690 Sf3b4 SNORA19 Sv2a
chr5:36500001-37000000	4.10	Sorcs2 Psapl1 2210406O10Rik Grpel1 Tada2b Ccdc96 Tbc1d14 D5Ertd579e
chr14:31000001-31500000	4.10	Cacna1d Dcp1a Tkt AC154646.1 Prkcd Rft1
chr14:122000001-122500000	4.10	Dock9 Ubac2 Gpr18 Gpr183 Timm8a2
chr16:19500001-20000000	4.08	Olfr167 Olfr168 Olfr169 Olfr170 Olfr171 Lamp3 B3gnt5 A930003A15Rik Klhl6
chr11:46000001-46500000	4.07	Cyfip2 C030019I05Rik Itk Gm12167 Fam71b Med7 2310031A07Rik Havcr2 Gm12169 Gm12171 BC053393 Dppa1 Gm4926 Timd2
chr3:52500001-53000000	4.06	U6 Cog6 Lhfp
chr16:33500001-34000000	4.05	Zfp148 Slc12a8 Heg1 Gm15658 Gm15657 Muc13 Itgb5 Umps Gm15829 Kalrn
chr10:95500001-96000000	4.04	Eea1 AC131596.1
chr10:43000001-43500000	4.03	Pdss2 Gm10281 Gm3699 Bend3 1700021F05Rik Cd24a F930017D23Rik
chr5:123500001-124000000	4.00	Gm17627 Tmem120b Rhof AI480526 Setd1b Hpd Psmd9 Wdr66 Gm15857 Gm15860 Bcl7a U1 Gm15747 Mlxip Il31 Lrrc43 Gm15751 Diablo B3gnt4 SCARNA20 Vps33a
chr17:34000001-34500000	3.98	Kifc1 BC033916 BC051226 Daxx Tapbp Zbtb22 Rgl2 H2-Ke2 Wdr46 B3galt4 Rps18 Vps52 U6 H2-K1 Ring1 Mir219-1 Mir219-1 H2-Ke6 Gm20427 Slc39a7 Rxrb Col11a2 H2-Oa Brd2 H2-DMa H2-DMb2 H2-DMb1 Psmb9 Psmb9 Tap1 Psmb8 Gm20496 Tap2 Gm15821 H2-Ob Gm20506 H2-Ab1 H2-Aa Gm20513 H2-Eb1 H2-Eb2 Gm11140 Btnl2
chr16:94500001-95000000	3.97	Hlcs Ripply3 Pigp Ttc3 U1 Dscr3 Dyrk1a Kcnj6
chr2:3500001-4000000	3.96	Fam107b Gm13185 Gm13180 Gm13191 Frmd4a
chr19:57000001-57500000	3.96	Afap1l2 Ablim1 B230217O12Rik Fam160b1
chr3:9500001-10000000	3.96	Zfp704 Pag1 Gm16337 5S_rRNA
chr13:93500001-94000000	3.96	Thbs4 Mtx3 Cmya5 Papd4
chr11:5000001-5500000	3.93	Rhbdd3 Emid1 Kremen1 U6 Znrf3 Gm11963 Xbp1 Ccdc117 SNORA17 Ankrd36
chr9:116000001-116500000	3.87	Tgfbr2 AC131777.1 Rbms3
chr9:32000001-32500000	3.81	Arhgap32 Kcnj5 Kcnj1 Fli1 U6 Ets1
chr16:93000001-93500000	3.80	Mir802
chr10:6000001-6500000	3.80	Akap12 U8 Mthfd1l U1 Plekhg1 5S_rRNA
chr17:28500001-29000000	3.80	Tulp1 Fkbp5 7SK E230001N04Rik 4930511I11Rik Gm749 Clps Lhfpl5 Srpk1 Slc26a8 Mapk14 Mapk13 Brpf3 Gm16190 Pnpla1
chr7:82500001-83000000	3.79	Akap13 U6 AC158749.1 Klhl25
chr11:54500001-55000000	3.78	Rapgef6 Cdc42se2 Gm12227 Gm12228 Lyrm7 U1 Hint1 Gpx3 Tnip1 Anxa6 Ccdc69 Gm2a Slc36a3 Gm12233 Slc36a2
chr4:33000001-33500000	3.74	Ankrd6 Rragd 4933421O10Rik Ube2j1 Gabrr2 Gabrr1 Pm20d2 Srsf12 Pnrc1 Gm11934 AL772272.1 Rngtt
chr4:135500001-136000000	3.73	Hmgcl Gale Lypla2 1110049F12Rik Tceb3 Gm13008 AL672076.1 Rpl11 BX530725.1 U6 Id3 E2f2 Asap3 Tcea3 Zfp46 Hnrnpr 2610528B01Rik 9130020K20Rik Gm17388 Htr1d
chr2:34500001-35000000	3.67	Gapvd1 Hspa5 Rabepk snoU13 Fbxw2 Psmd5 D730039F16Rik Phf19 Gm13448 U6 Traf1 Hc

		Gm13449 AI182371 Cep110
chr17:73500001-74000000	3.67	Lclat1 SNORA17 Capn13 Galnt14 D630014O11Rik
chr2:27000001-27500000	3.64	Gm13399 Dbh Sardh Gm17071 Vav2 AA645442 AL731552.1 Brd3 Wdr5 U6atac Gm13421
chr19:29000001-29500000	3.64	4430402I18Rik Ppapdc2 Cdc37l1 Gm10136 Ak3 Rcl1 Mir101b Jak2 Insl6 Rln1 5033414D02Rik Cd274 Pdcd1lg2
chr2:166500001-167000000	3.54	Prex1 7SK U6 Trp53rk Arfgef2 Cse1l Gm17096 Stau1 Ddx27 Znfx1 1500012F01Rik SNORD12 SNORD12 Snord12 Gm14290 Kcnb1
chr13:43000001-43500000	3.52	Phactr1 Gm15809 7SK Gm15813 Tbc1d7 Gfod1 Sirt5 Nol7 Ranbp9
		trans interactions from Igk viewpoint in Thymus
bin	z-score	genes in bin
chrY:2500001-3000000	8.41	Gm3395
		trans interactions from Igl viewpoint in Rag-/- pro-B
bin	z-score	genes in bin
		no statistically signifficant interactions
		trans interactions from Igl viewpoint in Rag/81X pre-B
bin	z-score	genes in bin
chr4:44500001-45000000	10.76	Gm19980 Pax5 AL772319.1 Gm12462 Zcchc7 AL805896.1 Gm12678 Gm12493 Gm12679 Grhpr
chr12:114500001-115000000	9.89	Ighg2c Ighg Ighg1 AI324046 Gm17421 Gm11029 Ighm AC073553.1 AC073553.2 AC073553.3 Gm16734 Gm16843 Gm16879 Gm16878 Gm16877 Gm16783 Gm17600 Gm16782 Gm17700 Gm16942 Gm17537 Gm17424 Gm16941 Gm17339 Gm17663 Gm16781 Gm17264 Gm16785 Gm17486 Gm16784 Gm17620 Gm16947 Adam6b Gm16967 Gm17483 Gm16968 Adam6a Gm17347 Gm16969 Gm16970 Gm16971 Gm16948 Gm16891 Ighv2-4 Gm17309 Gm16949 Gm16593 Gm16592 Gm16594 Gm16886
chr6:68500001-69000000	9.36	Igkv12-98 Igkv10-96 Igkv10-95 Igkv10-94 Igkv19-93 Igkv4-92 Igkv4-91 Igkv4-90 Igkv12-89 Igkv1-88 Igkv4-86 Igkv13-84 Igkv4-81 Igkv4-80 Igkv4-79
chr6:69000001-69500000	9.25	Igkv4-78 Igkv4-74 Igkv4-73 Igkv4-72 Igkv4-71 Igkv4-70 Igkv4-69 Igkv4-68 RNaseP_nuc Igkv4-63 Igkv4-62 Igkv4-61 Igkv4-59 Igkv4-58 AC156953.1 Igkv4-57-1
chr10:20500001-21000000	8.54	Ahi1 Myb Gm16786 AC153556.1
chr15:9500001-10000000	8.52	Spef2 7SK
chr12:115500001-116000000	8.32	Ighv3-8 Ighv12-3 Ighv1-5 Ighv10-3 Ighv1-7 Ighv15-2 Ighv1-9 Ighv1-12 Ighv1-18 Ighv1-19 Ighv1-20
chr3:52000001-52500000	8.04	Foxo1 RP24-337A16.1 Gm10293
chr9:70500001-71000000	8.04	Fam63b Gm10642 Adam10 Lipc CT025701.1 Gm3436 Aqp9
chr6:68000001-68500000	7.87	Igkv9-120 Igkv1-117 Igkv2-116 Igkv1-115 Igkv2-112 Igkv14-111 SNORA17 Igkv1-110 Igkv2-109 Igkv16-104 Igkv15-103 Igkv14-100 SNORA17 Igkv1-99
chr15:80500001-81000000	7.87	Fam83f Tnrc6b AC125540.1 Adsl Sgsm3 Mkl1 U4
chr17:29000001-29500000	7.76	Pnpla1 4930539E08Rik 1700030A11Rik Gm16191 Pxt1 Kctd20 Stk38 U2 Gm16196 Gm16195 Srsf3 Gm16197 Cdkn1a Gm16194 Rab44 Cpne5 Ppil1 BC004004 Pi16 Mtch1 Fgd2
chr11:45000001-45500000	6.94	Gm12160 Gm12162 SNORA17
chr19:33000001-33500000	6.86	7SK Rnls Gm7237
chr19:44000001-44500000	6.86	n-R5s21 Cpn1 Cyp2c44 Erlin1 Chuk Cwf19l1 SNORA12 Bloc1s2 Pkd2l1 Scd3 AC123853.1 Scd2 AC123853.2 Scd4 Scd1
chr17:4500001-5000000	6.83	U6 Arid1b
chr19:3500001-4000000	6.46	Ppp6r3 Lrp5 AC132452.1 1810055G02Rik Suv420h1 Gm16066 AC133523.1 Chka Tcirg1 Ndufs8 Aldh3b1 Unc93b1 1700055N04Rik Aldh3b2 Acy3 Tbx10
chr6:70500001-71000000	6.44	Igkv3-10 Igkv3-9 Igkv3-7 Gm16774 Igkv3-4 Igkv3-3 Igkv3-2 Igkv3-1 Igkj1 Igkj2 Igkj3 Igkj4 Igkj5 Igkc Rpia Eif2ak3 SNORA5 1700011F03Rik Foxi3 U1
chr11:86000001-86500000	6.44	Brip1 4632419I22Rik Ints2 Med13 U3 Y_RNA 5S_rRNA U6 Rnft1 Rps6kb1 Tubd1 Vmp1 Mir21 Ptrh2
chr15:80000001-80500000	6.35	Mgat3 Smcr7l Atf4 Rps19bp1 Cacna1i Enthd1 SNORA17 Grap2
chr9:64500001-65000000	6.35	Megf11 Rab11a Dennd4a SNORA17 Slc24a1 2010321M09Rik AC122463.1 Ptplad1 Dpp8 Igdcc4 Igdcc3 AC161366.1
chr6:69500001-70000000	6.24	Igkv4-57 Igkv4-56 Gm11143 Igkv4-55 Igkv4-53 Igkv4-50 Igkv5-48 Igkv12-47 Igkv12-46 Igkv5-45 Igkv12-44 Igkv5-43 Igkv12-41 Igkv5-39 Igkv12-38 Igkv5-37 Igkv18-36 Igkv1-35 AC154006.1
chr13:54000001-54500000	6.21	Drd1a Sfxn1 Hrh2 Gm16578 Cplx2
chr15:81000001-81500000	6.18	Mkl1 4930483J18Rik Mchr1 Slc25a17 St13 Xpnpep3 Dnajb7 Gm17025 Rbx1 Gm5218 Ep300 AC160528.1 U6 L3mbtl2
chr19:32000001-32500000	6.18	A1cf Asah2 Sgms1 2700046G09Rik
chr15:10000001-10500000	6.15	Prlr Agxt2 Dnajc21 Brix1 Rad1 Ttc23l Rai14
chr17:30000001-30500000	6.15	Mdga1 Gm16758 SNORA70 Zfand3 Btbd9 U6
chr17:31500001-32000000	6.13	Pde9a Wdr4 Ndufv3 4833413E03Rik Pknox1 AC166172.1 Cbs U2af1 Cryaa Sik1
chr12:115000001-115500000	6.07	Ighv11-2 Ighv14-3 Gm7005 Gm16987 Ighv9-2 Ighv9-3 Gm16842 Gm16841 Ighv3-3 Gm16839
chr19:46000001-46500000	5.90	9130011E15Rik 4930505N22Rik Hps6 Ldb1 Pprc1 Nolc1 Elovl3 Pitx3 Gbf1 Gm16726 Nfkb2 Psd Fbxl15 Cuedc2 Gm17393 Tmem180 Mir146b SNORA32 Actr1a Sufu
chr17:31000001-31500000	5.87	Dnahc8 Glp1r Umodl1 AC165951.1 Abcg1 5S_rRNA Tff3 Tff2 Gm15318 Tff1 Tmprss3 Ubash3a Rsph1 Slc37a1
chr11:5500001-6000000	5.79	Ankrd36 Mrps24 Urgcp 2210015D19Rik Dbnl Pgam2 Polm Aebp1 Pold2 Myl7 Gck Gm11967 Ykt6 Camk2b
chr1:38000001-38500000	5.76	Gm15457 Lyg1 7SK Txndc9 Eif5b Rev1 Aff3 Gm16150 Gm16151 Gm16152
chr15:9000001-9500000	5.73	1110020G09Rik Skp2 Lmbrd2 Ugt3a1 Ugt3a2 Capsl Il7r
chr19:41500001-42000000	5.68	U7 Lcor Gm340 AI606181 Slit1 7SK Arhgap19 Frat2 Rrp12 Pgam1 Exosc1
chr17:5500001-6000000	5.62	Zdhhc14 Snx9 Synj2
chr18:55000001-55500000	5.56	Zfp608 Gm17270 Gm4221 SNORA40 U6

chr11:5000001-5500000	5.48	Rhbdd3 Emid1 Kremen1 U6 Znrf3 Gm11963 Xbp1 Ccdc117 SNORA17 Ankrd36
chr17:28500001-29000000	5.45	Tulp1 Fkbp5 7SK E230001N04Rik 4930511I11Rik Gm749 Clps Lhfpl5 Srpk1 Slc26a8 Mapk14 Mapk13 Brpf3 Gm16190 Pnpla1
chr10:20000001-20500000	5.40	Mtap7 4933406P04Rik Bclaf1 Fam54a Pde7b 4930403O15Rik
chr12:81000001-81500000	5.34	Zfp36l1 Gm17591 2310015A10Rik Actn1 Gm17425 Gm17373 Gm17301 Dcaf5 Scarna3b
chr19:45000001-45500000	5.34	Fam178a U6 Sema4g Mrpl43 Peo1 Lzts2 AC132957.1 Pdzd7 Sfxn3 Kazald1 Tlx1 Gm20424 Lbx1 Btrc
chr14:32000001-32500000	5.31	Tnnc1 Nisch Tnnc1 Sema3g Phf7 Bap1 Dnahc1 Capn7 Sh3bp5 Mettl6 Eaf1 Colq 7SK Hacl1 Btd
chr13:23500001-24000000	5.26	Abt1 C230035I16Rik Btn1a1 Btn2a2 Gm11335 Hist1h4h Hist1h2af Hist1h3g Hist1h2bh Hist1h3f Hist1h4f Hist1h1d Hist1h3e Hist1h2ae Hist1h2bg Hist1h2bf Hist1h2ad Hist1h3d Gm17658 Hist1h4d Hist1h2be Gm11398 Hist1h1e U6 Hist1h2ac 5S_rRNA Hist1h2bc Hist1h1t Hist1h4c Hfe Hist1h1c Hist1h3c Hist1h2bb Hist1h2ab Hist1h3b 4930558J22Rik Hist1h4b Hist1h4a Hist1h3a Hist1h1a Trim38 Gm11337 Slc17a2 Slc17a3 Slc17a1 Slc17a4
chr15:84000001-84500000	5.20	Pnpla3 Samm50 Parvb SNORA48 Parvg 1810041L15Rik Ldoc1l
chr19:41000001-41500000	5.20	Blnk Dntt Opalin Tll2 Tm9sf3 Pik3ap1
chr9:32000001-32500000	5.17	Arhgap32 Kcnj5 Kcnj1 Fli1 U6 Ets1
chr17:34000001-34500000	5.17	Kifc1 BC033916 BC051226 Daxx Tapbp Zbtb22 Rgl2 H2-Ke2 Wdr46 B3galt4 Rps18 Vps52 U6 H2-K1 Ring1 Mir219-1 Mir219-1 H2-Ke6 Gm20427 Slc39a7 Rxrb Col11a2 H2-Oa Brd2 H2-DMa H2-DMb2 H2-DMb1 Psmb9 Psmb9 Tap1 Psmb8 Gm20496 Tap2 Gm15821 H2-Ob Gm20506 H2-Ab1 H2-Aa Gm20513 H2-Eb1 H2-Eb2 Gm11140 Btnl2
chr12:78000001-78500000	5.11	Fntb Max AC133174.1 Fut8 U6
chr12:80500001-81000000	5.11	Rad51l1
chr4:135500001-136000000	5.06	Hmgcl Gale Lypla2 1110049F12Rik Tceb3 Gm13008 AL672076.1 Rpl11 BX530725.1 U6 Id3 E2f2 Asap3 Tcea3 Zfp46 Hnrnpr 2610528B01Rik 9130020K20Rik Gm17388 Htr1d
chr11:86500001-87000000	5.06	Ptrh2 Cltc Dhx40 AL596111.1 Ypel2 SCARNA3 Gdpd1 Gm11479 1200011M11Rik Prr11 Fam33a Mir301 Gm11491 Trim37
chr19:4000001-4500000	5.06	Nudt8 Gm16312 Doc2g Ndufv1 Gstp1 Gstp2 BC021614 U3 Cabp2 Cdk2ap2 Pitpnm1 Aip Tmem134 Cabp4 Gpr152 Coro1b Ptprcap Rps6kb2 Carns1 Gm17552 Tbc1d10c Ppp1ca Rad9 Clcf1 AC109138.1 Pold4 Ssh3 Ankrd13d Adrbk1 Kdm2a Rhod A930001C03Rik Syt12 2010003K11Rik
chr8:125000001-125500000	5.00	Gm20388 Ctu2 Fam38a U6 Cdt1 Aprt Galns Trappc2l Pabpn1l Cbfa2t3 Gm10612 Acsf3 Gm16378 Cdh15 Ankrd11
chr10:19500001-20000000	4.97	U6 Slc35d3 Pex7 Map3k5 Mtap7
chr6:87000001-87500000	4.95	Gfpt1 D6Ertd527e Antxr1 n-R5s164 Gkn1 Gkn2 Gkn3 Bmp10 Arhgap25
chr9:66000001-66500000	4.95	Dapk2 Herc1 U6 Fbxl22 Usp3 Gm15563
chr13:41500001-42000000	4.95	Nedd9 AC154848.1 Tmem170b Gm5082 9530008L14Rik 1700061E18Rik U6
chr18:35500001-36000000	4.92	Sil1 Gm5239 Snhg4 SNORA74 Snora74a Matr3 Paip2 Slc23a1 2010001M09Rik Gm1614 Spata24 Dnajc18 1700066B19Rik Ecscr Tmem173 Gm16490 Ube2d2 Cxxc5
chr4:32000001-32500000	4.89	Map3k7 U4 Bach2 D130062J21Rik Gm11932
chr17:4000001-4500000	4.89	
chr13:44000001-44500000	4.86	Gm5083
chr12:101000001-101500000	4.86	2610021K21Rik Tdp1 Kcnk13 AC159243.1 Psmc1 BC002230 Gm10433 Calm1 Gm17302
chr1:36500001-37000000	4.78	Lman2l Cnnm4 Cnnm3 Ankrd23 Ankrd39 Sema4c D430040D24Rik Fam178b AC084389.1 Cox5b Actr1b Zap70 Tmem131
chr8:125500001-126000000	4.78	Gm20388 Ankrd11 U6 Spg7 Rpl13 Snord68 Cpne7 Sult5a1 Dpep1 Chmp1a 4732415M23Rik Cdk10 Spata2L 4933417D19Rik 1300018I17Rik Zfp276 AC155810.1 Fanca Spire2 Tcf25 AC122266.1 Mc1r Tubb3 Def8 SNORA63
chr12:86000001-86500000	4.78	Tmem90a Npc2 Isca2 Ltbp2 D030025P21Rik 1110018G07Rik Gm17139 Gm17193 Fcf1 Ylpm1 Prox2 Dlst Rps6kl1
chr2:30500001-31000000	4.75	9330198N18Rik Gm14486 Gm14488 AL928593.1 1700001O22Rik 4930527E20Rik Mettl11a Asb6 Prrx2 Ptges Tor1b Tor1a BC005624 Usp20 Fnbp1
chr19:44500001-45000000	4.75	Wnt8b Sec31b Ndufb8 Ndufb8 Hif1an Gm17704 Pax2 Gm20395 1700039E22Rik
chr1:37500001-38000000	4.75	Mgat4a 2010300C02Rik 4930556I23Rik Tsga10 Gm17715 Lipt1 Mitd1 Mrpl30 Lyg2 Gm15457
chr11:44500001-45000000	4.72	Ebf1 Gm12159 Gm12160
chr11:22500001-23000000	4.69	Gm17335 Gm12052 Gm12055 Gm12056 Commd1 B3gnt2 RP23-242C19.6 SNORA63 RP23-242C19.5 U6 Zrsr1 Cct4 Fam161a 5S_rRNA Gm12059
chr6:67500001-68000000	4.64	Igkv2-137 Igkv1-135 Igkv17-134 Igkv1-133 Igkv1-132 Igkv1-131 Igkv14-130 SNORA17 SNORA17 Igkv9-129 Igkv17-127 Igkv14-126 SNORA17 Igkv11-125 Igkv9-124 Igkv9-123 Igkv1-122 Igkv17-121 Igkv9-120
chr13:24500001-25000000	4.64	Cmah U6 Fam65b Gm11346 C530050E15Rik 1700016G14Rik Gmnn BC005537 SNORA32 Acot13 Tdp2 D130043K22Rik 4932702P03Rik Aldh5a1
chr13:112500001-113000000	4.64	Mier3 Gm15287 Map3k1 Gm15327 Gm15325 Gm15324 Gm15326 Gm15322 Gm15323
chr6:120500001-121000000	4.61	Cecr2 Slc25a18 Atp6v1e1 Bcl2l13 Bid Mical3 Mical3
chr9:21000001-21500000	4.61	Pde4a Gm16754 Keap1 S1pr5 Atg4d Kri1 Cdkn2d Ap1m2 AC122525.1 Slc44a2 Ilf3 Gm16853 Qtrt1 Dnm2 Mir199a-1 Tmed1 AB124611 Carm1 Yipf2 1810026J23Rik Mir1946b Smarca4
chr19:6000001-6500000	4.61	Capn1 Gm10814 Syvn1 Mrpl49 Fau Znhit2-ps Tm7sf2 1110014N23Rik Zfpl1 BC048609 Cdca5 Gm550 Naaladl1 Sac3d1 Snx15 Arl2 Batf2 n-R5s19 1700123I01Rik Gpha2 Ppp2r5b Atg2a Mir194-2 Mir192 Gm14963 Ehd1 Cdc42bpg Men1 Map4k2 Gm14966 U7 Sf1 Pygm Rasgrp2 Gm14965 Nrxn2 AC167245.1
chr7:17000001-17500000	4.55	Zc3h4 Tmem160 Npas1 n-R5s151 Grlf1 U6 Ceacam15 AC150681.1 Ceacam9 Ap2s1 Slc1a5 Fkrp Strn4 Prkd2 9330104G04Rik Dact3 Gng8 Ptgir
chr10:5500001-6000000	4.55	Esr1 SNORD88 RNase_MRP Gm221 U1 1700052N19Rik Rmnd1 Gm16153 Zbtb2 Akap12
chr15:36500001-37000000	4.55	Pabpc1 Ywhaz AC138604.1 Gm10384 Zfp706 Gm16631
chr17:45000001-45500000	4.55	Supt3h

chr4:133000001-133500000	4.52	Gm13257 Fam46b Trnp1 1810019J16Rik Gm17688 Nudc Nr0b2 Gpatch3 Gpn2 Sfn Zdhhc18 BX537327.1 Pigv Arid1a U4 Gm12974 Rps6ka1 Gm17623 Gm12977 U6
chr17:30500001-31000000	4.52	Btbd9 Gm9874 Glo1 Dnahc8 U6
chr6:70000001-70500000	4.50	Igkv7-33 Igkv6-32 Igkv8-30 Igkv6-29 Igkv8-28 AC159715.1 Igkv8-27 Igkv8-26 Igkv6-25 Igkv8-24 Igkv6-23 Igkv8-21 Igkv6-20 Igkv8-19 Igkv8-18 Igkv6-17 Igkv8-16 Igkv6-15 Gm10360 Igkv6-14 Igkv6-13 Igkv3-12
chr19:57000001-57500000	4.50	Afap1l2 Ablim1 B230217O12Rik Fam160b1
chr9:57500001-58000000	4.47	Cyp1a2 Cyp1a1 Edc3 Clk3 Gm17231 Arid3b Ubl7 Sema7a Gm17322 Cyp11a1 Ccdc33 Gm16130 Stra6 Gm16131
chr18:36000001-36500000	4.47	Cxxc5 AC141471.1 Psd2 Nrg2 Pura
chr2:27000001-27500000	4.44	Gm13399 Dbh Sardh Gm17071 Vav2 AA645442 AL731552.1 Brd3 Wdr5 U6atac Gm13421
chr9:7500001-8000000	4.44	Mmp10 Mmp8 Mmp27 Mmp20 AV064505 Mmp7 Gm10709 Tmem123 Birc2 C330006D17Rik Birc3 Yap1 RP23-349N15.1
chr10:118000001-118500000	4.44	Dyrk2 4932442E05Rik
chr11:6000001-6500000	4.44	Nudcd3 Npc1l1 Ddx56 Tmed4 n-R5s67 Ogdh Zmiz2 Ppia H2afv Purb AL646020.1 Purb Gm11973 Myo1g Gm11974 SNORA9 SNORA70 Ccm2 Nacad
chr15:5000001-5500000	4.41	C7 Card6 Rpl37 Snord72 Gm10250 Prkaa1 Gm15938 Ttc33 Ptger4
chr19:7000001-7500000	4.41	Kcnk4 Gpr137 Bad Plcb3 Ppp1r14b Fkbp2 Vegfb Dnajc4 Nudt22 Trpt1 Fermt3 Stip1 Macrod1 Flrt1 Otub1 Cox8a Naa40 U6 5S_rRNA Rcor2 Mark2 Gm17227 AI846148 2700081O15Rik
chr10:6000001-6500000	4.38	Akap12 U8 Mthfd1l U1 Plekhg1 5S_rRNA
chr14:31500001-32000000	4.38	Rft1 Sfmbt1 1700087M22Rik Tmem110 Mustn1 Itih4 Itih3 Itih1 Nek4 Spcs1 Glt8d1 Gnl3 Snord69 SNORD19B Snord19 Pbrm1 Gm5459 2010107H07Rik Nt5dc2 Stab1 Tnnc1 Nisch
chr17:24500001-25000000	4.38	Abca3 Gm10506 D330041H03Rik Rnps1 Eci1 Dnase1l2 E4f1 Pgp Mlst8 9930021D14Rik Caskin1 Traf7 Rab26 SNORD60 Pkd1 AC132367.1 Tsc2 Nthl1 Slc9a3r2 Npw Zfp598 Syngr3 Gfer Noxo1 Tbl3 Rnf151 Rps2 Snhg9 Snora78 Snora64 Ndufb10 Rpl3l Sepx1 Hs3st6 4930528F23Rik Hagh Fahd1
chr15:99500001-100000000	4.36	Accn2 Gm17349 Smarcd1 Gm17241 Gm16537 Gpd1 2310016M24Rik Lass5 Gm17058 Lima1 U6 Gm17057 1700030F18Rik U12 Larp4 Dip2b
chr5:31000001-31500000	4.33	Dpysl5 Mapre3 Gm15461 Tmem214 Agbl5 Ost4 Emilin1 Khk Cgref1 Abhd1 Preb Tcf23 Slc5a6 0610007C21Rik Cad Slc30a3 Gm9924 Dnajc5g Trim54 Gm15469 Ucn Mpv17 Gtf3c2 Eif2b4 Snx17
chr11:78500001-79000000	4.33	Nlk Fam58b AL591376.1 U6 1810012P15Rik Nos2 Lgals9 Ksr1 Gm11201
chr18:35000001-35500000	4.33	Reep2 Egr1 Gm17507 Etf1 Hspa9 SNORD63 SNORD63 Gm6724 Ctnna1 Lrrtm2 Sil1 AC121874.1 snoU13
chr11:98000001-98500000	4.30	Ikzf3 Fbxl20 Med1 Cdk12 AL591205.1 n-R5s73 Neurod2 Ppp1r1b 1700003D09Rik Stard3 Tcap Pnmt Pgap3 Erbb2 U6 1810046J19Rik Gm12352 Grb7 U2 Zpbp2 Ormdl3 Gm12 Gm12355 Gsdma3
chr15:99000001-99500000	4.30	Spats2 7SK Kcnh3 Mcrs1 AC161198.1 Fam186b Prpf40b Fmnl3 U6 Tmbim6 Nckap5l 4921518J05Rik Bcdin3d Faim2 Aqp2 Aqp5 Aqp6 Racgap1 AC139317.1
chr19:24500001-25000000	4.30	Pip5k1b 4930418C01Rik Fam122a E030010A14Rik Pgm5 Gm10053 Foxd4 Cbwd1
chr2:32500001-33000000	4.27	Ak1 Eng AL772271.5 AL772271.3 Fpgs Cdk9 AL772271.4 AL772271.1 Sh2d3c 6330409D20Rik Ttc16 Tor2a Ptrh1 1700019L03Rik Stxbp1 SNORA31 Gm13524 Gm13523 Fam129b Lrsam1 Rpl12 Snora65 Slc2a8 Garnl3 Ralgps1
chr5:34500001-35000000	4.27	Poln Haus3 U6 Mxd4 Zfyve28 Gm15513 Rnf4 Fam193a snoU13 Tnip2 Sh3bp2 U1 Add1 Mfsd10 Nop14 Gm15522
chr8:74500001-75000000	4.27	Zfp961 Cyp4f18 U2 Olfr372 Olfr373 Olfr374 5S_rRNA AC158898.2 Tpm4 Gm17371 Gm16091 Rab8a Hsh2d Cib3 Gm11034 Fam32a AC158898.1 Ap1m1 Gm10282 Klf2 Eps15l1 Calr3 1700030K09Rik Cherp
chr5:66000001-66500000	4.24	Pds5a U6 1700022K14Rik N4bp2 SNORA73 Rhoh Chrna9 9130230L23Rik AC115293.1 Rbm47
chr5:136500001-137000000	4.24	Dtx2 Upk3b 2310043J07Rik Rasa4 U12 Gm15701 Polr2j Lrwd1 Alkbh4 Orai2 Prkrip1 Sh2b2 Cux1 Gm16599
chr11:117500001-118000000	4.24	Tnrc6c Tmc6 Tmc8 Gm11723 Gm11724 6030468B19Rik Syngr2 Afmid Tk1 Birc5 Cldn27 Tha1 Gm11725 Socs3 Pgs1 Dnahc17 Gm11738 Cyth1
chr8:10500001-11000000	4.22	Myo16 3930402G23Rik Irs2
chr12:32500001-33000000	4.22	Cog5 SCARNA17 Hbp1 Prkar2b Pik3cg
chr19:5000001-5500000	4.19	Slc29a2 B3gnt1 Brms1 Rin1 Cd248 Tmem151a Yif1a Cnih2 Rab1b Klc2 Pacs1 Sf3b2 Gal3st3 Catsper1 Cst6 Banf1 Eif1ad Sart1 Tsga10ip 4930481A15Rik Drap1 AI837181 SNORD86 Fosl1 Ccdc85b Fibp Ctsw Efemp2 Mus81 Cfl1 Snx32
chr13:30500001-31000000	4.19	Uqcrfs1 4930519D14Rik Dusp22 Irf4 Exoc2
chr4:45000001-45500000	4.16	Grhpr Zbtb5 1700055D18Rik Polr1e Fbxo10 Tomm5 Gm10982 Frmpd1 2900093L17Rik Rg9mtd3 Exosc3 Dcaf10 Mcart1 AL772376.2 Mcart1 Shb
chr5:32500001-33000000	4.13	Plb1 Ppp1cb Gm15614 Yes1
chr5:137000001-137500000	4.13	Cux1 4731417B20Rik Myl10 Emid2 RP24-498F17.1 Rabl5 4933404O12Rik Fis1 Cldn15 Znhit1 Plod3 Mir702
chr12:80000001-80500000	4.13	Plek2 Tmem229b Plekhh1 Pigh Arg2 Vti1b Rdh11 Rdh12 Zfyve26 Rad51l1
chr17:29500001-30000000	4.13	Fgd2 Gm16912 Pim1 Gm17657 Tmem217 Tbc1d22b Ftsjd2 AC163629.1 0610038L08Rik Rnf8 1110021J02Rik Mdga1
chr19:29000001-29500000	4.13	4430402I18Rik Ppapdc2 Cdc37l1 Gm10136 Ak3 Rcl1 Mir101b Jak2 Insl6 Rln1 5033414D02Rik Cd274 Pdcd1lg2
chr13:43000001-43500000	4.08	Phactr1 Gm15809 7SK Gm15813 Tbc1d7 Gfod1 Sirt5 Nol7 Ranbp9
chr14:16500001-17000000	4.08	
chr9:44000001-44500000	4.02	Cbl Ccdc153 Pdzd3 Nlrx1 Abcg4 Hinfp C2cd2l Dpagt1 H2afx Hmbs Vps11 7SK Hyou1 SNORA40 Slc37a4 Trappc4 Rps25 Ccdc84 Foxr1 Upk2 Gm9830 U6 C030014I23Rik Bcl9l Cxcr5 Ddx6 Treh Phldb1

chr12:116500001-117000000	4.02	Gm9740 Gm16633 Ighv1-59 Gm16900 Gm9232 Ighv1-62-2 Gm9235 Ighv8-9 Ighv1-63 Gm16865 Ighv8-11 Gm16901 Ighv1-67 Gm16708 Ighv8-12 Ighv1-71 Gm16709
chr13:49000001-49500000	4.02	Fam120a C030044B11Rik Wnk2 Ninj1 1110007C09Rik Susd3 Fgd3 Bicd2
chr15:8000001-8500000	4.02	Wdr70 Nup155 2410089E03Rik U6 Nipbl
chr17:32500001-33000000	4.02	Wiz Gm17561 CT485616.1 Rasal3 A530088E08Rik Pglyrp2 Cyp4f39 Cyp4f17 Cyp4f16 Gm9705 Cyp4f40 Cyp4f15 Zfp871 Gm17115 Zfp811 U1 5S_rRNA Gm16684 Zfp799
chr10:44000001-44500000	3.99	Atg5 Mir1929 Prdm1 U6 U6
chr11:4000001-4500000	3.99	Sec14l2 Rnf215 AL807825.1 Ccdc157 Sf3a1 Tbc1d10a Gatsl3 Osm Lif Gm11959 Gm11958 U6 Hormad2 Mtmr3
chr9:7000001-7500000	3.96	Dync2h1 Dcun1d5 Mmp13 Mmp12 Mmp1b Mmp3 Mmp1a
chr10:43500001-44000000	3.91	Gm9034 Qrsl1 Rtn4ip1 Aim1 Atg5
chr11:4500001-5000000	3.91	Gm11032 Gm11961 Ascc2 Uqcr10 Zmat5 Cabp7 Nf2 Nipsnap1 Thoc5 Nefh Ap1b1 SNORD125 Gas2l1 Rasl10a Ewsr1 Rhbdd3 Gm11031
chr17:27000001-27500000	3.91	Gm17382 Gm20468 Kifc5b Phf1 Cuta AC144621.1 Syngap1 Zbtb9 Ggnbp1 Bak1 Itpr3 1700062I23Rik 2900010M23Rik Ip6k3 Lemd2 Gm17262 Gm10505
chr13:51000001-51500000	3.88	Y_RNA Spin1 Nxnl2 Hist1h2al
chr19:11000001-11500000	3.88	Gpr44 Ccdc86 Ms4a10 Ms4a15 AW112010 Ms4a8a Gm336 1700017D01Rik 1700025F22Rik Ms4a13 4930526L06Rik Ms4a12 Ms4a1 Ms4a5 Ms4a14 Ms4a7 Ms4a4c
chr6:52500001-53000000	3.85	Hibadh SNORA32 Tax1bp1 Jazf1 SCARNA20
chr5:32000001-32500000	3.82	Mrpl33 Bre 7SK Gm17130 Gm10463 Fosl2 U6
chr5:65000001-65500000	3.79	AC122043.1 Klf3 Tlr1 Tlr6 Fam114a1 Mir574 Tmem156 Klhl5
chr14:26000001-26500000	3.79	Gm17716 D930049A15Rik Zmiz1 AC154455.1 Gm17670 Gm10397
chr19:6500001-7000000	3.79	Nrxn2 Gm14964 Slc22a12 Gm14967 AC124394.1 2410152P15Rik Gm14968 Rps6ka4 Ccdc88b Prdx5 Trmt112 Esrra 1700019N12Rik
chr14:31000001-31500000	3.77	Cacna1d Dcp1a Tkt AC154646.1 Prkcd Rft1
chr17:32000001-32500000	3.74	Hsf2bp 7SK Rrp1b Pdxk-ps Gm17276 Notch3 Ephx3 Brd4 Gm17549 Akap8 Akap8l Wiz
chr17:35000001-35500000	3.74	Gm20547 C2 Zbtb12 Ehmt2 Slc44a4 Neu1 1110038B12Rik AC087117.3 AC087117.2 AC087117.1 Hspa1b Hspa1a Gm20481 Hspa1l Gm10501 Lsm2 D17H6S56E-5 Vars D17H6S56E-3 Ng23 Msh5 U6 Clic1 Ddah2 AU023871 Ly6g6c Ly6g6c Ly6g6d Ly6g6e Ly6g6f Abhd16a Ly6g5c Ly6g5b Csnk2b RP23-115O3.9 Gm20522 Gpank1 D17H6S53E Apom Bag6 Prrc2a SNORA38 Gm17705 Aif1 Lst1 Ltb Tnf Lta Nfkbil1 Gm16181 Atp6v1g2 Ddx39b SNORD83 SNORD83 CR974466.1 H2-D1 Gm18733 H2-Q2 H2-Q2
chr9:63000001-63500000	3.68	Map2k5 2300009A05Rik Gm16759 Iqch AC122057.1 Aagab Smad3
chr11:100500001-101000000	3.68	Zfp385c Gm11547 Dhx58 Kat2a Hspb9 Rab5c Kcnh4 Hcrt Ghdc 7SK Stat5b Stat5a Stat3 Ptrf Atp6v0a1 Naglu Hsd17b1 Coasy Mlx Psmc3ip Fam134c Tubg1
chr17:39500001-40000000	3.65	AC168268.1
chr19:46500001-47000000	3.57	Sufu Trim8 Arl3 Sfxn2 D19Wsu162e Cyp17a1 2010012O05Rik As3mt Cnnm2 Nt5c2

trans interactions from Igl viewpoint in Thymus

bin	z-score	genes in bin
chr19:43000001-43500000	10.01	Hpse2 5S_rRNA
chr19:52500001-53000000	8.99	
chr19:35500001-36000000	8.66	AC119801.1 SNORA17
chr19:17500001-18000000	8.21	Pcsk5 snoU13 U6 AC133509.2
chr19:15000001-15500000	7.42	
chr19:14000001-14500000	7.42	
chr19:19000001-19500000	7.42	Rorb SNORA17
chr19:26000001-26500000	7.42	U4
chr19:19500001-20000000	6.97	
chr19:30500001-31000000	6.97	Dkk1 Prkg1 7SK
chr19:22000001-22500000	6.86	Trpm3 SNORA17
chr19:48500001-49000000	6.86	Sorcs3
chr19:35000001-35500000	6.52	Kif20b Mir1950 SNORA17 AC102038.1
chr19:39000001-39500000	6.41	Hells Cyp2c55 AC100729.1 Cyp2c65 Cyp2c66 Cyp2c29 Cyp2c38
chr19:22500001-23000000	6.30	Trpm3 Mir204
chr19:25500001-26000000	6.18	Kank1 U6 Dmrt1 Dmrt3 Dmrt2
chr17:3500001-4000000	5.96	Tiam2 Tfb1m Cldn20 Nox3
chr19:51000001-51500000	5.73	U6
chr19:20500001-21000000	5.62	Aldh1a1 Aldh1a7 Tmc1
chr19:23500001-24000000	5.62	Mamdc2 1700028P14Rik Gm9493 SNORA17 Ptar1 Gm9938 Apba1
chr19:7500001-8000000	5.51	2700081O15Rik Rtn3 Atl3 Pla2g16 Lgals12 Hrasls5 Slc22a19 Slc22a26 Slc22a27
chr19:13000001-13500000	5.51	Olfr1449 Olfr1450 Olfr1451 Olfr1453 Olfr1454 Olfr1456-ps1 Olfr1457 Olfr1458 Olfr1459 Olfr1461 Olfr1462 Olfr1463 U6 Olfr1465 Olfr1466 Olfr1467 Olfr1469
chr19:20000001-20500000	5.17	SNORA71 Anxa1
chr19:39500001-40000000	5.06	Cyp2c38 Cyp2c39 Cyp2c67 Cyp2c68 Cyp2c40 Cyp2c69
chr17:14500001-15000000	4.95	Smoc2 Thbs2 Gm3222 U7 Wdr27
chrY:2500001-3000000	4.83	Gm3395
chr19:8000001-8500000	4.72	Slc22a27 AC122119.1 Slc22a28 Slc22a29 Slc22a30
chr6:5500001-6000000	4.27	Dync1i1 1700019G24Rik Slc25a13
chr9:3500001-4000000	4.16	Gucy1a2
chr17:4000001-4500000	4.16	
chr17:9500001-10000000	4.16	Gm17728 Pabpc6

trans interactions from Pax5 viewpoint in Rag-/- pro-B

bin	z-score	genes in bin

chr12:115500001-116000000	15.89	Ighv3-8 Ighv12-3 Ighv1-5 Ighv10-3 Ighv1-7 Ighv15-2 Ighv1-9 Ighv1-12 Gm17686 Gm16857 Gm16858 Ighv1-18 Ighv1-19 Ighv1-20 Gm16860
chr12:115000001-115500000	15.40	Ighv11-2 Ighv14-3 Ighv9-2 Ighv9-3 Gm16842 Gm16841 Ighv3-3 Gm16839
chr3:52000001-52500000	14.20	Foxo1 RP24-337A16.1 Gm10293
chr12:114500001-115000000	14.16	Ighg2c Ighg Ighg1 AI324046 Gm17421 Gm11029 Ighm AC073553.1 AC073553.2 AC073553.3 Gm16734 Gm16843 Gm16879 Gm16878 Gm16877 Gm16783 Gm17600 Gm16782 Gm17700 Gm16942 Gm17537 Gm17424 Gm16941 Gm17339 Gm17663 Gm16781 Gm17264 Gm16785 Gm17486 Gm16784 Gm17620 Gm16947 Adam6b Gm16967 Gm17483 Gm16968 Adam6a Gm17347 Gm16969 Gm16970 Gm16971 Gm16948 Gm16891 Ighv2-4 Gm17309 Gm16949 Gm16593 Gm16592 Gm16594 Gm16886
chr12:80500001-81000000	7.42	Rad51l1
chr9:61000001-61500000	7.34	Gm10655 Tle3
chr12:116500001-117000000	7.23	Ighv1-59 Ighv1-62-2 Gm9235 Ighv8-9 Ighv1-63 Gm16865 Ighv8-11 Gm16901 Ighv1-67 Gm16708 Ighv8-12 Ighv1-71 Gm16709
chr9:61500001-62000000	7.12	Rplp1 Kif23 Paqr5 7SK Glce AC123610.1
chr11:78500001-79000000	7.08	Nlk Fam58b AL591376.1 U6 1810012P15Rik Nos2 Lgals9 Ksr1 Gm11201
chr17:30000001-30500000	6.18	Mdga1 Gm16758 SNORA70 Zfand3 Btbd9 U6
chr12:116000001-116500000	6.07	Ighv1-23 Ighv1-24 Gm16717 Gm17539 Gm16965 Gm16735 Gm16715 Gm16716 Gm16964 Ighv1-42 Ighv1-43 Gm16966 Gm16830 Ighv8-5 Gm16829 Gm16828 AB069917 Ighv8-6 Ighv1-54 Gm16792 Gm16791
chr2:27000001-27500000	5.92	Gm13399 Dbh Sardh Gm17071 Vav2 AA645442 AL731552.1 Brd3 Wdr5 U6atac Gm13421
chr18:35000001-35500000	5.88	Reep2 Egr1 Gm17507 Etf1 Hspa9 SNORD63 SNORD63 Gm6724 Ctnna1 Lrrtm2 Sil1 AC121874.1 snoU13
chr9:44500001-45000000	5.81	Phldb1 SNORA2 Arcn1 Ift46 Tmem25 Ttc36 Mll1 U6atac Atp5l Ube4a Cd3g Cd3d Cd3e Mpzl2 Mpzl3 Amica1 Gm10684 Scn2b Scn4b Tmprss4 Gm17099 BC049352
chr13:44000001-44500000	5.77	Gm5083
chr17:26500001-27000000	5.70	Neurl1b Dusp1 Gm8225 1700049J03Rik Ergic1 AC122252.1 Gm17218 Atp6v0e A930001N09Rik Bnip1 Nkx2-5 Gm17382 Gm20468
chr10:20000001-20500000	5.47	Mtap7 4933406P04Rik Bclaf1 Fam54a Pde7b 4930403O15Rik
chr16:30500001-31000000	5.47	Tmem44 Lsg1 Fam43a U6 SNORA17 AI480653 Gm15742
chr15:80500001-81000000	5.43	Fam83f Tnrc6b AC125540.1 Adsl Sgsm3 Mkl1 U4
chr9:44000001-44500000	5.36	Cbl Ccdc153 Pdzd3 Nlrx1 Abcg4 Hinfp C2cd2l Dpagt1 H2afx Hmbs Vps11 7SK Hyou1 SNORA40 Slc37a4 Trappc4 Rps25 Ccdc84 Foxr1 Upk2 Gm9830 U6 C030014I23Rik Bcl9l Cxcr5 Ddx6 Treh Phldb1
chr19:45500001-46000000	5.32	Btrc Gm6807 Poll Dpcd Fbxw4 Gm17018 Fgf8 Npm3 Gm15491 Mgea5 Kcnip2 9130011E15Rik
chr12:81000001-81500000	5.21	Zfp36l1 Gm17591 2310015A10Rik Actn1 Gm17425 Gm17373 Gm17301 Dcaf5 Scarna3b
chr9:63500001-64000000	4.95	Smad3 Smad6 5S_rRNA 1110036E04Rik Lctl Zwilch
chr14:26000001-26500000	4.91	Gm17716 D930049A15Rik Zmiz1 AC154455.1 Gm17670 Gm10397
chr2:31000001-31500000	4.80	D330023K18Rik Gpr107 SNORA76 Gm13405 Ncs1 Hmcn2 Ass1 Fubp3 AL732564.1 Gm13425 Prdm12
chr16:92500001-93000000	4.80	Clic6 Runx1 Gm16801
chr2:30500001-31000000	4.76	9330198N18Rik Gm14486 Gm14488 AL928593.1 1700001O22Rik 4930527E20Rik Mettl11a Asb6 Prrx2 Ptges Tor1b Tor1a BC005624 Usp20 Fnbp1
chr15:82500001-83000000	4.76	Cyp2d37-ps Cyp2d40 Gm5062 Cyp2d26 Tcf20 AC129563.1 AW121686 Nfam1 Serhl Gm17206 Rrp7a Poldip3 U12 Cyb5r3
chr8:129000001-129500000	4.72	AC118255.1 Gm16983 Irf2bp2 Tomm20 SNORA14 Rbm34
chr9:62500001-63000000	4.72	Itga11 Fem1b Gm17400 Cln6 Gm10653 Calml4 Pias1 U1 U6 Skor1
chr17:28000001-28500000	4.57	Uhrf1bp1 Taf11 Anks1 Gm15597 Gm15598 Tcp11 4930526A20Rik Scube3 Zfp523 Def6 Ppard Fance Rpl10a Tead3 Tulp1
chr17:31500001-32000000	4.50	Pde9a Wdr4 Ndufv3 4833413E03Rik Pknox1 AC166172.1 Cbs U2af1 Cryaa Sik1
chr2:33000001-33500000	4.46	Ralgps1 Gm13528 SNORA48 Angptl2 AL845277.1 Zbtb34 Gm13536 Zbtb43 Gm13530 Lmx1b C130021I20Rik
chr17:29500001-30000000	4.38	Fgd2 Gm16912 Pim1 Gm17657 Tmem217 Tbc1d22b Ftsjd2 AC163629.1 0610038L08Rik Rnf8 1110021J02Rik Mdga1
chr2:26500001-27000000	4.12	5730588L14Rik Lcn4 Abo Surf6 Med22 Rpl7a SNORD24 SNORD36 SNORD36 SNORD36 Surf1 Surf2 Surf4 Gm711 Rexo4 Adamts13 5930434B04Rik Slc2a6 Gm13398 Tmem8c Adamtsl2 Fam163b

trans interactions from Pax5 viewpoint in Rag/81X pre-B

bin	z-score	genes in bin
chr12:115500001-116000000	27.82	Ighv3-8 Ighv12-3 Ighv1-5 Ighv10-3 Ighv1-7 Ighv15-2 Ighv1-9 Ighv1-12 Ighv1-18 Ighv1-19 Ighv1-20
chr3:52000001-52500000	24.03	Foxo1 RP24-337A16.1 Gm10293
chr12:114500001-115000000	20.57	Ighg2c Ighg Ighg1 Ighm Adam6b Adam6a Ighv2-4
chr12:115000001-115500000	17.37	Ighv11-2 Ighv14-3 Ighv9-2 Ighv9-3 Ighv3-3
chr12:114000001-114500000	17.20	Pld4 Ahnak2 BC022687 Cdca4 Gpr132 Gm17723 Jag2 Nudt14 Gm17274 Brf1 Btbd6 Pacs2 Tex22 Mta1 Crip2 Crip1 4930427A07Rik Tmem121 U6
chr15:80500001-81000000	16.44	Fam83f Tnrc6b AC125540.1 Adsl Sgsm3 Mkl1 U4
chr6:69000001-69500000	16.27	Igkv4-78 Igkv4-74 Igkv4-73 Igkv4-72 Igkv4-71 Igkv4-70 Igkv4-69 Igkv4-68 RNaseP_nuc Igkv4-63 Igkv4-62 Igkv4-61 Igkv4-59 Igkv4-58 AC156953.1 Igkv4-57-1
chr6:68500001-69000000	15.85	Igkv12-98 Igkv10-96 Igkv10-95 Igkv10-94 Igkv19-93 Igkv4-92 Igkv4-91 Igkv4-90 Igkv12-89 Igkv1-88 Gm11145 Igkv4-86 Igkv13-84 Igkv4-81 Igkv4-80 Igkv4-79
chr15:81000001-81500000	15.09	Mkl1 4930483J18Rik Mchr1 Slc25a17 St13 Xpnpep3 Dnajb7 Gm17025 Rbx1 Gm5218 Ep300 AC160528.1 U6 L3mbtl2
chr17:29000001-29500000	14.42	Pnpla1 4930539E08Rik 1700030A11Rik Gm16191 Pxt1 Kctd20 Stk38 U2 Gm16196 Gm16195 Srsf3 Gm16197 Cdkn1a Gm16194 Rab44 Cpne5 Ppil1 BC004004 Pi16 Mtch1 Fgd2

chr16:19000001-19500000	14.25	Iglc3 Iglv1 Iglc2 Iglv3 Iglv2 Olfr164 SNORA17 AC112681.1 Olfr165 SNORA17 Olfr166
chr9:70500001-71000000	13.32	Fam63b Gm10642 Adam10 Lipc CT025701.1 Gm3436 Aqp9
chr15:80000001-80500000	13.15	Mgat3 Smcr7l Atf4 Rps19bp1 Cacna1i Enthd1 SNORA17 Grap2
chr16:32000001-32500000	13.15	Senp5 Pak2 SNORA17 Pigx 1500031L02Rik Gm15729 Lrrc33 Bex6 Fbxo45 SNORA79 Wdr53 Mir1946a 2310010M20Rik Rnf168 AC087556.1 Ubxn7 Tm4sf19 Tctex1d2 Pcyt1a Osta Zdhhc19
chr12:116000001-116500000	12.82	Ighv1-23 Ighv1-24 Gm16717 Gm17539 Gm16965 Gm16735 Gm16715 Gm16716 Gm16964 Ighv1-42 Ighv1-43 Gm16966 Gm16830 Ighv8-5 Gm16829 Gm16828 AB069917 Ighv8-6 Ighv1-54 Gm16792 Gm16791
chr9:64500001-65000000	12.73	Megf11 Rab11a Dennd4a SNORA17 Slc24a1 2010321M09Rik AC122463.1 Ptplad1 Dpp8 Igdcc4 Igdcc3 AC161366.1
chr2:31000001-31500000	12.65	D330023K18Rik Gpr107 SNORA76 Gm13405 Ncs1 Hmcn2 Ass1 Fubp3 AL732564.1 Gm13425 Prdm12
chr12:80500001-81000000	12.48	Rad51l1
chr12:81000001-81500000	12.39	Zfp36l1 Gm17591 2310015A10Rik Actn1 Gm17425 Gm17373 Gm17301 Dcaf5 Scarna3b
chr6:68000001-68500000	12.14	Igkv9-120 Igkv1-117 Igkv2-116 Igkv1-115 Igkv2-112 Igkv14-111 SNORA17 Igkv1-110 Igkv2-109 Igkv16-104 Igkv15-103 Igkv14-100 SNORA17 Igkv1-99
chr6:70500001-71000000	11.97	Igkv3-10 Igkv3-9 Igkv3-7 Gm16774 Igkv3-4 Igkv3-3 Igkv3-2 Igkv3-1 Igkj1 Igkj2 Igkj3 Igkj4 Igkj5 Igkc Rpia Eif2ak3 SNORA5 1700011F03Rik Foxi3 U1
chr18:35500001-36000000	11.89	Sil1 Gm5239 Snhg4 SNORA74 Snora74a Matr3 Paip2 Slc23a1 2010001M09Rik Gm1614 Spata24 Dnajc18 1700066B19Rik Ecscr Tmem173 Gm16490 Ube2d2 Cxxc5
chr2:32000001-32500000	11.72	Prrc2b SNORD62 AL808027.3 Gm13610 Pomt1 Uck1 Swi5 Golga2 Dnm1 AL808027.1 AL808027.2 Ciz1 1110008P14Rik Lcn2 Ptges2 Slc25a25 Naif1 Gm13412 Fam102a Dpm2 9430097D07Rik Pip5kl1 Gm17343 St6galnac4 AL772271.2 St6galnac6 Ak1
chr13:23500001-24000000	11.64	Abt1 C230035I16Rik Btn1a1 Btn2a2 Gm11335 Hist1h4h Hist1h2af Hist1h3g Hist1h2bh Hist1h3f Hist1h4f Hist1h1d Hist1h3e Hist1h2ae Hist1h2bg Hist1h2bf Hist1h2ad Hist1h3d Gm17658 Hist1h4d Hist1h2be Gm11398 Hist1h1e U6 Hist1h2ac 5S_rRNA Hist1h2bc Hist1h1t Hist1h4c Hfe Hist1h1c Hist1h3c Hist1h2bb Hist1h2ab Hist1h3b 4930558J22Rik Hist1h4b Hist1h4a Hist1h3a Hist1h1a Trim38 Gm11337 Slc17a2 Slc17a3 Slc17a1 Slc17a4
chr9:44000001-44500000	11.64	Cbl Ccdc153 Pdzd3 Nlrx1 Abcg4 Hinfp C2cd2l Dpagt1 H2afx Hmbs Vps11 7SK Hyou1 SNORA40 Slc37a4 Trappc4 Rps25 Ccdc84 Foxr1 Upk2 Gm9830 U6 C030014I23Rik Bcl9l Cxcr5 Ddx6 Treh Phldb1
chr10:20500001-21000000	11.64	Ahi1 Myb Gm16786 AC153556.1
chr2:32500001-33000000	11.47	Ak1 Eng AL772271.5 AL772271.3 Fpgs Cdk9 AL772271.4 AL772271.1 Sh2d3c 6330409D20Rik Ttc16 Tor2a Ptrh1 1700019L03Rik Stxbp1 SNORA31 Gm13524 Gm13523 Fam129b Lrsam1 Rpl12 Snora65 Slc2a8 Garnl3 Ralgps1
chr2:34500001-35000000	11.38	Gapvd1 Hspa5 Rabepk snoU13 Fbxw2 Psmd5 D730039F16Rik Phf19 Gm13448 U6 Traf1 Hc Gm13449 AI182371 Cep110
chr6:87000001-87500000	11.13	Gfpt1 D6Ertd527e Antxr1 n-R5s164 Gkn1 Gkn2 Gkn3 Bmp10 Arhgap25
chr10:79500001-80000000	11.13	Polr2e Gpx4 Sbno2 Stk11 Dos Atp5d Midn Cirbp 1600002K03Rik Efna2 Mum1 Ndufs7 Gamt Dazap1 Gm15122 Rps15 Apc2 2310011J03Rik Pcsk4 Reep6 Adamtsl5 Plk5 Gm15123 Gm15124 Mex3d AC152062.1 Mbd3 Uqcr11 Tcf3 U6 Onecut3 AC152058.1 Atp8b3
chr16:32500001-33000000	11.04	Zdhhc19 Tfrc Tnk2 Gm10818 Muc4 Muc20 1700021K19Rik Fyttd1 Lrch3 Gm17106
chr19:45500001-46000000	11.04	Btrc Gm6807 Poll Dpcd Fbxw4 Gm17018 Fgf8 Npm3 Gm15491 Mgea5 Kcnip2 9130011E15Rik
chr16:31000001-31500000	10.96	AI480653 Acap2 Ppp1r2 Apod Bdh1 Gm15743
chr12:85500001-86000000	10.88	C130039O16Rik Gm5436 AC159649.1 Ptgr2 Zfp410 Fam161b Coq6 Entpd5 2900006K08Rik Aldh6a1 Lin52 Vsx2 Abcd4 Vrtn
chr13:43500001-44000000	10.79	Ranbp9 U6 Ccdc90a Rnf182 Cd83 U6
chr13:44000001-44500000	10.79	Gm5083
chr2:30500001-31000000	10.71	9330198N18Rik Gm14486 Gm14488 AL928593.1 1700001O22Rik 4930527E20Rik Mettl11a Asb6 Prrx2 Ptges Tor1b Tor1a BC005624 Usp20 Fnbp1
chr6:67500001-68000000	10.71	Igkv2-137 Igkv1-135 Igkv17-134 Igkv1-133 Igkv1-132 Igkv1-131 Igkv14-130 SNORA17 SNORA17 Igkv9-129 Igkv17-127 Igkv14-126 SNORA17 Igkv11-125 Igkv9-124 Igkv9-123 Igkv1-122 Igkv17-121 Igkv9-120
chr9:66000001-66500000	10.71	Dapk2 Herc1 U6 Fbxl22 Usp3 Gm15563
chr15:78500001-79000000	10.62	Elfn2 Mfng Card10 Cdc42ep1 Lgals2 Gm17481 Gga1 Sh3bp1 1700027A07Rik Pdxp Lgals1 Nol12 Triobp Gcat Ankrd54 Eif3l AL589670.1 Micall1 1700088E04Rik Polr2f Sox10 Gm10863
chr17:31000001-31500000	10.62	Dnahc8 Glp1r Umodl1 AC165951.1 Abcg1 5S_rRNA Tff3 Tff2 Gm15318 Tff1 Tmprss3 Ubash3a Rsph1 Slc37a1
chr11:78500001-79000000	10.54	Nlk Fam58b AL591376.1 U6 1810012P15Rik Nos2 Lgals9 Ksr1 Gm11201
chr12:116500001-117000000	10.54	Gm9740 Gm16633 Ighv1-59 Gm16900 Gm9232 Ighv1-62-2 Gm9235 Ighv8-9 Ighv1-63 Gm16865 Ighv8-11 Gm16901 Ighv1-67 Gm16708 Ighv8-12 Ighv1-71 Gm16709
chr17:31500001-32000000	10.45	Pde9a Wdr4 Ndufv3 4833413E03Rik Pknox1 AC166172.1 Cbs U2af1 Cryaa Sik1
chr19:46000001-46500000	10.37	9130011E15Rik 4930505N22Rik Hps6 Ldb1 Pprc1 Nolc1 Elovl3 Pitx3 Gbf1 Gm16726 Nfkb2 Psd Fbxl15 Cuedc2 Gm17393 Tmem180 Mir146b SNORA32 Actr1a Sufu
chr12:86000001-86500000	10.20	Tmem90a Npc2 Isca2 Ltbp2 D030025P21Rik 1110018G07Rik Gm17139 Gm17193 Fcf1 Ylpm1 Prox2 Dlst Rps6kl1
chr14:32000001-32500000	10.20	Tnnc1 Nisch Tnnc1 Sema3g Phf7 Bap1 Dnahc1 Capn7 Sh3bp5 Mettl6 Eaf1 Colq 7SK Hacl1 Btd
chr17:28500001-29000000	10.20	Tulp1 Fkbp5 7SK E230001N04Rik 4930511I11Rik Gm749 Clps Lhfpl5 Srpk1 Slc26a8 Mapk14 Mapk13 Brpf3 Gm16190 Pnpla1
chr7:108000001-108500000	10.12	Relt Arhgef17 AC150744.1 P2ry6 P2ry2 Fchsd2 Atg16l2 Stard10 RP24-126J17.2 Arap1
chr13:37500001-38000000	10.12	Ly86 Rreb1
chr14:31500001-32000000	10.12	Rft1 Sfmbt1 1700087M22Rik Tmem110 Mustn1 Itih4 Itih3 Itih1 Nek4 Spcs1 Glt8d1 Gnl3 Snord69 SNORD19B Snord19 Pbrm1 Gm5459 2010107H07Rik Nt5dc2 Stab1 Tnnc1 Nisch
chr1:133500001-134000000	10.03	Avpr1b Ctse 5430435G22Rik Slc26a9 Pm20d1 AC161805.1 Slc41a1 Rab7l1 Nucks1 Slc45a3 Elk4

		Mfsd4 Gm17288 U6
chr2:29500001-30000000	10.03	Rapgef1 Gm13420 Gm11129 Trub2 Gm13547 Coq4 Slc27a4 Urm1 Mir219-2 2600006K01Rik Cercam Odf2 U6 Gle1 Spna2 Wdr34 Set Pkn3 Zdhhc12 Zer1 Tbc1d13
chr9:65000001-65500000	10.03	Igdcc3 U5 U5 Parp16 Cilp Clpx AC110235.1 Pdcd7 Gm514 Rasl12 Ostb Mtfmt Spg21 Ankdd1a Plekho2 Pif1 Rbpms2
chr9:65500001-66000000	10.03	Rbpms2 Oaz2 Zfp609 Trip4 n-R5s85 2810417H13Rik U6 Csnk1g1 SNORA17 Ppib Snx22 Snx1 Fam96a
chr10:19500001-20000000	10.03	U6 Slc35d3 Pex7 Map3k5 Mtap7
chr17:34000001-34500000	9.95	Kifc1 BC033916 BC051226 Daxx Tapbp Zbtb22 Rgl2 H2-Ke2 Wdr46 B3galt4 Rps18 Vps52 U6 H2-K1 Ring1 Mir219-1 Mir219-1 H2-Ke6 Gm20427 Slc39a7 Rxrb Col11a2 H2-Oa Brd2 H2-DMa H2-DMb2 H2-DMb1 Psmb9 Psmb9 Tap1 Psmb8 Gm20496 Tap2 Gm15821 H2-Ob Gm20506 H2-Ab1 H2-Aa Gm20513 H2-Eb1 H2-Eb2 Gm11140 Btnl2
chr19:44000001-44500000	9.86	n-R5s21 Cpn1 Cyp2c44 Erlin1 Chuk Cwf19l1 SNORA12 Bloc1s2 Pkd2l1 Scd3 AC123853.1 Scd2 AC123853.2 Scd4 Scd1
chr1:136500001-137000000	9.78	Kdm5b Gm3834 Syt2 Ppp1r12b AC131591.1 Ube2t Lgr6
chr16:30500001-31000000	9.70	Tmem44 Lsg1 Fam43a U6 SNORA17 AI480653 Gm15742
chr11:86000001-86500000	9.61	Brip1 4632419I22Rik Ints2 Med13 U3 Y_RNA 5S_rRNA U6 Rnft1 Rps6kb1 Tubd1 Vmp1 Mir21 Ptrh2
chr11:86500001-87000000	9.61	Ptrh2 Cltc Dhx40 AL596111.1 Ypel2 SCARNA3 Gdpd1 Gm11479 1200011M11Rik Prr11 Fam33a Mir301 Gm11491 Trim37
chr13:112500001-113000000	9.61	Mier3 Gm15287 Map3k1 Gm15327 Gm15325 Gm15324 Gm15326 Gm15322 Gm15323
chr13:44500001-45000000	9.53	Jarid2 SNORA61
chr15:79500001-80000000	9.53	Tomm22 Josd1 Gm17487 Gtpbp1 n-R5s40 Sun2 Gm16575 Gm16576 Dnalc4 Nptxr Npcd Cbx6 Apobec3 Cbx7 Pdgfb Rpl3 Snord83b snoU83B U6 Syngr1 Tab1
chr15:81500001-82000000	9.53	L3mbtl2 Chadl Rangap1 Zc3h7b Gm17597 Tef Gm8444 Tob2 Tob2 Phf5a Aco2 Polr3h Csdc2 Pmm1 Gm5805 1700029P11Rik Xrcc6 Pppde2 Nhp2l1 4930407I10Rik Mei1 Ccdc134 Srebf2
chr16:30000001-30500000	9.53	4632428C04Rik Hes1 n-R5s32 Gm17516 Cpn2 Lrrc15 Gp5 Atp13a3
chr18:55000001-55500000	9.53	Zfp608 Gm17270 Gm4221 SNORA40 U6
chr6:69500001-70000000	9.53	Igkv4-57 Igkv4-56 Gm11143 Igkv4-55 Igkv4-53 Igkv4-50 Igkv5-48 Igkv12-47 Igkv12-46 Igkv5-45 Igkv12-44 Igkv5-43 Igkv12-41 Igkv5-39 Igkv12-38 Igkv5-37 Igkv18-36 Igkv1-35 AC154006.1
chr6:70000001-70500000	9.44	Igkv7-33 Igkv6-32 Igkv8-30 Igkv6-29 Igkv8-28 AC159715.1 Igkv8-27 Igkv8-26 Igkv6-25 Igkv8-24 Igkv6-23 Igkv8-21 Igkv6-20 Igkv8-19 Igkv8-18 Igkv6-17 Igkv8-16 Igkv6-15 Gm10360 Igkv6-14 Igkv6-13 Igkv3-12
chr5:136500001-137000000	9.44	Dtx2 Upk3b 2310043J07Rik Rasa4 U12 Gm15701 Polr2j Lrwd1 Alkbh4 Orai2 Prkrip1 Sh2b2 Cux1 Gm16599
chr8:123000001-123500000	9.36	Gse1 Gins2 Cox4nb Cox4i1 7SK Irf8
chr2:166000001-166500000	9.27	5S_rRNA Gm11466 Gm11467 Gm11468 Gm14268 5031425F14Rik Gm14267 Prex1 AL732357.1
chr17:5000001-5500000	9.27	Arid1b 5730437N04Rik AC166064.1 Zdhhc14
chr19:5500001-6000000	9.27	Snx32 Ovol1 Gm962 Rnaseh2c Kat5 Rela Sipa1 Pcnxl3 Map3k11 Kcnk7 Ehbp1l1 Gm16538 Fam89b Sssca1 Ltbp3 Scyl1 Malat1 Gm20417 Neat1 Gm9783 Frmd8 Slc25a45 Tigd3 Dpf2 Cdc42ep2 Pola2 Slc22a20 Capn1
chr5:123000001-123500000	9.19	Ift81 P2rx7 Gm10064 P2rx4 Camkk2 Anapc5 Rnf34 Kdm2b A930024E05Rik Orai1 Morn3 Gm17627
chr12:86500001-87000000	9.19	Pgf Eif2b2 Mlh3 Acyp1 Fam164c Nek9 Tmed10 Fos Jdp2
chr17:46000001-46500000	9.19	Vegfa Mrps18a Rsph9 Mad2l1bp Gtpbp2 Polh Xpo5 Mir693 U6 Polr1c Yipf3 Gm88 Tjap1 Gm17358 Dlk2 Abcc10
chr2:31500001-32000000	9.11	Prdm12 Exosc2 Gm13427 Abl1 Qrfp Fibcd1 Gm13441 Lamc3 Aif1l Gm13442 Nup214 Gm13609 Fam78a Gm16534 Ppapdc3
chr8:125000001-125500000	9.11	Gm20388 Ctu2 Fam38a U6 Cdt1 Aprt Galns Trappc2l Pabpn1l Cbfa2t3 Gm10612 Acsf3 Gm16378 Cdh15 Ankrd11
chr12:101500001-102000000	9.11	Ttc7b Rps6ka5
chr17:30500001-31000000	9.11	Btbd9 Gm9874 Glo1 Dnahc8 U6
chr5:65000001-65500000	9.02	AC122043.1 Klf3 Tlr1 Tlr6 Fam114a1 Mir574 Tmem156 Klhl5
chr2:167500001-168000000	9.02	Tmem189 Cebpb A530013C23Rik Gm14321 9230111E07Rik 1200007C13Rik Gm14319 Ptpn1 Fam65c Gm14236 AL831766.1 Pard6b Gm14235 E130018N17Rik
chr11:117500001-118000000	9.02	Tnrc6c Tmc6 Tmc8 Gm11723 Gm11724 6030468B19Rik Syngr2 Afmid Tk1 Birc5 Cldn27 Tha1 Gm11725 Socs3 Pgs1 Dnahc17 Gm11738 Cyth1
chr2:166500001-167000000	8.94	Prex1 7SK U6 Trp53rk Arfgef2 Cse1l Gm17096 Stau1 Ddx27 Znfx1 1500012F01Rik SNORD12 SNORD12 Snord12 Gm14290 Kcnb1
chr10:118000001-118500000	8.94	Dyrk2 4932442E05Rik
chr11:116000001-116500000	8.94	Mrpl38 Fbf1 SCARNA4 Acox1 2310004N24Rik Cdk3-ps Evpl Srp68 Galr2 Exoc7 Gm16831 n-R5s74 Foxj1 Rnf157 Fam100b Qrich2 Gm11739 Prpsap1 Sphk1 Ube2o Aanat Rhbdf2
chr19:46500001-47000000	8.94	Sufu Trim8 Arl3 Sfxn2 D19Wsu162e Cyp17a1 2010012O05Rik As3mt Cnnm2 Nt5c2
chr2:27000001-27500000	8.77	Gm13399 Dbh Sardh Gm17071 Vav2 AA645442 AL731552.1 Brd3 Wdr5 U6atac Gm13421
chr3:95500001-96000000	8.77	Ecm1 Tars2 Rprd2 U1 Prpf3 Gm16884 Mrps21 C920021L13Rik Gm129 BC028528 Aph1a Car14 Anp32e Plekho1 Vps45 Otud7b Mtmr11 Gm17690 Sf3b4 SNORA19 Sv2a
chr5:66000001-66500000	8.77	Pds5a U6 1700022K14Rik N4bp2 SNORA73 Rhoh Chrna9 9130230L23Rik AC115293.1 Rbm47
chr9:61000001-61500000	8.77	Gm10655 Tle3
chr17:29500001-30000000	8.77	Fgd2 Gm16912 Pim1 Gm17657 Tmem217 Tbc1d22b Ftsjd2 AC163629.1 0610038L08Rik Rnf8 1110021J02Rik Mdga1
chr12:80000001-80500000	8.68	Plek2 Tmem229b Plekhh1 Pigh Arg2 Vti1b Rdh11 Rdh12 Zfyve26 Rad51l1
chr17:26500001-27000000	8.68	Neurl1b Dusp1 Gm8225 1700049J03Rik Ergic1 AC122252.1 Gm17218 Atp6v0e A930001N09Rik Bnip1 Nkx2-5 Gm17382 Gm20468
chr17:28000001-28500000	8.68	Uhrf1bp1 Taf11 Anks1 Gm15597 Gm15598 Tcp11 4930526A20Rik Scube3 Zfp523 Def6 Ppard

		Fance Rpl10a Tead3 Tulp1
chr9:57500001-58000000	8.60	Cyp1a2 Cyp1a1 Edc3 Clk3 Gm17231 Arid3b Ubl7 Sema7a Gm17322 Cyp11a1 Ccdc33 Gm16130 Stra6 Gm16131
chr9:60500001-61000000	8.60	Lrrc49 B930082K07Rik Larp6 1700036A12Rik Uaca Gm9869
chr16:33000001-33500000	8.60	Lrch3 Gm17106 n-R5s33 Iqcg Rpl35a Lmln AC126023.1 Mir1947 RNaseP_nuc Osbpl11 Snx4 AC122247.1 1700007L15Rik Zfp148
chr15:99500001-100000000	8.52	Accn2 Gm17349 Smarcd1 Gm17241 Gm16537 Gpd1 2310016M24Rik Lass5 Gm17058 Lima1 U6 Gm17057 1700030F18Rik U12 Larp4 Dip2b
chr18:36000001-36500000	8.52	Cxxc5 AC141471.1 Psd2 Nrg2 Pura
chr17:30000001-30500000	8.43	Mdga1 Gm16758 SNORA70 Zfand3 Btbd9 U6
chr19:41000001-41500000	8.43	Blnk Dntt Opalin Tll2 Tm9sf3 Pik3ap1
chr3:51500001-52000000	8.35	Maml3 AC116729.1 n-R5s196
chr11:59500001-60000000	8.35	Mprip 1700007J10Rik Gm12264 Pld6 Flcn Gm16062 5S_rRNA Cops3 Nt5m Gm12714 1810063I02Rik 1700013G23Rik Med9 Rasd1 Pemt Rai1 4930412M03Rik
chr13:24000001-24500000	8.35	Slc17a4 Hist1h2ba Hist1h2aa Scgn Gm11339 Lrrc16a SNORA17 Cmah Gm11342 Gm11345
chr15:84000001-84500000	8.35	Pnpla3 Samm50 Parvb SNORA48 Parvg 1810041L15Rik Ldoc1l
chr17:45000001-45500000	8.35	Supt3h
chr1:136000001-136500000	8.26	Gm8618 Chit1 Chi3l1 Mybph Adora1 U6 Myog Ppfia4 Tmem183a 4933406M09Rik Cyb5r1 Adipor1 Klhl12 Gm11092 Rabif SNORA61 4931440L10Rik Kdm5b
chr2:35000001-35500000	8.26	Cep110 Rab14 Gm13605 Gsn Stom 4930568D16Rik 4930402F06Rik Ggta1 Gm13447 Gm13446 Dab2ip
chr11:68500001-69000000	8.26	Myh10 Ndel1 Rnf222 Rpl26 U6 Odf4 Arhgef15 Slc25a35 Rangrf Pfas AL645902.1 U6 1500010J02Rik Aurkb 9330160F10Rik 2310047M10Rik Tmem107 Snord118 U6 Vamp2 Per1 9130213A22Rik Hes7 Aloxe3 Alox12b Alox8
chr11:77000001-77500000	8.26	Efcab5 Ssh2 SNORD86 Ssh2 Coro6 Ankrd13b 2210008F06Rik Git1 Trp53i13 Abhd15 Gm10392 Taok1 SNORA17 Nufip2
chr12:101000001-101500000	8.26	2610021K21Rik Tdp1 Kcnk13 AC159243.1 Psmc1 BC002230 Gm10433 Calm1 Gm17302
chr13:45000001-45500000	8.26	Jarid2 Dtnbp1 U6 Gm9817 7SK Mylip
chr9:61500001-62000000	8.18	Rplp1 Kif23 Paqr5 7SK Glce AC123610.1
chr11:98000001-98500000	8.18	Ikzf3 Fbxl20 Med1 Cdk12 AL591205.1 n-R5s73 Neurod2 Ppp1r1b 1700003D09Rik Stard3 Tcap Pnmt Pgap3 Erbb2 U6 1810046J19Rik Gm12352 Grb7 U2 Zpbp2 Ormdl3 Gm12 Gm12355 Gsdma3
chr16:29500001-30000000	8.18	Atp13a4 Opa1 Gm17734 Gm16761 Gm1968
chr17:73500001-74000000	8.18	Lclat1 SNORA17 Capn13 Galnt14 D630014O11Rik
chr9:63000001-63500000	8.09	Map2k5 2300009A05Rik Gm16759 Iqch AC122057.1 Aagab Smad3
chr3:95000001-95500000	8.09	Gabpb2 Gm16740 Mllt11 Cdc42se1 Gm128 Bnipl Prune Fam63a Fam63a Anxa9 Gm10691 Lass2 Setdb1 Gm4349 Arnt Ctsk Ctss Hormad1 Golph3l Ensa Mcl1 Adamtsl4
chr6:52500001-53000000	8.09	Hibadh SNORA32 Tax1bp1 Jazf1 SCARNA20
chr10:21000001-21500000	8.01	Hbs1l Aldh8a1 1700021A07Rik snoU13 1700020N01Rik Gm5420
chr12:78000001-78500000	8.01	Fntb Max AC133174.1 Fut8 U6
chr15:9000001-9500000	8.01	1110020G09Rik Skp2 Lmbrd2 Ugt3a1 Ugt3a2 Capsl Il7r
chr11:5000001-5500000	7.93	Rhbdd3 Emid1 Kremen1 U6 Znrf3 Gm11963 Xbp1 Ccdc117 SNORA17 Ankrd36
chr1:166500001-167000000	7.93	Dpt Xcl1 AC133891.1
chr7:87000001-87500000	7.93	Ap3s2 Gm17512 5430400D12Rik 2610034B18Rik AC110903.1 Zfp710 Idh2 AC164075.1 Mir1965 Sema4b Cib1 D330012F22Rik Ttll13 Ngrn Vps33b Prc1 6330403N20Rik Rccd1 Unc45a Hddc3 Man2a2
chr2:30000001-30500000	7.84	Tbc1d13 Endog D2Wsu81e Ccbl1 Lrrc8a Phyhd1 Dolk Nup188 Gm14471 AL954388.2 Sh3glb2 AL954388.1 Fam73b Dolpp1 Crat Gm16323 Ppp2r4 Ier5l Gm14487 Cstad 9330198N18Rik
chr8:108000001-108500000	7.84	Zdhhc1 Hsd11b2 Atp6v0d1 Agrp Gm17380 Gm8841 Fam65a Mir1966 Ctcf AC127419.1 Rltpr Acd Pard6a E130303B06Rik 4933405L10Rik Gfod2 Ranbp10 AC152826.1 Tsnaxip1 Cenpt Thap11 Nutf2 Edc4 Nrn1l Pskh1 Ctrl Gm16156 Psmb10 Lcat Slc12a4 Dpep3
chr8:129000001-129500000	7.84	AC118255.1 Gm16983 Irf2bp2 Tomm20 SNORA14 Rbm34
chr11:79000001-79500000	7.84	Wsb1 Gm9964 Nf1 AU040972 Omg Evi2b Evi2a Rab11fip4 U6 Gm11202 U6 U6 4930542H20Rik
chr13:41500001-42000000	7.84	Nedd9 AC154848.1 Tmem170b Gm5082 9530008L14Rik 1700061E18Rik U6
chr14:31000001-31500000	7.84	Cacna1d Dcp1a Tkt AC154646.1 Prkcd Rft1
chr17:32000001-32500000	7.84	Hsf2bp 7SK Rrp1b Pdxk-ps Gm17276 Notch3 Ephx3 Brd4 Gm17549 Akap8 Akap8l Wiz
chr1:135000001-135500000	7.76	Pik3c2b Ppp1r15b Plekha6 Golt1a Kiss1 Ren1 Etnk2 Sox13 SNORA32
chr10:80000001-80500000	7.76	Atp8b3 Rexo1 Klf16 Gm17682 Fam108a Adat3 Scamp4 Csnk1g2 Btbd2 Mknk2 Gm17306 Mob3a Izumo4 Ap3d1 Dot1l Gm17151 Plekhj1 Sf3a2 Amh Jsrp1 Oaz1 Mir1982 Lingo3 Lsm7 3110056O03Rik Tmprss9 Timm13 Lmnb2 Gadd45b Gng7 Diras1 Gm16099 Slc39a3
chr12:100500001-101000000	7.76	Foxn3 3300002A11Rik Gm16956 2610021K21Rik
chr15:98500001-99000000	7.76	Rnd1 Ccdc65 Fkbp11 Arf3 Wnt10b Wnt1 Ddn B130046B21Rik Prkag1 Mll2 Rhebl1 Dhh Lmbr1l Tuba1b Tuba1a 4930578M01Rik Gm8973 Tuba1c Prph Troap C1ql4 Dnajc22 Spats2 SNORA40
chr15:97500001-98000000	7.67	Rpap3 Endou Rapgef3 Gm16257 Gm16256 Slc48a1 Hdac7 Gm17532 Vdr 7SK Tmem106c Col2a1 Senp1 SNORA17 Pfkm Asb8 AI836003
chr19:6000001-6500000	7.67	Capn1 Gm10814 Syvn1 Mrpl49 Fau Znhit2-ps Tm7sf2 1110014N23Rik Zfpl1 BC048609 Cdca5 Gm550 Naaladl1 Sac3d1 Snx15 Arl2 Batf2 n-R5s19 1700123I01Rik Gpha2 Ppp2r5b Atg2a Mir194-2 Mir192 Gm14963 Ehd1 Cdc42bpg Men1 Map4k2 Gm14966 U7 Sf1 Pygm Rasgrp2 Gm14965 Nrxn2 AC167245.1
chr19:33000001-33500000	7.67	7SK Rnls Gm7237
chr5:34500001-35000000	7.67	Poln Haus3 U6 Mxd4 Zfyve28 Gm15513 Rnf4 Fam193a snoU13 Tnip2 Sh3bp2 U1 Add1 Mfsd10 Nop14 Gm15522
chr7:134000001-134500000	7.67	Ino80e Hirip3 Taok2 Tmem219 U6 Kctd13 Sez6l2 Asphd1 D830044I16Rik Cdipt Mvp Gm20418 2900092E17Rik Prrt2 Maz Kif22 7SK Zg16 U6 AI467606 Qprt Spn AC122537.1 Cd2bp2 Tbc1d10b

		Mylpf Sept1 Zfp553 Zfp771 Dctpp1 Sephs2 Gm17511 Itgal Zfp768
chr19:3500001-4000000	7.67	Ppp6r3 Lrp5 AC132452.1 1810055G02Rik Suv420h1 Gm16066 AC133523.1 Chka Tcirg1 Ndufs8 Aldh3b1 Unc93b1 1700055N04Rik Aldh3b2 Acy3 Tbx10
chr3:88000001-88500000	7.59	AW047730 Gm3764 AC044864.2 AC044864.1 Rhbg Gm17285 1700021C14Rik Cct3 0610031J06Rik Tmem79 Smg5 Paqr6 Bglap-rs1 Bglap2 Gm6821 Bglap Pmf1 Slc25a44 Sema4a Lmna Mex3a Mir1905 Rab25 Lamtor2 Ubqln4 Ssr2 Arhgef2 Rxfp4 2810403A07Rik SCARNA15
chr16:93000001-93500000	7.59	Mir802
chr18:35000001-35500000	7.59	Reep2 Egr1 Gm17507 Etf1 Hspa9 SNORD63 SNORD63 Gm6724 Ctnna1 Lrrtm2 Sil1 AC121874.1 snoU13
chr5:36500001-37000000	7.50	Sorcs2 Psapl1 2210406O10Rik Grpel1 Tada2b Ccdc96 Tbc1d14 D5Ertd579e
chr5:122500001-123000000	7.50	Cux2 Gm15637 Myl2 Ccdc63 Ppp1cc Hvcn1 Tctn1 Pptc7 Rad9b Vps29 1500011H22Rik Gpn3 Arpc3 Anapc7 Atp2a2 U6
chr7:135000001-135500000	7.50	AC149222.1 Zfp668 Zfp646 Prss53 Vkorc1 Bckdk Myst1 Prss8 Prss36 Fus Gm17468 B230325K18Rik Pycard Gm15533 Trim72 U1 Itgam Itgax Itgad Cox6a2 9130023H24Rik Armc5 Tgfb1i1 Slc5a2 BC017158 AC124566.1
chr13:24500001-25000000	7.50	Cmah U6 Fam65b Gm11346 C530050E15Rik 1700016G14Rik Gmnn BC005537 SNORA32 Acot13 Tdp2 D130043K22Rik 4932702P03Rik Aldh5a1
chr15:99000001-99500000	7.50	Spats2 7SK Kcnh3 Mcrs1 AC161198.1 Fam186b Prpf40b Fmnl3 U6 Tmbim6 Nckap5l 4921518J05Rik Bcdin3d Faim2 Aqp2 Aqp5 Aqp6 Racgap1 AC139317.1
chr16:10500001-11000000	7.50	Ciita Dexi Clec16a Gm15558 Socs1 Tnp2 Prm3 Prm2 Prm1 Gm10343 Gm11172 Gm17410 A630055G03Rik Litaf AC164093.1 U1
chr7:107500001-108000000	7.50	Ppme1 C2cd3 Ucp3 Ucp2 Dnajb13 Chchd8 Mrpl48 D630004N19Rik Rab6 Plekhb1 Fam168a Gm3200 Relt
chr12:32500001-33000000	7.42	Cog5 SCARNA17 Hbp1 Prkar2b Pik3cg
chr16:31500001-32000000	7.42	Dlg1 SNORA48 Mfi2 Pigz Ncbp2 Senp5 AC124681.1
chr6:86500001-87000000	7.42	1600020E01Rik AC158662.1 Asprv1 Mxd1 Snrnp27 Gmcl1 Anxa4 Aak1 Nfu1 Gfpt1
chr19:37500001-38000000	7.42	Hhex U6 Exoc6 Cyp26c1 Cyp26a1 Myof
chr1:133000001-133500000	7.34	Dyrk3 Eif2d Rassf5 Ikbke Srgap2 AC109299.1 Fam72a Avpr1b
chr2:165500001-166000000	7.34	Eya2 Zmynd8 AL591712.1 BC046401 Gm11465 AL589902.1 Gm11463 Gm11464 Ncoa3 Sulf2
chr3:89500001-90000000	7.34	Adar Chrnb2 4632404H12Rik Ube2q1 She Il6ra Atp8b2 U1 Hax1 Ubap2l SNORA58 4933434E20Rik Gm16540 1700094D03Rik Mir190b Tpm3 Nup210l SNORA41
chr5:149500001-150000000	7.34	2210417A02Rik n-R5s179 4930505K14Rik Gm15407 Katnal1 Gm15410 Gm15406 8430423G03Rik 1810059H22Rik Gm15409 Gm15411 Gm15408 Hmgb1 5730422E09Rik AC122546.2 Uspl1
chr9:71500001-72000000	7.34	Cgnl1 Tcf12 Rpl15-ps2 U6
chr19:32000001-32500000	7.34	A1cf Asah2 Sgms1 2700046G09Rik
chr19:44500001-45000000	7.34	Wnt8b Sec31b Ndufb8 Ndufb8 Hif1an Gm17704 Pax2 Gm20395 1700039E22Rik
chr5:140500001-141000000	7.25	Mad1l1 Gm16122 Gm16121 Gm16120 Ftsj2 Nudt1 Snx8 Eif3b Chst12
chr11:5500001-6000000	7.25	Ankrd36 Mrps24 Urgcp 2210015D19Rik Dbnl Pgam2 Polm Aebp1 Pold2 Myl7 Gck Gm11967 Ykt6 Camk2b
chr11:118000001-118500000	7.25	Cyth1 U6 Usp36 Timp2 BC100451 Lgals3bp Cant1 C1qtnf1 Gm11747 Gm11748 Engase Rbfox3
chr15:100000001-100500000	7.25	Dip2b Atf1 Tmprss12 Gm5474 Mettl7a1 Mettl7a3 Mettl7a2 Slc11a2 Gm5475 n-R5s43 5330439K02Rik Letmd1 Csrnp2 Tcfcp2 Pou6f1 C330013E15Rik Dazap2 Smagp Bin2
chr19:41500001-42000000	7.25	U7 Lcor Gm340 AI606181 Slit1 7SK Arhgap19 Frat2 Rrp12 Pgam1 Exosc1
chr1:135500001-136000000	7.17	Snrpe Gm17713 Zc3h11a Lax1 Gm17678 Atp2b4 Optc Gm15851 Prelp Fmod Btg2
chr2:28000001-28500000	7.17	Gfi1b Olfm1 Gm13373 Gm347 1700007K13Rik Mrps2 Gbgt1 Gm10134 Ralgds Cel Gtf3c5 Gm13381 U6 AL731851.1 Tsc1
chr8:47500001-48000000	7.17	Acsl1 Mlf1ip Ccdc111 Casp3 Gm16675 Irf2
chr9:44500001-45000000	7.17	Phldb1 SNORA2 Arcn1 Ift46 Tmem25 Ttc36 Mll1 U6atac Atp5l Ube4a Cd3g Cd3d Cd3e Mpzl2 Mpzl3 Amica1 Gm10684 Scn2b Scn4b Tmprss4 Gm17099 BC049352
chr9:63500001-64000000	7.17	Smad3 Smad6 5S_rRNA 1110036E04Rik Lctl Zwilch
chr9:72000001-72500000	7.17	Gm7866 U6 Zfp280d BC065403 Mns1 Tex9 Tex9 AC111135.1 4930509E16Rik Rfx7 U6
chr10:19000001-19500000	7.17	Olig3 Ifngr1 Il22ra2 9230106D20Rik Il20ra
chr10:20000001-20500000	7.17	Mtap7 4933406P04Rik Bclaf1 Fam54a Pde7b 4930403O15Rik
chr17:27000001-27500000	7.17	Gm17382 Gm20468 Kifc5b Phf1 Cuta AC144621.1 Syngap1 Zbtb9 Ggnbp1 Bak1 Itpr3 1700062I23Rik 2900010M23Rik Ip6k3 Lemd2 Gm17262 Gm10505
chr1:88000001-88500000	7.08	Psmd1 Htr2b Armc9 Gm16341 B3gnt7 Gm5258 Ncl Snora75 SNORD20 Snord82 C130036L24Rik Nmur1 Rpl30-ps6 Ptma Pde6d Cops7b
chr1:166000001-166500000	7.08	Sell Selp Gm16587 Gm16548 F5 Slc19a2 4930455F23Rik Blzf1 Nme7 Atp1b1 Gm16608
chr2:29000001-29500000	7.08	Setx Ntng2 6530402F18Rik Med27 Gm13402 5S_rRNA Rapgef1
chr5:34000001-34500000	7.08	Tmem129 Tacc3 Fgfr3 Letm1 Whsc1 Whsc2 Gm1673 Nat8l Poln Haus3
chr1:134000001-134500000	7.00	Cdk18 Lemd1 Mir135b 1700037F24Rik Gm10188 Klhdc8a Nuak2 Tmcc2 Gm15849 Dstyk 6030442K20Rik Rbbp5 Tmem81 Cntn2 Nfasc
chr9:66500001-67000000	7.00	Car12 Aph1b Gm10647 BC050972 Aph1c Gm17098 Rab8b Rps27l Lactb U6 Tpm1 U1
chr10:18500001-19000000	7.00	Gm4922 Perp Tnfaip3
chr12:70500001-71000000	7.00	AC153658.1 Mettl21d Sos2 U6 L2hgdh Atp5s Cdkl1 Mir681 4930512B01Rik Map4k5 4931403G20Rik Atl1
chr17:26000001-26500000	7.00	Gm17480 Fam195a 0610011F06Rik Wfikkn1 Rab40c Gm16278 Pigq Nhlrc4 A930017K11Rik D630044L22Rik Solh 1700022N22Rik Rab11fip3 Decr2 Nme4 Tmem8 Mrpl28 Axin1 Pdia2 Arhgdig Rgs11 Itfg3 SNORA48 Luc7l
chr1:37500001-38000000	6.91	Mgat4a 2010300C02Rik 4930556I23Rik Tsga10 Gm17715 Lipt1 Mitd1 Mrpl30 Lyg2 Gm15457
chr5:32500001-33000000	6.91	Plb1 Ppp1cb Gm15614 Yes1
chr5:64500001-65000000	6.91	Pgm1 SNORA17 Tbc1d1
chr13:102500001-103000000	6.91	Pik3r1 7SK

chr15:78000001-78500000	6.91	Ift27 Pvalb Ncf4 Csf2rb2 Csf2rb Y_RNA 1700061J05Rik Tst Mpst Kctd17 Tmprss6 Il2rb C1qtnf6 Sstr3 Gm6723 Rac2 Cyth4
chr1:36500001-37000000	6.83	Lman2l Cnnm4 Cnnm3 Ankrd23 Ankrd39 Sema4c D430040D24Rik Fam178b AC084389.1 Cox5b Actr1b Zap70 Tmem131
chr5:123500001-124000000	6.83	Gm17627 Tmem120b Rhof AI480526 Setd1b Hpd Psmd9 Wdr66 Gm15857 Gm15860 Bcl7a U1 Gm15747 Mlxip Il31 Lrrc43 Gm15751 Diablo B3gnt4 SCARNA20 Vps33a
chr5:137000001-137500000	6.83	Cux1 4731417B20Rik Myl10 Emid2 RP24-498F17.1 Rabl5 4933404O12Rik Fis1 Cldn15 Znhit1 Plod3 Mir702
chr6:87500001-88000000	6.83	Prokr1 Aplf E230015B07Rik 1810020O05Rik AC158626.1 Ccdc48 Gm5879 Gp9 Rab43 Isy1 Cnbp Copg Gm16723 8430410A17Rik H1fx Gm5577 Rab7
chr10:43000001-43500000	6.83	Pdss2 Gm10281 Gm3699 Bend3 1700021F05Rik Cd24a F930017D23Rik
chr11:77500001-78000000	6.83	Nufip2 Cryba1 Myo18a Gm10277 Pipox Gm11190 Sez6 Phf12 A030003K02Rik Dhrs13 Flot2 Mir144 Mir451 Eral1 BC017647 Traf4 Nek8 Tlcd1 Rpl23a Snord42a Snord4a Snord42b AL591070.1
chr14:77000001-77500000	6.83	9030625A04Rik Ccdc122
chr8:10500001-11000000	6.75	Myo16 3930402G23Rik Irs2
chr14:22000001-22500000	6.75	Adk 7SK U6 Myst4 Dupd1
chr16:95500001-96000000	6.75	Kcnj15 Erg Ets2
chr12:83000001-83500000	6.75	Pcnx n-R5s62 Sipa1l1
chr2:34000001-34500000	6.66	Pbx3 C79798 Mapkap1
chr2:118000001-118500000	6.66	Fsip1 AL845495.1 A930104D05Rik Gpr176 1700054M17Rik 5S_rRNA Eif2ak4 Srp14 Bmf Bub1b Pak6
chr8:125500001-126000000	6.66	Gm20388 Ankrd11 U6 Spg7 Rpl13 Snord68 Cpne7 Sult5a1 Dpep1 Chmp1a 4732415M23Rik Cdk10 Spata2L 4933417D19Rik 1300018I17Rik Zfp276 AC155810.1 Fanca Spire2 Tcf25 AC122266.1 Mc1r Tubb3 Def8 SNORA63
chr9:70000001-70500000	6.66	Gm17406 Myo1e Ccnb2 Rnf111 SNORA20 U6 U6 AC158995.1 U6 Sltm Fam63b
chr10:59500001-60000000	6.66	Ascc1 Spock2 Chst3 AC155640.1 AC155640.2 Psap Cdh23 4632428N05Rik Gm17455
chr16:20000001-20500000	6.66	Klhl24 Yeats2 Map6d1 Parl Cyp2ab1 Abcc5 7SK Eif2b5
chr2:26000001-26500000	6.58	Notch1 Gm13553 Lhx3 Qsox2 C030048H21Rik C030048H21Rik 4932418E24Rik Gpsm1 Dnlz Card9 Gm13562 Snapc4 Gm13563 Sdccag3 Pmpca Inpp5e Sec16a 0610009E02Rik Gm13568 Notch1 Egfl7 Gm20532 Mir126 Agpat2 Fam69b Snhg7 Snora43 Snora17 5730588L14Rik
chr5:35000001-35500000	6.58	Nop14 Grk4 Mir467g Htt A930005I04Rik Rgs12 AC126447.1 Hgfac Dok7 Lrpap1
chr8:122500001-123000000	6.58	Gm20388 Crispld2 Gm15684 Zdhhc7 Gm15898 6430548M08Rik Fam92b
chr11:120000001-120500000	6.58	Slc38a10 Gm11769 2810410L24Rik Gm11770 2900052L18Rik Bahcc1 Gm11772 Actg1 AL669855.1 0610009L18Rik Fscn2 2310003H01Rik Nploc4 Tspan10 Pde6g 1810049H13Rik Ccdc137 Arl16 Hgs Mrpl12 Gm16755 Gm11788 Slc25a10 Gm11789 Gcgr Fam195b Dysfip1 P4hb Arhgdia Thoc4 Anapc11 Npb Pcyt2 Sirt7 Mafg Gm17586 Pycr1
chr19:32500001-33000000	6.58	Rpl9-ps6 Minpp1 Papss2 Atad1 Pten
chr2:119500001-120000000	6.49	Rtf1 SNORA44 Itpka Ltk Rpap1 U6 Tyro3 Mga Mapkbp1 Gm13999 Pla2g4b Spnb5 Ehd4 Pla2g4e
chr1:38000001-38500000	6.49	Gm15457 Lyg1 7SK Txndc9 Eif5b Rev1 Aff3 Gm16150 Gm16151 Gm16152
chr1:134500001-135000000	6.49	Nfasc SNORA17 Lrrn2 Mdm4 Pik3c2b
chr2:28500001-29000000	6.49	Tsc1 1700026L06Rik Ak8 AL731851.2 Gtf3c4 Ddx31 Barhl1 1700101E01Rik Ttf1 Gm13395 Gm13393 Setx
chr10:117000001-117500000	6.49	Cpm U6 Mdm2 Slc35e3 Nup107 Rap1b
chr11:115500001-116000000	6.49	Grb2 SNORA70 2310067B10Rik Caskin2 Tsen54 Llgl2 Myo15b Recql5 2210020M01Rik 1110017F19Rik Rpl29-ps3 Sap30bp Gm11721 Itgb4 B230344G16Rik Galk1 H3f3b Unk Unc13d Wbp2 Trim47 Trim65 Mrpl38
chr11:116500001-117000000	6.49	Cygb Gm11744 1810032O08Rik Snord1c snoR38 Snord1b Snord1a St6galnac2 Gm11735 St6galnac1 BC018473 Gm17558 Mxra7 Jmjd6 1110005A03Rik Srsf2 Mfsd11 Mgat5b Gm11728 Gm11731 2810008D09Rik SCARNA16 AL627205.1 Gm11730 Sec14l1 7SK
chr11:118500001-119000000	6.49	Rbfox3 Gm11750 AL591544.1 Gm11749 Enpp7 Cbx2 Cbx8 Gm17569 Cbx4 AL662835.1 Gm11754 Gm11755
chr16:24000001-24500000	6.49	1110054M08Rik Lpp U7
chr17:84500001-85000000	6.49	Zfp36l2 Thada U6 U6 Plekhh2
chr7:52500001-53000000	6.41	U6 1700039E15Rik Trpm4 Hrc Ppfia3 Mtag2 Lin7b Snrnp70 SNORA67 Kcna7 Ntf5 Lhb Ruvbl2 Gys1 Ftl1 AC151602.1 Bax Dhdh Tulp2 Nucb1 Ppp1r15a Plekha4 Gm16022 Hsd17b14 0610005C13Rik Bcat2 Fgf21 Fut1 Izumo1 Rasip1 Gm16047 Mamstr Fut2 Sec1 Ntn5 Car11 Dbp Sphk2 Rpl18 Fam83e Spaca4 Sult2b1 AC167242.1
chr11:45000001-45500000	6.41	Gm12160 Gm12162 SNORA17
chr17:5500001-6000000	6.41	Zdhhc14 Snx9 Synj2
chr7:108500001-109000000	6.32	Arap1 Pde2a Mir139 Art2a-ps Art2b Clpb Phox2a Inppl1 Folr2
chr2:35500001-36000000	6.32	Dab2ip Ttll11 9030204H09Rik Ndufa8 Morn5 Lhx6 Rbm18 Mrrf
chr10:83500001-84000000	6.32	Nuak1 4930463O16Rik Ckap4
chr19:4500001-5000000	6.32	Pcx Lrfn4 Rce1 Gm960 Spnb3 Rbm4b Rbm14 Ccs Ccdc87 Ctsf Actn3 Zdhhc24 Bbs1 U6 Dpp3 Peli3 Mrpl11 Npas4
chr19:10500001-11000000	6.32	Syt7 Lrrc10b 4930579J09Rik Sdhaf2 Cpsf7 Tmem216 Tmem138 Cybasc3 Dak Ddb1 Vwce Pga5 Vps37c Cd5 A430093F15Rik Cd6 Slc15a3 Tmem132a Tmem109 Prpf19 Zp1
chr10:44000001-44500000	6.24	Atg5 Mir1929 Prdm1 U6 U6
chr11:69000001-69500000	6.24	Alox8 Gucy2e U6 1700067G03Rik Cntrob Trappc1 Kcnab3 Gm16040 A030009H04Rik Chd3 SCARNA21 Gm17305 Cyb5d1 Lsmd1 Tmem88 Kdm6b 1700064E03Rik Dnahc2 6030455H03Rik Efnb3 Wrap53 Trp53 Atp1b2 Shbg Sat2 Fxr2 Mir467f Sox15 Mpdu1 Mir1934 Cd68 Eif4a1 SNORA67 snoU6-77 SNORA48 Senp3 2010012P19Rik BC096441 Tnfsf13 Tnfsf12
chr11:75500001-76000000	6.24	Crk Ywhae Gm16626 Doc2b Gm12339 Rph3al Gm16075 1700016K19Rik Fam101b Vps53 Glod4 Fam57a

chr14:62000001-62500000	6.24	Kpna3 Rps12-ps2 6330409N04Rik Trim13 Kcnrg Dleu2 AC154660.1 AC154660.2 Mir1196
chr9:96000001-96500000	6.15	Gk5 Tfdp2 Atp1b3 Gm17562 BC043934 Rnf7 Rasa2 n-R5s87
chr10:43500001-44000000	6.15	Gm9034 Qrsl1 Rtn4ip1 Aim1 Atg5
chr13:54500001-55000000	6.15	Gm16248 7SK Thoc3 4732471D19Rik 4833439L19Rik Arl10 AC155262.1 Nop16 Higd2a Cltb Faf2 Rnf44 Cdhr2 Gprin1 Sncb Gm16249 Eif4e1b Tspan17
chr13:55000001-55500000	6.15	5330429C05Rik 4930526F13Rik Unc5a Hk3 Uimc1 Zfp346 Gm17617 Fgfr4 Nsd1 Rab24 Prelid1 Mxd3 Lman2 Rgs14
chr17:4500001-5000000	6.15	U6 Arid1b
chr17:25000001-25500000	6.15	Hagh Igfals Nubp2 Spsb3 Eme2 Mapk8ip3 Mrps34 Nme3 Hn1l Cramp1l Ift140 Tmem204 Telo2 Ptx4 Clcn7 Ccdc154 Unkl Gnptg 0610007P22Rik Baiap3 AC122454.1 Ube2i Prss34 SNORA70 Prss28 Prss29 Gm8123 Tpsab1
chr17:35000001-35500000	6.15	Gm20547 C2 Zbtb12 Ehmt2 Slc44a4 Neu1 1110038B12Rik AC087117.3 AC087117.2 AC087117.1 Hspa1b Hspa1a Gm20481 Hspa1l Gm10501 Lsm2 D17H6S56E-5 Vars D17H6S56E-3 Ng23 Msh5 U6 Clic1 Ddah2 AU023871 Ly6g6c Ly6g6c Ly6g6d Ly6g6e Ly6g6f Abhd16a Ly6g5c Ly6g5b Csnk2b RP23-115O3.9 Gm20522 Gpank1 D17H6S53E Apom Bag6 Prrc2a SNORA38 Gm17705 Aif1 Lst1 Ltb Tnf Lta Nfkbil1 Gm16181 Atp6v1g2 Ddx39b SNORD83 SNORD83 CR974466.1 H2-D1 Gm18733 H2-Q2 H2-Q2
chr17:44500001-45000000	6.15	Runx2 Gm16317 Runx2 n-R5s27 9530072K05Rik Gm10497 Supt3h
chr19:5000001-5500000	6.15	Slc29a2 B3gnt1 Brms1 Rin1 Cd248 Tmem151a Yif1a Cnih2 Rab1b Klc2 Pacs1 Sf3b2 Gal3st3 Catsper1 Cst6 Banf1 Eif1ad Sart1 Tsga10ip 4930481A15Rik Drap1 AI837181 SNORD86 Fosl1 Ccdc85b Fibp Ctsw Efemp2 Mus81 Cfl1 Snx32
chr5:36000001-36500000	6.07	Htra3 Sh3tc1 Gm15650 Ablim2 Afap1 Sorcs2
chr6:51500001-52000000	6.07	Snx10 AC153877.1 Skap2
chr7:105500001-106000000	6.07	Tsku Gucy2d Lrrc32 U1 A630091E08Rik 2210018M11Rik Gm15506 Prkrir Wnt11
chr12:78500001-79000000	6.07	Fut8 U1 SNORA17
chr17:27500001-28000000	6.07	Grm4 Hmga1 AI413582 C130040N14Rik Nudt3 Rps10 Gm15420 Pacsin1 Spdef Gm15458 D17Wsu92e Snrpc Uhrf1bp1
chr17:32500001-33000000	6.07	Wiz Gm17561 CT485616.1 Rasal3 A530088E08Rik Pglyrp2 Cyp4f39 Cyp4f17 Cyp4f16 Gm9705 Cyp4f40 Cyp4f15 Zfp871 Gm17115 Zfp811 U1 5S_rRNA Gm16684 Zfp799
chr5:141000001-141500000	5.99	Chst12 Grifin Lfng Ttyh3 Iqce Baat1 Amz1 Gna12 Card11
chr6:39000001-39500000	5.99	Tbxas1 Parp12 4930599N23Rik Jhdm1d U6 Slc37a3 Rab19 Mkrn1 Gm10244 SNORA71 AC153624.1 Dennd2a 8030453O22Rik
chr9:64000001-64500000	5.99	Zwilch Rpl4 SNORD18 Snord16a SNORD18 SNORD16 SNORD18 Snapc5 Map2k1 AC160118.1 Uchl4 Tipin SCARNA14 Dis3l Megf11
chr9:108000001-108500000	5.99	Bsn F630040L22Rik Dag1 Nicn1 Amt Tcta Rhoa Gpx1 Usp4 1700102P08Rik Ccdc36 SNORA70 BC048562 Klhdc8b Ccdc71 Lamb2 Usp19 Qars Qrich1 Impdh2 Ndufaf3 CT010508.1 Mir425 Dalrd3 Wdr6 P4htm
chr10:116500001-117000000	5.99	Cct2 Frs2 SNORA13 Yeats4 9530003J23Rik Gm10936 Lyz2 Lyz1 Cpsf6
chr11:75000001-75500000	5.99	Dph1 Rtn4rl1 Rpa1 Smyd4 Serpinf1 Gm12336 Serpinf2 Wdr81 2210403K04Rik Tlcd2 Mir22 Prpf8 Rilp Scarf1 Slc43a2 AL591496.1 Pitpna 4931413K12Rik Inpp5k Myo1c Crk
chr11:78000001-78500000	5.99	Rab34 Proca1 Supt6h Sdf2 2610507B11Rik Gm11192 BC030499 Gm11193 Spag5 Aldoc Pigs Unc119 Foxn1 Gm11194 Slc13a2 Gm11195 Slc46a1 Sarm1 Vtn Sebox Tmem199 Poldip2 Tnfaip1 Ift20 Tmem97 SNORA70 Nlk
chr15:82500001-83000000	5.99	Cyp2d37-ps Cyp2d40 Gm5062 Cyp2d26 Tcf20 AC129563.1 AW121686 Nfam1 Serhl Gm17206 Rrp7a Poldip3 U12 Cyb5r3
chr17:47000001-47500000	5.99	A330017A19Rik Tbcc AC165289.1 Prph2 Ubr2 7SK Gm16494 Gm4945 Trerf1 5S_rRNA
chr18:34500001-35000000	5.99	Reep5 Pkd2l2 Fam13b n-R5s24 Wnt8a Nme5 4933408B17Rik Brd8 Kif20a Cdc23 n-R5s25 Gfra3 Cdc25c Gm3550 2010110K18Rik Fam53c Kdm3b Gm17557
chr7:107000001-107500000	5.90	Spcs2 Xrra1 Rnf169 RP23-428N8.1 Chrdl2 Pold3 Lipt2 Kcne3 Pgm2l1 P4ha3 Ppme1
chr11:119000001-119500000	5.90	Tbc1d16 Gm17433 Gm11753 Gm11752 Ccdc40 Gaa Eif4a3 Card14 Sgsh Slc26a11 Mir1932 Rnf213 A730011L01Rik Nptx1 Gm11762 Rptor
chr12:100000001-100500000	5.90	Zc3h14 Eml5 Ttc8 Rpl30-ps8 Foxn3
chr14:70500001-71000000	5.90	Bin3 2610301G19Rik 9930012K11Rik Pdlim2 Sorbs3 Gm16600 Ppp3cc Slc39a14 Piwil2 SNORA70 U11 Polr3d Mir320 Phyhip Bmp1 Sftpc Lgi3 Reep4 Hr Nudt18 Fam160b2
chr15:58500001-59000000	5.90	Fer1l6 Tmem65 U1 Gm5959 Trmt12 Rnf139 Tatdn1 Ndufb9 Mtss1
chr18:65000001-65500000	5.90	Nedd4l Mir122a Alpk2 F730048M01Rik
chr19:37000001-37500000	5.90	Btaf1 Cpeb3 CPEB3_ribozyme A330032B11Rik AC113124.1 March5 U6 Ide Kif11
chr6:31000001-31500000	5.82	Mir29a Mir29b-1 Gm13834 Gm13833 AB041803 2210408F21Rik Gm14532 Gm13845 Gm13844 Mkln1 Podxl
chr6:51000001-51500000	5.82	Mir148a Gm9953 Gm17725 Nfe2l3 Hnrnpa2b1 Cbx3 Snx10
chr11:98500001-99000000	5.82	Gsdma2 Gsdma Psmd3 Gm12356 Csf3 Med24 SNORD124 Thra Nr1d1 Msl1 Gm12359 Casc3 Rapgefl1 Wipf2 U6 Cdc6 Rara U6 Gjd3 Top2a SNORA42 SNORA32 Igfbp4 Tns4
chr15:74500001-75000000	5.82	Arc Jrk 4933427E11Rik Psca Lypd2 4930572J05Rik Slurp1 2300005B03Rik Lynx1 Ly6d Gm17189 Ly6k Gml Hemt1 Cyp11b1 Cyp11b2 2010109I03Rik Ly6e Ly6i Ly6a Ly6c1 Ly6c2 Ly6g
chr16:91500001-92000000	5.82	Ifnar1 Ifngr2 Tmem50b Gm15964 Dnajc28 Gart Son Donson Atp5o Gm10785 Cryzl1 Itsn1 U6 Gm15976 D430001F17Rik
chr19:7000001-7500000	5.82	Kcnk4 Gpr137 Bad Plcb3 Ppp1r14b Fkbp2 Vegfb Dnajc4 Nudt22 Trpt1 Fermt3 Stip1 Macrod1 Flrt1 Otub1 Cox8a Naa40 U6 5S_rRNA Rcor2 Mark2 Gm17227 AI846148 2700081O15Rik
chr3:52500001-53000000	5.82	U6 Cog6 Lhfp
chr11:68000001-68500000	5.82	Stx8 C78197 RP23-25D18.6 Ntn1 Gm12305 AL662894.1 Pik3r5 Pik3r6 Mfsd6l 4930535C22Rik Ccdc42
chr12:81500001-82000000	5.82	Dcaf5 Exd2 Gm16866 AC163282.1 Galntl1 U6 Erh Slc39a9 0610009B14Rik 3830431G21Rik Gm1568 Gm17242 4933426M11Rik Gm17461
chr13:93500001-94000000	5.82	Thbs4 Mtx3 Cmya5 Papd4

chr14:70000001-70500000	5.82	Gm16867 Loxl2 R3hcc1 Chmp7 4930480K23Rik Tnfrsf10b Rhobtb2 Pebp4 Egr3 Bin3
chr16:92500001-93000000	5.82	Clic6 Runx1 Gm16801
chr19:4000001-4500000	5.82	Nudt8 Gm16312 Doc2g Ndufv1 Gstp1 Gstp2 BC021614 U3 Cabp2 Cdk2ap2 Pitpnm1 Aip Tmem134 Cabp4 Gpr152 Coro1b Ptprcap Rps6kb2 Carns1 Gm17552 Tbc1d10c Ppp1ca Rad9 Clcf1 AC109138.1 Pold4 Ssh3 Ankrd13d Adrbk1 Kdm2a Rhod A930001C03Rik Syt12 2010003K11Rik
chr1:38500001-39000000	5.73	Aff3 Lonrf2 Chst10 Nms
chr2:24500001-25000000	5.73	Cacna1b Ehmt1 AL732525.1 Arrdc1 AL732525.2 Zmynd19 Wdr85 Mrpl41 Pnpla7 U6 U6 Nelf AL732585.1 Entpd8 Noxa1 Gm13387
chr5:31000001-31500000	5.73	Dpysl5 Mapre3 Gm15461 Tmem214 Agbl5 Ost4 Emilin1 Khk Cgref1 Abhd1 Preb Tcf23 Slc5a6 0610007C21Rik Cad Slc30a3 Gm9924 Dnajc5g Trim54 Gm15469 Ucn Mpv17 Gtf3c2 Eif2b4 Snx17
chr11:76500001-77000000	5.73	Tusc5 Gosr1 Cpd Tmigd1 Blmh U1 Slc6a4 Gm12343 Ccdc55 SNORA33 Mir423 Efcab5
chr11:100500001-101000000	5.73	Zfp385c Gm11547 Dhx58 Kat2a Hspb9 Rab5c Kcnh4 Hcrt Ghdc 7SK Stat5b Stat5a Stat3 Ptrf Atp6v0a1 Naglu Hsd17b1 Coasy Mlx Psmc3ip Fam134c Tubg1
chr11:115000001-115500000	5.73	Rab37 Slc9a3r1 Nat9 Tmem104 Grin2c AL603828.1 Fdxr Fads6 Otop2 Ush1g Otop3 C630004H02Rik Cdr2l Ict1 C920011F04Rik Atp5h Kctd2 4933422H20Rik AL645470.1 Gm11695 Slc16a5 Armc7 Nt5c Hn1 Sumo2 Nup85 Gga3 U6 Mrps7 Mif4gd Slc25a19 Gm17246
chr14:62500001-63000000	5.73	Dleu7 Rnaseh2b
chr16:33500001-34000000	5.73	Zfp148 Slc12a8 Heg1 Gm15658 Gm15657 Muc13 Itgb5 Umps Gm15829 Kalrn
chr16:93500001-94000000	5.73	Setd4 Cbr1 7SK Cbr3 Dopey2 2310043M15Rik Morc3 Chaf1b Cldn14
chr19:24500001-25000000	5.73	Pip5k1b 4930418C01Rik Fam122a E030010A14Rik Pgm5 Gm10053 Foxd4 Cbwd1
chr3:89000001-89500000	5.65	U6 Gba Mtx1 Thbs3 Mir92b Muc1 Trim46 Krtcap2 Dpm3 Slc50a1 Efna1 AC132327.1 Efna3 Gm15998 Efna4 4731419I09Rik Adam15 Dcst1 Zbtb7b Gm15417 Lenep Flad1 Cks1b Shc1 Pygo2 Pbxip1 Pmvk Kcnn3
chr6:52000001-52500000	5.65	Gm15055 Hoxa1 Gm15051 Hoxa2 Hoxa3 5730446D14Rik Hoxa3 Gm15050 2700086A05Rik 5730596B20Rik Hoxa4 Hoxa5 Hoxa6 Hoxa7 Hoxa9 RP23-329P9.11 Mir196b Hoxa10 Hoxa11 Hoxa11as Hoxa13 Gm15053 5730457N03Rik Evx1 Hibadh
chr6:67000001-67500000	5.65	E230016M11Rik A430010J10Rik Serbp1 Il12rb2 Il23r Tacstd2
chr13:55500001-56000000	5.65	Slc34a1 Pfn3 F12 Grk6 Prr7 Dbn1 Pdlim7 Dok3 Ddx41 Fam193b Tmed9 B4galt7 Gm15911 Caml Ddx46 B230219D22Rik Txndc15 Pcbd2 4930451E10Rik Catsper3 Pitx1
chr17:4000001-4500000	5.65	
chr17:46500001-47000000	5.65	Zfp318 7SK Crip3 Slc22a7 Gm5093 Ttbk1 Gm16736 BC048355 Cul9 Srf Ptk7 Klc4 Mrpl2 Cul7 Rrp36 Klhdc3 Mea1 Ppp2r5d Pex6 Gnmt Cnpy3 Ptcra 2310039H08Rik Rpl7l1 BC032203
chr19:57000001-57500000	5.65	Afap1l2 Ablim1 B230217O12Rik Fam160b1
chr2:26500001-27000000	5.65	5730588L14Rik Lcn4 Abo Surf6 Med22 Rpl7a SNORD24 SNORD36 SNORD36 SNORD36 Surf1 Surf2 Surf4 Gm711 Rexo4 Adamts13 5930434B04Rik Slc2a6 Gm13398 Tmem8c Adamtsl2 Fam163b
chr5:122000001-122500000	5.65	Aldh2 Acad12 Acad10 Brap Atxn2 Gm16552 Sh2b3 Fam109a Cux2 Gm15637
chr8:74500001-75000000	5.65	Zfp961 Cyp4f18 U2 Olfr372 Olfr373 Olfr374 5S_rRNA AC158898.2 Tpm4 Gm17371 Gm16091 Rab8a Hsh2d Cib3 Gm11034 Fam32a AC158898.1 Ap1m1 Gm10282 Klf2 Eps15l1 Calr3 1700030K09Rik Cherp
chr8:128000001-128500000	5.65	Sipa1l2 4933403G14Rik Ntpcr Pcnxl2 BC021891
chr11:22500001-23000000	5.65	Gm17335 Gm12052 Gm12055 Gm12056 Commd1 B3gnt2 RP23-242C19.6 SNORA63 RP23-242C19.5 U6 Zrsr1 Cct4 Fam161a 5S_rRNA Gm12059
chr16:24500001-25000000	5.65	Lpp Mir28 SNORA17
chr18:39500001-40000000	5.65	Arhgap26 Gm15337 Nr3c1 Gm10008 Pabpc2
chr5:107500001-108000000	5.56	Tgfbr3 U6 Brdt n-R5s173 Ephx4 Gm17202 Lpcat2b Btbd8 A830010M20Rik 1700028K03Rik Glmn
chr7:87500001-88000000	5.56	Man2a2 Fes Furin Blm Crtc3 Gm15880 Iqgap1
chr9:13500001-14000000	5.56	Maml2 Mtmr2 Cep57 Fam76b
chr10:94500001-95000000	5.56	Cradd Socs2 5730420D15Rik Mrpl42 Ube2n
chr11:97000001-97500000	5.56	Tbkbp1 Kpnb1 Gm11583 Npepps Gm11592 Mrpl45 Gpr179 Socs7 Arhgap23 4933428G20Rik Srcin1 Gm11611 Gm11612 2410003L11Rik E130012A19Rik
chr11:97500001-98000000	5.56	Gm11613 AL596123.1 Mllt6 Cisd3 Pcgf2 Psmb3 Pip4k2b Gm11614 Cwc25 Gm17413 1700001P01Rik Rpl23 Snora21 Lasp1 B230217C12Rik B230217C12Rik Fbxo47 Gm11630 Plxdc1 AL591209.1 Arl5c Cacnb1 Gm11629 Rpl19 Stac2 Fbxl20 Gm11632
chr14:26000001-26500000	5.56	Gm17716 D930049A15Rik Zmiz1 AC154455.1 Gm17670 Gm10397
chr19:47000001-47500000	5.56	Nt5c2 Ina Pcgf6 U6 Taf5 Usmg5 Pdcd11 Calhm2 Calhm1 Gm6970 Neurl1a Sh3pxd2a
chr3:87500001-88000000	5.48	Arhgef11 4933430H15Rik Pear1 Ntrk1 Insrr Sh2d2a Prcc Hdgf Mrpl24 Rrnad1 Isg20l2 Crabp2 Nes Bcan Hapln2 Gpatch4 Apoa1bp Ttc24 Iqgap3 Mef2d 1700113A16Rik
chr11:76000001-76500000	5.48	Glod4 Fam57a Gemin4 Dbil5 Rnmtl1 Nxn Timm22 Abr Gm16727 Bhlha9 Tusc5
chr15:102000001-102500000	5.48	Csad Zfp740 Itgb7 Rarg Gm9918 Mfsd5 Espl1 Pfdn5 Myg1 Aaas Sp7 U6 Gm17671 Sp1 Amhr2 Gm17403 U6 Prr13 Pcbp2 Map3k12 Gm10337 Tarbp2 Npff Atf7 Atf7 U6 Gm15430 Atp5g2
chr19:45000001-45500000	5.48	Fam178a U6 Sema4g Mrpl43 Peo1 Lzts2 AC132957.1 Pdzd7 Sfxn3 Kazald1 Tlx1 Gm20424 Lbx1 Btrc
chr19:58000001-58500000	5.48	Atrnl1 Gm16277 Gfra1
chr3:96000001-96500000	5.40	Bola1 Gm15444 Hist2h2ab Hist2h2ac Hist2h2be Hist2h2aa2 Hist2h2aa1 Hist2h3c1 Hist2h4 Hist2h3b Hist2h2bb Fcgr1 U1 Gm17667 Gm17580 U1 U1 Gm17575 Gm17587 4930477E14Rik Telomerase-vert U1 BC107364 U1 U1 U1 U1 Hfe2 Gm15441 Txnip Gm16253 Polr3gl Ankrd34a Lix1l 6330549D23Rik Rbm8a Pex11b Itga10 Rpl21-ps11 Ankrd35
chr8:97000001-97500000	5.40	Nlrc5 Cpne2 Fam192a Rspry1 Arl2bp Pllp 7SK Ccl22 Cx3cl1 Ccl17 Ciapin1 Coq9 Polr2c Dok4 Ccdc102a Gpr114
chr11:54000001-54500000	5.40	4933405E24Rik Csf2 Gm12223 Il3 Acsl6 Gm12224 4930404A10Rik Fnip1 U6 Rapgef6
chr11:60000001-60500000	5.40	Rai1 Srebf1 Tom1l2 Gm12265 Lrrc48 Atpaf2 4933439F18Rik Drg2 Myo15 Alkbh5 Gm17423

chr13:36000001-36500000	5.40	Ppp1r3g Lyrm4 Fars2
chr13:103000001-103500000	5.40	Cd180
chr15:10000001-10500000	5.40	Prlr Agxt2 Dnajc21 Brix1 Rad1 Ttc23l Rai14
chr15:36500001-37000000	5.40	Pabpc1 Ywhaz AC138604.1 Gm10384 Zfp706 Gm16631
chr17:25500001-26000000	5.40	Tpsb2 Tpsg1 Cacna1h Tekt4 Sstr5 Sox8 2810468N07Rik Lmf1 U6 Gng13 Chtf18 Rpusd1 Mslnl AC134908.1 Msln Narfl Haghl Ccdc78 Fam173a Metrn Gm17480 Fbxl16 Wdr24 Jmjd8 Stub1 AC159277.1 Rhbdl1 Rhot2 Wdr90
chr17:73000001-73500000	5.40	Ypel5 Lbh U6 Lclat1
chr18:4500001-5000000	5.40	AC121802.1 9430020K01Rik Gm10556 Svil
chr18:75000001-75500000	5.40	SNORA22 AC155261.1 Lipg Rpl17 SNORD58 SNORD58 SNORD58 BC031181 Dym
chr1:137000001-137500000	5.31	Lgr6 Ptprv Ptpn7 Arl8a 5S_rRNA Gm15445 Gpr37l1 Gm16606 Elf3 Rnpep Timm17a Lmod1 U6 Shisa4 Ipo9 Nav1 Gm4793
chr3:9500001-10000000	5.31	Zfp704 Pag1 Gm16337 5S_rRNA
chr5:115000001-115500000	5.31	Gm13790 BC057022 Trpv4 Gltp Tchp Git2 4930515G01Rik Ankrd13a 2610524H06Rik Gm20499 RP23-3M10.11 RP23-3M10.7 Gm13821 4930519G04Rik Gm9936 Oasl2 Gm13822 Oasl1 2210016L21Rik Hnf1a Gm13824 Gm13825 Sppl3
chr11:4000001-4500000	5.31	Sec14l2 Rnf215 AL807825.1 Ccdc157 Sf3a1 Tbc1d10a Gatsl3 Osm Lif Gm11959 Gm11958 U6 Hormad2 Mtmr3
chr11:79500001-80000000	5.31	Rab11fip4 Gm11205 Mir193 Mir365-2 U7 9130204K15Rik SNORA51 Utp6 Suz12 Gm16706 Crlf3 Atad5 1110002N22Rik Adap2 Gm11206 Rnf135
chr13:43000001-43500000	5.31	Phactr1 Gm15809 7SK Gm15813 Tbc1d7 Gfod1 Sirt5 Nol7 Ranbp9
chr14:64500001-65000000	5.31	Pinx1 Sox7 4930578I06Rik Rp1l1 Prss55 Prss51 4930471C04Rik Prss52 Gm17116 Msra
chr14:75000001-75500000	5.31	Htr2a Esd Lrch1 5031414D18Rik Lrrc63
chr15:82000001-82500000	5.31	Srebf2 Mir33 Tnfrsf13c Cenpm 1500009C09Rik Sept3 Wbp2nl AC104325.1 Naga Fam109b 1500032L24Rik n-R5s41 Ndufa6 Cyp2d22 Cyp2d11 Cyp2d10 AC113593.1 Cyp2d9 Gm5806 Cyp2d12 Cyp2d34
chr15:96000001-96500000	5.31	2610037D02Rik 4833422M21Rik Arid2 Scaf11 Slc38a1
chr16:17500001-18000000	5.31	Aifm3 Lztr1 Thap7 4930451C15Rik P2rx6 Slc7a4 Smpd4 Ccdc74a Med15 Rpl26-ps4 Klhl22 Scarf2 Car15 Gm20518 Dgcr2 Tssk1 Tssk2 Dgcr14 Gsc2 Slc25a1 Vpreb2
chr16:94500001-95000000	5.31	Hlcs Ripply3 Pigp Ttc3 U1 Dscr3 Dyrk1a Kcnj6
chr3:87000001-87500000	5.23	Fcrls Cd5l Fcrl1 Fcrl5 Etv3 SNORA17 AC139241.1 Arhgef11 Gm6570
chr3:88500001-89000000	5.23	2810403A07Rik SNORA42 Rit1 Gm17146 Gm10253 Syt11 Gon4l U1 Msto1 n-R5s197 Dap3 Ash1l U6 SNORA17 Rusc1 Fdps U6 Mir720 Pklr Hcn3 Clk2 Scamp3 Gm16069 Fam189b
chr7:106000001-106500000	5.23	Wnt11 Uvrag SNORA17 Dgat2 Mogat2 Gm16890 Mtap6 Serpinh1
chr7:106500001-107000000	5.23	Serpinh1 Gdpd5 Klhl35 Rps3 Snord15b Snord15a n-R5s156 Arrb1 Mir326 Gm4980 SNORA41 Slco2b1 Gm15635 Olfr520 Olfr521 F730035P03Rik Neu3 Spcs2
chr7:133500001-134000000	5.23	Lat Spns1 Nfatc2ip Cd19 Rabep2 Atp2a1 Sh2b1 Tufm Atxn2l Eif3c U6 U6 Cln3 Apobr Il27 Nupr1 2510046G10Rik Ccdc101 Sult1a1 Slx1b Bola2 Coro1a Mapk3 Gdpd3 Gm9967 Ypel3 Tbx6 Ppp4c Aldoa Gm15676 Fam57b 4930451I11Rik Doc2a Ino80e
chr9:107500001-108000000	5.23	Sema3b Gnai2 Slc38a3 Gnat1 Sema3f Rbm5 Rbm6 Mon1a U6 Mst1r 4921517D21Rik Camkv Traip Uba7 6230427J02Rik SNORA61 Cdhr4 Cdhr4 Ip6k1 Gmppb Rnf123 RP24-484G16.7 Amigo3 Mst1 Apeh Bsn
chr10:41000001-41500000	5.23	Fig4 Akd1 U6 Zbtb24 Mical1 Smpd2 Ppil6 Cd164 Ccdc162 Gm17196 5730435O14Rik AC161426.1 Cep57l1
chr11:49500001-50000000	5.23	Cnot6 AL606479.2 Gfpt2 Mapk9 AL606479.1 Rasgef1c Rnf130 Mir340 Tbc1d9b Gm12195 3010026O09Rik
chr11:119500001-120000000	5.23	Rptor SNORA31 A430071A18Rik Chmp6 Gm11767 Gm11766 Baiap2 Aatk Mir338 Azi1 AL807824.1 2410002I01Rik 1810043H04Rik Slc38a10
chr13:30500001-31000000	5.23	Uqcrfs1 4930519D14Rik Dusp22 Irf4 Exoc2
chr13:54000001-54500000	5.23	Drd1a Sfxn1 Hrh2 Gm16578 Cplx2
chr2:167000001-167500000	5.14	Kcnb1 1110018N20Rik Ptgis Gm14291 Gm17544 B4galt5 Slc9a8 Spata2 Rnf114 Snai1 Gm11476 Ube2v1 Tmem189 AL589870.1 Tmem189 Gm14320
chr5:121500001-122000000	5.14	Ptpn11 Rpl6 SNORA42 Gm15800 U1 Trafd1 Naa25 Erp29 Tmem116 Adam1b Adam1a Mapkapk5
chr6:38500001-39000000	5.14	Luc7l2 Gm17451 Klrg2 Clec2l Hipk2 Tbxas1 SNORA17
chr6:71000001-71500000	5.14	Thnsl2 Fabp1 Smyd1 Krcc1 Gm1070 Cd8b1 Cd8a Rmnd5a Rnf103 Chmp3
chr8:123500001-124000000	5.14	Gm20388 1110050K14Rik Foxf1a Mthfsd Foxc2
chr9:45000001-45500000	5.14	Tmprss4 BC049352 Il10ra 1700003G13Rik Tmprss13 Fxyd6 Fxyd2 4833428L15Rik Dscaml1 U6
chr10:39000001-39500000	5.14	Fyn Gm16364 Gm16365 Traf3ip2 E130307A14Rik Rev3l U6atac
chr11:117000001-117500000	5.14	Sec14l1 Sept9 Gm16045 Gm11729 Gm8624 Gm11732 Gm11733 Gm11734 AL672228.1 2900041M22Rik
chr17:33500001-34000000	5.14	Zfp101 Actl9 Adamts10 Myo1f Zfp414 Gm20507 Pram1 Hnrnpm March2 U6 Rab11b Gm17251 Angptl4 4931413I07Rik Kank3 Rps28 Ndufa7 Cd320
chr19:55500001-56000000	5.14	Vti1a 4930552P12Rik Tcf7l2
chr5:108000001-108500000	5.14	A830010M20Rik Glmn Rpap2 A930041C12Rik Gm17717 Gfi1 A430072P03Rik Evi5 1700013N18Rik Rpl5 Snord21 SNORA66 SNORA66 Fam69a Mtf2
chr9:21000001-21500000	5.14	Pde4a Gm16754 Keap1 S1pr5 Atg4d Kri1 Cdkn2d Ap1m2 AC122525.1 Slc44a2 Ilf3 Gm16853 Qtrt1 Dnm2 Mir199a-1 Tmed1 AB124611 Carm1 Yipf2 1810026J23Rik Mir1946b Smarca4
chr12:112000001-112500000	5.14	Wdr20a Stk30 4921507G05Rik Gm17712 Zfp839 Gm3452 Cinp Tecpr2 Ankrd9 Rcor1 4930595D18Rik Traf3
chr13:51000001-51500000	5.14	Y_RNA Spin1 Nxnl2 Hist1h2al
chr15:9500001-10000000	5.14	Spef2 7SK
chr15:83000001-83500000	5.14	Cyb5r3 A4galt Arfgap3 1700001L05Rik Pacsin2 Ttll1 AL583889.1 Bik Mcat Tspo Ttll12 Scube1
chr17:47500001-48000000	5.14	Mrps10 Guca1b Guca1a 1700001C19Rik AI661453 Taf8 Ccnd3 Bysl Med20 Med20 Usp49 Tomm6 Prickle4 Gm14872 Frs3 Gm14873 Pgc Tcfeb Mdfi U1 n-R5s28

chr1:54500001-55000000	5.06	Pgap1 Pgap1 Ankrd44 AC151572.1
chr6:113000001-113500000	5.06	Thumpd3 U6 Gt(ROSA)26Sor Setd5 Lhfpl4 Mtmr14 Gm16161 Cpne9 Brpf1 Gm15492 Ogg1 Camk1 Tada3 Arpc4 Ttll3 Rpusd3 Cidec Jagn1 Il17re Il17rc Creld1 Prrt3 Tmem111 AC153910.1 Fancd2 AC153589.1
chr8:127500001-128000000	5.06	Tsnax Disc1 AL672234.1 Gm16237 Sipa1l2
chr9:32000001-32500000	5.06	Arhgap32 Kcnj5 Kcnj1 Fli1 U6 Ets1
chr10:5000001-5500000	5.06	Syne1 Gm10097 AC161829.1 Esr1
chr11:85500001-86000000	5.06	Bcas3 8430403D17Rik AL596324.1 9530048J24Rik 5S_rRNA 2610027K06Rik Tbx2 Gm11444 Tbx4 AL592465.1 AL592465.2 Brip1
chr12:35000001-35500000	5.06	Hdac9
chr2:119000001-119500000	4.97	Dnajc17 Gm14137 Zfyve19 Ppp1r14d Spint1 Rhov Vps18 Gm14207 Dll4 Chac1 Ino80 Exd1 1500003O03Rik 1700020I14Rik Oip5 Nusap1 n-R5s204 Ndufaf1
chr2:153000001-153500000	4.97	Tm9sf4 Tspyl3 Plagl2 Pofut1 Kif3b 2500004C02Rik Asxl1 8430427H17Rik 4930404H24Rik Commd7 7530422B04Rik Dnmt3b
chr5:65500001-66000000	4.97	Klhl5 5S_rRNA Wdr19 Rfc1 Klb Rpl9 Lias Ugdh 1110003E01Rik Ube2k
chr9:43500001-44000000	4.97	Pvrl1 U6 Thy1 Rnf26 Usp2 Mfrp C1qtnf5 RP24-329C11.5 Gm3906 Gm10687 Mcam Cbl
chr9:57000001-57500000	4.97	Commd4 Trcg1 1700017B05Rik Gm5121 Ppcdc Scamp5 Rpp25 Cox5a Gm17596 2310046O06Rik Mpi Scamp2 Ulk3 Cplx3 Lman1l Csk
chr9:62500001-63000000	4.97	Itga11 Fem1b Gm17400 Cln6 Gm10653 Calml4 Pias1 U1 U6 Skor1
chr10:42500001-43000000	4.97	Sec63 RNaseP_nuc Scml4 Sobp Mir297-2 9030612E09Rik Pdss2
chr11:69500001-70000000	4.97	2010012P19Rik BC096441 Tnfsf12 Polr2a Amac1 Zbtb4 Chrnb1 Fgf11 Tmem102 4933402P03Rik Spem1 Nlgn2 1810027O10Rik Plscr3 Tnk1 Kctd11 Acap1 2810408A11Rik Neurl4 Gps2 Eif5a Ybx2 Slc2a4 Cldn7 Rai12 Ctdnep1 Gabarap Phf23 Dvl2 Acadvl Mir324 Dlg4 Asgr1 Asgr2 Mgl2 Clec10a
chr11:84500001-85000000	4.97	1700109G15Rik Gm11431 Mrm1 Dhrs11 4930502E09Rik Ggnbp2 Pigw Myo19 AL645623.1 Znhit3 Car4 Usp32 U6 1700125H20Rik
chr11:88000001-88500000	4.97	Cuedc1 Mrps23 1700106J16Rik Msi2 AL732539.1 Gm15893
chr11:95000001-95500000	4.97	Dlx4 A730090H04Rik Gm11515 Tac4 Myst2 Gm11520 Gm11521 Fam117a Slc35b1 Spop Nxph3 Ngfr Gm11528
chr13:113500001-114000000	4.97	Slc38a9 Slc38a9 Ppap2a Skiv2l2 Dhx29 Ccno Gm6320 Cdc20b Mir449c Mir449b Mir449a Gm10735 Gpx8 Gzma Gm9848 Gzmk Esm1
chr14:79500001-80000000	4.97	1300010F03Rik Zfp957 1190002H23Rik Naa16 AC124745.1 Mtrf1 Kbtbd7 Gm5465 Wbp4 Elf1 Sugt1
chr5:124000001-124500000	4.97	Vps33a Clip1 U2 Zcchc8 Rsrc2 Kntc1 Niacr1 Gpr81 Denr Ccdc62 Hip1r Vps37b
chr11:24000001-24500000	4.97	Bcl11a Gm12064 4930538E20Rik Gm12065 Gm12066 Gm12068 4933430M04Rik U6
chr15:66500001-67000000	4.97	Tg Gm17140 Sla Wisp1 Ndrg1 Gm17035 Gm2895 U7 St3gal1
chr14:55000001-55500000	4.89	Slc7a7 Mrpl52 Mmp14 Gm11067 U6 Lrp10 Rem2 Prmt5 Haus4 Jub U6 4931414P19Rik Psmb5 Mir686 Psmb11 Cdh24 CT009512.1 Gm17606 Acin1 4930579G18Rik 1700123O20Rik Cebpe Slc7a8 Gm10332 Homez Ppp1r3e
chr1:137500001-138000000	4.89	Nav1 Csrp1 Phlda3 Tnni1 Lad1 Tnnt2 Pkp1 Igfn1 Tmem9 Cacna1s
chr10:82000001-82500000	4.89	1190007I07Rik Tdg Glt8d2 Hcfc2 Nfyb 1700028I16Rik Txnrd1 Gm4799 Chst11
chr12:87000001-87500000	4.89	Batf n-R5s64 Mfsd7c 0610007P14Rik Ttll5 Gm17691 Tgfb3 1700019E19Rik
chr13:32500001-33000000	4.89	Mylk4 Wrnip1 D930007J09Rik Serpinb1a Serpinb1c
chr19:10000001-10500000	4.89	Fth1 Best1 Rab3il1 Fads3 Fads2 Fads1 Gm10143 Fen1 1810006K21Rik Gm98 Dagla Syt7 Gm17289
chr1:37000001-37500000	4.81	Rpl12-ps1 n-R5s210 Vwa3b Vwa3b Cnga3 Inpp4a 4930439A04Rik 6330578E17Rik Unc50 Mgat4a
chr6:48500001-49000000	4.81	Lrrc61 Rarres2 Gm5111 Repin1 Zfp775 AI854703 Gimap8 Gimap9 Gimap4 Gimap6 Gimap1 Gimap7 Gm3345 Gimap5 Gimap3 Tmem176b Tmem176a Gm7932 Abp1 1600015I10Rik SNORA17 Gm10242 Doxl2 Svs1 Gpnmb
chr8:73000001-73500000	4.81	Klhl26 Tmem59l Crlf1 2810428I15Rik Uba52 2810422J05Rik Fkbp8 Ell Isyna1 Ssbp4 Lrrc25 Gdf15 Pgpep1 Lsm4 Jund Gm11175 Pde4c Rab3a Mpv17l2 Ifi30 Pik3r2 Mast3 Il12rb1 Arrdc2 Kcnn1 A230052G05Rik Ccdc124 Slc5a5 Rpl18a Snora68 Mtap1s Mir1969 Gm10654
chr9:71000001-71500000	4.81	Aqp9 Aldh1a2 Grinl1a Grinl1a Gcom1 Cgnl1
chr10:74500001-75000000	4.81	Rab36 Bcr Specc1l Adora2a 1110038D17Rik Upb1 7SK Snrpd3
chr11:87000001-87500000	4.81	Trim37 Ppm1e U6 AL596130.1 Rad51c Tex14 U1 U1 U3 U6 U3 U3 U3 Gm11492 Sept4 Mtmr4 Hsf5 Rnf43
chr11:96500001-97000000	4.81	Skap1 2010300F17Rik Gm11537 Snx11 Cbx1 Nfe2l1 Copz2 Mir152 Gm11523 Cdk5rap3 D030028A08Rik Gm11525 Prr15l Pnpo Sp2 Sp6 Gm11532 Scrn2 Lrrc46 Mrpl10 Gm11574 Osbpl7 Tbx21 Tbkbp1
chr11:100000001-100500000	4.81	Krt19 Krt9 Krt14 Krt16 Krt17 Krt42 Gm14206 Gm12349 Eif1 Gast Hap1 RP23-392I3.14 Jup Gm12348 Leprel4 Fkbp10 Nt5c3l Klhl10 Klhl11 Acly Ttc25 Cnp Dnajc7 Nkiras2 Zfp385c
chr1:59000001-59500000	4.72	Trak2 Stradb Als2cr11 Gm17570 Als2cr11 SNORA17 Als2cr4 Mpp4 Als2 Cdk15
chr5:30500001-31000000	4.72	Hadhb Gpr113 Gm5299 Ept1 Ccdc164 Otof 1700001C02Rik Cib4 U6 Kcnk3 4930471M23Rik Cenpa
chr7:52000001-52500000	4.72	Zfp473 Vrk3 Atf5 Nup62 Il4i1 Tbc1d17 Akt1s1 Mir707 Pnkp Ptov1 Med25 Fuz Ap2a1 Tsks Cpt1c Prmt1 Gm15545 Bcl2l12 Irf3 Scaf1 Rras Prr12 Prrg2 Nosip Rcn3 Fcgrt Mir150 Rps11 Snord35b Rpl13a Snord35a Snord34 Snord33 Snord32a Flt3l Aldh16a1 Pih1d1 Slc17a7 Pth2 Ccdc155 Dkkl1 Tead2 Cd37
chr10:6000001-6500000	4.72	Akap12 U8 Mthfd1l U1 Plekhg1 5S_rRNA
chr13:52000001-52500000	4.72	Gm16767
chr14:21500001-22000000	4.72	Sec24c 6230400D17Rik Fut11 AC121599.1 Chchd1 2310021P13Rik Ndst2 Camk2g Plau Vcl Ap3m1 Adk
chr14:79000001-79500000	4.72	Dgkh SNORA40 1300010F03Rik
chr15:85500001-86000000	4.72	Mirlet7c-2 Mirlet7b Ppara 2210021J22Rik Pkdrej Ttc38 Gtse1 Trmu Celsr1 Gramd4 Gm15722

		Cerk 7SK
chr19:29000001-29500000	4.72	4430402I18Rik Ppapdc2 Cdc37l1 Gm10136 Ak3 Rcl1 Mir101b Jak2 Insl6 Rln1 5033414D02Rik Cd274 Pdcd1lg2
chr3:51000001-51500000	4.64	Ccrn4l Elf2 4930577N17Rik AC161183.1 4930583H14Rik Ndufc1 Naa15 Rab33b Setd7 5031434O11Rik Mgst2 Maml3 Gm10729
chr5:32000001-32500000	4.64	Mrpl33 Bre 7SK Gm17130 Gm10463 Fosl2 U6
chr6:146000001-146500000	4.64	Itpr2 Gm17706 4933424B01Rik
chr10:41500001-42000000	4.64	Cep57l1 Sesn1 Armc2 Foxo3
chr11:4500001-5000000	4.64	Gm11032 Gm11961 Ascc2 Uqcr10 Zmat5 Cabp7 Nf2 Nipsnap1 Thoc5 Nefh Ap1b1 SNORD125 Gas2l1 Rasl10a Ewsr1 Rhbdd3 Gm11031
chr13:45500001-46000000	4.64	Mylip U6 Gmpr Atxn1
chr16:4000001-4500000	4.64	Slx4 Gm15879 Dnase1 Trap1 AC132380.1 Crebbp Gm5766 AC132575.1 Adcy9 Srl
chr16:4500001-5000000	4.64	Srl Tcfap4 Glis2 Pam16 Coro7 Vasn Dnaja3 Nmral1 Hmox2 Gm15859 AC166903.1 5730403B10Rik Gm15835 4930562C15Rik Fam100a Mgrn1 Gm16861 Nudt16l1 Anks3 4930451G09Rik Sept12
chr17:45500001-46000000	4.64	Cdc5l B230354K17Rik Spats1 Gm9104 Aars2 Tcte1 Gm17441 Tmem151b Nfkbie Slc35b2 Hsp90ab1 Slc29a1 Gm17080 Gm7325 U6 Capn11 Tmem63b Gm16172 Mrpl14 Gm16862
chr19:40500001-41000000	4.64	Sorbs1 Aldh18a1 Gm16765 Tctn3 Entpd1 Ccnj E030007J07Rik Zfp518a
chr5:37000001-37500000	4.55	D5Ertd579e U6 SNORA17 Cno Mrfap1 Man2b2 Ppp2r2c 4933401P06Rik Wfs1 Jakmip1 Gm17286 5S_rRNA
chr7:17000001-17500000	4.55	Zc3h4 Tmem160 Npas1 n-R5s151 Grlf1 U6 Ceacam15 AC150681.1 Ceacam9 Ap2s1 Slc1a5 Fkrp Strn4 Prkd2 9330104G04Rik Dact3 Gng8 Ptgir
chr8:127000001-127500000	4.55	Cog2 Agt Capn9 2310022B05Rik Ttc13 Arv1 Fam89a Trim67 Gm16163 2810004N23Rik Gnpat Exoc8 Gm505 Egln1
chr9:103000001-103500000	4.55	Rab6b Srprb Trf Trf 1300017J02Rik Topbp1 Cdv3 5830418P13Rik Bfsp2 Gm16252 Tmem108 U6
chr9:118500001-119000000	4.55	Itga9 Gm2415 Gm16295 Ctdspl Mir26a-1 Vill Plcd1
chr10:42000001-42500000	4.55	7SK Lace1 7SK Snx3 Nr2e1 Ostm1 Gm15200 U7 Gm15199 Sec63 Gm17442
chr10:60500001-61000000	4.55	Pcbd1 Sgpl1 Tbata Adamts14 AC123530.1 Prf1 Rpl27a-ps1 X99384 Nodal Eif4ebp2 D830039M14Rik Lrrc20
chr10:80500001-81000000	4.55	Slc39a3 Sgta Thop1 Creb3l3 Map2k2 Zbtb7a Pias4 Eef2 Snord37 4930442H23Rik Dapk3 2310050B05Rik Itgb1bp3 Atcay AC155932.2 Zfr2 Matk Mrpl54 Apba3 AC155932.1 Tjp3 Pip5k1c Gm16315 2510012J08Rik Tbxa2r Gipc3 Hmg20b F630110N24Rik 4930404N11Rik Fzr1 Dohh 2210404O07Rik Nfic Gm16104 Celf5 Gm16105 Ncln S1pr4 Gna15 AC159474.1 Gna11
chr10:83000001-83500000	4.55	A230046K03Rik Appl2 1500009L16Rik
chr14:20500001-21000000	4.55	Nid2 2700060E02Rik Gng2 1810063B07Rik Kcnk5
chr1:130500001-131000000	4.47	Gm17699 U6
chr2:156500001-157000000	4.47	Dlgap4 4930405A21Rik Myl9 Gm14230 Tgif2 5430405H02Rik 4930518I15Rik 1110008F13Rik Sla2 Ndrg3 Dsn1 9830001H06Rik Gm1332 Samhd1 AL669828.1 Rbl1
chr3:90000001-90500000	4.47	Nup210l U6 Rps27 Rab13 Jtb Creb3l4 Slc39a1 Crtc2 Gm10973 Dennd4b Gatad2b Slc27a3 Ints3 Npr1 Gm16048 Ilf2 Snapin 2500003M10Rik S100a1 S100a13 S100a14 S100a16 U6 U1 S100a3 S100a4 S100a5 S100a6 S100a7a S100a8 S100a9
chr3:94500001-95000000	4.47	Cgn Selenbp2 Pogz Psmb4 U6 Selenbp1 Rfx5 B230398E01Rik Pi4kb A730011C13Rik Gm15265 Zfp687 4930481B07Rik Psmd4 Pip5k1a SNORD62 U6 Vps72 Tmod4 Scnm1 Lysmd1 Tnfaip8l2 Sema6c Gabpb2
chr7:31000001-31500000	4.47	Tbcb Polr2i Ovol3 Wdr62 Thap8 Clip3 Alkbh6 AI428936 Sdhaf1 E130208F15Rik Lrfn3 U2 Tyrobp Hcst Nfkbid Aplp1 Kirrel2 Nphs1 Nphs1as Prodh2 Gm1082 Arhgap33 BC053749 Hspb6 Lin37 Psenen U2af1l4 Gm17104 Tmem149 Wbp7 Zbtb32 Upk1a Cox6b1 Etv2 Rbm42 Haus5 Gm17478 4930479M11Rik 2200002J24Rik Gm4883 Atp4a
chr8:122000001-122500000	4.47	Slc38a8 Mbtps1 Hsdl1 Lrrc50 Taf1c Adad2 Kcng4 Wfdc1 Atp2c2 4632415K11Rik Cotl1 Klhl36 Usp10 Gm20388
chr10:94000001-94500000	4.47	Tmcc3 Gm16154 4932415G12Rik Ccdc41 Plxnc1 5S_rRNA AC159379.1 7SK
chr14:122000001-122500000	4.47	Dock9 Ubac2 Gpr18 Gpr183 Timm8a2
chr6:30000001-30500000	4.38	Nrf1 7SK Mir182 Mir96 Mir183 Ube2h 1700095J07Rik 5S_rRNA Zc3hc1 n-R5s161 Klhdc10 1700012C14Rik Tmem209 1700025E21Rik Cpa2
chr6:72000001-72500000	4.38	St3gal5 Atoh8 Sftpb Usp39 0610030E20Rik Tmem150a Rnf181 Vamp5 Vamp8 Gm17505 Gm17607 Ggcx Mat2a Sh2d6 Capg
chr7:31500001-32000000	4.38	Atp4a Tmem147 Gapdhs Sbsn Dmkn Krtdap Ffar2 Ffar3 Ffar1 Cd22 Mag Hamp2 Hamp Usf2 Gm17077 Gm4673 Lsr Fam187b Fxyd5 Fxyd7 Fxyd1 Lgi4 Fxyd3 Hpn Scn1b Gramd1a G630030J09Rik
chr12:112500001-113000000	4.38	Traf3 Amn A230087F16Rik Cdc42bpb A230065H16Rik 1200009I06Rik Gm10425 Tnfaip2 Gm266 Eif5 Snora28 2810029C07Rik Mark3 Ckb Trmt61a Bag5 2810002N01Rik Gm15995 Gm15996 Klc1
chr17:6000001-6500000	4.38	Synj2 Serac1 Gtf2h5 Tulp4 AC154650.1 n-R5s26 Tmem181a Dynlt1a Gm17692 Gm2792 Dynlt1b Tmem181b-ps
chr2:6000001-6500000	4.30	5430407P10Rik Echdc3 A230108P19Rik Gm13383 Usp6nl Gm13388 Gm13391 Celf2
chr2:33000001-33500000	4.30	Ralgps1 Gm13528 SNORA48 Angptl2 AL845277.1 Zbtb34 Gm13536 Zbtb43 Gm13530 Lmx1b C130021I20Rik
chr3:37500001-38000000	4.30	4930594O21Rik Spry1 Gm5148 SNORA17 SNORA17
chr3:86500001-87000000	4.30	Lrba Dclk2 U1 Cd1d2 Cd1d1 SNORA17 Kirrel
chr7:133000001-133500000	4.30	D430042O09Rik Gsg1l Xpo6 Gm17137 Sbk1 Gm10155
chr9:56500001-57000000	4.30	Lingo1 Odf3l1 Cspg4 Snx33 Imp3 Snupn Ptpn9 Gm10658 Sin3a 2700012I20Rik 2410133F24Rik Man2c1 Neil1 Gm16493
chr10:62000001-62500000	4.30	2510003E04Rik AC126428.1 Ddx21 Ddx50 Stox1 Ccar1 Snord98 Tet1 U6 7SK Slc25a16 SNORA70 Dna2 Rufy2 Gm16135 Hnrnph3 Pbld2

chr11:51500001-52000000	4.30	0610009B22Rik Sec24a SNORA48 Sar1b Phf15 Gm16953 AL669920.1 Cdkn2aipnl Ube2b Gm12204 Cdkl3 Gm12205 Ppp2ca AL935177.2 Gm17500 AL935177.1 Olfr1373
chr11:70500001-71000000	4.30	Camta2 Inca1 Kif1c Gm12320 AL596117.1 Zfp3 A430084P05Rik Rabep1 Nup88 Rpain C1qbp Dhx33 U6 Derl2 Mis12 6330403K07Rik Nlrp1a Nlrp1b
chr14:61000001-61500000	4.30	Spata13 C1qtnf9 Gm15919 Mipep
chr14:73500001-74000000	4.30	Rcbtb2 Gm17233 Rb1 Mir687 Lpar6 Itm2b Med4 Nudt15 Sucla2
chr15:98000001-98500000	4.30	AI836003 Olfr288 Olfr287 Olfr286 H1fnt Zfp641 Olfr285 Olfr284 Olfr283 Olfr282 Olfr281 Lalba Olfr279 2310037I24Rik Snora34 Snora2b Ccnt1 9330020H09Rik 4930415O20Rik Adcy6 Cacnb3 Ddx23 Rnd1
chr16:96000001-96500000	4.30	2810404F17Rik 1600002D24Rik Gm15340 Psmg1 Brwd1 Gm15342 1700093J21Rik Gm15341 Hmgn1 Wrb Gm15317 Lca5l Sh3bgr B3galt5
chr17:48000001-48500000	4.30	Foxp4 Gm15556 1700067P10Rik 9830107B12Rik A530064D06Rik Trem1 Trem3 Treml4 Treml2 B430306N03Rik Trem2 Treml1
chr17:84000001-84500000	4.30	Kcng3 Mta3 Haao C430042M11Rik 5S_rRNA
chr17:87500001-88000000	4.30	Socs5 AC129309.1 Mcfd2 4833418N02Rik Ttc7 Gm15978 0610012D04Rik 1700011E24Rik Calm2 SNORA17
chr2:72500001-73000000	4.22	8430437L04Rik 6430710C18Rik Sp3 AL844840.1 Gm11084 1700011J10Rik AL844840.2 Ola1
chr11:83500001-84000000	4.22	Gm11428 Expi 1100001G20Rik Heatr6 5S_rRNA Gm12576 7SK Hnf1b Ddx52 Synrg Dusp14 Tada2a Acaca Gm11437
chr12:16000001-16500000	4.22	AC102435.1
chr1:173500001-174000000	4.22	Cd244 Ly9 Slamf7 Cd48 U6 U6 Slamf1 Cd84 Gm10521 Slamf6 Vangl2 Nhlh1 Ncstn
chr8:124500001-125000000	4.22	Gm20388 Banp Gm22 Zfpm1 Trhr2 Zc3h18 Il17c Cyba Mvd Snai3 Rnf166 AC114917.1
chr11:106000001-106500000	4.22	Map3k3 Limd2 Gm10840 Strada U1 Ccdc47 Ddx42 Ftsj3 Psmc5 U6 Smarcd2 Tcam1 Gh Cd79b Scn4a 2310007L24Rik Icam2 Ern1 Snord104 SNORA76 Tex2 snosnR60_Z15
chr15:100500001-101000000	4.22	Cela1 Galnt6 1810009N23Rik Slc4a8 Scn8a Scn8a Ankrd33 Acvrl1 Gm16031
chr18:54500001-55000000	4.22	9430076G02Rik
chr1:138000001-138500000	4.13	Cacna1s Gm15850 Kif21b 2310006M14Rik 5730559C18Rik Gm17643 Gpr25 Gm17543 Camsap2 9230116N13Rik Ddx59 Kif14
chr7:135500001-136000000	4.13	Rgs10 Gm15503 Tial1 AC130474.1 Bag3 Inpp5f Mcmbp U6 Sec23ip n-R5s158 AC136741.1
chr11:95500001-96000000	4.13	Phb Gm17369 Gm9796 1110035M17Rik Zfp652 B130006D01Rik Phospho1 Abi3 Gngt2 Gm11527 4833417C18Rik B4galnt2 Gm11534 U1 Igf2bp1 AL606704.1 Gip U3 Snf8 Ube2z Atp5g1 U2 Calcoco2 Ttll6
chr15:76500001-77000000	4.13	Foxh1 Ppp1r16a Gpt Mfsd3 Recql4 Lrrc14 Lrrc24 C030006K11Rik Arhgap39 Gm17271 Zfp251 Zfp7 Commd5 Rpl8 Zfp647 1110038F14Rik Mb Apol6 U6 Rbfox2 1700109K24Rik
chr17:36000001-36500000	4.13	5530401N12Rik Nrm 2310014H01Rik Dhx16 2310061I04Rik Gm16279 Atat1 Mrps18b Ppp1r10 Mir1894 Abcf1 Mir877 Prr3 Gnl1 Gm20508 A930015D03Rik RP24-443D19.4 Gm17414 H2-T24 Gm17579 H2-T23 BC023719 H2-T22 Gm6034 Gm11127 H2-Bl H2-T10 RP23-108F2.4 H2-T9 Gm7030 Gm10499 2410017I17Rik Gm8909 RP23-108F2.6 RP23-108F2.2 H2-T3 7SK Gm20546 Rpp21 Trim39 H2-M10.2 H2-M10.1
chr18:68000001-68500000	4.13	Cep192 D18Ertd653e 4933403F05Rik Rnmt Mc5r
chr19:29500001-30000000	4.13	Pdcd1lg2 A930007I19Rik C030046E11Rik Ermp1 Mlana 9930021J03Rik 9930021J03Rik Ranbp6 Il33
chr2:155500001-156000000	4.05	Trpc4ap Edem2 Gm17581 Procr Mmp24 BC029722 Eif6 Gm16098 Fam83c Uqcc Gm15557 Gdf5 Cep250 6430550D23Rik Ergic3 Fer1l4 Spag4 Cpne1 Nfs1 Rbm12 Romo1 Rbm39
chr6:86000001-86500000	4.05	Add2 Tgfa Fam136a Snrpg Pcyox1 Tia1 C87436 A430078I02Rik Pcbp1 1600020E01Rik
chr7:120500001-121000000	4.05	Btbd10 Pth Gm17646 Far1 1700006P19Rik AC103664.1 Gm5600 Spon1
chr8:13500001-14000000	4.05	1700029H14Rik Rasa3 4932443I19Rik Cdc16 Upf3a AF366264 Zfp828 SNORA3 2410022L05Rik Gm7676 Fbxo25 2610019F03Rik
chr11:88500001-89000000	4.05	Msi2 C030037D09Rik Gm11493 Akap1 RP23-243J8.2 U6 4930405P13Rik Scpep1 AL646096.1 Gm15698 Coil Gm11496 Trim25 Dgke AL646096.2 A930013B10Rik Gm525 U6atac Gm11497 7SK
chr12:8500001-9000000	4.05	Rhob Slc7a15 Pum2 Gm4755 Sdc1 9930038B18Rik Laptm4a Matn3 Wdr35
chr19:34500001-35000000	4.05	Ch25h Gm16704 Lipa Ifit2 Ifit3 Gm14446 I830012O16Rik 2010002M12Rik Ifit1 Slc16a12 U1 Pank1 Mir107 AC113244.1 Kif20b
chr6:8000001-8500000	3.96	Col28a1 Mios Rpa3 Gm16039 Gm16055 Gm16043 7SK 2810488G03Rik SNORA65 Glcci1
chr15:59000001-59500000	3.96	Gm5045 Sqle E430025E21Rik Nsmce2 Trib1
chr19:6500001-7000000	3.96	Nrxn2 Gm14964 Slc22a12 Gm14967 AC124394.1 2410152P15Rik Gm14968 Rps6ka4 Ccdc88b Prdx5 Trmt112 Esrra 1700019N12Rik
chr1:193000001-193500000	3.96	Atf3 7SK D730003I15Rik Nenf Tmem206 Ppp2r5a Dtl Ints7
chr12:25500001-26000000	3.96	Mboat2 Kidins220 Id2
chr2:164000001-164500000	3.88	Wfdc5 A730032A03Rik Wfdc12 Wfdc15a Wfdc15b Svs2 Svs3b Svs4 Svs3a Svs6 Svs5 Slpi Matn4 Rbpjl Sdc4 Sys1 Gm14302 Dbndd2 Trp53tg5 Dbndd2 Pigt Gm14317 Wfdc2 Spint3 Wfdc6a Spinlw1 Wfdc8 U6 Wfdc6b SNORA17 Wfdc16 Wfdc9 Wfdc10 Wfdc11
chr5:66500001-67000000	3.88	Rbm47 Gm16885 AC132284.1 Nsun7 Apbb2 7SK
chr6:53500001-54000000	3.88	Creb5 Tril Gm16499 SNORA17 Cpvl Chn2
chr11:50000001-50500000	3.88	3010026O09Rik Sqstm1 Mgat4b Ltc4s Gm16641 Maml1 Canx Cby3 Mir804 Hnrnph1 Rufy1 7SK Gm12198 Adamts2
chr11:80000001-80500000	3.88	Rnf135 Rhot1 Rhbdl3 5730455P16Rik Zfp207 AL591146.1 Psmd11 Cdk5r1 Myo1d C030013C21Rik
chr8:26000001-26500000	3.79	Adam32 U6 Adam9 Tm2d2 Htra4 Gm16933 Plekha2 Tacc1
chr14:65000001-65500000	3.79	Msra A930011O12Rik Mir124a-1 AC134898.1 Kif13b SNORA36 Hmbox1
chr16:17000001-17500000	3.79	Mapk1 U6 1700056N10Rik Ypel1 Ppil2 Gm15585 2610318N02Rik Mir130b Mir301b Sdf2l1 Ccdc116 Gm15646 Ydjc Ube2l3 Gm15648 U6 Rimbp3 Hic2 Gm17625 Tmem191c Pi4ka Serpind1 U6 Snap29 Crkl U6 Aifm3

chr11:101000001-101500000	3.71	Tubg2 Plekhh3 Cntnap1 Ccr10 Ezh1 Ramp2 Vps25 Wnk4 Gm11615 Ccdc56 Cntd1 Becn1 Psme3 Aoc2 Aoc3 AL590969.1 G6pc U2 Aarsd1 Rundc1 Rpl27 Ifi35 Gm11626 Vat1 Rnd2 Brca1 Nbr1 Tmem106a Gm11634 U2 Gm11635 Rdm1 U2
chr10:44500001-45000000	3.63	AC156273.1 Gm4795 Prep AC159378.1 SNORA17
chr16:21500001-22000000	3.63	Vps8 AC133597.1 2510009E07Rik Ehhadh U6 1300002E11Rik Gm17439 Map3k13 2610020F03Rik Tmem41a Liph

trans interactions from Pax5 viewpoint in Thymus

bin	z-score	genes in bin
chr8:12000001-12500000	6.24	A230072I06Rik 7SK Gm5607 AC102525.1
chr14:34000001-34500000	5.40	SNORA17 Arhgap22 Gm15512 Mapk8 Gm626 Ptpn20 U6
chr12:114500001-115000000	5.23	Ighg2c Ighg Ighg1 Ighm Adam6 Ighv2-4
chr16:34000001-34500000	5.23	Kalrn
chr19:42500001-43000000	4.72	Crtac1 D19Ertd386e Gm16541 Loxl4 SNORA17 Pyroxd2 Hps1 Gm16244 Hpse2
chr19:43000001-43500000	4.72	Hpse2 5S_rRNA
chr17:4500001-5000000	4.55	U6 Arid1b
chr11:21500001-22000000	4.38	Wdpcp Otx1 Ehbp1
chr15:101500001-102000000	4.38	Krt6b Krt6a Krt5 Krt71 Krt74 Krt72-ps Krt73 Krt2 Krt1 Krt77 Krt76 Krt4 Krt79 Krt78 Krt8 Krt18 Eif4b Tenc1 Spryd3 Igfbp6 Soat2
chr16:34500001-35000000	4.38	Kalrn Ropn1 Ccdc14 Mylk
chr19:7500001-8000000	4.22	2700081O15Rik Rtn3 Atl3 Pla2g16 Lgals12 Hrasls5 Slc22a19 Slc22a26 Slc22a27
chr8:48000001-48500000	4.05	Enpp6 4930579M01Rik Stox2 4930448N21Rik Gm10083
chr2:27500001-28000000	3.88	Rxra 2810430I11Rik Col5a1 Gm13372 Fcnb Gm13371 F730016J06Rik
chr11:22000001-22500000	3.88	Ehbp1 Gm12050 Gm12051 Tmem17
chr19:59000001-59500000	3.88	Eno4 4930506M07Rik Vax1 Kcnk18 Slc18a2 Pdzd8 Rps12-ps3 Emx2os

trans interactions from Foxo1 viewpoint in Rag-/- pro-B

bin	z-score	genes in bin
chr4:44500001-45000000	19.67	Gm19980 Pax5 AL772319.1 Gm12462 Zcchc7 AL805896.1 Gm12678 Gm12493 Gm12679 Grhpr
chr12:115500001-116000000	17.54	Ighv3-8 Ighv12-3 Gm16930 Gm16695 Gm17000 Gm16696 Gm16694 Ighv1-5 Ighv10-3 Ighv1-7 Ighv15-2 Ighv1-9 Ighv1-12 Gm17686 Gm16857 Gm16858 Ighv1-18 Ighv1-19 Ighv1-20 Gm16860
chr12:115000001-115500000	16.97	Ighv11-2 Ighv14-3 Gm7005 Gm16987 Ighv9-2 Ighv9-3 Gm16842 Gm16841 Ighv3-3 Gm16839
chr12:114500001-115000000	12.48	Ighg2c Ighg Ighg1 AI324046 Gm17421 Gm11029 Ighm AC073553.1 AC073553.2 AC073553.3 Gm16734 Gm16843 Gm16879 Gm16878 Gm16877 Gm16783 Gm17600 Gm16782 Gm17700 Gm16942 Gm17537 Gm17424 Gm16941 Gm17339 Gm17663 Gm16781 Gm17264 Gm16785 Gm17486 Gm16784 Gm17620 Gm16947 Adam6b Gm16967 Gm17483 Gm16968 Adam6a Gm17347 Gm16969 Gm16970 Gm16971 Gm16948 Gm16891 Ighv2-4 Gm17309 Gm16949 Gm16593 Gm16592 Gm16594 Gm16886
chr9:61000001-61500000	11.02	Gm10655 Tle3
chr8:10500001-11000000	10.90	Myo16 3930402G23Rik Irs2
chr13:37500001-38000000	10.34	Ly86 Rreb1
chr12:80500001-81000000	9.33	Rad51l1
chr16:19000001-19500000	8.99	Iglc3 Iglv1 Iglc2 Iglv3 Iglv2 Olfr164 SNORA17 AC112681.1 Olfr165 SNORA17 Olfr166
chr8:129000001-129500000	8.88	AC118255.1 Gm16983 Irf2bp2 Tomm20 SNORA14 Rbm34
chr12:78000001-78500000	8.32	Fntb Max AC133174.1 Fut8 U6
chr10:20500001-21000000	8.21	Ahi1 Myb Gm16786 AC153556.1
chr16:24000001-24500000	8.21	1110054M08Rik Lpp U7
chr12:86500001-87000000	8.09	Pgf Eif2b2 Mlh3 Acyp1 Fam164c Nek9 Tmed10 Fos Jdp2
chr12:81000001-81500000	7.98	Zfp36l1 Gm17591 2310015A10Rik Actn1 Gm17425 Gm17373 Gm17301 Dcaf5 Scarna3b
chr12:116500001-117000000	7.98	Ighv1-59 Ighv1-62-2 Ighv8-9 Ighv1-63 Ighv8-11 Ighv1-67 Ighv8-12 Ighv1-71
chr12:116000001-116500000	7.64	Ighv1-23 Ighv1-24 Ighv1-42 Ighv1-43 Ighv8-5 Ighv8-6 Ighv1-54
chr13:112500001-113000000	7.42	Mier3 Gm15287 Map3k1 Gm15327 Gm15325 Gm15324 Gm15326 Gm15322 Gm15323
chr11:44500001-45000000	7.31	Ebf1 Gm12159 Gm12160
chr13:23500001-24000000	7.31	Abt1 C230035I16Rik Btn1a1 Btn2a2 Gm11335 Hist1h4h Hist1h2af Hist1h3g Hist1h2bh Hist1h3f Hist1h4f Hist1h1d Hist1h3e Hist1h2ae Hist1h2bg Hist1h2bf Hist1h2ad Hist1h3d Gm17658 Hist1h4d Hist1h2be Gm11398 Hist1h1e U6 Hist1h2ac 5S_rRNA Hist1h2bc Hist1h1t Hist1h4c Hfe Hist1h1c Hist1h3c Hist1h2bb Hist1h2ab Hist1h3b 4930558J22Rik Hist1h4b Hist1h4a Hist1h3a Hist1h1a Trim38 Gm11337 Slc17a2 Slc17a3 Slc17a1 Slc17a4
chr16:93000001-93500000	7.31	Mir802
chr9:71500001-72000000	7.19	Cgnl1 Tcf12 Rpl15-ps2 U6
chr19:32000001-32500000	7.08	A1cf Asah2 Sgms1 2700046G09Rik
chr17:44500001-45000000	6.97	Runx2 Gm16317 Runx2 n-R5s27 9530072K05Rik Gm10497 Supt3h
chr15:80500001-81000000	6.97	Fam83f Tnrc6b AC125540.1 Adsl Sgsm3 Mkl1 U4
chr18:36000001-36500000	6.75	Cxxc5 AC141471.1 Psd2 Nrg2 Pura
chr17:29000001-29500000	6.41	Pnpla1 4930539E08Rik 1700030A11Rik Gm16191 Pxt1 Kctd20 Stk38 U2 Gm16196 Gm16195 Srsf3 Gm16197 Cdkn1a Gm16194 Rab44 Cpne5 Ppil1 BC004004 Pi16 Mtch1 Fgd2
chr15:9000001-9500000	6.30	1110020G09Rik Skp2 Lmbrd2 Ugt3a1 Ugt3a2 Capsl Il7r
chr19:10500001-11000000	6.30	Syt7 Lrrc10b 4930579J09Rik Sdhaf2 Cpsf7 Tmem216 Tmem138 Cybasc3 Dak Ddb1 Vwce Pga5 Vps37c Cd5 A430093F15Rik Cd6 Slc15a3 Tmem132a Tmem109 Prpf19 Zp1
chr10:19000001-19500000	6.18	Olig3 Ifngr1 Il22ra2 9230106D20Rik Il20ra
chr16:32000001-32500000	6.18	Senp5 Pak2 SNORA17 Pigx 1500031L02Rik Gm15729 Lrrc33 Bex6 Fbxo45 SNORA79 Wdr53 Mir1946a 2310010M20Rik Rnf168 AC087556.1 Ubxn7 Tm4sf19 Tctex1d2 Pcyt1a Osta Zdhhc19
chr17:26500001-27000000	6.18	Neurl1b Dusp1 Gm8225 1700049J03Rik Ergic1 AC122252.1 Gm17218 Atp6v0e A930001N09Rik Bnip1 Nkx2-5 Gm17382 Gm20468
chr10:21000001-21500000	5.85	Hbs1l Aldh8a1 1700021A07Rik snoU13 1700020N01Rik Gm5420

chr9:61500001-62000000	5.73	Rplp1 Kif23 Paqr5 7SK Glce AC123610.1
chr10:19500001-20000000	5.73	U6 Slc35d3 Pex7 Map3k5 Mtap7
chr16:94500001-95000000	5.73	Hlcs Ripply3 Pigp Ttc3 U1 Dscr3 Dyrk1a Kcnj6
chr2:27000001-27500000	5.62	Gm13399 Dbh Sardh Gm17071 Vav2 AA645442 AL731552.1 Brd3 Wdr5 U6atac Gm13421
chr4:45000001-45500000	5.62	Grhpr Zbtb5 1700055D18Rik Polr1e Fbxo10 Tomm5 Gm10982 Frmpd1 2900093L17Rik Rg9mtd3 Exosc3 Dcaf10 Mcart1 AL772376.2 Mcart1 Shb
chr12:114000001-114500000	5.62	Pld4 Ahnak2 BC022687 Cdca4 Gpr132 Gm17723 Jag2 Nudt14 Gm17274 Brf1 Btbd6 Pacs2 Tex22 Mta1 Crip2 Crip1 4930427A07Rik Tmem121 U6
chr15:57500001-58000000	5.62	Zhx2 Gm16006 9330154K18Rik Derl1 Wdr67 Fam83a 9130401M01Rik SNORA2 Zhx1 Atad2 Wdyhv1 U7 SNORA11
chr19:41000001-41500000	5.62	Blnk Dntt Opalin Tll2 Tm9sf3 Pik3ap1
chr5:32500001-33000000	5.51	Plb1 Ppp1cb Gm15614 Yes1
chr9:44500001-45000000	5.51	Phldb1 SNORA2 Arcn1 Ift46 Tmem25 Ttc36 Mll1 U6atac Atp5l Ube4a Cd3g Cd3d Cd3e Mpzl2 Mpzl3 Amica1 Gm10684 Scn2b Scn4b Tmprss4 Gm17099 BC049352
chr10:20000001-20500000	5.51	Mtap7 4933406P04Rik Bclaf1 Fam54a Pde7b 4930403O15Rik
chr13:41500001-42000000	5.51	Nedd9 AC154848.1 Tmem170b Gm5082 9530008L14Rik 1700061E18Rik U6
chr2:18500001-19000000	5.40	Commd3 Bmi1 Gm13334 BC061194 RP23-396N6.7 Pip4k2a 4930426L09Rik
chr9:45000001-45500000	5.40	Tmprss4 BC049352 Il10ra 1700003G13Rik Tmprss13 Fxyd6 Fxyd2 4833428L15Rik Dscaml1 U6
chr12:32500001-33000000	5.40	Cog5 SCARNA17 Hbp1 Prkar2b Pik3cg
chr16:30000001-30500000	5.40	4632428C04Rik Hes1 n-R5s32 Gm17516 Cpn2 Lrrc15 Gp5 Atp13a3
chr1:38500001-39000000	5.28	Aff3 Lonrf2 Chst10 Nms
chr12:35500001-36000000	5.28	4921508M14Rik SNORA17 Prps1l1 7SK Snx13 Mir680-3
chr15:84000001-84500000	5.28	Pnpla3 Samm50 Parvb SNORA48 Parvg 1810041L15Rik Ldoc1l
chr16:21500001-22000000	5.28	Vps8 AC133597.1 2510009E07Rik Ehhadh U6 1300002E11Rik Gm17439 Map3k13 2610020F03Rik Tmem41a Liph
chr19:57000001-57500000	5.17	Afap1l2 Ablim1 B230217O12Rik Fam160b1
chr11:24000001-24500000	5.06	Bcl11a Gm12064 4930538E20Rik Gm12065 Gm12066 Gm12068 4933430M04Rik U6
chr14:32000001-32500000	5.06	Tnnc1 Nisch Tnnc1 Sema3g Phf7 Bap1 Dnahc1 Capn7 Sh3bp5 Mettl6 Eaf1 Colq 7SK Hacl1 Btd
chr16:24500001-25000000	5.06	Lpp Mir28 SNORA17
chr17:86500001-87000000	5.06	Srbd1 Prkce Gm10309
chr1:37500001-38000000	4.95	Mgat4a 2010300C02Rik 4930556I23Rik Tsga10 Gm17715 Lipt1 Mitd1 Mrpl30 Lyg2 Gm15457
chr5:36500001-37000000	4.95	Sorcs2 Psapl1 2210406O10Rik Grpel1 Tada2b Ccdc96 Tbc1d14 D5Ertd579e
chr11:68000001-68500000	4.95	Stx8 C78197 RP23-25D18.6 Ntn1 Gm12305 AL662894.1 Pik3r5 Pik3r6 Mfsd6l 4930535C22Rik Ccdc42
chr14:77000001-77500000	4.95	9030625A04Rik Ccdc122
chr16:29500001-30000000	4.95	Atp13a4 Opa1 Gm17734 Gm16761 Gm1968
chr13:24000001-24500000	4.83	Slc17a4 Hist1h2ba Hist1h2aa Scgn Gm11339 Lrrc16a SNORA17 Cmah Gm11342 Gm11345
chr16:30500001-31000000	4.83	Tmem44 Lsg1 Fam43a U6 SNORA17 AI480653 Gm15742
chr10:6000001-6500000	4.83	Akap12 U8 Mthfd1l U1 Plekhg1 5S_rRNA
chr12:83000001-83500000	4.83	Pcnx n-R5s62 Sipa1l1
chr13:52000001-52500000	4.83	Gm16767
chr16:92500001-93000000	4.83	Clic6 Runx1 Gm16801
chr17:31500001-32000000	4.83	Pde9a Wdr4 Ndufv3 4833413E03Rik Pknox1 AC166172.1 Cbs U2af1 Cryaa Sik1
chr13:28500001-29000000	4.72	2610307P16Rik
chr16:49500001-50000000	4.72	Ift57 Gm15518 Gm16619 Cd47
chr17:28500001-29000000	4.61	Tulp1 Fkbp5 7SK E230001N04Rik 4930511I11Rik Gm749 Clps Lhfpl5 Srpk1 Slc26a8 Mapk14 Mapk13 Brpf3 Gm16190 Pnpla1
chr18:55000001-55500000	4.61	Zfp608 Gm17270 Gm4221 SNORA40 U6
chr9:63500001-64000000	4.50	Smad3 Smad6 5S_rRNA 1110036E04Rik Lctl Zwilch
chr15:59000001-59500000	4.50	Gm5045 Sqle E430025E21Rik Nsmce2 Trib1
chr16:11000001-11500000	4.50	Litaf Gm4262 Snn Txndc11 Zc3h7a mmu-mir-689-2 U1 4930509G22Rik Rsl1d1 2610020C07Rik Gspt1 Mir1945 Tnfrsf17 Snx29 Snx29
chr17:5500001-6000000	4.50	Zdhhc14 Snx9 Synj2
chr19:3500001-4000000	4.50	Ppp6r3 Lrp5 AC132452.1 1810055G02Rik Suv420h1 Gm16066 AC133523.1 Chka Tcirg1 Ndufs8 Aldh3b1 Unc93b1 1700055N04Rik Aldh3b2 Acy3 Tbx10
chr19:45500001-46000000	4.50	Btrc Gm6807 Poll Dpcd Fbxw4 Gm17018 Fgf8 Npm3 Gm15491 Mgea5 Kcnip2 9130011E15Rik
chr18:35000001-35500000	4.38	Reep2 Egr1 Gm17507 Etf1 Hspa9 SNORD63 SNORD63 Gm6724 Ctnna1 Lrrtm2 Sil1 AC121874.1 snoU13
chr10:41500001-42000000	4.27	Cep57l1 Sesn1 Armc2 Foxo3
chr19:29000001-29500000	4.27	4430402I18Rik Ppapdc2 Cdc37l1 Gm10136 Ak3 Rcl1 Mir101b Jak2 Insl6 Rln1 5033414D02Rik Cd274 Pdcd1lg2
chr16:33000001-33500000	4.16	Lrch3 Gm17106 n-R5s33 Iqcg Rpl35a Lmln AC126023.1 Mir1947 RNaseP_nuc Osbpl11 Snx4 AC122247.1 1700007L15Rik Zfp148
chr9:57500001-58000000	4.05	Cyp1a2 Cyp1a1 Edc3 Clk3 Gm17231 Arid3b Ubl7 Sema7a Gm17322 Cyp11a1 Ccdc33 Gm16130 Stra6 Gm16131

trans interactions from Foxo1 viewpoint in Rag/81X pre-B

bin	z-score	genes in bin
chr4:44500001-45000000	28.05	Gm19980 Pax5 AL772319.1 Gm12462 Zcchc7 AL805896.1 Gm12678 Gm12493 Gm12679 Grhpr
chr12:115500001-116000000	25.91	Ighv3-8 Ighv12-3 Gm16930 Gm16695 Gm17000 Gm16696 Gm16694 Ighv1-5 Ighv10-3 Ighv1-7 Ighv15-2 Ighv1-9 Ighv1-12 Gm17686 Gm16857 Gm16858 Ighv1-18 Ighv1-19 Ighv1-20 Gm16860
chr11:44500001-45000000	25.57	Ebf1 Gm12159 Gm12160
chr4:32000001-32500000	20.52	Map3k7 U4 Bach2 D130062J21Rik Gm11932
chr11:45000001-45500000	18.72	Gm12160 Gm12162 SNORA17
chr6:68500001-69000000	16.92	Igkv12-98 Gm16637 Igkv10-96 Igkv10-95 Igkv10-94 Igkv19-93 Igkv4-92 Igkv4-91 Igkv4-90

		Igkv12-89 Igkv1-88 Gm11145 Igkv4-86 Igkv13-84 Igkv4-81 Igkv4-80 Igkv4-79
chr6:68000001-68500000	16.92	Igkv9-120 Igkv1-117 Igkv2-116 Igkv1-115 Igkv2-112 Igkv14-111 SNORA17 Igkv1-110 Igkv2-109 Igkv16-104 Igkv15-103 Igkv14-100 SNORA17 Igkv1-99
chr6:69000001-69500000	15.96	Igkv4-78 Igkv4-74 Igkv4-73 Igkv4-72 Igkv4-71 Igkv4-70 Igkv4-69 Igkv4-68 RNaseP_nuc Igkv4-63 Igkv4-62 Igkv4-61 Igkv4-59 Igkv4-58 AC156953.1 Igkv4-57-1
chr6:69500001-70000000	15.57	Igkv4-57 Igkv4-56 Gm11143 Igkv4-55 Igkv4-53 Igkv4-50 Igkv5-48 Igkv12-47 Igkv12-46 Igkv5-45 Igkv12-44 Igkv5-43 Igkv12-41 Igkv5-39 Igkv12-38 Igkv5-37 Igkv18-36 Igkv1-35 AC154006.1
chr12:114500001-115000000	14.84	Ighg2c Ighg Ighg Ighm Adam6b Adam6a Ighv2-4
chr6:67500001-68000000	14.78	Igkv2-137 Igkv1-135 Igkv17-134 Igkv1-133 Igkv1-132 Igkv1-131 Igkv14-130 SNORA17 SNORA17 Igkv9-129 Igkv17-127 Igkv14-126 SNORA17 Igkv11-125 Igkv9-124 Igkv9-123 Igkv1-122 Igkv17-121 Igkv9-120
chr4:32500001-33000000	12.98	Bach2 7SK BC024582 Gja10 Casp8ap2 Mdn1 Lyrm2 Ankrd6
chr6:70500001-71000000	12.76	Igkv3-10 Igkv3-9 Igkv3-7 Gm16774 Igkv3-4 Igkv3-3 Igkv3-2 Igkv3-1 Igkj1 Igkj2 Igkj3 Igkj4 Igkj5 Igkc Rpia Eif2ak3 SNORA5 1700011F03Rik Foxi3 U1
chr12:116000001-116500000	12.70	Ighv1-23 Ighv1-24 Gm16717 Gm17539 Gm16965 Gm16735 Gm16715 Gm16716 Gm16964 Ighv1-42 Ighv1-43 Gm16966 Gm16830 Ighv8-5 Gm16829 Gm16828 AB069917 Ighv8-6 Ighv1-54 Gm16792 Gm16791
chr12:115000001-115500000	12.14	Ighv11-2 Ighv14-3 Gm7005 Gm16987 Ighv9-2 Ighv9-3 Gm16842 Gm16841 Ighv3-3 Gm16839
chr16:19000001-19500000	12.08	Iglc3 Iglv1 Iglc2 Iglv3 Iglv2 Olfr164 SNORA17 AC112681.1 Olfr165 SNORA17 Olfr166
chr6:99000001-99500000	11.97	Foxp1 Eif4e3 AC152987.1
chr15:80500001-81000000	11.86	Fam83f Tnrc6b AC125540.1 Adsl Sgsm3 Mkl1 U4
chr13:37500001-38000000	11.47	Ly86 Rreb1
chr5:136500001-137000000	11.30	Dtx2 Upk3b 2310043J07Rik Rasa4 U12 Gm15701 Polr2j Lrwd1 Alkbh4 Orai2 Prkrip1 Sh2b2 Cux1 Gm16599
chr17:5000001-5500000	11.24	Arid1b 5730437N04Rik AC166064.1 Zdhhc14
chr19:33000001-33500000	11.24	7SK Rnls Gm7237
chr17:4500001-5000000	11.13	U6 Arid1b
chr12:81000001-81500000	10.85	Zfp36l1 Gm17591 2310015A10Rik Actn1 Gm17425 Gm17373 Gm17301 Dcaf5 Scarna3b
chr12:80500001-81000000	10.79	Rad51l1
chr15:9500001-10000000	10.62	Spef2 7SK
chr13:41500001-42000000	10.23	Nedd9 AC154848.1 Tmem170b Gm5082 9530008L14Rik 1700061E18Rik U6
chr1:38500001-39000000	10.17	Aff3 Lonrf2 Chst10 Nms
chr1:166500001-167000000	10.12	Dpt Xcl1 AC133891.1
chr12:101000001-101500000	10.12	2610021K21Rik Tdp1 Kcnk13 AC159243.1 Psmc1 BC002230 Gm10433 Calm1 Gm17302
chr8:129000001-129500000	9.95	AC118255.1 Gm16983 Irf2bp2 Tomm20 SNORA14 Rbm34
chr13:44000001-44500000	9.78	Gm5083
chr9:70500001-71000000	9.78	Fam63b Gm10642 Adam10 Lipc CT025701.1 Gm3436 Aqp9
chr10:44000001-44500000	9.67	Atg5 Mir1929 Prdm1 U6 U6
chr12:101500001-102000000	9.61	Ttc7b Rps6ka5
chr13:24500001-25000000	9.61	Cmah U6 Fam65b Gm11346 C530050E15Rik 1700016G14Rik Gmnn BC005537 SNORA32 Acot13 Tdp2 D130043K22Rik 4932702P03Rik Aldh5a1
chr15:81000001-81500000	9.56	Mkl1 4930483J18Rik Mchr1 Slc25a17 St13 Xpnpep3 Dnajb7 Gm17025 Rbx1 Gm5218 Ep300 AC160528.1 U6 L3mbtl2
chr17:5500001-6000000	9.44	Zdhhc14 Snx9 Synj2
chr6:70000001-70500000	9.39	Igkv7-33 Igkv6-32 Igkv8-30 Igkv6-29 Igkv8-28 AC159715.1 Igkv8-27 Igkv8-26 Igkv6-25 Igkv8-24 Igkv6-23 Igkv8-21 Igkv6-20 Igkv8-19 Igkv8-18 Igkv6-17 Igkv8-16 Igkv6-15 Gm10360 Igkv6-14 Igkv6-13 Igkv3-12
chr13:112500001-113000000	9.39	Mier3 Gm15287 Map3k1 Gm15327 Gm15325 Gm15324 Gm15326 Gm15322 Gm15323
chr8:125000001-125500000	9.33	Gm20388 Ctu2 Fam38a U6 Cdt1 Aprt Galns Trappc2l Pabpn1l Cbfa2t3 Gm10612 Acsf3 Gm16378 Cdh15 Ankrd11
chr10:94500001-95000000	9.16	Cradd Socs2 5730420D15Rik Mrpl42 Ube2n
chr13:23500001-24000000	9.16	Abt1 C230035I16Rik Btn1a1 Btn2a2 Gm11335 Hist1h4h Hist1h2af Hist1h3g Hist1h2bh Hist1h3f Hist1h4f Hist1h1d Hist1h3e Hist1h2ae Hist1h2bg Hist1h2bf Hist1h2ad Hist1h3d Gm17658 Hist1h4d Hist1h2be Gm11398 Hist1h1e U6 Hist1h2ac 5S_rRNA Hist1h2bc Hist1h1t Hist1h4c Hfe Hist1h1c Hist1h3c Hist1h2bb Hist1h2ab Hist1h3b 4930558J22Rik Hist1h4b Hist1h4a Hist1h3a Hist1h1a Trim38 Gm11337 Slc17a2 Slc17a3 Slc17a1 Slc17a4
chr12:116500001-117000000	9.11	Gm9740 Gm16633 Ighv1-59 Gm16900 Gm9232 Ighv1-62-2 Gm9235 Ighv8-9 Ighv1-63 Gm16865 Ighv8-11 Gm16901 Ighv1-67 Gm16708 Ighv8-12 Ighv1-71 Gm16709
chr1:38000001-38500000	9.05	Gm15457 Lyg1 7SK Txndc9 Eif5b Rev1 Aff3 Gm16150 Gm16151 Gm16152
chr5:137000001-137500000	8.94	Cux1 4731417B20Rik Myl10 Emid2 RP24-498F17.1 Rabl5 4933404O12Rik Fis1 Cldn15 Znhit1 Plod3 Mir702
chr16:30000001-30500000	8.88	4632428C04Rik Hes1 n-R5s32 Gm17516 Cpn2 Lrrc15 Gp5 Atp13a3
chr15:9000001-9500000	8.82	1110020G09Rik Skp2 Lmbrd2 Ugt3a1 Ugt3a2 Capsl Il7r
chr2:167500001-168000000	8.77	Tmem189 Cebpb A530013C23Rik Gm14321 9230111E07Rik 1200007C13Rik Gm14319 Ptpn1 Fam65c Gm14236 AL831766.1 Pard6b Gm14235 E130018N17Rik
chr17:29000001-29500000	8.77	Pnpla1 4930539E08Rik 1700030A11Rik Gm16191 Pxt1 Kctd20 Stk38 U2 Gm16196 Gm16195 Srsf3 Gm16197 Cdkn1a Gm16194 Rab44 Cpne5 Ppil1 BC004004 Pi16 Mtch1 Fgd2
chr19:41000001-41500000	8.71	Blnk Dntt Opalin Tll2 Tm9sf3 Pik3ap1
chr15:59000001-59500000	8.66	Gm5045 Sqle E430025E21Rik Nsmce2 Trib1
chr6:87000001-87500000	8.60	Gfpt1 D6Ertd527e Antxr1 n-R5s164 Gkn1 Gkn2 Gkn3 Bmp10 Arhgap25
chr12:114000001-114500000	8.54	Pld4 Ahnak2 BC022687 Cdca4 Gpr132 Gm17723 Jag2 Nudt14 Gm17274 Brf1 Btbd6 Pacs2 Tex22 Mta1 Crip2 Crip1 4930427A07Rik Tmem121 U6
chr4:135500001-136000000	8.49	Hmgcl Gale Lypla2 1110049F12Rik Tceb3 Gm13008 AL672076.1 Rpl11 BX530725.1 U6 Id3 E2f2 Asap3 Tcea3 Zfp46 Hnrnpr 2610528B01Rik 9130020K20Rik Gm17388 Htr1d

chr17:86500001-87000000	8.49	Srbd1 Prkce Gm10309
chr12:100500001-101000000	8.43	Foxn3 3300002A11Rik Gm16956 2610021K21Rik
chr16:30500001-31000000	8.38	Tmem44 Lsg1 Fam43a U6 SNORA17 AI480653 Gm15742
chr4:59000001-59500000	8.32	Dnajc25 Gm20503 Gng10 AI481877 Gm12594 Ugcg Gm12596 Susd1 Rod1
chr16:10500001-11000000	8.32	Ciita Dexi Clec16a Gm15558 Socs1 Tnp2 Prm3 Prm2 Prm1 Gm10343 Gm11172 Gm17410 A630055G03Rik Litaf AC164093.1 U1
chr12:86500001-87000000	8.32	Pgf Eif2b2 Mlh3 Acyp1 Fam164c Nek9 Tmed10 Fos Jdp2
chr4:132500001-133000000	8.26	Fgr Ahdc1 Gm10151 Wasf2 7SK Gpr3 Cd164l2 Map3k6 Sytl1 Tmem222 Wdtc1 Slc9a1 AL671882.1
chr14:32000001-32500000	8.26	Tnnc1 Nisch Tnnc1 Sema3g Phf7 Bap1 Dnahc1 Capn7 Sh3bp5 Mettl6 Eaf1 Colq 7SK Hacl1 Btd
chr2:166000001-166500000	8.21	5S_rRNA Gm11466 Gm11467 Gm11468 Gm14268 5031425F14Rik Gm14267 Prex1 AL732357.1
chr10:20500001-21000000	8.21	Ahi1 Myb Gm16786 AC153556.1
chr19:41500001-42000000	8.21	U7 Lcor Gm340 AI606181 Slit1 7SK Arhgap19 Frat2 Rrp12 Pgam1 Exosc1
chr7:87000001-87500000	8.15	Ap3s2 Gm17512 5430400D12Rik 2610034B18Rik AC110903.1 Zfp710 Idh2 AC164075.1 Mir1965 Sema4b Cib1 D330012F22Rik Ttll13 Ngrn Vps33b Prc1 6330403N20Rik Rccd1 Unc45a Hddc3 Man2a2
chr14:31000001-31500000	8.15	Cacna1d Dcp1a Tkt AC154646.1 Prkcd Rft1
chr17:4000001-4500000	8.15	
chr15:80000001-80500000	8.09	Mgat3 Smcr7l Atf4 Rps19bp1 Cacna1i Enthd1 SNORA17 Grap2
chr5:66000001-66500000	8.04	Pds5a U6 1700022K14Rik N4bp2 SNORA73 Rhoh Chrna9 9130230L23Rik AC115293.1 Rbm47
chr11:59500001-60000000	8.04	Mprip 1700007J10Rik Gm12264 Pld6 Flcn Gm16062 5S_rRNA Cops3 Nt5m Gm12714 1810063I02Rik 1700013G23Rik Med9 Rasd1 Pemt Rai1 4930412M03Rik
chr18:35500001-36000000	7.93	Sil1 Gm5239 Snhg4 SNORA74 Snora74a Matr3 Paip2 Slc23a1 2010001M09Rik Gm1614 Spata24 Dnajc18 1700066B19Rik Ecscr Tmem173 Gm16490 Ube2d2 Cxxc5
chr9:66000001-66500000	7.87	Dapk2 Herc1 U6 Fbxl22 Usp3 Gm15563
chr10:19500001-20000000	7.87	U6 Slc35d3 Pex7 Map3k5 Mtap7
chr10:79500001-80000000	7.87	Polr2e Gpx4 Sbno2 Stk11 Dos Atp5d Midn Cirbp 1600002K03Rik Efna2 Mum1 Ndufs7 Gamt Dazap1 Gm15122 Rps15 Apc2 2310011J03Rik Pcsk4 Reep6 Adamtsl5 Plk5 Gm15123 Gm15124 Mex3d AC152062.1 Mbd3 Uqcr11 Tcf3 U6 Onecut3 AC152058.1 Atp8b3
chr11:86000001-86500000	7.81	Brip1 4632419I22Rik Ints2 Med13 U3 Y_RNA 5S_rRNA U6 Rnft1 Rps6kb1 Tubd1 Vmp1 Mir21 Ptrh2
chr12:70500001-71000000	7.81	AC153658.1 Mettl21d Sos2 U6 L2hgdh Atp5s Cdkl1 Mir681 4930512B01Rik Map4k5 4931403G20Rik Atl1
chr17:30000001-30500000	7.64	Mdga1 Gm16758 SNORA70 Zfand3 Btbd9 U6
chr5:64500001-65000000	7.59	Pgm1 SNORA17 Tbc1d1
chr9:57500001-58000000	7.59	Cyp1a2 Cyp1a1 Edc3 Clk3 Gm17231 Arid3b Ubl7 Sema7a Gm17322 Cyp11a1 Ccdc33 Gm16130 Stra6 Gm16131
chr4:45500001-46000000	7.53	Shb AL772376.1 U6 Gm12408 Gm829 Gm12410 Gm12409 Aldh1b1 Igfbpl1 1300002K09Rik E230008N13Rik Tdrd7
chr13:51000001-51500000	7.53	Y_RNA Spin1 Nxnl2 Hist1h2al
chr19:32000001-32500000	7.53	A1cf Asah2 Sgms1 2700046G09Rik
chr4:133000001-133500000	7.53	Gm13257 Fam46b Trnp1 1810019J16Rik Gm17688 Nudc Nr0b2 Gpatch3 Gpn2 Sfn Zdhhc18 BX537327.1 Pigv Arid1a U4 Gm12974 Rps6ka1 Gm17623 Gm12977 U6
chr5:65000001-65500000	7.48	AC122043.1 Klf3 Tlr1 Tlr6 Fam114a1 Mir574 Tmem156 Klhl5
chr13:43500001-44000000	7.48	Ranbp9 U6 Ccdc90a Rnf182 Cd83 U6
chr15:10000001-10500000	7.48	Prlr Agxt2 Dnajc21 Brix1 Rad1 Ttc23l Rai14
chr16:29500001-30000000	7.48	Atp13a4 Opa1 Gm17734 Gm16761 Gm1968
chr7:134000001-134500000	7.42	Ino80e Hirip3 Taok2 Tmem219 U6 Kctd13 Sez6l2 Asphd1 D830044I16Rik Cdipt Mvp Gm20418 2900092E17Rik Prrt2 Maz Kif22 7SK Zg16 U6 AI467606 Qprt Spn AC122537.1 Cd2bp2 Tbc1d10b Mylpf Sept1 Zfp553 Zfp771 Dctpp1 Sephs2 Gm17511 Itgal Zfp768
chr13:24000001-24500000	7.42	Slc17a4 Hist1h2ba Hist1h2aa Scgn Gm11339 Lrrc16a SNORA17 Cmah Gm11342 Gm11345
chr19:55500001-56000000	7.42	Vti1a 4930552P12Rik Tcf7l2
chr1:37500001-38000000	7.36	Mgat4a 2010300C02Rik 4930556I23Rik Tsga10 Gm17715 Lipt1 Mitd1 Mrpl30 Lyg2 Gm15457
chr2:166500001-167000000	7.36	Prex1 7SK U6 Trp53rk Arfgef2 Cse1l Gm17096 Stau1 Ddx27 Znfx1 1500012F01Rik SNORD12 SNORD12 Snord12 Gm14290 Kcnb1
chr11:45500001-46000000	7.36	F630206G17Rik AL645948.1 Clint1 Lsm11 Thg1l Sox30 Gm12166 Adam19 Gm16033 Gm16034 Nipal4
chr2:45000001-45500000	7.31	Gm13479
chr16:92500001-93000000	7.31	Clic6 Runx1 Gm16801
chr19:37500001-38000000	7.31	Hhex U6 Exoc6 Cyp26c1 Cyp26a1 Myof
chr4:134500001-135000000	7.25	Gm16225 Runx3 Gm16224 Clic4 Gm12984 Srrm1 A330049M08Rik Rcan3 Mir700 Gm15979
chr19:45500001-46000000	7.14	Btrc Gm6807 Poll Dpcd Fbxw4 Gm17018 Fgf8 Npm3 Gm15491 Mgea5 Kcnip2 9130011E15Rik
chr9:61000001-61500000	7.14	Gm10655 Tle3
chr16:11000001-11500000	7.14	Litaf Gm4262 Snn Txndc11 Zc3h7a mmu-mir-689-2 U1 4930509G22Rik Rsl1d1 2610020C07Rik Gspt1 Mir1945 Tnfrsf17 Snx29 Snx29
chr7:135000001-135500000	7.03	AC149222.1 Zfp668 Zfp646 Prss53 Vkorc1 Bckdk Myst1 Prss8 Prss36 Fus Gm17468 B230325K18Rik Pycard Gm15533 Trim72 U1 Itgam Itgax Itgad Cox6a2 9130023H24Rik Armc5 Tgfb1i1 Slc5a2 BC017158 AC124566.1
chr2:35500001-36000000	6.97	Dab2ip Ttll11 9030204H09Rik Ndufa8 Morn5 Lhx6 Rbm18 Mrrf
chr2:32000001-32500000	6.97	Prrc2b SNORD62 AL808027.3 Gm13610 Pomt1 Uck1 Swi5 Golga2 Dnm1 AL808027.1 AL808027.2 Ciz1 1110008P14Rik Lcn2 Ptges2 Slc25a25 Naif1 Gm13412 Fam102a Dpm2 9430097D07Rik Pip5kl1 Gm17343 St6galnac4 AL772271.2 St6galnac6 Ak1
chr5:34500001-35000000	6.91	Poln Haus3 U6 Mxd4 Zfyve28 Gm15513 Rnf4 Fam193a snoU13 Tnip2 Sh3bp2 U1 Add1 Mfsd10 Nop14 Gm15522

chr6:52500001-53000000	6.91	Hibadh SNORA32 Tax1bp1 Jazf1 SCARNA20
chr10:118000001-118500000	6.91	Dyrk2 4932442E05Rik
chr1:166000001-166500000	6.80	Sell Selp Gm16587 Gm16548 F5 Slc19a2 4930455F23Rik Blzf1 Nme7 Atp1b1 Gm16608
chr7:139500001-140000000	6.80	Fgfr2 Chst15 Oat Nkx1-2 Gm16764 Lhpp Gm15582 Fam53b
chr4:134000001-134500000	6.75	1700021N21Rik Stmn1 AL669982.1 Paqr7 2610002D18Rik Fam54b Sepn1 Man1c1 Ldlrap1 AL645531.1 Tmem57 Rhd Tmem50a D4Wsu53e Syf2
chr14:77000001-77500000	6.63	9030625A04Rik Ccdc122
chr16:95500001-96000000	6.63	Kcnj15 Erg Ets2
chr9:71500001-72000000	6.58	Cgnl1 Tcf12 Rpl15-ps2 U6
chr2:30500001-31000000	6.52	9330198N18Rik Gm14486 Gm14488 AL928593.1 1700001O22Rik 4930527E20Rik Mettl11a Asb6 Prrx2 Ptges Tor1b Tor1a BC005624 Usp20 Fnbp1
chr4:44000001-44500000	6.52	Clta Gne U1 Gm12503 Gm12504 Rnf38 AL805952.1 Melk SNORA17
chr8:47500001-48000000	6.52	Acsl1 Mlf1ip Ccdc111 Casp3 Gm16675 Irf2
chr11:54500001-55000000	6.52	Rapgef6 Cdc42se2 Gm12227 Gm12228 Lyrm7 U1 Hint1 Gpx3 Tnip1 Anxa6 Ccdc69 Gm2a Slc36a3 Gm12233 Slc36a2
chr11:98500001-99000000	6.52	Gsdma2 Gsdma Psmd3 Gm12356 Csf3 Med24 SNORD124 Thra Nr1d1 Msl1 Gm12359 Casc3 Rapgefl1 Wipf2 U6 Cdc6 Rara U6 Gjd3 Top2a SNORA42 SNORA32 Igfbp4 Tns4
chr11:100500001-101000000	6.52	Zfp385c Gm11547 Dhx58 Kat2a Hspb9 Rab5c Kcnh4 Hcrt Ghdc 7SK Stat5b Stat5a Stat3 Ptrf Atp6v0a1 Naglu Hsd17b1 Coasy Mlx Psmc3ip Fam134c Tubg1
chr14:26000001-26500000	6.52	Gm17716 D930049A15Rik Zmiz1 AC154455.1 Gm17670 Gm10397
chr17:34000001-34500000	6.52	Kifc1 BC033916 BC051226 Daxx Tapbp Zbtb22 Rgl2 H2-Ke2 Wdr46 B3galt4 Rps18 Vps52 U6 H2-K1 Ring1 Mir219-1 Mir219-1 H2-Ke6 Gm20427 Slc39a7 Rxrb Col11a2 H2-Oa Brd2 H2-DMa H2-DMb2 H2-DMb1 Psmb9 Psmb9 Tap1 Psmb8 Gm20496 Tap2 Gm15821 H2-Ob Gm20506 H2-Ab1 H2-Aa Gm20513 H2-Eb1 H2-Eb2 Gm11140 Btnl2
chr5:149500001-150000000	6.46	2210417A02Rik n-R5s179 4930505K14Rik Gm15407 Katnal1 Gm15410 Gm15406 8430423G03Rik 1810059H22Rik Gm15409 Gm15411 Gm15408 Hmgb1 5730422E09Rik AC122546.2 Uspl1
chr8:125500001-126000000	6.46	Gm20388 Ankrd11 U6 Spg7 Rpl13 Snord68 Cpne7 Sult5a1 Dpep1 Chmp1a 4732415M23Rik Cdk10 Spata2L 4933417D19Rik 1300018I17Rik Zfp276 AC155810.1 Fanca Spire2 Tcf25 AC122266.1 Mc1r Tubb3 Def8 SNORA63
chr13:44500001-45000000	6.46	Jarid2 SNORA61
chr4:45000001-45500000	6.46	Grhpr Zbtb5 1700055D18Rik Polr1e Fbxo10 Tomm5 Gm10982 Frmpd1 2900093L17Rik Rg9mtd3 Exosc3 Dcaf10 Mcart1 AL772376.2 Mcart1 Shb
chr6:145500001-146000000	6.46	Ifltd1 Tuba3b Gm15704 Rassf8 Rassf8 Bhlhe41 Sspn Gm15705
chr4:132000001-132500000	6.41	Med18 snoU13 Sesn2 Gm12981 Atpif1 Gm12999 Dnajc8 U6 Ptafr Eya3 Xkr8 Smpdl3b Rpa2 BC013712 Ppp1r8 SCARNA1 Stx12 Fam76a U6
chr6:86500001-87000000	6.35	1600020E01Rik AC158662.1 Asprv1 Mxd1 Snrnp27 Gmcl1 Anxa4 Aak1 Nfu1 Gfpt1
chr11:5500001-6000000	6.35	Ankrd36 Mrps24 Urgcp 2210015D19Rik Dbnl Pgam2 Polm Aebp1 Pold2 Myl7 Gck Gm11967 Ykt6 Camk2b
chr11:117500001-118000000	6.35	Tnrc6c Tmc6 Tmc8 Gm11723 Gm11724 6030468B19Rik Syngr2 Afmid Tk1 Birc5 Cldn27 Tha1 Gm11725 Socs3 Pgs1 Dnahc17 Gm11738 Cyth1
chr17:26500001-27000000	6.35	Neurl1b Dusp1 Gm8225 1700049J03Rik Ergic1 AC122252.1 Gm17218 Atp6v0e A930001N09Rik Bnip1 Nkx2-5 Gm17382 Gm20468
chr14:122000001-122500000	6.35	Dock9 Ubac2 Gpr18 Gpr183 Timm8a2
chr2:32500001-33000000	6.30	Ak1 Eng AL772271.5 AL772271.3 Fpgs Cdk9 AL772271.4 AL772271.1 Sh2d3c 6330409D20Rik Ttc16 Tor2a Ptrh1 1700019L03Rik Stxbp1 SNORA31 Gm13524 Gm13523 Fam129b Lrsam1 Rpl12 Snora65 Slc2a8 Garnl3 Ralgps1
chr10:83500001-84000000	6.30	Nuak1 4930463O16Rik Ckap4
chr11:44000001-44500000	6.30	Gm12154 Il12b Ublcp1 AL669944.1 Rnf145 4930597A21Rik Ebf1 Gm12158
chr4:8500001-9000000	6.24	Rab2a Chd7
chr9:32000001-32500000	6.24	Arhgap32 Kcnj5 Kcnj1 Fli1 U6 Ets1
chr11:86500001-87000000	6.24	Ptrh2 Cltc Dhx40 AL596111.1 Ypel2 SCARNA3 Gdpd1 Gm11479 1200011M11Rik Prr11 Fam33a Mir301 Gm11491 Trim37
chr18:75000001-75500000	6.24	SNORA22 AC155261.1 Lipg Rpl17 SNORD58 SNORD58 SNORD58 BC031181 Dym
chr18:80500001-81000000	6.18	Gm16997 Ctdp1 Nfatc1 Atp9b
chr17:31000001-31500000	6.18	Dnahc8 Glp1r Umodl1 AC165951.1 Abcg1 5S_rRNA Tff3 Tff2 Gm15318 Tff1 Tmprss3 Ubash3a Rsph1 Slc37a1
chr11:22500001-23000000	6.13	Gm17335 Gm12052 Gm12055 Gm12056 Commd1 B3gnt2 RP23-242C19.6 SNORA63 RP23-242C19.5 U6 Zrsr1 Cct4 Fam161a 5S_rRNA Gm12059
chr12:78000001-78500000	6.13	Fntb Max AC133174.1 Fut8 U6
chr16:32500001-33000000	6.13	Zdhhc19 Tfrc Tnk2 Gm10818 Muc4 Muc20 1700021K19Rik Fyttd1 Lrch3 Gm17106
chr1:36500001-37000000	6.07	Lman2l Cnnm4 Cnnm3 Ankrd23 Ankrd39 Sema4c D430040D24Rik Fam178b AC084389.1 Cox5b Actr1b Zap70 Tmem131
chr9:70000001-70500000	6.07	Gm17406 Myo1e Ccnb2 Rnf111 SNORA20 U6 U6 AC158995.1 U6 Sltm Fam63b
chr16:24000001-24500000	6.07	1110054M08Rik Lpp U7
chr5:36500001-37000000	6.07	Sorcs2 Psapl1 2210406O10Rik Grpel1 Tada2b Ccdc96 Tbc1d14 D5Ertd579e
chr17:31500001-32000000	6.01	Pde9a Wdr4 Ndufv3 4833413E03Rik Pknox1 AC166172.1 Cbs U2af1 Cryaa Sik1
chr13:93500001-94000000	6.01	Thbs4 Mtx3 Cmya5 Papd4
chr15:58500001-59000000	6.01	Fer1l6 Tmem65 U1 Gm5959 Trmt12 Rnf139 Tatdn1 Ndufb9 Mtss1
chr9:116000001-116500000	5.96	Tgfbr2 AC131777.1 Rbms3
chr17:45000001-45500000	5.96	Supt3h
chr2:35000001-35500000	5.90	Cep110 Rab14 Gm13605 Gsn Stom 4930568D16Rik 4930402F06Rik Ggta1 Gm13447 Gm13446 Dab2ip
chr4:133500001-134000000	5.90	Hmgn2 Dhdds Lin28a Gm13061 Gm13060 Aim1l Cd52 Ubxn11 Sh3bgrl3 Ccdc21 Gm17345

		Gm7534 Catsper4 Cnksr1 Zfp593 E130218I03Rik Grrp1 Pdik1l Trim63 Slc30a2 Extl1 Pafah2
chr10:117000001-117500000	5.90	Cpm U6 Mdm2 Slc35e3 Nup107 Rap1b
chr14:79500001-80000000	5.90	1300010F03Rik Zfp957 1190002H23Rik Naa16 AC124745.1 Mtrf1 Kbtbd7 Gm5465 Wbp4 Elf1 Sugt1
chr8:123000001-123500000	5.85	Gse1 Gins2 Cox4nb Cox4i1 7SK Irf8
chr9:44000001-44500000	5.85	Cbl Ccdc153 Pdzd3 Nlrx1 Abcg4 Hinfp C2cd2l Dpagt1 H2afx Hmbs Vps11 7SK Hyou1 SNORA40 Slc37a4 Trappc4 Rps25 Ccdc84 Foxr1 Upk2 Gm9830 U6 C030014I23Rik Bcl9l Cxcr5 Ddx6 Treh Phldb1
chr11:118000001-118500000	5.85	Cyth1 U6 Usp36 Timp2 BC100451 Lgals3bp Cant1 C1qtnf1 Gm11747 Gm11748 Engase Rbfox3
chr16:33500001-34000000	5.85	Zfp148 Slc12a8 Heg1 Gm15658 Gm15657 Muc13 Itgb5 Umps Gm15829 Kalrn
chr17:28500001-29000000	5.85	Tulp1 Fkbp5 7SK E230001N04Rik 4930511I11Rik Gm749 Clps Lhfpl5 Srpk1 Slc26a8 Mapk14 Mapk13 Brpf3 Gm16190 Pnpla1
chr17:73000001-73500000	5.85	Ypel5 Lbh U6 Lclat1
chr9:60500001-61000000	5.79	Lrrc49 B930082K07Rik Larp6 1700036A12Rik Uaca Gm9869
chr10:19000001-19500000	5.79	Olig3 Ifngr1 Il22ra2 9230106D20Rik Il20ra
chr16:94500001-95000000	5.79	Hlcs Ripply3 Pigp Ttc3 U1 Dscr3 Dyrk1a Kcnj6
chr17:84500001-85000000	5.79	Zfp36l2 Thada U6 U6 Plekhh2
chr9:65000001-65500000	5.79	Igdcc3 U5 U5 Parp16 Cilp Clpx AC110235.1 Pdcd7 Gm514 Rasl12 Ostb Mtfmt Spg21 Ankdd1a Plekho2 Pif1 Rbpms2
chr9:103000001-103500000	5.79	Rab6b Srprb Trf Trf 1300017J02Rik Topbp1 Cdv3 5830418P13Rik Bfsp2 Gm16252 Tmem108 U6
chr17:50000001-50500000	5.79	Kif6 Gm16554 Rftn1 AY702103 Dazl
chr10:6000001-6500000	5.73	Akap12 U8 Mthfd1l U1 Plekhg1 5S_rRNA
chr10:39000001-39500000	5.73	Fyn Gm16364 Gm16365 Traf3ip2 E130307A14Rik Rev3l U6atac
chr12:86000001-86500000	5.73	Tmem90a Npc2 Isca2 Ltbp2 D030025P21Rik 1110018G07Rik Gm17139 Gm17193 Fcf1 Ylpm1 Prox2 Dlst Rps6kl1
chr12:100000001-100500000	5.73	Zc3h14 Eml5 Ttc8 Rpl30-ps8 Foxn3
chr16:32000001-32500000	5.73	Senp5 Pak2 SNORA17 Pigx 1500031L02Rik Gm15729 Lrrc33 Bex6 Fbxo45 SNORA79 Wdr53 Mir1946a 2310010M20Rik Rnf168 AC087556.1 Ubxn7 Tm4sf19 Tctex1d2 Pcyt1a Osta Zdhhc19
chr17:29500001-30000000	5.68	Fgd2 Gm16912 Pim1 Gm17657 Tmem217 Tbc1d22b Ftsjd2 AC163629.1 0610038L08Rik Rnf8 1110021J02Rik Mdga1
chr2:34500001-35000000	5.62	Gapvd1 Hspa5 Rabepk snoU13 Fbxw2 Psmd5 D730039F16Rik Phf19 Gm13448 U6 Traf1 Hc Gm13449 AI182371 Cep110
chr7:17000001-17500000	5.62	Zc3h4 Tmem160 Npas1 n-R5s151 Grlf1 U6 Ceacam15 AC150681.1 Ceacam9 Ap2s1 Slc1a5 Fkrp Strn4 Prkd2 9330104G04Rik Dact3 Gng8 Ptgir
chr7:133500001-134000000	5.62	Lat Spns1 Nfatc2ip Cd19 Rabep2 Atp2a1 Sh2b1 Tufm Atxn2l Eif3c U6 U6 Cln3 Apobr Il27 Nupr1 2510046G10Rik Ccdc101 Sult1a1 Slx1b Bola2 Coro1a Mapk3 Gdpd3 Gm9967 Ypel3 Tbx6 Ppp4c Aldoa Gm15676 Fam57b 4930451I11Rik Doc2a Ino80e
chr18:39500001-40000000	5.62	Arhgap26 Gm15337 Nr3c1 Gm10008 Pabpc2
chr18:54500001-55000000	5.62	9430076G02Rik
chr19:46500001-47000000	5.62	Sufu Trim8 Arl3 Sfxn2 D19Wsu162e Cyp17a1 2010012O05Rik As3mt Cnnm2 Nt5c2
chr2:165500001-166000000	5.56	Eya2 Zmynd8 AL591712.1 BC046401 Gm11465 AL589902.1 Gm11463 Gm11464 Ncoa3 Sulf2
chr5:123000001-123500000	5.56	Ift81 P2rx7 Gm10064 P2rx4 Camkk2 Anapc5 Rnf34 Kdm2b A930024E05Rik Orai1 Morn3 Gm17627
chr6:120500001-121000000	5.56	Cecr2 Slc25a18 Atp6v1e1 Bcl2l13 Bid Mical3 Mical3
chr8:122500001-123000000	5.56	Gm20388 Crispld2 Gm15684 Zdhhc7 Gm15898 6430548M08Rik Fam92b
chr11:77000001-77500000	5.56	Efcab5 Ssh2 SNORD86 Ssh2 Coro6 Ankrd13b 2210008F06Rik Git1 Trp53i13 Abhd15 Gm10392 Taok1 SNORA17 Nufip2
chr12:80000001-80500000	5.56	Plek2 Tmem229b Plekhh1 Pigh Arg2 Vti1b Rdh11 Rdh12 Zfyve26 Rad51l1
chr18:55000001-55500000	5.56	Zfp608 Gm17270 Gm4221 SNORA40 U6
chr19:57000001-57500000	5.56	Afap1l2 Ablim1 B230217O12Rik Fam160b1
chr10:116500001-117000000	5.51	Cct2 Frs2 SNORA13 Yeats4 9530003J23Rik Gm10936 Lyz2 Lyz1 Cpsf6
chr13:103000001-103500000	5.51	Cd180
chr2:27000001-27500000	5.40	Gm13399 Dbh Sardh Gm17071 Vav2 AA645442 AL731552.1 Brd3 Wdr5 U6atac Gm13421
chr6:8000001-8500000	5.40	Col28a1 Mios Rpa3 Gm16039 Gm16055 Gm16043 7SK 2810488G03Rik SNORA65 Glcci1
chr11:74500001-75000000	5.40	Pafah1b1 U6 Mettl16 Mnt Sgsm2 Tsr1 Snord91a SNORD91 Srr Smg6 U6 Gm12333 Hic1 1700016P03Rik Mir212 Mir132 Ovca2 Dph1
chr15:36500001-37000000	5.40	Pabpc1 Ywhaz AC138604.1 Gm10384 Zfp706 Gm16631
chr16:31000001-31500000	5.40	AI480653 Acap2 Ppp1r2 Apod Bdh1 Gm15743
chr1:182000001-182500000	5.34	Cdc42bpa Adck3 Psen2 Gm5069 Itpkb 6330403A02Rik Parp1
chr1:182500001-183000000	5.34	Parp1 Lin9 Mixl1 Acbd3 AC167020.1 H3f3a Gm17275 Gm16067 U6 BC031781 Lefty2 Pycr2 Lefty1 Tmem63a 2210411M09Rik Ephx1 9130409I23Rik
chr5:65500001-66000000	5.34	Klhl5 5S_rRNA Wdr19 Rfc1 Klb Rpl9 Lias Ugdh 1110003E01Rik Ube2k
chr7:108000001-108500000	5.34	Relt Arhgef17 AC150744.1 P2ry6 P2ry2 Fchsd2 Atg16l2 Stard10 RP24-126J17.2 Arap1
chr9:72000001-72500000	5.34	Gm7866 U6 Zfp280d BC065403 Mns1 Tex9 Tex9 AC111135.1 4930509E16Rik Rfx7 U6
chr12:85500001-86000000	5.34	C130039O16Rik Gm5436 AC159649.1 Ptgr2 Zfp410 Fam161b Coq6 Entpd5 2900006K08Rik Aldh6a1 Lin52 Vsx2 Abcd4 Vrtn
chr4:11000001-11500000	5.28	2310030N02Rik Gm11827 Trp53inp1 Ccne2 Ints8 Dpy19l4 U1 Gm16652 Esrp1 Gm17283 1110037F02Rik Gm11831 Rad54b
chr10:43500001-44000000	5.28	Gm9034 Qrsl1 Rtn4ip1 Aim1 Atg5
chr11:6000001-6500000	5.28	Nudcd3 Npc1l1 Ddx56 Tmed4 n-R5s67 Ogdh Zmiz2 Ppia H2afv Purb AL646020.1 Purb Gm11973 Myo1g Gm11974 SNORA9 SNORA70 Ccm2 Nacad
chr11:88000001-88500000	5.28	Cuedc1 Mrps23 1700106J16Rik Msi2 AL732539.1 Gm15893
chr4:33000001-33500000	5.28	Ankrd6 Rragd 4933421O10Rik Ube2j1 Gabrr2 Gabrr1 Pm20d2 Srsf12 Pnrc1 Gm11934 AL772272.1 Rngtt

chr5:141000001-141500000	5.28	Chst12 Grifin Lfng Ttyh3 Iqce Baat1 Amz1 Gna12 Card11
chr10:43000001-43500000	5.28	Pdss2 Gm10281 Gm3699 Bend3 1700021F05Rik Cd24a F930017D23Rik
chr1:133000001-133500000	5.23	Dyrk3 Eif2d Rassf5 Ikbke Srgap2 AC109299.1 Fam72a Avpr1b
chr11:11500001-12000000	5.23	4930512M02Rik Gm11999 Ikzf1 Gm12000 Fignl1 Ddc 1700042O10Rik SCARNA4 Grb10 U1
chr15:81500001-82000000	5.23	L3mbtl2 Chadl Rangap1 Zc3h7b Gm17597 Tef Gm8444 Tob2 Tob2 Phf5a Aco2 Polr3h Csdc2 Pmm1 Gm5805 1700029P11Rik Xrcc6 Pppde2 Nhp2l1 4930407I10Rik Mei1 Ccdc134 Srebf2
chr19:5500001-6000000	5.23	Snx32 Ovol1 Gm962 Rnaseh2c Kat5 Rela Sipa1 Pcnxl3 Map3k11 Kcnk7 Ehbp1l1 Gm16538 Fam89b Sssca1 Ltbp3 Scyl1 Malat1 Gm20417 Neat1 Gm9783 Frmd8 Slc25a45 Tigd3 Dpf2 Cdc42ep2 Pola2 Slc22a20 Capn1
chr5:108000001-108500000	5.17	A830010M20Rik Glmn Rpap2 A930041C12Rik Gm17717 Gfi1 A430072P03Rik Evi5 1700013N18Rik Rpl5 Snord21 SNORA66 SNORA66 Fam69a Mtf2
chr8:10500001-11000000	5.17	Myo16 3930402G23Rik Irs2
chr10:92500001-93000000	5.17	4930485B16Rik Cdk17 Mir1931 Elk3 Lta4h Hal Amdhd1
chr11:75000001-75500000	5.17	Dph1 Rtn4rl1 Rpa1 Smyd4 Serpinf1 Gm12336 Serpinf2 Wdr81 2210403K04Rik Tlcd2 Mir22 Prpf8 Rilp Scarf1 Slc43a2 AL591496.1 Pitpna 4931413K12Rik Inpp5k Myo1c Crk
chr13:52000001-52500000	5.17	Gm16767
chr9:13500001-14000000	5.11	Maml2 Mtmr2 Cep57 Fam76b
chr10:18500001-19000000	5.11	Gm4922 Perp Tnfaip3
chr14:70000001-70500000	5.11	Gm16867 Loxl2 R3hcc1 Chmp7 4930480K23Rik Tnfrsf10b Rhobtb2 Pebp4 Egr3 Bin3
chr16:33000001-33500000	5.11	Lrch3 Gm17106 n-R5s33 Iqcg Rpl35a Lmln AC126023.1 Mir1947 RNaseP_nuc Osbpl11 Snx4 AC122247.1 1700007L15Rik Zfp148
chr17:28000001-28500000	5.11	Uhrf1bp1 Taf11 Anks1 Gm15597 Gm15598 Tcp11 4930526A20Rik Scube3 Zfp523 Def6 Ppard Fance Rpl10a Tead3 Tulp1
chr19:24500001-25000000	5.11	Pip5k1b 4930418C01Rik Fam122a E030010A14Rik Pgm5 Gm10053 Foxd4 Cbwd1
chr8:108000001-108500000	5.11	Zdhhc1 Hsd11b2 Atp6v0d1 Agrp Gm17380 Gm8841 Fam65a Mir1966 Ctcf AC127419.1 Rltpr Acd Pard6a E130303B06Rik 4933405L10Rik Gfod2 Ranbp10 AC152826.1 Tsnaxip1 Cenpt Thap11 Nutf2 Edc4 Nrn1l Pskh1 Ctrl Gm16156 Psmb10 Lcat Slc12a4 Dpep3
chr16:24500001-25000000	5.11	Lpp Mir28 SNORA17
chr2:5500001-6000000	5.06	Camk1d Cdc123 Nudt5 Gm13199 Sec61a2 Gm13267 Dhtkd1 Upf2
chr2:37500001-38000000	5.06	Strbp BX545905.1 Crb2 Dennd1a
chr7:87500001-88000000	5.06	Man2a2 Fes Furin Blm Crtc3 Gm15880 Iqgap1
chr15:57500001-58000000	5.06	Zhx2 Gm16006 9330154K18Rik Derl1 Wdr67 Fam83a 9130401M01Rik SNORA2 Zhx1 Atad2 Wdyhv1 U7 SNORA11
chr9:64500001-65000000	5.00	Megf11 Rab11a Dennd4a SNORA17 Slc24a1 2010321M09Rik AC122463.1 Ptplad1 Dpp8 Igdcc4 Igdcc3 AC161366.1
chr1:130500001-131000000	4.95	Gm17699 U6
chr2:31000001-31500000	4.95	D330023K18Rik Gpr107 SNORA76 Gm13405 Ncs1 Hmcn2 Ass1 Fubp3 AL732564.1 Gm13425 Prdm12
chr13:93000001-93500000	4.95	Msh3 Dhfr C030017D09Rik Ankrd34b Fam151b Zfyve16 Spz1 Serinc5
chr2:167000001-167500000	4.89	Kcnb1 1110018N20Rik Ptgis Gm14291 Gm17544 B4galt5 Slc9a8 Spata2 Rnf114 Snai1 Gm11476 Ube2v1 Tmem189 AL589870.1 Tmem189 Gm14320
chr5:140500001-141000000	4.89	Mad1l1 Gm16122 Gm16121 Gm16120 Ftsj2 Nudt1 Snx8 Eif3b Chst12
chr10:59500001-60000000	4.89	Ascc1 Spock2 Chst3 AC155640.1 AC155640.2 Psap Cdh23 4632428N05Rik Gm17455
chr13:43000001-43500000	4.89	Phactr1 Gm15809 7SK Gm15813 Tbc1d7 Gfod1 Sirt5 Nol7 Ranbp9
chr18:61000001-61500000	4.83	Tcof1 Arsi Camk2a Slc6a7 Cdx1 Pdgfrb Csf1r Hmgxb3 U6 Slc26a2 Pde6a Ppargc1b
chr10:21000001-21500000	4.78	Hbs1l Aldh8a1 1700021A07Rik snoU13 1700020N01Rik Gm5420
chr11:95000001-95500000	4.78	Dlx4 A730090H04Rik Gm11515 Tac4 Myst2 Gm11520 Gm11521 Fam117a Slc35b1 Spop Nxph3 Ngfr Gm11528
chr13:102500001-103000000	4.78	Pik3r1 7SK
chr14:31500001-32000000	4.78	Rft1 Sfmbt1 1700087M22Rik Tmem110 Mustn1 Itih4 Itih3 Itih1 Nek4 Spcs1 Glt8d1 Gnl3 Snord69 SNORD19B Snord19 Pbrm1 Gm5459 2010107H07Rik Nt5dc2 Stab1 Tnnc1 Nisch
chr15:78500001-79000000	4.78	Elfn2 Mfng Card10 Cdc42ep1 Lgals2 Gm17481 Gga1 Sh3bp1 1700027A07Rik Pdxp Lgals1 Nol12 Triobp Gcat Ankrd54 Eif3l AL589670.1 Micall1 1700088E04Rik Polr2f Sox10 Gm10863
chr19:32500001-33000000	4.78	Rpl9-ps6 Minpp1 Papss2 Atad1 Pten
chr19:46000001-46500000	4.78	9130011E15Rik 4930505N22Rik Hps6 Ldb1 Pprc1 Nolc1 Elovl3 Pitx3 Gbf1 Gm16726 Nfkb2 Psd Fbxl15 Cuedc2 Gm17393 Tmem180 Mir146b SNORA32 Actr1a Sufu
chr2:118000001-118500000	4.72	Fsip1 AL845495.1 A930104D05Rik Gpr176 1700054M17Rik 5S_rRNA Eif2ak4 Srp14 Bmf Bub1b Pak6
chr4:149000001-149500000	4.72	Clstn1 Pik3cd Tmem201 Slc25a33 Gm13068 Gm16188 Gm13073 n-R5s193 snoZ178 Spsb1 Gm13070 H6pd Gm13067 Mir34a Gpr157 Gm13093 Slc2a5
chr9:21000001-21500000	4.72	Pde4a Gm16754 Keap1 S1pr5 Atg4d Kri1 Cdkn2d Ap1m2 AC122525.1 Slc44a2 Ilf3 Gm16853 Qtrt1 Dnm2 Mir199a-1 Tmed1 AB124611 Carm1 Yipf2 1810026J23Rik Mir1946b Smarca4
chr11:46000001-46500000	4.67	Cyfip2 C030019I05Rik Itk Gm12167 Fam71b Med7 2310031A07Rik Havcr2 Gm12169 Gm12171 BC053393 Dppa1 Gm4926 Timd2
chr14:22000001-22500000	4.67	Adk 7SK U6 Myst4 Dupd1
chr9:96000001-96500000	4.61	Gk5 Tfdp2 Atp1b3 Gm17562 BC043934 Rnf7 Rasa2 n-R5s87
chr11:106000001-106500000	4.61	Map3k3 Limd2 Gm10840 Strada U1 Ccdc47 Ddx42 Ftsj3 Psmc5 U6 Smarcd2 Tcam1 Gh Cd79b Scn4a 2310007L24Rik Icam2 Ern1 Snord104 SNORA76 Tex2 snosnR60_Z15
chr16:96000001-96500000	4.61	2810404F17Rik 1600002D24Rik Gm15340 Psmg1 Brwd1 Gm15342 1700093J21Rik Gm15341 Hmgn1 Wrb Gm15317 Lca5l Sh3bgr B3galt5
chr2:118500001-119000000	4.55	Pak6 Gm1337 Plcb2 5430417L22Rik A430105I19Rik Phgr1 Disp2 D2Ertd750e Gm14091 Gm14090 Ivd Bahd1 Chst14 Gm14089 Ccdc32 Rpusd2 Casc5 Rad51 Fam82a2 Gchfr Dnajc17
chr11:119000001-119500000	4.55	Tbc1d16 Gm17433 Gm11753 Gm11752 Ccdc40 Gaa Eif4a3 Card14 Sgsh Slc26a11 Mir1932 Rnf213 A730011L01Rik Nptx1 Gm11762 Rptor

chr1:193000001-193500000	4.50	Atf3 7SK D730003I15Rik Nenf Tmem206 Ppp2r5a Dtl Ints7
chr9:61500001-62000000	4.50	Rplp1 Kif23 Paqr5 7SK Glce AC123610.1
chr10:20000001-20500000	4.50	Mtap7 4933406P04Rik Bclaf1 Fam54a Pde7b 4930403O15Rik
chr10:80000001-80500000	4.50	Atp8b3 Rexo1 Klf16 Gm17682 Fam108a Adat3 Scamp4 Csnk1g2 Btbd2 Mknk2 Gm17306 Mob3a Izumo4 Ap3d1 Dot1l Gm17151 Plekhj1 Sf3a2 Amh Jsrp1 Oaz1 Mir1982 Lingo3 Lsm7 3110056O03Rik Tmprss9 Timm13 Lmnb2 Gadd45b Gng7 Diras1 Gm16099 Slc39a3
chr4:59500001-60000000	4.44	Rod1 AL824704.1 Hsdl2 E130308A19Rik 1110054O05Rik Snx30 Gm12542 Slc46a2 Mup4 Mup6
chr6:128500001-129000000	4.44	BC048546 Klrb1a Gm5884 Clec2j Clec2h Klrb1 Klrb1c Klrb1b Gm17395 BC035044 Clec2i Clec2g Gm15987 BC064078 Klrb1f
chr11:5000001-5500000	4.44	Rhbdd3 Emid1 Kremen1 U6 Znrf3 Gm11963 Xbp1 Ccdc117 SNORA17 Ankrd36
chr16:20000001-20500000	4.44	Klhl24 Yeats2 Map6d1 Parl Cyp2ab1 Abcc5 7SK Eif2b5
chr12:16000001-16500000	4.44	AC102435.1
chr1:54500001-55000000	4.38	Pgap1 Pgap1 Ankrd44 AC151572.1
chr5:32500001-33000000	4.38	Plb1 Ppp1cb Gm15614 Yes1
chr5:115500001-116000000	4.38	Sppl3 Gm10401 Gm13826 Acads Unc119b Mlec Cabp1 Pop5 Rnf10 Coq5 Dynll1 Gm13830 Srsf9 Gatc Triap1 Cox6a1 4930401G09Rik Gm13832 Msi1 4930430O22Rik Pla2g1b Sirt4 U4 U4 Pxn Gm13840
chr11:49500001-50000000	4.38	Cnot6 AL606479.2 Gfpt2 Mapk9 AL606479.1 Rasgef1c Rnf130 Mir340 Tbc1d9b Gm12195 3010026O09Rik
chr1:40000001-40500000	4.33	Map4k4 Gm16894 Il1r2 Il1r1 Il1rl2 Il1rl1
chr6:52000001-52500000	4.33	Gm15055 Hoxa1 Gm15051 Hoxa2 Hoxa3 5730446D14Rik Hoxa3 Gm15050 2700086A05Rik 5730596B20Rik Hoxa4 Hoxa5 Hoxa6 Hoxa7 Hoxa9 RP23-329P9.11 Mir196b Hoxa10 Hoxa11 Hoxa11as Hoxa13 Gm15053 5730457N03Rik Evx1 Hibadh
chr10:5500001-6000000	4.33	Esr1 SNORD88 RNase_MRP Gm221 U1 1700052N19Rik Rmnd1 Gm16153 Zbtb2 Akap12
chr11:87500001-88000000	4.33	Rnf43 U6 1110028F11Rik Supt4h1 A430104N18Rik Mir142 Bzrap1 Mpo Gm11505 Lpo Mks1 Epx Olfr462 Olfr463 Olfr464 Gm11503 Dynll2 Gm11508 2010015M23Rik Srsf1 Gm15892 Vezf1 2210416O15Rik Cuedc1
chr15:66500001-67000000	4.33	Tg Gm17140 Sla Wisp1 Ndrg1 Gm17035 Gm2895 U7 St3gal1
chr17:73500001-74000000	4.33	Lclat1 SNORA17 Capn13 Galnt14 D630014O11Rik
chr18:65000001-65500000	4.33	Nedd4l Mir122a Alpk2 F730048M01Rik
chr4:57000001-57500000	4.27	6430704M03Rik Epb4.1l4b Gm12530 Ptpn3 Gm12536 1700042G15Rik Palm2
chr8:74500001-75000000	4.27	Zfp961 Cyp4f18 U2 Olfr372 Olfr373 Olfr374 5S_rRNA AC158898.2 Tpm4 Gm17371 Gm16091 Rab8a Hsh2d Cib3 Gm11034 Fam32a AC158898.1 Ap1m1 Gm10282 Klf2 Eps15l1 Calr3 1700030K09Rik Cherp
chr10:42500001-43000000	4.27	Sec63 RNaseP_nuc Scml4 Sobp Mir297-2 9030612E09Rik Pdss2
chr19:29000001-29500000	4.27	4430402I18Rik Ppapdc2 Cdc37l1 Gm10136 Ak3 Rcl1 Mir101b Jak2 Insl6 Rln1 5033414D02Rik Cd274 Pdcd1lg2
chr10:74500001-75000000	4.22	Rab36 Bcr Specc1l Adora2a 1110038D17Rik Upb1 7SK Snrpd3
chr11:75500001-76000000	4.22	Crk Ywhae Gm16626 Doc2b Gm12339 Rph3al Gm16075 1700016K19Rik Fam101b Vps53 Glod4 Fam57a
chr1:89500001-90000000	4.16	Inpp5d Atg16l1 SCARNA6 Scarna6 5830472F04Rik Sag Dgkd Usp40 AC087801.1 Ugt1a10 RP23-324B17.1 Ugt1a9 Ugt1a8 Ugt1a7c Ugt1a6a Ugt1a6b
chr2:119000001-119500000	4.16	Dnajc17 Gm14137 Zfyve19 Ppp1r14d Spint1 Rhov Vps18 Gm14207 Dll4 Chac1 Ino80 Exd1 1500003O03Rik 1700020I14Rik Oip5 Nusap1 n-R5s204 Ndufaf1
chr8:122000001-122500000	4.16	Slc38a8 Mbtps1 Hsdl1 Lrrc50 Taf1c Adad2 Kcng4 Wfdc1 Atp2c2 4632415K11Rik Cotl1 Klhl36 Usp10 Gm20388
chr13:42000001-42500000	4.16	Hivep1 Edn1
chr13:52500001-53000000	4.16	Diras2 Sykb Auh
chr14:73000001-73500000	4.16	Fndc3a Gm16549 Cysltr2
chr17:27500001-28000000	4.16	Grm4 Hmga1 AI413582 C130040N14Rik Nudt3 Rps10 Gm15420 Pacsin1 Spdef Gm15458 D17Wsu92e Snrpc Uhrf1bp1
chr5:122500001-123000000	4.10	Cux2 Gm15637 Myl2 Ccdc63 Ppp1cc Hvcn1 Tctn1 Pptc7 Rad9b Vps29 1500011H22Rik Gpn3 Arpc3 Anapc7 Atp2a2 U6
chr6:39000001-39500000	4.10	Tbxas1 Parp12 4930599N23Rik Jhdm1d U6 Slc37a3 Rab19 Mkrn1 Gm10244 SNORA71 AC153624.1 Dennd2a 8030453O22Rik
chr18:56500001-57000000	4.10	Gramd3 Aldh7a1 Phax 1700065I17Rik Lmnb1 March3 Gm15345
chr8:127500001-128000000	4.10	Tsnax Disc1 AL672234.1 Gm16237 Sipa1l2
chr13:113000001-113500000	4.10	Ankrd55 U2 Il6st Il31ra Ddx4 Slc38a9
chr14:65000001-65500000	4.10	Msra A930011O12Rik Mir124a-1 AC134898.1 Kif13b SNORA36 Hmbox1
chr6:145000001-145500000	4.05	Bcat1 Gm15687 Lrmp Casc1 Gm15543 Lyrm5 Kras Gm15706 7SK 2010013B24Rik Ifltd1 SNORA17 1700073E17Rik Gm15499 SNORA17
chr8:26000001-26500000	4.05	Adam32 U6 Adam9 Tm2d2 Htra4 Gm16933 Plekha2 Tacc1
chr11:98000001-98500000	4.05	Ikzf3 Fbxl20 Med1 Cdk12 AL591205.1 n-R5s73 Neurod2 Ppp1r1b 1700003D09Rik Stard3 Tcap Pnmt Pgap3 Erbb2 U6 1810046J19Rik Gm12352 Grb7 U2 Zpbp2 Ormdl3 Gm12 Gm12355 Gsdma3
chr1:156500001-157000000	3.99	Cacna1e Gm9530 Ier5 Mr1
chr5:37000001-37500000	3.99	D5Ertd579e U6 SNORA17 Cno Mrfap1 Man2b2 Ppp2r2c 4933401P06Rik Wfs1 Jakmip1 Gm17286 5S_rRNA
chr18:34000001-34500000	3.93	Epb4.1l4a U7 SNORA17 U7 Apc Srp19
chr18:65500001-66000000	3.93	Alpk2 AC102240.1 Malt1 AC102240.2 Zfp532 5330437I02Rik Sec11c
chr19:29500001-30000000	3.93	Pdcd1lg2 A930007I19Rik C030046E11Rik Ermp1 Mlana 9930021J03Rik 9930021J03Rik Ranbp6 Il33
chr6:51000001-51500000	3.88	Mir148a Gm9953 Gm17725 Nfe2l3 Hnrnpa2b1 Cbx3 Snx10
chr14:69500001-70000000	3.88	Stc1 Rps2-ps5 1700092C10Rik Nkx2-6 Nkx3-1 Slc25a37 D930020E02Rik Gm16677 Entpd4

		Gm16867
chr1:37000001-37500000	3.82	Rpl12-ps1 n-R5s210 Vwa3b Vwa3b Cnga3 Inpp4a 4930439A04Rik 6330578E17Rik Unc50 Mgat4a
chr2:22500001-23000000	3.82	Gad2 AL928693.1 1700092C17Rik Apbb1ip Pdss1 SNORA42 Abi1 Acbd5 Mastl
chr7:120500001-121000000	3.82	Btbd10 Pth Gm17646 Far1 1700006P19Rik AC103664.1 Gm5600 Spon1
chr7:134500001-135000000	3.82	Zfp747 9130019O22Rik E430018J23Rik Zfp764 Zfp688 Zfp689 B130055M24Rik Prr14 Fbrs Srcap AC122417.1 Snora30 Srcap Phkg2 Gm166 Rnf40 Zfp629 Bcl7c Mir762 Ctf1 Ctf2 Fbxl19 Orai3 Setd1a Hsd3b7 Stx1b Stx4a
chr18:68000001-68500000	3.82	Cep192 D18Ertd653e 4933403F05Rik Rnmt Mc5r
chr19:44000001-44500000	3.82	n-R5s21 Cpn1 Cyp2c44 Erlin1 Chuk Cwf19l1 SNORA12 Bloc1s2 Pkd2l1 Scd3 AC123853.1 Scd2 AC123853.2 Scd4 Scd1
chr6:48500001-49000000	3.77	Lrrc61 Rarres2 Gm5111 Repin1 Zfp775 AI854703 Gimap8 Gimap9 Gimap4 Gimap6 Gimap1 Gimap7 Gm3345 Gimap5 Gimap3 Tmem176b Tmem176a Gm7932 Abp1 1600015I10Rik SNORA17 Gm10242 Doxl2 Svs1 Gpnmb
chr7:107500001-108000000	3.77	Ppme1 C2cd3 Ucp3 Ucp2 Dnajb13 Chchd8 Mrpl48 D630004N19Rik Rab6 Plekhb1 Fam168a Gm3200 Relt
chr7:135500001-136000000	3.77	Rgs10 Gm15503 Tial1 AC130474.1 Bag3 Inpp5f Mcmbp U6 Sec23ip n-R5s158 AC136741.1
chr12:87000001-87500000	3.77	Batf n-R5s64 Mfsd7c 0610007P14Rik Ttll5 Gm17691 Tgfb3 1700019E19Rik
chr13:45000001-45500000	3.77	Jarid2 Dtnbp1 U6 Gm9817 7SK Mylip
chr16:49500001-50000000	3.77	Ift57 Gm15518 Gm16619 Cd47
chr2:29500001-30000000	3.65	Rapgef1 Gm13420 Gm11129 Trub2 Gm13547 Coq4 Slc27a4 Urm1 Mir219-2 2600006K01Rik Cercam Odf2 U6 Gle1 Spna2 Wdr34 Set Pkn3 Zdhhc12 Zer1 Tbc1d13
chr13:20000001-20500000	3.65	Elmo1
chr13:29500001-30000000	3.65	Cdkal1 AL512647.1 E2f3

trans interactions from Foxo1 viewpoint in Thymus

bin	z-score	genes in bin
chr10:28000001-28500000	10.79	Ptprk Themis
chr9:71500001-72000000	10.45	Cgnl1 Tcf12 Rpl15-ps2 U6
chr15:80500001-81000000	10.45	Fam83f Tnrc6b AC125540.1 Adsl Sgsm3 Mkl1 U4
chr17:52000001-52500000	10.29	
chr16:24000001-24500000	10.12	1110054M08Rik Lpp U7
chr1:139500001-140000000	9.95	SNORA17 A130050O07Rik Mir181a-1 Mir181b-1 5S_rRNA Ptprc
chr1:140000001-140500000	9.95	Ptprc Atp6v1g3 Nek7
chr9:72000001-72500000	9.27	Gm7866 U6 Zfp280d BC065403 Mns1 Tex9 Tex9 AC111135.1 4930509E16Rik Rfx7 U6
chr10:19000001-19500000	9.27	Olig3 Ifngr1 Il22ra2 9230106D20Rik Il20ra
chr18:81500001-82000000	8.94	
chr1:139000001-139500000	8.77	U6 SNORA17
chr9:112000001-112500000	8.77	Arpp21 Mir128-2 2310075C17Rik 2900079G21Rik SNORA17
chr17:51000001-51500000	8.43	Tbc1d5 U4
chr5:64500001-65000000	8.26	Pgm1 SNORA17 Tbc1d1
chr18:33000001-33500000	8.09	Wdr36 2310026I22Rik Camk4 U6 Stard4
chr8:35500001-36000000	7.93	Dusp4 Tnks
chr17:5000001-5500000	7.93	Arid1b 5730437N04Rik AC166064.1 Zdhhc14
chr4:6500001-7000000	7.76	SNORA17 Tox Gm11802
chr6:99000001-99500000	7.76	Foxp1 Eif4e3 AC152987.1
chr10:18500001-19000000	7.76	Gm4922 Perp Tnfaip3
chr17:5500001-6000000	7.76	Zdhhc14 Snx9 Synj2
chr13:23500001-24000000	7.59	Abt1 C230035I16Rik Btn1a1 Btn2a2 Gm11335 Hist1h4h Hist1h2af Hist1h3g Hist1h2bh Hist1h3f Hist1h4f Hist1h1d Hist1h3e Hist1h2ae Hist1h2bg Hist1h2bf Hist1h2ad Hist1h3d Gm17658 Hist1h4d Hist1h2be Gm11398 Hist1h1e U6 Hist1h2ac 5S_rRNA Hist1h2bc Hist1h1t Hist1h4c Hfe Hist1h1c Hist1h3c Hist1h2bb Hist1h2ab Hist1h3b 4930558J22Rik Hist1h4b Hist1h4a Hist1h3a Hist1h1a Trim38 Gm11337 Slc17a2 Slc17a3 Slc17a1 Slc17a4
chr7:87500001-88000000	7.42	Man2a2 Fes Furin Blm Crtc3 Gm15880 Iqgap1
chr11:5000001-5500000	7.25	Rhbdd3 Emid1 Kremen1 U6 Znrf3 Gm11963 Xbp1 Ccdc117 SNORA17 Ankrd36
chr17:51500001-52000000	7.25	Satb1
chr8:36000001-36500000	7.08	Tnks Ppp1r3b
chr13:28500001-29000000	7.08	2610307P16Rik
chr13:44000001-44500000	7.08	Gm5083
chr16:93000001-93500000	7.08	Mir802
chr5:65000001-65500000	6.91	AC122043.1 Klf3 Tlr1 Tlr6 Fam114a1 Mir574 Tmem156 Klhl5
chr12:70500001-71000000	6.75	AC153658.1 Mettl21d Sos2 U6 L2hgdh Atp5s Cdkl1 Mir681 4930512B01Rik Map4k5 4931403G20Rik Atl1
chr15:80000001-80500000	6.75	Mgat3 Smcr7l Atf4 Rps19bp1 Cacna1i Enthd1 SNORA17 Grap2
chr10:20500001-21000000	6.75	Ahi1 Myb Gm16786 AC153556.1
chr12:117000001-117500000	6.58	Ighv1-73 Ighv8-14 Ighv1-83 Ighv1-84 Ighv1-85 Zfp386 Gm17626 Vipr2 U6 Wdr60
chr18:35500001-36000000	6.58	Sil1 Gm5239 Snhg4 SNORA74 Snora74a Matr3 Paip2 Slc23a1 2010001M09Rik Gm1614 Spata24 Dnajc18 1700066B19Rik Ecscr Tmem173 Gm16490 Ube2d2 Cxxc5
chr18:39500001-40000000	6.58	Arhgap26 Gm15337 Nr3c1 Gm10008 Pabpc2
chr19:32000001-32500000	6.58	A1cf Asah2 Sgms1 2700046G09Rik
chr11:86000001-86500000	6.58	Brip1 4632419I22Rik Ints2 Med13 U3 Y_RNA 5S_rRNA U6 Rnft1 Rps6kb1 Tubd1 Vmp1 Mir21 Ptrh2
chr13:91500001-92000000	6.41	A830009L08Rik Ssbp2 4833422C13Rik SNORA17 Acot12 7SK Zcchc9 Ckmt2
chr18:5000001-5500000	6.41	Svil Gm16954 Zfp438 Gm10125
chr2:9500001-10000000	6.24	Gm13218 Gata3 Gm13256 4930412O13Rik 9230102O04Rik Gm13262 Taf3 Atp5c1 SNORA17

chr9:94500001-95000000	6.24	U6 Slc9a9 Gm16262
chr13:37500001-38000000	6.24	Ly86 Rreb1
chr16:32000001-32500000	6.24	Senp5 Pak2 SNORA17 Pigx 1500031L02Rik Gm15729 Lrrc33 Bex6 Fbxo45 SNORA79 Wdr53 Mir1946a 2310010M20Rik Rnf168 AC087556.1 Ubxn7 Tm4sf19 Tctex1d2 Pcyt1a Osta Zdhhc19
chr10:122000001-122500000	6.07	Ppm1h Mirlet7i Mon2
chr12:86500001-87000000	6.07	Pgf Eif2b2 Mlh3 Acyp1 Fam164c Nek9 Tmed10 Fos Jdp2
chr12:115500001-116000000	6.07	Ighv3-8 Ighv12-3 Ighv1-5 Ighv10-3 Ighv1-7 Ighv15-2 Ighv1-9 Ighv1-12 Gm17686 Gm16857 Gm16858 Ighv1-18 Ighv1-19 Ighv1-20 Gm16860
chr15:59000001-59500000	6.07	Gm5045 Sqle E430025E21Rik Nsmce2 Trib1
chr1:39000001-39500000	5.90	Nms Pdcl3 Npas2 Rpl31 Tbc1d8
chr2:18500001-19000000	5.90	Commd3 Bmi1 Gm13334 BC061194 RP23-396N6.7 Pip4k2a 4930426L09Rik
chr4:7000001-7500000	5.90	8430436N08Rik
chr6:134500001-135000000	5.90	Lrp6 Mansc1 Loh12cr1 Dusp16 Crebl2 Gpr19 Cdkn1b Apold1 Ddx47
chr12:108500001-109000000	5.90	3110018I06Rik 4930465M20Rik Gm15208
chr12:114000001-114500000	5.90	Pld4 Ahnak2 BC022687 Cdca4 Gpr132 Gm17723 Jag2 Nudt14 Gm17274 Brf1 Btbd6 Pacs2 Tex22 Mta1 Crip2 Crip1 4930427A07Rik Tmem121 U6
chr13:112500001-113000000	5.90	Mier3 Gm15287 Map3k1 Gm15327 Gm15325 Gm15324 Gm15326 Gm15322 Gm15323
chr14:26000001-26500000	5.90	Gm17716 D930049A15Rik Zmiz1 AC154455.1 Gm17670 Gm10397
chr16:92500001-93000000	5.90	Clic6 Runx1 Gm16801
chr1:60500001-61000000	5.73	Abi2 Raph1 AL683804.1 Cd28 Gm11579 2310016D23Rik Ctla4
chr1:182000001-182500000	5.73	Cdc42bpa Adck3 Psen2 Gm5069 Itpkb 6330403A02Rik Parp1
chr4:59000001-59500000	5.73	Dnajc25 Gm20503 Gng10 AI481877 Gm12594 Ugcg Gm12596 Susd1 Rod1
chr5:136500001-137000000	5.73	Dtx2 Upk3b 2310043J07Rik Rasa4 U12 Gm15701 Polr2j Lrwd1 Alkbh4 Orai2 Prkrip1 Sh2b2 Cux1 Gm16599
chr11:117500001-118000000	5.73	Tnrc6c Tmc6 Tmc8 Gm11723 Gm11724 6030468B19Rik Syngr2 Afmid Tk1 Birc5 Cldn27 Tha1 Gm11725 Socs3 Pgs1 Dnahc17 Gm11738 Cyth1
chr1:38000001-38500000	5.56	Gm15457 Lyg1 7SK Txndc9 Eif5b Rev1 Aff3 Gm16150 Gm16151 Gm16152
chr1:158000001-158500000	5.56	Fam163a Tdrd5 Nphs2 9430070O13Rik Gm2000 Soat1 Abl2
chr9:107500001-108000000	5.56	Sema3b Gnai2 Slc38a3 Gnat1 Sema3f Rbm5 Rbm6 Mon1a U6 Mst1r 4921517D21Rik Camkv Traip Uba7 6230427J02Rik SNORA61 Cdhr4 Cdhr4 Ip6k1 Gmppb Rnf123 RP24-484G16.7 Amigo3 Mst1 Apeh Bsn
chr11:96500001-97000000	5.56	Skap1 2010300F17Rik Gm11537 Snx11 Cbx1 Nfe2l1 Copz2 Mir152 Gm11523 Cdk5rap3 D030028A08Rik Gm11525 Prr15l Pnpo Sp2 Sp6 Gm11532 Scrn2 Lrrc46 Mrpl10 Gm11574 Osbpl7 Tbx21 Tbkbp1
chr12:3500001-4000000	5.56	Asxl2 Dtnb CR974568.1 Gm20448 Dnmt3a Gm10485 AC159324.1 Pomc Efr3b
chr12:100500001-101000000	5.56	Foxn3 3300002A11Rik Gm16956 2610021K21Rik
chr14:16500001-17000000	5.56	
chr14:54000001-54500000	5.56	Gm13952 Gm13953 Trav6-3 Gm13946 Gm13945 Trav7-4 Gm13950 Gm13947 Trav6-5 Trav10 Gm16981 Gm10908 Gm17011 Gm16980 Gm5770 Gm16591 Gm16979 Gm17002 Tcra-V8 Gm14498 Trav13-2 Trav14-2 Trav15-2-dv6-2 Trav3-3 Trav9-4 Gm13908 Trav5-4 Gm13909 Trav7-6 Gm14031 Gm13896 Gm13934 Gm13933 Trav3-4 B230359F08Rik Trav17 Trav18 Gm13893 Gm14030 Gm13892
chr14:55000001-55500000	5.56	Slc7a7 Mrpl52 Mmp14 Gm11067 U6 Lrp10 Rem2 Prmt5 Haus4 Jub U6 4931414P19Rik Psmb5 Mir686 Psmb11 Cdh24 CT009512.1 Gm17606 Acin1 4930579G18Rik 1700123O20Rik Cebpe Slc7a8 Gm10332 Homez Ppp1r3e
chr15:81000001-81500000	5.56	Mkl1 4930483J18Rik Mchr1 Slc25a17 St13 Xpnpep3 Dnajb7 Gm17025 Rbx1 Gm5218 Ep300 AC160528.1 U6 L3mbtl2
chr17:84500001-85000000	5.56	Zfp36l2 Thada U6 U6 Plekhh2
chr18:68000001-68500000	5.56	Cep192 D18Ertd653e 4933403F05Rik Rnmt Mc5r
chr19:33000001-33500000	5.56	7SK Rnls Gm7237
chr19:46500001-47000000	5.56	Sufu Trim8 Arl3 Sfxn2 D19Wsu162e Cyp17a1 2010012O05Rik As3mt Cnnm2 Nt5c2
chr1:38500001-39000000	5.40	Aff3 Lonrf2 Chst10 Nms
chr1:167500001-168000000	5.40	Adcy10 SNORA18 Mpzl1 Rcsd1 Creg1 Gm16565 5S_rRNA Cd247 U6 Pou2f1 Gm17444
chr5:66000001-66500000	5.40	Pds5a U6 1700022K14Rik N4bp2 SNORA73 Rhoh Chrna9 9130230L23Rik AC115293.1 Rbm47
chr8:125000001-125500000	5.40	Gm20388 Ctu2 Fam38a U6 Cdt1 Aprt Galns Trappc2l Pabpn1l Cbfa2t3 Gm10612 Acsf3 Gm16378 Cdh15 Ankrd11
chr11:59500001-60000000	5.40	Mprip 1700007J10Rik Gm12264 Pld6 Flcn Gm16062 5S_rRNA Cops3 Nt5m Gm12714 1810063I02Rik 1700013G23Rik Med9 Rasd1 Pemt Rai1 4930412M03Rik
chr12:25500001-26000000	5.40	Mboat2 Kidins220 Id2
chr13:49000001-49500000	5.40	Fam120a C030044B11Rik Wnk2 Ninj1 1110007C09Rik Susd3 Fgd3 Bicd2
chr13:113000001-113500000	5.40	Ankrd55 U2 Il6st Il31ra Ddx4 Slc38a9
chr14:54500001-55000000	5.40	Trdv1 Trdv2-1 Gm17015 Trdv4 Trdd1 7SK Trdd2 Trdj1 Trdj2 Trdv5 Gm17363 Gm17534 Traj59 Traj58 Gm16768 Gm16769 Gm17471 Gm17479 Gm16772 Gm16773 Gm16924 Gm17007 Gm17012 Gm16923 Gm16928 Gm16927 Gm16926 Gm16925 Gm16922 Gm16921 Gm16668 Gm16669 Gm16670 Gm16671 Gm17610 Gm16664 Gm16665 Gm16666 Gm16667 Gm17008 Gm16672 Gm16819 Gm16820 Gm16817 Gm16818 Gm16823 Gm16824 Gm16821 Gm16822 Gm16815 Gm16816 Gm16655 Gm17009 Gm17010 Gm16656 Gm16658 Gm16657 Gm16660 Gm16659 Gm16654 Gm16653 Gm16918 Gm16919 Gm16920 Traj5 Gm16915 Gm16916 Traj2 Traj1 Trac Dad1 Abhd4 Olfr49 Oxa1l Slc7a7
chr15:36500001-37000000	5.40	Pabpc1 Ywhaz AC138604.1 Gm10384 Zfp706 Gm16631
chr16:10500001-11000000	5.40	Ciita Dexi Clec16a Gm15558 Socs1 Tnp2 Prm3 Prm2 Prm1 Gm10343 Gm11172 Gm17410 A630055G03Rik Litaf AC164093.1 U1
chr17:87000001-87500000	5.40	Prkce U6 Epas1 1700090G07Rik Atp6v1e2 Rhoq Pigf Cript SNORA40
chr19:32500001-33000000	5.40	Rpl9-ps6 Minpp1 Papss2 Atad1 Pten

chr4:7500001-8000000	5.06	8430436N08Rik Gm11795 SNORA17
chr4:133000001-133500000	5.06	Gm13257 Fam46b Trnp1 1810019J16Rik Gm17688 Nudc Nr0b2 Gpatch3 Gpn2 Sfn Zdhhc18 BX537327.1 Pigv Arid1a U4 Gm12974 Rps6ka1 Gm17623 Gm12977 U6
chr5:137000001-137500000	5.06	Cux1 4731417B20Rik Myl10 Emid2 RP24-498F17.1 Rabl5 4933404O12Rik Fis1 Cldn15 Znhit1 Plod3 Mir702
chr8:35000001-35500000	5.06	Rbpms AC123616.1 Gm9951 Dctn6 Gm17702 Mboat4 Leprotl1 Tmem66 AC134443.1 Gm4889
chr13:43500001-44000000	5.06	Ranbp9 U6 Ccdc90a Rnf182 Cd83 U6
chr18:6000001-6500000	5.06	Arhgap12 Kif5b Gm17036 Rpl27-ps3 Epc1 Mir1893
chr18:81000001-81500000	5.06	Atp9b AC117949.1 Sall3 U6
chr4:132500001-133000000	4.89	Fgr Ahdc1 Gm10151 Wasf2 7SK Gpr3 Cd164l2 Map3k6 Sytl1 Tmem222 Wdtc1 Slc9a1 AL671882.1
chr17:29000001-29500000	4.89	Pnpla1 4930539E08Rik 1700030A11Rik Gm16191 Pxt1 Kctd20 Stk38 U2 Gm16196 Gm16195 Srsf3 Gm16197 Cdkn1a Gm16194 Rab44 Cpne5 Ppil1 BC004004 Pi16 Mtch1 Fgd2
chr2:11000001-11500000	4.89	U4 Prkcq Gm13293 Gm13291 Pfkfb3
chr6:119500001-120000000	4.89	Erc1 3110021A11Rik 4930540M05Rik Rad52 Wnk1 Mir706 Mir706
chr9:66000001-66500000	4.89	Dapk2 Herc1 U6 Fbxl22 Usp3 Gm15563
chr10:19500001-20000000	4.89	U6 Slc35d3 Pex7 Map3k5 Mtap7
chr10:39500001-40000000	4.89	Rev3l Gm17645 4930547M16Rik 2010001E11Rik G630090E17Rik BC021785 AI317395 Gm8055 Slc16a10 SNORA17 Rpf2 Gtf3c6 U3
chr11:67500001-68000000	4.89	Gas7 Glp2r Rcvrn Gm12302 Dhrs7c Usp43 9130017K11Rik Wdr16 Stx8 5S_rRNA
chr11:86500001-87000000	4.89	Ptrh2 Cltc Dhx40 AL596111.1 Ypel2 SCARNA3 Gdpd1 Gm11479 1200011M11Rik Prr11 Fam33a Mir301 Gm11491 Trim37
chr11:96000001-96500000	4.89	Ttll6 Gm11535 Hoxb13 Gm11538 Gm53 Mir196a-1 Mir196a-1 Hoxb9 Hoxb8 Hoxb7 0610040B09Rik Hoxb6 Hoxb5 Hoxb4 Mir10a Mir10a Hoxb3 Gm11536 Hoxb3os Hoxb2 Hoxb1 Gm11529 Skap1
chr17:50500001-51000000	4.89	Plcl2 Gm7334 Tbc1d5
chr18:36000001-36500000	4.89	Cxxc5 AC141471.1 Psd2 Nrg2 Pura
chr18:61000001-61500000	4.89	Tcof1 Arsi Camk2a Slc6a7 Cdx1 Pdgfrb Csf1r Hmgxb3 U6 Slc26a2 Pde6a Ppargc1b
chr19:45500001-46000000	4.89	Btrc Gm6807 Poll Dpcd Fbxw4 Gm17018 Fgf8 Npm3 Gm15491 Mgea5 Kcnip2 9130011E15Rik
chr1:39500001-40000000	4.72	Tbc1d8 U3 D1Bwg0212e Gm15832 Snord89 Rnf149 SNORA33 Creg2 D930019O06Rik Rfx8 Gm3646 Map4k4
chr1:43500001-44000000	4.72	Nck2 1500015O10Rik Uxs1 SNORA17 AC125134.1 Tpp2
chr4:32000001-32500000	4.72	Map3k7 U4 Bach2 D130062J21Rik Gm11932
chr9:32500001-33000000	4.72	Ets1
chr9:44000001-44500000	4.72	Cbl Ccdc153 Pdzd3 Nlrx1 Abcg4 Hinfp C2cd2l Dpagt1 H2afx Hmbs Vps11 7SK Hyou1 SNORA40 Slc37a4 Trappc4 Rps25 Ccdc84 Foxr1 Upk2 Gm9830 U6 C030014I23Rik Bcl9l Cxcr5 Ddx6 Treh Phldb1
chr9:116000001-116500000	4.72	Tgfbr2 AC131777.1 Rbms3
chr10:18000001-18500000	4.72	Nhsl1 Hebp2 D10Bwg1379e Gm4922
chr10:41000001-41500000	4.72	Fig4 Akd1 U6 Zbtb24 Mical1 Smpd2 Ppil6 Cd164 Ccdc162 Gm17196 5730435O14Rik AC161426.1 Cep57l1
chr11:3000001-3500000	4.72	Pisd-ps1 Sfi1 Gm11399 Drg1 Gm12735 Eif4enif1 Patz1 Gm12592 Gm11944 Pik3ip1 Limk2 Gm11948 Rnf185 8430429K09Rik U8 Pla2g3 Inpp5j Selm Smtn Gm11946 Gm11947
chr11:31500001-32000000	4.72	Bod1 D630024D03Rik Gm12107 Cpeb4 4930524B15Rik Nsg2 Gm12108
chr12:83000001-83500000	4.72	Pcnx n-R5s62 Sipa1l1
chr12:101500001-102000000	4.72	Ttc7b Rps6ka5
chr12:108000001-108500000	4.72	1700013N06Rik Gm16087 Gm16086 Gm16085 Gm16084 Gm2800
chr16:4500001-5000000	4.72	Srl Tcfap4 Glis2 Pam16 Coro7 Vasn Dnaja3 Nmral1 Hmox2 Gm15859 AC166903.1 5730403B10Rik Gm15835 4930562C15Rik Fam100a Mgrn1 Gm16861 Nudt16l1 Anks3 4930451G09Rik Sept12
chr16:95500001-96000000	4.72	Kcnj15 Erg Ets2
chr18:5500001-6000000	4.72	Gm10125 Zeb1 AC127028.1
chr19:3500001-4000000	4.72	Ppp6r3 Lrp5 AC132452.1 1810055G02Rik Suv420h1 Gm16066 AC133523.1 Chka Tcirg1 Ndufs8 Aldh3b1 Unc93b1 1700055N04Rik Aldh3b2 Acy3 Tbx10
chr19:55500001-56000000	4.72	Vti1a 4930552P12Rik Tcf7l2
chr1:37500001-38000000	4.55	Mgat4a 2010300C02Rik 4930556I23Rik Tsga10 Gm17715 Lipt1 Mitd1 Mrpl30 Lyg2 Gm15457
chr1:173500001-174000000	4.55	Cd244 Ly9 Slamf7 Cd48 U6 U6 Slamf1 Cd84 Gm10521 Slamf6 Vangl2 Nhlh1 Ncstn
chr4:32500001-33000000	4.55	Bach2 7SK BC024582 Gja10 Casp8ap2 Mdn1 Lyrm2 Ankrd6
chr5:107500001-108000000	4.55	Tgfbr3 U6 Brdt n-R5s173 Ephx4 Gm17202 Lpcat2b Btbd8 A830010M20Rik 1700028K03Rik Glmn
chr6:33500001-34000000	4.55	Exoc4 Gm13853 Lrguk
chr9:61000001-61500000	4.55	Gm10655 Tle3
chr14:16000001-16500000	4.55	Lrrc3b Gm17628
chr18:34500001-35000000	4.55	Reep5 Pkd2l2 Fam13b n-R5s24 Wnt8a Nme5 4933408B17Rik Brd8 Kif20a Cdc23 n-R5s25 Gfra3 Cdc25c Gm3550 2010110K18Rik Fam53c Kdm3b Gm17557
chr1:36500001-37000000	4.38	Lman2l Cnnm4 Cnnm3 Ankrd23 Ankrd39 Sema4c D430040D24Rik Fam178b AC084389.1 Cox5b Actr1b Zap70 Tmem131
chr6:8000001-8500000	4.38	Col28a1 Mios Rpa3 Gm16039 Gm16055 Gm16043 7SK 2810488G03Rik SNORA65 Glcci1
chr6:33000001-33500000	4.38	Chchd3 U6 Exoc4
chr8:108500001-109000000	4.38	Dpep3 Dpep2 SNORA75 Dus2l Ddx28 Nfatc3 Esrp2 1810019D21Rik AC133195.1 Pla2g15 Slc7a6 Slc7a6os Prmt7 Gm17245 Smpd3 Gm10629 Zfp90
chr15:58500001-59000000	4.38	Fer1l6 Tmem65 U1 Gm5959 Trmt12 Rnf139 Tatdn1 Ndufb9 Mtss1
chr15:74500001-75000000	4.38	Arc Jrk 4933427E11Rik Psca Lypd2 4930572J05Rik Slurp1 2300005B03Rik Lynx1 Ly6d Gm17189 Ly6k Gml Hemt1 Cyp11b1 Cyp11b2 2010109I03Rik Ly6e Ly6i Ly6a Ly6c1 Ly6c2 Ly6g
chr2:5500001-6000000	4.22	Camk1d Cdc123 Nudt5 Gm13199 Sec61a2 Gm13267 Dhtkd1 Upf2

chr6:52500001-53000000	4.22	Hibadh SNORA32 Tax1bp1 Jazf1 SCARNA20
chr7:135000001-135500000	4.22	AC149222.1 Zfp668 Zfp646 Prss53 Vkorc1 Bckdk Myst1 Prss8 Prss36 Fus Gm17468 B230325K18Rik Pycard Gm15533 Trim72 U1 Itgam Itgax Itgad Cox6a2 9130023H24Rik Armc5 Tgfb1i1 Slc5a2 BC017158 AC124566.1
chr12:101000001-101500000	4.22	2610021K21Rik Tdp1 Kcnk13 AC159243.1 Psmc1 BC002230 Gm10433 Calm1 Gm17302
chr15:96000001-96500000	4.22	2610037D02Rik 4833422M21Rik Arid2 Scaf11 Slc38a1
chr19:5000001-5500000	4.22	Slc29a2 B3gnt1 Brms1 Rin1 Cd248 Tmem151a Yif1a Cnih2 Rab1b Klc2 Pacs1 Sf3b2 Gal3st3 Catsper1 Cst6 Banf1 Eif1ad Sart1 Tsga10ip 4930481A15Rik Drap1 AI837181 SNORD86 Fosl1 Ccdc85b Fibp Ctsw Efemp2 Mus81 Cfl1 Snx32
chrX:156000001-156500000	4.22	A830080D01Rik Sh3kbp1 Map3k15
chr8:129000001-129500000	4.22	AC118255.1 Gm16983 Irf2bp2 Tomm20 SNORA14 Rbm34
chr11:75500001-76000000	4.22	Crk Ywhae Gm16626 Doc2b Gm12339 Rph3al Gm16075 1700016K19Rik Fam101b Vps53 Glod4 Fam57a
chr16:4000001-4500000	4.22	Slx4 Gm15879 Dnase1 Trap1 AC132380.1 Crebbp Gm5766 AC132575.1 Adcy9 Srl
chr17:30000001-30500000	4.22	Mdga1 Gm16758 SNORA70 Zfand3 Btbd9 U6
chr2:30500001-31000000	4.05	9330198N18Rik Gm14486 Gm14488 AL928593.1 1700001O22Rik 4930527E20Rik Mettl11a Asb6 Prrx2 Ptges Tor1b Tor1a BC005624 Usp20 Fnbp1
chr4:8500001-9000000	4.05	Rab2a Chd7
chr4:11000001-11500000	4.05	2310030N02Rik Gm11827 Trp53inp1 Ccne2 Ints8 Dpy19l4 U1 Gm16652 Esrp1 Gm17283 1110037F02Rik Gm11831 Rad54b
chr4:133500001-134000000	4.05	Hmgn2 Dhdds Lin28a Gm13061 Gm13060 Aim1l Cd52 Ubxn11 Sh3bgrl3 Ccdc21 Gm17345 Gm7534 Catsper4 Cnksr1 Zfp593 E130218I03Rik Grrp1 Pdik1l Trim63 Slc30a2 Extl1 Pafah2
chr8:23500001-24000000	4.05	Slc25a15 Mrps31 AI316807 Slc20a2 Gm17491 Vdac3 Dkk4 Polb Gm17362 Ikbkb Gm15346 Plat Ap3m2 1700041G16Rik U6 Myst3
chr11:106000001-106500000	4.05	Map3k3 Limd2 Gm10840 Strada U1 Ccdc47 Ddx42 Ftsj3 Psmc5 U6 Smarcd2 Tcam1 Gh Cd79b Scn4a 2310007L24Rik Icam2 Ern1 Snord104 SNORA76 Tex2 snosnR60_Z15
chr12:35500001-36000000	4.05	4921508M14Rik SNORA17 Prps1l1 7SK Snx13 Mir680-3
chr13:44500001-45000000	4.05	Jarid2 SNORA61
chr15:36000001-36500000	4.05	Rgs22 Fbxo43 U1 Polr2k Spag1 U6 Rnf19a Rpl7a-ps3 Ankrd46 Snx31
chr2:71500001-72000000	3.88	Gm1631 Gm13647 Itga6 Gm13663 Gm17250 Gm13662 Pdk1 Gm13746 Rapgef4 SNORA17 Gm13634
chr5:108000001-108500000	3.88	A830010M20Rik Glmn Rpap2 A930041C12Rik Gm17717 Gfi1 A430072P03Rik Evi5 1700013N18Rik Rpl5 Snord21 SNORA66 SNORA66 Fam69a Mtf2
chr5:122500001-123000000	3.88	Cux2 Gm15637 Myl2 Ccdc63 Ppp1cc Hvcn1 Tctn1 Pptc7 Rad9b Vps29 1500011H22Rik Gpn3 Arpc3 Anapc7 Atp2a2 U6
chr14:21500001-22000000	3.88	Sec24c 6230400D17Rik Fut11 AC121599.1 Chchd1 2310021P13Rik Ndst2 Camk2g Plau Vcl Ap3m1 Adk
chr16:24500001-25000000	3.88	Lpp Mir28 SNORA17
chr1:36000001-36500000	3.71	Hs6st1 Uggt1 Neurl3 Arid5a 4632411B12Rik Fer1l5 Lman2l
chr10:127500001-128000000	3.71	Ptges3 Baz2a Atp5b SNORD59 AC131120.1 Rbms2 Gls2 Spryd4 Mip Gm17292 Timeless Apon Apof Stat2 Il23a U6 Pan2 Cnpy2 AC090489.2 Cs U8 Coq10a Ankrd52 AC090489.1 Gm17201 Slc39a5 Obfc2b Rnf41 SCARNA11 Smarcc2 Myl6 Myl6b A430046D13Rik Esyt1 Zc3h10 Pa2g4
chr12:56000001-56500000	3.71	Baz1a Gm20403 U6 2700097O09Rik Srp54b Srp54a Fam177a 1700047I17Rik2 Srp54c Ppp2r3c 1110008L16Rik Psma6
chr12:109000001-109500000	3.71	Gm15208 Bcl11b Setd3 Ccnk Ccdc85c

trans interactions from Il7r viewpoint in Rag-/- pro-B

bin	z-score	genes in bin
chr11:22500001-23000000	13.49	Gm17335 Gm12052 Gm12055 Gm12056 Commd1 B3gnt2 RP23-242C19.6 SNORA63 RP23-242C19.5 U6 Zrsr1 Cct4 Fam161a 5S_rRNA Gm12059
chr11:24000001-24500000	12.70	Bcl11a Gm12064 4930538E20Rik Gm12065 Gm12066 Gm12068 4933430M04Rik U6
chr8:10500001-11000000	12.14	Myo16 3930402G23Rik Irs2
chr10:20500001-21000000	11.69	Ahi1 Myb Gm16786 AC153556.1
chr10:6000001-6500000	11.47	Akap12 U8 Mthfd1l U1 Plekhg1 5S_rRNA
chr4:44500001-45000000	10.57	Gm19980 Pax5 AL772319.1 Gm12462 Zcchc7 AL805896.1 Gm12678 Gm12493 Gm12679 Grhpr
chr13:23500001-24000000	10.23	Abt1 C230035I16Rik Btn1a1 Btn2a2 Gm11335 Hist1h4h Hist1h2af Hist1h3g Hist1h2bh Hist1h3f Hist1h4f Hist1h1d Hist1h3e Hist1h2ae Hist1h2bg Hist1h2bf Hist1h2ad Hist1h3d Gm17658 Hist1h4d Hist1h2be Gm11398 Hist1h1e U6 Hist1h2ac 5S_rRNA Hist1h2bc Hist1h1t Hist1h4c Hfe Hist1h1c Hist1h3c Hist1h2bb Hist1h2ab Hist1h3b 4930558J22Rik Hist1h4b Hist1h4a Hist1h3a Hist1h1a Trim38 Gm11337 Slc17a2 Slc17a3 Slc17a1 Slc17a4
chr17:5000001-5500000	9.78	Arid1b 5730437N04Rik AC166064.1 Zdhhc14
chr16:19000001-19500000	9.44	Gm10088 Iglc3 Iglv1 Iglc2 Iglv3 Iglv2 Olfr164 SNORA17 AC112681.1 Olfr165 SNORA17 Olfr166
chr5:3000001-3500000	9.33	Cdk6 Gm17590
chr10:5500001-6000000	9.33	Esr1 SNORD88 RNase_MRP Gm221 U1 1700052N19Rik Rmnd1 Gm16153 Zbtb2 Akap12
chr9:7000001-7500000	8.99	Dync2h1 Dcun1d5 Mmp13 Mmp12 Mmp1b Mmp3 Mmp1a
chr11:44500001-45000000	8.88	Ebf1 Gm12159 Gm12160
chr3:52000001-52500000	8.54	Foxo1 RP24-337A16.1 Gm10293
chr4:8500001-9000000	8.54	Rab2a Chd7
chr17:4500001-5000000	8.54	U6 Arid1b
chr11:11500001-12000000	8.32	4930512M02Rik Gm11999 Ikzf1 Gm12000 Fignl1 Ddc 1700042O10Rik SCARNA4 Grb10 U1
chr19:33000001-33500000	8.32	7SK Rnls Gm7237
chr19:32000001-32500000	8.21	A1cf Asah2 Sgms1 2700046G09Rik
chr9:13500001-14000000	7.98	Maml2 Mtmr2 Cep57 Fam76b
chr3:21500001-22000000	7.87	Tbl1xr1
chr19:29000001-29500000	7.76	4430402I18Rik Ppapdc2 Cdc37l1 Gm10136 Ak3 Rcl1 Mir101b Jak2 Insl6 Rln1 5033414D02Rik

		Cd274 Pdcd1lg2
chr10:13500001-14000000	7.64	Aig1 U6 Hivep2 Gm8330 SNORA17
chr5:3500001-4000000	7.53	Cdk6 Fam133b n-R5s169 1700109H08Rik C030048B08Rik Pex1 Gatad1 AC090443.1 4930511M11Rik Ankib1 AC022236.1 Krit1 4932412H11Rik Mterf Akap9
chr14:15000001-15500000	7.42	Olfr720 Olfr31 Il3ra Olfr721-ps1
chr16:4000001-4500000	7.19	Slx4 Gm15879 Dnase1 Trap1 AC132380.1 Crebbp Gm5766 AC132575.1 Adcy9 Srl
chr4:11500001-12000000	6.86	Rad54b Rad54b Gm11832 Gem Cdh17 7SK AL772167.1 Pdp1 1700123M08Rik Gm10604 Gm17454 Gm11840 Gm11842 Tmem67
chr17:4000001-4500000	6.86	
chr3:9500001-10000000	6.75	Zfp704 Pag1 Gm16337 5S_rRNA
chr16:4500001-5000000	6.75	Srl Tcfap4 Glis2 Pam16 Coro7 Vasn Dnaja3 Nmral1 Hmox2 Gm15859 AC166903.1 5730403B10Rik Gm15835 4930562C15Rik Fam100a Mgrn1 Gm16861 Nudt16l1 Anks3 4930451G09Rik Sept12
chr18:55000001-55500000	6.75	Zfp608 Gm17270 Gm4221 SNORA40 U6
chr11:4000001-4500000	6.63	Sec14l2 Rnf215 AL807825.1 Ccdc157 Sf3a1 Tbc1d10a Gatsl3 Osm Lif Gm11959 Gm11958 U6 Hormad2 Mtmr3
chr10:16000001-16500000	6.52	
chr13:20000001-20500000	6.52	Elmo1
chr19:3500001-4000000	6.52	Ppp6r3 Lrp5 AC132452.1 1810055G02Rik Suv420h1 Gm16066 AC133523.1 Chka Tcirg1 Ndufs8 Aldh3b1 Unc93b1 1700055N04Rik Aldh3b2 Acy3 Tbx10
chr19:11500001-12000000	6.52	Ms4a4c Ms4a4b Ms4a6c Gm8369 Ms4a6b Ms4a4d Gm10212 Ms4a6d SNORA17 Ms4a2 Ms4a3 Plac1l Oosp1 SCARNA17 SCARNA18 Gm97 Gif Mrpl16 Stx3 Olfr1417 Olfr1418 Olfr1419 Olfr1420 Patl1
chr2:11000001-11500000	6.30	U4 Prkcq Gm13293 Gm13291 Pfkfb3
chr14:16500001-17000000	6.30	
chr11:5000001-5500000	6.18	Rhbdd3 Emid1 Kremen1 U6 Znrf3 Gm11963 Xbp1 Ccdc117 SNORA17 Ankrd36
chr11:8500001-9000000	6.07	Tns3 Pkd1l1 Hus1 Sun3 Gm11992
chr10:19000001-19500000	5.96	Olig3 Ifngr1 Il22ra2 9230106D20Rik Il20ra
chr14:18500001-19000000	5.96	Thrb 7SK
chr19:21000001-21500000	5.85	Tmc1 Zfand5 Gda
chr9:14000001-14500000	5.73	Sesn3 Endod1 Kdm4d Cwc15 Amotl1
chr9:22500001-23000000	5.62	Bbs9
chr12:36500001-37000000	5.62	Agr3 Agr2 Tspan13 Gm5434 Bzw2 Ankmy2 1700108M19Rik
chr4:10500001-11000000	5.51	1700123O12Rik AL672160.1 2610301B20Rik Plekhf2 2310030N02Rik
chr10:7500001-8000000	5.51	BC013529 B430219N15Rik 6530403G13Rik Ppil4 Zc3h12d AC159137.1 SNORA40 Tab2 Ust
chr11:6000001-6500000	5.51	Nudcd3 Npc1l1 Ddx56 Tmed4 n-R5s67 Ogdh Zmiz2 Ppia H2afv Purb AL646020.1 Purb Gm11973 Myo1g Gm11974 SNORA9 SNORA70 Ccm2 Nacad
chr11:26000001-26500000	5.51	5730522E02Rik 5730522E02Rik U1 Fancl Vrk2 Gm6899
chr19:58000001-58500000	5.51	Atrnl1 Gm16277 Gfra1
chr4:3500001-4000000	5.40	Tmem68 Tgs1 SNORA18 2210414B05Rik Lyn Gm17726 SNORA17 Rps20 snoU54 SNORA17 Mos Plag1 Chchd7 Gm11808 Sdr16c5 Sdr16c6
chr19:27000001-27500000	5.28	Vldlr Kcnv2 D19Bwg1357e
chr17:21500001-22000000	5.06	Zfp677 Zfp54 Zfp51 Gm17372 Zfp53 9330136K24Rik Zfp52 Zfp948 3110052M02Rik Gm10509 Gm10226 Zfp760 Zfp229 Zfp820
chr1:13000001-13500000	4.95	Prdm14 Ncoa2 U6
chr2:3000001-3500000	4.95	Fam171a1 Nmt2 U4 Rpp38 Acbd7 Olah Meig1 Dclre1c Suv39h2 Gm13184 Hspa14 Hspa14 Cdnf
chr12:114500001-115000000	4.95	Ighg2c Ighg Ighg1 Ighm Adam6b Adam6a Ighv2-4
chr10:21500001-22000000	4.61	Gm6846 SNORD23 Sgk1 4930444G20Rik E030030I06Rik H60b Raet1c
chr19:23500001-24000000	4.50	Mamdc2 1700028P14Rik Gm9493 SNORA17 Ptar1 Gm9938 Apba1
chr3:10000001-10500000	4.38	Fabp5 Gm9833 Pmp2 Fabp9 Fabp4 Fabp12 Impa1 Slc10a5 Zfand1 Chmp4c Snx16
chr14:15500001-16000000	4.38	Slc4a7 Nek10

trans interactions from Il7r viewpoint in Rag/81X pre-B

bin	z-score	genes in bin
chr16:19000001-19500000	17.03	Gm10088 Iglc3 Iglv1 Iglc2 Iglv3 Iglv2 Olfr164 SNORA17 AC112681.1 Olfr165 SNORA17 Olfr166
chr4:44500001-45000000	16.86	Gm19980 Pax5 AL772319.1 Gm12462 Zcchc7 AL805896.1 Gm12678 Gm12493 Gm12679 Grhpr
chr13:23500001-24000000	16.36	Abt1 C230035I16Rik Btn1a1 Btn2a2 Gm11335 Hist1h4h Hist1h2af Hist1h3g Hist1h2bh Hist1h3f Hist1h4f Hist1h1d Hist1h3e Hist1h2ae Hist1h2bg Hist1h2bf Hist1h2ad Hist1h3d Gm17658 Hist1h4d Hist1h2be Gm11398 Hist1h1e U6 Hist1h2ac 5S_rRNA Hist1h2bc Hist1h1t Hist1h4c Hfe Hist1h1c Hist1h3c Hist1h2bb Hist1h2ab Hist1h3b 4930558J22Rik Hist1h4b Hist1h4a Hist1h3a Hist1h1a Trim38 Gm11337 Slc17a2 Slc17a3 Slc17a1 Slc17a4
chr3:52000001-52500000	16.19	Foxo1 RP24-337A16.1 Gm10293
chr6:68000001-68500000	15.18	Igkv9-120 Igkv1-117 Igkv2-116 Igkv1-115 Igkv2-112 Igkv14-111 SNORA17 Igkv1-110 Igkv2-109 Igkv16-104 Igkv15-103 Igkv14-100 SNORA17 Igkv1-99
chr12:115500001-116000000	15.18	Ighv3-8 Ighv12-3 Gm16930 Gm16695 Gm17000 Gm16696 Gm16694 Ighv1-5 Ighv10-3 Ighv1-7 Ighv15-2 Ighv1-9 Ighv1-12 Gm17686 Gm16857 Gm16858 Ighv1-18 Ighv1-19 Ighv1-20 Gm16860
chr4:32000001-32500000	14.84	Map3k7 U4 Bach2 D130062J21Rik Gm11932
chr11:44500001-45000000	14.67	Ebf1 Gm12159 Gm12160
chr11:45000001-45500000	14.50	Gm12160 Gm12162 SNORA17
chr11:22500001-23000000	14.33	Gm17335 Gm12052 Gm12055 Gm12056 Commd1 B3gnt2 RP23-242C19.6 SNORA63 RP23-242C19.5 U6 Zrsr1 Cct4 Fam161a 5S_rRNA Gm12059
chr17:5000001-5500000	13.66	Arid1b 5730437N04Rik AC166064.1 Zdhhc14
chr6:68500001-69000000	13.49	Igkv12-98 Gm16637 Igkv10-96 Igkv10-95 Igkv10-94 Igkv19-93 Igkv4-92 Igkv4-91 Igkv4-90 Igkv12-89 Igkv1-88 Gm11145 Igkv4-86 Igkv13-84 Igkv4-81 Igkv4-80 Igkv4-79
chr19:33000001-33500000	13.15	7SK Rnls Gm7237

chr19:32500001-33000000	12.98	Rpl9-ps6 Minpp1 Papss2 Atad1 Pten
chr17:4500001-5000000	12.98	U6 Arid1b
chr6:69000001-69500000	12.82	Igkv4-78 Igkv4-74 Igkv4-73 Igkv4-72 Igkv4-71 Igkv4-70 Igkv4-69 Igkv4-68 RNaseP_nuc Igkv4-63 Igkv4-62 Igkv4-61 Igkv4-59 Igkv4-58 AC156953.1 Igkv4-57-1
chr19:32000001-32500000	12.82	A1cf Asah2 Sgms1 2700046G09Rik
chr10:20500001-21000000	12.65	Ahi1 Myb Gm16786 AC153556.1
chr6:70500001-71000000	11.80	Igkv3-10 Igkv3-9 Igkv3-7 Gm16774 Igkv3-4 Igkv3-3 Igkv3-2 Igkv3-1 Igkj1 Igkj2 Igkj3 Igkj4 Igkj5 Igkc Rpia Eif2ak3 SNORA5 1700011F03Rik Foxi3 U1
chr10:5500001-6000000	11.13	Esr1 SNORD88 RNase_MRP Gm221 U1 1700052N19Rik Rmnd1 Gm16153 Zbtb2 Akap12
chr11:11500001-12000000	11.13	4930512M02Rik Gm11999 Ikzf1 Gm12000 Fignl1 Ddc 1700042O10Rik SCARNA4 Grb10 U1
chr12:115000001-115500000	10.79	Ighv11-2 Ighv14-3 Gm7005 Gm16987 Ighv9-2 Ighv9-3 Gm16842 Gm16841 Ighv3-3 Gm16839
chr4:32500001-33000000	10.29	Bach2 7SK BC024582 Gja10 Casp8ap2 Mdn1 Lyrm2 Ankrd6
chr11:45500001-46000000	10.29	F630206G17Rik AL645948.1 Clint1 Lsm11 Thg1l Sox30 Gm12166 Adam19 Gm16033 Gm16034 Nipal4
chr13:24500001-25000000	10.29	Cmah U6 Fam65b Gm11346 C530050E15Rik 1700016G14Rik Gmnn BC005537 SNORA32 Acot13 Tdp2 D130043K22Rik 4932702P03Rik Aldh5a1
chr12:16000001-16500000	10.12	AC102435.1
chr13:37500001-38000000	10.12	Ly86 Rreb1
chr17:5500001-6000000	9.95	Zdhhc14 Snx9 Synj2
chr12:116000001-116500000	9.78	Ighv1-23 Ighv1-24 Ighv1-42 Ighv1-43 Gm16966 Gm16830 Ighv8-5 Gm16829 Gm16828 AB069917 Ighv8-6 Ighv1-54 Gm16792 Gm16791
chr19:55500001-56000000	9.61	Vti1a 4930552P12Rik Tcf7l2
chr4:3500001-4000000	9.44	Tmem68 Tgs1 SNORA18 2210414B05Rik Lyn Gm17726 SNORA17 Rps20 snoU54 SNORA17 Mos Plag1 Chchd7 Gm11808 Sdr16c5 Sdr16c6
chr13:41500001-42000000	9.44	Nedd9 AC154848.1 Tmem170b Gm5082 9530008L14Rik 1700061E18Rik U6
chr19:41000001-41500000	9.44	Blnk Dntt Opalin Tll2 Tm9sf3 Pik3ap1
chr11:24000001-24500000	9.27	Bcl11a Gm12064 4930538E20Rik Gm12065 Gm12066 Gm12068 4933430M04Rik U6
chr19:7000001-7500000	9.27	Kcnk4 Gpr137 Bad Plcb3 Ppp1r14b Fkbp2 Vegfb Dnajc4 Nudt22 Trpt1 Fermt3 Stip1 Macrod1 Flrt1 Otub1 Cox8a Naa40 U6 5S_rRNA Rcor2 Mark2 Gm17227 AI846148 2700081O15Rik
chr19:11500001-12000000	9.27	Ms4a4c Ms4a4b Ms4a6c Gm8369 Ms4a6b Ms4a4d Gm10212 Ms4a6d SNORA17 Ms4a2 Ms4a3 Plac1l Oosp1 SCARNA17 SCARNA18 Gm97 Gif Mrpl16 Stx3 Olfr1417 Olfr1418 Olfr1419 Olfr1420 Patl1
chr1:38000001-38500000	8.94	Gm15457 Lyg1 7SK Txndc9 Eif5b Rev1 Aff3 Gm16150 Gm16151 Gm16152
chr6:8000001-8500000	8.94	Col28a1 Mios Rpa3 Gm16039 Gm16055 Gm16043 7SK 2810488G03Rik SNORA65 Glcci1
chr12:114500001-115000000	8.94	Ighg2c Ighg Ighg1 Ighm Adam6b Adam6a Ighv2-4
chr10:6000001-6500000	8.77	Akap12 U8 Mthfd1l U1 Plekhg1 5S_rRNA
chr12:8500001-9000000	8.60	Rhob Slc7a15 Pum2 Gm4755 Sdc1 9930038B18Rik Laptm4a Matn3 Wdr35
chr19:24500001-25000000	8.60	Pip5k1b 4930418C01Rik Fam122a E030010A14Rik Pgm5 Gm10053 Foxd4 Cbwd1
chr8:47500001-48000000	8.43	Acsl1 Mlf1ip Ccdc111 Casp3 Gm16675 Irf2
chr19:37500001-38000000	8.43	Hhex U6 Exoc6 Cyp26c1 Cyp26a1 Myof
chr9:32000001-32500000	8.43	Arhgap32 Kcnj5 Kcnj1 Fli1 U6 Ets1
chr9:13500001-14000000	8.26	Maml2 Mtmr2 Cep57 Fam76b
chr11:21000001-21500000	8.26	Peli1 7SK Vps54 SNORA17 Ugp2 Mir1933 Gm12043 4932414J04Rik Mdh1 AL663049.1 Wdpcp
chr19:3500001-4000000	8.26	Ppp6r3 Lrp5 AC132452.1 1810055G02Rik Suv420h1 Gm16066 AC133523.1 Chka Tcirg1 Ndufs8 Aldh3b1 Unc93b1 1700055N04Rik Aldh3b2 Acy3 Tbx10
chr6:67500001-68000000	8.09	Igkv2-137 Igkv1-135 Igkv17-134 Igkv1-133 Igkv1-132 Igkv1-131 Igkv14-130 SNORA17 SNORA17 Igkv9-129 Igkv17-127 Igkv14-126 SNORA17 Igkv11-125 Igkv9-124 Igkv9-123 Igkv1-122 Igkv17-121 Igkv9-120
chr13:24000001-24500000	8.09	Slc17a4 Hist1h2ba Hist1h2aa Scgn Gm11339 Lrrc16a SNORA17 Cmah Gm11342 Gm11345
chr18:55000001-55500000	8.09	Zfp608 Gm17270 Gm4221 SNORA40 U6
chr11:5000001-5500000	7.93	Rhbdd3 Emid1 Kremen1 U6 Znrf3 Gm11963 Xbp1 Ccdc117 SNORA17 Ankrd36
chr8:10500001-11000000	7.93	Myo16 3930402G23Rik Irs2
chr9:7500001-8000000	7.93	Mmp10 Mmp8 Mmp27 Mmp20 AV064505 Mmp7 Gm10709 Tmem123 Birc2 C330006D17Rik Birc3 Yap1 RP23-349N15.1
chr11:6000001-6500000	7.93	Nudcd3 Npc1l1 Ddx56 Tmed4 n-R5s67 Ogdh Zmiz2 Ppia H2afv Purb AL646020.1 Purb Gm11973 Myo1g Gm11974 SNORA9 SNORA70 Ccm2 Nacad
chr11:23500001-24000000	7.93	0610010F05Rik 5S_rRNA Pex13 Pus10 Rel U1 Papolg Gm12061 A830031A19Rik Gm12063 Bcl11a Gm12064
chr16:4500001-5000000	7.93	Srl Tcfap4 Glis2 Pam16 Coro7 Vasn Dnaja3 Nmral1 Hmox2 Gm15859 AC166903.1 5730403B10Rik Gm15835 4930562C15Rik Fam100a Mgrn1 Gm16861 Nudt16l1 Anks3 4930451G09Rik Sept12
chr18:39500001-40000000	7.93	Arhgap26 Gm15337 Nr3c1 Gm10008 Pabpc2
chr19:25000001-25500000	7.93	Cbwd1 SNORA19 Dock8 SNORA24 Kank1
chr9:70500001-71000000	7.76	Fam63b Gm10642 Adam10 Lipc CT025701.1 Gm3436 Aqp9
chr16:4000001-4500000	7.76	Slx4 Gm15879 Dnase1 Trap1 AC132380.1 Crebbp Gm5766 AC132575.1 Adcy9 Srl
chr19:44000001-44500000	7.76	n-R5s21 Cpn1 Cyp2c44 Erlin1 Chuk Cwf19l1 SNORA12 Bloc1s2 Pkd2l1 Scd3 AC123853.1 Scd2 AC123853.2 Scd4 Scd1
chr2:3000001-3500000	7.59	Fam171a1 Nmt2 U4 Rpp38 Acbd7 Olah Meig1 Dclre1c Suv39h2 Gm13184 Hspa14 Hspa14 Cdnf
chr6:69500001-70000000	7.59	Igkv4-57 Igkv4-56 Gm11143 Igkv4-55 Igkv4-53 Igkv4-50 Igkv5-48 Igkv12-47 Igkv12-46 Igkv5-45 Igkv12-44 Igkv5-43 Igkv12-41 Igkv5-39 Igkv12-38 Igkv5-37 Igkv18-36 Igkv1-35 AC154006.1
chr2:3500001-4000000	7.42	Fam107b Gm13185 Gm13180 Gm13191 Frmd4a
chr10:19500001-20000000	7.42	U6 Slc35d3 Pex7 Map3k5 Mtap7
chr11:44000001-44500000	7.42	Gm12154 Il12b Ublcp1 AL669944.1 Rnf145 4930597A21Rik Ebf1 Gm12158
chr13:44000001-44500000	7.42	Gm5083

chr4:8500001-9000000	7.25	Rab2a Chd7
chr16:10500001-11000000	7.25	Ciita Dexi Clec16a Gm15558 Socs1 Tnp2 Prm3 Prm2 Prm1 Gm10343 Gm11172 Gm17410 A630055G03Rik Litaf AC164093.1 U1
chr1:13500001-14000000	7.25	Tram1 Lactb2 Xkr9 SNORA17 7SK
chr19:21500001-22000000	7.25	Gda Gm3443 1110059E24Rik Fam108b Tmem2
chr1:13000001-13500000	7.08	Prdm14 Ncoa2 U6
chr3:19000001-19500000	7.08	Armc1 Mtfr1 Pde7a Gm16093 7SK Dnajc5b U1
chr6:52500001-53000000	7.08	Hibadh SNORA32 Tax1bp1 Jazf1 SCARNA20
chr1:37500001-38000000	6.91	Mgat4a 2010300C02Rik 4930556I23Rik Tsga10 Gm17715 Lipt1 Mitd1 Mrpl30 Lyg2 Gm15457
chr2:6500001-7000000	6.91	Celf2 Gm13389 Gm10855 Gm10115 7SK Gm17437
chr2:11500001-12000000	6.91	Rbm17 Gm17355 Gm17490 Il2ra Il15ra Fbxo18 Ankrd16
chr4:45000001-45500000	6.91	Grhpr Zbtb5 1700055D18Rik Polr1e Fbxo10 Tomm5 Gm10982 Frmpd1 2900093L17Rik Rg9mtd3 Exosc3 Dcaf10 Mcart1 AL772376.2 Mcart1 Shb
chr9:7000001-7500000	6.91	Dync2h1 Dcun1d5 Mmp13 Mmp12 Mmp1b Mmp3 Mmp1a
chr16:11000001-11500000	6.91	Litaf Gm4262 Snn Txndc11 Zc3h7a mmu-mir-689-2 U1 4930509G22Rik Rsl1d1 2610020C07Rik Gspt1 Mir1945 Tnfrsf17 Snx29 Snx29
chr16:24000001-24500000	6.91	1110054M08Rik Lpp U7
chr16:29500001-30000000	6.91	Atp13a4 Opa1 Gm17734 Gm16761 Gm1968
chr3:60000001-60500000	6.75	Mbnl1
chr4:11000001-11500000	6.75	2310030N02Rik Gm11827 Trp53inp1 Ccne2 Ints8 Dpy19l4 U1 Gm16652 Esrp1 Gm17283 1110037F02Rik Gm11831 Rad54b
chr16:31000001-31500000	6.75	AI480653 Acap2 Ppp1r2 Apod Bdh1 Gm15743
chr10:18500001-19000000	6.58	Gm4922 Perp Tnfaip3
chr11:30500001-31000000	6.58	Acyp2 Gm12100 Psme4 Gpr75 Erlec1 Asb3 Chac2
chr12:32500001-33000000	6.58	Cog5 SCARNA17 Hbp1 Prkar2b Pik3cg
chr13:30500001-31000000	6.58	Uqcrfs1 4930519D14Rik Dusp22 Irf4 Exoc2
chr19:57000001-57500000	6.58	Afap1l2 Ablim1 B230217O12Rik Fam160b1
chr2:5500001-6000000	6.58	Camk1d Cdc123 Nudt5 Gm13199 Sec61a2 Gm13267 Dhtkd1 Upf2
chr5:20500001-21000000	6.58	Ptpn12 SNORA40 Pion Ccdc146 Fgl2 Fam185a Fbxl13
chr17:4000001-4500000	6.58	
chr5:65000001-65500000	6.41	AC122043.1 Klf3 Tlr1 Tlr6 Fam114a1 Mir574 Tmem156 Klhl5
chr6:8500001-9000000	6.41	Gm16039 Glcci1 Ica1 Nxph1
chr10:39000001-39500000	6.41	Fyn Gm16364 Gm16365 Traf3ip2 E130307A14Rik Rev3l U6atac
chr11:5500001-6000000	6.41	Ankrd36 Mrps24 Urgcp 2210015D19Rik Dbnl Pgam2 Polm Aebp1 Pold2 Myl7 Gck Gm11967 Ykt6 Camk2b
chr16:32000001-32500000	6.41	Senp5 Pak2 SNORA17 Pigx 1500031L02Rik Gm15729 Lrrc33 Bex6 Fbxo45 SNORA79 Wdr53 Mir1946a 2310010M20Rik Rnf168 AC087556.1 Ubxn7 Tm4sf19 Tctex1d2 Pcyt1a Osta Zdhhc19
chr18:35500001-36000000	6.41	Sil1 Gm5239 Snhg4 SNORA74 Snora74a Matr3 Paip2 Slc23a1 2010001M09Rik Gm1614 Spata24 Dnajc18 1700066B19Rik Ecscr Tmem173 Gm16490 Ube2d2 Cxxc5
chr19:45500001-46000000	6.41	Btrc Gm6807 Poll Dpcd Fbxw4 Gm17018 Fgf8 Npm3 Gm15491 Mgea5 Kcnip2 9130011E15Rik
chr3:9500001-10000000	6.24	Zfp704 Pag1 Gm16337 5S_rRNA
chr5:9000001-9500000	6.24	4930420K17Rik Dmtf1 U2 Gm15734 9330182L06Rik Mir879 Grm3
chr6:67000001-67500000	6.24	E230016M11Rik A430010J10Rik Serbp1 Il12rb2 Il23r Tacstd2
chr11:46000001-46500000	6.24	Cyfip2 C030019I05Rik Itk Gm12167 Fam71b Med7 2310031A07Rik Havcr2 Gm12169 Gm12171 BC053393 Dppa1 Gm4926 Timd2
chr19:16000001-16500000	6.24	Psat1 Cep78 C130060C02Rik Rpl37-ps1 Gnaq
chr19:58000001-58500000	6.24	Atrnl1 Gm16277 Gfra1
chr1:36500001-37000000	6.07	Lman2l Cnnm4 Cnnm3 Ankrd23 Ankrd39 Sema4c D430040D24Rik Fam178b AC084389.1 Cox5b Actr1b Zap70 Tmem131
chr5:21000001-21500000	6.07	Fbxl13 Lrrc17 Gm6543 Armc10 Napepld Pmpcb Dnajc2 Psmc2 Slc26a5 Reln Gm10475
chr16:21500001-22000000	6.07	Vps8 AC133597.1 2510009E07Rik Ehhadh U6 1300002E11Rik Gm17439 Map3k13 2610020F03Rik Tmem41a Liph
chr19:10500001-11000000	6.07	Syt7 Lrrc10b 4930579J09Rik Sdhaf2 Cpsf7 Tmem216 Tmem138 Cybasc3 Dak Ddb1 Vwce Pga5 Vps37c Cd5 A430093F15Rik Cd6 Slc15a3 Tmem132a Tmem109 Prpf19 Zp1
chr19:34000001-34500000	6.07	U6 Lipf Lipk Lipn AC165239.1 Lipm Ankrd22 Stambpl1 Acta2 Fas AC157912.1
chr2:22500001-23000000	5.90	Gad2 AL928693.1 1700092C17Rik Apbb1ip Pdss1 SNORA42 Abi1 Acbd5 Mastl
chr3:51500001-52000000	5.90	Maml3 AC116729.1 n-R5s196
chr4:59000001-59500000	5.90	Dnajc25 Gm20503 Gng10 AI481877 Gm12594 Ugcg Gm12596 Susd1 Rod1
chr14:16500001-17000000	5.90	
chr16:20000001-20500000	5.90	Klhl24 Yeats2 Map6d1 Parl Cyp2ab1 Abcc5 7SK Eif2b5
chr16:24500001-25000000	5.90	Lpp Mir28 SNORA17
chr16:30000001-30500000	5.90	4632428C04Rik Hes1 n-R5s32 Gm17516 Cpn2 Lrrc15 Gp5 Atp13a3
chr16:95500001-96000000	5.90	Kcnj15 Erg Ets2
chr19:10000001-10500000	5.90	Fth1 Best1 Rab3il1 Fads3 Fads2 Fads1 Gm10143 Fen1 1810006K21Rik Gm98 Dagla Syt7 Gm17289
chr19:29000001-29500000	5.90	4430402I18Rik Ppapdc2 Cdc37l1 Gm10136 Ak3 Rcl1 Mir101b Jak2 Insl6 Rln1 5033414D02Rik Cd274 Pdcd1lg2
chr19:34500001-35000000	5.90	Ch25h Gm16704 Lipa Ifit2 Ifit3 Gm14446 I830012O16Rik 2010002M12Rik Ifit1 Slc16a12 U1 Pank1 Mir107 AC113244.1 Kif20b
chr19:41500001-42000000	5.90	U7 Lcor Gm340 AI606181 Slit1 7SK Arhgap19 Frat2 Rrp12 Pgam1 Exosc1
chr13:28500001-29000000	5.90	2610307P16Rik
chr6:99000001-99500000	5.73	Foxp1 Eif4e3 AC152987.1
chr11:54500001-55000000	5.73	Rapgef6 Cdc42se2 Gm12227 Gm12228 Lyrm7 U1 Hint1 Gpx3 Tnip1 Anxa6 Ccdc69 Gm2a Slc36a3 Gm12233 Slc36a2

chr13:3500001-4000000	5.73	Gdi2 BC016423 Asb13 5S_rRNA Calml3 Calm4 Net1 Tubal3 Ucn3 AC139323.1
chr14:17000001-17500000	5.73	Oxsm Ngly1 Top2b Rarb
chr14:32000001-32500000	5.73	Tnnc1 Nisch Tnnc1 Sema3g Phf7 Bap1 Dnahc1 Capn7 Sh3bp5 Mettl6 Eaf1 Colq 7SK Hacl1 Btd
chr17:29000001-29500000	5.73	Pnpla1 4930539E08Rik 1700030A11Rik Gm16191 Pxt1 Kctd20 Stk38 U2 Gm16196 Gm16195 Srsf3 Gm16197 Cdkn1a Gm16194 Rab44 Cpne5 Ppil1 BC004004 Pi16 Mtch1 Fgd2
chr18:4500001-5000000	5.73	AC121802.1 9430020K01Rik Gm10556 Svil
chr18:6000001-6500000	5.73	Arhgap12 Kif5b Gm17036 Rpl27-ps3 Epc1 Mir1893
chr18:15000001-15500000	5.73	Taf4b Kctd1
chr19:53500001-54000000	5.73	5830416P10Rik 4833407H14Rik Dusp5 Nutf2-ps1 Smc3 Rbm20 Gm16299 Pdcd4
chr12:4500001-5000000	5.56	Gm3625 Itsn2 Gm17541 4930417G10Rik A830093I24Rik U6 U6 Pfn4 0610009D07Rik Fkbp1b BC068281 Mfsd2b Ubxn2a Atad2b
chr12:80500001-81000000	5.56	Rad51l1
chr12:81000001-81500000	5.56	Zfp36l1 Gm17591 2310015A10Rik Actn1 Gm17425 Gm17373 Gm17301 Dcaf5 Scarna3b
chr2:6000001-6500000	5.56	5430407P10Rik Echdc3 A230108P19Rik Gm13383 Usp6nl Gm13388 Gm13391 Celf2
chr2:45000001-45500000	5.56	Gm13479
chr8:26000001-26500000	5.56	Adam32 U6 Adam9 Tm2d2 Htra4 Gm16933 Plekha2 Tacc1
chr11:32000001-32500000	5.56	Gm12108 Il9r Snrnp25 Rhbdf1 Nprl3 Mpg Hba-x Hba-a1 Hbq1b Hba-a2 Hbq1a Sh3pxd2b Ubtd2 Efcab9 Stk10
chr11:34000001-34500000	5.56	Gm12121 Foxi1 Dock2 4930403D09Rik Fam196b
chr16:17000001-17500000	5.56	Mapk1 U6 1700056N10Rik Ypel1 Ppil2 Gm15585 2610318N02Rik Mir130b Mir301b Sdf2l1 Ccdc116 Gm15646 Ydjc Ube2l3 Gm15648 U6 Rimbp3 Hic2 Gm17625 Tmem191c Pi4ka Serpind1 U6 Snap29 Crkl U6 Aifm3
chr17:50500001-51000000	5.56	Plcl2 Gm7334 Tbc1d5
chr19:12500001-13000000	5.56	Pfpl Mpeg1 Dtx4 Fam111a A330040F15Rik Gm4952 Glyat U6 Olfr1442 Olfr1443 Keg1 Gm15962 Cntf Zfp91 Lpxn Gm5244 Olfr1444 Olfr1445 Olfr1446 Olfr1447 Olfr1448
chr19:46500001-47000000	5.56	Sufu Trim8 Arl3 Sfxn2 D19Wsu162e Cyp17a1 2010012O05Rik As3mt Cnnm2 Nt5c2
chr1:14000001-14500000	5.40	Eya1 AC156988.1
chr5:36500001-37000000	5.40	Sorcs2 Psapl1 2210406O10Rik Grpel1 Tada2b Ccdc96 Tbc1d14 D5Ertd579e
chr16:30500001-31000000	5.40	Tmem44 Lsg1 Fam43a U6 SNORA17 AI480653 Gm15742
chr19:37000001-37500000	5.40	Btaf1 Cpeb3 CPEB3_ribozyme A330032B11Rik AC113124.1 March5 U6 Ide Kif11
chr4:45500001-46000000	5.23	Shb AL772376.1 U6 Gm12408 Gm829 Gm12410 Gm12409 Aldh1b1 Igfbpl1 1300002K09Rik E230008N13Rik Tdrd7
chr4:57000001-57500000	5.23	6430704M03Rik Epb4.1l4b Gm12530 Ptpn3 Gm12536 1700042G15Rik Palm2
chr9:61500001-62000000	5.23	Rplp1 Kif23 Paqr5 7SK Glce AC123610.1
chr10:5000001-5500000	5.23	Syne1 Gm10097 AC161829.1 Esr1
chr12:25500001-26000000	5.23	Mboat2 Kidins220 Id2
chr12:35500001-36000000	5.23	4921508M14Rik SNORA17 Prps1l1 7SK Snx13 Mir680-3
chr12:70500001-71000000	5.23	AC153658.1 Mettl21d Sos2 U6 L2hgdh Atp5s Cdkl1 Mir681 4930512B01Rik Map4k5 4931403G20Rik Atl1
chr16:33500001-34000000	5.23	Zfp148 Slc12a8 Heg1 Gm15658 Gm15657 Muc13 Itgb5 Umps Gm15829 Kalrn
chr16:36500001-37000000	5.23	Casr 7SK Cd86 Ildr1 Slc15a2 AC117662.1 Eaf2 Iqcb1 Golgb1 Golgb1 4930565N06Rik Hcls1 Fbxo40
chr17:15500001-16000000	5.23	Dll1 A930024N18Rik Fam120b Psmb1 Tbp Pdcd2 Prdm9 Chd1 Rgmb U6
chr17:44500001-45000000	5.23	Runx2 Gm16317 Runx2 n-R5s27 9530072K05Rik Gm10497 Supt3h
chr18:24000001-24500000	5.23	Mapre2 Zfp397 Zscan30 Zfp35 Zfp191 Ino80c Galnt1
chr19:15500001-16000000	5.23	U6 Psat1
chr4:10500001-11000000	5.06	1700123O12Rik AL672160.1 2610301B20Rik Plekhf2 2310030N02Rik
chr4:58500001-59000000	5.06	Lpar1 Gm12580 Olfr267 AI314180 AL805972.1 Zkscan16 Ptgr1
chr5:3000001-3500000	5.06	Cdk6 Gm17590
chr5:64500001-65000000	5.06	Pgm1 SNORA17 Tbc1d1
chr11:4500001-5000000	5.06	Gm11032 Gm11961 Ascc2 Uqcr10 Zmat5 Cabp7 Nf2 Nipsnap1 Thoc5 Nefh Ap1b1 SNORD125 Gas2l1 Rasl10a Ewsr1 Rhbdd3 Gm11031
chr11:29000001-29500000	5.06	Pnpt1 A630052C17Rik Smek2 Ccdc104 U6atac Ccdc88a Prorsd1 Gm12089 Mtif2 Rps27a 1700034F02Rik Gm12088
chr12:4000001-4500000	5.06	Efr3b Dnajc27 Adcy3 Cenpo 2410017P09Rik Ncoa1 5S_rRNA 7SK
chr12:35000001-35500000	5.06	Hdac9
chr14:21500001-22000000	5.06	Sec24c 6230400D17Rik Fut11 AC121599.1 Chchd1 2310021P13Rik Ndst2 Camk2g Plau Vcl Ap3m1 Adk
chr16:19500001-20000000	5.06	Olfr167 Olfr168 Olfr169 Olfr170 Olfr171 Lamp3 B3gnt5 A930003A15Rik Klhl6
chr17:3500001-4000000	5.06	Tiam2 Tfb1m Cldn20 Nox3
chr17:45000001-45500000	5.06	Supt3h
chr17:73500001-74000000	5.06	Lclat1 SNORA17 Capn13 Galnt14 D630014O11Rik
chr19:4500001-5000000	5.06	Pcx Lrfn4 Rce1 Gm960 Spnb3 Rbm4b Rbm14 Ccs Ccdc87 Ctsf Actn3 Zdhhc24 Bbs1 U6 Dpp3 Peli3 Mrpl11 Npas4
chr19:38000001-38500000	5.06	Myof I830134H01Rik Cep55 SNORA42 O3far1 Rbp4 Pde6c 5730455O13Rik Lgi1 Tmem20
chr17:26500001-27000000	4.89	Neurl1b Dusp1 Gm8225 1700049J03Rik Ergic1 AC122252.1 Gm17218 Atp6v0e A930001N09Rik Bnip1 Nkx2-5 Gm17382 Gm20468
chr18:5500001-6000000	4.89	Gm10125 Zeb1 AC127028.1
chr19:56500001-57000000	4.89	Casp7 9930023K05Rik Dclre1a Nhlrc2 Adrb1 Gm6990 A630007B06Rik Tdrd1 Vwa2 Afap1l2
chr7:26000001-26500000	4.89	Dedd2 Zfp526 Gsk3a 9130221H12Rik Erf Cic Pafah1b3 Prr19 Tmem145 Megf8 Cnfn Lipe 4732471J01Rik Cxcl17 Ceacam1 Ceacam2 Gm7092 Atp5sl B3gnt8 Bckdha Exosc5 Tmem91 B9d2 Tgfb1 Ccdc97
chr9:21000001-21500000	4.89	Pde4a Gm16754 Keap1 S1pr5 Atg4d Kri1 Cdkn2d Ap1m2 AC122525.1 Slc44a2 Ilf3 Gm16853 Qtrt1 Dnm2 Mir199a-1 Tmed1 AB124611 Carm1 Yipf2 1810026J23Rik Mir1946b Smarca4

chr10:21500001-22000000	4.89	Gm6846 SNORD23 Sgk1 4930444G20Rik E030030I06Rik H60b Raet1c
chr10:43500001-44000000	4.89	Gm9034 Qrsl1 Rtn4ip1 Aim1 Atg5
chr11:4000001-4500000	4.89	Sec14l2 Rnf215 AL807825.1 Ccdc157 Sf3a1 Tbc1d10a Gatsl3 Osm Lif Gm11959 Gm11958 U6 Hormad2 Mtmr3
chr11:75000001-75500000	4.89	Dph1 Rtn4rl1 Rpa1 Smyd4 Serpinf1 Gm12336 Serpinf2 Wdr81 2210403K04Rik Tlcd2 Mir22 Prpf8 Rilp Scarf1 Slc43a2 AL591496.1 Pitpna 4931413K12Rik Inpp5k Myo1c Crk
chr12:117000001-117500000	4.89	Gm16810 Ighv1-73 Gm16710 Ighv8-14 Gm16811 Gm16813 Gm16746 Gm16812 Gm16814 Gm16711 Gm16747 Ighv1-83 Ighv1-84 Ighv1-85 Zfp386 Gm17626 Vipr2 U6 Wdr60
chr17:44000001-44500000	4.89	Rcan2 7SK Enpp5 Enpp4 Clic5
chr18:54500001-55000000	4.89	9430076G02Rik
chr19:40500001-41000000	4.89	Sorbs1 Aldh18a1 Gm16765 Tctn3 Entpd1 Ccnj E030007J07Rik Zfp518a
chr4:9000001-9500000	4.72	U6 Gm17240 Clvs1 Gm11816 Gm11817 Asph
chr5:3500001-4000000	4.72	Cdk6 Fam133b n-R5s169 1700109H08Rik C030048B08Rik Pex1 Gatad1 AC090443.1 4930511M11Rik Ankib1 AC022236.1 Krit1 4932412H11Rik Mterf Akap9
chr5:66000001-66500000	4.72	Pds5a U6 1700022K14Rik N4bp2 SNORA73 Rhoh Chrna9 9130230L23Rik AC115293.1 Rbm47
chr6:5000001-5500000	4.72	Ppp1r9a Pon1 Pon3 Pon2 Asb4 Pdk4
chr9:14000001-14500000	4.72	Sesn3 Endod1 Kdm4d Cwc15 Amotl1
chr10:43000001-43500000	4.72	Pdss2 Gm10281 Gm3699 Bend3 1700021F05Rik Cd24a F930017D23Rik
chr12:86500001-87000000	4.72	Pgf Eif2b2 Mlh3 Acyp1 Fam164c Nek9 Tmed10 Fos Jdp2
chr13:51000001-51500000	4.72	Y_RNA Spin1 Nxnl2 Hist1h2al
chr18:36000001-36500000	4.72	Cxxc5 AC141471.1 Psd2 Nrg2 Pura
chr19:5500001-6000000	4.72	Snx32 Ovol1 Gm962 Rnaseh2c Kat5 Rela Sipa1 Pcnxl3 Map3k11 Kcnk7 Ehbp1l1 Gm16538 Fam89b Sssca1 Ltbp3 Scyl1 Malat1 Gm20417 Neat1 Gm9783 Frmd8 Slc25a45 Tigd3 Dpf2 Cdc42ep2 Pola2 Slc22a20 Capn1
chr3:14500001-15000000	4.55	Slc7a12 Lrrcc1 E2f5 1810022K09Rik Car13 Car1 Car3 Car2
chr5:8500001-9000000	4.55	Rundc3b Abcb1a Gm5106 Abcb1b Abcb4 Crot Gm15611
chr11:20500001-21000000	4.55	Sertad2 Aftph 1110067D22Rik Gm12037 SNORA65 Peli1
chr13:32000001-32500000	4.55	Gmds Gm11381
chr13:42000001-42500000	4.55	Hivep1 Edn1
chr14:62000001-62500000	4.55	Kpna3 Rps12-ps2 6330409N04Rik Trim13 Kcnrg Dleu2 AC154660.1 AC154660.2 Mir1196
chr17:50000001-50500000	4.55	Kif6 Gm16554 Rftn1 AY702103 Dazl
chr2:34500001-35000000	4.38	Gapvd1 Hspa5 Rabepk snoU13 Fbxw2 Psmd5 D730039F16Rik Phf19 Gm13448 U6 Traf1 Hc Gm13449 AI182371 Cep110
chr9:14500001-15000000	4.38	Piwil4 Gm10706 Fut4 1700012B09Rik Ankrd49 Mre11a Gm16302 Gpr83 Folr4 Panx1 Hephl1
chr11:11000001-11500000	4.38	Vwc2 5S_rRNA Zpbp SNORA24 4930415F15Rik Gm11998 4930512M02Rik
chr11:86000001-86500000	4.38	Brip1 4632419I22Rik Ints2 Med13 U3 Y_RNA 5S_rRNA U6 Rnft1 Rps6kb1 Tubd1 Vmp1 Mir21 Ptrh2
chr17:8000001-8500000	4.38	Fndc1 D030054H15Rik Tagap Rsph3a Gm1604A SCARNA3 Rnaset2a Fgfr1op Ccr6 Brp44l 4930506C21Rik
chr18:38500001-39000000	4.38	5S_rRNA Ndfip1 AC134576.1 Spry4 Arhgap26 9630014M24Rik Fgf1
chr19:29500001-30000000	4.38	Pdcd1lg2 A930007I19Rik C030046E11Rik Ermp1 Mlana 9930021J03Rik 9930021J03Rik Ranbp6 Il33
chr19:60500001-61000000	4.38	Prlhr 2700078E11Rik AC108409.1 Nanos1 Eif3a SNORA19 SNORA19 Fam45a Sfxn4 Prdx3 Grk5
chr6:7500001-8000000	4.22	Tac1 Asns C1galt1 SNORA3 Col28a1
chr9:11000001-11500000	4.22	CT009748.1
chr9:37000001-37500000	4.22	Tmem218 Slc37a2 Gm10177 Ccdc15 Hepacam Robo4 Robo3 BC024479 Esam Vsig2 Nrgn Spa17 Siae Tbrg1 Panx3
chr12:16500001-17000000	4.22	Lpin1 Ntsr2 Greb1 AC157352.1 E2f6 Rock2 SNORA32 Pqlc3
chr12:36500001-37000000	4.22	Agr3 Agr2 Tspan13 Gm5434 Bzw2 Ankmy2 1700108M19Rik
chr18:80500001-81000000	4.22	Gm16997 Ctdp1 Nfatc1 Atp9b
chr19:46000001-46500000	4.22	9130011E15Rik 4930505N22Rik Hps6 Ldb1 Pprc1 Nolc1 Elovl3 Pitx3 Gbf1 Gm16726 Nfkb2 Psd Fbxl15 Cuedc2 Gm17393 Tmem180 Mir146b SNORA32 Actr1a Sufu
chr11:53500001-54000000	4.22	Rad50 7SK Il5 Gm12214 Irf1 Gm17334 Gm12216 Gm11006 Slc22a5 Slc22a21 Slc22a4 Pdlim4 P4ha2 4933405E24Rik
chr17:51500001-52000000	4.22	Satb1
chr19:36000001-36500000	4.22	Htr7 Rpp30 Ankrd1 Pcgf5 U6
chr19:45000001-45500000	4.22	Fam178a U6 Sema4g Mrpl43 Peo1 Lzts2 AC132957.1 Pdzd7 Sfxn3 Kazald1 Tlx1 Gm20424 Lbx1 Btrc
chr19:47500001-48000000	4.22	Sh3pxd2a Obfc1 Slk Gm16068 Col17a1 SNORA17 U6 Sfr1 Wdr96 Gsto1 Gsto2 Itprip AC126679.1
chr5:32000001-32500000	4.05	Mrpl33 Bre 7SK Gm17130 Gm10463 Fosl2 U6
chr7:82500001-83000000	4.05	Akap13 U6 AC158749.1 Klhl25
chr13:112500001-113000000	4.05	Mier3 Gm15287 Map3k1 Gm15327 Gm15325 Gm15324 Gm15326 Gm15322 Gm15323
chr19:53000001-53500000	4.05	Xpnpep1 Add3 U6 Mxi1 Gm10197 Smndc1
chr1:54500001-55000000	3.88	Pgap1 Pgap1 Ankrd44 AC151572.1
chr7:52500001-53000000	3.88	U6 1700039E15Rik Trpm4 Hrc Ppfia3 Mtag2 Lin7b Snrnp70 SNORA67 Kcna7 Ntf5 Lhb Ruvbl2 Gys1 Ftl1 AC151602.1 Bax Dhdh Tulp2 Nucb1 Ppp1r15a Plekha4 Gm16022 Hsd17b14 0610005C13Rik Bcat2 Fgf21 Fut1 Izumo1 Rasip1 Gm16047 Mamstr Fut2 Sec1 Ntn5 Car11 Dbp Sphk2 Rpl18 Fam83e Spaca4 Sult2b1 AC167242.1
chr8:13500001-14000000	3.88	1700029H14Rik Rasa3 4932443I19Rik Cdc16 Upf3a AF366264 Zfp828 SNORA3 2410022L05Rik Gm7676 Fbxo25 2610019F03Rik
chr8:73000001-73500000	3.88	Klhl26 Tmem59l Crlf1 2810428I15Rik Uba52 2810422J05Rik Fkbp8 Ell Isyna1 Ssbp4 Lrrc25 Gdf15 Pgpep1 Lsm4 Jund Gm11175 Pde4c Rab3a Mpv17l2 Ifi30 Pik3r2 Mast3 Il12rb1 Arrdc2 Kcnn1 A230052G05Rik Ccdc124 Slc5a5 Rpl18a Snora68 Mtap1s Mir1969 Gm10654
chr8:74500001-75000000	3.88	Zfp961 Cyp4f18 U2 Olfr372 Olfr373 Olfr374 5S_rRNA AC158898.2 Tpm4 Gm17371 Gm16091

		Rab8a Hsh2d Cib3 Gm11034 Fam32a AC158898.1 Ap1m1 Gm10282 Klf2 Eps15l1 Calr3 1700030K09Rik Cherp
chr11:78500001-79000000	3.88	Nlk Fam58b AL591376.1 U6 1810012P15Rik Nos2 Lgals9 Ksr1 Gm11201
chr11:86500001-87000000	3.88	Ptrh2 Cltc Dhx40 AL596111.1 Ypel2 SCARNA3 Gdpd1 Gm11479 1200011M11Rik Prr11 Fam33a Mir301 Gm11491 Trim37
chr12:56500001-57000000	3.88	Psma6 Nfkbia Aldoart2 Insm2 Ralgapa1 AC159624.1 Brms1l
chr14:20500001-21000000	3.88	Nid2 2700060E02Rik Gng2 1810063B07Rik Kcnk5
chr14:77000001-77500000	3.88	9030625A04Rik Ccdc122
chr18:54000001-54500000	3.88	Csnk1g3 Gm5507

trans interactions from Il7r viewpoint in Thymus

bin	z-score	genes in bin
chr19:21000001-21500000	6.58	Tmc1 Zfand5 Gda
chr12:115000001-115500000	6.41	Ighv11-2 Ighv14-3 Gm7005 Gm16987 Ighv9-2 Ighv9-3 Gm16842 Gm16841 Ighv3-3 Gm16839
chr19:11500001-12000000	5.40	Ms4a4c Ms4a4b Ms4a6c Gm8369 Ms4a6b Ms4a4d Gm10212 Ms4a6d SNORA17 Ms4a2 Ms4a3 Plac1l Oosp1 SCARNA17 SCARNA18 Gm97 Gif Mrpl16 Stx3 Olfr1417 Olfr1418 Olfr1419 Olfr1420 Patl1
chr11:11500001-12000000	5.23	4930512M02Rik Gm11999 Ikzf1 Gm12000 Fignl1 Ddc 1700042O10Rik SCARNA4 Grb10 U1
chr12:115500001-116000000	5.23	Ighv3-8 Ighv12-3 Ighv1-5 Ighv10-3 Ighv1-7 Ighv15-2 Ighv1-9 Ighv1-12 Gm17686 Gm16857 Gm16858 Ighv1-18 Ighv1-19 Ighv1-20 Gm16860
chr17:3000001-3500000	5.23	SNORA40 Pisd-ps2 Scaf8 Tiam2
chr14:11000001-11500000	4.89	Fhit CT485999.1 SNORA73
chr19:23500001-24000000	4.89	Mamdc2 1700028P14Rik Gm9493 SNORA17 Ptar1 Gm9938 Apba1
chr19:26500001-27000000	4.89	Smarca2 Gm815
chr5:8500001-9000000	4.72	Rundc3b Abcb1a Gm5106 Abcb1b Abcb4 Crot Gm15611
chr10:16500001-17000000	4.72	U6
chr13:10000001-10500000	4.72	Gm16950
chr13:9000001-9500000	4.55	AC125484.1 Larp4b 7SK Dip2c Gm17294
chr16:19000001-19500000	4.55	Iglc3 Iglv1 Iglc2 Iglv3 Iglv2 Olfr164 SNORA17 AC112681.1 Olfr165 SNORA17 Olfr166
chr19:15500001-16000000	4.55	U6 Psat1
chr19:31000001-31500000	4.55	Prkg1 Cstf2t
chr16:51500001-52000000	4.38	U7
chr19:21500001-22000000	4.38	Gda Gm3443 1110059E24Rik Fam108b Tmem2
chr19:27000001-27500000	4.38	Vldlr Kcnv2 D19Bwg1357e
chr19:27500001-28000000	4.38	D19Bwg1357e SNORA48 Rfx3
chr19:58000001-58500000	4.38	Atrnl1 Gm16277 Gfra1
chr12:15500001-16000000	4.22	Trib2 Gm5432
chr12:26000001-26500000	4.22	5S_rRNA
chr11:11000001-11500000	4.22	Vwc2 5S_rRNA Zpbp SNORA24 4930415F15Rik Gm11998 4930512M02Rik
chr19:14500001-15000000	4.22	Tle4 U4
chr4:9000001-9500000	3.88	U6 Gm17240 Clvs1 Gm11816 Gm11817 Asph
chr9:13500001-14000000	3.88	Maml2 Mtmr2 Cep57 Fam76b
chr14:19500001-20000000	3.88	Ube2e2 SNORA17
chr19:17000001-17500000	3.88	Prune2 Gcnt1 Rfk
chr19:35000001-35500000	3.88	Kif20b Mir1950 SNORA17 AC102038.1
chr6:70500001-71000000	3.71	Igkv3-10 Igkv3-9 Igkv3-7 Gm16774 Igkv3-4 Igkv3-3 Igkv3-2 Igkv3-1 Igkj1 Igkj2 Igkj3 Igkj4 Igkj5 Igkc Rpia Eif2ak3 SNORA5 1700011F03Rik Foxi3 U1
chr18:12500001-13000000	3.71	Lama3 Gm17506 5S_rRNA Ttc39c Mir1948 Cabyr Osbpl1a
chr19:11000001-11500000	3.71	Gpr44 Ccdc86 Ms4a10 Ms4a15 AW112010 Ms4a8a Gm336 1700017D01Rik 1700025F22Rik Ms4a13 4930526L06Rik Ms4a12 Ms4a1 Ms4a5 Ms4a14 Ms4a7 Ms4a4c
chr19:23000001-23500000	3.71	Trpm3 C330002G04Rik 2410080I02Rik Klf9 Mir1192 Smc5 U6 Mamdc2

trans interactions from Rag1/2 viewpoint in Rag-/- pro-B

bin	z-score	genes in bin
chrX:103000001-103500000	179.87	Atrx U2 U6 Magt1 Cox7b Atp7a Tlr13 Pgk1 Taf9b Fnd3c2
chr12:115500001-116000000	5.85	Ighv3-8 Ighv12-34 Ighv1-5 Ighv10-3 Ighv1-7 Ighv15-2 Ighv1-9 Ighv1-12 Gm17686 Gm16857 Gm16858 Ighv1-18 Ighv1-19 Ighv1-20 Gm16860
chr5:149500001-150000000	5.17	Katnal1 Hmgb1 Uspl1

trans interactions from Rag1/2 viewpoint in Rag/81X pre-B

bin	z-score	genes in bin
chrX:103000001-103500000	163.06	Atrx U2 U6 Magt1 Cox7b Atp7a Tlr13 Pgk1 Taf9b Fnd3c2
chr12:115500001-116000000	11.13	Ighv3-8 Ighv12-3 Ighv1-5 Ighv10-3 Ighv1-7 Ighv15-2 Ighv1-9 Ighv1-12 Gm17686 Gm16857 Gm16858 Ighv1-18 Ighv1-19 Ighv1-20 Gm16860
chr1:185500001-186000000	8.43	Gm8214 Dusp10 1700056E22Rik
chr14:122000001-122500000	8.26	Dock9 Ubac2 Gpr18 Gpr183 Timm8a2
chr8:129000001-129500000	8.09	AC118255.1 Gm16983 Irf2bp2 Tomm20 SNORA14 Rbm34
chr6:134500001-135000000	7.93	Lrp6 Mansc1 Loh12cr1 Dusp16 Crebl2 Gpr19 Cdkn1b Apold1 Ddx47
chr12:118500001-119000000	7.93	Ptprn2 Rapgef5 5S_rRNA
chr5:149500001-150000000	7.59	Katnal1 Hmgb1 Uspl1
chr6:129000001-129500000	7.25	Klrb1f Clec2e Klrb1-ps1 U7 Clec2d 2310001H17Rik Cd69 4922502D21Rik Clec12a Clec12b Clec1a Clec1b Clec9a Clec7a Olr1 D630042F21Rik 1700101I11Rik Gabarapl1
chr1:97000001-97500000	6.91	Fam174a U7 St8sia4
chr12:114500001-115000000	6.75	Ighg2c Ighg Ighg1 Ighm Adam6b Adam6a Ighv2-4
chr13:112500001-113000000	6.58	Mier3 Gm15287 Map3k1 Gm15327 Gm15325 Gm15324 Gm15326 Gm15322 Gm15323

chr6:70500001-71000000	6.41	Igkv3-10 Igkv3-9 Igkv3-7 Gm16774 Igkv3-4 Igkv3-3 Igkv3-2 Igkv3-1 Igkj1 Igkj2 Igkj3 Igkj4 Igkj5 Igkc Rpia Eif2ak3 SNORA5 1700011F03Rik Foxi3 U1
chr6:134000001-134500000	6.41	Etv6 Gm17088 Gm17089 Bcl2l14 Lrp6
chr9:116000001-116500000	6.41	Tgfbr2 AC131777.1 Rbms3
chr13:108500001-109000000	6.41	Zswim6 AC165250.1 2810008M24Rik Ndufaf2 Ercc8
chr3:136000001-136500000	6.07	Ppp3ca
chr3:143500001-144000000	6.07	Lmo4
chr8:127500001-128000000	6.07	Tsnax Disc1 AL672234.1 Gm16237 Sipa1l2
chr1:194500001-195000000	5.90	Hhat U5 A730013G03Rik Sertad4 Gm15867 Syt14 7SK Diexf Irf6 A130010J15Rik
chr1:195000001-195500000	5.90	A130010J15Rik Traf3ip3 Gm15872 4930570N18Rik 1600010F14Rik Hsd11b1 G0s2 Lamb3 Camk1g 4631405K08Rik Mir205
chr13:117500001-118000000	5.90	Parp8
chr10:96000001-96500000	5.56	Btg1 AC152946.1
chr12:101500001-102000000	5.56	Ttc7b Rps6ka5
chr1:196500001-197000000	5.40	Plxna2 AC162447.1 7SK Cd34 Gm16897 A330023F24Rik Mir29b-2 Mir29c Cd46 Cr1l Cr2
chr6:68500001-69000000	5.40	Igkv12-98 Gm16637 Igkv10-96 Igkv10-95 Igkv10-94 Igkv19-93 Igkv4-92 Igkv4-91 Igkv4-90 Igkv12-89 Igkv1-88 Gm11145 Igkv4-86 Igkv13-84 Igkv4-81 Igkv4-80 Igkv4-79
chr10:116000001-116500000	5.40	Cnot2 Gm16913 Gm239 Rab3ip D630029K05Rik Gm10271 Best3 Lrrc10 Cct2
chr12:116000001-116500000	5.40	Ighv1-23 Ighv1-24 Gm16717 Gm17539 Gm16965 Gm16735 Gm16715 Gm16716 Gm16964 Ighv1-42 Ighv1-43 Gm16966 Gm16830 Ighv8-5 Gm16829 Gm16828 AB069917 Ighv8-6 Ighv1-54 Gm16792 Gm16791
chr12:117000001-117500000	5.40	Gm16810 Ighv1-73 Gm16710 Ighv8-14 Gm16811 Gm16813 Gm16746 Gm16812 Gm16814 Gm16711 Gm16747 Ighv1-83 Ighv1-84 Ighv1-85 Zfp386 Gm17626 Vipr2 U6 Wdr60
chr10:110500001-111000000	5.23	Gm5428 U6 Osbpl8 Bbs10 Nap1l1 SNORA48 Gm5176 Phlda1
chr10:120500001-121000000	5.23	Wif1 Tbc1d30 Gns Rassf3 Tbk1
chr5:151000001-151500000	5.06	Fry snoU13 Zar1l Brca2 U4 U6 N4bp2l1 N4bp2l2 Pds5b
chr8:129500001-130000000	5.06	AC115706.1 U1 Pard3
chr10:94500001-95000000	5.06	Cradd Socs2 5730420D15Rik Mrpl42 Ube2n
chr13:109000001-109500000	5.06	Elovl7 Gm2822 Depdc1b Pde4d Gm9000
chr13:115500001-116000000	5.06	Mocs2 Itga2 Itga1 Pelo U6
chr3:135500001-136000000	4.89	Slc39a8 Bank1
chr6:146500001-147000000	4.89	4933424B01Rik Fgfr1op2 Tm7sf3 Med21 4930479D17Rik Stk38l Arntl2 1700023A16Rik Ppfibp1 1700034J05Rik Rep15 Mrps35
chr9:118500001-119000000	4.89	Itga9 Gm2415 Gm16295 Ctdspl Mir26a-1 Vill Plcd1
chr6:99000001-99500000	4.72	Foxp1 Eif4e3 AC152987.1
chr12:116500001-117000000	4.72	Ighv1-59 Gm16900 Gm9232 Ighv1-62-2 Gm9235 Ighv8-9 Ighv1-63 Gm16865 Ighv8-11 Gm16901 Ighv1-67 Gm16708 Ighv8-12 Ighv1-71 Gm16709
chr14:105500001-106000000	4.72	Rbm26 Gm17066 U6 Ndfip2 U6 4930449E01Rik 9330188P03Rik
chr6:145000001-145500000	4.55	Bcat1 Gm15687 Lrmp Casc1 Gm15543 Lyrm5 Kras Gm15706 7SK 2010013B24Rik Ifltd1 SNORA17 1700073E17Rik Gm15499 SNORA17
chr6:148000001-148500000	4.55	Far2 Gm16583 Ergic2 Gm17216 Tmtc1 Rps4y2
chr7:151500001-152000000	4.55	Shank2 Gm14372 Cttn Gm14376 Ppfia1 Gm10574 Fadd Ano1 Gm10152 AC149593.1
chr13:110000001-110500000	4.55	Pde4d Mir582
chr1:166500001-167000000	4.38	Dpt Xcl1 AC133891.1
chr3:148500001-149000000	4.38	Lphn2 U6 Gm9912 Gm10287
chr7:152000001-152500000	4.38	Fgf3 Fgf4 Gm17685 Fgf15 AC161763.1 Oraov1 Ccnd1 Tpcn2 Mrgprf
chr11:109000001-109500000	4.22	E030025P04Rik Rgs9 Gm11696 Gna13 9930022D16Rik Amz2 Gm15642 Slc16a6 mmu-mir-1194 Arsg U6 Wipi1 Gm11685
chr4:120500001-121000000	3.88	Nfyc AL606904.1 Rims3 U6 Dem1 Zfp69 Smap2 Col9a2 Zmpste24 SNORA18 U1 Tmco2 7SK Rlf Gm12888
chr14:119000001-119500000	3.88	Abcc4 SNORA17 Cldn10 n-R5s51 Dzip1 Dnajc3 Uggt2 Gm16835
chr17:84500001-85000000	3.88	Zfp36l2 Thada U6 U6 Plekhh2

trans interactions from Rag1/2 viewpoint in Thymus

bin	z-score	genes in bin
chr12:115500001-116000000	20.74	Ighv3-8 Ighv12-3 Ighv1-5 Ighv10-3 Ighv1-7 Ighv15-2 Ighv1-9 Ighv1-12 Gm17686 Gm16857 Gm16858 Ighv1-18 Ighv1-19 Ighv1-20 Gm16860
chr12:116500001-117000000	12.48	Ighv1-59 Ighv1-62-2 Ighv8-9 Ighv1-63 Gm16865 Ighv8-11 Gm16901 Ighv1-67 Gm16708 Ighv8-12 Ighv1-71 Gm16709
chr12:117000001-117500000	10.29	Ighv1-73 Ighv8-14 Ighv1-83 Ighv1-84 Ighv1-85 Zfp386 Gm17626 Vipr2 U6 Wdr60
chr6:134500001-135000000	9.61	Lrp6 Mansc1 Loh12cr1 Dusp16 Crebl2 Gpr19 Cdkn1b Apold1 Ddx47
chr12:116000001-116500000	9.27	Ighv1-23 Ighv1-24 Ighv1-42 Ighv1-43 Gm16966 Gm16830 Ighv8-5 Gm16829 Gm16828 AB069917 Ighv8-6 Ighv1-54 Gm16792 Gm16791
chr14:54500001-55000000	9.11	Trdv1 Trdv2-1 Gm17015 Trdv4 Trdd1 7SK Trdd2 Trdj1 Trdj2 Trdv5 Gm17363 Gm17534 Traj59 Traj58 Traj5 Gm16915 Gm16916 Traj2 Traj1 Trac Dad1 Abhd4 Olfr49 Oxa1l Slc7a7
chr12:115000001-115500000	8.77	Ighv11-2 Ighv14-3 Ighv9-2 Ighv9-3 Gm16842 Gm16841 Ighv3-3 Gm16839
chr1:179000001-179500000	8.60	Akt3 Gm17407 Zfp238
chr4:144500001-145000000	8.26	Dhrs3 Vps13d Vps13d Tnfrsf1b Tnfrsf8
chr3:135000001-135500000	7.59	Nhedc2 Nhedc1 Cisd2 4930539J05Rik Ube2d3 Manba Nfkb1 Gm9799 Slc39a8
chr14:122000001-122500000	7.08	Dock9 Ubac2 Gpr18 Gpr183 Timm8a2
chr6:67000001-67500000	6.75	E230016M11Rik A430010J10Rik Serbp1 Il12rb2 Il23r Tacstd2
chr10:122000001-122500000	6.75	Ppm1h Mirlet7i Mon2
chr14:16500001-17000000	6.75	
chr3:142000001-142500000	6.58	Pdlim5 Gbp5 Gbp7 Gbp3 Gbp1 Gbp2 Ccbl2 Gm15540 Gtf2b U6 Pkn2 SNORA17
chr3:143500001-144000000	6.58	Lmo4

chr18:89000001-89500000	6.58	Socs6 Rttn Cd226 Dok6
chr10:96000001-96500000	6.41	Btg1 AC152946.1
chr10:92500001-93000000	6.24	4930485B16Rik Cdk17 Mir1931 Elk3 Lta4h Hal Amdhd1
chr16:48500001-49000000	6.24	Morc1 Trat1 Retnlb Retnla Retnlg Dzip3 U6 C330027C09Rik
chr12:114500001-115000000	6.07	Ighg2c Ighg Ighg1 Ighv2-4
chr14:79500001-80000000	6.07	1300010F03Rik Zfp957 1190002H23Rik Naa16 AC124745.1 Mtrf1 Kbtbd7 Gm5465 Wbp4 Elf1 Sugt1
chr3:52000001-52500000	5.90	Foxo1 RP24-337A16.1 Gm10293
chr13:108500001-109000000	5.90	Zswim6 AC165250.1 2810008M24Rik Ndufaf2 Ercc8
chr10:98500001-99000000	5.73	Poc1b Galnt4 Phxr2 Gm16239 Dusp6 B530045E10Rik Gad1-ps
chr1:195000001-195500000	5.56	A130010J15Rik Traf3ip3 Gm15872 4930570N18Rik 1600010F14Rik Hsd11b1 G0s2 Lamb3 Camk1g 4631405K08Rik Mir205
chr16:49500001-50000000	5.56	Ift57 Gm15518 Gm16619 Cd47
chr3:144000001-144500000	5.23	Hs2st1 Sep15 SNORA2 Sh3glb1 Clca1 Clca2 Clca4
chr18:56500001-57000000	5.23	Gramd3 Aldh7a1 Phax 1700065I17Rik Lmnb1 March3 Gm15345
chr6:145000001-145500000	4.72	Bcat1 Gm15687 Lrmp Casc1 Gm15543 Lyrm5 Kras Gm15706 7SK 2010013B24Rik Ifltd1 SNORA17 1700073E17Rik Gm15499 SNORA17
chr16:91000001-91500000	4.55	Synj1 4930404I05Rik Gcfc1 4931406G06Rik 4932438H23Rik Gm9881 Olig2 Olig1 Gm15966 U4 Ifnar2 Il10rb A930006K02Rik Ifnar1
chr6:135000001-135500000	4.38	Gprc5a Gprc5d Hebp1 SNORA17 8430419L09Rik Gsg1 Pbp2 Emp1
chr10:117000001-117500000	4.38	Cpm U6 Mdm2 Slc35e3 Nup107 Rap1b
chr5:150000001-150500000	4.22	Uspl1 AC122546.1 Alox5ap n-R5s180 BC028471 6330406I15Rik Gm20488 4930588N13Rik Gm15997 Wdr95 Hsph1 B3galtl
chr17:80000001-80500000	4.22	Fam82a1 4921513D11Rik Cyp1b1 Atl2 Hnrpll U6
chr6:67500001-68000000	4.22	Igkv2-137 Igkv1-135 Igkv17-134 Igkv1-133 Igkv1-132 Igkv1-131 Igkv14-130 SNORA17 SNORA17 Igkv9-129 Igkv17-127 Igkv14-126 SNORA17 Igkv11-125 Igkv9-124 Igkv9-123 Igkv1-122 Igkv17-121 Igkv9-120
chr3:75000001-75500000	3.88	Serpini2 Pdcd10 Serpini1
chr14:105500001-106000000	3.88	Rbm26 Gm17066 U6 Ndfip2 U6 4930449E01Rik 9330188P03Rik

Appendix B

Summary of z-scores for all 0.5Mb bins that showed a significant (z-score > 3.5) trans interaction with at least one of the seven viewpoints in at least one cell type.

	Rag-/- pro-B							Rag/81X pre-B							Thymus						
Bin	Igh	Igk	Igl	Pax5	Foxo1	Il7r	Rag1/2	Igh	Igk	Igl	Pax5	Foxo1	Il7r	Rag1/2	Igh	Igk	Igl	Pax5	Foxo1	Il7r	Rag1/2
chr4:44500001-45000000	15.33	1.63	3.04	na	19.67	10.57	0.67	12.11	13.46	10.76	na	28.05	16.86	3.20	1.09	1.16	1.01	na	1.01	3.37	1.35
chr11:44500001-45000000	13.77	2.09	1.35	2.47	7.31	8.88	0.22	17.25	15.46	4.72	3.04	25.57	14.67	2.53	0.72	0.41	0.79	3.37	0.67	1.18	0.84
chr16:92500001-93000000	12.72	0.95	na	4.80	4.83	2.36	1.35	8.29	4.57	na	5.82	7.31	3.37	2.87	3.76	0.67	na	0.84	5.90	0.17	2.70
chr8:129000001-129500000	12.45	0.49	2.40	4.72	8.88	1.80	3.37	5.21	6.66	2.36	7.84	9.95	2.70	8.09	1.81	0.94	1.24	0.51	4.22	0.67	2.36
chr16:93000001-93500000	12.26	0.69	na	1.69	7.31	2.02	1.57	7.91	3.80	na	7.59	0.67	2.53	1.52	3.86	0.71	na	1.18	7.08	0.51	3.37
chr3:52000001-52500000	11.46	2.30	1.69	14.20	na	8.54	2.92	8.07	13.84	8.04	24.03	na	16.19	2.70	1.70	0.56	0.79	0.34	na	1.69	5.90
chr13:112500001-113000000	10.29	0.63	1.50	3.45	7.42	2.47	2.02	6.32	7.14	4.64	9.61	9.39	4.05	6.58	2.57	0.54	0.90	1.18	5.90	0.67	na
chr5:136500001-137000000	9.58	0.83	0.82	2.02	2.59	0.56	0.45	6.80	5.76	4.24	9.44	11.30	1.35	2.02	1.09	1.22	0.67	0.67	5.73	0.84	2.19
chr10:118000001-118500000	9.56	1.38	1.39	1.72	3.37	1.46	1.35	5.17	5.45	4.44	8.94	6.91	2.70	3.04	2.54	0.45	0.56	0.17	3.37	0.84	na
chr9:61000001-61500000	8.75	0.74	2.47	7.34	11.02	1.91	0.00	3.97	4.46	3.40	8.77	7.14	2.53	0.00	0.30	1.21	0.56	0.84	4.55	0.67	0.51
chr1:38500001-39000000	8.72	0.82	0.00	3.30	5.28	2.92	0.67	10.47	6.38	3.37	5.73	10.17	3.04	1.69	3.16	0.92	0.22	0.17	5.40	0.34	0.67
chr2:166000001-166500000	8.58	1.24	0.56	2.36	3.37	0.34	na	4.38	5.01	2.50	9.27	8.21	3.20	na	0.18	1.37	1.12	0.51	1.35	1.01	na
chr6:99000001-99500000	8.45	na	1.24	2.32	3.48	1.69	2.02	8.68	na	2.50	3.20	11.97	5.73	4.72	2.42	na	1.01	0.84	7.76	0.34	2.19
chr5:149500001-150000000	8.42	0.43	1.27	2.10	2.47	0.90	5.17	5.23	5.54	3.23	7.34	6.46	2.70	7.59	1.28	0.57	1.01	0.51	3.37	0.34	3.04
chr16:94500001-95000000	8.21	0.33	na	1.35	5.73	2.47	2.70	6.48	3.97	na	5.31	5.79	2.02	3.20	2.83	0.38	na	0.00	3.37	0.34	2.19
chr16:95500001-96000000	8.11	0.54	na	2.89	3.26	2.36	1.12	7.18	5.46	na	6.75	6.63	5.90	2.70	2.51	0.70	na	2.87	4.72	0.67	2.36
chr5:137000001-137500000	7.87	0.54	1.46	2.51	3.37	0.67	0.45	6.69	5.60	4.13	6.83	8.94	2.19	3.20	1.17	1.05	1.01	0.67	5.06	0.51	1.18
chr6:120500001-121000000	7.85	na	0.45	1.87	2.36	2.47	2.25	4.43	na	4.61	2.70	5.56	3.20	2.36	0.61	na	1.12	0.84	2.19	0.51	1.52
chr8:125000001-125500000	7.72	1.21	1.61	2.29	2.70	0.90	1.35	5.32	5.49	5.00	9.11	9.33	3.20	2.70	0.60	1.40	1.12	0.67	5.40	0.84	1.18
chr1:38000001-38500000	7.64	0.35	3.30	2.25	3.37	2.92	0.67	10.30	6.10	5.76	6.49	9.05	8.94	1.52	3.36	0.84	0.56	1.35	5.56	0.34	0.34
chr4:149500001-150000000	7.63	0.65	0.45	na	2.47	0.56	2.92	4.69	2.84	2.00	na	2.70	2.02	1.85	1.54	0.84	0.45	na	3.04	0.17	2.36
chr11:117500001-118000000	7.55	0.99	0.75	2.14	1.46	0.67	1.57	4.30	5.60	4.24	9.02	6.35	2.53	3.37	0.25	1.15	0.90	0.67	5.73	0.51	1.18
chr19:58000001-58500000	7.52	2.83	2.02	1.69	3.37	5.51	1.80	4.31	3.49	2.70	5.48	3.15	6.24	1.52	3.14	0.86	0.90	2.36	3.37	4.38	0.84
chr15:80500001-81000000	7.22	0.53	2.62	5.43	6.97	na	0.67	4.92	6.69	7.87	16.44	11.86	na	1.52	1.75	0.79	0.67	0.67	10.45	na	1.69
chr4:134500001-135000000	7.21	0.74	0.07	na	2.70	0.67	0.90	4.97	4.29	3.04	na	7.25	3.20	3.20	0.84	1.08	1.12	na	2.70	0.67	0.34
chr13:37500001-38000000	7.13	0.49	2.02	2.36	10.34	3.37	0.22	3.46	6.96	3.15	10.12	11.47	10.12	1.52	0.99	0.88	1.01	0.67	6.24	0.00	3.04
chr4:149000001-149500000	7.04	1.39	0.52	na	2.70	0.45	1.35	4.50	3.12	3.37	na	4.72	1.01	2.19	1.04	1.27	0.90	na	3.04	0.51	1.35
chr3:130500001-131000000	7.02	1.00	0.82	0.86	na	0.90	2.47	3.03	1.71	1.91	2.61	na	1.35	2.87	1.01	1.09	1.12	1.01	na	0.67	2.70
chr11:77000001-77500000	7.01	0.67	1.65	1.01	2.02	1.35	0.22	4.25	5.17	2.98	8.26	5.56	2.53	1.01	0.37	1.32	0.90	0.34	3.20	0.17	0.51
chr4:133000001-133500000	6.97	1.00	1.12	na	3.04	0.56	0.45	4.27	5.62	4.52	na	7.53	1.85	2.19	0.58	1.31	0.90	na	5.06	0.67	1.52
chr11:78500001-79000000	6.95	0.39	2.21	7.08	0.67	1.35	1.12	3.15	4.12	4.33	10.54	2.70	3.88	1.01	0.39	1.10	1.01	1.01	3.37	0.51	1.52
chr17:86500001-87000000	6.92	0.61	0.79	3.11	5.06	1.69	2.25	5.01	4.26	2.14	2.70	8.49	3.20	3.20	1.44	0.42	0.34	1.01	3.04	0.84	2.70
chr3:136000001-136500000	6.75	0.54	0.30	0.30	na	0.45	2.02	4.73	3.31	0.73	1.94	na	0.67	6.07	3.48	1.18	0.67	0.51	na	0.51	3.04

chr15:80000001-80500000	6.60	0.87	2.06	2.70	3.37	na	0.45	4.31	5.07	6.35	13.15	8.09	na	0.84	1.35	1.23	1.12	0.84	6.75	na	0.84
chr9:116000001-116500000	6.56	0.92	2.17	2.25	3.26	1.80	3.37	4.24	3.87	3.23	3.37	5.96	3.04	6.41	2.37	0.78	0.79	0.34	4.72	0.67	2.36
chr13:52000001-52500000	6.53	0.57	2.32	3.37	4.83	2.36	0.22	3.36	5.16	3.18	4.72	5.17	3.04	2.02	0.47	0.99	0.34	1.35	3.04	0.67	1.35
chr8:125500001-126000000	6.49	1.33	1.01	3.37	1.91	1.12	0.45	3.44	3.30	4.78	6.66	6.46	3.20	1.52	0.63	1.32	1.01	0.34	2.87	0.51	0.34
chr6:129000001-129500000	6.48	na	0.60	0.79	2.59	1.01	0.67	4.26	na	2.30	2.53	2.92	1.85	7.25	4.63	na	0.67	0.84	2.53	0.34	2.02
chr4:134000001-134500000	6.43	0.86	0.71	na	3.04	0.56	0.90	4.04	4.64	3.43	na	6.75	2.02	1.18	0.86	1.11	1.01	na	2.53	0.67	1.69
chr11:118000001-118500000	6.40	1.05	0.90	2.59	2.25	0.56	0.45	3.92	3.49	2.81	7.25	5.85	1.85	1.18	0.40	1.24	0.56	0.67	1.85	0.34	1.18
chr1:182000001-182500000	6.37	0.93	1.05	0.86	1.12	0.34	0.45	3.33	2.84	2.36	2.11	5.34	1.52	2.70	1.12	0.96	1.01	0.17	5.73	0.67	3.20
chr8:123000001-123500000	6.35	0.75	1.12	2.96	2.36	0.67	0.67	3.87	4.34	3.46	9.36	5.85	2.19	2.87	0.35	1.14	0.67	0.67	3.04	0.67	3.37
chr1:179000001-179500000	6.33	0.92	0.34	0.41	2.59	0.67	3.37	3.70	2.62	0.42	2.28	3.37	1.01	3.37	5.12	0.87	0.56	0.67	1.52	0.67	8.60
chr9:66000001-66500000	6.31	0.26	1.57	2.36	3.37	1.91	0.45	4.36	5.02	4.95	10.71	7.87	2.70	2.53	0.82	0.99	0.67	0.34	4.89	0.34	0.17
chr17:29000001-29500000	6.31	0.75	2.02	1.35	6.41	1.12	0.22	3.90	8.18	7.76	14.42	8.77	5.73	2.02	0.80	1.04	0.90	0.51	4.89	0.67	0.17
chr6:87000001-87500000	6.21	na	0.64	3.37	2.02	1.01	0.67	5.30	na	4.95	11.13	8.60	3.04	1.01	1.49	na	0.90	0.17	2.70	0.67	3.20
chr13:102500001-103000000	6.21	1.09	2.25	2.02	3.15	1.91	2.70	5.03	3.43	2.28	6.91	4.78	2.53	1.69	2.48	0.38	0.45	0.17	1.52	1.18	1.69
chr19:33000001-33500000	6.17	0.96	3.04	3.37	2.02	8.32	0.90	3.03	7.38	6.86	7.67	11.24	13.15	0.84	2.06	0.42	0.79	1.01	5.56	1.85	2.02
chr9:121500001-122000000	6.10	1.05	1.01	2.81	1.91	1.35	2.70	3.11	1.76	1.52	3.12	3.32	1.85	2.70	1.19	0.22	1.12	0.84	1.85	0.84	2.02
chr11:86000001-86500000	6.06	0.66	0.97	3.45	3.48	2.25	1.12	4.66	5.35	6.44	9.61	7.81	4.38	1.01	0.16	1.11	1.12	0.84	6.58	0.51	1.18
chr7:139500001-140000000	6.05	0.36	0.41	1.12	2.81	0.79	3.15	5.19	3.40	2.25	2.87	6.80	1.85	3.04	1.00	0.50	0.34	0.67	1.69	0.67	0.67
chr11:86500001-87000000	5.94	0.67	1.31	1.35	3.04	1.46	0.67	3.37	6.00	5.06	9.61	6.24	3.88	2.02	0.35	0.92	0.90	0.51	4.89	0.51	1.18
chr17:30000001-30500000	5.94	0.72	3.11	6.18	2.70	2.14	0.45	4.83	4.37	6.15	8.43	7.64	2.02	1.18	2.27	0.95	0.79	1.01	4.22	0.17	0.34
chr4:135500001-136000000	5.93	1.02	0.56	na	3.04	0.45	0.67	3.09	3.73	5.06	na	8.49	2.19	3.20	0.46	0.99	0.67	na	2.02	0.17	1.69
chr14:122000001-122500000	5.89	0.23	0.45	2.21	2.36	0.79	3.37	4.51	4.10	1.74	4.47	6.35	3.04	8.26	2.85	0.25	0.67	1.18	2.87	0.84	7.08
chr9:61500001-62000000	5.86	0.70	2.59	7.12	5.73	2.36	0.67	2.97	3.35	2.92	8.18	4.50	5.23	0.84	0.57	1.07	1.12	0.67	1.85	1.18	1.01
chr1:133500001-134000000	5.75	1.04	0.19	2.25	2.70	0.79	0.45	4.52	3.46	2.42	10.03	2.02	1.35	1.85	1.24	0.56	1.01	0.51	2.53	0.34	2.36
chr1:166500001-167000000	5.70	0.58	0.19	0.79	1.24	1.46	2.47	6.89	8.34	2.19	7.93	10.12	2.36	4.38	2.77	0.45	0.79	0.34	1.52	0.17	1.18
chr11:100500001-101000000	5.69	0.85	0.94	2.85	2.59	0.79	0.90	2.69	2.98	3.68	5.73	6.52	2.19	1.01	0.10	1.33	1.24	0.67	3.04	0.51	1.01
chr7:108000001-108500000	5.68	0.68	1.54	3.04	3.37	2.36	0.67	4.03	5.02	3.37	10.12	5.34	3.20	3.20	1.49	0.92	0.56	0.51	2.36	1.18	1.18
chr2:167500001-168000000	5.64	1.35	0.19	1.61	0.67	0.56	na	4.62	4.48	2.28	9.02	8.77	1.01	na	0.43	1.34	1.01	0.34	1.35	0.00	na
chr17:84500001-85000000	5.61	0.28	1.61	3.04	2.70	2.14	1.12	4.23	3.34	2.87	6.49	5.79	3.37	3.88	2.16	0.48	0.56	1.01	5.56	0.84	2.70
chr16:24000001-24500000	5.55	0.58	na	1.69	8.21	3.37	2.47	4.07	4.78	na	6.49	6.07	6.91	1.52	1.83	0.76	na	0.34	10.12	0.51	1.35
chr1:193000001-193500000	5.41	0.76	0.45	0.97	1.35	0.56	2.70	4.42	2.98	2.11	3.96	4.50	1.35	2.36	1.58	0.15	0.67	0.84	2.19	0.34	2.70
chr6:87500001-88000000	5.34	na	1.09	1.57	2.36	1.46	0.45	3.39	na	3.04	6.83	2.98	1.52	1.69	0.85	na	0.90	0.67	2.53	0.17	0.67
chr3:103500001-104000000	5.32	0.33	0.90	1.35	na	0.79	0.67	2.49	1.93	1.94	3.12	na	1.18	2.87	1.28	0.81	1.01	0.17	na	0.67	1.85
chr9:118500001-119000000	5.30	0.85	1.54	2.02	3.15	1.01	0.90	3.76	2.47	1.91	4.55	3.37	1.52	4.89	2.09	0.47	0.79	0.51	3.37	0.17	2.02
chr4:133500001-134000000	5.28	1.42	0.75	na	2.59	0.45	0.45	3.09	3.32	3.06	na	5.90	2.53	1.35	0.30	1.14	0.90	na	4.05	0.67	1.18
chr16:32000001-32500000	5.28	0.56	na	3.37	6.18	2.70	1.12	4.69	4.78	na	13.15	5.73	6.41	1.69	1.23	1.22	na	0.67	6.24	0.51	1.01
chr2:166500001-167000000	5.23	1.62	0.94	1.65	3.37	0.45	na	3.32	3.54	2.39	8.94	7.36	2.19	na	0.33	1.23	1.12	1.01	2.53	0.67	na
chr11:120000001-120500000	5.17	1.36	0.90	0.79	3.48	0.56	0.22	2.01	1.38	3.37	6.58	3.09	1.18	1.18	0.15	1.32	1.01	1.18	0.67	0.51	0.51
chr1:89500001-90000000	5.15	1.01	0.90	3.04	2.70	2.14	0.45	3.48	2.71	3.01	3.37	4.16	2.53	2.36	0.56	1.21	1.01	0.84	1.52	0.51	1.01
chr17:29500001-30000000	5.12	0.70	1.54	4.38	1.69	0.56	0.45	3.15	4.75	4.13	8.77	5.68	3.04	2.19	0.55	1.20	0.79	1.18	1.85	0.67	0.34
chr18:68000001-68500000	5.10	0.44	2.70	3.45	2.70	1.01	0.90	2.47	2.88	1.49	4.13	3.82	3.37	2.19	1.67	0.82	0.67	0.84	5.56	0.34	3.37
chr6:145500001-146000000	5.06	na	0.52	0.49	1.01	1.01	2.25	4.97	na	2.33	3.20	6.46	2.19	2.53	2.47	na	0.67	1.52	1.85	0.67	2.02
chr4:132500001-133000000	5.05	1.38	1.16	na	1.35	1.01	1.35	3.58	3.48	3.20	na	8.26	1.35	2.70	0.31	1.37	0.79	na	4.89	1.01	1.69
chr8:127500001-128000000	5.01	0.48	0.64	3.45	2.36	0.11	1.12	3.05	2.77	1.24	5.06	4.10	0.51	6.07	1.16	0.79	1.12	0.51	1.52	0.34	2.19
chr7:121500001-122000000	4.96	0.23	0.75	2.02	2.25	0.67	2.92	2.70	2.59	1.80	2.95	2.47	1.35	3.04	3.23	0.02	1.12	0.51	1.18	0.17	3.37
chr17:31000001-31500000	4.95	0.82	2.40	1.69	3.26	1.12	0.90	3.24	5.07	5.87	10.62	6.18	3.37	0.84	0.36	1.32	0.45	0.67	3.20	0.51	0.34
chr1:173500001-174000000	4.93	0.83	0.49	0.34	1.24	0.79	1.12	4.89	4.52	1.91	4.22	3.43	2.19	2.87	1.20	0.56	0.90	0.51	4.55	0.34	3.20
chr4:135000001-135500000	4.88	1.19	0.41	na	2.25	1.01	0.45	3.86	3.48	1.94	na	2.02	1.85	1.01	0.68	1.07	0.90	na	2.70	0.51	1.01
chr13:54000001-54500000	4.87	0.15	2.62	2.70	2.70	2.59	0.22	2.60	3.08	6.21	5.23	2.70	3.04	1.85	0.43	0.13	0.45	2.36	0.51	0.34	0.84

chr17:32000001-32500000	4.86	0.78	3.00	3.00	2.92	1.35	0.67	2.69	3.13	3.74	7.84	3.37	2.02	0.84	0.59	1.04	0.67	0.17	2.02	0.34	0.67
chr11:116000001-116500000	4.86	1.33	0.75	1.12	2.25	0.00	0.67	3.31	3.44	3.32	8.94	3.04	2.53	1.35	0.31	1.50	1.01	0.67	3.37	0.84	0.17
chr3:51500001-52000000	4.83	0.35	1.05	2.70	na	3.37	0.22	3.45	3.49	2.02	8.35	na	5.90	0.84	0.75	0.97	0.67	0.51	na	0.67	2.36
chr10:94500001-95000000	4.80	0.39	0.34	1.46	2.70	1.01	3.37	3.17	4.36	1.80	5.56	9.16	3.37	5.06	1.30	0.11	0.67	0.51	0.17	0.67	1.69
chr3:135500001-136000000	4.79	0.47	0.52	0.11	na	0.34	1.35	3.04	2.25	1.74	1.18	na	0.67	4.89	2.55	0.43	0.56	0.17	na	1.01	1.35
chr6:145000001-145500000	4.77	na	0.71	0.52	1.46	0.79	3.15	4.04	na	2.75	1.85	4.05	1.35	4.55	2.08	na	0.67	0.84	2.70	0.67	4.72
chr13:41500001-42000000	4.73	0.62	1.35	3.19	5.51	1.35	0.45	4.74	7.67	4.95	7.84	10.23	9.44	2.87	0.82	0.14	0.11	1.35	2.36	2.36	1.01
chr16:30000001-30500000	4.72	0.33	na	1.35	5.40	2.70	1.12	4.06	6.23	na	9.53	8.88	5.90	0.84	1.41	0.56	na	0.17	1.35	0.67	0.84
chr16:33500001-34000000	4.71	0.16	na	2.70	3.04	1.35	0.67	4.43	4.05	na	5.73	5.85	5.23	1.01	2.41	0.67	na	1.52	2.53	1.69	2.02
chr16:32500001-33000000	4.68	0.73	na	3.11	3.48	2.59	0.22	4.31	4.29	na	11.04	6.13	3.37	2.02	1.83	1.00	na	0.51	3.37	0.67	1.35
chr6:128500001-129000000	4.67	na	0.37	1.50	1.57	1.12	2.92	5.28	na	2.89	3.04	4.44	3.04	2.70	3.46	na	0.79	0.67	2.19	0.34	2.36
chr17:87000001-87500000	4.66	0.53	0.56	1.80	2.36	0.22	1.35	3.23	2.72	1.18	2.70	3.04	1.69	2.53	2.66	0.19	0.45	0.67	5.40	0.84	1.69
chr4:132000001-132500000	4.65	1.29	1.12	na	1.91	0.22	0.67	2.71	3.20	2.42	na	6.41	1.35	1.52	0.31	1.24	1.12	na	2.36	0.17	1.52
chr13:102000001-102500000	4.59	0.64	0.67	2.21	2.70	0.67	0.45	3.40	3.08	2.53	2.87	2.87	2.02	1.69	4.09	0.33	0.90	0.51	2.70	0.84	1.69
chr10:92500001-93000000	4.53	0.30	0.37	1.42	0.90	0.90	2.47	2.57	3.07	2.25	3.20	5.17	1.52	0.84	0.94	0.83	0.79	0.67	3.37	0.17	6.24
chr14:65000001-65500000	4.43	0.15	1.31	2.40	3.26	0.90	1.57	3.32	1.91	2.50	3.79	4.10	1.69	1.01	0.91	0.55	0.22	0.67	3.04	0.51	1.35
chr1:166000001-166500000	4.35	0.74	0.49	0.67	0.90	0.22	2.02	3.35	4.12	3.15	7.08	6.80	1.69	2.36	2.52	0.29	0.79	0.67	2.36	0.67	2.70
chr13:103000001-103500000	4.29	0.35	1.27	0.82	2.25	1.46	3.15	4.66	4.52	2.30	5.40	5.51	2.53	3.04	1.96	0.40	0.56	0.51	1.18	0.17	1.35
chr16:96500001-97000000	4.26	1.33	na	1.35	2.70	1.57	2.02	3.34	2.31	na	2.70	2.98	0.67	2.53	2.35	0.41	na	1.35	1.18	1.52	1.52
chr16:91000001-91500000	4.10	0.23	na	2.29	2.14	1.24	2.02	4.16	2.76	na	3.04	2.98	2.19	3.04	2.24	0.32	na	3.37	1.18	1.01	4.55
chr16:30500001-31000000	4.09	0.67	na	5.47	4.83	2.02	0.90	4.43	5.75	na	9.70	8.38	5.40	2.02	1.41	0.99	na	0.17	1.35	0.67	0.34
chr9:122000001-122500000	4.08	0.39	1.05	2.06	0.90	0.22	1.57	2.07	0.67	0.42	1.85	1.69	0.51	1.35	1.50	0.33	0.45	0.34	0.67	0.34	1.69
chr7:106000001-106500000	4.05	0.92	0.82	0.97	1.80	1.57	0.67	2.96	1.59	1.85	5.23	1.91	1.35	0.84	0.90	0.86	0.67	0.84	2.02	0.17	0.51
chr2:163000001-163500000	3.97	1.21	0.79	0.52	1.24	0.22	na	2.83	0.98	0.98	1.26	2.81	0.17	na	0.66	0.69	0.90	0.17	0.51	0.51	na
chr4:32000001-32500000	3.14	0.71	2.06	na	2.70	1.69	0.22	19.82	12.00	4.89	na	20.52	14.84	3.20	1.41	0.59	0.56	na	4.72	1.69	1.69
chr4:32500001-33000000	1.92	0.49	2.10	na	2.36	2.92	0.90	18.89	7.97	2.11	na	12.98	10.29	1.85	1.38	0.45	0.56	na	4.55	2.02	3.04
chr11:45000001-45500000	2.60	1.26	2.25	0.82	2.02	2.02	0.90	13.28	14.62	6.94	6.41	18.72	14.50	2.70	0.54	0.93	2.36	1.69	0.34	1.52	0.17
chr4:33000001-33500000	0.72	0.12	0.41	na	1.35	3.15	1.35	7.04	3.74	2.56	na	5.28	3.37	1.18	1.78	0.19	0.90	na	3.37	1.52	2.87
chr11:44000001-44500000	3.04	0.55	1.31	1.05	3.04	3.26	0.67	5.85	5.47	3.26	1.35	6.30	7.42	0.67	0.47	0.10	0.34	3.04	1.52	2.19	0.67
chr6:68500001-69000000	1.22	na	1.95	2.36	1.69	2.70	1.35	5.74	na	9.36	15.85	16.92	13.49	5.40	0.25	na	0.67	1.01	0.51	1.69	0.84
chr2:45000001-45500000	2.34	2.47	1.35	0.79	2.36	2.02	na	5.67	7.42	2.67	2.70	7.31	5.56	na	1.84	0.71	0.22	0.84	0.51	2.19	na
chr18:55000001-55500000	2.41	1.83	3.37	1.80	4.61	6.75	0.22	5.59	7.12	5.56	9.53	5.56	8.09	2.87	2.76	1.26	1.01	0.51	1.52	3.04	2.02
chr16:91500001-92000000	3.28	0.40	na	2.10	3.04	1.91	1.35	5.52	2.93	na	5.82	3.15	2.87	2.70	2.18	0.54	na	0.67	3.04	0.34	1.85
chr16:19000001-19500000	2.83	2.83	na	3.37	8.99	9.44	1.35	5.51	10.18	na	14.25	12.08	17.03	3.04	0.12	1.57	na	1.85	0.17	4.55	1.01
chr11:45500001-46000000	0.72	0.57	0.67	0.30	0.79	2.36	0.67	5.51	5.69	2.56	2.95	7.36	10.29	1.18	0.38	0.26	0.45	2.70	0.67	2.36	0.00
chr1:37500001-38000000	2.70	0.55	2.10	3.04	4.95	2.92	0.45	5.36	5.36	4.75	6.91	7.36	6.91	0.67	1.44	1.02	0.34	0.17	4.55	0.67	1.01
chr16:93500001-94000000	3.47	0.82	na	1.50	1.24	0.45	0.67	5.20	3.33	na	5.73	2.98	2.19	1.01	2.43	0.73	na	0.84	2.19	1.01	1.52
chr1:136500001-137000000	2.80	1.05	0.52	1.46	2.14	0.56	0.90	5.13	3.23	3.37	9.78	3.15	1.69	0.67	1.34	1.13	0.56	0.84	1.85	0.67	0.67
chr13:44000001-44500000	2.41	0.10	3.26	5.77	1.35	2.36	0.45	4.81	6.76	4.86	10.79	9.78	7.42	1.35	1.16	0.63	0.45	0.17	7.08	0.00	1.01
chr16:96000001-96500000	2.80	0.37	na	1.50	1.46	0.79	1.12	4.80	3.30	na	4.30	4.61	0.84	3.04	0.99	1.17	na	0.51	3.37	1.01	2.87
chr6:69000001-69500000	0.92	na	1.99	1.05	1.24	2.47	2.47	4.78	na	9.25	16.27	15.96	12.82	3.04	0.29	na	0.45	1.35	0.34	0.84	0.17
chr9:70500001-71000000	3.18	0.49	2.44	1.35	2.02	2.36	0.90	4.75	9.16	8.04	13.32	9.78	7.76	2.36	0.49	0.68	0.22	1.01	1.69	0.51	0.17
chr13:103500001-104000000	2.71	0.27	0.82	1.16	1.35	0.67	0.90	4.75	3.21	1.77	3.20	3.48	1.85	2.36	1.37	0.53	0.45	1.18	0.34	0.17	1.52
chr13:93000001-93500000	2.19	0.25	0.41	0.86	1.69	0.67	1.35	4.73	4.48	1.88	3.37	4.95	3.20	2.36	1.79	0.29	0.34	1.18	2.87	0.17	3.37
chr4:59000001-59500000	3.18	0.70	1.27	na	2.25	2.36	0.67	4.56	5.73	3.26	na	8.32	5.90	1.18	1.51	0.26	0.90	na	5.73	1.35	3.37
chr4:45000001-45500000	2.84	0.57	1.42	na	5.62	2.36	0.00	4.55	4.25	4.16	na	6.46	6.91	1.69	0.52	0.30	0.34	na	0.51	0.34	2.02
chr18:54500001-55000000	1.43	1.34	2.55	1.72	2.36	3.15	1.12	4.53	5.59	3.15	4.22	5.62	4.89	2.87	1.46	1.63	2.25	2.53	0.51	1.52	0.67
chr4:45500001-46000000	2.89	0.37	0.90	na	3.37	2.14	0.45	4.49	2.46	2.42	na	7.53	5.23	1.69	0.50	0.53	0.56	na	1.35	0.67	0.51
chr3:143500001-144000000	0.81	0.57	0.94	0.30	na	0.56	2.02	4.44	4.59	2.56	3.37	na	1.35	6.07	3.16	0.29	0.11	0.17	na	0.67	6.58

chr17:4500001-5000000	1.22	0.97	2.29	2.06	3.48	8.54	0.22	4.41	8.25	6.83	6.15	11.13	12.98	2.70	1.11	0.48	1.69	4.55	1.85	2.70	1.18
chr13:44500001-45000000	3.04	0.46	2.21	1.35	3.37	2.47	1.12	4.37	5.09	3.37	9.53	6.46	3.04	1.01	1.58	1.15	0.67	0.84	4.05	0.34	1.18
chr13:93500001-94000000	2.23	0.35	0.19	0.94	1.57	0.79	0.90	4.37	3.96	2.98	5.82	6.01	3.37	1.69	1.52	0.82	0.11	0.51	1.01	0.17	2.36
chr6:70500001-71000000	1.91	na	1.31	2.81	2.70	3.37	3.15	4.36	na	6.44	11.97	12.76	11.80	6.41	1.39	na	0.11	3.04	1.69	3.71	2.70
chr3:95500001-96000000	3.23	0.91	0.45	3.22	na	0.79	0.45	4.35	4.11	3.04	8.77	na	2.19	3.04	0.95	1.15	1.01	0.34	na	0.67	0.84
chr1:156500001-157000000	3.31	0.84	0.60	0.45	1.35	0.45	2.25	4.34	3.00	1.77	2.78	3.99	1.18	2.19	0.32	1.21	0.79	0.67	1.85	0.34	2.53
chr15:81000001-81500000	3.18	0.44	1.87	2.70	3.37	na	0.45	4.32	5.39	6.18	15.09	9.56	na	2.36	1.24	1.10	1.01	0.17	5.56	na	1.35
chr14:62500001-63000000	3.37	0.30	1.87	2.36	2.92	1.46	1.12	4.29	3.22	2.47	5.73	3.43	1.35	2.36	1.75	0.45	0.67	0.84	1.01	0.34	0.84
chr6:146000001-146500000	3.28	na	0.56	0.37	1.24	0.45	0.67	4.29	na	1.24	4.64	3.32	0.67	3.37	2.05	na	0.45	0.51	3.20	0.17	2.87
chr7:135000001-135500000	3.08	1.20	0.79	1.57	2.36	0.34	1.12	4.24	5.33	3.15	7.50	7.03	2.36	2.70	0.33	1.16	0.79	0.17	4.22	0.51	0.84
chr14:77000001-77500000	3.47	0.24	1.05	2.55	4.95	1.35	1.80	4.21	4.24	2.89	6.83	6.63	3.88	2.53	2.08	0.60	0.45	0.84	2.53	0.51	2.02
chr10:117000001-117500000	2.79	0.31	0.56	1.20	1.57	0.45	2.70	4.18	4.63	2.70	6.49	5.90	0.17	1.69	1.74	0.83	1.01	0.51	2.36	0.67	4.38
chr18:35500001-36000000	3.47	0.69	2.36	3.04	3.37	2.92	0.67	4.10	4.41	4.92	11.89	7.93	6.41	1.01	2.23	0.34	0.45	2.19	6.58	1.69	0.67
chr6:68000001-68500000	1.38	na	1.12	1.80	3.48	1.57	1.35	4.09	na	7.87	12.14	16.92	15.18	3.37	0.09	na	1.69	0.84	0.00	0.67	2.70
chr6:52500001-53000000	1.93	na	2.02	3.04	2.70	2.36	0.45	4.05	na	3.85	8.09	6.91	7.08	1.85	0.77	na	1.01	0.67	4.22	1.18	2.36
chr16:20000001-20500000	3.12	0.71	na	3.30	3.15	1.35	0.22	4.05	4.53	na	6.66	4.44	5.90	1.35	1.53	0.07	na	0.17	1.85	2.19	2.53
chr6:148000001-148500000	3.03	na	0.60	0.49	0.79	0.67	2.02	4.01	na	1.12	2.45	1.18	1.01	4.55	1.78	na	0.34	1.01	0.67	0.17	1.69
chr1:134000001-134500000	2.65	1.27	0.86	1.65	1.35	0.22	0.22	3.91	1.87	2.81	7.00	3.37	1.35	1.69	0.27	1.05	0.79	0.17	0.34	0.51	0.34
chr19:45500001-46000000	2.51	0.21	3.30	5.32	4.50	2.36	0.90	3.90	4.83	3.04	11.04	7.14	6.41	0.17	1.04	1.04	0.45	0.51	4.89	0.67	1.35
chr1:135000001-135500000	3.47	1.10	0.97	3.30	2.59	0.67	0.22	3.88	1.85	2.30	7.76	3.15	1.18	1.18	1.19	1.32	1.01	0.17	2.02	0.67	1.01
chr17:30500001-31000000	2.95	0.86	2.06	3.34	3.37	1.24	0.67	3.87	2.68	4.52	9.11	3.26	2.87	0.17	1.38	1.09	1.01	1.01	2.19	0.34	0.51
chr6:98500001-99000000	1.67	na	0.26	0.26	1.01	1.12	1.80	3.85	na	0.65	0.67	1.35	0.84	0.51	1.97	na	1.12	0.51	3.04	1.01	0.84
chr1:133000001-133500000	2.79	0.65	0.52	0.97	2.81	0.45	1.35	3.85	3.45	3.06	7.34	5.23	1.69	2.70	2.38	0.92	0.79	0.51	3.04	0.00	2.53
chr16:29500001-30000000	3.45	0.22	na	2.02	4.95	2.02	0.22	3.82	5.29	na	8.18	7.48	6.91	1.35	1.28	0.49	na	1.01	2.02	1.01	0.34
chr9:71500001-72000000	3.37	0.79	1.69	2.70	7.19	1.69	0.45	3.79	4.79	3.37	7.34	6.58	2.02	3.04	1.75	0.80	0.56	0.34	10.45	0.34	1.52
chr6:86500001-87000000	3.08	na	0.37	2.47	3.37	0.90	0.45	3.79	na	1.26	7.42	6.35	2.02	2.02	1.38	na	1.24	0.17	2.70	0.51	1.52
chr10:116500001-117000000	3.15	0.60	0.41	0.90	1.01	0.56	0.67	3.77	3.37	2.39	5.99	5.51	2.36	1.52	2.36	0.35	0.56	1.01	2.70	0.51	2.02
chr16:31000001-31500000	2.65	0.70	na	2.62	2.02	1.91	0.45	3.74	4.26	na	10.96	5.40	6.75	2.02	1.64	0.62	na	0.67	2.53	1.01	0.67
chr14:79500001-80000000	3.07	0.34	0.86	1.05	3.37	1.46	2.02	3.72	4.47	2.36	4.97	5.90	2.02	2.36	1.37	0.99	0.79	0.51	2.70	0.17	6.07
chr2:30500001-31000000	2.65	1.16	1.09	4.76	1.69	1.12	na	3.72	3.36	4.75	10.71	6.52	2.87	na	0.22	1.27	0.90	0.67	4.05	0.67	na
chr13:113000001-113500000	2.89	0.76	0.64	1.65	1.01	0.90	1.35	3.71	2.37	1.32	3.37	4.10	1.35	2.36	2.13	0.07	1.01	1.01	5.40	0.51	2.36
chr16:92000001-92500000	2.76	0.24	na	1.42	2.92	0.34	0.67	3.70	2.12	na	2.70	2.87	1.35	2.53	2.65	0.10	na	2.36	1.18	0.51	0.67
chr18:55500001-56000000	1.90	1.55	1.95	1.24	2.14	3.04	0.67	3.67	4.93	3.43	3.37	2.70	2.02	2.87	3.36	1.27	0.67	1.18	2.02	2.19	3.04
chr7:129500001-130000000	2.85	0.45	0.60	0.26	0.56	0.56	1.35	3.67	1.81	0.53	1.26	2.98	1.01	1.18	0.62	0.76	0.56	0.67	2.02	0.67	1.01
chr1:136000001-136500000	3.38	1.42	0.52	2.17	0.90	0.34	0.45	3.62	1.62	3.12	8.26	3.04	0.34	1.01	0.62	1.23	0.56	0.84	1.52	0.51	1.18
chr17:31500001-32000000	3.32	0.49	1.57	4.50	4.83	0.67	0.22	3.62	5.22	6.13	10.45	6.01	2.02	1.01	0.63	1.20	0.67	0.84	1.85	0.17	0.17
chr18:35000001-35500000	3.18	0.55	3.00	5.88	4.38	2.70	0.67	3.53	2.72	4.33	7.59	3.04	3.37	1.52	2.25	0.29	0.45	3.37	3.04	1.18	0.67
chr18:89000001-89500000	1.20	2.74	0.41	0.19	0.22	1.24	0.90	1.17	0.84	0.53	0.00	0.28	0.67	2.36	6.86	1.37	0.11	0.67	2.53	1.52	6.58
chr9:112000001-112500000	3.19	2.89	0.79	0.37	1.01	1.35	0.67	1.72	1.87	0.00	0.34	0.11	0.51	3.20	5.52	0.25	0.34	0.84	8.77	0.67	1.35
chr8:130500001-131000000	3.39	1.95	2.51	1.24	1.35	0.90	3.15	2.95	2.22	0.39	2.45	1.69	0.17	3.20	5.43	0.47	0.22	1.18	3.04	0.84	3.04
chr17:51000001-51500000	1.74	1.09	1.24	1.50	2.25	2.36	0.90	1.72	2.51	1.80	2.19	1.18	3.37	1.52	5.23	0.25	0.45	0.51	8.43	0.51	1.52
chr4:144500001-145000000	1.46	1.05	0.52	na	0.34	0.34	2.70	2.80	1.11	0.20	na	0.45	0.34	2.53	5.17	0.67	0.67	na	0.67	0.34	8.26
chr9:94500001-95000000	0.83	1.16	0.22	0.45	0.34	1.01	3.15	1.18	0.63	0.11	0.84	0.11	0.17	1.18	5.02	0.39	0.56	0.34	6.24	0.51	1.01
chr16:76000001-76500000	0.58	1.37	na	0.22	0.56	0.79	1.80	1.63	0.87	na	0.25	0.17	0.84	1.18	4.87	0.43	na	0.51	2.70	1.35	3.37
chr4:6500001-7000000	0.20	0.85	3.11	na	1.46	2.70	0.00	0.50	1.64	1.32	na	0.73	3.04	1.01	4.84	1.00	0.22	na	7.76	2.19	2.70
chr16:76500001-77000000	0.59	0.82	na	0.41	0.67	1.01	0.90	1.51	0.41	na	0.25	0.11	0.51	1.69	4.84	0.94	na	0.34	2.36	3.20	3.04
chr4:97500001-98000000	2.65	1.38	0.64	na	2.47	1.57	3.37	1.68	1.48	0.48	na	0.96	0.51	3.04	4.72	1.00	0.34	na	3.04	0.67	3.37
chr3:142000001-142500000	2.60	0.57	0.86	0.49	na	0.79	3.15	2.57	1.11	0.11	1.01	na	0.51	3.37	4.69	1.19	0.90	0.34	na	0.51	6.58
chr1:145500001-146000000	0.33	1.03	1.24	0.60	0.79	0.67	1.12	1.65	1.12	0.28	0.42	0.28	1.35	2.87	4.54	0.16	0.34	0.67	1.01	0.67	3.37

chr10:96000001-96500000	1.59	2.12	0.67	1.20	1.69	0.67	2.02	2.87	2.85	1.29	2.87	2.92	2.87	5.56	4.40	0.60	0.79	0.84	1.69	0.34	6.41
chr7:65500001-66000000	0.28	1.27	0.30	0.34	1.12	1.12	0.22	0.21	0.48	0.11	0.08	0.51	0.84	1.01	4.36	0.86	0.11	0.17	0.67	1.01	3.20
chr8:130000001-130500000	2.34	1.48	0.79	0.67	0.56	0.90	2.02	2.27	1.74	1.49	1.18	1.07	1.52	2.70	4.35	0.56	0.34	1.01	1.18	0.34	3.37
chr14:105500001-106000000	1.38	0.97	0.41	0.22	0.56	0.11	1.35	1.95	1.71	0.48	0.17	0.62	0.84	4.72	4.28	1.46	0.34	0.34	0.51	1.85	3.88
chr5:63000001-63500000	0.40	0.69	0.67	0.45	0.11	1.12	0.45	0.49	1.43	0.56	1.10	0.28	1.18	1.18	4.27	0.74	0.67	1.01	1.69	0.84	1.85
chr3:60000001-60500000	2.36	1.77	2.55	1.87	na	1.69	1.12	3.38	5.19	2.61	3.12	na	6.75	3.20	4.25	0.45	0.22	0.51	na	1.69	2.87
chr8:84000001-84500000	0.72	1.60	1.24	0.60	0.79	0.45	0.67	1.53	1.98	0.79	0.93	1.07	2.53	0.17	4.18	1.08	0.34	0.67	2.53	2.36	2.70
chr1:178500001-179000000	1.73	0.50	0.82	0.45	0.56	0.56	0.45	1.71	0.61	0.08	0.51	1.07	0.00	3.04	4.17	0.53	0.11	0.67	0.34	0.67	3.04
chr10:122000001-122500000	1.63	0.91	0.52	0.34	0.11	0.56	0.67	1.69	1.13	0.11	0.08	1.18	0.51	2.87	3.88	0.07	0.90	0.67	6.07	0.34	6.75
chr6:143500001-144000000	0.97	na	0.15	0.34	0.34	0.56	1.57	1.41	na	0.45	0.34	0.22	0.17	1.01	3.87	na	0.11	1.01	0.51	0.51	1.18
chr10:129500001-129993255	2.01	3.23	0.97	0.45	0.34	0.45	3.37	2.98	2.11	0.20	0.17	0.90	0.34	1.69	3.85	1.64	0.45	0.84	0.84	0.51	1.85
chr4:87500001-88000000	1.97	1.28	0.41	na	1.35	1.35	0.67	1.65	1.77	0.96	na	2.36	3.20	2.87	3.77	0.59	0.34	na	2.87	1.01	2.70
chr15:50500001-51000000	0.76	2.82	2.02	0.30	0.11	na	1.35	0.09	1.90	0.59	0.84	0.67	na	1.52	3.76	1.54	0.90	0.51	0.84	na	2.70
chr2:139500001-140000000	0.22	0.90	1.01	0.60	0.34	0.67	na	0.20	0.33	0.53	0.59	0.79	0.51	na	3.75	0.35	0.45	1.01	0.51	0.84	na
chr14:103500001-104000000	2.27	0.63	0.52	0.07	0.90	0.45	1.57	2.67	2.58	1.21	1.94	2.02	1.52	3.37	3.68	1.29	0.79	1.01	2.02	1.85	3.04
chr3:135000001-135500000	2.89	0.99	1.05	0.79	na	0.67	1.57	3.48	1.37	0.28	2.53	na	0.84	3.37	3.68	0.07	1.01	0.67	na	0.67	7.59
chr1:97000001-97500000	1.03	1.68	0.19	0.30	0.45	1.12	1.80	2.60	3.18	1.18	0.17	1.24	1.52	6.91	3.67	1.60	0.56	0.84	0.34	0.51	2.53
chr19:50500001-51000000	0.44	4.94	1.12	0.34	0.34	0.79	0.67	0.60	0.21	0.53	0.34	0.67	0.67	0.00	0.53	3.43	3.15	0.34	0.51	1.69	0.67
chr11:111500001-112000000	2.02	4.57	0.97	1.35	0.34	0.34	1.12	1.02	1.25	0.28	0.34	0.17	0.34	1.01	1.31	2.22	1.69	0.51	0.17	0.34	0.34
chr11:92500001-93000000	0.35	4.51	0.37	0.64	0.67	0.34	0.22	0.14	0.31	0.51	0.67	0.56	0.17	0.34	0.22	1.45	0.34	1.18	0.51	0.17	0.34
chr11:91500001-92000000	0.45	4.37	0.45	0.60	0.67	0.22	0.67	0.08	0.49	0.67	0.59	0.67	0.67	0.34	0.26	1.60	1.01	0.51	0.67	0.51	0.17
chr19:48500001-49000000	0.34	3.91	1.09	0.41	0.45	0.11	0.67	0.60	0.08	0.08	0.25	0.22	0.67	0.67	0.72	2.83	6.86	2.36	0.67	1.35	0.67
chr12:115500001-116000000	na	1.65	3.48	15.89	17.54	2.92	5.85	na	11.56	8.32	27.82	25.91	15.18	11.13	na	1.81	0.22	2.36	6.07	5.23	20.74
chr15:9500001-10000000	1.64	1.94	3.37	3.00	3.37	na	0.45	3.39	8.55	8.52	5.14	10.62	na	0.67	1.02	1.37	2.47	2.36	0.17	na	0.51
chr12:114500001-115000000	na	0.84	2.81	14.16	12.48	4.95	3.15	na	7.68	9.89	20.57	14.84	8.94	6.75	na	0.29	0.34	5.23	1.69	3.37	6.07
chr12:115000001-115500000	na	0.67	1.01	15.40	16.97	1.35	3.37	na	7.42	6.07	17.37	12.14	10.79	3.04	na	1.38	1.24	3.20	1.85	6.41	8.77
chr12:81000001-81500000	na	0.61	1.65	5.21	7.98	3.26	0.45	na	7.13	5.34	12.39	10.85	5.56	3.20	na	0.69	0.34	0.51	3.37	0.34	2.19
chr17:5000001-5500000	1.96	0.62	1.87	2.47	1.35	9.78	0.45	3.32	6.76	3.37	9.27	11.24	13.66	0.67	2.04	0.38	0.56	1.18	7.93	1.18	1.35
chr12:80500001-81000000	na	0.15	2.32	7.42	9.33	3.48	1.12	na	6.57	5.11	12.48	10.79	5.56	1.35	na	0.68	0.67	1.01	3.37	0.51	1.01
chr10:20500001-21000000	3.28	0.33	3.11	3.04	8.21	11.69	0.67	3.11	6.22	8.54	11.64	8.21	12.65	1.18	1.09	0.86	0.45	0.34	6.75	0.34	1.69
chr13:24500001-25000000	1.93	0.53	1.57	3.34	3.37	2.02	1.35	2.65	6.06	4.64	7.50	9.61	10.29	0.84	0.34	0.94	1.01	0.17	2.87	0.17	2.02
chr5:64500001-65000000	2.40	0.64	0.75	2.70	2.36	1.69	0.22	3.22	6.04	3.37	6.91	7.59	5.06	2.02	1.13	0.96	1.01	0.51	8.26	0.51	3.37
chr19:41000001-41500000	2.60	0.31	1.50	2.02	5.62	2.02	0.90	2.79	6.03	5.20	8.43	8.71	9.44	1.52	0.86	0.25	0.90	1.69	2.36	0.67	1.01
chr12:116000001-116500000	na	0.33	1.39	6.07	7.64	1.01	2.92	na	5.84	3.06	12.82	12.70	9.78	5.40	na	0.71	0.11	1.35	2.70	2.87	9.27
chr15:10000001-10500000	1.20	1.21	2.02	2.40	3.26	na	0.45	2.63	5.83	6.15	5.40	7.48	na	0.17	1.03	1.38	2.47	2.36	1.69	na	0.00
chr10:44000001-44500000	1.19	0.72	0.64	0.52	2.25	3.04	1.35	2.75	5.82	3.99	6.24	9.67	3.37	2.02	0.72	0.36	0.56	0.17	0.84	0.17	0.34
chr19:32000001-32500000	2.31	0.56	2.51	3.37	7.08	8.21	0.45	2.30	5.69	6.18	7.34	7.53	12.82	3.04	2.54	0.25	0.22	0.34	6.58	2.70	2.53
chr19:32500001-33000000	2.41	0.40	2.02	2.89	3.37	1.35	0.67	2.21	5.56	2.87	6.58	4.78	12.98	1.18	1.74	0.72	0.56	0.84	5.40	1.69	2.53
chr17:4000001-4500000	0.50	0.53	3.37	1.76	2.02	6.86	0.67	2.86	5.53	4.89	5.65	8.15	6.58	0.84	0.32	1.63	4.16	3.37	0.51	2.19	0.67
chr5:65000001-65500000	2.55	0.48	0.52	2.81	3.15	2.25	0.45	3.22	5.51	3.79	9.02	7.48	6.41	1.35	0.91	0.97	1.12	1.01	6.91	0.84	2.70
chr13:23500001-24000000	3.34	1.08	1.87	2.36	7.31	10.23	1.12	2.80	5.42	5.26	11.64	9.16	16.36	2.70	1.04	0.26	0.34	2.19	7.59	2.36	3.04
chr12:101500001-102000000	na	0.17	1.27	1.84	3.37	2.25	0.90	na	5.35	3.37	9.11	9.61	3.37	5.56	na	0.44	0.79	0.84	4.72	0.51	2.53
chr12:100500001-101000000	na	0.34	0.64	2.40	2.70	1.91	1.80	na	5.18	2.53	7.76	8.43	2.70	2.36	na	0.68	0.56	0.67	5.56	0.51	1.69
chr12:101000001-101500000	na	0.40	0.49	0.86	2.25	0.79	1.57	na	5.05	4.86	8.26	10.12	2.70	2.53	na	0.50	0.45	0.34	4.22	0.51	1.69
chr11:22500001-23000000	1.56	0.72	2.14	1.87	1.35	13.49	0.45	1.28	5.03	4.69	5.65	6.13	14.33	1.01	0.59	0.17	0.34	0.34	2.70	1.85	3.20
chr8:47500001-48000000	2.26	0.51	1.27	2.81	3.37	3.37	0.22	2.58	5.03	2.92	7.17	6.52	8.43	3.37	1.21	0.49	0.56	2.19	2.70	2.53	1.18
chr19:37500001-38000000	3.04	0.41	2.92	2.66	2.14	2.02	0.22	2.39	5.03	2.92	7.42	7.31	8.43	0.34	0.57	0.39	3.37	3.37	0.84	2.02	0.51
chr15:9000001-9500000	1.51	1.27	1.69	2.70	6.30	na	0.45	2.46	5.03	5.73	8.01	8.82	na	1.69	1.62	1.22	2.59	3.04	2.02	na	2.02
chr17:5500001-6000000	0.94	0.23	2.14	1.57	4.50	2.70	0.67	3.12	5.00	5.62	6.41	9.44	9.95	0.51	1.93	0.95	0.79	1.69	7.76	0.84	0.34

chr16:10500001-11000000	1.87	0.23	na	3.34	3.04	3.48	0.45	2.84	4.90	na	7.50	8.32	7.25	0.17	0.86	0.72	na	0.67	5.40	1.01	2.87
chr13:43500001-44000000	3.32	0.57	1.24	1.69	2.70	2.36	0.22	3.45	4.86	2.78	10.79	7.48	3.04	1.35	1.20	0.76	0.90	0.34	5.06	0.17	1.18
chr13:30500001-31000000	2.22	0.47	1.87	2.70	3.37	2.70	0.67	1.78	4.85	4.19	5.23	3.04	6.58	1.18	0.85	0.25	0.34	0.67	2.70	1.01	1.52
chr7:87000001-87500000	3.47	0.74	0.94	3.45	3.04	1.46	0.67	3.40	4.83	2.02	7.93	8.15	2.02	0.17	0.56	0.80	0.90	0.17	2.70	0.51	1.35
chr13:24000001-24500000	1.69	0.28	1.72	2.17	4.83	1.80	0.45	2.57	4.83	2.92	8.35	7.42	8.09	0.51	0.09	0.96	0.00	1.01	1.52	0.67	0.67
chr17:73000001-73500000	3.13	0.47	0.86	2.62	3.26	1.69	1.57	2.80	4.78	3.09	5.40	5.85	2.36	2.70	0.73	0.21	0.34	0.84	3.04	0.67	2.36
chr13:51000001-51500000	2.43	0.20	1.80	2.32	2.36	2.25	0.67	2.22	4.73	3.88	5.14	7.53	4.72	1.69	0.41	0.33	0.79	0.34	0.17	0.67	0.17
chr4:8500001-9000000	0.95	0.15	1.54	na	3.37	8.54	0.22	2.54	4.72	3.40	na	6.24	7.25	2.53	1.32	0.41	0.22	na	4.05	1.85	1.18
chr19:41500001-42000000	2.17	0.45	0.60	1.35	2.70	2.59	0.45	3.07	4.68	5.68	7.25	8.21	5.90	0.34	0.58	0.26	0.34	0.84	1.69	1.69	0.67
chr15:36500001-37000000	2.99	0.33	1.35	2.02	3.37	na	1.35	2.35	4.67	4.55	5.40	5.40	na	1.85	1.83	0.30	0.34	0.51	5.40	na	2.02
chr5:66000001-66500000	2.95	0.70	0.94	3.04	2.36	1.80	0.67	2.76	4.61	4.24	8.77	8.04	4.72	2.36	0.80	1.07	1.01	0.67	5.40	0.51	1.01
chr14:32000001-32500000	1.83	1.03	1.16	2.40	5.06	2.14	0.45	3.14	4.60	5.31	10.20	8.26	5.73	2.53	0.19	1.08	0.56	0.67	3.04	0.51	0.51
chr15:58500001-59000000	2.23	0.21	1.31	2.70	2.70	na	0.45	1.90	4.55	3.40	5.90	6.01	na	0.67	0.92	1.08	0.22	1.52	4.38	na	1.85
chr18:39500001-40000000	2.68	2.49	3.34	2.02	2.70	2.02	2.70	2.80	4.54	3.04	5.65	5.62	7.93	2.53	3.44	0.35	0.22	0.51	6.58	2.53	3.04
chr12:86500001-87000000	na	0.62	1.20	0.67	8.09	2.36	0.90	na	4.52	3.04	9.19	8.32	4.72	2.53	na	0.68	1.12	0.51	6.07	0.84	0.51
chr12:16000001-16500000	na	2.12	2.02	1.20	1.35	2.70	1.12	na	4.49	3.37	4.22	4.44	10.12	1.35	na	1.17	1.46	0.67	2.36	2.02	1.69
chr19:55500001-56000000	3.28	1.78	1.65	2.02	3.37	2.02	1.57	2.94	4.46	2.87	5.14	7.42	9.61	3.04	1.83	0.85	1.01	2.02	4.72	3.04	1.35
chr4:59500001-60000000	2.55	0.38	0.97	na	1.91	1.80	0.90	2.98	4.44	2.56	na	4.44	3.37	3.37	0.90	0.73	0.22	na	2.87	0.51	1.85
chr11:98000001-98500000	3.08	0.63	1.80	2.44	2.70	0.79	0.45	2.67	4.40	4.30	8.18	4.05	3.04	1.52	0.25	1.35	0.79	0.84	3.04	0.84	0.17
chr14:16500001-17000000	0.23	1.60	1.95	0.64	1.80	6.30	0.90	1.13	4.39	4.08	2.45	2.53	5.90	1.35	2.43	0.22	0.45	0.67	5.56	1.35	6.75
chr1:14000001-14500000	0.95	1.47	1.91	1.42	3.37	2.70	0.67	2.24	4.34	3.04	2.19	3.04	5.40	2.36	0.11	0.97	1.57	3.04	0.34	1.35	0.34
chr11:11500001-12000000	0.72	0.61	2.02	1.87	3.15	8.32	0.45	1.23	4.32	3.01	2.02	5.23	11.13	1.52	1.89	0.54	0.11	3.04	2.36	5.23	2.53
chr12:116500001-117000000	na	0.28	1.09	7.23	7.98	2.70	2.47	na	4.32	4.02	10.54	9.11	2.70	4.72	na	0.59	0.56	1.01	2.70	2.02	12.48
chr1:13500001-14000000	0.89	0.29	1.69	1.95	3.04	2.81	0.67	1.56	4.30	3.37	2.95	3.37	7.25	2.19	0.76	1.19	1.01	1.85	1.35	2.19	0.67
chr12:70500001-71000000	na	0.37	1.69	2.81	2.70	3.26	0.90	na	4.26	2.70	7.00	7.81	5.23	2.36	na	0.60	0.56	0.34	6.75	0.51	1.69
chr15:59000001-59500000	3.47	0.55	0.86	3.37	4.50	na	1.80	2.89	4.24	3.15	3.96	8.66	na	2.70	1.99	0.80	0.90	0.67	6.07	na	1.69
chr10:19500001-20000000	3.14	0.37	2.40	1.35	5.73	3.37	0.45	2.65	4.24	4.97	10.03	7.87	7.42	0.84	1.22	0.94	0.79	0.00	4.89	0.84	1.69
chr10:5500001-6000000	1.41	0.75	2.10	2.36	2.92	9.33	0.90	1.84	4.20	4.55	2.87	4.33	11.13	1.18	0.99	0.24	0.34	0.84	0.67	1.52	1.01
chr5:36500001-37000000	1.38	0.59	0.97	2.92	4.95	2.25	0.45	2.84	4.10	2.78	7.50	6.07	5.40	0.84	0.16	0.83	0.79	1.01	2.53	0.17	2.02
chr14:31000001-31500000	2.84	0.16	1.72	2.96	3.26	1.69	0.67	2.76	4.10	3.77	7.84	8.15	2.70	0.67	1.06	0.41	0.67	2.02	2.53	1.01	0.34
chr16:19500001-20000000	2.51	1.08	na	3.45	2.70	0.00	1.12	3.47	4.08	na	3.20	2.70	5.06	0.67	1.29	0.31	na	1.01	1.35	1.52	0.84
chr11:46000001-46500000	1.35	0.42	0.79	0.30	2.92	3.48	0.45	3.44	4.07	2.87	2.78	4.67	6.24	0.84	0.50	0.56	0.67	0.34	1.52	2.70	1.52
chr3:52500001-53000000	2.29	0.48	1.12	2.21	na	2.36	0.45	2.36	4.06	2.36	5.82	na	2.70	1.18	0.38	0.78	0.56	0.84	na	0.34	1.52
chr10:95500001-96000000	1.61	0.83	0.37	0.26	0.56	0.79	2.47	2.81	4.04	1.38	2.78	3.37	1.18	3.37	3.44	0.10	0.45	0.17	1.18	0.51	3.37
chr10:43000001-43500000	2.57	0.71	1.54	2.66	3.04	3.15	1.12	2.25	4.03	3.37	6.83	5.28	4.72	2.53	0.92	0.16	0.22	0.51	2.70	0.84	2.02
chr5:123500001-124000000	3.13	1.46	0.45	1.54	2.59	1.01	0.45	3.38	4.00	3.48	6.83	3.37	2.36	2.02	0.46	1.36	1.01	0.67	3.37	0.51	0.34
chr17:34000001-34500000	2.68	1.47	0.75	2.06	2.25	2.70	0.45	1.84	3.98	5.17	9.95	6.52	3.37	1.18	0.25	1.40	1.12	1.01	0.84	0.34	0.00
chr2:3500001-4000000	0.23	0.69	2.25	0.90	2.36	2.70	na	0.53	3.96	3.12	2.70	3.37	7.42	na	0.86	0.19	0.00	0.51	3.37	1.18	na
chr19:57000001-57500000	3.01	0.47	1.95	3.37	5.17	1.69	0.90	2.87	3.96	4.50	5.65	5.56	6.58	1.85	1.39	0.23	0.90	0.51	2.70	1.18	0.17
chr3:9500001-10000000	2.23	0.71	1.87	2.10	na	6.75	0.90	1.60	3.96	2.98	5.31	na	6.24	1.52	1.50	0.09	1.01	0.34	na	2.02	3.37
chr11:5000001-5500000	0.79	0.64	2.02	2.59	2.02	6.18	0.45	2.34	3.93	5.48	7.93	4.44	7.93	0.00	0.75	1.16	1.12	0.34	7.25	0.51	1.69
chr9:32000001-32500000	0.96	0.88	1.69	1.65	2.36	3.04	0.67	1.70	3.81	5.17	5.06	6.24	8.43	2.19	0.82	0.50	0.67	0.17	3.37	1.35	1.69
chr10:6000001-6500000	0.72	0.99	2.77	1.57	4.83	11.47	0.67	1.64	3.80	4.38	4.72	5.73	8.77	0.67	0.78	0.61	0.11	1.52	2.87	2.87	0.67
chr17:28500001-29000000	2.70	1.26	0.56	3.37	4.61	0.34	0.45	3.40	3.80	5.45	10.20	5.85	1.35	0.17	0.58	1.07	0.79	0.51	3.37	0.67	0.51
chr7:82500001-83000000	2.48	0.25	0.37	1.69	2.14	1.35	1.80	2.23	3.79	2.45	2.87	3.48	4.05	3.37	2.40	0.53	0.67	0.17	3.04	0.51	1.69
chr11:54500001-55000000	2.27	0.97	1.54	3.07	2.70	2.70	0.90	1.77	3.78	2.95	3.04	6.52	5.73	0.67	0.09	1.23	1.01	0.34	2.70	0.84	0.84
chr2:34500001-35000000	3.27	1.10	0.67	2.55	3.04	3.37	na	3.13	3.67	3.37	11.38	5.62	4.38	na	0.62	1.14	0.90	0.51	2.70	0.67	na
chr17:73500001-74000000	2.50	1.36	0.64	2.14	3.04	1.24	2.47	3.47	3.67	3.40	8.18	4.33	5.06	1.69	1.22	0.49	0.45	1.69	1.18	2.53	2.87
chr2:27000001-27500000	3.04	0.39	2.47	5.92	5.62	2.59	na	3.07	3.64	4.44	8.77	5.40	2.70	na	0.57	0.94	0.11	0.67	3.20	0.67	na

chr19:29000001-29500000	2.41	0.78	1.57	3.41	4.27	7.76	0.67	1.60	3.64	4.13	4.72	4.27	5.90	1.35	1.86	0.39	0.67	1.35	2.02	2.87	2.02
chr13:43000001-43500000	2.30	0.73	1.39	2.36	3.15	2.02	0.90	2.72	3.52	4.08	5.31	4.89	3.37	1.35	0.51	1.02	0.56	0.34	1.69	0.17	1.01
chrY:2500001-3000000	0.42	1.93	1.72	0.34	0.56	0.56	0.45	0.66	0.58	0.51	0.42	0.79	0.17	0.67	0.41	8.41	4.83	1.18	0.00	0.51	0.84
chr19:44000001-44500000	2.01	0.40	2.70	2.02	3.37	1.80	0.90	2.42	3.23	6.86	9.86	3.82	7.76	0.00	0.89	0.13	1.24	2.02	3.04	1.52	1.18
chr19:3500001-4000000	1.55	0.54	1.35	3.37	4.50	6.52	0.45	1.97	3.23	6.46	7.67	2.36	8.26	1.52	1.08	0.71	0.56	0.34	4.72	0.67	0.51
chr9:64500001-65000000	2.70	0.55	1.16	2.47	3.37	0.67	0.00	2.71	2.98	6.35	12.73	5.00	3.04	0.51	0.36	1.09	0.34	1.35	1.85	0.34	0.67
chr6:69500001-70000000	0.50	na	0.82	1.01	0.79	2.47	2.92	3.46	na	6.24	9.53	15.57	7.59	2.36	0.41	na	0.45	0.51	0.34	1.01	1.18
chr19:46000001-46500000	2.81	0.49	1.87	3.26	2.36	1.80	0.45	3.38	3.11	5.90	10.37	4.78	4.22	1.35	1.36	0.90	0.67	1.01	2.36	0.34	1.01
chr11:5500001-6000000	0.34	1.11	1.72	1.46	1.91	3.37	0.67	2.04	3.03	5.79	7.25	6.35	6.41	0.34	0.37	0.70	0.90	0.67	3.20	0.34	0.67
chr10:20000001-20500000	2.26	0.38	2.51	5.47	5.51	3.37	0.67	2.34	2.42	5.40	7.17	4.50	3.04	0.34	1.84	0.57	0.22	2.19	2.70	1.52	1.01
chr19:45000001-45500000	1.60	0.69	2.29	3.15	1.91	1.01	0.67	2.54	2.97	5.34	5.48	3.37	4.22	0.34	0.99	1.05	0.56	1.69	3.04	0.84	0.51
chr15:84000001-84500000	3.37	0.40	1.87	3.37	5.28	na	0.67	2.61	3.08	5.20	8.35	2.70	na	1.85	0.36	0.95	0.22	1.01	1.18	na	0.84
chr12:78000001-78500000	na	0.60	2.77	3.37	8.32	3.26	1.57	na	3.37	5.11	8.01	6.13	3.04	2.87	na	0.28	0.56	0.67	1.69	1.01	2.36
chr19:4000001-4500000	0.93	1.30	0.56	2.44	2.81	2.70	0.90	1.42	2.56	5.06	5.82	3.37	2.70	0.17	0.23	1.41	1.01	0.34	2.02	0.51	1.01
chr1:36500001-37000000	2.51	0.66	1.95	3.19	3.04	3.48	0.45	3.35	3.10	4.78	6.83	6.07	6.07	0.84	0.93	0.81	1.01	0.17	4.38	0.51	1.69
chr12:86000001-86500000	na	0.93	1.16	2.32	3.37	1.01	0.67	na	3.07	4.78	10.20	5.73	2.70	1.52	na	0.66	0.90	0.84	1.85	0.51	2.36
chr19:44500001-45000000	1.37	0.35	2.59	2.25	2.14	1.91	0.45	1.70	1.51	4.75	7.34	2.19	3.04	0.84	0.81	0.09	1.57	1.69	0.67	2.02	0.34
chr6:67500001-68000000	0.87	na	1.27	0.97	2.25	3.15	1.57	3.25	na	4.64	10.71	14.78	8.09	2.53	0.11	na	1.12	2.19	0.51	2.36	4.22
chr9:21000001-21500000	0.70	1.50	0.22	1.84	1.57	3.37	0.67	1.31	1.94	4.61	5.14	4.72	4.89	0.34	0.12	1.32	0.90	0.67	3.04	0.51	1.18
chr19:6000001-6500000	1.28	1.31	1.31	2.59	2.59	0.79	0.67	2.11	1.98	4.61	7.67	3.20	2.70	0.17	0.14	1.04	0.56	0.34	2.02	0.51	0.34
chr7:17000001-17500000	0.59	0.72	0.79	1.95	2.59	2.81	0.45	1.69	2.76	4.55	4.55	5.62	2.70	0.67	0.22	1.06	0.34	0.34	1.35	0.17	0.51
chr17:45000001-45500000	2.99	0.34	2.17	3.48	3.37	2.59	0.90	2.82	3.39	4.55	8.35	5.96	5.06	0.67	1.30	0.28	0.34	1.18	2.36	1.01	0.67
chr6:70000001-70500000	0.52	na	1.27	0.86	1.69	2.36	1.57	3.04	na	4.50	9.44	9.39	3.37	3.37	0.44	na	1.12	1.18	0.51	2.19	1.01
chr9:57500001-58000000	3.25	1.29	1.72	2.70	4.05	1.46	0.67	2.22	3.49	4.47	8.60	7.59	3.37	1.69	0.22	1.07	0.79	0.84	3.37	0.51	1.52
chr18:36000001-36500000	2.79	0.11	2.55	3.30	6.75	3.26	0.90	2.41	3.28	4.47	8.52	3.48	4.72	1.35	1.83	0.07	0.67	2.36	4.89	1.69	2.02
chr9:7500001-8000000	0.31	0.43	2.81	0.97	2.02	2.70	0.67	0.40	2.83	4.44	2.95	2.02	7.93	2.19	1.01	0.70	0.67	2.19	1.52	3.04	0.84
chr11:6000001-6500000	0.71	0.89	1.57	1.91	2.92	5.51	0.90	1.31	2.57	4.44	2.70	5.28	7.93	0.51	0.51	0.79	0.79	0.34	2.70	0.84	0.67
chr15:5000001-5500000	0.28	0.93	1.09	0.86	1.57	na	0.67	1.34	3.34	4.41	2.61	3.26	na	0.84	3.18	0.31	0.67	1.01	3.37	na	2.53
chr19:7000001-7500000	1.74	1.28	1.27	2.59	3.37	2.70	0.67	1.18	2.56	4.41	5.82	3.37	9.27	0.34	0.55	1.16	0.67	0.51	3.04	0.51	0.51
chr14:31500001-32000000	2.07	0.62	0.64	2.51	2.81	2.59	0.90	2.28	2.32	4.38	10.12	4.78	2.70	0.00	0.95	0.77	0.45	1.69	3.04	1.18	1.52
chr17:24500001-25000000	1.17	1.34	1.31	2.36	3.04	1.01	0.45	1.30	1.00	4.38	3.20	3.32	3.37	0.00	0.15	1.26	0.22	1.18	3.20	0.84	0.00
chr15:99500001-100000000	3.47	0.74	1.31	2.17	2.92	na	0.67	3.49	2.79	4.36	8.52	2.70	na	1.01	1.39	0.83	0.56	1.35	1.52	na	1.69
chr5:31000001-31500000	0.97	1.00	1.31	2.55	2.92	2.02	0.67	1.80	1.62	4.33	5.73	3.04	2.19	0.34	0.17	0.72	0.56	1.52	2.70	0.17	0.84
chr15:99000001-99500000	3.30	0.97	0.49	2.74	1.12	na	0.67	2.60	1.56	4.30	7.50	1.97	na	1.18	0.43	1.24	0.67	0.34	2.19	na	0.00
chr19:24500001-25000000	1.35	0.58	2.29	2.17	3.15	1.35	0.45	2.03	3.06	4.30	5.73	5.11	8.60	0.84	0.43	0.32	2.02	1.85	2.02	3.04	0.51
chr2:32500001-33000000	3.24	1.08	2.06	2.70	3.37	0.56	na	3.17	3.22	4.27	11.47	6.30	1.35	na	0.69	1.07	0.90	1.01	2.36	0.34	na
chr5:34500001-35000000	2.88	1.06	1.54	2.81	2.36	1.57	1.12	2.68	2.74	4.27	7.67	6.91	3.37	0.17	0.39	0.77	1.12	0.34	3.20	0.84	1.85
chr8:74500001-75000000	1.47	1.02	1.16	1.27	2.25	1.12	0.45	1.91	2.91	4.27	5.65	4.27	3.88	1.01	0.13	1.11	0.90	0.34	1.18	0.00	2.02
chr8:10500001-11000000	3.45	0.70	2.02	3.15	10.90	12.14	1.12	1.74	3.25	4.22	6.75	5.17	7.93	1.52	0.63	0.47	0.45	3.37	0.84	2.02	0.51
chr12:32500001-33000000	na	0.16	1.05	2.02	5.40	2.02	0.67	na	3.49	4.22	7.42	3.37	6.58	2.02	na	0.25	0.22	0.17	1.35	3.20	1.69
chr19:5000001-5500000	0.95	1.10	1.61	1.35	2.47	2.59	0.90	1.52	1.20	4.19	6.15	1.80	3.04	0.84	0.49	1.26	0.56	0.17	4.22	0.34	0.17
chr5:32500001-33000000	3.42	0.96	2.66	3.04	5.51	1.35	0.45	2.70	2.42	4.13	6.91	4.38	2.70	0.67	0.55	0.74	0.56	0.84	1.01	0.84	0.51
chr12:80000001-80500000	na	0.88	1.20	3.19	3.04	0.90	0.67	na	2.37	4.13	8.68	5.56	3.37	2.87	na	0.62	0.67	1.35	2.02	0.84	0.51
chr9:44000001-44500000	2.51	1.06	1.39	5.36	3.37	3.15	0.45	2.10	3.34	4.02	11.64	5.85	3.37	1.85	0.39	1.11	1.12	1.01	4.72	0.67	1.01
chr13:49000001-49500000	3.01	0.80	0.67	2.92	1.35	2.92	0.67	2.07	3.01	4.02	3.46	3.37	3.20	0.51	0.20	1.08	0.79	0.34	5.40	0.84	1.18
chr15:8000001-8500000	0.70	0.54	1.01	1.46	2.14	na	0.45	1.28	2.96	4.02	2.53	3.37	na	1.01	1.45	0.05	0.79	0.84	3.20	na	1.69
chr17:32500001-33000000	2.31	0.95	1.05	3.48	2.70	0.45	0.45	1.89	1.66	4.02	6.07	1.29	3.04	0.67	0.89	0.97	0.34	1.52	0.84	1.01	0.34
chr11:4000001-4500000	0.88	1.02	1.84	2.47	3.37	6.63	0.67	0.64	1.85	3.99	5.31	1.69	4.89	0.67	1.02	0.53	0.45	2.02	2.87	2.19	0.17
chr9:7000001-7500000	0.55	1.24	1.80	0.41	2.25	8.99	0.45	0.83	3.17	3.96	2.19	2.42	6.91	1.85	0.84	2.07	2.36	2.87	0.67	3.37	0.00

chr10:43500001-44000000	2.65	0.33	0.60	1.99	2.70	1.69	0.45	1.42	3.42	3.91	6.15	5.28	4.89	0.84	0.53	0.34	0.45	0.34	1.69	0.84	0.67
chr11:4500001-5000000	0.33	1.13	0.79	1.87	2.25	1.35	0.67	1.14	1.30	3.91	4.64	2.81	5.06	0.67	0.13	1.25	0.90	0.34	3.37	1.18	0.51
chr17:27000001-27500000	3.12	0.98	1.69	3.04	2.36	1.57	0.45	1.74	1.91	3.91	7.17	3.26	2.36	0.51	0.36	1.31	0.45	0.67	2.02	0.34	0.00
chr19:11000001-11500000	0.75	0.64	2.74	1.54	1.69	2.36	0.90	1.19	3.27	3.88	3.20	2.14	3.04	1.18	1.81	0.35	1.35	2.70	0.67	3.71	0.17
chr5:32000001-32500000	1.91	0.15	3.48	2.89	3.48	2.02	0.67	3.17	1.96	3.82	4.64	1.91	4.05	0.51	0.92	0.74	1.12	2.19	1.69	1.01	0.17
chr14:26000001-26500000	2.22	0.08	2.25	4.91	3.37	1.69	0.22	2.56	2.53	3.79	5.56	6.52	3.04	0.67	0.78	0.99	0.67	0.84	5.90	1.18	0.84
chr19:6500001-7000000	0.58	1.62	0.64	1.84	2.25	1.01	0.67	0.50	0.55	3.79	3.96	2.30	3.20	0.51	0.12	1.30	0.67	0.67	0.17	0.84	0.67
chr17:35000001-35500000	2.76	1.33	1.54	2.51	2.92	0.34	0.67	1.71	1.94	3.74	6.15	3.20	3.04	0.67	0.20	1.18	0.90	0.34	1.85	0.67	1.35
chr9:63000001-63500000	2.41	0.81	1.84	2.36	3.04	1.35	0.67	3.26	2.76	3.68	8.09	3.37	2.70	1.01	1.01	0.79	0.67	0.51	3.20	1.52	0.84
chr17:39500001-40000000	0.43	1.05	1.99	0.19	0.56	3.37	0.90	0.37	0.30	3.65	0.93	0.34	1.35	0.34	0.16	0.34	2.59	0.51	0.34	3.37	0.00
chr19:46500001-47000000	2.64	0.40	0.67	3.41	3.04	2.02	1.12	2.78	2.88	3.57	8.94	5.62	5.56	1.01	0.75	1.00	0.67	0.51	5.56	0.17	1.69
chr19:43000001-43500000	0.34	2.80	3.00	0.79	0.56	1.57	0.45	0.29	0.14	0.59	0.25	0.51	0.67	0.34	0.27	1.32	10.01	4.72	0.51	3.04	0.67
chr19:52500001-53000000	0.36	3.41	1.72	0.19	0.34	0.67	0.67	0.39	0.20	0.76	0.25	0.79	0.00	0.67	0.31	3.21	8.99	0.34	0.51	1.18	0.67
chr19:35500001-36000000	0.15	2.72	2.92	0.37	0.56	1.80	0.67	0.46	0.10	1.21	0.34	0.51	0.17	0.17	0.24	1.85	8.66	1.69	0.51	3.04	0.51
chr19:17500001-18000000	0.45	0.80	1.57	0.34	0.34	1.69	1.12	0.52	0.26	0.48	0.08	0.45	0.84	0.67	0.57	1.72	8.21	2.87	0.84	1.35	0.51
chr19:15000001-15500000	0.57	0.62	0.41	0.56	0.90	1.12	0.45	0.47	0.27	0.70	0.25	0.28	1.85	0.67	0.57	1.83	7.42	1.01	0.51	1.85	0.67
chr19:14000001-14500000	0.51	1.69	3.07	1.12	0.56	2.70	0.45	0.21	0.23	0.90	0.51	0.17	1.18	1.18	0.03	1.98	7.42	1.01	0.34	2.36	0.34
chr19:19000001-19500000	0.50	2.24	1.84	0.26	0.56	1.46	0.45	0.66	0.40	0.20	0.59	0.45	0.00	0.67	0.75	2.62	7.42	0.51	0.34	1.18	0.67
chr19:26000001-26500000	0.30	1.28	2.51	0.52	0.11	1.91	0.90	0.60	0.14	0.45	0.17	0.62	0.34	0.51	0.39	1.98	7.42	1.18	0.00	1.69	0.34
chr19:19500001-20000000	0.35	2.11	0.94	0.52	0.67	2.70	0.45	0.83	0.50	0.67	0.34	0.28	0.84	0.34	0.71	1.95	6.97	0.67	0.67	1.01	0.67
chr19:30500001-31000000	0.55	0.66	1.46	0.82	0.34	1.24	0.45	0.34	0.40	0.65	0.59	0.22	0.84	0.51	0.15	1.66	6.97	2.02	0.51	3.37	0.17
chr19:22000001-22500000	0.36	1.11	1.20	0.30	0.34	0.90	0.90	0.13	1.22	1.12	0.84	0.00	2.70	0.67	0.36	1.32	6.86	0.51	0.51	3.04	0.67
chr19:35000001-35500000	0.35	1.74	2.62	1.05	0.34	1.57	0.45	0.46	0.09	0.84	0.42	0.39	0.00	0.34	0.46	1.03	6.52	3.20	0.17	3.88	0.17
chr19:39000001-39500000	0.34	1.88	1.42	0.22	0.45	0.79	0.45	0.51	0.33	0.11	0.51	0.45	0.67	0.00	0.43	1.00	6.41	1.18	0.67	2.36	0.67
chr19:22500001-23000000	0.37	1.47	1.16	0.26	0.56	1.35	0.90	0.53	0.07	0.90	0.25	0.34	1.18	0.17	0.40	2.55	6.30	0.84	0.17	1.18	0.51
chr19:25500001-26000000	0.37	0.69	1.31	0.41	0.34	1.35	0.90	0.13	0.69	1.88	1.01	0.62	1.35	0.51	0.52	1.39	6.18	2.36	0.67	1.85	0.67
chr17:3500001-4000000	0.36	1.92	2.66	0.56	1.69	2.70	0.67	1.45	3.13	3.37	2.87	1.52	5.06	0.34	0.38	2.63	5.96	2.36	0.34	3.04	0.67
chr19:51000001-51500000	0.34	3.49	0.60	0.64	0.45	0.67	0.45	0.51	0.20	0.56	0.42	0.28	0.51	0.34	0.44	2.77	5.73	0.34	0.34	0.34	0.34
chr19:20500001-21000000	0.31	1.39	1.35	0.52	0.56	1.57	0.45	0.32	0.16	1.57	0.17	0.67	2.53	0.51	0.51	2.22	5.62	1.69	0.34	3.37	0.67
chr19:23500001-24000000	0.22	0.67	1.24	1.01	0.34	4.50	0.22	0.15	0.38	0.59	1.18	0.11	1.35	1.01	0.20	1.38	5.62	2.53	0.84	4.89	1.35
chr19:7500001-8000000	0.52	0.46	2.02	1.57	1.24	1.91	0.67	0.09	0.69	2.45	2.02	0.73	3.37	0.17	0.79	0.56	5.51	4.22	1.18	2.02	0.67
chr19:13000001-13500000	0.51	2.02	1.42	0.49	0.34	1.35	0.45	0.66	0.40	0.17	0.34	0.56	0.67	0.34	0.39	2.33	5.51	1.69	0.51	1.85	0.51
chr19:20000001-20500000	0.37	1.02	1.46	0.34	0.22	2.02	0.22	0.73	0.44	0.28	0.25	0.17	1.01	0.34	0.33	1.86	5.17	0.67	0.34	2.53	0.34
chr19:39500001-40000000	0.55	1.63	0.60	0.34	0.56	0.00	0.67	0.80	0.64	0.45	0.51	0.67	0.34	0.17	0.83	0.75	5.06	0.51	0.67	0.51	0.51
chr17:14500001-15000000	0.52	0.98	1.72	0.30	0.79	2.36	0.90	0.40	0.12	0.25	0.67	0.34	1.18	0.67	0.20	0.86	4.95	2.36	0.67	2.02	0.00
chr19:8000001-8500000	0.35	0.88	2.25	1.16	0.67	2.70	0.67	0.47	0.34	2.08	0.51	0.51	1.52	0.67	0.40	0.79	4.72	2.70	0.34	1.85	0.34
chr6:5500001-6000000	0.68	na	0.45	0.26	0.34	1.57	0.45	0.63	na	0.53	0.25	0.28	1.35	0.34	0.56	na	4.27	0.84	0.51	2.53	0.67
chr9:3500001-4000000	0.67	0.38	0.97	0.37	0.56	1.57	0.45	0.72	0.31	0.39	0.51	0.17	0.34	0.67	0.69	1.95	4.16	0.51	0.51	0.34	0.34
chr17:9500001-10000000	0.50	1.29	3.04	0.30	0.34	1.24	0.90	0.69	0.27	0.22	0.51	0.67	0.34	0.17	0.45	2.69	4.16	2.53	0.00	1.35	0.34
chr9:44500001-45000000	2.55	1.01	0.56	5.81	5.51	2.92	0.22	2.41	3.12	3.06	7.17	3.37	2.36	0.84	0.40	1.16	1.01	0.67	3.37	0.34	0.67
chr17:26500001-27000000	2.51	0.42	2.70	5.70	6.18	2.92	0.00	3.22	3.29	2.92	8.68	6.35	4.89	0.51	0.71	0.99	0.22	1.35	2.53	0.34	0.17
chr9:63500001-64000000	2.31	0.96	1.54	4.95	4.50	1.24	0.90	2.92	2.85	2.98	7.17	3.32	1.85	1.52	0.24	1.24	0.22	0.34	2.36	0.67	0.51
chr2:31000001-31500000	2.95	1.06	1.01	4.80	2.47	0.67	na	3.17	3.09	3.37	12.65	4.95	1.35	na	0.69	1.33	0.56	1.18	1.52	0.00	na
chr15:82500001-83000000	1.88	0.55	2.62	4.76	3.15	na	0.67	2.45	2.10	3.48	5.99	2.75	na	0.34	1.27	0.53	1.24	3.20	1.52	na	1.35
chr9:62500001-63000000	2.75	1.05	1.84	4.72	3.04	0.67	0.90	1.88	0.92	2.47	4.97	2.19	2.53	0.17	0.46	1.15	0.34	0.67	1.85	0.34	0.67
chr17:28000001-28500000	3.43	1.09	0.67	4.57	3.37	0.56	0.67	3.15	2.77	3.15	8.68	5.11	2.02	0.84	0.42	1.15	1.12	0.17	2.70	0.84	0.34
chr2:33000001-33500000	1.80	1.21	1.72	4.46	2.92	0.90	na	1.97	1.42	3.40	4.30	2.36	1.69	na	0.64	1.17	0.79	0.67	0.84	0.84	na
chr2:26500001-27000000	2.16	0.96	2.25	4.12	3.37	0.22	na	1.47	1.54	3.23	5.65	2.53	1.01	na	0.42	1.33	0.67	1.01	2.87	1.18	na
chr12:114000001-114500000	na	1.06	0.97	2.02	5.62	0.67	1.80	na	3.42	3.20	17.20	8.54	2.02	3.37	na	0.47	0.67	1.85	5.90	1.18	2.36

chr2:32000001-32500000	2.89	1.16	1.01	2.14	2.70	1.24	na	2.61	2.48	2.73	11.72	6.97	3.37	na	0.14	1.42	1.01	0.67	1.85	0.67	na
chr10:79500001-80000000	2.92	1.53	0.45	2.21	2.14	0.34	0.45	1.90	2.38	3.37	11.13	7.87	3.37	1.01	0.05	1.23	1.01	1.35	2.02	0.17	2.36
chr12:85500001-86000000	na	0.88	1.12	2.70	3.37	1.01	0.45	na	3.05	2.61	10.88	5.34	2.02	0.34	na	1.09	0.90	0.34	2.36	1.01	0.51
chr15:78500001-79000000	2.26	1.22	0.37	2.70	3.26	na	0.22	2.22	2.51	3.48	10.62	4.78	na	0.34	0.57	1.27	1.12	0.51	2.87	na	0.17
chr2:29500001-30000000	2.86	1.07	1.39	2.70	3.37	0.79	na	2.47	2.05	3.37	10.03	3.65	1.52	na	0.15	1.37	0.90	0.17	0.84	0.17	na
chr9:65000001-65500000	3.21	1.08	1.20	2.02	3.37	0.79	0.90	2.45	2.61	2.70	10.03	5.79	1.35	1.69	0.33	1.17	0.34	0.51	2.36	0.17	1.01
chr9:65500001-66000000	3.37	0.86	0.71	2.77	3.04	1.35	0.45	2.67	1.62	2.81	10.03	3.37	1.85	1.01	0.75	1.28	0.90	0.51	2.02	0.17	0.51
chr15:79500001-80000000	3.48	1.01	0.60	2.14	2.14	na	0.67	2.41	1.78	3.04	9.53	2.36	na	1.01	0.66	1.28	1.01	0.51	2.87	na	0.67
chr15:81500001-82000000	2.19	1.39	0.90	1.80	3.15	na	0.67	2.16	3.29	3.48	9.53	5.23	na	1.18	0.18	1.40	0.79	0.51	3.20	na	0.67
chr19:5500001-6000000	2.09	1.38	1.61	2.32	3.15	1.57	0.22	2.03	2.50	3.15	9.27	5.23	4.72	0.67	0.08	1.21	1.12	0.84	3.04	0.17	1.18
chr5:123000001-123500000	3.28	1.39	0.60	2.66	2.81	1.35	0.45	3.08	3.42	3.46	9.19	5.56	1.52	3.04	0.44	1.20	1.01	0.67	3.37	1.01	0.51
chr17:46000001-46500000	3.37	0.35	1.69	2.92	1.91	2.36	0.90	2.75	1.94	3.43	9.19	3.37	2.70	1.01	0.71	1.09	0.67	1.35	1.18	0.17	0.67
chr2:31500001-32000000	3.37	1.51	1.80	2.70	3.15	0.90	na	2.18	2.35	2.73	9.11	2.36	1.35	na	0.10	1.26	1.12	0.34	1.69	0.34	na
chr9:60500001-61000000	3.18	0.39	1.95	2.70	3.37	1.46	0.45	2.91	2.79	3.18	8.60	5.79	2.70	0.84	0.78	1.13	0.67	0.84	3.37	0.51	0.34
chr16:33000001-33500000	2.72	0.97	na	2.51	4.16	1.01	0.67	3.06	2.42	na	8.60	5.11	2.36	1.01	1.32	0.91	na	0.34	1.85	0.34	1.18
chr11:59500001-60000000	2.89	1.06	1.24	2.02	2.02	0.56	0.67	2.26	2.97	1.91	8.35	8.04	2.87	1.35	0.45	1.29	0.67	0.67	5.40	0.51	0.17
chr2:35000001-35500000	2.91	0.51	1.61	2.06	2.92	2.47	na	3.29	3.37	2.95	8.26	5.90	2.70	na	0.49	1.28	0.34	0.51	3.37	0.51	na
chr11:68500001-69000000	3.23	0.69	1.35	2.70	3.37	2.70	0.67	2.13	2.63	3.32	8.26	3.37	3.20	1.01	0.14	1.28	0.90	0.51	2.87	0.67	0.34
chr13:45000001-45500000	2.46	0.43	1.31	3.26	2.02	1.35	0.22	2.98	3.12	3.26	8.26	3.77	1.69	0.84	1.85	0.73	0.45	0.51	2.87	1.69	0.84
chr3:95000001-95500000	3.43	1.13	1.12	1.76	na	0.90	0.22	2.22	1.89	2.05	8.09	na	1.18	1.35	0.03	1.25	0.79	0.34	na	0.34	0.51
chr10:21000001-21500000	2.09	0.39	2.21	2.96	5.85	2.70	1.12	2.08	3.26	3.32	8.01	4.78	2.02	0.84	0.65	0.95	0.90	0.84	2.36	0.51	1.18
chr2:30000001-30500000	3.16	1.34	1.27	3.11	2.70	0.45	na	1.98	2.18	2.95	7.84	3.04	1.85	na	0.16	1.32	0.90	0.67	1.69	0.84	na
chr8:108000001-108500000	2.86	0.86	0.41	1.87	2.70	0.34	0.90	2.86	2.61	3.48	7.84	5.11	3.37	1.18	0.42	1.13	0.67	0.17	3.20	0.34	1.69
chr11:79000001-79500000	3.47	0.91	0.30	3.19	2.47	1.01	0.67	3.08	2.74	3.06	7.84	3.04	2.02	1.18	0.24	0.94	1.24	0.67	2.70	0.51	0.67
chr10:80000001-80500000	2.99	1.49	0.30	1.35	2.14	0.67	0.22	1.86	2.44	1.55	7.76	4.50	3.20	0.84	0.11	1.20	1.12	0.84	3.04	0.17	0.67
chr15:98500001-99000000	2.65	0.81	0.64	2.40	1.57	na	0.67	2.87	1.92	2.64	7.76	2.81	na	0.84	0.26	1.14	1.24	0.51	3.04	na	0.51
chr15:97500001-98000000	2.82	1.17	0.97	1.95	2.36	na	0.90	2.65	1.63	1.63	7.67	1.91	na	1.52	0.25	1.27	0.90	0.17	0.51	na	1.85
chr7:134000001-134500000	3.47	1.33	0.41	1.80	2.25	0.67	0.90	2.96	3.36	2.98	7.67	7.42	1.35	2.87	0.15	1.30	0.90	1.18	3.04	0.67	2.19
chr3:88000001-88500000	2.96	1.45	0.41	1.76	na	1.01	0.22	2.30	1.80	2.89	7.59	na	1.52	2.19	0.27	1.25	0.90	1.01	na	1.01	0.34
chr5:122500001-123000000	2.84	1.24	0.45	1.05	2.25	0.56	0.90	2.12	3.42	2.36	7.50	4.10	3.37	0.84	0.28	1.40	0.90	0.51	3.88	0.67	1.01
chr7:107500001-108000000	2.99	0.92	0.49	1.50	2.59	0.56	0.00	2.69	1.87	3.37	7.50	3.77	1.85	1.52	0.90	0.90	1.24	0.51	2.70	0.51	0.00
chr16:31500001-32000000	2.22	0.90	na	2.47	2.02	0.90	0.45	3.45	2.36	na	7.42	2.98	3.37	0.67	1.63	0.85	na	1.01	0.67	1.01	0.17
chr2:165500001-166000000	2.51	1.58	0.75	1.57	1.12	0.45	na	2.39	3.40	2.50	7.34	5.56	0.84	na	0.19	1.45	1.24	0.51	1.85	0.84	na
chr3:89500001-90000000	2.44	1.01	0.67	2.17	na	1.12	0.45	2.32	2.49	2.19	7.34	na	1.69	0.67	0.59	1.09	0.67	1.18	na	0.17	1.18
chr5:140500001-141000000	3.37	1.11	1.09	1.35	3.37	0.67	0.90	2.80	1.92	3.34	7.25	4.89	2.19	1.18	1.07	1.34	1.12	1.18	2.36	0.34	2.19
chr15:100000001-100500000	3.47	0.34	2.32	0.67	3.26	na	0.90	3.26	2.42	2.59	7.25	3.04	na	1.01	0.83	1.11	0.90	0.17	2.36	na	0.51
chr1:135500001-136000000	3.28	1.02	0.49	2.55	1.35	0.56	0.45	3.43	2.15	2.78	7.17	3.37	1.18	0.67	1.17	0.99	0.22	0.34	2.02	0.84	0.34
chr2:28000001-28500000	1.89	0.89	1.27	3.04	2.92	0.56	na	1.95	1.33	1.46	7.17	2.70	1.69	na	0.42	0.83	0.22	2.36	0.84	0.34	na
chr9:72000001-72500000	2.70	0.31	1.05	2.77	1.57	2.02	0.22	3.06	3.46	2.81	7.17	5.34	1.69	0.84	1.55	1.05	1.01	0.67	9.27	0.00	2.19
chr10:19000001-19500000	2.34	0.83	1.42	2.92	6.18	5.96	0.45	2.11	3.24	3.18	7.17	5.79	3.37	3.04	0.70	1.04	0.90	1.01	9.27	0.34	1.69
chr1:88000001-88500000	2.62	1.00	0.64	1.54	1.24	0.67	0.90	2.96	3.38	2.50	7.08	3.37	2.02	2.36	0.34	0.98	1.01	0.51	3.37	0.17	1.52
chr2:29000001-29500000	3.25	0.76	1.24	2.36	3.48	0.79	na	2.50	1.65	3.04	7.08	2.14	1.85	na	0.45	1.13	0.56	1.85	1.85	0.51	na
chr5:34000001-34500000	2.53	0.85	2.21	2.70	2.70	2.14	0.67	2.49	2.20	3.01	7.08	3.04	0.84	0.84	0.17	1.01	0.56	1.85	1.85	0.17	0.34
chr9:66500001-67000000	3.01	0.67	1.65	3.22	3.37	1.35	0.67	1.29	1.62	2.73	7.00	2.02	2.36	0.51	0.31	0.99	0.79	0.67	3.37	0.51	1.35
chr10:18500001-19000000	1.81	0.30	1.24	3.04	3.04	2.70	1.12	1.23	2.99	3.37	7.00	5.11	6.58	1.01	1.39	0.66	0.79	1.35	7.76	0.51	2.36
chr17:26000001-26500000	1.82	0.95	1.42	2.70	3.37	1.57	0.45	1.71	1.14	3.37	7.00	2.59	3.37	0.34	0.09	1.32	0.11	0.34	1.85	0.67	0.67
chr15:78000001-78500000	2.38	1.08	1.31	3.22	2.02	na	0.22	2.16	2.39	2.47	6.91	3.15	na	0.84	0.86	1.26	0.56	1.52	2.36	na	0.34
chr11:77500001-78000000	2.41	1.04	1.80	2.17	2.02	0.90	0.22	2.81	2.30	2.92	6.83	3.26	1.35	0.67	0.25	1.43	1.01	0.51	2.53	0.67	0.17
chr14:22000001-22500000	1.69	0.66	2.29	2.44	3.48	2.70	1.12	1.71	2.33	2.05	6.75	4.67	3.04	1.18	1.49	0.16	0.56	1.69	1.69	0.34	1.18

chr12:83000001-83500000	na	0.54	2.81	2.47	4.83	1.46	0.90	na	3.14	2.89	6.75	3.32	3.20	2.36	na	0.71	0.90	0.17	4.72	0.51	1.35
chr2:34000001-34500000	1.63	0.26	2.25	3.00	2.25	1.46	na	2.38	1.26	3.04	6.66	1.80	1.01	na	1.35	0.85	0.22	2.36	2.70	0.84	na
chr2:118000001-118500000	2.05	1.41	0.52	0.75	1.24	0.22	na	2.22	3.20	1.66	6.66	4.72	1.35	na	0.03	1.39	0.79	0.51	1.52	0.84	na
chr9:70000001-70500000	2.57	0.27	1.42	1.46	2.47	2.47	0.22	2.58	3.44	3.15	6.66	6.07	2.36	0.17	0.58	0.92	0.34	1.01	2.19	0.84	0.84
chr10:59500001-60000000	2.36	0.93	0.45	1.99	3.48	1.12	0.45	2.26	2.44	3.32	6.66	4.89	2.19	1.35	0.29	1.36	1.01	0.51	2.53	0.34	1.35
chr2:26000001-26500000	2.16	1.20	1.01	1.69	2.02	1.01	na	1.90	1.09	3.09	6.58	3.43	2.70	na	0.23	1.18	0.56	0.67	2.19	0.17	na
chr5:35000001-35500000	1.63	0.74	2.02	3.11	3.37	2.47	0.22	2.15	1.08	2.92	6.58	2.87	1.69	0.51	0.52	1.06	0.34	3.37	1.35	0.51	0.17
chr8:122500001-123000000	2.89	1.22	0.49	2.02	2.36	0.56	0.90	3.44	3.11	2.25	6.58	5.56	0.84	2.70	0.22	1.30	1.01	0.00	2.36	0.51	2.87
chr2:119500001-120000000	3.02	1.39	0.64	1.42	0.90	0.56	na	2.61	2.00	3.37	6.49	3.37	0.67	na	0.38	0.88	1.01	0.51	1.35	0.67	na
chr1:134500001-135000000	2.56	0.97	0.75	1.09	1.91	0.34	0.67	2.81	1.17	1.55	6.49	1.57	0.51	0.17	0.42	0.94	0.45	1.35	0.51	0.51	1.01
chr2:28500001-29000000	2.75	0.86	1.87	3.04	2.47	0.90	na	2.08	1.29	1.85	6.49	2.42	0.67	na	0.53	0.88	0.67	1.52	2.02	0.67	na
chr11:115500001-116000000	3.22	1.52	0.64	0.97	0.45	0.34	0.45	2.29	1.84	2.28	6.49	3.37	1.69	1.69	0.16	1.49	1.12	1.35	1.85	0.51	0.34
chr11:116500001-117000000	3.19	1.48	0.30	1.31	1.46	1.01	1.12	2.59	1.17	3.40	6.49	1.80	1.69	0.67	0.35	1.26	0.56	0.67	1.69	0.17	0.34
chr11:118500001-119000000	3.37	0.70	1.27	2.66	2.14	0.22	0.67	2.66	1.87	1.66	6.49	3.04	0.67	0.67	0.48	1.31	0.22	2.36	1.69	0.51	0.51
chr7:52500001-53000000	1.23	0.90	0.94	1.42	1.69	1.24	0.67	1.66	1.58	1.74	6.41	3.37	3.88	1.35	0.13	0.84	1.01	0.17	1.35	0.34	0.00
chr7:108500001-109000000	2.83	1.21	0.75	1.42	0.67	0.67	0.67	2.36	1.73	2.45	6.32	1.74	1.52	0.51	0.94	1.18	0.67	0.84	1.85	0.67	1.18
chr2:35500001-36000000	2.91	0.81	1.05	2.77	3.37	2.25	na	2.31	3.26	1.60	6.32	6.97	2.70	na	0.17	1.03	0.67	0.84	1.69	0.00	na
chr10:83500001-84000000	2.99	0.37	0.49	1.76	1.80	0.90	1.12	3.30	3.37	3.20	6.32	6.30	1.35	2.53	0.31	0.38	0.67	0.84	0.17	0.17	0.34
chr19:4500001-5000000	1.08	0.76	2.02	3.48	2.59	3.37	0.67	1.84	1.63	3.37	6.32	3.37	5.06	0.67	0.95	0.56	0.45	2.53	1.85	0.51	0.34
chr19:10500001-11000000	0.77	1.06	1.20	2.29	6.30	3.37	0.90	1.14	1.76	2.70	6.32	2.02	6.07	0.67	0.30	0.70	0.56	0.17	2.87	0.34	1.69
chr11:69000001-69500000	1.61	1.56	0.22	2.06	2.14	1.01	0.67	1.04	0.99	2.50	6.24	2.53	1.52	0.51	0.59	1.60	1.12	0.51	0.34	0.84	0.34
chr11:75500001-76000000	2.51	0.89	0.75	3.11	2.02	1.35	0.45	2.88	2.14	1.57	6.24	4.22	1.35	0.17	0.40	1.10	0.90	0.34	4.22	0.34	0.17
chr14:62000001-62500000	3.28	0.30	2.47	2.70	3.04	2.47	0.45	3.30	3.46	3.37	6.24	2.36	4.55	1.35	1.76	0.29	0.67	1.01	3.20	1.52	3.20
chr9:96000001-96500000	3.08	0.15	1.16	1.87	2.70	1.69	1.57	2.90	2.88	2.36	6.15	4.61	1.35	3.37	2.11	0.70	0.79	0.51	2.36	0.34	3.37
chr13:54500001-55000000	2.06	1.23	0.49	1.24	2.47	2.14	0.45	1.81	2.43	2.14	6.15	2.87	3.20	0.84	0.38	0.78	0.34	0.17	1.18	0.67	1.18
chr13:55000001-55500000	2.16	1.30	0.97	2.44	2.70	1.01	0.90	1.85	1.63	3.01	6.15	2.64	1.35	1.18	0.34	0.88	0.34	1.01	2.19	0.17	1.01
chr17:25000001-25500000	1.08	1.10	2.51	2.36	2.14	2.92	0.22	1.18	0.62	2.92	6.15	1.18	1.85	0.00	0.11	1.33	1.12	0.67	0.17	0.67	0.00
chr17:44500001-45000000	2.17	0.49	2.47	2.92	6.97	3.15	1.57	3.11	3.00	3.37	6.15	3.37	5.23	1.35	1.62	0.19	0.67	2.36	2.19	1.52	1.69
chr5:36000001-36500000	1.09	0.96	0.79	2.40	2.92	2.36	0.67	1.79	1.53	3.32	6.07	3.32	2.02	0.17	0.23	1.18	0.90	1.18	1.01	0.84	1.18
chr6:51500001-52000000	1.90	na	1.76	3.15	1.46	0.67	0.90	2.66	na	2.02	6.07	1.80	2.87	0.51	0.35	na	0.56	0.84	0.67	0.67	0.34
chr7:105500001-106000000	2.79	0.67	0.64	2.85	1.91	0.45	1.80	2.36	0.88	1.60	6.07	2.25	1.35	1.01	1.07	0.72	0.90	0.51	2.53	0.34	1.18
chr12:78500001-79000000	na	0.47	2.51	2.02	2.70	3.48	0.45	na	2.18	1.32	6.07	1.52	3.20	1.01	na	0.32	0.11	1.18	3.20	1.18	1.01
chr17:27500001-28000000	1.95	1.39	1.46	2.89	2.36	0.56	0.90	1.90	1.91	3.01	6.07	4.16	2.36	0.51	0.17	1.49	0.79	0.34	0.51	0.34	0.67
chr5:141000001-141500000	3.47	1.03	0.49	1.61	1.91	0.56	0.90	3.14	2.71	1.80	5.99	5.28	0.00	1.69	0.62	1.00	1.12	0.84	3.20	0.84	2.53
chr6:39000001-39500000	0.71	na	0.71	2.51	1.35	2.59	0.67	1.59	na	2.05	5.99	4.10	1.85	0.84	0.35	na	0.79	0.51	1.52	0.84	0.84
chr9:64000001-64500000	2.19	1.11	1.20	3.37	1.57	0.79	0.90	1.71	1.04	1.85	5.99	0.84	0.84	0.51	0.36	1.19	0.56	1.01	0.17	0.34	0.67
chr9:108000001-108500000	3.12	1.57	0.56	1.65	1.69	0.34	0.45	2.04	1.22	2.11	5.99	3.48	0.67	1.69	0.33	1.33	0.79	0.67	2.19	0.67	1.69
chr11:75000001-75500000	3.37	1.29	1.65	2.92	2.70	1.35	0.45	3.05	2.70	1.63	5.99	5.17	4.89	1.35	0.08	1.26	1.01	1.18	3.37	0.84	0.84
chr11:78000001-78500000	3.48	1.17	2.36	3.48	3.15	0.11	0.22	2.38	1.38	2.75	5.99	3.04	1.69	1.52	0.30	0.97	1.01	0.67	2.36	0.34	0.17
chr17:47000001-47500000	2.01	0.92	0.71	0.90	1.12	0.79	0.45	1.38	0.74	2.67	5.99	1.80	1.35	0.84	0.46	1.03	0.79	0.84	2.02	0.84	0.17
chr18:34500001-35000000	1.28	0.87	0.64	3.11	2.36	2.25	2.02	1.80	1.63	2.73	5.99	3.48	3.04	1.69	1.26	0.31	0.67	1.01	4.55	0.51	1.01
chr7:107000001-107500000	3.37	0.98	0.56	1.87	1.57	0.34	0.67	2.86	0.95	1.57	5.90	2.53	1.35	0.17	1.17	1.06	0.79	0.84	3.04	0.51	1.18
chr11:119000001-119500000	3.17	1.44	0.56	1.24	1.57	0.34	0.45	2.73	2.59	1.38	5.90	4.55	0.67	1.18	0.17	1.36	1.24	0.34	0.67	0.00	0.51
chr12:100000001-100500000	na	0.53	0.22	1.27	1.46	1.01	0.67	na	3.28	2.84	5.90	5.73	3.20	3.04	na	0.33	0.34	0.34	1.69	0.51	2.53
chr14:70500001-71000000	3.31	0.87	0.75	1.65	2.81	0.79	1.12	2.75	2.98	2.95	5.90	3.15	2.36	2.19	0.85	0.90	1.01	0.51	3.04	0.67	2.53
chr18:65000001-65500000	2.11	0.78	1.01	2.02	1.46	1.12	0.90	2.35	3.00	2.64	5.90	4.33	2.02	2.02	1.20	0.26	0.45	1.18	1.69	0.84	2.19
chr19:37000001-37500000	1.69	0.20	2.55	2.14	2.02	0.67	0.67	1.68	2.39	3.15	5.90	2.19	5.40	0.00	0.95	0.13	2.02	1.85	0.84	3.37	0.67
chr6:31000001-31500000	1.92	na	2.81	2.17	3.04	1.69	0.22	1.83	na	1.83	5.82	3.32	3.37	0.17	1.30	na	0.22	1.52	2.53	1.01	1.01
chr6:51000001-51500000	2.77	na	3.00	1.01	2.70	1.91	1.12	2.43	na	3.20	5.82	3.88	3.20	1.01	0.34	na	0.56	0.67	0.51	0.51	0.67

chr11:98500001-99000000	2.70	1.36	0.64	1.99	0.56	0.22	0.22	2.25	2.41	2.30	5.82	6.52	3.37	1.18	0.15	1.45	1.12	0.67	2.87	0.51	1.18
chr15:74500001-75000000	2.06	0.46	1.42	2.21	3.04	na	1.12	2.20	2.83	3.37	5.82	3.15	na	1.01	0.28	0.75	0.90	0.67	4.38	na	2.70
chr11:68000001-68500000	2.50	0.51	0.97	2.36	4.95	1.91	0.90	2.40	2.22	2.33	5.82	3.15	3.37	1.35	0.14	1.20	1.24	0.17	3.04	0.34	1.69
chr12:81500001-82000000	na	1.30	1.95	3.22	1.57	0.79	0.90	na	0.64	0.84	5.82	2.42	1.18	0.17	na	1.03	0.34	0.51	0.84	0.34	0.17
chr14:70000001-70500000	3.11	1.02	0.56	1.84	2.36	0.22	0.90	3.12	3.07	2.22	5.82	5.11	1.69	2.19	1.29	0.82	0.45	1.01	1.52	0.34	1.85
chr2:24500001-25000000	1.01	0.60	1.91	1.50	2.81	2.47	na	1.03	0.87	2.61	5.73	2.59	1.52	na	0.24	1.05	0.56	0.17	1.52	0.84	na
chr11:76500001-77000000	2.26	1.14	1.27	3.34	2.36	0.79	0.67	2.65	2.06	2.64	5.73	3.37	0.67	0.00	0.28	1.08	0.56	0.34	1.69	0.51	0.34
chr11:115000001-115500000	3.12	1.42	0.26	0.52	0.79	0.79	0.22	2.39	1.45	2.08	5.73	2.59	2.36	1.18	0.52	1.54	1.12	0.67	1.01	0.67	2.70
chr3:89000001-89500000	2.21	1.03	0.64	1.42	na	0.79	0.67	2.40	1.23	2.22	5.65	na	0.67	0.84	0.41	1.29	1.24	1.52	na	0.34	0.84
chr6:52000001-52500000	1.86	na	1.95	3.15	2.70	0.79	0.22	3.31	na	2.11	5.65	4.33	2.87	0.51	0.13	na	0.56	0.67	0.51	0.84	1.01
chr6:67000001-67500000	1.19	na	0.90	1.35	3.04	2.70	3.37	2.38	na	3.01	5.65	2.98	6.24	1.69	3.42	na	0.45	1.69	2.53	2.36	6.75
chr13:55500001-56000000	1.91	1.04	0.64	1.01	1.91	1.12	0.90	1.86	1.80	3.04	5.65	2.08	2.19	1.85	0.23	1.27	0.45	1.01	1.52	0.84	1.18
chr17:46500001-47000000	1.71	1.19	0.97	1.46	1.69	1.12	0.67	2.22	1.52	2.50	5.65	3.04	1.52	0.17	0.35	1.02	0.90	0.84	2.87	0.51	0.67
chr5:122000001-122500000	1.47	1.43	0.60	2.36	1.46	0.34	0.22	1.74	0.95	2.36	5.65	2.59	0.51	0.67	0.45	1.10	1.01	0.51	1.35	0.17	1.69
chr8:128000001-128500000	3.04	0.78	0.52	1.42	1.69	0.11	0.90	3.02	1.83	1.60	5.65	1.74	2.53	3.20	0.95	0.50	0.90	1.35	0.67	0.51	1.52
chr16:24500001-25000000	3.34	1.00	na	2.81	5.06	3.04	0.67	3.27	3.50	na	5.65	5.11	5.90	1.35	1.81	0.71	na	0.67	3.88	0.84	0.84
chr5:107500001-108000000	2.99	0.37	1.16	2.81	3.04	0.79	1.80	2.77	3.36	2.64	5.56	3.04	1.52	1.18	1.60	0.61	0.79	1.18	4.55	0.51	3.37
chr7:87500001-88000000	2.60	1.21	0.90	3.15	1.46	1.01	0.67	2.91	2.87	2.67	5.56	5.06	2.02	0.84	0.68	1.15	1.01	0.51	7.42	0.67	3.37
chr9:13500001-14000000	0.79	0.73	2.55	1.16	3.37	7.98	0.22	1.40	3.50	3.18	5.56	5.11	8.26	0.84	1.16	0.40	0.67	0.84	3.20	3.88	1.35
chr11:97000001-97500000	3.36	1.48	0.41	3.15	1.80	0.56	0.45	2.35	2.09	2.36	5.56	3.37	1.85	0.34	0.22	1.52	0.90	0.51	2.87	0.34	0.34
chr11:97500001-98000000	2.48	1.38	0.52	1.65	0.79	1.24	0.67	1.95	2.26	2.73	5.56	3.37	1.18	2.19	0.33	1.33	1.12	0.67	3.37	0.34	0.84
chr19:47000001-47500000	0.68	0.48	0.49	2.14	1.91	1.69	0.67	1.56	1.69	2.30	5.56	2.59	2.19	0.34	1.11	0.46	0.56	1.52	2.19	0.34	1.01
chr3:87500001-88000000	3.08	1.58	0.56	1.91	na	1.01	0.45	1.92	1.28	1.71	5.48	na	0.17	0.17	0.08	1.14	1.12	0.84	na	0.67	1.01
chr11:76000001-76500000	1.88	1.59	0.52	1.35	1.91	0.56	0.90	2.14	0.92	1.71	5.48	2.70	0.34	0.51	0.17	1.26	1.12	0.17	1.18	0.00	0.84
chr15:102000001-102500000	3.18	0.63	1.87	1.35	1.69	na	1.12	2.03	1.59	3.01	5.48	2.81	na	1.69	0.74	0.98	0.79	0.51	3.20	na	1.52
chr3:96000001-96500000	3.44	1.40	0.49	2.06	na	0.90	0.45	2.15	3.22	2.92	5.40	na	2.19	0.67	0.25	0.99	1.01	1.35	na	0.67	1.01
chr8:97000001-97500000	2.36	0.61	0.56	1.20	1.91	0.67	1.12	1.94	1.63	2.61	5.40	3.37	2.36	1.85	1.30	0.62	0.34	0.51	2.19	0.17	3.04
chr11:54000001-54500000	2.82	0.58	1.09	2.85	3.26	2.59	0.22	1.38	1.05	1.77	5.40	1.52	2.53	0.34	0.81	0.96	0.67	0.51	3.20	0.34	1.01
chr11:60000001-60500000	2.03	1.12	1.24	1.91	3.26	1.01	0.45	1.56	1.22	2.33	5.40	3.04	2.36	0.51	0.17	1.10	1.01	0.67	2.02	0.84	0.51
chr13:36000001-36500000	1.43	0.21	0.75	1.57	2.02	1.46	0.45	1.81	2.71	2.95	5.40	2.25	3.37	0.67	0.89	0.41	0.67	0.51	2.70	1.35	1.52
chr17:25500001-26000000	0.39	1.59	2.10	2.81	2.81	0.90	0.90	1.36	1.21	3.37	5.40	2.08	2.70	0.84	0.27	1.19	0.34	1.18	0.51	0.34	0.34
chr18:4500001-5000000	0.50	0.60	0.97	0.97	2.02	3.37	0.45	1.96	3.22	2.70	5.40	3.37	5.73	1.85	1.93	0.29	0.67	1.18	3.20	2.36	1.01
chr18:75000001-75500000	2.64	0.54	1.16	1.35	1.69	0.90	2.25	2.82	2.21	1.46	5.40	6.24	3.04	2.70	1.25	0.36	0.56	0.51	2.53	1.35	3.20
chr1:137000001-137500000	2.47	1.29	0.30	0.82	1.35	0.45	0.45	3.10	0.97	1.10	5.31	1.24	0.00	0.84	0.73	0.84	0.34	0.34	1.35	0.51	0.17
chr5:115000001-115500000	2.60	1.50	0.49	2.66	2.59	0.56	0.45	2.32	2.34	2.22	5.31	3.15	1.18	1.52	0.27	1.28	0.90	0.34	2.70	0.51	0.84
chr11:79500001-80000000	2.97	0.79	0.75	1.01	1.57	0.56	0.67	1.87	1.26	2.25	5.31	1.46	1.85	0.51	0.07	1.23	0.45	0.51	1.35	0.67	0.67
chr14:64500001-65000000	2.81	0.45	0.79	2.96	3.26	0.22	0.67	2.04	0.90	1.69	5.31	2.08	1.01	0.51	1.38	0.55	0.79	1.18	1.69	0.17	1.18
chr14:75000001-75500000	3.08	0.31	0.82	1.50	0.90	1.46	1.12	3.10	3.43	2.16	5.31	2.02	2.36	3.37	1.58	0.32	0.56	0.67	2.02	0.67	2.02
chr15:82000001-82500000	1.97	0.24	1.91	1.95	1.24	na	0.45	1.75	1.54	3.26	5.31	3.37	na	0.17	0.56	1.02	0.90	1.85	1.18	na	0.67
chr15:96000001-96500000	2.53	0.93	1.09	1.42	3.26	na	0.90	2.85	3.31	2.95	5.31	2.70	na	2.70	1.63	0.59	0.56	0.00	4.22	na	2.19
chr16:17500001-18000000	2.17	1.15	na	3.30	2.02	1.69	0.45	2.64	1.62	na	5.31	2.87	3.04	0.34	1.41	0.48	na	0.17	2.36	0.17	0.84
chr3:87000001-87500000	2.95	0.46	1.72	2.06	na	1.01	0.67	2.08	1.76	2.45	5.23	na	2.02	1.18	0.79	0.54	0.56	0.84	na	0.51	0.00
chr3:88500001-89000000	3.04	1.25	0.45	1.87	na	0.67	0.00	2.13	1.26	1.83	5.23	na	1.01	1.35	0.07	1.37	1.24	0.67	na	1.01	0.51
chr7:106500001-107000000	2.22	0.83	1.31	2.66	2.36	1.80	0.45	2.56	1.57	1.88	5.23	2.87	1.85	0.17	1.05	0.82	0.56	1.52	2.70	0.51	0.00
chr7:133500001-134000000	2.02	1.59	1.01	1.39	0.67	0.90	1.35	2.99	2.55	2.84	5.23	5.62	1.18	0.84	0.15	1.33	1.01	1.18	2.70	0.84	0.84
chr9:107500001-108000000	3.44	1.51	0.71	1.01	1.24	0.90	0.67	2.86	1.87	2.05	5.23	3.37	2.70	2.53	0.35	1.23	1.12	0.67	5.56	1.01	0.67
chr10:41000001-41500000	1.37	0.69	1.09	1.69	1.91	1.24	0.90	1.28	1.88	3.46	5.23	2.81	3.37	1.35	0.77	0.75	0.90	1.01	4.72	0.84	2.36
chr11:49500001-50000000	1.31	0.97	1.35	2.25	1.80	2.59	1.12	1.97	2.93	2.84	5.23	4.38	2.70	2.02	0.11	0.91	0.56	1.18	2.36	0.84	1.69
chr11:119500001-120000000	3.03	1.15	1.50	0.90	0.79	0.34	0.90	1.99	1.11	1.35	5.23	2.08	0.51	0.51	0.12	1.47	1.12	0.67	1.01	0.84	1.18

chr2:167000001-167500000	2.51	1.35	0.60	0.90	2.70	0.67	na	3.01	2.98	1.66	5.14	4.89	0.17	na	0.19	1.30	1.24	0.51	1.35	0.67	na
chr5:121500001-122000000	1.81	1.37	0.11	1.27	0.90	0.45	0.45	1.42	0.30	1.74	5.14	1.46	1.01	1.01	0.10	1.31	1.01	0.17	1.35	0.34	1.18
chr6:38500001-39000000	1.03	na	1.42	3.45	3.37	3.15	0.00	2.16	na	2.92	5.14	2.92	2.70	1.01	0.54	na	0.45	1.52	1.52	2.02	0.17
chr6:71000001-71500000	0.72	na	0.79	0.19	0.67	1.12	1.12	1.89	na	2.19	5.14	0.84	0.84	1.69	0.81	na	0.67	0.34	2.70	0.34	3.37
chr8:123500001-124000000	2.49	0.79	0.67	1.87	2.14	0.79	0.90	2.30	1.30	1.63	5.14	1.63	0.51	1.35	0.12	1.21	0.79	2.70	0.84	0.67	0.00
chr9:45000001-45500000	2.24	0.70	0.64	3.45	5.40	1.24	1.12	0.90	0.94	2.70	5.14	3.26	2.19	0.34	0.11	1.30	0.34	1.01	0.84	0.00	0.51
chr10:39000001-39500000	3.28	0.71	1.42	3.37	2.02	3.15	0.45	1.96	3.32	2.19	5.14	5.73	6.41	0.84	1.70	0.15	0.34	0.34	3.20	0.67	1.01
chr11:117000001-117500000	3.37	1.22	0.41	2.40	2.25	0.34	0.67	2.55	1.73	1.94	5.14	3.15	1.01	0.67	0.53	1.37	1.01	0.51	1.69	0.67	0.34
chr17:33500001-34000000	2.78	0.81	2.36	2.25	1.69	1.69	0.45	1.51	1.50	3.37	5.14	1.52	1.01	0.51	0.00	1.32	0.90	1.52	1.52	0.51	1.35
chr5:108000001-108500000	2.64	0.78	0.60	1.12	3.15	1.69	0.22	2.28	3.47	2.19	5.14	5.17	2.19	1.01	1.08	0.77	0.90	0.34	3.88	0.67	3.37
chr12:112000001-112500000	na	0.63	0.90	1.76	1.24	0.56	1.35	na	1.87	2.45	5.14	1.85	2.70	1.52	na	1.05	1.01	0.17	3.04	0.51	2.70
chr15:83000001-83500000	1.70	0.99	1.39	2.32	2.36	na	0.67	1.57	1.56	2.56	5.14	1.63	na	0.84	0.31	0.83	0.79	2.19	0.67	na	1.52
chr17:47500001-48000000	1.28	1.23	0.07	1.65	1.69	1.24	0.45	1.77	1.62	2.16	5.14	2.36	3.04	1.01	0.65	1.31	0.67	0.67	2.87	0.84	1.01
chr1:54500001-55000000	2.99	0.37	1.24	1.80	2.14	3.04	1.12	2.76	3.00	2.42	5.06	4.38	3.88	1.35	1.89	0.39	0.56	0.17	2.36	0.00	1.35
chr6:113000001-113500000	2.94	na	0.79	1.20	2.47	0.90	0.45	2.80	na	1.43	5.06	2.36	3.20	2.36	0.58	na	0.90	0.67	2.19	1.01	2.70
chr10:5000001-5500000	0.73	0.93	1.99	1.91	1.91	3.37	0.90	1.43	3.04	3.32	5.06	3.15	5.23	1.01	1.11	0.42	0.45	0.67	2.70	2.19	2.02
chr11:85500001-86000000	1.93	0.88	0.86	2.47	2.36	0.56	0.45	3.39	1.68	3.20	5.06	1.97	1.01	1.01	0.63	1.12	0.45	2.02	0.84	0.34	0.67
chr12:35000001-35500000	na	1.16	2.06	1.27	2.47	2.02	0.67	na	3.32	1.77	5.06	3.15	5.06	1.85	na	1.76	2.02	2.36	0.34	2.02	0.17
chr2:119000001-119500000	1.58	1.56	0.45	0.34	0.90	0.45	na	1.60	1.05	0.73	4.97	4.16	0.17	na	0.24	1.28	0.79	1.01	2.36	0.51	na
chr2:153000001-153500000	2.22	1.36	0.19	0.86	3.15	0.67	na	2.59	1.50	0.93	4.97	3.26	0.34	na	0.55	1.22	1.01	0.51	3.04	0.51	na
chr5:65500001-66000000	1.31	1.26	0.64	0.90	2.59	0.79	0.45	2.15	2.82	2.67	4.97	5.34	2.02	0.51	0.45	0.90	0.56	0.34	2.87	0.00	0.67
chr9:43500001-44000000	0.22	0.97	1.54	2.62	1.91	1.46	0.45	0.51	0.35	1.12	4.97	1.24	0.84	0.34	0.21	1.14	0.79	0.67	2.36	0.00	0.00
chr9:57000001-57500000	3.01	0.82	0.79	3.34	3.04	1.12	0.45	2.14	2.56	2.70	4.97	3.15	1.52	0.51	0.03	1.24	0.67	0.51	2.87	0.51	0.67
chr10:42500001-43000000	1.75	0.37	1.16	2.25	2.92	1.69	0.45	1.79	2.17	3.37	4.97	4.27	3.04	1.18	0.65	0.36	0.34	2.02	2.19	2.19	1.18
chr11:69500001-70000000	1.78	1.26	0.34	1.95	1.69	1.24	0.45	1.47	1.12	2.81	4.97	1.57	1.69	0.34	0.64	1.52	0.90	0.84	1.35	0.67	0.84
chr11:84500001-85000000	2.18	0.26	1.87	1.61	1.35	0.45	0.45	1.65	0.75	2.05	4.97	0.84	1.18	0.00	0.02	1.27	0.56	0.67	0.67	0.34	0.34
chr11:88000001-88500000	2.79	0.74	1.01	1.24	2.47	0.79	1.35	2.77	3.23	2.00	4.97	5.28	3.37	1.52	0.30	1.27	0.90	1.35	2.53	0.51	1.01
chr11:95000001-95500000	1.93	0.82	0.75	2.02	1.80	0.90	0.67	2.36	2.04	1.52	4.97	4.78	1.01	1.35	0.25	1.21	0.34	0.34	2.70	0.51	0.34
chr13:113500001-114000000	1.61	0.50	0.34	0.90	1.01	0.34	3.37	2.25	1.11	0.93	4.97	0.67	1.01	3.37	1.69	0.57	0.67	0.17	3.37	0.51	1.69
chr5:124000001-124500000	2.23	1.50	0.90	1.57	2.14	0.45	0.22	2.43	1.41	2.22	4.97	3.15	1.18	1.35	0.30	1.27	1.24	1.18	2.19	0.84	0.17
chr11:24000001-24500000	1.48	0.66	3.04	2.14	5.06	12.70	0.67	0.90	3.43	2.98	4.97	3.37	9.27	1.35	0.18	0.14	1.80	2.70	0.51	2.19	0.51
chr15:66500001-67000000	2.55	0.13	0.45	1.99	2.70	na	0.45	1.60	3.21	2.92	4.97	4.33	na	2.70	1.70	0.66	0.34	0.17	2.02	na	3.20
chr14:55000001-55500000	2.61	1.04	0.86	2.36	2.14	0.90	0.90	1.62	1.75	1.29	4.89	2.25	3.37	2.87	0.51	1.14	0.79	0.67	5.56	0.84	1.18
chr1:137500001-138000000	2.44	1.33	0.94	1.20	0.34	0.22	0.45	2.63	0.59	1.21	4.89	3.32	0.84	2.19	0.95	1.17	0.79	0.67	2.87	0.17	1.18
chr10:82000001-82500000	3.36	0.57	0.34	2.51	1.91	0.34	0.67	1.80	2.27	2.81	4.89	2.53	1.52	1.52	1.10	0.29	0.56	0.67	2.02	0.67	2.53
chr12:87000001-87500000	na	0.53	0.30	2.55	2.70	1.24	0.90	na	1.27	2.05	4.89	3.77	1.35	1.18	na	0.89	0.67	0.51	2.36	0.51	1.35
chr13:32500001-33000000	1.01	0.39	0.79	2.06	2.14	1.69	0.22	0.80	2.31	1.41	4.89	1.52	3.20	0.84	0.27	0.17	0.45	1.85	0.84	1.52	0.67
chr19:10000001-10500000	0.98	0.84	2.32	2.59	2.25	3.37	0.22	0.58	1.88	2.70	4.89	1.85	5.90	2.02	0.35	0.57	1.57	1.85	0.67	2.19	1.18
chr1:37000001-37500000	2.66	0.72	1.27	1.35	2.02	1.91	0.22	3.27	2.79	2.33	4.81	3.82	2.19	0.67	1.20	0.89	0.56	0.84	2.36	0.84	0.67
chr6:48500001-49000000	2.70	na	0.97	2.47	2.02	3.26	0.67	1.53	na	2.98	4.81	3.77	1.35	0.51	0.07	na	0.45	1.69	1.18	0.51	2.19
chr8:73000001-73500000	1.12	1.26	0.34	0.45	2.14	1.12	0.67	1.25	1.69	2.28	4.81	3.43	3.88	2.02	0.30	1.23	1.12	0.67	1.69	0.34	0.51
chr9:71000001-71500000	0.59	0.50	0.37	2.14	0.45	0.67	0.90	1.43	1.44	2.05	4.81	1.91	1.35	0.67	0.88	0.85	0.11	1.52	1.18	1.35	0.34
chr10:74500001-75000000	1.78	0.41	0.86	1.12	1.69	1.12	0.90	2.08	2.58	2.42	4.81	4.22	3.37	2.36	0.29	0.77	0.79	0.51	1.01	0.34	1.18
chr11:87000001-87500000	2.76	1.23	0.45	1.24	2.02	0.79	0.45	2.68	2.63	2.36	4.81	3.09	1.85	0.51	0.25	1.38	1.01	1.01	2.87	0.84	0.34
chr11:96500001-97000000	2.64	1.53	0.30	2.21	2.36	0.45	0.45	1.55	0.67	0.45	4.81	1.91	1.01	0.51	0.78	1.33	0.90	0.51	5.56	0.34	0.00
chr11:100000001-100500000	3.16	0.79	1.27	2.36	2.02	0.79	0.67	1.89	1.89	1.49	4.81	3.04	2.02	0.51	0.22	1.05	0.56	2.02	1.85	0.51	0.34
chr1:59000001-59500000	1.68	0.72	0.64	2.25	0.67	0.79	0.45	1.89	1.88	2.28	4.72	2.47	2.87	0.17	0.94	0.55	0.56	0.67	2.70	0.34	2.36
chr5:30500001-31000000	0.23	0.76	1.24	1.39	1.24	1.91	0.67	1.01	1.23	2.05	4.72	1.74	1.52	0.84	0.05	0.70	0.45	3.04	1.01	0.34	0.17
chr7:52000001-52500000	1.12	1.32	0.19	1.46	1.69	1.12	0.67	0.97	1.25	1.97	4.72	2.36	2.70	0.67	0.58	1.25	0.90	0.34	1.18	0.17	0.34

chr14:21500001-22000000	1.30	0.89	0.64	2.85	2.25	1.91	0.67	1.77	1.77	2.50	4.72	2.87	5.06	1.85	1.18	0.48	0.45	0.34	3.88	0.67	1.85
chr14:79000001-79500000	1.45	0.42	0.52	0.97	1.91	0.79	1.12	2.45	3.18	2.11	4.72	3.37	3.04	3.20	2.00	0.21	0.45	0.00	2.70	1.35	0.51
chr15:85500001-86000000	1.14	0.97	0.71	0.75	1.12	na	0.67	1.44	1.91	1.29	4.72	3.32	na	1.18	0.11	1.33	1.01	0.84	2.70	na	0.67
chr3:51000001-51500000	0.64	0.86	0.75	1.01	na	2.36	1.35	1.42	2.25	1.32	4.64	na	3.37	0.00	0.60	0.69	0.45	0.51	na	0.17	2.70
chr10:41500001-42000000	2.25	0.59	1.09	3.26	4.27	2.25	0.67	0.97	1.99	1.85	4.64	2.64	1.01	0.51	0.67	0.85	0.79	0.84	3.37	0.34	1.85
chr13:45500001-46000000	3.00	0.62	2.44	3.15	2.70	1.46	0.45	2.05	1.94	1.57	4.64	3.32	2.19	0.84	1.09	0.72	0.34	1.01	2.19	0.34	0.34
chr16:4000001-4500000	1.07	0.64	na	0.82	2.36	7.19	0.67	2.13	2.04	na	4.64	3.04	7.76	0.51	1.87	0.63	na	0.51	4.22	1.18	1.52
chr16:4500001-5000000	0.98	0.58	na	2.25	2.59	6.75	0.90	2.13	3.19	na	4.64	3.37	7.93	1.69	0.68	1.03	na	1.01	4.72	1.18	1.18
chr17:45500001-46000000	1.62	1.56	0.75	1.72	2.02	1.35	0.67	1.72	1.24	3.37	4.64	2.36	2.87	0.67	0.12	1.39	0.90	1.01	2.70	0.34	0.34
chr19:40500001-41000000	2.97	0.41	2.06	2.89	2.02	3.04	0.90	1.47	2.95	3.43	4.64	3.04	4.89	0.84	1.03	0.20	0.45	0.34	1.35	0.67	1.18
chr5:37000001-37500000	0.96	0.52	0.82	1.99	2.81	3.26	0.45	1.70	1.77	2.84	4.55	3.99	3.37	0.34	0.06	0.87	0.90	0.67	2.19	0.51	0.67
chr8:127000001-127500000	2.70	0.55	0.86	1.65	1.80	1.01	1.12	1.89	0.44	2.11	4.55	0.96	0.17	1.52	0.62	1.21	0.79	0.51	1.85	0.67	1.18
chr9:103000001-103500000	2.70	0.20	0.86	2.59	3.37	0.90	1.80	3.41	3.00	1.69	4.55	5.79	2.53	3.37	0.90	0.43	1.01	0.84	1.85	0.84	2.70
chr10:42000001-42500000	1.04	0.28	0.94	1.72	1.57	1.01	0.45	1.00	1.31	2.30	4.55	2.14	3.04	0.67	0.24	0.79	0.34	0.84	3.37	0.67	1.01
chr10:60500001-61000000	1.82	0.36	1.12	2.02	1.80	0.56	0.45	1.41	0.93	1.55	4.55	3.43	3.37	0.67	0.48	1.13	0.45	0.67	1.69	0.34	1.18
chr10:80500001-81000000	1.14	1.97	0.75	0.82	1.24	0.34	0.22	0.80	0.85	1.38	4.55	2.98	2.02	0.84	0.47	1.56	1.24	0.67	1.69	1.01	0.67
chr10:83000001-83500000	1.82	0.71	1.01	1.31	0.56	0.34	0.22	1.84	1.14	0.98	4.55	1.41	1.18	1.85	0.14	0.18	0.22	0.17	0.67	1.52	2.87
chr2:156500001-157000000	3.14	1.28	0.37	0.49	0.67	0.34	na	2.34	0.99	1.52	4.47	1.97	1.01	na	0.17	1.17	0.90	0.51	1.52	0.67	na
chr3:90000001-90500000	3.00	0.75	0.52	1.54	na	0.90	0.67	1.95	1.19	2.56	4.47	na	0.84	2.36	0.33	0.94	0.34	0.67	na	0.17	2.70
chr3:94500001-95000000	1.98	0.58	0.34	1.12	na	0.67	0.67	1.51	1.11	1.52	4.47	na	0.84	0.51	0.36	0.93	0.56	0.51	na	0.34	1.85
chr7:31000001-31500000	0.40	1.31	0.37	1.27	0.56	1.24	0.45	0.69	1.32	2.56	4.47	2.25	3.04	0.34	0.23	1.21	1.24	0.51	0.34	0.51	0.34
chr10:94000001-94500000	2.63	0.51	0.22	0.64	1.91	0.11	0.22	2.13	2.35	1.46	4.47	2.70	2.02	2.70	1.14	0.47	0.34	0.84	0.34	0.51	1.35
chr6:30000001-30500000	1.29	na	1.20	1.61	2.14	1.57	0.45	1.51	na	2.39	4.38	3.37	3.37	0.67	0.45	na	1.01	0.00	1.18	1.18	0.84
chr6:72000001-72500000	1.10	na	0.34	1.42	1.57	1.01	0.45	2.07	na	1.74	4.38	2.47	0.67	0.34	0.21	na	0.67	0.67	1.18	0.17	1.52
chr7:31500001-32000000	0.61	0.25	0.41	0.34	1.24	0.67	0.22	1.19	1.64	2.39	4.38	2.75	3.37	0.34	0.44	0.79	0.67	0.34	0.34	1.85	0.67
chr12:112500001-113000000	na	1.54	0.56	1.09	1.46	0.45	0.90	na	0.50	1.15	4.38	2.02	0.67	0.67	na	1.15	0.67	0.51	0.67	0.34	0.17
chr17:6000001-6500000	0.43	1.68	1.09	0.86	1.01	1.24	0.67	0.60	0.87	1.35	4.38	2.19	3.04	0.17	0.13	1.29	0.67	0.84	1.85	0.51	0.67
chr3:37500001-38000000	3.46	1.26	2.70	1.69	na	2.36	0.45	1.91	3.28	2.02	4.30	na	2.53	2.02	1.86	0.32	0.45	0.84	na	1.85	2.19
chr3:86500001-87000000	3.27	0.41	1.57	2.62	na	0.67	1.57	2.52	2.15	3.26	4.30	na	0.67	3.20	1.66	0.63	0.34	0.84	na	1.35	1.52
chr7:133000001-133500000	1.94	0.66	0.67	0.52	0.79	0.45	1.57	2.16	1.44	1.35	4.30	3.09	0.00	1.52	0.28	1.16	1.12	1.35	2.87	0.34	0.34
chr9:56500001-57000000	1.80	0.88	2.17	2.70	2.92	1.12	0.45	1.24	0.85	2.30	4.30	2.53	2.36	1.69	0.25	1.37	0.67	0.17	2.02	0.17	0.17
chr10:62000001-62500000	1.52	0.94	0.82	2.36	1.91	1.24	0.90	1.64	1.45	1.80	4.30	2.19	1.35	0.67	0.33	1.06	1.01	0.51	1.35	0.00	2.36
chr11:51500001-52000000	2.40	1.07	1.05	2.51	3.15	1.69	0.90	1.34	1.82	2.81	4.30	3.04	3.04	1.01	0.27	1.28	0.90	0.51	2.36	0.67	1.69
chr11:70500001-71000000	1.66	0.67	1.24	2.44	1.57	1.24	0.45	0.51	0.58	1.29	4.30	1.74	1.01	0.51	0.11	1.02	0.34	1.01	0.51	0.51	0.17
chr14:61000001-61500000	1.92	0.72	1.16	1.09	1.69	1.12	0.67	1.48	0.90	1.91	4.30	2.42	1.01	1.01	0.62	0.36	1.01	0.51	0.67	0.51	1.01
chr14:73500001-74000000	2.12	0.74	0.22	1.65	2.59	1.35	2.02	2.58	2.93	2.28	4.30	3.65	1.01	3.37	1.31	0.45	0.90	0.84	2.36	0.51	3.20
chr15:98000001-98500000	2.79	0.13	1.50	1.91	1.57	na	0.90	1.78	1.06	2.00	4.30	0.96	na	1.18	0.76	0.32	0.45	2.70	0.51	na	1.01
chr17:48000001-48500000	1.85	0.84	0.67	0.64	2.36	1.91	0.22	1.10	1.64	2.02	4.30	3.20	2.53	0.00	0.34	0.97	0.56	1.18	1.18	0.34	0.34
chr17:84000001-84500000	2.63	0.58	0.52	1.65	1.01	0.67	0.67	2.12	2.14	1.57	4.30	2.59	3.37	3.20	1.05	0.88	1.01	0.84	3.37	0.17	1.85
chr17:87500001-88000000	3.18	0.55	0.79	1.72	2.25	0.67	2.70	3.36	3.22	1.35	4.30	3.37	2.19	2.70	1.58	0.68	0.67	0.67	2.02	0.67	2.36
chr2:72500001-73000000	2.89	0.21	0.64	2.36	2.02	1.46	na	2.92	3.08	1.91	4.22	2.92	1.35	na	0.84	0.85	1.01	0.51	2.53	0.51	na
chr11:83500001-84000000	2.32	1.13	1.84	2.85	3.37	0.34	0.45	1.55	1.33	1.71	4.22	2.19	0.84	0.51	0.15	1.16	0.45	1.85	0.34	0.51	0.67
chr8:124500001-125000000	3.37	1.66	0.41	1.84	1.35	0.34	0.22	2.73	1.23	1.29	4.22	2.47	1.01	0.34	0.43	1.08	0.56	0.51	0.51	0.67	1.18
chr15:100500001-101000000	2.71	0.64	0.75	2.44	2.36	na	0.45	1.79	0.79	2.16	4.22	2.53	na	1.35	0.39	0.69	0.56	0.84	2.70	na	0.51
chr1:138000001-138500000	1.42	1.17	0.67	0.37	1.57	0.45	0.45	2.72	1.17	1.38	4.13	2.98	0.84	1.18	1.81	0.93	1.01	0.84	2.87	0.51	0.34
chr11:95500001-96000000	2.34	1.25	1.05	1.99	2.47	0.56	0.45	1.78	1.19	1.46	4.13	2.08	1.18	0.67	0.56	1.17	1.12	0.84	2.70	0.34	0.34
chr15:76500001-77000000	1.14	0.53	1.61	2.32	2.02	na	0.00	1.15	0.80	1.60	4.13	2.36	na	0.34	0.14	1.12	0.67	1.85	0.84	na	0.34
chr17:36000001-36500000	1.88	0.40	1.95	2.74	2.70	3.04	0.90	1.45	1.55	3.15	4.13	2.75	2.87	1.35	0.32	0.99	0.34	0.34	2.53	0.51	2.19
chr2:155500001-156000000	3.12	1.54	0.67	1.09	1.01	0.67	na	1.79	0.65	1.10	4.05	2.08	0.84	na	0.35	1.26	0.67	0.67	2.87	0.84	na

chr6:86000001-86500000	2.19	na	0.49	2.14	0.22	0.11	0.45	1.64	na	1.15	4.05	1.97	2.02	1.35	0.24	na	0.56	0.67	1.69	0.34	0.00
chr11:88500001-89000000	1.66	0.34	0.37	1.99	1.01	1.46	1.12	1.93	2.60	0.90	4.05	3.20	2.70	1.35	0.61	1.08	0.79	0.00	2.87	0.67	1.01
chr2:164000001-164500000	3.18	1.20	0.37	0.86	1.12	0.56	na	3.25	2.22	1.91	3.88	2.30	1.52	na	0.13	0.57	0.45	0.51	0.51	0.34	na
chr5:66500001-67000000	0.64	1.14	0.52	1.95	1.35	2.25	0.22	1.04	0.77	1.60	3.88	1.12	1.35	2.02	0.83	0.83	0.67	0.51	1.85	0.34	0.51
chr6:53500001-54000000	1.69	na	1.65	2.70	3.37	2.36	0.90	1.86	na	3.12	3.88	1.85	1.69	0.67	0.25	na	0.79	2.53	0.34	1.85	0.67
chr11:50000001-50500000	1.54	0.48	1.46	1.72	2.14	1.35	0.67	0.45	1.12	0.93	3.88	3.37	2.53	0.67	0.19	1.09	0.34	0.51	2.36	1.35	1.01
chr11:80000001-80500000	1.85	1.09	0.94	2.25	1.35	0.67	0.00	0.99	1.15	1.57	3.88	3.09	2.36	1.18	0.37	1.37	1.01	0.51	1.52	0.34	0.17
chr11:101000001-101500000	3.10	1.10	1.09	1.57	1.69	0.45	0.45	1.68	1.06	1.21	3.71	2.92	1.01	0.17	0.27	1.25	1.12	0.00	0.84	0.84	0.34
chr10:44500001-45000000	0.32	0.47	0.52	0.11	1.12	1.24	0.90	0.66	1.59	1.18	3.63	1.97	2.53	1.69	0.39	0.22	0.67	0.51	0.84	0.67	0.51
chr8:12000001-12500000	0.29	0.57	0.75	1.31	1.01	1.57	0.67	0.15	0.52	0.70	1.52	0.00	0.67	1.85	0.29	0.68	1.57	6.24	0.67	1.85	0.67
chr14:34000001-34500000	1.32	0.17	2.29	0.82	3.04	1.69	0.22	1.10	1.12	1.66	2.36	2.64	2.53	1.35	0.16	0.09	1.12	5.40	0.67	0.67	0.51
chr16:34000001-34500000	1.64	0.15	na	2.51	2.47	1.46	0.45	1.16	0.64	na	1.60	1.07	1.18	2.02	1.51	0.22	na	5.23	1.18	2.70	0.51
chr19:42500001-43000000	0.17	1.09	2.36	1.09	1.01	1.69	0.45	0.18	0.16	1.71	0.59	1.46	1.18	0.51	0.34	0.10	1.80	4.72	1.01	2.53	0.00
chr11:21500001-22000000	0.33	0.23	1.80	0.41	0.67	2.59	0.67	0.32	0.45	0.25	0.59	0.51	1.85	0.51	0.13	0.66	3.48	4.38	1.35	3.20	0.17
chr15:101500001-102000000	1.41	0.73	0.75	2.70	1.91	na	0.90	1.37	0.33	1.60	2.53	1.74	na	0.34	0.12	0.63	0.67	4.38	0.67	na	0.17
chr16:34500001-35000000	1.06	0.28	na	1.99	2.02	0.56	0.67	0.65	0.19	na	2.02	0.45	1.52	0.67	0.76	0.36	na	4.38	0.51	2.02	0.00
chr8:48000001-48500000	0.44	0.27	0.37	0.52	1.12	1.01	0.90	0.37	1.92	1.46	2.53	2.30	1.69	1.52	0.17	0.53	1.35	4.05	1.52	0.67	0.34
chr2:27500001-28000000	0.90	0.96	2.44	2.77	2.92	1.01	na	1.27	0.40	1.63	3.37	0.62	1.01	na	0.46	0.95	0.56	3.88	0.67	0.51	na
chr11:22000001-22500000	0.41	0.50	1.80	0.22	0.67	2.81	0.67	0.50	0.42	1.24	0.42	0.51	1.01	0.67	0.33	0.44	1.12	3.88	0.51	3.04	0.00
chr19:59000001-59500000	1.54	2.19	1.46	1.80	2.70	2.36	1.80	0.76	1.62	1.49	2.70	1.52	1.85	2.87	0.91	0.94	1.46	3.88	0.67	3.04	1.85
chr15:57500001-58000000	2.95	0.33	1.87	2.92	5.62	na	0.45	2.17	2.73	2.25	3.37	5.06	na	2.19	0.58	0.28	1.01	0.67	3.37	na	3.04
chr2:18500001-19000000	1.90	0.34	2.14	2.36	5.40	2.70	na	1.40	2.57	2.89	3.04	2.36	3.20	na	0.99	0.65	1.24	0.17	5.90	0.17	na
chr12:35500001-36000000	na	0.35	2.14	2.62	5.28	1.69	0.45	na	3.30	2.11	3.20	2.92	5.23	1.85	na	0.76	0.45	0.67	4.05	2.53	2.19
chr16:21500001-22000000	2.41	0.54	na	1.80	5.28	1.01	0.45	2.23	2.61	na	3.63	2.70	6.07	0.84	1.95	0.54	na	1.69	2.87	1.85	1.01
chr13:28500001-29000000	2.12	0.91	3.37	3.07	4.72	3.04	1.35	1.79	3.42	2.59	3.20	3.04	5.90	0.34	2.10	0.52	0.90	0.67	7.08	0.67	2.70
chr16:49500001-50000000	3.20	0.66	na	1.95	4.72	2.59	0.90	3.19	3.16	na	3.46	3.77	2.36	2.70	3.13	0.10	na	1.52	2.36	1.01	5.56
chr16:11000001-11500000	1.35	0.49	na	2.32	4.50	3.26	0.67	2.40	3.40	na	2.70	7.14	6.91	0.34	0.37	0.76	na	0.84	2.36	1.18	2.36
chr4:44000001-44500000	1.87	0.80	1.91	na	1.91	1.91	0.90	3.48	2.25	2.98	na	6.52	3.37	0.84	0.24	0.40	0.11	na	0.51	0.51	0.51
chr18:80500001-81000000	3.04	0.39	1.12	2.51	1.35	2.02	1.35	3.42	3.29	1.57	3.04	6.18	4.22	2.70	1.78	1.08	0.67	0.34	3.20	0.34	0.51
chr17:50000001-50500000	0.81	0.46	0.56	1.27	0.34	2.25	0.45	1.96	2.78	2.50	2.70	5.79	4.55	2.70	2.19	0.84	0.67	0.17	3.37	1.18	1.18
chr6:8000001-8500000	0.57	na	1.65	1.35	1.24	0.67	0.45	1.26	na	3.37	3.96	5.40	8.94	2.02	1.34	na	0.45	1.18	4.38	2.19	3.04
chr11:74500001-75000000	2.41	0.74	0.30	1.05	2.92	1.01	0.45	1.67	1.25	2.16	3.37	5.40	2.36	1.01	0.18	1.08	0.90	0.17	3.37	0.34	0.84
chr1:182500001-183000000	3.47	1.45	0.86	0.41	0.67	0.56	1.35	3.30	2.39	1.38	3.37	5.34	0.67	2.02	0.71	1.13	1.01	0.84	2.87	0.51	2.36
chr4:11000001-11500000	0.62	0.50	1.24	na	2.92	2.02	0.67	1.45	3.08	2.36	na	5.28	6.75	0.84	0.84	0.31	1.01	na	4.05	1.52	3.04
chr2:5500001-6000000	0.52	0.57	1.72	2.02	2.92	3.37	na	1.44	2.35	3.04	3.37	5.06	6.58	na	1.20	0.50	0.56	0.51	4.22	1.52	na
chr2:37500001-38000000	1.13	0.34	0.11	2.44	2.36	1.91	na	2.26	2.15	2.05	3.46	5.06	2.19	na	1.09	0.29	1.35	0.67	2.36	0.84	na
chr1:130500001-131000000	2.70	0.25	0.45	1.39	1.69	0.34	2.47	2.63	3.44	1.60	4.47	4.95	2.36	0.84	1.54	0.63	0.79	0.51	3.37	0.17	1.85
chr18:61000001-61500000	1.58	0.90	0.64	0.82	2.47	1.24	1.12	1.96	2.31	3.06	3.46	4.83	2.19	1.69	0.75	0.45	0.67	1.01	4.89	0.34	2.36
chr11:106000001-106500000	2.31	1.06	0.60	1.50	1.57	0.22	1.35	2.37	2.31	2.00	4.22	4.61	2.36	0.51	0.23	1.19	1.24	0.84	4.05	0.34	2.02
chr2:118500001-119000000	1.23	1.60	0.41	0.75	0.45	0.45	na	2.02	1.99	1.18	2.02	4.55	0.67	na	0.16	1.35	1.12	0.67	3.37	0.51	na
chr5:115500001-116000000	3.25	1.54	1.09	1.24	1.12	0.34	0.45	2.33	2.13	2.42	3.37	4.38	1.01	1.69	0.11	1.23	1.24	0.17	1.85	0.67	0.51
chr1:40000001-40500000	2.10	0.68	1.57	1.31	3.04	1.35	0.67	2.10	2.46	2.70	2.87	4.33	1.18	0.51	0.69	0.81	0.45	1.52	0.84	1.01	0.00
chr11:87500001-88000000	2.97	0.78	0.22	1.35	2.14	1.35	1.12	2.86	2.45	1.80	3.20	4.33	2.87	1.85	0.15	1.33	0.90	0.67	2.19	0.67	1.01
chr4:57000001-57500000	1.93	0.60	0.60	na	3.15	2.25	1.12	2.31	1.74	2.19	na	4.27	5.23	0.67	0.75	0.26	0.67	na	1.18	1.18	0.51
chr8:122000001-122500000	1.87	1.36	0.19	1.35	1.91	0.56	0.90	1.97	1.48	1.41	4.47	4.16	1.01	1.35	0.39	1.09	1.12	0.67	3.04	0.84	2.19
chr13:42000001-42500000	0.86	0.51	0.79	2.36	1.46	2.47	0.67	1.85	2.60	3.09	3.12	4.16	4.55	1.52	0.38	0.67	0.56	1.01	1.85	1.01	0.34
chr13:52500001-53000000	3.12	0.61	1.69	1.46	2.70	1.46	0.45	2.80	2.72	2.81	3.46	4.16	3.37	0.34	0.39	0.86	0.45	0.17	2.70	1.01	0.84
chr14:73000001-73500000	3.03	1.11	1.57	1.95	1.91	0.79	0.45	2.87	3.20	2.30	3.37	4.16	2.70	2.02	1.26	0.21	0.90	0.00	1.18	1.18	1.52
chr18:56500001-57000000	1.04	0.55	0.67	1.65	1.46	2.70	0.90	2.05	3.14	1.91	3.37	4.10	1.85	2.19	1.68	0.34	0.79	0.67	1.69	1.01	5.23

chr8:26000001-26500000	1.27	0.29	1.01	2.02	0.90	2.70	0.90	1.50	1.78	3.18	3.79	4.05	5.56	0.34	0.41	0.21	0.45	1.35	1.01	2.02	2.02
chr18:34000001-34500000	1.40	0.37	2.92	2.17	2.47	2.47	0.45	1.47	2.20	2.14	3.04	3.93	3.04	0.51	1.24	0.69	0.45	2.36	1.35	0.67	0.00
chr18:65500001-66000000	1.66	0.35	2.70	1.72	1.69	1.80	1.12	2.47	2.91	3.26	2.36	3.93	2.87	2.53	0.82	0.65	0.67	1.35	2.02	0.51	0.67
chr19:29500001-30000000	1.64	0.33	2.47	3.48	2.36	3.37	0.45	1.18	2.15	2.19	4.13	3.93	4.38	2.02	1.41	0.14	1.24	0.67	3.37	2.19	1.18
chr14:69500001-70000000	2.36	0.23	0.30	1.39	1.24	0.67	0.45	3.20	2.81	2.61	3.37	3.88	2.36	1.69	1.53	0.10	0.45	1.85	2.70	0.51	3.04
chr2:22500001-23000000	0.96	0.81	1.27	1.31	2.47	3.37	na	1.34	2.58	2.45	3.04	3.82	5.90	na	1.06	0.18	0.45	0.34	2.70	0.51	na
chr7:120500001-121000000	2.65	0.65	1.24	1.27	1.24	0.34	1.80	2.88	2.25	2.64	4.05	3.82	0.34	2.53	1.49	0.17	0.67	1.18	2.36	0.51	1.85
chr7:134500001-135000000	2.94	1.65	0.60	1.31	0.45	0.45	0.45	2.41	1.98	1.43	3.37	3.82	1.01	1.35	0.10	1.40	1.01	0.67	2.53	0.84	2.19
chr7:135500001-136000000	3.17	0.60	0.41	0.71	1.24	0.90	1.57	2.78	2.31	1.74	4.13	3.77	0.34	0.84	0.81	1.00	0.56	0.67	2.87	0.67	2.19
chr13:20000001-20500000	0.93	0.26	2.55	1.16	2.59	6.52	0.67	1.01	2.44	2.42	3.12	3.65	3.04	0.51	0.72	0.21	0.45	0.34	3.37	2.02	2.02
chr13:29500001-30000000	0.73	0.37	1.35	1.27	1.01	2.47	1.80	1.26	2.74	1.97	2.11	3.65	2.36	1.52	1.01	0.38	0.11	0.67	1.52	1.01	0.84
chr10:28000001-28500000	0.29	2.65	1.91	0.15	0.79	1.91	0.45	0.38	0.86	0.20	0.42	0.17	1.18	0.51	2.97	0.21	0.56	0.51	10.79	1.01	2.87
chr17:52000001-52500000	0.82	1.08	1.05	0.37	1.46	1.57	0.67	0.77	1.60	0.31	0.67	0.11	1.35	0.84	1.43	0.64	0.90	1.01	10.29	0.51	0.34
chr1:139500001-140000000	1.75	0.39	0.49	0.34	1.24	0.22	2.02	3.22	2.25	1.01	1.26	1.97	0.51	2.70	2.56	1.04	1.12	1.01	9.95	0.67	2.02
chr1:140000001-140500000	1.33	0.43	0.71	0.30	0.79	0.56	1.80	2.22	1.68	0.45	1.60	2.30	0.34	3.37	2.34	0.82	1.01	0.51	9.95	0.67	1.35
chr18:81500001-82000000	1.35	1.36	2.32	2.21	1.24	2.36	2.92	1.38	1.22	0.67	1.77	0.11	0.34	3.04	2.51	0.79	0.22	0.84	8.94	0.51	2.53
chr1:139000001-139500000	0.49	0.36	0.56	0.19	0.67	0.34	0.90	1.48	0.10	0.25	0.51	0.51	0.34	0.84	3.36	0.83	1.01	0.51	8.77	0.51	1.01
chr18:33000001-33500000	0.27	0.76	1.31	0.45	0.56	1.24	0.67	0.40	0.22	0.45	0.51	0.34	0.17	0.17	3.16	0.23	0.67	0.51	8.09	0.34	1.01
chr8:35500001-36000000	1.49	0.34	1.27	2.21	2.92	3.37	1.12	0.74	1.39	1.94	2.11	1.91	3.20	0.67	1.34	0.45	1.12	1.01	7.93	0.34	2.53
chr17:51500001-52000000	1.56	1.29	1.42	0.52	1.69	1.46	2.02	1.80	2.98	3.40	1.85	1.63	4.22	1.18	3.40	0.67	1.12	0.34	7.25	1.01	1.18
chr8:36000001-36500000	0.91	0.71	1.69	1.27	2.70	3.37	0.45	1.06	2.02	1.60	3.04	2.19	2.19	1.69	1.65	0.45	0.45	0.51	7.08	0.84	2.19
chr12:117000001-117500000	na	0.19	1.76	2.36	2.81	1.80	2.25	na	1.77	1.07	2.19	2.59	4.89	5.40	na	0.21	0.79	0.67	6.58	1.69	10.29
chr13:91500001-92000000	2.98	0.60	0.71	1.76	1.35	0.56	2.02	1.88	1.86	1.18	1.52	1.24	2.53	2.70	2.87	0.26	0.90	0.17	6.41	0.17	3.37
chr18:5000001-5500000	0.49	0.56	2.40	1.57	2.36	2.02	0.45	1.02	1.68	2.39	2.19	3.09	2.36	0.34	2.49	0.15	0.45	0.51	6.41	1.52	1.52
chr2:9500001-10000000	0.42	0.84	1.99	1.09	0.79	3.04	na	0.10	1.18	0.93	0.93	0.51	2.19	na	2.30	0.17	0.79	0.17	6.24	2.02	na
chr1:39000001-39500000	1.50	0.45	0.64	1.20	2.02	1.35	0.90	1.43	0.87	1.43	2.28	1.85	2.36	0.17	1.68	1.04	0.79	1.18	5.90	0.34	0.67
chr4:7000001-7500000	0.47	1.39	2.21	na	1.24	3.48	0.00	0.22	1.09	0.62	na	0.28	1.85	0.51	3.12	0.26	0.34	na	5.90	1.85	2.87
chr6:134500001-135000000	3.37	na	0.56	1.05	1.01	0.56	2.70	3.34	na	1.29	3.46	3.37	1.18	7.93	2.85	na	0.67	1.52	5.90	0.67	9.61
chr12:108500001-109000000	na	1.01	0.75	0.34	0.34	0.56	0.67	na	0.40	0.67	0.42	0.51	0.67	0.67	na	1.11	1.24	0.84	5.90	0.51	3.20
chr1:60500001-61000000	3.47	0.31	1.39	1.99	2.14	1.69	0.90	2.18	2.79	2.92	3.37	1.91	2.19	1.85	1.92	0.58	0.56	0.84	5.73	0.67	3.37
chr1:158000001-158500000	1.13	1.25	0.94	0.67	0.79	0.45	0.90	1.32	0.34	0.45	0.84	1.07	0.34	0.67	0.76	1.07	0.90	1.01	5.56	0.84	1.69
chr12:3500001-4000000	na	0.78	0.67	0.71	2.25	0.67	0.67	na	1.08	1.94	2.95	2.08	2.36	0.67	na	0.24	0.34	1.69	5.56	2.87	1.18
chr14:54000001-54500000	0.68	1.09	0.49	1.46	1.69	0.11	0.90	0.12	0.38	0.00	1.43	0.67	0.00	1.01	0.94	0.36	1.12	0.34	5.56	1.35	2.36
chr1:167500001-168000000	2.31	0.75	0.37	0.71	0.90	0.34	1.35	2.14	1.99	0.65	2.02	2.64	0.51	2.02	3.08	0.65	0.90	0.51	5.40	0.67	2.70
chr12:25500001-26000000	na	0.31	1.57	2.06	3.37	3.48	1.57	na	2.09	2.14	3.96	3.04	5.23	1.35	na	0.45	0.67	0.67	5.40	1.69	1.85
chr14:54500001-55000000	2.66	0.55	1.39	3.30	2.92	1.80	0.45	1.67	0.89	1.71	2.61	1.91	1.69	1.01	1.95	0.35	1.01	0.17	5.40	1.01	9.11
chr4:7500001-8000000	0.42	0.86	0.45	na	0.45	2.59	0.45	0.15	0.95	1.66	na	0.90	2.19	1.52	3.25	1.34	0.45	na	5.06	3.37	2.19
chr8:35000001-35500000	0.80	0.69	0.75	1.65	2.81	2.81	0.67	0.67	1.34	2.14	3.29	2.30	2.36	0.51	1.29	0.69	0.67	0.34	5.06	0.67	2.53
chr18:6000001-6500000	0.40	0.22	1.42	0.90	1.12	2.70	0.45	1.03	1.23	2.75	2.19	1.85	5.73	1.69	1.37	0.57	0.90	0.17	5.06	2.87	0.67
chr18:81000001-81500000	1.30	0.82	1.42	1.12	1.01	1.46	3.15	1.27	0.95	1.07	1.01	0.56	1.18	2.02	1.78	1.13	0.79	0.51	5.06	0.67	1.01
chr2:11000001-11500000	0.94	0.53	1.27	1.46	2.92	6.30	na	0.77	2.36	2.89	2.61	2.98	2.36	na	0.66	0.43	0.45	0.51	4.89	0.34	na
chr6:119500001-120000000	2.89	na	0.56	2.06	1.24	0.22	2.25	1.74	na	1.94	1.85	2.08	0.84	0.84	1.16	na	1.01	0.34	4.89	0.51	2.53
chr10:39500001-40000000	1.29	0.71	0.75	2.74	1.69	2.81	0.22	0.92	1.33	2.70	2.87	3.37	2.36	2.02	1.24	0.86	1.12	0.84	4.89	0.67	0.00
chr11:67500001-68000000	1.52	0.66	1.69	2.89	3.15	1.91	0.67	1.39	1.20	2.33	3.20	2.25	1.52	0.51	0.14	0.89	0.22	1.69	4.89	0.67	0.67
chr11:96000001-96500000	2.54	1.26	0.49	2.14	1.24	0.11	0.45	1.14	0.25	1.74	3.12	0.11	0.51	0.17	1.54	1.17	1.01	0.34	4.89	0.17	0.51
chr17:50500001-51000000	2.33	0.84	0.71	1.72	2.47	2.81	1.35	2.31	2.48	1.74	2.95	3.09	5.56	1.52	3.13	0.27	0.79	0.00	4.89	2.19	2.02
chr1:39500001-40000000	1.35	0.49	1.31	2.62	2.70	2.92	0.22	3.32	2.24	2.11	3.37	3.43	2.02	0.17	1.36	0.45	0.90	0.67	4.72	1.18	0.67
chr1:43500001-44000000	0.63	0.76	0.97	1.09	1.80	2.14	0.22	0.92	1.59	1.12	1.60	2.19	0.84	1.01	1.26	0.25	1.12	0.51	4.72	1.85	3.04
chr9:32500001-33000000	0.62	0.64	2.21	1.61	3.37	2.59	1.12	1.04	2.59	1.49	2.87	3.48	2.36	1.18	0.95	0.79	0.90	0.67	4.72	0.34	2.36

chr10:18000001-18500000	0.36	0.90	1.16	1.50	1.01	2.36	0.67	0.03	0.34	0.65	2.02	0.96	1.18	0.51	1.60	0.89	0.56	1.35	4.72	2.36	1.01
chr11:31500001-32000000	0.19	0.43	0.86	0.37	1.12	1.80	0.90	0.28	0.89	1.63	1.43	1.80	3.37	0.34	1.03	0.23	0.45	1.35	4.72	1.18	1.35
chr12:108000001-108500000	na	1.12	0.90	0.64	0.45	0.45	0.22	na	0.64	0.56	0.67	0.45	0.67	0.34	na	1.23	0.79	0.67	4.72	0.67	1.85
chr18:5500001-6000000	1.05	0.78	2.74	1.54	2.47	3.37	0.90	1.20	2.24	2.30	3.37	3.04	4.89	1.01	2.38	0.26	0.45	0.51	4.72	1.35	0.84
chr6:33500001-34000000	0.73	na	2.10	1.65	1.57	2.47	0.67	0.75	na	0.79	1.35	0.34	0.51	0.51	2.55	na	0.45	0.34	4.55	1.35	1.69
chr14:16000001-16500000	0.55	1.27	1.20	0.30	0.11	2.47	0.90	0.19	1.18	0.76	0.34	0.45	1.18	0.17	1.88	0.60	0.56	0.67	4.55	1.35	2.53
chr6:33000001-33500000	0.43	na	2.81	0.94	0.90	1.35	0.67	0.58	na	1.10	1.60	0.34	1.35	0.51	2.18	na	0.79	0.17	4.38	1.85	0.84
chr8:108500001-109000000	1.99	0.83	0.71	1.05	1.46	0.56	1.80	2.18	1.83	3.37	3.37	3.15	2.70	2.36	0.74	0.99	0.79	1.35	4.38	0.51	0.84
chrX:156000001-156500000	3.49	0.82	0.34	0.19	1.24	0.34	0.67	3.27	1.67	0.98	1.26	1.69	1.18	1.01	1.43	1.08	0.90	1.01	4.22	0.67	1.85
chr8:23500001-24000000	0.51	0.53	1.09	2.14	2.36	1.35	0.45	0.74	1.19	2.47	1.77	3.04	3.37	1.35	0.60	0.30	0.56	1.52	4.05	0.51	1.18
chr15:36000001-36500000	0.38	0.80	1.05	1.46	0.56	na	0.90	0.36	0.81	1.83	2.02	1.29	na	1.85	1.04	0.59	0.79	0.51	4.05	na	2.02
chr2:71500001-72000000	2.62	1.04	0.71	2.21	2.25	0.90	na	1.98	1.29	0.87	3.37	1.74	2.02	na	0.77	1.00	1.12	0.67	3.88	0.84	na
chr1:36000001-36500000	0.90	0.38	0.45	1.57	2.25	1.35	0.45	1.43	1.57	2.19	2.28	2.14	3.20	0.00	0.75	0.88	0.67	0.84	3.71	0.17	0.17
chr10:127500001-128000000	3.15	1.19	0.49	0.37	1.12	0.22	1.12	3.22	1.48	2.75	2.70	2.87	0.51	3.20	0.35	1.09	1.01	1.35	3.71	0.34	2.87
chr12:56000001-56500000	na	1.23	0.56	1.16	1.91	3.37	0.67	na	1.01	2.19	2.87	2.64	3.20	1.69	na	0.87	0.90	1.35	3.71	0.34	0.34
chr12:109000001-109500000	na	0.19	0.67	0.64	0.79	0.45	0.90	na	0.52	0.28	0.17	0.34	0.67	0.00	na	1.16	1.01	0.51	3.71	0.51	1.18
chr5:3000001-3500000	0.34	0.55	1.31	1.20	1.80	9.33	0.45	0.14	0.77	1.38	0.84	1.24	5.06	0.34	0.68	0.60	1.57	0.17	0.17	2.70	1.01
chr3:21500001-22000000	0.87	1.66	2.36	1.24	na	7.87	0.67	0.67	2.88	1.91	2.19	na	3.04	1.85	2.94	0.61	0.56	0.34	na	2.53	2.70
chr10:13500001-14000000	2.41	0.48	2.59	2.44	3.37	7.64	0.67	1.15	3.10	2.36	2.45	3.04	3.04	1.85	1.70	0.41	0.79	0.67	2.70	0.67	2.87
chr5:3500001-4000000	0.15	0.60	2.36	0.45	2.02	7.53	0.22	0.25	1.16	2.33	1.69	0.56	4.72	1.18	0.81	0.68	0.56	2.19	3.20	2.02	1.01
chr14:15000001-15500000	0.75	0.49	2.51	1.31	2.92	7.42	0.22	0.22	1.11	2.61	1.18	1.85	2.36	0.67	0.36	0.99	2.02	0.67	0.34	2.19	0.67
chr4:11500001-12000000	0.64	0.75	3.04	na	1.12	6.86	0.45	1.17	2.10	3.06	na	1.91	3.37	2.19	0.91	1.58	0.79	na	0.17	3.37	0.51
chr10:16000001-16500000	0.58	1.54	1.76	0.07	1.69	6.52	0.90	0.24	1.62	2.22	0.84	0.45	2.87	0.67	0.31	1.29	2.59	1.35	0.34	1.69	0.34
chr19:11500001-12000000	0.77	0.85	1.80	0.52	2.81	6.52	0.90	0.73	3.16	3.04	3.37	3.09	9.27	0.51	1.52	0.89	1.69	2.53	1.85	5.40	2.19
chr11:8500001-9000000	0.30	0.50	1.65	1.31	1.57	6.07	0.67	0.15	1.27	1.18	1.18	1.91	3.37	0.17	0.69	0.36	0.56	3.37	0.84	2.53	0.84
chr14:18500001-19000000	0.20	0.84	2.32	0.75	1.69	5.96	1.12	0.15	0.58	2.16	1.01	1.29	1.52	0.34	1.49	0.80	0.67	1.85	1.01	3.04	2.53
chr19:21000001-21500000	0.07	1.18	2.21	0.67	0.79	5.85	0.00	0.49	1.91	1.74	1.52	1.12	3.04	1.18	1.47	1.11	2.92	1.35	1.85	6.58	0.34
chr9:14000001-14500000	0.63	0.51	1.65	2.10	3.48	5.73	0.67	0.72	2.59	1.97	3.29	3.26	4.72	0.84	1.04	0.17	0.34	2.02	1.85	2.36	2.70
chr9:22500001-23000000	0.47	0.59	1.61	0.90	0.90	5.62	0.67	0.29	1.25	2.16	2.02	1.01	0.84	0.67	0.19	0.30	1.12	2.36	0.51	1.52	0.84
chr12:36500001-37000000	na	0.54	1.12	0.52	1.91	5.62	0.90	na	1.62	2.02	1.94	2.59	4.22	1.01	na	0.52	0.45	0.84	2.36	2.53	0.84
chr4:10500001-11000000	0.46	0.28	1.20	na	1.01	5.51	0.90	1.39	2.68	2.16	na	2.92	5.06	0.51	0.69	0.12	0.56	na	1.35	0.51	1.18
chr10:7500001-8000000	0.81	0.37	2.06	1.16	2.47	5.51	0.22	0.66	1.86	1.94	1.85	2.42	2.70	1.52	0.82	0.10	0.45	0.34	2.70	2.19	2.36
chr11:26000001-26500000	0.36	0.84	1.87	0.64	0.90	5.51	0.22	0.08	1.02	1.26	0.17	0.00	2.53	0.67	0.43	0.55	0.90	3.04	0.84	2.19	0.51
chr4:3500001-4000000	0.44	0.39	2.59	na	1.91	5.40	0.22	0.81	3.11	2.16	na	2.81	9.44	1.52	0.56	0.80	1.57	na	1.52	2.87	1.52
chr19:27000001-27500000	1.55	0.81	2.70	2.47	2.47	5.28	0.45	0.27	1.35	1.63	1.26	0.51	1.85	1.69	1.55	1.27	2.59	1.69	1.85	4.38	0.84
chr17:21500001-22000000	0.30	0.42	2.02	0.94	0.90	5.06	1.35	0.18	1.17	1.35	1.35	1.29	2.70	1.01	0.78	0.47	0.22	0.51	0.34	1.18	1.01
chr1:13000001-13500000	0.89	0.36	2.02	2.21	2.02	4.95	0.67	1.93	3.38	1.94	2.53	3.43	7.08	1.01	0.87	0.15	0.34	1.52	2.02	2.02	1.52
chr2:3000001-3500000	0.06	1.02	1.57	1.12	1.12	4.95	na	0.16	2.24	1.10	1.52	2.36	7.59	na	0.66	0.40	0.34	1.85	1.85	1.85	na
chr10:21500001-22000000	1.60	0.64	1.72	2.14	3.37	4.61	0.45	0.80	2.00	2.87	3.04	3.37	4.89	1.01	0.32	1.07	0.34	0.67	2.36	0.17	0.34
chr3:10000001-10500000	0.28	0.42	1.72	1.12	na	4.38	0.67	0.77	2.24	1.88	3.04	na	3.37	0.51	2.10	0.56	0.56	3.04	na	2.36	0.51
chr14:15500001-16000000	0.24	0.40	2.14	1.24	1.35	4.38	0.45	0.17	1.38	1.60	1.77	1.07	3.04	0.00	1.66	0.76	0.11	0.84	1.85	1.69	2.19
chr12:8500001-9000000	na	0.43	1.20	2.44	3.04	2.70	0.67	na	3.20	3.04	4.05	3.04	8.60	0.84	na	0.57	0.11	1.01	1.69	2.70	2.70
chr11:21000001-21500000	0.62	0.39	1.09	2.51	2.47	3.37	0.22	0.82	2.38	2.45	3.29	2.98	8.26	1.35	1.42	0.29	0.67	0.84	3.04	2.70	2.53
chr11:23500001-24000000	0.59	0.39	1.05	0.86	1.91	1.35	0.45	0.58	1.42	2.87	2.87	2.81	7.93	1.18	0.55	0.31	0.45	1.01	1.69	2.36	0.67
chr19:25000001-25500000	0.42	0.26	1.57	1.27	1.35	2.02	0.22	1.58	2.47	3.20	3.20	3.04	7.93	0.17	0.63	0.16	0.67	0.34	1.69	2.19	0.00
chr19:21500001-22000000	0.34	0.36	1.99	0.97	2.36	3.37	0.45	0.43	2.43	2.30	1.18	1.74	7.25	1.52	0.95	0.33	1.57	0.84	1.35	4.38	0.34
chr3:19000001-19500000	0.29	0.40	1.50	1.12	na	2.59	0.67	1.02	3.31	2.98	3.12	na	7.08	2.87	1.36	0.75	0.11	0.84	na	3.37	1.85
chr2:6500001-7000000	0.78	1.95	2.29	1.65	1.80	2.70	na	1.11	2.59	3.26	0.67	3.15	6.91	na	2.41	0.96	0.11	0.84	3.37	2.02	na
chr2:11500001-12000000	0.74	0.43	1.80	1.24	2.02	3.37	na	1.09	2.81	2.39	2.87	2.36	6.91	na	0.20	0.41	0.34	0.51	2.36	0.51	na

chr11:30500001-31000000	0.20	0.51	2.02	1.12	0.90	2.36	0.22	0.05	1.55	1.21	1.85	1.85	6.58	1.18	0.31	0.85	0.67	2.19	1.01	2.36	1.35
chr5:20500001-21000000	0.51	0.49	0.64	1.09	2.25	2.70	1.35	0.92	2.17	2.56	2.19	2.47	6.58	1.18	0.60	0.14	0.34	2.02	0.67	1.35	0.17
chr6:8500001-9000000	0.53	na	0.75	0.86	1.91	3.37	0.67	0.57	na	2.11	1.52	3.04	6.41	1.01	0.74	na	0.90	0.84	1.35	1.52	0.34
chr5:9000001-9500000	0.22	0.16	2.36	0.45	1.91	3.48	0.22	0.54	2.50	2.73	2.78	1.35	6.24	0.51	0.77	1.49	1.35	0.84	1.18	2.36	0.67
chr19:16000001-16500000	0.79	0.25	1.72	1.27	1.24	3.37	0.90	0.68	1.97	2.14	1.26	1.46	6.24	1.01	1.56	0.42	3.15	3.20	1.35	3.04	1.85
chr5:21000001-21500000	0.36	0.28	0.97	0.90	1.24	2.81	0.67	0.64	1.75	1.77	2.61	2.14	6.07	1.01	0.62	0.03	0.45	2.02	1.01	1.85	2.19
chr19:34000001-34500000	1.45	0.24	2.14	1.91	2.02	3.04	0.67	0.86	2.70	3.34	2.53	2.25	6.07	1.69	1.36	0.31	1.24	1.01	1.35	2.19	0.84
chr19:34500001-35000000	1.12	0.37	1.27	2.77	3.15	2.70	0.22	0.89	2.54	3.04	4.05	2.75	5.90	0.67	0.96	0.46	0.56	0.84	1.35	3.37	0.00
chr13:3500001-4000000	0.58	0.45	0.64	0.34	0.56	3.26	0.45	0.19	1.69	1.88	1.60	1.57	5.73	0.17	0.10	0.94	0.90	1.35	0.51	1.85	0.34
chr14:17000001-17500000	0.45	0.54	2.06	0.71	1.12	2.70	1.35	0.64	1.58	1.66	1.43	2.02	5.73	1.18	1.75	0.49	0.67	1.52	2.02	2.53	2.70
chr18:15000001-15500000	0.95	0.31	0.75	1.72	1.91	2.70	1.12	0.32	1.44	1.10	1.26	1.97	5.73	0.17	1.50	0.15	0.45	0.67	2.87	2.87	3.04
chr19:53500001-54000000	1.87	0.30	1.35	1.61	3.37	2.70	1.12	0.94	1.93	2.11	2.02	3.09	5.73	3.37	0.53	0.73	0.56	0.84	1.69	0.67	1.18
chr12:4500001-5000000	na	0.78	1.01	1.54	2.02	3.37	0.67	na	0.75	1.85	2.78	2.59	5.56	1.85	na	0.52	0.34	1.69	1.18	2.02	1.18
chr2:6000001-6500000	0.63	0.49	1.76	1.31	2.70	2.02	na	1.73	3.30	1.97	4.30	3.37	5.56	na	1.30	0.40	0.34	0.84	2.53	1.85	na
chr11:32000001-32500000	0.43	0.56	0.49	1.27	2.25	2.81	0.67	0.70	1.37	1.55	2.70	3.26	5.56	1.01	0.83	0.29	0.45	1.52	2.36	2.53	1.18
chr11:34000001-34500000	0.43	0.46	0.56	0.34	1.91	1.80	0.67	0.66	1.12	1.69	2.02	2.19	5.56	0.67	1.12	0.10	0.45	1.35	2.70	0.84	0.84
chr16:17000001-17500000	1.87	0.55	na	2.02	3.48	3.26	0.67	2.26	2.04	na	3.79	3.37	5.56	1.52	1.08	1.11	na	1.85	3.04	1.01	1.52
chr19:12500001-13000000	0.41	0.42	1.20	0.26	0.45	2.70	0.67	0.27	0.84	0.76	0.08	0.11	5.56	0.51	0.59	0.52	1.80	1.01	1.35	3.37	0.34
chr16:36500001-37000000	0.93	0.42	na	1.12	1.57	1.80	0.67	1.24	1.59	na	1.60	1.57	5.23	2.53	0.83	0.17	na	2.87	0.17	3.04	0.84
chr17:15500001-16000000	0.19	0.23	1.57	1.01	0.22	2.70	0.90	0.19	1.44	1.85	1.26	1.01	5.23	0.34	0.52	0.27	0.22	0.17	1.01	2.19	2.53
chr18:24000001-24500000	0.31	0.85	1.01	1.09	1.12	2.02	1.12	0.72	1.85	3.04	3.04	2.81	5.23	2.02	1.63	1.36	1.12	2.19	2.02	3.37	2.02
chr19:15500001-16000000	0.43	0.93	2.10	0.60	0.67	2.14	0.90	0.14	1.35	1.94	0.76	0.79	5.23	1.01	0.30	1.73	3.15	1.85	0.34	4.55	0.00
chr4:58500001-59000000	1.94	0.28	0.86	na	2.36	0.67	0.45	2.33	3.25	2.75	na	2.70	5.06	2.53	0.98	0.07	0.34	na	1.01	0.51	0.51
chr11:29000001-29500000	0.25	0.82	1.31	0.45	0.67	3.37	0.45	0.16	1.18	1.43	1.69	0.79	5.06	0.67	1.07	0.40	0.79	1.52	1.69	2.19	0.34
chr12:4000001-4500000	na	0.80	1.05	1.16	1.24	3.04	1.12	na	1.41	2.81	3.20	2.30	5.06	0.00	na	0.07	0.56	2.02	3.04	2.87	0.51
chr19:38000001-38500000	1.06	0.27	1.46	1.20	0.79	2.70	0.90	0.82	2.46	3.32	3.04	2.81	5.06	0.51	0.32	0.51	2.47	3.37	0.67	2.87	0.34
chr19:56500001-57000000	1.08	0.90	2.36	2.21	1.24	1.46	1.35	1.27	1.66	2.56	3.46	1.01	4.89	1.18	1.58	0.37	1.80	2.87	1.69	2.19	1.35
chr7:26000001-26500000	0.75	1.02	0.34	0.79	1.46	1.57	0.45	0.69	1.80	3.06	2.87	2.98	4.89	0.34	0.45	1.10	0.90	0.84	1.35	0.67	0.51
chr17:44000001-44500000	1.02	0.23	0.56	0.86	1.46	1.57	0.00	1.49	1.47	0.73	3.29	2.36	4.89	1.18	0.60	0.51	1.35	2.87	0.17	0.51	0.17
chr4:9000001-9500000	0.39	0.31	0.64	na	0.90	3.37	0.22	0.72	1.76	2.05	na	1.69	4.72	1.18	1.18	0.88	2.47	na	1.18	3.88	0.67
chr6:5000001-5500000	0.47	na	2.77	0.45	1.57	2.02	0.45	0.19	na	2.73	1.60	1.12	4.72	0.51	0.84	na	1.12	2.36	1.01	3.37	0.84
chr3:14500001-15000000	0.29	0.89	1.24	1.20	na	1.35	0.67	0.25	2.68	1.69	1.60	na	4.55	2.36	0.55	1.24	0.67	1.35	na	2.36	0.67
chr5:8500001-9000000	0.23	0.85	2.96	0.22	1.35	3.37	0.22	0.61	1.80	2.08	2.02	1.35	4.55	0.34	2.01	1.27	0.45	1.35	1.85	4.72	3.04
chr11:20500001-21000000	0.34	0.53	1.91	1.24	2.47	2.02	0.45	0.50	1.05	2.53	1.85	2.08	4.55	0.67	1.39	0.26	0.45	0.34	2.36	2.19	2.19
chr13:32000001-32500000	1.54	0.40	1.99	2.21	2.92	3.04	0.67	0.63	1.50	1.77	2.95	1.24	4.55	1.18	0.53	0.12	1.01	1.35	0.84	1.35	0.51
chr9:14500001-15000000	0.22	0.63	0.52	0.34	1.24	2.02	0.45	0.23	0.59	0.98	0.67	1.29	4.38	1.18	0.90	0.26	1.01	1.52	3.20	0.67	1.85
chr11:11000001-11500000	0.41	0.12	0.52	0.60	1.57	1.01	0.67	0.37	1.64	0.87	0.59	1.85	4.38	0.67	1.20	0.98	1.24	0.34	3.37	4.22	2.70
chr17:8000001-8500000	0.57	0.84	0.97	1.31	2.02	3.37	0.45	0.46	0.94	2.22	3.46	2.87	4.38	0.51	0.13	1.26	0.22	0.84	2.02	0.51	0.84
chr18:38500001-39000000	1.76	0.44	1.12	1.84	2.81	0.67	0.45	1.25	1.30	1.21	3.12	1.97	4.38	1.01	0.65	0.22	0.45	3.20	3.04	1.35	2.87
chr19:60500001-61000000	2.04	1.24	2.40	3.00	1.46	3.48	1.35	1.14	2.11	2.84	2.11	1.91	4.38	2.19	0.98	0.79	1.12	1.35	0.67	2.36	1.52
chr6:7500001-8000000	0.35	na	1.27	0.49	0.79	3.37	0.45	0.24	na	2.36	0.76	0.84	4.22	0.17	0.58	na	0.34	2.19	0.84	2.02	1.01
chr9:11000001-11500000	1.00	1.11	1.12	0.56	0.34	2.36	0.90	0.21	1.31	0.39	0.25	0.56	4.22	0.34	1.15	1.14	1.46	0.17	0.34	1.01	0.17
chr9:37000001-37500000	0.36	0.34	1.12	0.90	3.04	1.57	0.67	0.47	1.57	2.50	2.28	2.02	4.22	0.51	0.63	0.45	0.22	1.35	0.84	2.02	1.35
chr12:16500001-17000000	na	0.60	0.67	0.52	1.12	3.04	0.45	na	1.27	1.41	1.52	2.25	4.22	1.01	na	0.63	0.45	1.35	1.01	2.53	1.01
chr11:53500001-54000000	1.44	1.20	0.56	3.04	3.37	3.04	0.45	1.13	2.15	1.66	3.04	3.37	4.22	0.84	0.32	0.81	1.01	0.67	2.53	0.34	0.67
chr19:36000001-36500000	1.79	1.01	2.59	2.21	3.37	3.37	0.22	0.57	1.35	2.92	3.37	2.30	4.22	1.18	0.95	0.15	1.80	0.17	1.18	2.02	1.01
chr19:47500001-48000000	0.98	0.71	0.75	1.69	1.80	2.02	0.90	1.55	1.52	2.33	3.20	2.64	4.22	1.52	1.48	0.52	0.34	1.18	3.04	1.85	0.67
chr19:53000001-53500000	1.02	1.15	1.12	0.64	2.02	2.70	1.12	1.02	2.71	2.95	3.12	2.75	4.05	1.69	0.47	0.25	1.01	2.19	2.70	1.85	1.01
chr8:13500001-14000000	0.35	0.83	1.35	1.65	1.91	3.04	0.00	0.15	0.64	3.37	4.05	2.47	3.88	0.84	0.10	0.67	0.67	0.84	2.19	0.84	1.18

chr12:56500001-57000000	na	0.42	0.97	1.16	2.47	2.47	0.90	na	2.03	2.95	2.45	2.25	3.88	0.51	na	0.03	0.34	1.85	2.36	1.18	1.18
chr14:20500001-21000000	0.67	0.49	1.76	1.91	2.02	3.48	0.67	1.02	1.67	2.73	4.55	3.09	3.88	1.18	0.83	0.18	0.34	1.85	2.02	0.51	2.53
chr18:54000001-54500000	0.86	0.10	1.27	0.75	1.12	0.67	0.67	2.12	3.00	2.53	3.37	1.69	3.88	0.00	1.33	0.68	0.45	0.84	0.84	0.84	2.70
chr17:3000001-3500000	0.45	0.85	2.17	0.56	0.79	3.37	0.67	0.23	1.00	2.14	1.94	1.24	3.04	0.17	0.38	0.30	2.14	2.19	0.84	5.23	0.34
chr14:11000001-11500000	0.32	2.32	1.61	0.34	0.22	3.37	0.67	0.44	2.02	0.90	1.18	0.56	3.04	1.52	2.21	1.32	0.90	0.00	1.69	4.89	1.18
chr19:26500001-27000000	0.28	0.53	1.72	1.39	1.80	3.15	0.67	0.19	0.54	2.64	2.53	1.41	2.70	1.01	1.10	0.50	2.02	1.52	1.01	4.89	0.84
chr10:16500001-17000000	0.20	1.09	1.50	1.20	1.12	0.67	0.22	0.52	2.15	2.70	0.93	1.24	3.37	1.52	0.77	1.15	2.14	1.52	0.34	4.72	0.34
chr13:10000001-10500000	0.19	1.38	2.59	0.64	1.01	2.70	0.67	0.11	1.55	0.53	0.25	0.67	2.70	0.51	0.40	1.62	1.46	0.34	1.35	4.72	0.17
chr13:9000001-9500000	0.34	0.60	1.87	1.01	2.14	2.02	0.67	0.20	1.33	0.93	0.93	1.57	3.20	0.51	0.64	0.30	0.34	2.19	1.35	4.55	1.18
chr19:31000001-31500000	0.45	1.00	3.11	0.94	1.57	0.67	0.45	0.17	0.53	0.98	0.17	0.73	2.02	0.17	1.46	0.63	2.59	2.02	1.01	4.55	0.84
chr16:51500001-52000000	0.42	2.51	na	0.30	1.12	0.79	1.35	1.88	1.82	na	0.17	0.67	2.36	1.01	3.02	1.07	na	0.17	1.69	4.38	0.67
chr19:27500001-28000000	0.25	1.70	2.92	1.54	1.57	2.59	0.45	0.13	0.56	1.29	0.51	0.34	1.69	0.17	1.02	1.17	2.70	3.37	0.67	4.38	0.51
chr12:15500001-16000000	na	1.06	1.20	0.52	0.90	1.24	0.45	na	2.09	1.80	2.28	2.02	3.37	1.52	na	1.04	1.12	1.01	1.01	4.22	2.02
chr12:26000001-26500000	na	0.79	2.36	1.50	0.45	2.36	0.90	na	1.49	1.43	1.94	1.91	1.01	0.84	na	0.47	0.45	0.17	2.02	4.22	1.18
chr19:14500001-15000000	0.42	1.26	1.84	0.41	1.12	2.81	1.35	0.10	1.14	0.51	1.52	0.39	1.85	0.17	1.26	1.34	2.25	2.36	0.34	4.22	0.17
chr14:19500001-20000000	0.63	1.31	2.29	0.30	0.22	1.24	0.45	0.66	0.28	0.56	0.67	0.51	1.01	0.34	1.12	1.64	0.90	2.19	1.35	3.88	1.52
chr19:17000001-17500000	0.33	0.24	1.20	0.75	0.90	2.47	0.22	0.19	0.84	2.28	1.94	1.35	3.04	0.67	0.15	0.32	3.15	3.20	0.67	3.88	0.67
chr18:12500001-13000000	0.14	0.32	0.79	0.34	2.47	1.80	0.67	0.34	0.36	1.66	1.69	0.79	2.19	1.18	0.55	0.33	2.02	1.85	2.19	3.71	0.51
chr19:23000001-23500000	0.12	0.92	2.55	1.20	1.80	3.37	0.67	0.20	0.49	0.98	0.59	0.62	2.19	1.35	0.69	1.45	3.04	1.01	0.17	3.71	0.67
chrX:103000001-103500000	1.38	0.73	0.19	0.07	0.11	0.45	179.87	1.02	0.41	0.45	0.34	0.62	0.84	163.06	0.35	1.29	0.56	0.84	0.34	0.51	1.52
chr1:185500001-186000000	1.38	0.78	0.64	0.67	0.67	0.22	2.25	2.76	1.53	0.90	1.35	1.18	0.67	8.43	2.34	0.38	1.12	0.67	2.36	0.51	2.36
chr12:118500001-119000000	na	1.22	1.80	2.85	3.37	1.35	2.02	na	2.93	2.87	3.04	3.15	2.19	7.93	na	0.70	0.34	1.18	0.51	1.01	1.35
chr6:134000001-134500000	2.60	na	0.60	0.45	0.79	0.45	2.70	2.53	na	0.17	0.76	1.29	0.51	6.41	2.19	na	1.12	1.01	1.18	0.17	2.70
chr13:108500001-109000000	1.27	0.70	0.41	0.52	1.01	0.45	2.02	1.46	1.23	0.34	0.93	0.96	0.00	6.41	2.63	1.16	0.67	0.00	2.19	0.67	5.90
chr1:194500001-195000000	1.55	0.85	0.56	0.34	0.56	0.34	0.67	2.22	0.49	0.51	0.34	1.07	0.51	5.90	2.77	0.09	0.45	0.67	1.52	0.34	2.70
chr1:195000001-195500000	2.31	0.56	0.60	0.41	0.34	0.67	3.37	1.72	0.50	0.08	0.42	0.84	0.00	5.90	2.31	0.18	0.79	0.34	2.19	0.51	5.56
chr13:117500001-118000000	1.23	1.67	0.11	0.64	0.56	0.45	1.12	2.51	2.68	0.39	1.01	1.69	1.18	5.90	3.28	0.91	0.56	0.51	0.84	0.84	1.35
chr1:196500001-197000000	2.17	1.12	0.22	0.56	0.34	0.34	3.37	2.34	0.68	0.20	0.51	0.45	0.34	5.40	3.24	0.72	0.22	0.84	0.34	0.00	3.37
chr10:116000001-116500000	1.96	0.27	1.01	0.56	1.01	0.56	2.02	2.05	1.85	1.85	2.19	1.35	2.36	5.40	1.87	0.50	0.79	0.84	1.35	0.51	2.36
chr10:110500001-111000000	0.86	0.24	1.09	0.26	0.22	0.56	2.47	1.82	1.95	0.98	0.67	1.35	1.35	5.23	2.41	0.07	1.01	0.17	1.18	0.51	2.53
chr10:120500001-121000000	1.56	0.57	0.45	0.64	0.67	0.45	1.80	1.59	0.49	0.70	1.10	0.84	0.34	5.23	1.25	0.34	0.45	0.51	0.51	0.51	2.02
chr5:151000001-151500000	2.60	0.81	1.01	0.75	0.90	0.34	1.35	3.48	1.59	0.87	1.43	1.18	0.34	5.06	2.53	0.20	0.22	0.67	0.84	0.17	1.69
chr8:129500001-130000000	1.48	0.88	2.02	0.71	0.79	0.67	0.90	1.44	0.02	0.70	1.26	0.39	0.34	5.06	1.90	0.41	0.34	1.35	0.67	0.17	1.52
chr13:109000001-109500000	1.65	1.28	0.71	0.86	0.56	0.67	2.70	1.45	1.30	0.67	0.76	0.56	0.84	5.06	1.60	0.54	0.45	0.00	0.34	0.34	1.01
chr13:115500001-116000000	0.80	1.26	0.41	0.30	0.11	0.79	1.35	1.58	1.38	0.51	0.93	0.51	0.34	5.06	2.28	0.93	0.34	1.18	0.51	0.00	1.52
chr6:146500001-147000000	2.85	na	0.67	1.01	1.01	0.45	2.25	3.28	na	1.29	2.02	1.63	0.67	4.89	1.88	na	0.79	0.51	0.67	0.51	3.04
chr7:151500001-152000000	1.79	0.66	0.41	1.27	0.56	0.45	0.90	1.63	0.13	0.59	1.85	0.79	0.00	4.55	0.76	0.37	0.11	2.19	0.51	0.51	1.35
chr13:110000001-110500000	1.27	0.78	0.41	0.30	0.45	0.34	1.80	2.38	1.25	1.12	0.76	0.17	1.52	4.55	2.45	1.13	0.34	0.34	0.51	0.51	2.53
chr3:148500001-149000000	2.26	0.38	0.52	0.30	na	0.45	2.25	2.34	0.80	0.37	0.17	na	0.34	4.38	2.46	0.46	0.22	0.84	na	0.67	0.34
chr7:152000001-152500000	2.51	1.09	0.30	0.82	1.91	0.22	1.35	2.07	0.28	0.28	1.77	0.17	0.67	4.38	0.85	0.47	0.34	0.00	0.84	0.17	0.84
chr11:109000001-109500000	2.75	0.21	0.00	1.12	2.14	0.45	2.02	2.56	1.94	0.59	1.35	1.46	1.18	4.22	1.65	0.55	0.45	2.36	2.19	0.17	1.35
chr4:120500001-121000000	1.49	0.36	0.71	na	1.12	0.11	1.57	1.54	0.87	0.73	na	2.42	1.85	3.88	1.21	0.18	0.00	na	1.01	0.51	1.35
chr14:119000001-119500000	2.70	0.24	0.94	0.49	1.12	0.34	1.12	2.24	2.39	1.07	2.36	1.80	0.84	3.88	2.45	0.34	0.34	0.51	3.37	0.84	2.70
chr16:48500001-49000000	0.29	0.34	na	1.09	0.45	1.01	0.45	0.70	0.35	na	0.00	0.11	1.69	0.00	3.30	0.56	na	0.34	3.20	2.19	6.24
chr10:98500001-99000000	1.82	0.78	0.71	0.75	1.12	0.45	1.57	2.71	3.00	1.24	1.52	2.42	2.53	3.37	2.98	0.32	1.12	0.84	1.69	0.34	5.73
chr3:144000001-144500000	1.86	0.51	0.64	0.56	na	0.67	0.45	2.03	1.09	0.70	0.67	na	0.67	3.20	2.97	0.29	0.79	0.51	na	0.67	5.23
chr6:135000001-135500000	2.50	na	0.82	0.37	0.67	0.45	2.70	1.38	na	0.31	0.34	0.22	0.00	2.02	1.43	na	0.56	0.00	1.18	0.67	4.38
chr5:150000001-150500000	3.13	0.31	0.37	1.24	1.69	1.24	3.15	2.08	1.36	1.55	1.69	3.09	1.01	3.37	0.84	0.81	0.90	1.01	2.02	0.67	4.22
chr17:80000001-80500000	2.02	0.37	0.64	1.27	0.67	1.01	1.57	2.05	2.19	1.07	2.70	2.59	2.70	3.37	1.87	0.66	0.67	0.51	3.37	1.01	4.22

chr3:75000001-75500000	0.78	0.79	0.60	0.15	na	2.02	0.90	0.78	1.61	0.51	1.35	na	2.19	2.36	2.91	0.98	0.22	0.34	na	1.01	3.88